Journal of Geophysical Research

VOLUME 64 OCTOBER 1959 NUMBER 10

THE SCIENTIFIC PUBLICATION
OF THE AMERICAN GEOPHYSICAL UNION

Journal of Geophysical Research

An International Scientific Publication

This Journal welcomes original scientific contributions on the physics of the earth and its environment.

Manuscripts should be transmitted to J. A. Peoples, Jr., Geology Department, University of Kansas, Lawrence, Kansas. Authors' institutions, if in the United States or Canada, are requested to pay a publication charge of $15 per page, which, if honored, entitles them to 100 free reprints.

Subscriptions to the *Journal of Geophysical Research* and *Transactions, AGU* are included in membership dues.

Non-member subscriptions, *Journal of Geophysical Research*. . $16 for the calendar year 1959, $2 per copy; $20 for the calendar year 1960, $2.25 per copy

Non-member subscriptions, *Transactions, AGU*. . . . . $4 per calendar year, $1.25 per copy

Subscriptions, renewals, and orders for back numbers should be addressed to American Geophysical Union, 1515 Massachusetts Ave., Northwest, Washington 5, D. C. Suggestions to authors are available on request.

Advertising Representative: Howland and Howland, Inc., 114 East 32nd St., New York 16, N. Y.

Beginning with the January 1959 issue (Vol. 64, No. 1) the *Journal of Geophysical Research* is published monthly by the American Geophysical Union, the U. S. National Committee of the International Union of Geodesy and Geophysics organized under the National Academy of Sciences-National Research Council as the U. S. national adhering body. Publication of this journal is supported by the National Science Foundation and the Carnegie Institution of Washington. The new monthly combines the type of scientific material formerly published in the bi-monthly *Transactions, American Geophysical Union*, and the quarterly *Journal of Geophysical Research*. The *Transactions, American Geophysical Union* will continue as a quarterly publication for Union business and items of interest to members of the Union.

Published monthly by the American Geophysical Union from 1407 Sherwood Avenue, Richmond, Virginia. Second class postage paid at Richmond, Virginia.

WRITTEN BY THE WIND

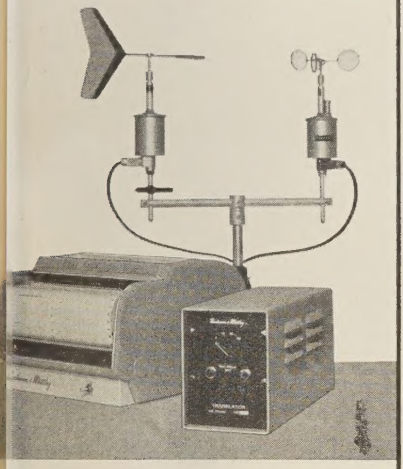

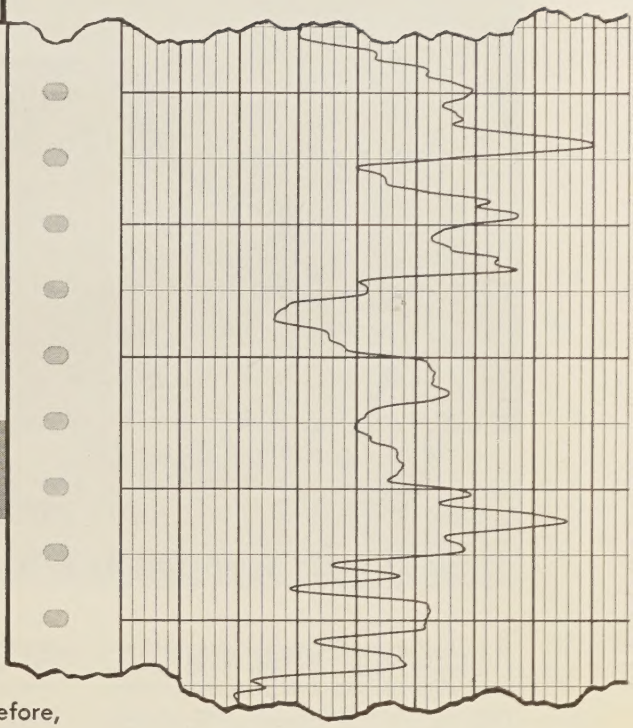

High resolution recording system

Sliced up thinner than ever before, the wind can record itself with a new maximum of resolution in the Beckman & Whitley Type F System. This not only permits a more intimate documentation of the features of the winds, but, even where detailed records are not required, offers many advantages for fixed-station and system-telemetering uses.

Operating from standard 115-volt 60-cps supply, the Type F can be used in portable applications where the increased resolution is needed, by the addition of an accessory battery-operated power supply.

Sample chart illustrated, produced by typical recorder shown, reveals fine, smooth detail recorded where maximum chart width is six miles per hour at a chart speed of 6-in. per min. Translator unit, designed for either bench-top or rack mounting, permits instantaneous switching between the four scales calibrated to maxima of 6, 12, 30, and 60 miles per hour.

For further information write:

Beckman & Whitley INC.

SAN CARLOS 15, CALIFORNIA

CUT EXPLORATION COSTS . . .
SAVE 50% to 80% IN POWER, WEIGHT, SIZE

Texas Instruments Incorporated has developed a completely new, high-performance seismograph around the functional magic of transistors.

YOU SAVE ON PORTAGE AND TRANSPORTATION . . . For the first time, a 24-channel seismograph, complete with control and test circuitry, is contained in a compact, *one-man* portable case 18" x 26" x 8" weighing only 57 pounds. Other systems require from three to six cases for components performing the same functions. Also, the entire seismograph system, with camera and magnetic recorder (*TECHNO's* new all-transistorized magnetic recorder is a highly compatible system with the EXPLORER) may be mounted in one Jeep or transported in one helicopter trip.

YOU SAVE ON POWER . . . the EXPLORER requires only one 12-volt battery and consumes nine amperes (normally only six amperes after first breaks) . . . no warmup time is required. This is better than a five-to-one power savings over other present seismographs.

YOU SAVE ON MAINTENANCE . . . after initial system checks, 80 per cent of all amplifier difficulties are attributable to vacuum tubes. Transistors used in the EXPLORER, for practical purposes, have infinite life.

Furthermore, the EXPLORER offers a wide practical frequency range, 5 to 200 cps; broad dynamic range; and wide operational latitude in AGC speeds, initial suppression, filtering, inputs, outputs, and test circuitry.

The EXPLORER is literally *jumps* ahead of the exploration industry . . . it pays for itself in REDUCED OPERATING COSTS, INCREASED PRODUCTION, and UNEQUALLED RELIABILITY.

Write for complete EXPLORER information . . . specify Bulletin S-324.

TEXAS INSTRUMENTS
INCORPORATED
GEOSCIENCES AND INSTRUMENTATION DIVISION
3609 BUFFALO SPEEDWAY • HOUSTON, TEXAS
CABLE: TEXINS

Other TI/GSID Products
- Complete Seismic Instrumentation
- TI Worden Gravity Meters
- Measurement and Control Systems
- "tracti-riter" Recorders and Accessories
- Automatic Test Equipment

(TI handles export sales and service for TECHNO transistorized recorder)

MINIATURIZED RAYDIST DM SYSTEM

SAVES OIL COMPANY THOUSANDS OF DOLLARS

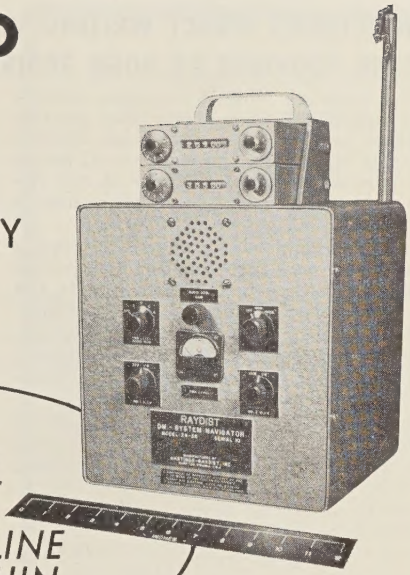

HYDROGRAPHIC AND GEOPHYSICAL SURVEY ALONG 75 MILES OF COASTLINE COMPLETED WITHIN 40 WORKING DAYS

The Pacific Petroleum Company, an affiliate of Richfield Oil, selected the new, miniaturized Raydist Type DM system for use in a geological survey off the coast of Peru.

According to the Chief Geophysicist for the survey, the selection of Raydist over other position determining systems resulted in an over-all savings of thousands of dollars.

Since time was limited, the equipment was shipped by air from Hampton, Virginia, to Peru, South America. Raydist, weighing only one-tenth of competitive systems, saved $4,000 in shipping costs alone. Within twenty-four hours after clearing customs, Raydist was on the job.

The new, miniaturized Raydist system saved many days of installation time since the small, light, battery-operated shore stations can be set up within thirty minutes.

Raydist, maintained by only two operators, saved additional transportation costs and also reduced the logistics problem especially important in this remote area.

Raydist provided a continuous permanent record of the vessel's position with relation to two selected shore sites which enabled the survey boat to return to any point at a later date with extreme accuracy.

Raydist left Hampton, Virginia, on December 10 and returned home February 2 after having completed a hydrographic survey along a 75 mile coastline in Peru, South America.

An observer from another oil company, after seeing Raydist in operation, said, "I was favorably impressed by the portability and compactness of the system. I was also favorably impressed by the apparent accuracy and repeatability of the system. The whole set-up appeared efficient, and I feel sure it would be of value in our operation."

In case after case, Raydist has proved itself a superior tool for all hydrographic operations. We welcome your inquiries.

HASTINGS-RAYDIST, INCORPORATED

TEL: PARK 3-6531 HAMPTON, VIRGINIA

Journal of
GEOPHYSICAL RESEARCH

VOLUME 64 OCTOBER, 1959 No. 10

Analytic and Experimental Electrical Conductivity between the Stratosphere and the Ionosphere

R. E. BOURDEAU,[1] E. C. WHIPPLE, JR.,[1] AND J. F. CLARK[1]

U. S. Naval Research Laboratory
Washington, D. C.

Abstract—Data on atmospheric conductivity obtained experimentally in the altitude region between 35 and 80 km by use of rocket-borne Gerdien condensers are presented. Analytic expressions based on ion equilibrium and ionization by cosmic rays only are derived for comparison. The experimental technique is described, and several factors that might influence the measurements are evaluated.

There is good agreement between the measured and predicted values of negative conductivity at altitudes up to 50 km. Low conductivity values observed between 50 and 80 km are attributed to ionic diffusion to particulate matter, the reduction agreeing quantitatively with that calculated from present estimates of the radius and concentration of noctilucent cloud particles. It is suggested that meteoritic dust may be an important agent for electron destruction in the ionosphere.

Introduction—The electrical conductivity of the atmosphere has been investigated extensively in the troposphere and stratosphere below 30 km and in the ionosphere above 80 km. It is an important parameter in the electrical balance of the lower atmosphere, particularly in the troposphere, where investigations have shown the influence of the positive-to-negative conductivity ratio on the charge accumulated by rain droplets [*Gunn*, 1957]. Earlier balloon measurements by *Wigand* [1914] and *Gish and Sherman* [1936] have been extended to almost 30 km by *Woessner, Cobb, and Gunn* [1958] and by *Stergis and others* [1955].

It is well known that conductivity in the ionosphere is larger than in the stratosphere, partly because of photo-ionization processes that begin to be effective at about 80 km. The general nature and structure of the ionosphere between 80 and 300 km have been well established by an effective combination of ground-based radio probing and rocket-borne experiments. Recently the subject has been thoroughly reviewed by *Chapman* [1956].

However, a gap in both theory and experiment has existed between 30 and 80 km. This altitude range includes part of the *D* region; normal *D*-layer radio soundings indicate a reflection from near the 80-km altitude, but the physical processes involved are not well understood [*Mitra*, 1952]. The purposes of this paper are (1) to extend the analytic determination of conductivity up to 80 km, and (2) to present and compare with theory the results of conductivity measurements between 35 and 80 km obtained on November 21, 1950, at White Sands, New Mexico, from the Viking 5 rocket.

Analytic determination of conductivity—Expressions for conductivity as a function of altitude can be derived from the equilibrium equation for ion density:

$$n = (q/\alpha)^{1/2} \qquad (1)$$

[1] Now with the National Aeronautics and Space Administration, Washington 25, D. C.

where q is the rate of ion-pair production and α is Thomson's ion-ion volume recombination coefficient. It is assumed that the free electron concentration is negligible compared with that of the negative ion and that there is but one species each of positive and negative ions. The polar conductivity due to either positive or negative ions is given by

$$\lambda = nek \tag{2}$$

where e is the elementary charge and k is the appropriate positive or negative ionic mobility.

Both k and α are known functions of pressure and temperature and therefore of altitude. Since k is inversely proportional to density its altitude dependence can be obtained from

$$k = k_0(760/p)(T/273) \tag{3}$$

where k_0 is the mobility at standard conditions (NTP), p the pressure in millimeters of mercury, and T the absolute temperature.

The recombination coefficient α is appropriate to air at pressures from 1 atmosphere to 10^{-3} mm Hg and has been expressed as a function of air density by *Loeb* [1955]:

$$\alpha = 1.73 \times 10^{-7}(273/T)^{3/2} \cdot (1/m_m)^{1/2}(2w - w^2) \tag{4}$$

where m_m is the molecular weight of the ions relative to hydrogen, and w is a density-dependent probability function given by

$$w = 1 - (2/x^2)[1 - e^{-x}(x + 1)] = \sum_{n=1}^{\infty} \frac{(-1)^{n+1}2(m + 1)x^n}{(n + 2)!} \tag{5}$$

The parameter x is given by

$$x = 8.1 \times 10^{-4}(273/T)^2(p/760)(1/L_0) \tag{6}$$

where L_0 is the ionic mean free path at NTP.

Values for L_0 and m_m of 2.55×10^{-6} cm and 110 AMU, respectively, have been determined from Langevin's mobility equation [*Loeb*, 1955] and known values of α [*Thomson and Thomson*, 1928] and k at NTP. For this paper, the conductivity for positive (λ_+) and negative (λ_-) ions is considered separately by substituting values of 1.4 and 1.8 cm^2/volt-sec. for k_0 in equation 3. These are representative of values obtained experimentally by numerous investigators. Thus from equations 1, 2, 3, and 4 we have

$$\lambda_+ = 1.75 \times 10^{-16}(760/p) \cdot (T/273)^{7/4}[q/(2w - w^2)]^{1/2} \tag{7}$$

$$\lambda_- = 2.25 \times 10^{-16}(760/p) \cdot (T/273)^{7/4}[q/(2w - w^2)]^{1/2} \tag{8}$$

Since w is a function of pressure and temperature, it remains only to determine the altitude dependence of q. Other authors have been interested mainly in balloon altitudes. *Kraakevik* [1957] and *Stergis and others* [1955] use experimental values of q obtained from balloon-borne ionization chambers. *Woessner and others* [1958] use a mass ionization equation, $q = B\rho I$, where B is a mass ionization coefficient, ρ the air density, and I the cosmic-ray intensity. The equation they develop for λ as a function of altitude, however, cannot be used at high altitudes since they assume an exponential increase of cosmic-ray intensity with decreasing pressure. This assumption is true at White Sands only below about 20 km.

In order to predict λ at higher altitudes the assumption is made here that the curve q_0 (ion pairs per cubic centimeter per second reduced to NTP) versus altitude has the same shape as the cosmic-ray counting rate for a single Geiger counter. This assumption, which is equivalent to the mass ionization equation, was shown to be valid at lower altitudes by *Neher and Pickering* [1942] from simultaneous ionization and counter observations. The assumption is approximately valid at higher altitudes where groups of particles register only once in the counter. The resultant error in the conductivity should be small, however, since λ is proportional to $q^{1/2}$. By comparing low-altitude ionization data [*Millikan, Neher, and Pickering*, 1944; *Biehl and Neher*, 1950] at 41° north magnetic latitude with the smoothed composite curve of counting rate versus altitude obtained at White Sands by *Gangnes, Jenkins, and Van Allen* [1949], a conversion factor between q_0 and counting rate of 5.6 ions/cm^3 per count/sec was realized. This conversion factor was then applied to the above counter data to obtain q_0 versus altitude up to 80 km. Since the ambient ionization rate is proportional to the density,

onductivity is given by

$$_{++} = 1.75 \times 10^{-16}(760/p)^{1/2} \cdot (T/273)^{5/4}[q_0/(2w - w^2)]^{1/2} \quad (9)$$

$$_{--} = 2.25 \times 10^{-16}(760/p)^{1/2} \cdot (T/273)^{5/4}[q_0/(2w - w^2)]^{1/2} \quad (10)$$

Two major assumptions are made in the preceding analysis. The first is that cosmic radiation is the only source of ionization (no collisional or photo-ionization). If this were not valid, then, in the absence of other compensating factors, the experimental values of both polar conductivities would be higher than predicted.

The second assumption is that the contribution of free electrons to the negative conductivity is negligible, which implies either that detachment of electrons from negative ions can be neglected, or that the mean lifetime of the free electrons is short, or both. The latter implication was investigated and found to be valid on the basis of *Hill's* curve of capture coefficient versus altitude [1958] and the same assumption of ionization by cosmic rays only. *Chapman and Little's* assumption of a constant capture coefficient with altitude [1957] yields a relatively constant and negligible value of 10^{-6} for the ratio of electron to negative ion density between 35 and 80 km. Even if the free electron density is significant, it is shown in the next section that the experimental values of negative conductivity would still correctly measure the contribution of the negative ions to the total negative conductivity.

Predicted values of conductivity are affected to a smaller extent by the assumption that the nature of the ions is the same at all altitudes. It is probable that the complex ions (clusters) formed in air at sea level are broken up into simpler molecules at lower pressures. Rocket ion spectroscopy data [*Johnson and others*, 1958] indicates that the ionic molecular weight at the highest altitude of interest here is in the neighborhood of 32 AMU. If an ion mass of 32 AMU is used, a value for k_0 of 2.5 cm²/volt-sec is computed from Langevin's point center of force equation [*Loeb*, 1955]; and a value for L_0 of 1.53×10^{-5} cm is obtained by using this value of k_0 in the expression for α at NTP. The net effect is to increase the predicted values of λ_+ and λ_- by factors of approximately 3.2 and 2.5 respectively.

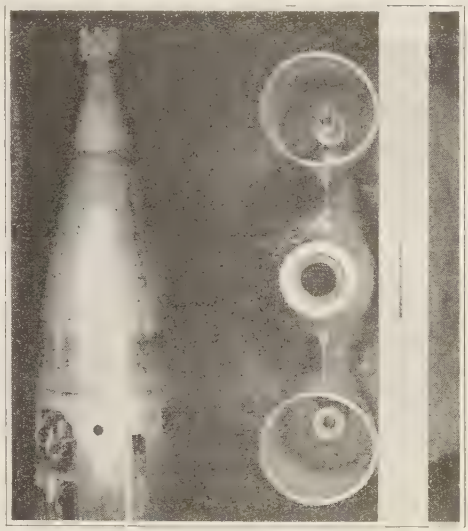

FIG. 1—Dual Gerdien condensers on nose cone of Viking rocket.

Experimental determination of conductivity —Two Gerdien condensers were mounted beside each other on the nose of the rocket with their axes parallel to the longitudinal axis of the rocket (Fig. 1). The potential of the central electrode relative to the outer cylinder in each condenser was programmed in 12.5-volt steps from −100 to +100 volts, and the resultant current was measured and telemetered. During each of the 18 voltage steps four amplifier input resistors were commutated so that a current to the central electrode ranging from 10^{-9} to 10^{-5} amp could be measured with an ac-

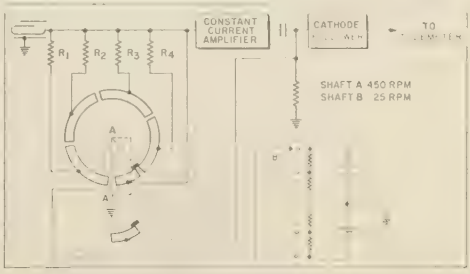

FIG. 2—Block diagram of electronic system.

curacy of approximately 10 per cent. A current-voltage curve for each polarity was obtained in 1.2 seconds.

A block diagram of the electronic system is given in Figure 2. Immediately after each change in its potential, the central electrode was connected directly to the potential source for about 10 milliseconds before the four input resistors were commutated. This had two beneficial effects: (1) by providing an amplifier input zero voltage reference, errors due to cathode follower drift were eliminated; and (2) by charging and discharging the Gerdien condenser through a negligible impedance, the effects of displacement currents were removed. Long-term drift in the amplifier was circumvented by the use of condenser coupling between it and the cathode follower. High currents through the larger input resistors caused overloading of the amplifier. The slow recovery of the cathode follower which otherwise would have occurred was eliminated by commutating the resistors in order of increasing resistance and then discharging the coupling condenser synchronously with the discharge of the Gerdien condenser.

The usual relation for computing conductivity from the volt-ampere curve is:

$$\lambda = (\epsilon_0/C)\ dI/dV \qquad (11)$$

where ϵ_0 is the dielectric constant of air and C the capacitance of the condenser (3.2 mmf). The expression is assumed to be valid as long as the ionic mean free path is small compared with the dimensions of the condenser. At about 80 km, the mean free path is 0.6 cm (the diameter of the central cylinder), photo-ionization starts to take place, a positive ion sheath forms about the rocket, and the condenser functions as a Langmuir probe. For these reasons, data above 80 km are not reported here.

The measurement of conductivity from a high-speed rocket is at least an order of magnitude more difficult than measurements made from aircraft and balloons. The factors affecting the interpretation of the volt-ampere curves which airplane and balloon experimenters have considered are re-evaluated here for the rocket case.

A sufficiently large charge on the rocket itself would reduce the measured conductivity of the same polarity. When *Kraakevik's* airplane results [1958] are extrapolated to higher altitudes and larger air flows, the critical vehicle potential (relative to the surrounding atmosphere) below which the measurement is essentially unaffected falls exponentially with altitude but is still greater than 100 volts at 80 km. An electric field meter was flown simultaneously with the conductivity apparatus described here. Its measured field due to the charge on the rocket over the altitude range considered here was less than the instrument's maximum sensitivity of 50 volts/meter. It is possible to compute from this an upper limit for the vehicle potential by approximating the rocket shape with a prolate spheroid [*Clark*, 1957]. Thus a value of rocket potential of less than 55 volts was indirectly obtained. These data show that any charge on the rocket did not influence the measured conductivity.

Shock-wave effects which do not exist for slow-moving aircraft must be critically examined in the present case of a rocket traveling with a speed greater than Mach 4. The increase in air density ρ in passing through the shock front should cause only second-order effects, however, since the ion density in the affected region increases proportionally whereas the mobility decreases inversely as ρ. This assumes that the lifetime of an ion is much greater than the time the ion spends in the shock-affected region, a justifiable assumption since the lifetime of an ion at sea level is several minutes and increases with altitude.

The measured conductivity is independent of air flow as long as the applied potential is less than that required for current saturation. This critical voltage, V_c, at which all the ions entering the Gerdien condenser are collected is proportional to u/k, the ratio of air flow to

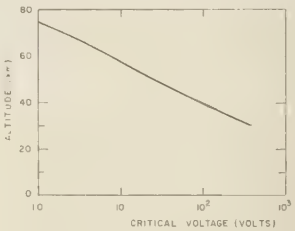

FIG. 3—Analytic values of critical voltage (V_c) versus altitude.

mobility, and is plotted against altitude in Figure 3. All the volt-ampere curves obtained below 80 km were approximately linear. Although the resolution was not good enough to detect small departures from linearity it can be stated with confidence that the expected saturation did not occur.

At least two possible phenomena could raise the value of V_o. If the quantity u_ρ were constant through the shock-affected region (mass transport equation), V_o would be unchanged, but the convergence of the flow lines around the rocket causes u_ρ to increase at the condensers and thereby raises V_o. If the shock wave increases ρ by a factor r, it would increase the critical voltage by not more than $r^{2/3}$. Immediately behind the shock front, r may have a value as high as 5. Thus, increases in V_o due to the shock wave do not explain completely the absence of saturation above 55 km.

Another possibility is that the effective collection area of the condenser with its relatively exposed central electrode increases with applied potential, especially at the higher altitudes. Such an increase in collection area would cause the condenser to behave similarly to an isolated unipolar collector which never saturates. The observed linearity of the volt-ampere curves at all altitudes for voltages greater than the computed value of V_o indicates that the increased collection area affected only V_o and not the effective capacitance C in equation 11.

Another possible effect of the shock wave is the production of ions by thermal ionization. At speeds above Mach 4 the temperature just behind the shock front may be as high as 1200°A. Other investigators have detected ionization behind pellets moving at speeds above 1 km/sec at sea-level pressure [*Partridge and Harris*, 1957; *Hendricks*, 1957]. *Saha's* equation [1920] yields 10^7 ions/cm^3 for 1200°A at 68 km, but its applicability may be questioned since it is an equation for a system in chemical equilibrium. Such large ion densities would certainly have caused larger currents than were observed below 80 km. Similarly, breakdown of the air would have resulted in larger currents than were observed.

Finally, it should be noted that the negative conductivity computed from (11) will not include the contribution of free electrons. Their high mobility would result in their collection at the lowest applied positive potential so that the net effect on the current-voltage characteristic beyond the zero voltage point would be to displace the negative current away from the abscissa by a fixed amount. Such displacements were not observed below 80 km.

Discussion of results—The rocket was launched at 1018 MST and reached a peak altitude of 174 km 4 minutes later. Excellent trajectory and aspect data were obtained, and all the research instrumentation performed well. The axes of the Gerdien condensers did not deviate from the flight path by more than 21° below 80 km. This amount of deviation has a negligible effect on the air flow through the condenser. Current-voltage characteristics were obtained until the rocket broke up on the downward leg. The day was free of any unusual solar or geomagnetic disturbances. The local meteorological conditions were exceptionally good, with no clouds visible from the launching site.

Predicted values of positive and negative conductivity from equations 9 and 10 using pressure and temperature data published by the *Rocket Panel* [1952] are shown as the solid curves in Figure 4. The dashed curve is the predicted conductivity for an ionic molecular weight of 32 AMU as indicated in the second section. Superimposed are the experimental rocket values computed from the slopes of the best straight lines through the points obtained on the volt-ampere characteristics. The points below 30 km are the results of *Woessner, Cobb, and Gunn* [1958].

The experimental rocket conductivity values

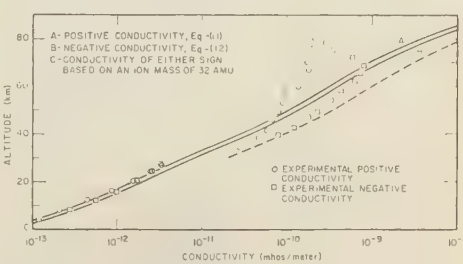

FIG. 4—Conductivity versus altitude. Experimental points below 30 km are from *Woessner, Cobb and Gunn* [1958]. Observed values above 30 km were obtained during the rocket ascent.

lie close to the dashed curve up to 40 km, indicating that the ion mass is considerably less than that of the complex ion of the lower atmosphere, although the ambient ion above 30 km may be actually complex with its breakup occurring in the shock wave.

There are two striking features in the experimental data above 40 km: (1) both λ_+ and λ_- increase more slowly with altitude than was expected; (2) the negative-to-positive conductivity ratio increases with altitude up to about 70 km, at which altitude λ_- drops off sharply until at 80 km λ_+ and λ_- are nearly equal and a factor of 50 less than expected.

There is no correlation between the conductivity ratio and the angle that the condenser axes made with the sun's position vector. Thus the difference cannot be explained by the effects of sunlight.

The most likely explanation for the different behavior of λ_+ and λ_- below 60 km is that the mobility of the positive ion decreased inside the condenser. It is known that the mobility of positive molecular oxygen and nitrogen ions decreases for high values of E/p, where E is the electric field and p the pressure [*Varney*, 1953]. Thus λ_+ inside the Gerdien condenser would be reduced from its value outside. Allowance for this effect brings the positive conductivity into much better agreement with the negative conductivity values below 60 km.

The decrease in positive-ion mobility at high E/p is a charge-exchange phenomenon which does not occur in general for negative ions. There is instead the possibility of electron detachment from O_2^- at high E/p which would cause an increase in the effective mobility [*Loeb*, 1955]. However, this effect is ruled out by the observed linearity of the volt-ampere curves at all altitudes.

The most probable explanation for the observed low conductivities is the presence of particulate matter in the atmosphere. There is considerable interest at the present time in this phenomenon because of *Bowen's* suggestion [1953] of an effect of meteor dust on rainfall. *Ludlam* [1957] attributes the occurrence of noctilucent clouds at 80 km to dust layers, and *Bigg* [1956] claims to have detected dust at the 80-km temperature minimum by observations of twilight scattering. Since the combination coefficient for the destruction of ions by diffusion to particles depends only on the temperature and the available particle surface area above 30 km whereas Thomson's volume recombination coefficient is roughly proportional to the pressure, the diffusion process will predominate at high altitudes even if the particle concentration is very low.

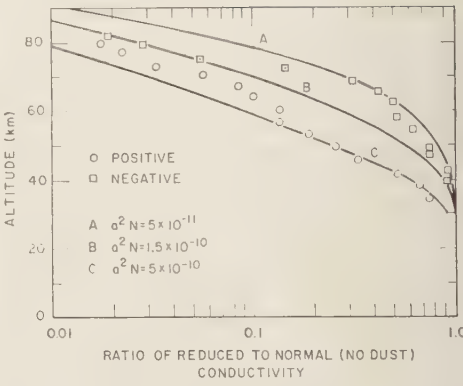

FIG. 5—Effect of particulate matter on conductivity. N is the particle concentration per cubic centimeter and a the particle radius in centimeters.

Computed ratios of reduced to normal (no particulate matter) conductivity for various radii and concentrations of particles are plotted as solid lines in Figure 5. The individual points are the ratios of the experimental to the predicted conductivity (dashed curve) of Figure 4. An ion equilibrium equation of the following form was assumed:

$$q = \alpha n^2 + \eta n N \qquad (12)$$

where N is the particle concentration and η the combination coefficient for ions diffusing to spherical particles. The appropriate value for η in this situation is

$$\eta = \pi a^2 \bar{c} \qquad (13)$$

where a is the particle radius and $\bar{c}$ the most probable thermal velocity of the ion. The expression for η given by (13) can also be derived from a more general treatment by *Gunn* [1954] by considering the case when the ionic mean free path is larger than the particle radius and the equilibrium charge on the particle is zero

It is evident from the figure that a concentra-
on of only 1 particle per cm^3 with a radius of
$^{-5}$ cm would cause the kind of reduction that
as observed. These values agree with Ludlam's
timate of concentration and radius for the
rticles composing noctilucent clouds.

In the presence of a few free electrons one
ould expect the particles to acquire a negative
harge, which means that to maintain zero
pace charge n_- must be less than n_+. In such
case the measured negative-to-positive con-
uctivity ratio should decrease as it is observed
do above 60 km. The possibility of this effect
being studied further.

Conclusions—1. Predicted values of conduc-
vity are derived for altitudes up to 80 km for
n masses of 110 and 32 AMU on the assump-
on that cosmic rays are the only source of
nization. The good agreement between rocket
easurements of negative conductivity in the
titude range from 35 to 50 km and the pre-
cted values for an ion mass of 32 AMU indi-
tes that at least for this flight cosmic rays
ere the only source of ionization and that the
llected ions in this region are smaller than
e complex ions known to exist in the lower
mosphere.

2. An unexpectedly high negative-to-positive
nductivity ratio was observed above 40 km.
he high ratio between 40 and 60 km was most
kely introduced by the measuring apparatus
the form of a decrease of the positive-ion
obility in the electric field of the condenser
these low pressures.

3. The measured values of both positive and
gative conductivities are much lower than
redicted at altitudes above 50 km. It is sug-
sted that the presence of particulate matter
responsible for this reduction. The amount
the reduction agrees quantitatively with the
fect calculated from present estimates of the
dius and concentration of noctilucent parti-
es. Since dust has been observed to altitudes
at least 200 km after meteor showers [*Zach-
ov*, 1957] it may be an important agent for
ectron destruction in the ionosphere that has
itherto been overlooked.

4. The integrated columnar resistance of the
mosphere between 40 and 80 km, computed
ther from the analytic or experimental con-
uctivity, contributes less than 1 per cent to
previous estimates of the total columnar re-
sistance [*Kraakevik*, 1958].

5. These measurements should be extended
to study diurnal and latitude variations of ion
density in the 30 to 80-km region. It would be
desirable to modify the experiment so as to
definitely obtain saturation currents. Such meas-
urements would be particularly interesting be-
low an aurora to investigate the increase in ion
density from auroral X rays suggested by *Chap-
man and Little* [1957]. An experiment to
measure ionization rate should be flown simul-
taneously.

Acknowledgments—This project was originated by T. R. Burnight, former head of the Ionosphere Section of the Rocket Sonde Branch at the U. S. Naval Research Laboratory. The authors wish to thank E. M. Trent for her part in reducing and plotting many of the data. The Physical Science Laboratory of the New Mexico College of Agriculture and Mechanic Arts also assisted in this respect. The helpful discussions with G. P. Serbu during the preparation of the paper are also acknowledged.

References

Biehl, A. T., and H. V. Neher, The latitude and longitude effects in cosmic rays over the United States and Canada at 30,000 feet, *Phys. Rev., 78,* 172–173, 1950.

Bigg, E. K., The detection of atmospheric dust and temperature inversions by twilight scattering, *J. Meteorol., 13,* 262-268, 1956.

Bowen, E. G., The influence of meteoritic dust on rainfall, *Australian J. Phys., 6,* 490–497, 1953.

Chapman, S., The electrical conductivity of the ionosphere: a review, *Nuovo Cimento, 4,* Suppl., 1385–1412, 1956.

Chapman, S., and C. G. Little, The nondeviative absorption of high-frequency radio waves in auroral latitudes, *J. Atmospheric and Terrest. Phys., 10,* 20-31, 1957.

Clark, J. F., Airborne measurement of atmospheric potential gradient, *J. Geophys. Research, 62,* 617–628, 1957.

Gangnes, A. V., J. F. Jenkins, Jr., and J. A. Van Allen, The cosmic-ray intensity above the atmosphere, *Phys. Rev., 75,* 57–69, 1949.

Gish, O. H., and K. L. Sherman, The National Geographic Society— U. S. Army Air Corps stratosphere flight of 1935 in the balloon Explorer II, *Natl. Geog. Soc., Stratosphere Series,* no. 2, 94–116, 1936.

Gunn, R., Diffusion charging of atmospheric droplets by ions, and the resulting combination coefficients, *J. Meteorol., 11,* 339–347, 1954.

Gunn, R., The electrification of precipitation and thunderstorms, *Proc. IRE, 45,* 1331–1359, 1957.

Hendricks, C. D. Jr., Ionization by ultra-speed pellets, *J. Appl. Phys., 28,* 1339–1341, 1957.

Hill, E. L., Free electrons in the lower atmosphere, *Recent Advances in Atmospheric Electricity,* Pergammon Press, New York, 1958.

Johnson, C. Y., E. B. Meadows, and J. C. Holmes, Ion composition of the arctic ionosphere, *J. Geophys. Research, 63,* 443–444, 1958.

Kraakevik, J. H., *The electrical conductivity and current density in the troposphere,* University Microfilms, Ann Arbor, 1957; Doctoral Dissertation Series, pub. no. 21,526.

Kraakevik, J. H., The airborne measurement of atmospheric conductivity, *J. Geophys. Research, 63,* 161–169, 1958.

Loeb, L. B., *Basic Processes of Gaseous Electronics,* University of California Press, Berkeley, 1012 pp., 1955.

Ludlam, F. H., Noctilucent clouds, *Tellus, 9,* 341–364, 1957.

Millikan, R. A., H. V. Neher, and W. H. Pickering, Further studies on the origin of cosmic rays, *Phys. Rev., 66,* 295–302, 1944.

Mitra, S. K., *The Upper Atmosphere,* The Asiatic Society, Calcutta, 713 pp., 1952.

Neher, H. V., and W. H. Pickering, Results of a high altitude cosmic-ray survey near the magnetic equator, *Phys. Rev., 61,* 407–413, 1942.

Partridge, W. S., and L. D. Harris, Ionization in the trail of high-velocity pellets, *J. Appl. Phys. 28,* 1269–1271, 1957.

The Rocket Panel, Pressures, densities, and temperatures in the upper atmosphere, *Phys Rev., 88,* 1027–1032, 1952.

Saha, M. N., Ionization in the solar chromosphere *Phil. Mag., 40,* 472–488, 1920.

Stergis, C. G., S. C. Coroniti, A. Nazarek, D. E Kotas, D. W. Seymour, and J. V. Werme, Conductivity measurements in the stratosphere *J. Atmospheric and Terrest. Phys., 6,* 233–242 1955.

Thomson, J. J., and G. P. Thomson, *Conduction of Electricity through Gases,* vol. I, Cambridg University Press, London, 491 pp., 1928.

Varney, R. N., Drift velocity of ions in oxygen nitrogen, and carbon monoxide, *Phys. Rev., 89* 708–711, 1953.

Wigand, A., Measurements of the electrical conductivity in the free atmosphere up to 9,000 meters in height, *Terrestrial Magnetism and Atmospheric Elec., 19,* 93–101, 1914.

Woessner, R. H., W. E. Cobb, and R. Gunn Simultaneous measurements of the positive and negative light-ion conductivities to 26 kilometers, *J. Geophys. Research, 63,* 171–180, 1958

Zacharov, I., Dämmerungsmessungen im Laufe der Perseiden 1953, *Bull. Astr. Inst. Czech., 8* 135–142, 1957.

Measurements of Ionospheric Electron Content by the Lunar Radio Technique

SIEGFRIED J. BAUER AND FRED B. DANIELS

U. S. Army Signal Research and Development Laboratory
Fort Monmouth, New Jersey

Abstract—Measurements of the Faraday rotation of lunar radio echoes on a frequency of 151 Mc/s are used to determine the time variation in the total ionospheric electron content. Absolute values of ionospheric electron content are determined from these measurements in conjunction with information on the electron content below the F_2 peak computed from vertical-incidence sounding data. Diurnal, day-to-day, and seasonal variations in the total electron content are presented. The ratio n_a:n_b of the number of electrons above the F_2 peak to that below is found to be in the order of 4 to 5 during three summer nights (June) before sunrise and about equal to 3 after sunrise. For two days in November the ratio n_a:n_b is found to be equal to about three both before and after sunrise. Possibilities of inferring other characteristics of the upper ionosphere from observed variations in the total electron content are briefly discussed.

INTRODUCTION

Since the early days of moon radar it has een noted that moon radio echoes are subject o two distinct types of fading. The rapid fad- ng (with periods of seconds) was ascribed to ne librations of the moon; the longer-period ading was considered to be of ionospheric rigin. *Murray and Hargreaves* [1954] first ointed out that the slow fading of moon echoes an be explained as the result of the rotation f the plane of polarization of the radio waves s they pass through the ionosphere (the Fara- ay effect). *Browne et al.* [1956] showed that neasuring the angular rotation of the plane of olarization of lunar radio reflections would ield information on the integrated electron ontent of the ionosphere. Such measurements n two closely spaced frequencies were made y *Evans* [1956, 1957], which, however, were andicapped in giving time variation since bservations were limited to a short time inter- al near lunar transit. Consequently, the re- ults of several days' observations had to be ombined to get a continuous curve. Recently he authors presented results of continuous neasurements of the Faraday rotation on a ingle frequency (151 Mc/s) during one night *Bauer and Daniels,* 1958]. The present paper ives results of additional measurements of his type.

THEORY AND METHOD

For radio waves of a frequency much higher than the plasma, gyro, and collision frequencies, and when the direction of propagation is not too nearly perpendicular to the earth's magnetic field, the quasi-longitudinal approximation of the Appleton-Hartree formula applies. Under these conditions, a linearly polarized wave upon entering the ionosphere is split into two circularly polarized components having opposite rotations and different phase velocities, which causes a rotation of the phase vector of the resultant along the path. For the two-way path from the earth to the moon, the total rotation is given by

$$\Phi = 4.72 \times 10^4 f^{-2} \cdot \int_{h_1}^{h_2} NB \cos\theta \sec\delta \, dh \text{ radians}$$

where N is the number of electrons per cubic centimeter, B is the magnetic field strength in gauss, θ is the angle between the propagation path and the earth's magnetic field, δ is the zenith angle of the propagation path, f is the frequency of the radio wave in cycles per second, and h_1 and h_2 are the height limits within which the electron density is great enough to contribute appreciably to the total rotation. A detailed derivation of the above expression

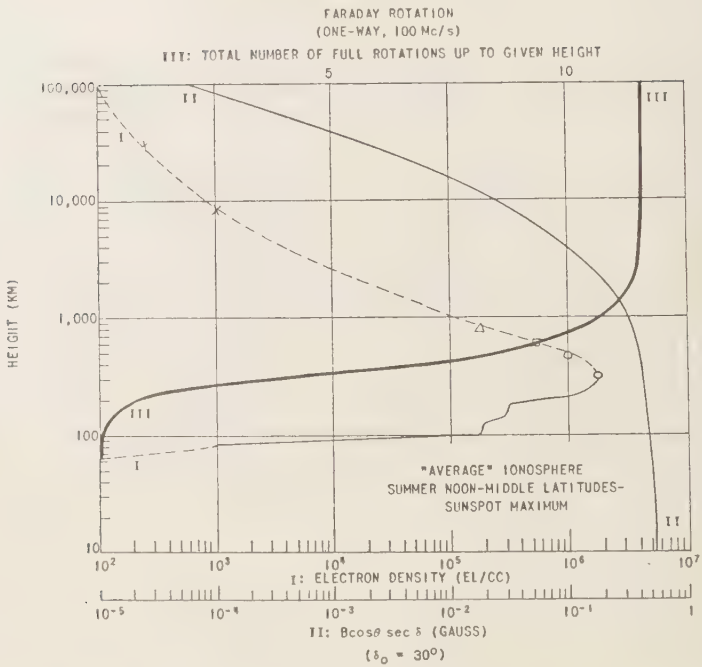

FIG. 1.—Computed Faraday rotation for an ionospheric model compiled from recent rocket, satellite, and whistler data [*Townsend*, 1959].

has been given elsewhere [*Daniels and Bauer*, 1959].

Figure 1 shows the computed Faraday rotation (at 100 Mc/s) for a one-way path for an electron-density profile based on the one compiled from recent United States and U.S.S.R. rocket, satellite, and whistler data [*Townsend*, 1958]. A simple magnetic dipole field and an oblique path (elevation angle of 60°) have been assumed. The cumulative Faraday rotation was calculated by numerical integration. Since $B \cos \theta \sec \delta$ varies only slightly with height within the lower 1000 km, it can be removed from the integral. If a mean value of $B \cos \theta \sec \delta$ representing a height of about 350 km is adopted, the total Faraday rotation computed by means of the generally used formula

$$\Phi = 4.72 \times 10^4 f^{-2} \overline{B \cos \theta \sec \delta} \int_{h_1}^{h_2} N \, dh$$

is in good agreement with the exact value obtained by numerical integration. (For the assumed model there is no appreciable contribution to the Faraday rotation above $h_2 \simeq 2500$ km.)

Since the Faraday rotation at 151 Mc/s is a multiple of π radians, it cannot be determined unambiguously at this frequency. One way to determine the total electron content unambiguously is to use two closely spaced frequencies [*Evans*, 1957] or a frequency greater than 400 Mc/s for which the total rotation is less than π radians at the time of minimum electron content.

Our measurements of the Faraday rotation were made by rotating the receiving dipole and thus introducing sharp nulls in the received signal and observing the shift of the minimum with respect to the dipole's position [*Daniels and Bauer*, 1958]. To remove the ambiguity in the total number of rotations at 151 Mc/s and therefore in the total electron content, we make use of independent information regarding the electron content up to the F_2 maximum, together with certain theoretical considerations. The total electron content as measured by Faraday rotation can be expressed as

$$n_F = \int_{h_1}^{h_2} N\,dh = \int_{h_1}^{h_m} N\,dh + \int_{h_m}^{h_2} N\,dh$$

here h_m is the height of the F_2-layer maximum. Rewriting the above expression,

$$n_F = n_b + n_a$$

here n_b is the electron content below the F_2 eak and n_a is that above the peak.

For nighttime conditions and neglecting diffsion, we may write the equation of continuity or any height level)

$$dN(h)/dt = -\beta(h)N(h)$$

or a realistic approach, we must consider β as function of height, and thus

$$\frac{dn_F}{dt} = -\int_{h_1}^{h_2} \beta(h)N(h)\,dh$$

ccording to the mean value theorem, we can rite

$$\frac{dn_F}{dt} = -\beta_F \int_{h_1}^{h_2} N(h)\,dh = -\beta_F n_F$$

here β_F is a representative mean value. The me considerations apply also for n_b and n_a.

It is known from theoretical studies [*Burkard,* 58] that the following relation holds between e scale height at the F_2 peak and n_a and N_m he electron density at the F_2 peak)

$$H_m = R'T_m \propto (n_a/N_m)$$

here H_m is the scale height and T_m the temperure at the F_2 peak, and R' is the gas constant rresponding to the atmospheric composition the F_2 peak. If we assume that the temperare at the F_2 peak does not change during a ven time interval, we deduce from the above pression that

$$\beta_a = \beta_m$$

here β_a is the effective quasi-attachment coeffient of the region above the F_2 peak, and β_m at at the F_2 peak. Using an approximation to e continuity equation, we can now write for e ratio of the electron content above the F_2 eak to that below

$$n_a/n_b \approx (\beta_b/\beta_m)(\kappa - 1)$$

where

$$\kappa = \frac{\Delta n_F/\Delta t}{\Delta n_b/\Delta t}$$

all of which quantities can be determined experimentally. Thus

$$\bar{n}_F \approx \bar{n}_b[1 + (\beta_b/\beta_m)(\kappa - 1)]$$

where $\bar{n}_F$ and $\bar{n}_b$ are representative mean values over the time interval Δt.

Observational Results

Total electron content vs. subpeak electron content—The variation in the total electron content was derived from continuous Faraday rotation measurements on a frequency of 151 Mc/s. Since our measurements were made with a bistatic radar, the transmitter being located at Belmar, N. J., and the receiver at Urbana, Ill., the propagation path traversed the ionosphere at two different points. Because of the changing intersection points, the total electron content has been plotted as a function of the local civil time midway between the two penetration points (taken at the level of the F_2 peak). The subpeak electron content is based on vertical-sounding data at Washington, D. C., and was computed by the Central Radio Propagation Laboratory of the National Bureau of Standards. The plotted values of the subpeak electron content are three-point moving averages of the original data. The absolute scale for the total electron content was computed from the subpeak values by using the method described above. For each of the curves of measured variation in relative value of total electron content, a time interval Δt was selected which corresponded to a reasonably smooth variation in subpeak electron content, justifying the assumption of a linear law of electron loss. For this time interval, the quantities required for the adjustment to the absolute scale were determined from experimental data. At the midpoint of the selected time interval, the absolute value of total electron content was obtained by multiplying the value of subpeak electron content by the correction factor determined by β_b, β_m, and κ. The entire curve of measured variation in total electron content was then replotted so that the computed absolute value point fell on the curve.

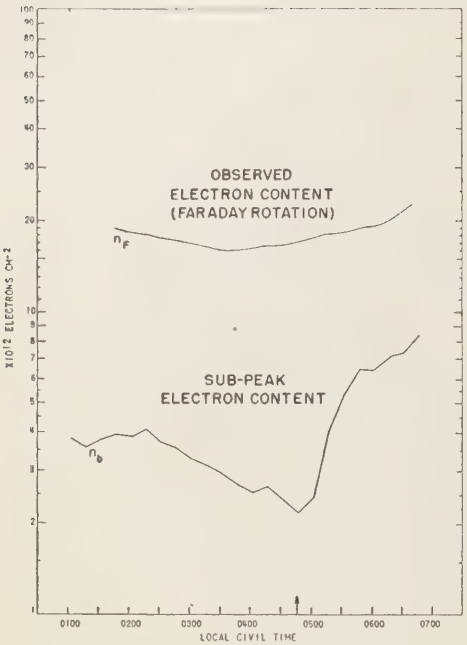

FIG. 2—Time variation in total and subpeak electron content, June 5, 1958.

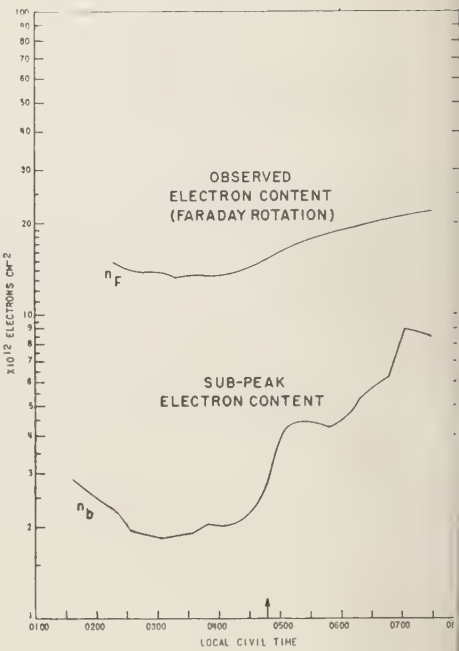

FIG. 4—Time variation in total and subpeak elec tron content, June 8, 1958.

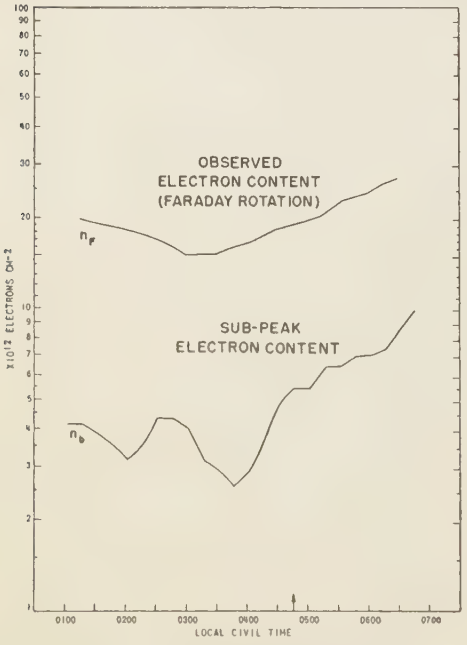

FIG. 3—Time variation in total and subpeak electron content, June 6, 1958.

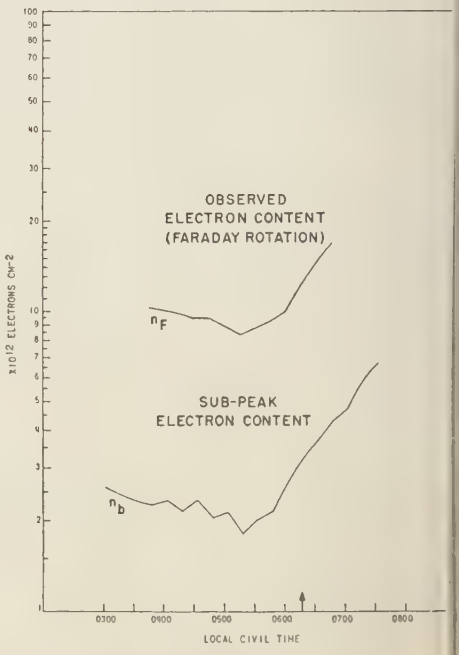

FIG. 5—Time variation in total and subpeak ele tron content, November 5, 1958.

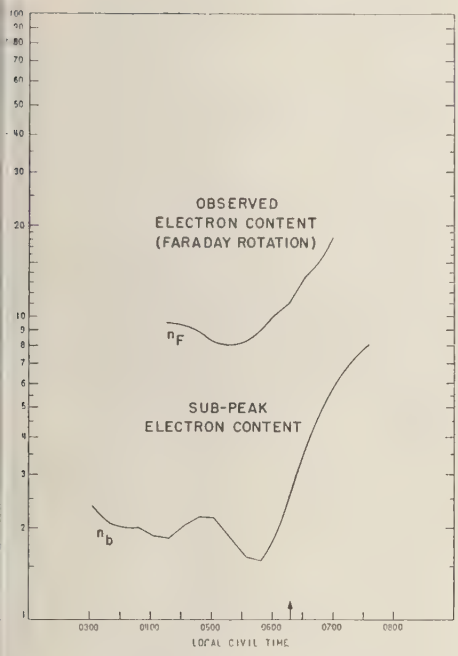

FIG. 6—Time variation in total and subpeak electron content, November 6, 1958.

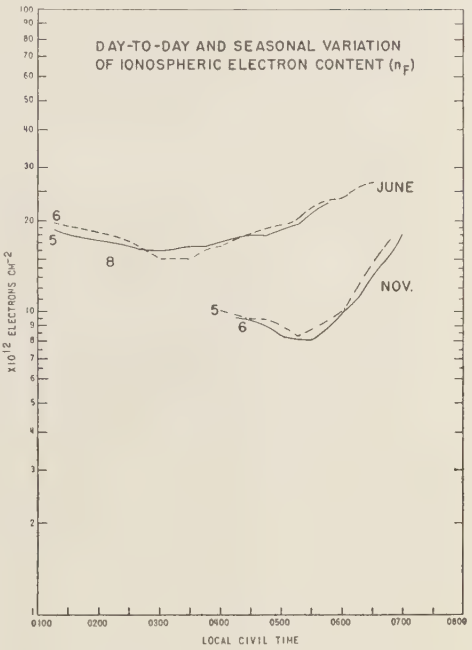

FIG. 7—Comparison of variations in total electron content for June and November 1958.

Figures 2 to 6 show the total electron content nd the subpeak electron content for three days n June 1958 and two days in November 1958. 'or the two days in November the variations n the total electron content followed quite losely the variations in the subpeak electron ontent. The ratio n_a/n_b is approximately equal o 3 throughout the run. For the three days in ummer, however, the variation in the total lectron content is much smoother and exhibits more shallow trough than that of the subpeak. 'he ratio n_a/n_b is in the order of 4 to 5 before unrise at the earth's surface, and about equal o 3 afterward. The obvious reason for the igher ratio is that during June the upper egions of the ionosphere are illuminated by the un much earlier than the lower ionosphere. 'he electron loss in the upper region is therefore partially balanced by electron production, whereas in the lower region only a loss of lectrons occurs.

Day-to-day and seasonal variations—In Figure 7 the variations in the total electron content 'or all five days are plotted. It is obvious that he general shape of the curves for the two lays in November is very similar, although there is a slight day-to-day change in the absolute values.

For the three days in summer, the day-to-day variation between June 5 and June 6 is very small. However, on June 6 the rate of decrease and increase of the total electron content is greater. It should be noted that on June 6 the positive phase of an ionospheric storm occurred. (Fredericksburg, Va., reported the onset of a moderately severe magnetic storm on June 6, 1958, at 0000 EST.) June 7 was one of the five magnetically disturbed days of the month, but unfortunately no measurements were made on this day. On June 8 the total electron content appeared to be lower than on the other two days, but this may also have been due to inaccuracy in adjustment of the absolute scale.

Discussion of Results and Conclusions

Although our method provides very accurate observations of the time variation in the total electron content, the absolute values obtained are subject to inaccuracies, particularly during the summer (because of some of the assumptions made). During summer nights the electron loss in the upper regions of the ionosphere is

partly balanced by electron production beginning soon after midnight. This could explain the fact that during the summer nights the ratio n_a/n_b is higher than during the winter. After sunrise, this ratio seems to average about 3 both in summer and winter.

The time variations in the electron content of the entire ionosphere show a much smoother behavior than those below the F_2 peak. This is due to the fact that any changes in the electron distribution with height average out over the entire ionospheric column, whereas the subpeak electron content measures the number of electrons in a column of unit cross section up to a height which changes irregularly with time.

The relationship between scale height at the F_2 peak and n_a and N_m could be used to determine temperature fluctuations at the F_2 peak. We did not attempt this, however, since we made use of the assumption that no such temperature variation occurred in determining our absolute values of n_F. If the total electron content is measured unambiguously (for example, by using two frequencies), the result could be used to establish the extent of possible temperature variations. The absolute value of the scale height at the F_2 peak, however, can only be determined from the above type of data if assumptions about the temperature profile are made [*Burkard*, 1958].

Acknowlegments—We are indebted to the Central Radio Propagation Laboratory of the National Bureau of Standards, and especially J. W. Wright, for providing us with values of the subpeak electron content. We also wish to acknowledge the assistance of H. D. Webb of the University of Illinois for maintaining and operating the receiving facility, and of Alan S. Gross and his staff of the U. S. Army Signal Research and Development Laboratory, who operated the transmitter. The assistance of Mary Tate in computing the results is also gratefully acknowledged.

References

Bauer, S. J., and F. B. Daniels, Ionospheric parameters deduced from the Faraday rotation of lunar radio reflections, *J. Geophys. Research, 63*, 439–442, 1958.

Browne, I. C., J. V. Evans, J. K. Hargreaves, and W. A. S. Murray, Radio echoes from the moon, *Proc. Phys. Soc. London, B, 69*, 901–920, 1956.

Burkard, O., Studien zum neuen Modell der Ionosphäre, I, *Geofis. pura e appl., 41 (III)*, 133–140, 1958.

Daniels, F. B., and S. J. Bauer, Measurements of the ionospheric Faraday effect by radio waves reflected from the moon, *Nature, 181*, 1392–1393, 1958.

Daniels, F. B., and S. J. Bauer, The ionospheric Faraday effect and its applications, *J. Franklin Inst., 267*, 187–200, 1959.

Evans, J. V., The measurement of the electron content of the ionosphere by the lunar radio echo method, *Proc. Phys. Soc. London, B, 69*, 953–955, 1956.

Evans, J. V., The electron content of the ionosphere, *J. Atmospheric and Terrestrial Phys., 11*, 259–271, 1957.

Murray, W. A. S., and J. K. Hargreaves, Lunar radio echoes and the Faraday effect in the ionosphere, *Nature, 173*, 944–945, 1954.

Townsend, J. W., Soviet papers presented at the rocket and satellite symposium, *Science, 129*, 80–84, 1959.

(Manuscript received May 20, 1959; revised July 22, 1959.)

Detection of an Electrical Current in the Ionosphere above Greenland[1]

LAURENCE J. CAHILL, JR.[2]

Department of Physics
State University of Iowa
Iowa City, Iowa

Abstract—During a magnetic storm on 6 August 1957, a rocket-borne magnetometer was launched near the coast of Greenland. The time and location of the flight and the magnetic measurements obtained provide evidence that the rocket entered the postulated sheet current flowing across the polar cap. An estimate is made of the magnitude of the detected current.

Introduction—The results of an investigation electrical currents in the ionosphere near the gnetic equator have been previously reported *hill*, 1959]. An investigation of ionospheric rents in the polar regions was also under- en as part of the same IGY project. During latter investigation one rocket-borne mag- ometer was launched while a magnetic storm s in progress and was successful in reaching lower ionosphere.

The magnetometer and the methods of launch- ; and of receiving data were identical to those d in the equatorial flights. The rockoon, ate University of Iowa Number 59, left the ck of the USS *Plymouth Rock* (LSD-29) at 03 Universal Time (1203 local time) on 6 gust 1957. The ship was then at 56° 09′ West gitude, 63° 56′ North latitude (Fig. 1). The ket fired at 1723 UT when the balloon reached altitude of 23 km.

The flight record—The magnetic field measure- nts plotted against altitude in Figure 2 have en corrected to remove the effects, on the parent proton precession frequency, of a ation (14 cps) of the rocket about its longi- dinal axis. The rotation rate and sense were nitored by photoelectric cells mounted in the le of the rocket. The individual measurements ver 200 during the complete flight) do not more than $\pm 20\gamma$ from the lines shown and the error in the absolute values of the measurements is not more than $\pm 20\gamma$. The decrease of the magnetic field in the portion of the record below 90 km followed approximately the inverse cube law. An additional decrease occurred during the flight because of horizontal motion of the rocket to the southeast, toward a region of lower total field intensity. This explains the divergence of the upward and downward records in Figure 2. A rather abrupt change in slope of

FIG. 1—Map of a portion of the Davis Strait showing the location of SUI Flight 59.

[1] Assisted by the National Academy of Sciences d the National Science Foundation through S/IGY Project 10.1.

[2] Now at the University of New Hampshire, urham, New Hampshire.

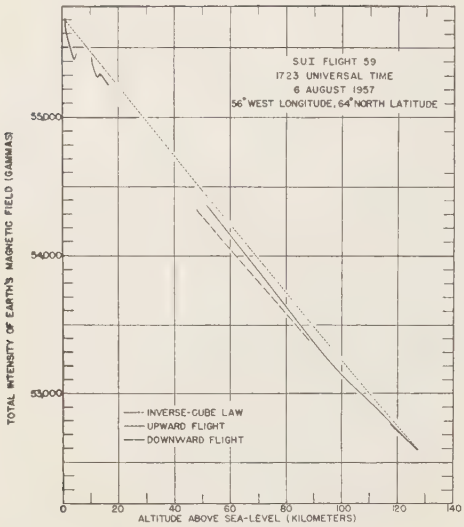

FIG. 2—Flight 59; magnetic field intensity versus altitude.

the upward flight record between 90 km and 100 km indicates entrance into an electrical current sheet. Figure 3 shows the record above 90 km in greater detail with the inverse cube decrease removed. The measurements indicate that the same general features of the current were encountered on both the upward and downward portions of the flight even though the two portions were separated horizontally by several kilometers. This fact and the relatively abrupt change of slope indicate that a current sheet of large lateral extent was entered. Approach to a narrow ribbon or filament of current would result in changes of a different nature [*Meredith and others*, 1958]. The gap in the record from 117 km to 92 km on the downward flight was caused when the angle between the magnetic field vector and the magnetometer coil became too small to allow reliable measurements. Rough measurements of precession frequencies obtained for this section with a narrow-band frequency analyzer indicate that the upward record was essentially retraced. At the peak altitude there was not a definite return to the slope of the record at lower altitudes; hence the current layer was not completely penetrated. The fluctuations of the measurements near peak altitude were probably in part, due to time variations in the magnetic field. These time variations became more evident at peak where the rocket was changing altitude more slowly.

Interpretation—Interpretation of the flight record is more difficult for Flight 59 than for the equatorial flights since at this location the dip angle is approximately 80°. The contribution of a horizontal current sheet to the total magnetic field **F** is that of a small horizontal vector added to a much larger, and nearly vertical, vector. The departure, at the peak of the flight record, from the decrease expected in the absence of current, is $90 \pm 20\gamma$. The smallest change in the horizontal magnetic field that could cause this change in **F** is $90\gamma \times \sec 80°$ or 520γ. This change would occur if the horizontal disturbance vector were exactly parallel to the horizontal component of **F** but in opposition below the current sheet.

Since the horizontal component **H** has a true azimuth of 315° (the magnetic variation is 45°W

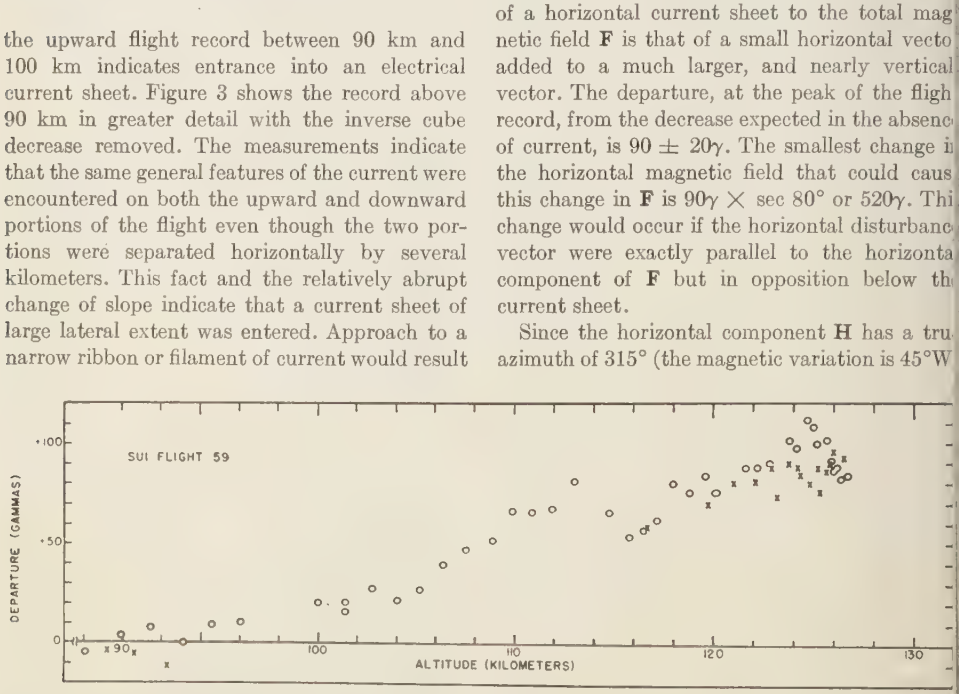

DEPARTURE OF MEASUREMENTS FROM INVERSE CUBE VS. ALTITUDE

FIG. 3—Flight 59; departure from decrease expected in absence of ionospheric currents (circles indicate upward flight measurement, crosses downward flight).

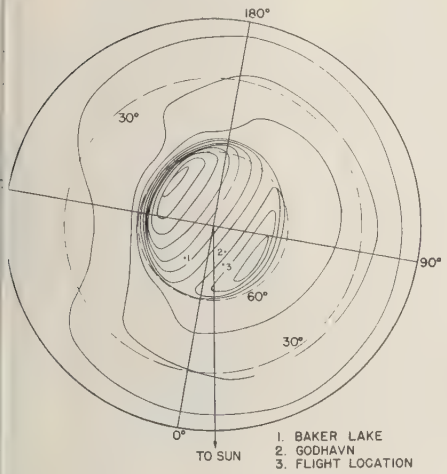

FIG. 4—Current diagram for northern hemisphere, for magnetic storm of May 1, 1933, at 00 UT. The diagram is centered on the north geomagnetic pole and the zero meridian shown is that through the geographic pole. The current flow is clockwise in the dawn side of the auroral zone and counter-clockwise in the twilight side. The flow between adjacent current lines is 200,000 amperes (after *Vestine*).

the flight location the direction of a current sheet producing the minimum change in **H** would be 225° true azimuth. A current producing a change in **H** of 520γ during the rocket flight would result in a contribution to the ground level variation in **H** of 260γ.

Only two-thirds of the total ground-level variation is thought to be due to overhead currents; thus the total ground level variation that might be observed would be 390 $\pm$ 90γ. A larger ground level variation would be expected in the vicinity of the flight location, however, since the current layer was apparently not completely penetrated. If the current direction were appreciably different from 225°, the current density and the ground level variation in **H** would have to be larger to be consistent with the observed 90γ change in **F**. If the azimuth were as little as 165°, the current density necessary would have to be twice as great as in the minimum case and would produce a ground-level variation of at least 780γ.

The locations of two ground level magnetic observatories are shown in Figure 4 with relation to the current system believed responsible for magnetic variations observed during magnetic storms. This figure, prepared by *Vestine* [1947] is an electrical current representation of surface magnetic variations occurring during one specific magnetic storm. Although a current representation of the 6 August storm may differ in detail the general features may well be similar to those of Figure 4. The magnetic records are now available for the two observatories plotted in Figure 4 and these records are reproduced in Figures 5 and 6. The Baker Lake observatory is in approximately the same geomagnetic latitude as the flight location, but farther west. The main features of the DS variation seen at Baker Lake would be observed earlier at the flight location. Godhavn is only slightly east of the flight location in geomagnetic longitude, but 5° farther north. The variation in **H** observed at Baker Lake at flight time was approximately 500γ and that at Godhavn approximately 300γ. The minimum ground-level variation in **H** at the flight location, 390 $\pm$ 90γ, inferred from the rocket measurements, is in reasonable agreement with the Godhavn variation. Some lack of agreement might be expected because of local differences in overhead current densities at the two separated locations.

The most simple explanation of the rocket

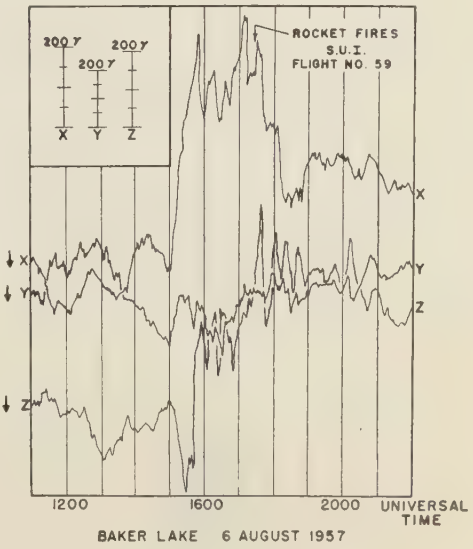

FIG. 5—Magnetic record, August 6, 1957, Baker Lake, Canada (96°W, 64°N).

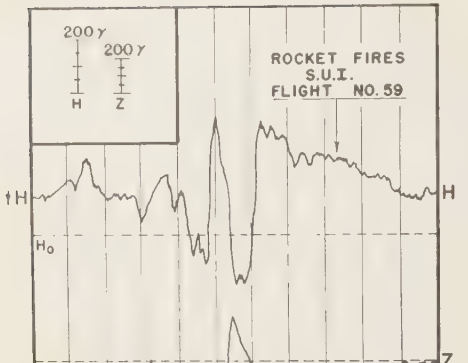

FIG. 6—Magnetic record, August 6, 1957, Godhavn, Greenland (54°W, 69°N).

flight results is that they were produced by a horizontal current layer flowing in a southwesterly direction. The possibility cannot be ruled out, however, that, with relation to the current system of the 6 August storm, the flight location is farther south than for the storm shown in Figure 4. The higher current density, necessary to explain the rocket results, could then be due to the increase in density as the polar cap current funneled into the eastward flowing auroral arc. In this case the current direction might be toward the south or even the southeast.

It should be further noted that although the above interpretation is the most simple one, consistent with both the rocket data and ground-level observations, other current systems could produce the field changes observed during the rocket flight. For example, another possible current system, pointed out to the author by McNish, is a horizontal, circular current pancake-shaped. The rocket magnetometer, ascending through the center of the pancake would encounter changes in **Z**. The changes in **Z**, necessary to account for the observed **H** changes, would be small since **Z** is nearly parallel to **F**. The current density of the system could be much lower than that of the assumed horizontal current sheet.

The average current density of the layer detected, assuming the 225° azimuth, is approximately 11 amperes/km². The current density appears to vary with height but the results do not disagree with the conductivity expected in polar regions [*Baker and Martyn*, 1952]. The applicable conductivity, for the case of a nearly vertical magnetic field, has a broad maximum from 90 km to 130 km.

Acknowledgments—The encouragement and assistance of James A. Van Allen are gratefully acknowledged. The considerable cooperation of the crew of the USS *Plymouth Rock* was essential in conducting the flights. Dr. Karl Anderson of the Meteorologisk Institut, Denmark, was kind enough to supply the Godhavn magnetic records and the Baker Lake records were obtained from the Dominion Observatory, Canada, through the U. S. Coast and Geodetic Survey.

REFERENCES

BAKER, W. G., AND D. F. MARTYN, Conductivity of the ionosphere, *Nature, 170,* 1090–1092, 1952.

CAHILL, L. J., JR., Investigation of the equatorial electrojet by rocket magetometer, *J. Geophys. Research, 64,* 489–503, 1959.

MEREDITH, L. H., L. R. DAVIS, J. P. HEPPNER, AND O. E. BERG, Rocket auroral investigations, *IGY Rocket Report Series, 1,* 169–178, 30 July 1958.

VESTINE, E. H., L. LAPORTE, I. LANGE, AND W. E. SCOTT, *Carnegie Inst. Wash. Publ. 580,* 370, 1947.

(Manuscript received July 8, 1959; revised August 6, 1959.)

The Southern Auroral Zone in Geomagnetic Longitude Sector 20°E

S. EVANS

Scott Polar Research Institute, Cambridge, England

AND

G. M. THOMAS

Department of Natural Philosophy, University of Edinburgh, Scotland

Abstract—Visual auroral observations from the Halley Bay, Shackleton, and Southice, antarctic bases, are tabulated to show how the frequency of occurrence of aurora varied with the geomagnetic latitude, from 63° to 79°, in the sector 20°E during the IGY. The distribution of quiet arcs, and its diurnal variation, are given particular attention. The center of the quiet arc zone is found to be at geomagnetic latitude 71.7°; the interquartile range is 2°.

Introduction—The longitudes between 0° and °W geographic, to which this paper refers, e those in which we may expect the auroral ne to be at the highest geographic latitudes the southern hemisphere. Scattered visual servations of aurora australis were collected *White and Geddes* [1939], and a tentative roral zone was drawn. No data were availa- e from these longitudes, but the part of the ne that was delineated lay between circles of dius 20° and 25° about the geomagnetic axis int.

Vestine and Snyder [1945] derived a zone maximum disturbance daily variation, S_d. ney took the observations from thirteen mag- tic stations and extrapolated from each along e geomagnetic meridian according to the havior observed in the northern hemisphere. ne zone so derived was closely circular within e limits 21° to 25° about the axis point.

Among theoretical treatments of the problem king account of more than a simple centered pole field is that of *Quenby and Webber* 959]. Their zone is highly asymmetrical and the sector of interest passes close to the ographic south pole, about 12° from the axis int.

Hultqvist [1959] has recently produced a ries of lines of constant auroral frequency for ie northern hemisphere, which conform most osely to data so far published [*Vestine*, 1944]. e uses a spherical harmonic analysis of the earth's magnetic field including terms up to the fifth order. It is to be hoped that the computations will be extended to the southern hemisphere.

Definition of the zone—There have been a number of definitions of the auroral zone. Apart from those based on magnetic disturbance effects, there are first Fritz's isochasms [see *Vestine*, 1944]. These specify the number of days in the year on which aurora can be seen at any point. The disadvantage of this method is that each point describes the maximum activity, during local darkness, over an area of approximately 1000-km radius visible from the site. For this reason it has been recommended that the figure given should relate only to the occurrence of aurora in the zenith; this method does not make full use of the available information in regions where observing stations may be widely spaced.

Alternatively one might specify the fraction of the number of hours of observation that aurora is visible—or is visible in the zenith. These are quite different parameters from the previous ones because of the marked diurnal variation of occurrence frequency. For the same reason they are greatly influenced by the diurnal distribution of observing times. In all these cases the zone itself may move, with periods varying from 1 day to 11 years; for example, a Universal Time variation as the inclination of the magnetic axis to the earth-

sun line changes might reasonably be effected.

These methods of defining an auroral zone result from attempts to utilize data collected from many sources, of differing reliability, over a period of years. From an unbroken period of systematic observation at a single station, however, the distribution of occurrence in latitude may be derived with some certainty. In this paper independent and overlapping results from three stations are compared.

The results presented are based on observations from Royal Society Base, Halley Bay, and the transantarctic bases at Shackleton and Southice. Halley Bay is in lat. 75°31′S, long. 26°36′W; the geomagnetic coordinates are $\Phi = 65.8°S$, $\Lambda = 24°E$. A continuous watch was kept during darkness in the southern winters of 1956, 1957, and 1958. Shackleton is in lat. 77°51′S, long. 37°16′W; the geomagnetic coordinates are $\Phi = 67.5°S$, Λ 16°E. Regular records were made at the times of the three-hourly meteorological observations during 1956 and 1957. Additional notes were made at other times of prominent displays. Southice is in lat. 81°57′S, long. 28°48′W; the geomagnetic coordinates are $\Phi = 71.7°S$, $\Lambda = 16°E$. Regular notes were made at 00, 06, 12, and 18 hr UT and occasionally at other times during 1957. Thus the observations cover an interesting range of values of Φ in the same longitude sector. Coverage unfortunately does not extend to the region where we may expect to find the inner auroral zone reported by *Fel'dshteyn* [1959] in the northern hemisphere. Results from Vostok-I (72°08′S, 93°35′E) in 1957 have been used by *Aver'janov* [1959] to support the existence of this inner zone in the south at $\Phi = 82.7°$.

Halley Bay observations—At Halley Bay an examination of the sky was made at each quarter hour UT and more frequently if required. This procedure was followed for all the observations recorded here; consequently the visual data are best suited to analysis for systematic effects. Tabular presentation is used to show the diurnal behavior, the differences from year to year, and the geographical extent of auroral activity. General correlations with other phenomena become apparent in this way, but individual correlations cannot be sought. (The photographic data on the other hand are sporadic but capable of supplying great detail on individual favorable occasions.)

Either a fixed or a hand alidade was used for elevation measurements, as unaided estimates are notoriously unreliable at low elevations. Readings were taken to the nearest degree, and it may be assumed that they are accurate to this order for the whole range. Bearings were read from a simple horizontal circle and were commonly taken only on quiet arcs.

The average behavior of a display resembled that described by many observers just to the south of the northern auroral zone. Quiet arcs tend to lie almost stationary for long periods in a narrow range of latitudes. Any increase in activity is likely to show itself first by an equatorward drift of the arc, which may later break into rays or bands. A short period of rapidly moving forms, with bright coloration, gives way to diffuse surfaces and pulsation. Amorphous patches of luminosity may litter the sky for many hours without any noticeable change after a display of this kind. Classification of forms has been reduced to arcs, rays, bands and surfaces. Although borderline forms will occur from time to time, these four are so distinct that they surely result from four different physical processes in action.

Elevation was measured on the meridian from the southern horizon through the zenith. For a quiet arc, the maximum elevation of the lower border is sufficient to specify the position. These are the elevations used in Table 1. In each column is entered the number of quarter-hourly periods in which any arcs were observed in the elevation range given in the extreme left-hand column. (For the 1956 data half-hourly periods have been used.) The total number of periods in which observations were made in clear sky conditions is entered at the bottom of each column. Thus, up to four occurrences (two in 1956) may be recorded in a single hour in any elevation group. The extreme right-hand column gives the geomagnetic latitude in which the arc is overhead, assuming a height of 100 km. Figure 1 illustrates the number of arcs occurring in each degree of latitude, on the same assumption, for all hours added together. The narrowness of the distributions is striking. It is suggested that the inter-

quartile range is the most suitable definition of the "quiet arc zone."

The diurnal variation in the latitude of the quiet arc zone has been investigated by plotting the median elevations for each hour, as shown in Figure 2(a). The median upper and lower elevation limits for all other forms are plotted in Figure 2 (*b*). Points to note here are as

TABLE 1—*Occurrence of arcs*

Elevation, degrees	Hourly intervals, UT 18/19	19/20	20/21	21/22	22/23	23/24	00/01	01/02	02/03	03/04	04/05	05/06	06/07	07/08	08/09	09/10	Totals	Latitude
								1956										
1								2	1								3	75
2							1			•							1	74
3			1	1	1	2	1	1			1						8	73
4–5		1	1	2	4	1	7	3	5	5	4	1	1	1	1		37	72
6–7					3	8	5	5	4	3	6	4	4				42	71
8–10	1	1	1	1	2	9	9	6	6	8	3	7	4	2	1		61	70
11–15			1		3	6	4	4	9	4	3	1	2				37	69
16–23			1		1	3	1	3	2	1	1						13	68
24–40					1	3	2	2	1	1	2	3					15	67
41–90						3	1	1	2	2	2	1					12	66
91–140				1		1	2	3	3	2	1						13	65
No. observations	30	52	62	68	72	74	78	78	78	78	76	74	64	28	22			
								1957										
1		1	2	2			2	2	1						1		11	75
2	2		2	3	5	6	7	2	4								31	74
3	2	3	5	11	15	9	8	6	8	5	4	4	3	3	1	3	90	73
4–5	2	1	9	27	27	39	30	28	33	23	20	18	10	12	13	6	298	72
6–7	2		4	15	12	9	18	26	15	12	12	5	8	7	2	1	148	71
8–10				9	6	13	14	11	18	14	15	10	10	8	3		131	70
11–15				1	2	2	4	5	3	9	6	4	7	2			45	69
16–23				2	1	3	1	5	7	3	1	1					24	68
24–40				1		2	3	1	2								9	67
41–90					1		4	1	1								7	66
91–140																		65
141–180							2	4	2								8	64
No. observations	29	64	121	164	174	181	180	188	175	160	149	138	124	97	68	19		

TABLE 1—*Occurrence of arcs*—(Continued)

Elevation, degrees	Hourly intervals, UT 18/19	19/20	20/21	21/22	22/23	23/24	00/01	01/02	02/03	03/04	04/05	05/06	06/07	07/08	08/09	09/10	Totals	Latitude
								1958										
1	2		1	1	1		1										6	75
2	1	1	2	2	1	4	3					1		3		1	19	74
3	2	13	14	15	12	17	17	5	3	2		1			2		103	73
4–5	4	17	21	31	36	39	35	22	16	12	22	37	32	15	8	3	350	72
6–7	1	2	4	17	11	20	11	7	15	6	15	20	12	9	4		154	71
8–10		2	1	7	4	11	12	14	12	14	10	8	11	8	2		116	70
11–15				5	3	1	5	4	8	11	18	3	4	3			65	69
16–23				2		1	2	5	7	7	6	3	3	1			37	68
24–40							1	3		5	1						10	67
41–90							1	1									2	66
91–140																		65
141–180								1		1							2	64
No. observations	21	54	93	150	153	165	163	148	154	152	159	147	135	87	69	25		

follows. First, regular diurnal movements were evidently small, within a range of 2° of latitude. Thus no appreciable broadening of the latitudinal distribution of arcs results from summing the observation from all hours, as in Figure 1. These are the distributions that should be compared with those from Shackleton and Southice described below. Second, in Figure 2(*a*), there is a systematic difference between the median elevations in 1956 and those in 1957 and 1958; it is unfortunate that the observer on the station was changed in the interval when this difference, if real, occurred. A small movement is common to all three years, with a phase such that the zone is at the lowest latitude at 03–06 hr UT or around 03 hr LT. Results from other longitudes would be of considerable interest here. Finally, all other forms clearly occur more frequently to the equatorial side of the arc zone. Since other forms occur at times of greater disturbance they are distributed more widely in latitudes.

Transantarctic expedition observations—In the analysis of the observations from Shackleton and Southice it was convenient to divide th sky into the *Z*, *N*, and *D* regions used b *Stoffregen* [1959] for Ascaplots. The *Z* regio is a circle of radius 60° about the zenith. *I* is the belt between 10° elevation and 30° ele vation to the geomagnetic north, and *S* sim ilarly to the south. Two extra regions *NH* an *SH* below 10° elevation to the north and sout have been added for this analysis, though thei value is rather limited. Observations below 30 elevation to the east and west are ignore Each of the regions used is roughly of equa area and 3° of latitude in width on a surfac 100 km above the earth. Table 2 shows th number of occurrences of aurora under th nearest hour UT to which they were made. Th first figure in each column is the total numbe of occurrences of any form; the followin figure in parentheses relates to arcs only. Onl the predominant form has been recorded i arriving at these figures. The total number o occasions on which observations were made i clear sky conditions is entered at the botto of each column. Since only a small diurn

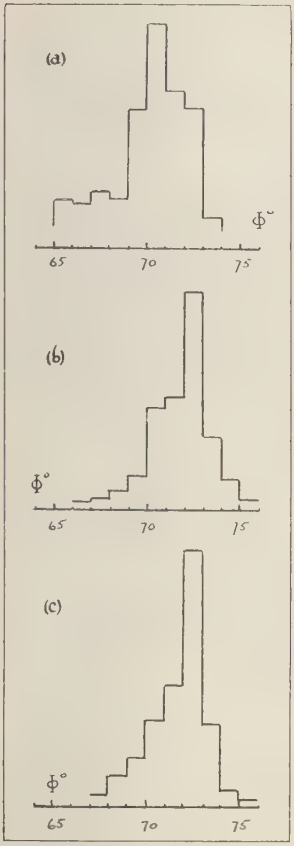

Fig. 1—Number of occasions on which quiet cs were observed from Halley Bay in each egree of geomagnetic latitude. For ordinates see able 1. (*a*) 1956, (*b*) 1957, (*c*) 1958.

ariation in latitude was found at Halley Bay, ne figures for all hours may be added together s has been done in the right-hand column. hese are the figures illustrated in Figure 3.

The Quiet Arc Zone—The histograms in Figres 1 and 3 should be compared. The Halley ay distributions are narrower, but this may e assumed to be due to the narrower sky visions used (1° against 3°). It is reassuring find that the median latitudes of the arc one derived from the three bases in the same eason, 1957, are very close. They are 71.8° Halley Bay), 71° (Shackleton), and 72° (Southe). This finding confirms to a certain extent

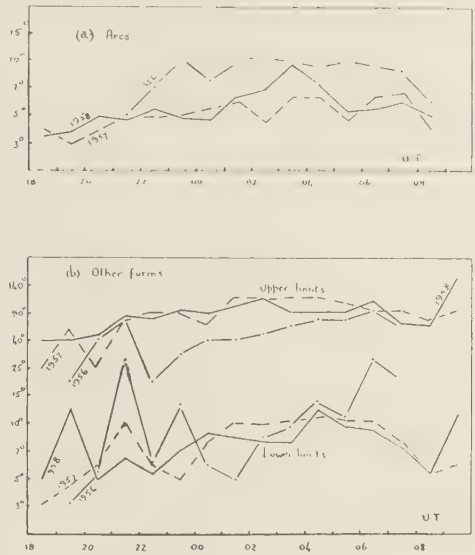

Fig. 2—Median elevations, in degrees on a nonlinear scale, against UT at Halley Bay 1956 to 1958. (*a*) Center of quiet arcs; (b) upper and lower limits of all other forms.

the constant height assumed for the arcs. At the low elevations frequently measured at Halley Bay the latitudes derived are rather sensitive to the height chosen. At Southice, the flat-topped distribution suggests that there may have been some saturation, which could have arisen because aurora of lower luminance would be visible at higher elevations.

A mean of the three latitudes, weighted according to the number of observations used in deriving each, is $\Phi = 71.7°$. The interquartile range is 2°, corresponding to an area around lat. 81.5°S, long. 20°W geographic, where the magnetic dip is 70° (magnetic latitude, 54°). The mean figure derived by Vestine in the north was $\Phi = 70.0°$ along the zero magnetic meridan. The interquartile range was approximately 8°, but Vestine's figures relate to all auroral forms, not to arcs alone.

Systematic movements of arcs—In Figure 4(*a*) and (*b*), the distributions of true bearings of the centers of quiet arcs are shown for Halley Bay and Shackleton. The true bearings of geomagnetic and local magnetic south are shown by the letters *g* and *l* respectively. Few

TABLE 2—*T.A.E. data*

(*a*) Shackleton, 1956

Region	Hours, UT										Total
	18	19	20	21	22	23	00	01	02	03	
NH	0	—	—	0	0	0	0	0	0	—	0(0)
N	0	—	—	0	0	1(0)	1(0)	0	1(0)	—	3(0)
Z	0	—	—	0	2(1)	3(0)	3(0)	1(1)	2(1)	—	11(3)
S	0	—	—	2(2)	5(4)	5(3)	8(6)	5(4)	5(3)	—	30(22)
SH	0	—	—	1(1)	1(1)	4(3)	7(6)	4(4)	2(2)	—	19(17)
No. observations	28	0	0	33	6	10	36	10	5	0	

(*c*) Southice, 1957

Region	Hours, UT				Total
	18	00	06	12	
NH	0	9(8)	13(6)	0	22(14)
N	0	15(7)	28(7)	3(0)	46(14)
Z	1(1)	24(8)	21(4)	3(1)	49(14)
S	6(3)	22(12)	14(6)	1(0)	43(21)
SH	3(2)	9(6)	10(6)	1(1)	23(15)
No. observations	109	112	124	120	

(*b*) Shackleton, 1957

Region	Hours, UT															Total
	18	19	20	21	22	23	00	01	02	03	04	05	06	07	08	
NH	0	—	0	0	0	0	1(0)	1(0)	0	2(0)	1(0)	0	1(0)	0	—	6(0)
N	0	—	0	2(2)	0	0	7(6)	2(0)	1(0)	5(2)	3(2)	1(0)	4(1)	0	—	25(13)
Z	0	—	1(0)	2(0)	3(0)	3(3)	16(11)	7(2)	7(2)	25(8)	5(1)	4(1)	21(6)	0	—	94(34)
S	1(1)	—	0	9(6)	7(4)	4(2)	28(22)	13(9)	8(4)	31(15)	6(3)	6(3)	20(11)	0	—	133(80)
SH	2(2)	—	0	10(8)	3(3)	3(3)	22(20)	3(1)	2(1)	8(6)	2(1)	2(1)	8(5)	0	—	65(51)
No. observations	56	0	1	64	10	8	88	18	12	68	11	10	62	1	0	

other stations have such a large difference between the two directions, and the overriding influence of the dipole field is clearly shown.

Figure 4(*c*) shows the effect of separating the bearings into hourly intervals, which are plotted horizontally. Mean bearings for the hour are plotted vertically, revealing a distinct movement of the center, or closest point, of the arcs. Note that, in spite of the inclination of the magnetic axis, neither this movement nor the possible north-south movement shown in Figure 2 would be produced by a zone fixed with reference to the surface of the earth. Consider, however, the effect of a zone which is eccentric in local time coordinates as illustrated schematically in Figure 5. *G* is the geomagnetic south pole. The observer at Halley Bay moves round the outer circle at a constant radius of 24° from *G*. The fact that the geomagnetic axis direction oscillates in space need not affect this simple argument. Let us suppose that the auroral zone is circular, with center, *Z*, shifted 2° from *G* along the local time meridian 02 hr. Then at 02 hr the zone will clearly be 2° closer to the observer than at 20 hr LT (04 hr and 22 hr UT respectively at Halley Bay; see Figure 2). Second, the closest point of the zone at 20 hr LT is in the direction 5°E of S geomagnetic. At 02 hr LT it is due S, and at 08 hr it is 5°W of S. These are the phase and the order of magnitude of the movement shown in Figure 4(*c*). An equally distinct motion of the same kind was detected by *Harang* [1945] in the northern hemisphere, though he did not offer this simple explanation. He found that at Tromsö the direction was stationary at about 18 hr LT and thereafter moved towards the west, passing through geomagnetic north at 00 hr LT. This permits of the same explanation as given above except that the eccentricity should be a shift along the local time meridian 00 hr LT, a result not too different in phase from ours. *Alfven*

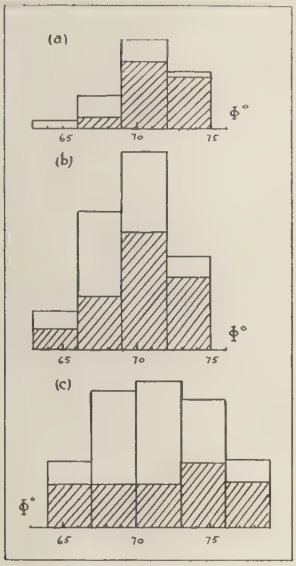

Fig. 3—Number of occasions on which aurora s observed in different geomagnetic latitude ions. The shaded portion refers to arcs only. r ordinates see Table 2. (*a*) Shackleton Base, 6; (*b*) Shackleton Base, 1957; (*c*) Southice, 57.

955] predicted an eccentricity in local co-linates on theoretical grounds, but the phase s quite different. On Alfven's theory the zone tends to the lowest latitudes at 18 hr LT. The rotation of arcs observed by *Weill* [1958]

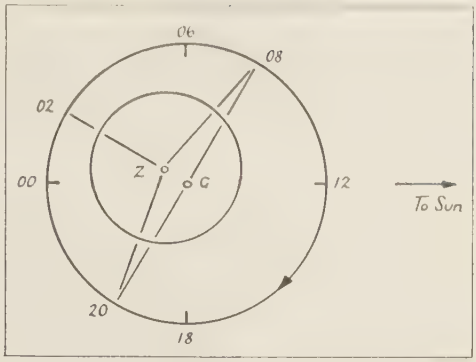

Fig. 5—The effect of an eccentric auroral zone.

in Adélie Land is different in character. Dumont d'Urville, to which his observations refer, is inside the auroral zone, and it seems likely that the orientation of arcs reflects the pattern of disturbance current across the polar cap.

More detailed tabulation of the original visual observations is to be published in the Royal Society volumes of observations for Halley Bay. The program of all-sky photography will also be described therein. Some results for 1956 have been published already [*Evans*, 1959]. The 1957 and 1958 films are now being analyzed.

Acknowledgments—This work formed part of the program of the British National Committee for the International Geophysical Year. Thanks are due to the Royal Society for the original

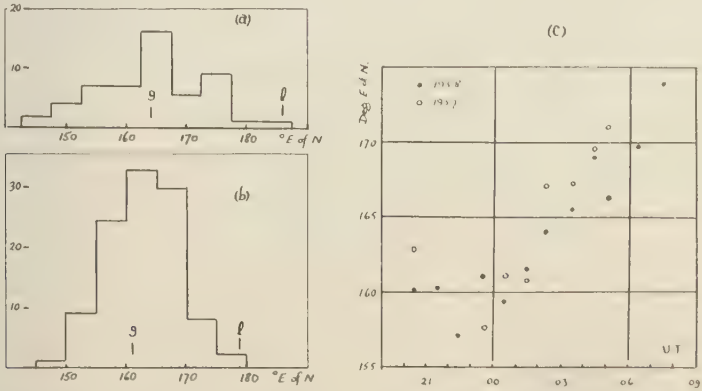

Fig. 4—Distribution of true bearings of the centers of quiet arcs measured E of N. (*a*) om Shackleton, 1957, (*b*) from Halley Bay, 1958, *g* and *l* mark the directions of geomagnetic and al magnetic south respectively; (*c*) mean bearings for each hourly interval UT at Halley Bay.

data obtained at Halley Bay and to the Trans-antarctic Expedition for making and supplying the visual notes from Shackleton and Southice. All the original records are now lodged inW. D. C.-C, Edinburgh, under the supervision of Mr. J. Paton, who has taken a keen interest in the analysis throughout and whose advice is much appreciated.

References

Alfven, H., On the electric field theory of magnetic storms and aurorae, *Tellus, 7,* 50–64, 1955.

Aver'janov, V. G., Preliminary auroral results from Vostok-I, *Bull. Soviet Antarctic Exped.,* no. 5, pp. 46–47, 1959.

Evans, S., Horizontal movements of visual auroral features, *J. Atmospheric and Terrest. Phys.,* in publication, 1959.

Fel'dshteyn, Ya. I., Distribution of aurorae in the circumpolar region, *Izvest. Akad. Nauk S.S.S.R., Ser. Geofiz.,* no. 1, pp. 170–171, 1959; translation, U. S. Dept. Commerce Info. Soviet Bloc, IGC, Feb. 20, 1959.

Harang, L., A study of auroral arcs and draperies, *Terrestrial Magnetism and Atmospheric Ele 50,* 297–306, 1945.

Hultqvist, B., Auroral isochasms, *Nature, 1* 1478–1479, 1959.

Quenby, J. J., and W. R. Webber, Cosmic r cut-off rigidities, *Phil. Mag., 4,* 90–113, 1959

Stoffregen, W., *Uppsala Ionospheric Observato Rept.,* no. 5, 1959.

Vestine, E. H., The geographical incidence aurora and magnetic disturbance, northe hemisphere, *Terrestial Magnetism and Atm pheric Elec., 49,* 77–102, 1944.

Vestine, E. H., and E. J. Snyder, Aurora a magnetic disturbances, southern hemisphe *Terrestrial Magnetism and Atmospheric El 50,* 105–124, 1945.

Weill, G., Aspects de l'aurore observée à la ba Dumont-d'Urville in Terre Adélie, *Compt. ren 246,* 2925–2927, 1958.

White, F. G. W., and M. Geddes, Antarctic zo of maximum auroral frequency, *Terrestr Magnetism and Atmospheric Elec., 44,* 367–3 1939.

(Manuscript received July 7, 1959.)

Antarctic Auroral Observations, Ellsworth Station, 1957

J. M. MALVILLE

High Altitude Observatory
Boulder, Colorado

Abstract—Auroral observations made during the Antarctic winter of 1957 are summarized. The data discussed include daily variation, east-west drift, and hydrogen emission. From a comparison of observations made at Ellsworth and the South Pole evidence is obtained of a spiraling zone of maximum auroral activity.

ntroduction—As part of the United States Y program in the Antarctic, observations of orae were carried out during the winter nths of 1957 at Ellsworth Station (geomag-ic latitude 67°). The data which will be ussed were obtained by four types of ob-vations:

1) IGY spectrograph. This high-speed, low-persion spectrograph was designed as an omatic patrol instrument. Its slit, 2° wide 180° long was aligned along the geomag-ic meridian. During its seven months of ration 778 spectrograms were obtained, 508 which contained auroral lines.

2) Meridian photometer. This photometer, ploying an interference filter peaked at 7A, was part of the automatic system of patrol spectrograph, and was used to give independent measure of 5577A intensity ng the geomagnetic meridian.

3) All-sky camera. The all-sky camera, con-mirror type, was used to obtain photo-phs of the entire sky.

4) Visual observations. The visual observa-ns were made according to the North Ameri-procedure [*Chapman*, 1957]. The altitude auroral forms lying along the geomagnetic ridian was determined by means of an lade, and readings were generally taken ry fifteen minutes during eight to twelve rs of the night.

Observations—Ellsworth Station, geomagnetic latitude of 23°, lies close to the auroral zone predicted by *Vestine* [1954]. Visual observa-ns yield a value of 76 per cent for the quency of clear nights on which aurorae were observed in any part of the sky. Another value for the auroral frequency may be obtained from the patrol-spectrograph data. Although faint and short-lived aurorae are not detected by the spectrograph, it does not rely upon spot checks of the sky; moreover, it can detect auroral radiation through a thin overcast. The spectrograph was operated continuously on 116 nights between the limits of nautical twilight, and auroral spectrograms were recorded for 86 per cent of the nights. It is interesting to note the high percentage of nights showing hydrogen emission; on 70 per cent of the nights during which aurorae were observed, hydrogen was detected.

Neither of the two figures for the auroral frequency has been corrected for the variation of the number of dark hours during the winter. This correction is undoubtedly small, as auroral displays occurred most frequently near midnight, local time. The daily variation of all visible aurorae at Ellsworth is shown in Figure 1. This figure also shows the variation of hydrogen emission during the night. Like the over-all

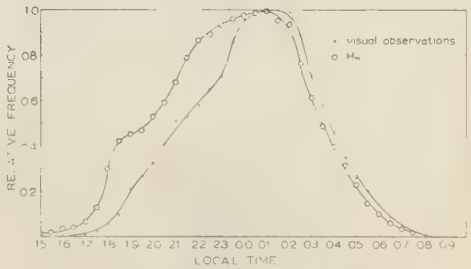

FIG. 1—Daily variation of all visible aurorae at Ellsworth.

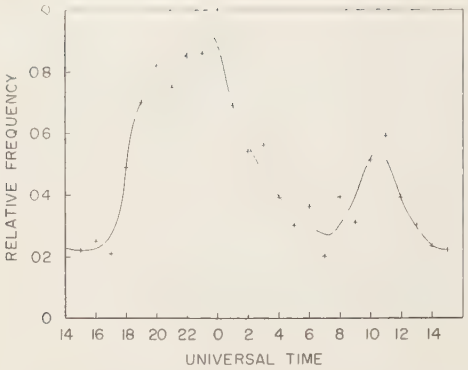

FIG. 2—Daily variation of all visible aurorae at the South Pole (courtesy of A. U. Landolt).

auroral activity, this appears to be roughly symmetrical with respect to geomagnetic midnight.

The daily variation of aurorae at Ellsworth is typical of stations lying outside the auroral zone, where, as a general rule, the maximum probability of occurrence is at geomagnetic midnight. However, such is apparently not the case for stations lying well within the zone. This is evidenced by Figure 2 which gives the daily variation of all visible aurorae at the South Pole. A unique feature of the South Pole variation is the existence of two maxima separated by approximately twelve hours. In addition, the time of the largest maximum precedes geomagnetic midnight by nine hours. This fact is in agreement with observations at Ellsworth that the time of maximum becomes earlier as one approaches the geomagnetic pole. The geomagnetic times of maxima for six altitude intervals at Ellsworth and for two at the Pole are shown in Figure 3. These quantities were obtained by assuming an elevation of 100 km for the lower border of all aurorae. The sky was then divided into nine altitude intervals corresponding to 4° of latitude to the south and to the north. For instance, aurorae with lower borders lying between 10°, 14°, 21°, 32°, and 62° above the southern horizon were assumed to be overhead for observers respectively 1°, 2°, 3°, and 4° to the south.

The sense of the spiral in Figure 3 is the same as was predicted by *Störmer's* [1955] line of precipitation for negative particles. Similar data for the Northern Hemisphere for times of

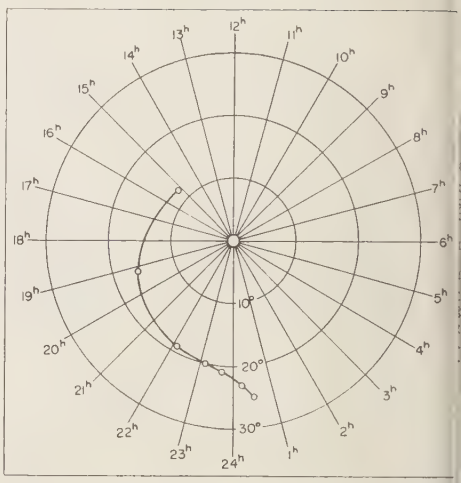

FIG. 3—Geomagnetic times of the maximum probability for the occurrence of overhead aurora in different geomagnetic co-latitudes.

radio blackout [*Agy*, 1954; *Meek*, 1952] an for times of maxima of geomagnetic disturb ances [*Nikolski*, 1956] as discussed by *Hop* [1956] show isochrons (lines connecting loca tions where events occur at identical times spiraling in the same sense as Störmer's pre cipitation spiral for positive particles.

Meek [1955], after analyzing the magneti data from the Polar Year of 1932–1933 foun evidence in the Arctic of two spiraling zone having approximately the same pitch but op posite sense. Meek qualitatively explained the spirals as resulting from Störmer precipitatio zones for electrons and protons.

As the South Pole and Ellsworth lie near th same geomagnetic meridian, Figure 3 may po sibly be transformed into an isochron pl possessing the same sense as Störmer's precip tation spiral for positive particles. One mus however, be cautious in interpreting these da in terms of the Störmer theory. The applic bility of the theory for auroral and geomagnet phenomena may be seriously questioned. T problem of the influence of the earth's magnet field on a moving ion cloud is likely to be si nificantly different from that considered Störmer, namely that of a single charged par cle moving in a dipole field. *Chapman and Fe raro* [1940] have calculated the maximum lowable density of the solar stream for t

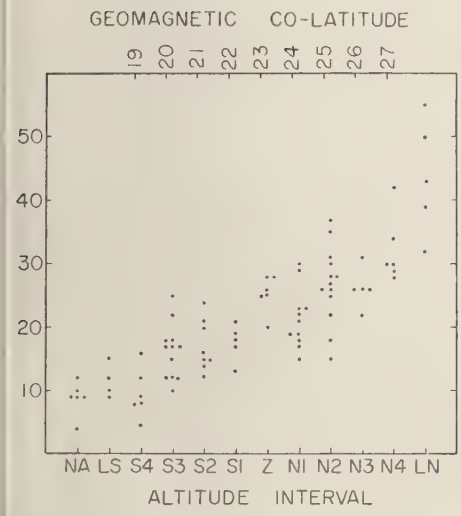

Fig. 4—Variation of northward limit of auroral ne with Lerwick K index. NA, no aurora; LS, wer border of aurora less than 10° above south- n horizon; S4, S3, etc., see *Chapman* (1957)

örmer theory to be applicable. They found at the ion density must be of the order of $^{-6}$ cm^{-3} before the mutual attraction of the as becomes negligable and the ions gain any eedom of motion in a dipole field. This density negligible compared with densities of 10^3 as/cm^3 as predicted for solar streams from met tail motions, and from zodiacal light servations [*Biermann,* 1957]. Moreover the eory itself is not an unqualified success in antitatively explaining auroral morphology. r instance protons must possess an energy about 5 Mev or a velocity of 10^{10} cm/sec to ach 23° from the geomagnetic pole and ereby produce aurorae down to heights of km. Similarly, electrons must have energies 300 Mev or velocities close to that of light *törmer,* 1955] resulting also in extremely low rorae. Such a difference in energy and veloc- between proton and electron beams seems likely, and consequently the Störmer theory pears inadequate to explain the spirals. Also, electrons and protons were precipitating ng different Störmer spirals, as suggested by eek, the daily variation of hydrogen emission ould not be roughly the same as that of the er-all auroral activity (Fig. 1). In addition, e existence of auroral arcs with large exten-

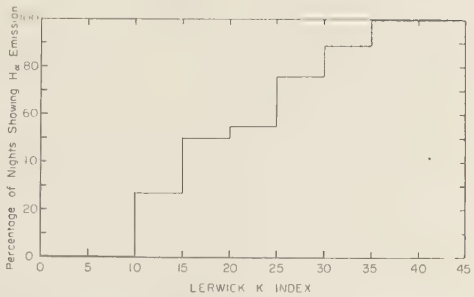

Fig. 5—Percentage of nights showing Hα emission.

sions in longitude is, according to the Störmer theory, in contradiction to single emitting regions on the sun. Shifting the coordinates of Figure 3 from geomagnetic pole to either the eccentric dipole or the dip pole does not alter the essential nature of the spiral of Figure 3.

Observations based on aurorae that appear over the entire sky are not adequate for determining realistic isochasms of auroral activity. The two figures of 76 per cent and 86 per cent for Ellsworth are, for instance, averaged over some 17° of latitude. In addition, the actual location of the auroral zone is far from static. Figure 4 shows the northward limit of the auroral zone; that is, the latitude of the most northerly aurora observed at Ellsworth during a 24-hour interval, as plotted against the magnetic K index of Lerwick (geomagnetic latitude 62.5°). The 24-hour interval used in the analysis was centered about local midnight at Ellsworth. The general northward motion of the zone with increasing K index does not, however, imply an expansion of the radius of the entire zone. A comparison of records obtained at Ellsworth and at the South Pole, two stations lying on opposite sides of the auroral zone, shows that apparently the width of the

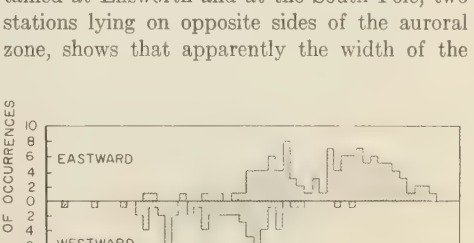

Fig. 6—Direction of drift of aurorae.

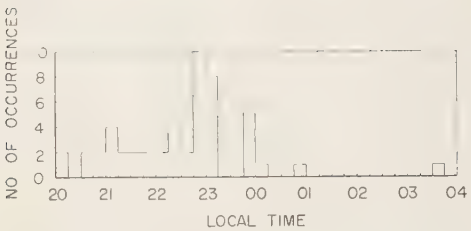

FIG. 7—Daily variation of frequency of type B aurorae.

zone rather than its radius expands with increasing magnetic disturbance.

The percentage of nights showing hydrogen emission similarly increases with increasing Lerwick K index (Fig. 5). For instance, of the 21 nights for which $K \geq 30$, only one night had no hydrogen emission. This correlation is considerably better than that observed by *Gal'perin* [1959] and is very striking in that it involves the K index from a locality close to the *northern* auroral zone.

Through the combination of all-sky camera records and visual observations, the variation of the direction of drift of auroral features has been determined for the southern auroral zone (Fig. 6). The drift toward the sunlit hemisphere is in the same direction as in the Northern Hemisphere [*Meinel and Schulte*, 1953; *Bullough and Kaiser* 1955]. With regard to Figure 6 it should be pointed out that the westward drift in the evening hours is primarily connected with type B and similarly active aurorae which occur at time of break-up. The eastward drift in the morning is slower than the westward drift and involves the diffuse forms characteristic of the morning hours. The type B aurora (red lower border) appears mainly in the evening hours (Fig. 7).

Figure 8 shows the variation of 5577A throughout the night of June 4/5, 1957. It will be noted that before the two major break-ups, hydrogen emission was present and that it disappeared soon after the appearance of rayed arcs. This behavior of hydrogen is well shown by Figure 9 which gives the results of a series of spectrograms for the night of May 24/25, 1957.

Summary—In this paper some varied auroral phenomena, observed by the author during a stay in the Antarctic, are described. The direction of auroral drift in the Southern Hemisphere, undetermined previous to the IGY, is shown to be in the same direction as in the Northern Hemisphere. The close similarity of geomagnetic phenomena in the Northern and Southern Hemispheres is demonstrated by the

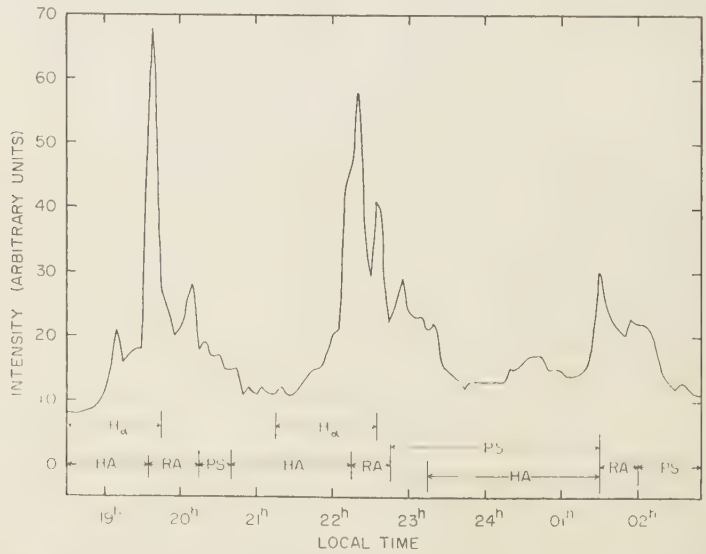

FIG. 8—Meridian photometer measurements in 5577A, June 4/5, 1957; HA, homogeneous arc; RA rayed arc; PS, pulsating surface; Hα, hyrogen emission.

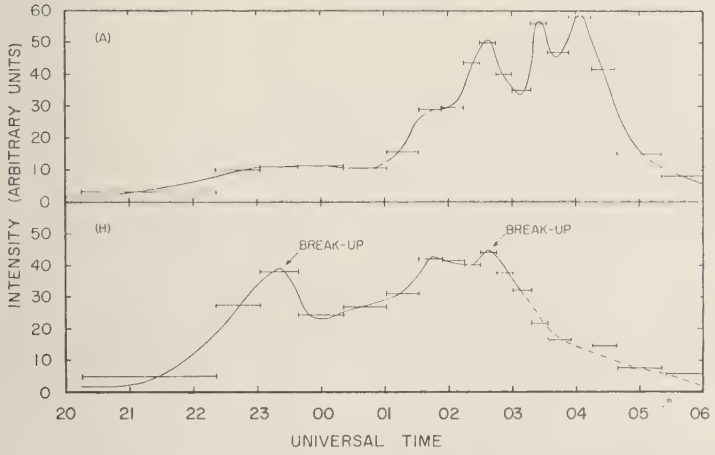

FIG. 9—Intensity measurements of 18 patrol-spectrograph exposures, May 24/25, 1957. (A) N'_2 — 3914A; (B) Hα.

orrelation between the Lerwick K index and atures of the southern auroral zone.

Hydrogen emission appears not to be the re occurrence it was once thought to be, as it as present during 70 per cent of the nights of uroral activity and shows a close correlation ith the magnetic K index.

The use of data from both Ellsworth and the outh Pole makes possible a determination of e time of maximum probability for the oc- urrence of overhead aurorae for eight geo- agnetic latitudes ranging from 27°S to 12°S. his analysis indicates a spiraling zone of maxi- um activity. In the Northern Hemisphere bservations involving times of radio blackout id geomagnetic disturbances indicate the ex- tence of two spirals of opposite sense. An terpretation of the spirals in terms of the örmer theory appears, at present, to be ijustified.

Acknowledgment—It is a pleasure to thank W. Chamberlain, S. Chapman, and S. Matsu- ita for their helpful discussions and F. E. Roach id J. W. Warwick for critically reading the man- cript. I am also very grateful to A. U. Landolt r making available to me his auroral data from e South Pole.

REFERENCES

GY, V., The location of the auroral absorption zone, *J. Geophys. Research, 59,* 267–272, 1954.

BIERMANN, L., Solar corpuscular radiation and the interplanetary gas, *Observatory, 77,* 109–110, 1957.

BULLOUGH K. AND T. R. KAISER, Radio reflections from aurorae II, *J. Atmospheric and Terrest. Phys. 6,* 198–214, 1955.

CHAPMAN, S., Visual auroral observation, *Annals of the IGY,* Vol. IV, 41–103, 1957.

CHAPMAN, S. AND V. C. A. FERRARO, The theory of the first phase of a geomagnetic storm, *Terrestrial Magnetism and Atmospheric Electricity, 45,* 245–268, 1940.

GAL'PERIN, G. I., Hydrogen emission and the two types of auroral spectra, *Planetary and Space Sci., 1,* 57–62, 1959.

HOPE, E. R., Spiral pattern of solar corpuscular precipitation, *Nature, 177,* 571–572, 1956.

MEEK, J. H., Ionospheric disturbances in Canada, *J. Geophys. Research, 57,* 177–190, 1952.

MEEK, J. H., The location and shape of the auroral zone, *J. Atmospheric and Terrest. Phys., 6,* 313–321, 1955.

MEINEL, A. B. AND D. H. SCHULTE, A note on auroral motions, *Ap. J., 117,* 454–455, 1953.

NIKOLSKI, A. P., Geographical distribution of magnetic disturbances in the circumpolar region of the Arctic, *Doklady Akad. Nauk. SSSR, 109,* 939–942, 1956.

STÖRMER, C., The polar aurora, The Clarendon Press, Oxford, 403 pp., 1955.

VESTINE, E. H., Winds in the upper atmosphere deduced from the dynamo theory of geomagnetic disturbances, *J. Geophys. Research, 59,* 93–128, 1954.

(Manuscript received April 18, 1959; revised July 6, 1959.)

Geomagnetic Oscillations at Middle Latitudes

Part I. The Observational Data

ELWOOD MAPLE

Geophysics Research Directorate
U. S. Air Force Cambridge Research Center
Bedford, Massachusetts

Abstract—Oscillations are defined as comprising only the more regular of the short-period geomagnetic fluctuations (periods from 1 to 200 seconds) and may be recognized as representing electromagnetic energy in narrow frequency bandwidths and identified by objective criteria. The characteristics of these oscillations, as indicated by the available observational data, are examined with a view toward the eventual identification of their resonant sources. Three distinct frequency 'bands' are observed. Two of them, a 20-sec band (that is, oscillations having similar characteristics and having periods centered at about 20 sec) and a 70-sec band, are predominantly daytime phenomena, whereas the third, an 8-sec band, occurs at night. The 8-sec oscillations show a strong positive correlation, both in amplitude and duration, with the K index; this correlation is less pronounced for the 20-sec band and is absent (or perhaps negative) for the 70-sec band. An additional nighttime band containing periods longer than about 95 sec is not yet definitely established.

INTRODUCTION

The 'rapid' or 'short-period' geomagnetic fluc-ations in the frequency range of about 1 to)05 cps (periods from 1 to 200 sec) exhibit a lde variety of characteristics which suggest ferent physical mechanisms for their sources. ıe term 'oscillations' is here restricted to mean *ly* the more regular of these fluctuations; at is, those which may be recognized as repre-ıting electromagnetic energy in narrow fre-ency bands. The frequent appearance on ısitive magnetograms of these trains of waves, netimes with quite pure sinusoidal wave-ms, has been a major factor in arousing the erest of many investigators. However, ob-tive measures of their quasi-sinusoidal char-ter have seldom been used in the analysis of ə records.

A resonant source (or sources) for the oscilla-ns is definitely indicated, as has been pointed t by *Holmberg* [1951]. Objective criteria de-ned to select from the records only those asi-sinusoidal fluctuations which indicate such source were used by *Chernosky and others* 954] in an analysis of high-sensitivity, rapid-n recordings from Tucson. The resulting clear-t description of many characteristics of the oscillations illustrates the value of intensive analysis of comparatively short time intervals as a supplement to studies of much longer recording intervals for which such detailed analysis is not practicable.

In the present paper some of the observational data are further examined to clarify the conditions (time of day, degree of magnetic disturbance) favorable for the appearance of oscillations of various periods. This is based principally on the data from Tucson, Arizona, both because the method of analysis was most suitable and because the original Tucson records, as well as the results of the previous scaling, have been available for further study. The results of *Holmberg* [1951, 1953] from Eskdalemuir, Scotland, are also quite useful, although definite selection rules were not used in scaling the records. In each case the vertical component of the oscillations was recorded and a large, buried, horizontal loop was used as a detector. The work of other investigators, whose results are usually in less suitable form, is considered briefly.

In Part II the probable origins of the oscillations will be considered. Comparison of the observational data with the results of certain iono-

spheric studies and with hydromagnetic theories strongly suggests (as previously reported more briefly) [*Maple*, 1954] that both an excitation mechanism (source of energy) and a resonant mechanism (acting as a bandpass filter) are involved in the production of the oscillations and that both mechanisms are located in the ionosphere.

Definition of Oscillations

The rapid geomagnetic fluctuations include, in addition to the quasi-sinusoidal oscillations, other characteristic waveforms such as the impulsive wavetrains which are damped out within a few cycles after an impulsive beginning and which show varying 'periods' between successive maxima. Also, irregular or 'random' fluctuations are probably always present, although often masked by other types of fluctuations. Separate study of these various types is needed to clarify the conditions favorable for their appearance, since different physical mechanisms are to be expected as their origins.

The criteria adopted here to define an oscillation (which were also those used by *Chernosky and others* [1954] to define a 'constant frequency' oscillation) are that it consist of three or more consecutive cycles whose periods are equal to within ±10 per cent and have amplitudes at least twice those of any shorter-period fluctuations which may be superposed in order to eliminate doubtful cases.

These criteria are probably the least stringent which should be used in detailed studies of the usual pen-and-ink or photographic traces. The designations 'pc,' 'pt,' etc., which are now in use may be as detailed as is practicable in handling large quantities of records. For intensive studies, however, they do not appear to effect an adequate separation of the various types of fluctuations. *Holmberg's* [1951] discussion of the ratio of bandwidth to midband frequency of the oscillations in the Eskdalemuir records would suggest criteria similar to those used here. At Eskdalemuir, however, modifications would have been needed to allow for the superposition of oscillations of different periods, a phenomenon not observed at Tucson.

The Oscillations at Tucson, Arizona

Results of previous analysis—Fluctuations in the vertical component of magnetic field with periods from 1 to 60 sec at Tucson (geomagnetic latitude $\lambda = +40°$) were described by *Chernosky and others* [1954]. The discussion here is concerned only with what were termed 'constant frequency' oscillations (see above) which constituted the major portion of the oscillatory activity.

The intensive analysis of the Tucson records covered the 12-day interval from May 22 to June 2, 1947, during which 9.1 days of usable records having a sensitivity of 0.005 gammas/mm and a time scale of 150 mm/minute were obtained. For analysis, the oscillations were divided into six groups with center periods of 5, 10, 15, 20, 25, and 30 sec. No appreciable activity having periods between 32 and 60 sec was observed. For each 15-minute time interval of the records, the amplitude (measured by the peak-to-peak value of the third-largest cycle of oscillation) and the duration (number of minutes the oscillations were in progress) were recorded for each period group. (Note that oscillations of more than one period group could occur in a single 15-min interval.)

Oscillations appeared about 20 per cent of the time at Tucson and had amplitudes which were approximately proportional to their periods. Periods of about 20 sec occurred most often. Contour plots of average amplitudes and of durations as functions of oscillation period and local clock hours were given, and the division of the oscillations into day and night activity according to period was clearly shown. The relationship of the activity to the K index was also indicated. These and other features of the previous analysis are discussed more fully below.

Further analysis of the previously scaled data—The occurrences of the oscillations are related to both time of day and K index, as indicated by the examples of Figure 1, and it is desirable to separate the two effects as far as possible. The division of the oscillatory activity into separate day and night bands is further illustrated in Figure 2 (sunrise and sunset were at 05h and 19h).

The term *bands* designates what are judged to be physically significant divisions of the oscillations according to observed characteristics. The bands are to be distinguished from the period *groups* which were chosen merely for

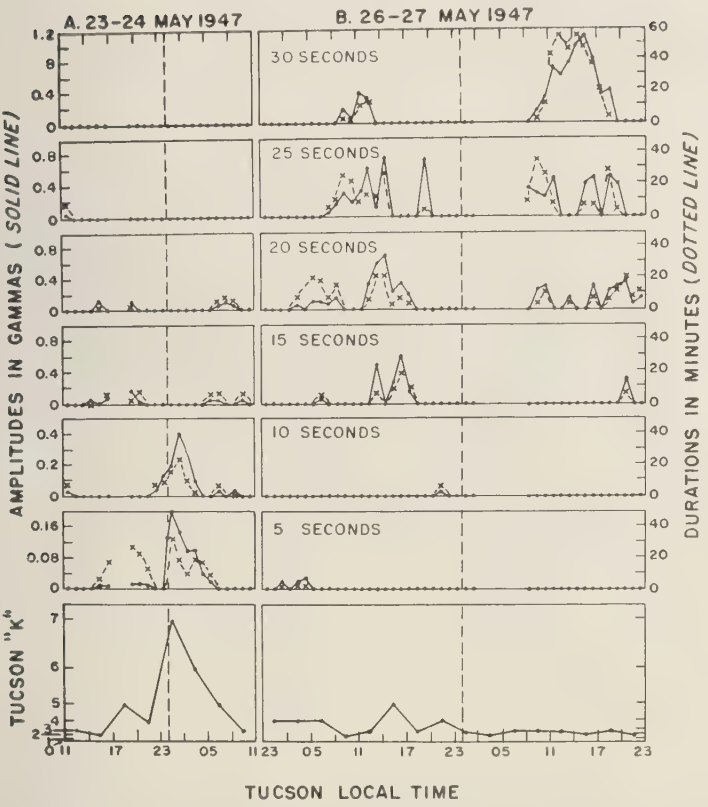

FIG. 1—Occurrence patterns of 2- to 32-sec period oscillations on the most active days at Tucson, Arizona. A. Activity in 'nighttime' period groups on May 23–24, 1947. B. Strong oscillations in 'daytime' period groups on May 26–27, 1947. The oscillations are divided into six groups designated by their central periods. For each hour, the peak-to-peak amplitude of the third-largest cycle of oscillation and the number of minutes of activity are shown for each period group. The Tucson K index is shown on a scale expanded to be approximately linear in gammas.

convenience in the scaling and analysis of the records.

The 'nighttime' band, which may also be termed the '8-second' band, includes periods from 2 to 12 sec (the 5- and 10-sec groups) and is centered at about an 8-sec period. The daytime' band, or '20-second' band, includes periods from 13 to 32 sec (the 15- to 30-sec groups).

From Table 1, which includes data from only those hours favorable for the appearance of the nighttime band (20h to 05h), it is clear that these oscillations are closely related to the degree of magnetic disturbance. The threshold level for their appearance in the present data is at $K = 3$, and both the percentage activity and the amplitudes increased rapidly with increasing K index. During the night hours, no oscillations in this band were observed with a K of 2 or less, while six of the eight 3-hour intervals having a K of 3 showed activity, as did all the intervals having a K of 4 or more. (Note that amplitudes are given in units of 10^{-7} oersted $= 10^{-2}$ gamma.)

Fig. 1A shows the largest occurrence of activity in the 8-sec band with K indices of 7 and 6. The figure suggests that the 5-sec oscillations on the afternoon of May 23 (the only occurrence of this period group during daylight hours) might be a precursor of the disturbance

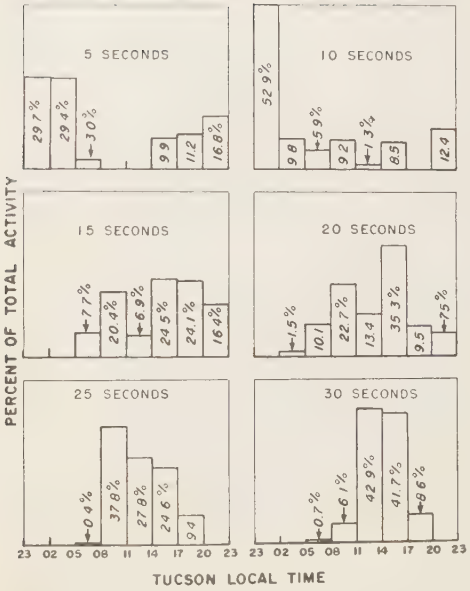

FIG. 2—Occurrence of the 2- to 32-sec oscillations at Tucson as a function of local time. For each period group, designated by its central period, the percentage of its total activity which occurred in each 3-hour interval of the day is shown.

to follow. There were four other small daytime occurrences in the 10-sec group, indicating that the 'daytime' oscillations in the 20-sec band occasionally have periods shorter than 13 sec.

Of the total activity in the 8-sec band, 62 per cent occurred on the night of May 23–24. The correlation with the K index, however, on this and other nights, indicates that the behavior observed is fairly representative of times of large magnetic disturbance.

The daytime oscillations in the 20-sec band showed a gradual change, both in times of occurrence and in relationship to K index, as their periods increased. The 15- and 20-sec groups occurred from 05h to 23h (Fig. 2), with the 20-sec group being more concentrated in the 08h to 17h interval. Activity in these groups occurred several times after sunset (20h to 23h), but such activity was observed only once, and with small amplitude, in the early morning hours before sunrise (23h to 05h). Ninety per cent of the activity of the 25-sec group was between 08h and 17h, and 85 per cent of the oscillations in the 30-sec group occurred in the 6-hour interval from 11h to 17h.

During the times favorable for their appearance, oscillations in the 15- and 20-sec groups increased both in amplitude and percentage activity with increasing K index up to $K = 5$ (Table 2), although not as rapidly as did the nighttime oscillations. The data are inconclusive for K's above 5, since only one occurred ($K = 6$ at 20h to 23h). The oscillations in the 25-sec group increased in magnitude up to $K = 5$, but the maximum percentage activity was shown at $K = 2$ and 3. The 30-sec group showed both maximum amplitude and maximum percentage activity at $K = 2$ and 3.

Of the observed activity in the 30-sec group, 73 per cent occurred on May 27, when it was almost continuous from 11h to 17h (Fig. 1B), and there was little indication of what conditions were particularly favorable at that time. The 15-, 20-, and 25-sec activity was more evenly spread over the 12-day interval, and it seems more probable that the measurement interval is a representative one for these period groups.

Periods from 55 to 200 seconds—The Tucson records have been scaled for oscillations having periods from 33 to 200 sec (which were not previously reported). The fluxmeter equipment had not been calibrated for long periods, but a few fluctuations were found which had durations of about 5 minutes and amplitudes which could be read with reasonable accuracy on both the fluxmeter records and the magnetograms of the Tucson Magnetic Observatory (operated by the U. S. Coast and Geodetic Survey). The comparison indicated that the amplitudes read from the fluxmeter records were about 20 per cent low for these fluctuations, which were comparable to oscillations having half-periods of about 300 sec. The expected error for periods of 55 and 200 sec would therefore not be more than about 3 and 10 per cent, respectively.

Only one oscillation was found which had a period between 33 and 55 sec, so the slower oscillations stand apart from the 8-sec and 20-sec bands discussed above.

The comparatively few (72 total) oscillations which were found (Fig. 3) had amplitudes which were roughly proportional to their periods (Fig. 4). The oscillations consist of two

TABLE 1—*Variation of 8-second band oscillations with K-index data for night hours (20h to 05h) only*

Item		Tucson K Index				
		0, 1	2, 3	4, 5	6, 7	All (0 to 7)
Number of intervals scaled	{ 3 hour*	6	11	7	3	27
	{15 min.	68	123	84	35	310
5-second period group						
Number of active intervals	{ 3 hour	0	6	5	2	13
	{15 min.	0	8	11	15	34
Percentage activity	{All†	0	1.0	4.7	18.7	3.8
	{Active	...	16	36	44	35
Mean amplitude§	{All	0	0.15	0.94	4.4	0.82
	{Active	...	2.5	7.2	10.3	7.4
Largest amplitude		0	3	25	20	25
10-sec period group						
Number of active intervals	{ 3 hour	0	2	4	3	9
	{15 min.	0	5	13	14	32
Percentage activity	{All	0	0.7	2.4	13.9	2.5
	{Active	...	16	15	34	24
Mean amplitudes	{All	0	0.11	0.60	6.34	0.80
	{Active	...	2.8	3.8	15.9	8.9
Largest amplitude		0	5	10	40	40

*The number of 3-hour intervals (scaled and Active) are listed to give a more direct comparison with the 3-hour K index; any 3-hour interval for which data were available for 2 hours or more (8 or more 15-min intervals) is included.

†'All' and 'Active' imply, respectively, all the intervals scaled or only those intervals showing oscillatory activity for the particular period group.

‡Percentage activity is the percentage of total time (in All or in only the Active 15-min intervals) during which oscillations of a particular period group were in progress.

§Amplitudes are given in units of 10^{-7} oersted (= 10^{-2} gamma) and are based on the original tabulations of the peak-to-peak values of the third-largest cycle of oscillation of each period group for each 15-min interval. Mean amplitudes are the averages for All or for only the Active 15-min intervals.

verlapping bands, a daytime or 80-sec band (that is, centered at about an 80-sec period) and a nighttime band with periods greater than 95 sec. Periods greater than 145 sec appeared almost entirely at night, particularly in the early morning hours (Fig. 3), and showed a positive correlation with the K index both in frequency of occurrence and in amplitude (Fig. 4). These characteristics are quite similar to those of the 8-sec nighttime band.

The oscillations having periods between 55 and 95 sec appeared chiefly during daylight and evening hours, the only two occurrences in the early morning hours being of small amplitude. They showed no positive correlation with the K index. The largest oscillations occurred at K = 1 or 2, and a larger percentage of the activity occurred with $K \leq 3$ than would be expected on a random basis. Their occurrence pattern thus resembles that of the 20-sec daytime band, but the relationship to the K index is not the same.

The transition or 'overlap' region appears between 95 and 145 sec. In their relationship to the K index, the daylight and evening occurrences in this group are similar to those having periods less than 95 sec, whereas the smaller number of early morning occurrences resemble the oscillations having periods greater than 145 sec.

It should be noted that although the quasi-sinusoidal character of the Tucson oscillations indicated resonance effects throughout the 2- to 200-sec period range, these effects appeared less

TABLE 2—*Variation of 20-second band oscillations with K-index daytime period groups*

Item		Tucson *K* Index				
		0, 1	2, 3	4, 5	6, 7	All (0 to 7)
05h to 23h only:						
Number of intervals scaled	3 hour	6	36	15	1	58
	15 min.	79	420	169	11	679
08h to 20h only:						
Number of intervals scaled	3 hour	4	27	10	0	41
	15 min.	58	320	110	0	489
A. 15-sec period group 05h to 23h only						
Number of active intervals	3 hour	0	13	12	1	26
	15 min.	0	36	23	1	60
Percentage activity	All	0	2.6	4.2	1.8	2.7
	Active	...	31	31	20	30
Mean amplitudes	All	0	1.1	2.3	2.3	1.3
	Active	...	12.7	17.1	25.0	14.6
Largest amplitudes		0	50	70	25	70
B. 20-sec period group 05h to 23h only						
Number of active intervals	3 hour	2	26	11	0	39
	15 min.	5	75	41	0	121
Percentage activity	All	2.8	5.6	10.6	0	6.4
	Active	44	31	44	...	36
Mean amplitudes	All	0.8	2.0	6.9	0	3.1
	Active	11.8	11.3	28.5	...	17.1
Largest amplitudes		15	60	90	0	90
C. 25-sec period group 08h to 20h only						
Number of active intervals	3 hour	3	19	2	...	24
	15 min.	7	67	11	...	85
Percentage activity	All	3.8	8.9	5.9	...	7.6
	Active	31	43	60	...	44
Mean amplitudes	All	0.6	3.5	4.2	...	3.3
	Active	5.3	16.6	41.9	...	18.9
Largest amplitudes		9	70	75	...	75
D. 30-sec period group 08h to 20h only						
Number of active intervals	3 hour	3	13	2	...	18
	15 min.	7	47	3	...	57
Percentage activity	All	2.8	8.2	1.3	...	6.0
	Active	23	54	49	...	51
Mean amplitudes	All	0.7	6.1	0.3	...	4.1
	Active	5.6	40.9	12.3	...	35.2
Largest amplitudes		10	110	18	...	110

Notes: See Table 1.

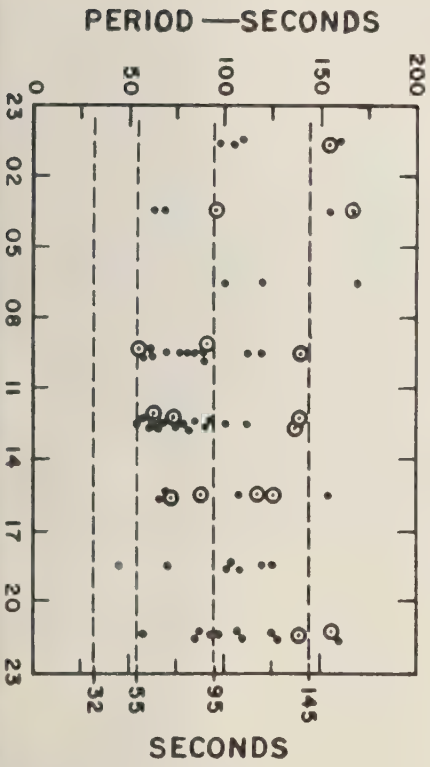

FIG. 3—Occurrence of oscillation periods from to 200 sec at Tucson. Each point shows the riod and time of day (by 3-hour intervals) of oscillation consisting of 3 or more consecutive cles; circled points indicate 5 or more consecu- e cycles.

onounced in all respects for the periods eater than 55 sec. Only 518 minutes of activity ere found in the 80-sec band and the 'periods 95 seconds' band combined, compared with 35 minutes in the 8-sec band and 1943 minutes the 20-sec band. Amplitudes were approxiately proportional to periods in both the 2- 32-sec period range and the 55- to 200-sec riod range. However, the amplitudes at 60 c (0.17 gammas, Fig. 4) were only about one- lf of those at 30 sec (0.35 gammas, Table 2). Also, in the 8- and 20-sec bands a large per- ntage of the oscillations (perhaps close to 50 r cent) would have met more stringent defini- on criteria, such as 5 or more consecutive cles having periods equal to within ±5 per

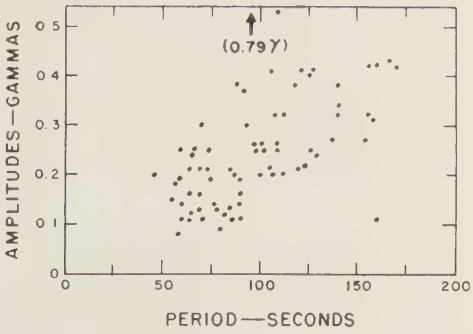

FIG. 4—Amplitudes as a function of periods for the 33- to 200-sec oscillations at Tucson. Amplitudes shown are the peak-to-peak values of the third-largest cycle of each oscillation.

cent. Only 15 of the slower oscillations (circled on Fig. 3) lasted for 5 or more cycles, and few would have met the ±5 per cent requirements on the periods.

The simultaneous occurrence of oscillations belonging to two different frequency bands, reported to be common at some other stations, was not observed at Tucson. Inspection of the records indicates that this negative result was not caused by the scaling rules used.

THE OSCILLATIONS AT ESKDALEMUIR, SCOTLAND

Holmberg [1951, 1953] has analyzed the oscillations with periods from about 5 to 120 sec in the Eskdalemuir ($\lambda = +58°$) records for the intervals near the equinoxes and solstices of 1926–1927. The 'midband frequency' for each hour of each day was determined by the average number of cycles occurring per second, each observation representing 'the mean of at least 5 cycles and often as many as 20 or more.' The maximum intensity was measured by the mean amplitude of the two largest consecutive cycles in the hour. In most cases, the actual duration of the oscillatory activity was not determined.

Rapid oscillations with average periods of about 8 sec occurred at Eskdalemuir during times of large magnetic disturbance. These oscillations were near the limit of time-resolution of the records and were not analyzed further.

No correlation was found between magnetic disturbance and the oscillations having periods between 15 and 120 sec. This may have been due to the use of *'C'* figures and maximum daily

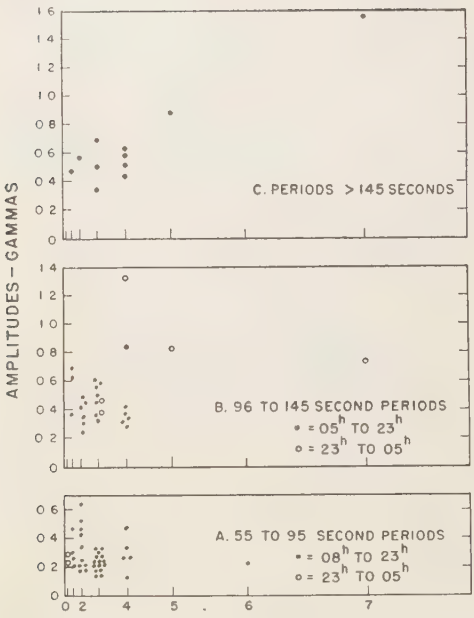

FIG. 5—Amplitudes of the 55- to 200-sec oscillations as a function of Tucson K index according to period group. Amplitudes shown are the peak-to-peak values of the largest cycles of each oscillation and average about twice the values shown in Fig. 4.

ranges of the elements rather than the three-hour K index. It may also have been due partly to the consideration of all oscillation periods together, since the correlation with K index at Tucson varied greatly with period.

The amplitudes of the Eskdalemuir oscillations were proportional to their periods in the 15- to 120-sec range. During the daylight hours these oscillations tended to divide into two separate frequency bands which were centered at about 20- and 70-sec periods. Oscillations in the two bands frequently appeared to be superimposed. The most frequent period in the latter band varied with the season, being about 60 sec in winter, 70 sec at the equinox, and 80 sec in the summer. There appeared to be a similar variation in the 20-sec band, though it was not so readily apparent from the plots which were given.

At the summer solstice, which gives the best comparison with the summer data from Tucson the separation of the daytime oscillations into the two frequency bands was very pronounced and few oscillations with periods between 3 and 60 sec appeared. During the night, the oscillations were much less numerous than during the day; those which did occur at night were mostly in the early morning from midnight to sunrise, with very few in the late evening after sunset. All frequencies occurred at night with periods between 20 and 45 sec being most common.

Other Observations at Middle and Low Latitudes

Extensive historical descriptions have been given by *Holmberg* [1951], *Coulomb* [1954] and *Kato and Watanabe* [1957b]. Only a selected few of the previous results are listed briefly here. Local times are used throughout. *Eschenhagen* [1897] (Potsdam, $\lambda = +52°$) reported all periods from about 12 to more than 100 sec during daylight hours the most frequent period was about 30 sec and the pulsations sometimes lasted for 3 or 4 hours; periods longer than 1 min were usually observed at night, the duration usually being less than ½ hour. *Van Bemmelen* [1908] (Batavia, $\lambda = -18°$) observed 'spasms' (too rapid to be resolved on the records) with a maximum frequency of occurrence at 23h to 24h and a secondary maximum at 14h. Pulsations 1- to 4-min period had their maximum occurrence around midnight with a secondary maximum near noon. *De Moidrey* [1917] (Lukiapang, $\lambda = +20°$) found that pulsations of 1- to 2.5-min periods occurred most frequently near midnight with a weak secondary maximum near noon; periods between 1 and 1.5 min occurred more frequently during daylight hours than did the longer periods.

Johnston [1937] (Watheroo, $\lambda = -42°$) observed that pulsations of 20- to 30-sec period were more closely related to magnetic disturbance than were the slower pulsations of 30- to 80-sec periods. *El Wakil* [1937] (Meanook, $\lambda = +62°$) reported pulsations of 30- to 40-sec periods lasting for a few hours, generally in the early afternoon. *Utashiro* [1950] (Onagawa, $\lambda = +28°$) reported 'sinusoidal regular micro pulsations' having periods greater than 20 sec which occurred most frequently in the daytime

th maximum occurrence at 07h to 08h. roitskaya [1953] (Alma Ata, $\lambda = +34°$) ob- rved 'continuous oscillations' of 10- to 40-sec riods occurring from about 03h to 19h with maximum at about 11h, and 'oscillatory rsts' of 40- to 63-sec periods occurring from out 18h to 06h with a maximum at about h. *Kato and Watanabe* [1957a] found that e periods of *Pc* pulsations observed for large lues of *Kp* were usually shorter than those served for small values of *Kp*.

Only one paper is in definite disagreement th the Tucson and Eskdalemuir results. *idder* [1926] (Irkutsk, $\lambda = +41°$) described scillations' of 4- to 15-sec periods occurring ost frequently from 12h to 19h and 'oscilla- ns' of 30- to 45-sec periods occurring at all urs with a slight maximum during night urs. These results are unique and unexplained ong the middle latitude data; a possible re- ionship of the 4- to 15-sec periods with micro- sms was indicated.

Troitskaya reported that 'oscillations' oc- rred simultaneously on earth-current records m several stations extending over the longi- de range from 34°E to 142°E, and because of e similarity between earth-current and mag- tic data at Alma Ata (the only one of the ations where magnetic measurements were de) she concluded that the magnetic oscilla- ns were universal time phenomena. This con- sion is in disagreement with the observational ta of others, although the Alma Ata magnetic ta agrees with the other observations.

Summary

Most of the other observations at middle lati- des appear to be in good qualitative agree- nt with the Tucson and Eskdalemuir results. ecific agreement with many of the other udies is difficult to establish because of lack adequate distinction between oscillations (in e sense of this paper) and non-oscillatory fluc- ations. Also, the more rapid oscillations would t have been resolved on most of the earlier cords; since oscillation amplitudes vary with equency, the frequency distribution of the ob- rved oscillations can also be a function of the nsitivity of the records. With these reserva- ns, the other studies may be said to greatly tend the time interval and geographical area considered and thus confirm the general fea- tures of the Tucson and Eskdalemuir results.

The 20-second and 70-second bands—The oc- currence of two distinct daytime bands of geo- magnetic oscillations which are essentially local- time phenomena over a wide range of longitudes is rather firmly established. It is clear that these bands are predominantly daytime phenomena in the summer at both Tucson and Eskdalemuir, which differ in longitude by 107°, and their maximum occurrence is during local daylight hours for all seasons of the year at Eskdalemuir. This local-time dependence is also confirmed by many observations at other locations. The type of dependence on *K* index observed at Tucson is also confirmed, in a general way, by other observations; that is, the 20-sec band shows a positive correlation which is strongest for the shorter periods, while the correlation is absent (or perhaps even negative) for the 70-sec band.

There is a lack of complete agreement on the range of periods and hours of maximum occur- rence for the two bands. Some variation with latitude, longitude, and season probably exists; the lack is also due in part, however, to different methods of scaling the records. In the Tucson records, for example, only one oscillation having a period between 32 and 55 sec was found, but a number of other fluctuations were observed which resembled oscillations but did not meet the objective criteria which had been adopted.

The 8-second band—This nighttime band at Tucson, which contained periods from 2 to 12 sec and showed a strong positive correlation with *K* index, also appeared to depend strongly on local time. There are, however, no compar- able data from other locations to confirm this.

The 'periods > 95 seconds' band—The exist- ence of this nighttime band as a common or widespread phenomenon is not yet firmly estab- lished. It was not observed at Eskdalemuir, and it is not known how many of the nighttime 'pulsations' at Batavia and Lukiapang would have met the criteria for oscillations. The im- pulsive wavetrains observed at night at Eskdale- muir (which were *not* oscillations) also appeared with smoother waveforms at Tucson, and it seems possible that this type of fluctuation would occasionally be regular enough at the lower latitudes to account for the few occurrences of such 'oscillations' at Tucson.

Nature of the sources of the oscillations—The records suggest, to the author at least, that two separate mechanisms, each having midband frequencies and bandwidths which vary with time, are required for the production of the oscillations. Under this hypothesis, oscillations would appear only when the excitation mechanism (source of energy) supplied appreciable energy within the more narrow bandwidth of the resonant mechanism.

In the Tucson records, the 'irregular' fluctuations suggested random noise modified by a band-pass filter whose bandwidth and frequency of maximum transmission varied with time of day and degree of magnetic disturbance. The bandwidth of these irregular fluctuations was usually much wider than that of the oscillations, but there were times when this distinction was not so clear cut. It sometimes appeared, for example, that an excitation mechanism was supplying a large portion of its energy in the 33- to 55-sec period range, but that a narrow-band resonant mechanism in that range was lacking.

On the basis of the magnetic records alone, other interpretations are, of course, possible. Justification for the criteria used to separate the various types of fluctuations must ultimately depend on the utility of the results in the identification of the sources.

Acknowledgments—Thanks are expressed to the U. S. Naval Ordnance Laboratory, Silver Spring, Maryland, for making available both the Tucson magnetic records and the results of the orginal scaling of the records.

References

Chernosky, E. J., E. Maple, and R. M. Coon, Rapid geomagnetic fluctuations at Tucson, Arizona, *Trans. Am. Geophys. Union, 35,* 711–721, 1954.

Coulomb, J., Les pulsations du champ magnetique terrestre, *Annuaire pour l'An 1954,* Bureau des Longitudes, Paris, 1954.

De Moidrey, J., Pulsations magnétiques à Zikawei et à Lukiapang, *Terrest. Magnetism and Atmospheric Elec., 22,* 113–120, 1917.

El Wakil, M. A., Pulsations of the earth's magnetic field, Ph.D. thesis, London Univ., 1937.

Eschenhagen, M., On minute, rapid, periodic changes of the earth's magnetism, *Terrest. Magnetism and Atmospheric Elec., 2,* 105–114, 1897.

Holmberg, E. R. R., A discussion of the origin of rapid periodic fluctuations of the geomagnetic field and a new analysis of observational material, Ph.D. thesis, London Univ., 1951.

Holmberg, E. R. R., Rapid periodic fluctuations of the geomagnetic field—I., *Monthly Notices Roy. Astron. Soc., Geophys. Suppl., 6,* 467–481, 1953.

Johnson, H. F., Watheroo, *IATME Bull. 10, Trans. Edinburgh Meeting* 1936, 261, IUGG, Copenhagen, 1937.

Kato, Y., and T. Watanabe, Studies on geomagnetic pulsation, Pc, *Sci. Repts. Tohoku Univ., Ser. 5, Geophys., 8,* 111–132, 1957a.

Kato, Y., and T. Watanabe, A survey of observational knowledge of the geomagnetic pulsation, *Sci. Repts. Tohoku Univ., Ser. 5, Geophys., 8,* 157–185, 1957b.

Maple, E., Sub-audio-frequency oscillations of the geomagnetic field: 0.01 to 1 cps (abstr.), *Trans. Am. Geophys. Union, 35,* 371, 1954.

Pödder, A., Micro-magnetic oscillations as observed at the Magnetical Section of the Observatory of Irkutsk (Zouy), 1925, *Terrest. Magnetism and Atmospheric Elec., 31,* 103–112, 1926.

Troitskaya, V. A., Two oscillatory modes of the terrestrial magnetic field and their diurnal GMT cycle, *Doklady Akad. Nauk SSSR, 93,* 261, 1953 translated by E. R. Hope in Defence Research Board (Canada) Publ. T 174 R.

Utashiro, S., On the character of the micropulsation in the magnetic storm, *J. Geomag. Geoelec., 1,* 59–66, 1950.

Van Bemmelen, W., Appendix, *Batavia Obs. Magn. Met. Obs., 29* (for 1906), 1908.

(Manuscript received March 23, 1959.)

Geomagnetic Oscillations at Middle Latitudes

Part II. Sources of the Oscillations

ELWOOD MAPLE

Geophysics Research Directorate
U. S. Air Force Cambridge Research Center
Bedford, Massachusetts

Abstract—The observed characteristics of the oscillations, quasi-sinusoidal geomagnetic fluctuations having periods from 1 to 200 seconds, are compared with theories of their origins and with observations of other ionospheric phenomena. The results favor the hypothesis of intra-layer hydromagnetic resonance in the ionosphere as the source mechanism and suggest that the 'daytime' oscillations comprising the 20- and 70-sec bands arise in the E region, whereas the 'nighttime' 8-sec band originates in the F region. Simultaneous studies of the different phenomena are needed to confirm these results and to furnish data for comparisons with further developments of the theory.

Introduction—The regular waveforms of the cillations represent electromagnetic energy in rrow frequency bands and definitely indicate sonant mechanisms for their sources. An origin the upper atmosphere was suggested quite rly [*Terada,* 1917], but origins outside the nosphere, such as the 'ring current' or charged rticles traveling in Störmer orbits, have also en considered for some time. Recent theoretal work has dealt with hydromagnetic hypothes of various types. The observed characterics of the oscillations, which were examined Part I of this paper, are here compared th the theories and with the results of other pes of ionospheric studies. As previously reorted more briefly [*Maple,* 1954], this sugsts hydromagnetic origins in both the E and F gions of the ionosphere.

Evidence against extra-ionospheric sources—istant sources outside the ionosphere could not ve produced the cases of simultaneous occurnce of different oscillation frequencies at staons separated by only 200 km [*Holmberg,* 51], and the postulation of more than one pe of source is at present unwarranted. The urce may, however, have considerable lateral tent; the frequencies were usually the same 200 km and were occasionally the same for station separation of 2000 km. *Duffus and and* [1958] found that oscillations were somenes (but only rarely) coherent for a separation of almost 5000 km; work with more closely spaced stations is under way (H. J. Duffus, 1959, private communication) and may furnish conclusive evidence for non-auroral-zone stations.

At middle-latitude stations, it is clear that the oscillations in the 20- and 70-sec bands are predominantly daytime phenomena over a wide geographical range, whereas the 8-sec band at Tucson was restricted almost entirely to the nighttime hours [*Part I*]. These large diurnal variations, dependent on local time, seem quite unlikely for sources external to the ionosphere.

Ashour and Price [1948] computed the effects of uniform magnetic fields externally applied to the non-uniform ionospheric shell, the mean integrated conductivity of the ionosphere being taken as 10^{-7} emu, and the maximum and minimum values as 6.1×10^{-7} and 3.2×10^{-8} emu. For 120-sec-period inducing fields parallel to the earth's axis, the amplitudes at the surface were reduced by a factor of 5 or more, and the computed vertical components at middle latitudes were about an order of magnitude larger at local midnight than at local noon. These computations indicate that the shielding effect would be appreciable for the shorter oscillation periods considered here, although it might be negligible for the longest periods. The diurnal variation required of an external source for the 20-sec band would thus be increased, and the

currents required would appear to be unreasonably large.

In the absence of definite evidence favoring extra-ionospheric sources, the sum of these arguments is quite convincing. It appears very unlikely that purely electromagnetic or hydrodynamic mechanisms within the earth-ionosphere system could account for the production of oscillations having the observed range of periods [*Holmberg*, 1951], and hydromagnetic processes remain.

The hydromagnetic hypotheses—It now seems fairly certain that several types of short-period geomagnetic fluctuations originate in hydromagnetic processes, but the theory as applied to the ionosphere is still under development and its present predictions are not necessarily final. Of the several hypotheses advanced in recent years, most are not applicable to the oscillations, although they may well apply to other types of fluctuations.

The variation of period with latitude predicted by the theory of *Obayashi and Jacobs* [1958], who considered the propagation of Alfvén waves along the geomagnetic lines of force, is not observed for the oscillations. Although wavetrains several cycles long which show a slow, regular change in the period of oscillation suggestive of the hypothesis of 'solar whistlers' [*Menzel and Gold*, 1958] are occasionally observed, they represent a small portion of the total oscillatory activity in the frequency bands considered here and could probably be accounted for in other ways.

The hypothesis of hydromagnetic oscillations of the outer atmosphere might account for some of the characteristics of the oscillations [*Kato and Akasofu*, 1956; *Kato and Watanabe*, 1957], but other observed characteristics would not appear to be allowed. Among the latter are the existence of more than two distinct frequency bands, the diurnal variations in period within the two daytime bands, and the occurrence within a single hour of appreciably different oscillation periods within the 20-sec band [*Part I*].

Hydromagnetic resonance within one or more of the ionospheric layers was first suggested by *Holmberg* [1951]. The natural periods which he estimated were too long, and the estimated attenuations were too great, and in each case the situation was least favorable in the E region. He therefore concluded that the two daytime bands were probably caused by the two modes of propagation of hydromagnetic waves in the F region.

Using later ionospheric data, *Lehnert* [1956] discussed the intra-layer hypothesis and concluded that all periods from about 1 sec to over 200 sec might be possible except that the damping distance computed for normal ionospheric conditions was too small to allow the required resonance effects. However, if the conductivities in the auroral zone were sometimes enhanced by a factor of about 10 or more (as at times of magnetic disturbance), he considered that the 'giant pulsations' observed in the zone might well result from this mechanism. If neutral particles are excluded in the computation of effective densities, the estimated hydromagnetic wave velocities become much larger than those used by Lehnert [*Dessler*, 1958].

The intra-layer resonance hypothesis—This is the only hypothesis which at present shows promise of accounting for all the observed characteristics of the oscillations. A major theoretical objection to the hypothesis is the computed high attenuation of hydromagnetic waves, particularly in the lower portion of the ionosphere. Rejection of the hypothesis on this basis, in view of other points in its favor, would appear to be premature.

Four frequency bands are allowed if both the transverse and the longitudinal modes of propagation are allowed in both the E and F regions. The similar diurnal variations of the 20- and 70-sec bands suggest an origin in the same ionospheric region, which would leave the 8-sec nighttime band for the other region. If the periods > 95 sec band should become more firmly established, its periods would not appear to fit readily into the theory as a second nighttime band.

If the two daytime bands originate within the same region, the Alfvén-wave band should predominate at the higher middle latitudes, and the longitudinal-wave band (probably the shorter-period band) should be the stronger at lower latitudes [*Holmberg*, 1951]. At Eskdalemuir ($\lambda = +58°$), amplitudes increased with period throughout the 15- to 120-sec period range. At Tucson ($\lambda = +40°$), amplitudes in

ased with period in each of the daytime ds, but the amplitudes at 60 sec (lower edge the 70-sec band) were only about half those 30 sec (upper edge of the 20-sec band). The sec-band oscillations were also less numerous l less persistent at Tucson than at Eskdale- ir [*Part I*]. The 70-sec band was stronger n the 20-sec band at White Oak, Maryland = +51°), as would be expected [*Austin l Maple,* 1954].

ystematic variations of the oscillation pe- ls are observed. At Eskdalemuir, the most quent period within the 70-sec band varied m about 60 sec at winter solstice to 70 sec equinox to 80 sec at summer solstice. At both kdalemuir and Tucson, the periods in both 20-sec and 70-sec bands varied with time day, the longest periods favoring the early ernoon hours and shorter periods being more mon earlier and later in the day. Under the ra-layer resonance hypothesis, normal varia- ns of the ionospheric regions might account a part, but probably not all, of the observed iod variations. There is considerable evi- ce, however, that discontinuities within the ions might often be more effective in produc- reflections than, for example, the boundaries the tops of the daytime F_1 or E regions.

n addition to sporadic E and spread F which e long been observed, vertical profiles of ization density from rocket measurements White Sands show that the daytime E region composed of 'blobs' rather than being a uni- m, continuous layer [*Pfister and Ulwick,* 8]. Finally, the currents associated with the rnal variations of field have sometimes been nd in discrete layers within the E region *ahill,* 1959]. The effective thickness for hy- magnetic resonance may therefore be ap- ciably less than, and may also vary more lely and more rapidly than, the thickness of ionospheric region itself. The intra-layer othesis thus shows promise of accounting the variations of period which can occur hin a single hour as well as the more sys- atic variations listed above.

region origin of the 8-sec band—These oscil- ons occurred at Tucson chiefly during the ht and were most numerous in the early rning (23h to 05h) when sporadic E is least valent in that area. When large oscillations occurred on May 23–24, 1947 [*Part I,* Fig. 1*A*], the original White Sands ionograms showed low limiting frequencies for sporadic E, particularly from 01h to 05h when the oscillations were strongest. This band can hardly be attributed, then, to sources below the F region, and arguments against more distant sources have already been presented.

The close correlation, both in amplitude and duration, of the 8-sec oscillations with the local K index invites comparison with radio star scintillations. The velocities of the moving irregularities of F-region ionization involved increase with K index [*Hewish,* 1952; *Little and Maxwell,* 1952]. Velocities greater than 300 m/s (and therefore scintillation durations of about 10 secs or less) occur only with K indices of 4 or more. Scintillation amplitudes show a pronounced diurnal variation with a maximum soon after local midnight; the half-amplitude times are about 22h and 04h, and amplitudes are very small between 12h and 18h [*Ryle and Hewish,* 1950]. This striking similarity to the diurnal variation of the 8-sec oscillations suggests a closer relationship than a mere mutual dependence on geomagnetic disturbance.

If the moving ionospheric irregularities served as their excitation mechanism, these oscillations would then appear only at times of magnetic disturbance when the excitation was near the resonant frequency of the ionospheric region. This type of relationship would account for the oscillations being much more regular and indicative of resonance than the scintillations themselves. It would also be consistent with the intra-layer hypothesis, although no theoretical basis for relating specific ionospheric velocities and oscillation frequencies is presently available.

Hines [1955] and *Dessler* [1958] have suggested the reverse effect, that moving F-region irregularities might be produced by hydromagnetic waves, but geomagnetic effects corresponding to cases other than the one cited above have not been reported.

E-region origin of the daytime bands—At least one of the three frequency bands would be attributed to the E region under the intra-layer hypothesis, and the daytime E region would appear as a likely source for the daytime occurrences of the 20- and 70-sec bands (for the present, the high attenuation predicted by pres-

ent theory is ignored), whereas their much less frequent nocturnal occurrences would require sporadic *E*. At Tucson, the daytime bands appeared several times after sunset (20h to 23h) when nocturnal sporadic *E* is most prevalent in that area. The original ionograms, although insufficient for any attempt at a detailed correlation, show that the daytime frequencies did occur at Tucson on evenings when the limiting frequency of nocturnal sporadic *E* at White Sands was comparatively high.

Each of the daytime bands at Tucson occurred only once, and with small amplitude, in the early morning hours before sunrise (23h to 05h) when nocturnal sporadic *E* is least prevalent and when the 8-sec nighttime band was most active. At Eskdalemuir the nocturnal appearances of the daytime bands were much more frequent in the early morning hours than in the late evening. Nocturnal sporadic *E* shows the same reversal of most frequent occurrence from late evening at White Sands to early morning at Slough, England [*CRPL-F Bulletins*, 1951–53], and this reversal from lower to upper middle latitudes is characteristic of the data from many ionospheric stations [*Peterson*, 1954]. This again suggests an *E*-region origin for the daytime bands.

Within the 20-sec band (13- to 32-sec periods) at Tucson, correlation with *K* index was strong for the shorter periods but became weaker for the longer periods. However, even the 28- to 32-sec periods, which were most active for *K* indices of 2 and 3, did not favor very quiet conditions, and the excitation of the entire band thus appears to be related to the *K* index. Turbulence would appear to be the only suitable excitation mechanism; it would be consistent with the intra-layer hypothesis and would be restricted to the *E* region. It would also agree with the inference of separate excitation and resonance mechanisms drawn from the magnetic records. Turbulence, increasing with magnetic disturbance, might also tend to reduce the effective layer thickness for resonance as required, since the shorter periods here attributed to the daytime *E* region are the same as those attributed to nocturnal sporadic *E*. The role of turbulent wind motion in the *E* region in the production of radio star scintillations has been suggested [*Dagg*, 1957], the small amplitudes of daytime scintillations being attributed to the inhibit of turbulent flow by large temperature gra ents. The almost continuous oscillatory activ at 28- to 32-sec periods for six hours (11h 17h) on May 27, 1947 [*Part I, Fig.* 1*B*], in cated very stable conditions in the ionosphe the shorter-period activity in the 20-sec ba which favored earlier or later hours and hig *K* indices, tended to be less continuous, s gesting more variable conditions.

Most of the conductivity of the ionosph may be attributed to the *E* region. Computati based on the same conductivities listed ab (which are about a factor of 3 larger than la estimates [*Chapman*, 1956]) indicate that i constant-amplitude magnetic dipole were os lating at a 30-sec period at *F*-region heig the amplitudes at the surface would be ab one-fifth as large at local noon as at local n night. This indicates that the daytime shield effect would be appreciable for the sho periods in the 20-sec band if the sources of nite size required for the oscillations were ab the *E* region. The 8-sec band was more shar restricted to the night hours than were the ra radio star scintillations, its only occurrence d ing daylight hours being of small amplitu this could also have resulted from the expec shielding effect.

'Giant pulsations' in the auroral zone—detailed discussion is possible here, but th appears to be no reason for postulating a ferent type of source for these intense os lations. Different occurrence patterns would expected because of different ionospheric co tions; for example, *E*-region ionization and c ductivity in the auroral zone are often grea at night than during the day at times of geom netic disturbance.

Conclusion—The intra-layer resonance pothesis shows promise of accounting for all presently known characteristics of the geom netic oscillations, although a major objection such resonance appears in the present hyd magnetic theory.

The arguments developed from comparis with other ionospheric phenomena indic sources in both the *E* and *F* regions, but arguments are at present necessarily specu tive, largely because of the lack of simultane geomagnetic and ionospheric data. The

sion does, however, show that suitably cor-ıted measurements could yield positive in-ımation of the type needed for comparison :h the theory, which is currently undergoing ›id development.

An observational program designed to inves-ate the correlation of the 8-sec band of oscil-ions with rapid radio star scintillations is be- initiated; information on the postulated *E*-ion shielding effect should also result.

Acknowledgments—Thanks are expressed to the ntral Radio Propagation Laboratory, U. S. Na-nal Bureau of Standards, for making available original ionograms from White Sands.

References

HOUR, A. A., AND A. T. PRICE, The induction of lectric currents in a non-uniform ionosphere, *Proc. Roy. Soc. A., 195,* 198–224, 1948.

STIN, W. E., AND E. MAPLE, Sub-audio-frequency fluctuations of the earth's magnetic field t White Oak, Maryland (abstr.), *Trans. Am. Geophys. Union, 35,* 371, 1954.

HILL, L. J., JR., Investigation of the equatorial lectrojet by rocket magnetometer, *J. Geophys. Research, 64,* 489–503, 1959.

APMAN, S., The electrical conductivity of the onosphere: A review, *Nuovo cimento Suppl., 4,* 385–1412, 1956.

RPL-F BULLETINS, Ionospheric data, Central Radio Propagation Lab., US Natl. Bur. Standards, Washington, D. C., 1951–1953.

GG, M., The origin of ionospheric irregularities esponsible for radio-star scintillations and spread-F, *J. Atmospheric and Terrest. Phys., 11,* 133–150, 1957.

SSLER, A. J., Large amplitude hydromagnetic waves above the ionosphere, *J. Geophys. Research, 63,* 507–511, 1958.

FFUS, H. J., AND J. A. SHAND, Some observations of geomagnetic micropulsations, *Can. J. Phys., 36,* 508–526, 1958.

WISH, A., The diffraction of galactic radio waves as a method of investigating the irregular structure of the ionosphere, *Proc. Roy. Soc. A., 214,* 494–514, 1952.

HINES, C. O., Hydromagnetic resonance in ionospheric waves, *J. Atmospheric and Terrest. Phys., 7,* 14–30, 1955.

HOLMBERG, E. R. R., A discussion of the origin of rapid periodic fluctuations of the geomagnetic field and a new analysis of observational material, Ph.D. thesis, London Univ., 1951.

KATO, T., AND S. AKASOFU, Outer atmosphere oscillation and geomagnetic micropulsation, *Sci. Repts. Tohoku Univ., Ser. 5, Geophys., 7,* 103–124, 1956.

KATO, T., AND T. WATANABE, Studies on geomagnetic pulsation, Pc, *Sci. Repts. Tohoku Univ., Ser. 5, Geophys., 8,* 111–132, 1957.

LEHNERT, B., Magneto-hydrodynamic waves in the ionosphere and their application to giant pulsations, *Tellus, 8,* 241–251, 1956.

LITTLE, C. G., AND A. MAXWELL, Scintillation of radio stars during aurorae and magnetic storms, *J. Atmospheric and Terrest. Phys., 2,* 356–360, 1952.

MAPLE, E., Sub-audio-frequency oscillations of the geomagnetic field: 0.01 to 1 c/s (abstr.), *Trans. Am. Geophys. Union, 35,* 371, 1954.

MENZEL, D. H., AND T. GOLD, Solar whistlers, Radio Noise Spectrum Symposium, Cambridge, Mass., 1958.

OBAYASHI, T., AND J. A. JACOBS, Geomagnetic pulsations and the earth's outer atmosphere, *Geophys. J., 1,* 53–63, 1958.

PETERSON, A. M., Geographical and temporal variations of sporadic-E occurrence (abstr.), URSI Meeting, Washington, D. C., 1954.

PFISTER, W., AND J. C. ULWICK, The analysis of rocket experiments in terms of electron-density distributions, *J. Geophys. Research, 63,* 315–333, 1958.

RYLE, M., AND A. HEWISH, The effects of the terrestrial ionosphere on the radio waves from discrete sources in the galaxy, *Monthly Notices Roy. Astron. Soc., 110,* 381–394, 1950.

TERADA, T., On rapid periodic variations of terrestrial magnetism, *J. Coll. Sci. Imp. Univ. Tokyo, 37,* 1, 1917.

(Manuscript received March 23, 1959; revised July 13, 1959.)

Note on Conjugate Points of Geomagnetic Field Lines for Some Selected Auroral and Whistler Stations of the IGY

E. H. Vestine

The RAND Corporation
Santa Monica, California

Abstract—A method for computing field lines in space is used to derive conjugate points of some auroral and magnetic stations of the IGY. The study uses a total of 48 coefficients with computations done on an electronic computer.

Introduction—It has often been suggested that ionospheric events, whether auroral or geomagnetic, may be interlinked via lines of force of the geomagnetic field [*Störmer,* 1907; *Alfvén,* 1950; *Singer,* 1957; *Ahmed and Scott,* 1955; *Storey,* 1953; *Maeda and Kimura,* 1956; *Helliwell and Morgan,* 1959]. Since the geomagnetic field of internal origin in the atmosphere and beyond can be computed from the geomagnetic field values at ground level [*Chapman and Bartels,* 1940; *Vestine and others,* 1947], it is theoretically possible to compute the terminus or intersection of any line of force with the earth's surface when a particular point on the line is specified. Thus the conjugate point in the opposite hemisphere to that of a particular auroral station can be estimated. If another auroral station exists near the conjugate it may be of considerable interest to compare observations at the two stations.

In lightning discharges a radio propagation effect known as a whistler arises, which is explained ordinarily as due to propagation along a geomagnetic field line back and forth between northern and southern hemispheres [*Storey,* 1953; *Maeda and Kimura,* 1956; *Helliwell and Morgan,* 1959].

It may be argued that magnetic fields due to ring currents, and concentrated electric currents flowing in the polar ionosphere, may so distort the geomagnetic field lines that calculation of the lines of force of the earth's main field may not be feasible. These fields may add local distortions in the field values. The localized fields of origin within the atmosphere or beyond the atmosphere may affect the various phenomena studied. Abrupt changes in direction or other complications in field structure along the path of motion may disrupt a plasma moving along a geomagnetic field line or may so redirect it that it never reaches regions above the conjugate point on the line. In the low atmosphere, however, the magnetic fields arising in the atmosphere seldom contribute as much as 1 per cent of field in low latitudes.

The principal difficulties encountered in computing field lines are related to the incompleteness of survey data used for constructing surface magnetic charts and to the large and uncertain effects of geomagnetic secular changes. Since secular changes in some ocean areas may be in error by as much as 100 gammas per annum, errors as great as 1000 gammas in charted main field values may accumulate in a few decades. It is therefore necessary that surface and airborne magnetic surveys be undertaken at suitable intervals if reliable computed values of magnetic field lines are to be obtained. For this and other reasons present plans for a worldwide magnetic survey by sea, air (including satellites), and land as a deferred item of the program of the International Geophysical Year are of importance. Errors naturally are likely to increase also if it becomes necessary to integrate field lines at very great distances above the earth's surface, when the geomagnetic field becomes very weak and the path of integration used to estimate the position of a line of force becomes very long. A study has not been made of the errors accumulated under these circumstances, but obviously the precision of determination of field parameters is reduced.

Method of computation of field lines—Field lines were computed by a method originally due

TABLE 1—*Estimated latitude* (ϕ), *longitude* (λ), *and height* (h) *above the earth's surface of points o geomagnetic field line, using harmonics to degree and order 6, epoch 1955.0*

Station	ϕ deg	ϕ min	λ deg	λ min	h, km
Anchorage, Alaska	61	10N	149	55W	0
	2	54N	168	45W	19810
	53	19S	172	04E	0
College, Alaska	64	51N	147	50W	0
	2	58N	169	49W	28050
	56	34S	168	26E	0
Nome, Alaska	64	30N	165	26W	0
	5	23N	177	31E	20840
	51	42S	161	29E	0
Unalaska, Alaska	53	53N	166	32W	0
	4	46N	178	4W	9140
	42	52S	169	48E	0
Battle Creek, Mich.	42	19N	85	11W	0
	11	58S	88	25W	13060
	66	20S	110	56W	0
Boulder, Colo.	40	3N	105	18W	0
	7	55S	114	31W	8590
	54	29S	132	48W	0
Gainesville, Fla.	29	39N	82	21W	0
	12	37S	84	53W	5310
	54	55S	97	35W	0
Hanover, N. H.	43	42N	72	18W	0
	12	51S	68	39W	14960
	72	28S	83	42W	0
Key West, Fla.	24	33N	81	48W	0
	12	33S	84	19W	3660
	49	40S	94	27W	0
Seattle, Wash.	47	39N	122	18W	0
	3	41S	136	2W	11520
	53	32S	155	44W	0
Stanford, Calif.	37	26N	122	10W	0
	4	9S	131	52W	5490
	44	50S	145	0W	0
Washington, D. C.	38	55N	77	4W	0
	12	56S	76	37W	10620
	66	32S	92	53W	0
Silver Hill, D. C.	38	50N	76	57W	0
	12	57S	76	27W	10560
	66	29S	92	35W	0
Father Point, Que.	48	5N	68	5W	0
	12	25S	61	12W	20280
	77	6S	72	5W	0
Frobisher Bay, N. W. T.	63	20N	67	20W	0
	11	33S	54	49W	84510
	88	49S	165	0E	0
Knob Lake, Que.	54	48N	66	49W	0
	11	58S	57	27W	34810
	83	11S	69	38W	0
Bermuda	32	22N	64	40W	0
	13	9S	59	18W	6580
	62	19S	61	30W	0
Argentia, Newfoundland	47	18N	54	0W	0
	10	31S	40	55W	15850
	72	42S	26	32W	0
Baker Lake, Can.	64	18N	96	0W	0
	8	53S	110	20W	90170
	75	33S	173	47W	0
Davis Strait (shipboard)	67	0N	58	0W	0
	9	51S	35	54W	109900
	85	1S	77	20E	0
Ft. Churchill, Manitoba	58	46N	94	10W	0
	9	46S	104	24W	49240
	74	22S	154	34W	0
Harmon, Newfoundland	48	44N	58	34W	0
	11	18S	46	46W	19020
	76	8S	37	43W	0
Sachs Harbor, Can.	72	0N	125	30W	0
	0	36N	160	30W	101420
	66	55S	161	34E	0
Saskatoon, Saskatchewan	52	8N	106	40W	0
	7	13S	119	59W	21610
	64	5S	150	1W	0
St. Johns, Newfoundland	47	33N	52	40W	0
	10	14S	39	6W	15760
	72	11S	23	10W	0
Narssarssuak, Greenland	61	11N	45	25W	0
	8	3S	24	8W	41900
	79	0S	22	41E	0
Adak, Aleutian Islands	51	33N	176	39W	0
	5	51N	174	49E	7010
	38	28S	165	11E	0
Anchorage, Alaska	61	10N	149	59W	0
	2	54N	168	48W	19790

Station	ϕ deg	ϕ min	λ deg	λ min	h, km
	53	18S	172	2E	0
Annette, Alaska	55	2N	131	34W	0
	1	5S	149	4W	1700
	55	20S	170	58W	0
Attu, Aleutian Islands	52	50N	173	11W	0
	5	32N	177	8E	792
	40	20S	166	33E	0
Barrow, Alaska	71	18N	156	47W	0
	5	13N	177	8E	4456
	58	38S	156	16E	0
Barter Island, Alaska	70	7N	143	40W	0
	3	11N	172	11W	5062
	61	4S	161	52E	0
Bethel, Alaska	60	47N	161	43W	0
	4	36N	177	31W	1614
	49	41S	166	50E	0
Big Delta, Alaska	64	9N	145	51W	0
	2	32N	167	42W	2734
	56	40S	170	9E	0
Cold Bay, Alaska	55	12N	162	43W	0
	4	20N	175	37W	1050
	44	58S	171	2E	0
Fort Greeley, Alaska	63	59N	145	43W	0
	2	31N	167	27W	2701
	56	36S	170	26E	0
King Salmon, Alaska	58	41N	156	39W	0
	3	44N	172	33W	1471
	49	26S	171	21E	0
Kodiak, Alaska	57	45N	152	31W	0
	3	2N	168	48W	1457
	49	57S	174	24E	0
Kotzebue, Alaska	66	52N	162	38W	0
	5	17N	177	43E	2656
	54	10S	160	5E	0
Healey, Alaska	66	40N	162	30W	0
	5	15N	177	58E	2614
	54	3S	160	22E	0
Matanuska, Alaska	61	34N	149	16W	0
	2	50N	168	30W	2069
	53	48S	171	55E	0
McGrath, Alaska	62	58N	155	37W	0
	3	56N	174	19W	2097
	53	0S	167	27E	0
Naknek, Alaska	58	44N	157	2W	0
	3	47N	172	52W	1468
	49	21S	171	6E	0
Northway, Alaska	62	58N	141	57W	0
	1	45N	163	36W	2655
	57	6S	173	22E	0
Pt. Barrow, Alaska	68	20N	166	45W	0
	5	57N	173	39E	2880
	54	24S	156	46E	0
Point Hope, Alaska	68	20N	166	45W	0
	5	57N	173	39E	2880
	54	24S	156	46E	0
Sitka, Alaska	57	3N	135	20W	0
	0	8S	153	47W	1853
	55	19S	175	39W	0
St. Paul Island, Alaska	57	9N	170	13W	0
	5	25N	177	52E	1110
	44	37S	165	26E	0
Yukutat, Alaska	59	31N	139	40W	0
	0	57N	159	12W	2078
	55	29S	178	58E	0
Ft. Yukon, Alaska	66	34N	145	18W	0
	2	48N	169	25W	3441
	58	27S	166	59E	0
Lemon Creek Glacier, Alaska	58	0N	134	0W	0
	0	18S	153	8W	2050
	56	29S	176	11W	0
Mt. Michelson, Alaska	69	0N	144	0W	0
	3	1N	171	2W	4479
	60	19S	163	38E	0
Cape Adare, Antarctica	71	17S	170	15E	0
	4	17S	136	47W	11740
	69	0N	109	16W	0
Fifth Station, Knox Coast, Antarctica	66	0S	110	0W	0
	11	59S	88	1W	1261
	41	49N	84	54W	0
Campbell Island, Antarctica	52	32S	168	59E	0
	3	45N	172	55W	1962
	61	58N	154	38W	0

Block and Herlofson [1956]. In their study, ed on terms up to and including the second er and degree of spherical harmonic repre- ations of the main field, they gave conjugate nts for many of the existing magnetic ob- ratories. The present study extends their re- ts, using a total of 48 coefficients so that ms of degree and order 6 are included; the puting was done on an IBM–704 electronic puter. It also extends a study by *Vestine Sibley* [1959] based on the first 8 Gauss fficients, the method there described having n followed again with extension to 48 co- ients. The coefficients are those derived re- tly by *Finch and Leaton* [1957] from the tish Admiralty world isomagnetic charts for 5.

The details covering these and other calcula- ns will be given in a later, more extended blication.

Conjugates of auroral and magnetic stations— eginning has been made in deriving conju- e points for a number of North American oral and magnetic stations. Table 1, compiled m IGY sources, lists a number of such sta- ns with the conjugate point (at ground level) each. If charged particles moving along the s of force cause visible auroral rays above a tion, auroral rays may also appear above conjugate point in the opposite hemisphere. will be of interest to check this possibility by ans of IGY data. Simultaneity in auroral nts may be influenced too by magnetic field engths at auroral levels above each station. less the earth's main field is of suitable ength above each station, conditions may be avorable for simultaneous auroral events at ugate stations. Thus the condition that par- es be reflected above each station may be ermined by an approximate equation due Alfvén of the form

$$F/\sin^2 \alpha = \text{constant} \qquad (1)$$

ere F is the total geomagnetic intensity and he pitch angle for particles of a given energy. hough the pitch angles α may change as the ult of scattering in the ionosphere so that par- es may penetrate to levels other than those accord with equation 1, in general, simul- neous enduring aurora at each station are more ely to be observed when F at a given height above each station is the same. Of course, even when the value F is much greater at a northern station, aurora may be noted simultaneously at the conjugate station in the southern hemisphere. Particles arriving above the southern station will then be quickly absorbed within the lower ionosphere, and the generating plasma moving along the lines of force will be drained off. Enduring aurora due to a plasma trapped in the field, when not continuously supplied, will then be of short duration. If an aurora endures for a considerable time a continuous source of supply may be indicated. Useful estimates of main field values within the atmosphere have been derived by *Vestine and others* [1947].

In post-IGY planning it has also been proposed that a scientific laboratory or field station should be set up at either end of a line of force of the geomagnetic field. For such planning purposes the use of the dipole approximation to the earth's field may lead to gross errors in position in some regions. In Table 1 an interesting possibility is Campbell Island in the Antarctic, for which a convenient calculated location is found about 150 km west of Anchorage in Alaska.

Table 1 also lists conjugates for whistler stations of the IGY. These are included for the convenience of workers in the area, though coarser estimates of conjugate points than those afforded by the 48-coefficient series may serve almost as well.

Conjugates of points on the northern auroral zone have been derived previously using the first 8 Gauss coefficients. It is hoped to present results based on the full series of terms in a future investigation.

Acknowledgment—The research on which this report is based was aided by a grant to The RAND Corporation from the National Science Foundation.

References

Ahmed, S. M., and W. E. Scott, Time relationship of small magnetic disturbances in Arctic and Antarctic, *J. Geophys. Research, 60,* 147–154, 1955.

Alfvén, H., *Cosmical Electrodynamics, International Series of Monographs on Physics,* Clarendon Press, Oxford, 1950.

Block, L., and N. Herlofson, Numerical integration of geomagnetic field lines, *Tellus, 8,* 210–214, 1956.

Chapman, S., and J. Bartels, *Geomagnetism,* vols. 1 and 2, Oxford, 1940.

Finch, H. F., and B. R. Leaton, The earth's main magnetic field—epoch 1955.0, *Monthly Notices Roy. Astron. Soc., Geophys. Suppl., 7,* 314–317, 1957.

Helliwell, R. A., and M. G. Morgan, Atmospheric whistlers, *Proc. IRE, 47,* 200–208, 1959.

Maeda, K., and I. Kimura, A theoretical investigation on the propagation path of the whistling atmospherics, *Rep. Ionosphere Research Japan, 10,* 105–123, 1956.

Singer, S. F., A new model of magnetic storms and aurorae, *Trans. Am. Geophys. Union, 38,* 175–190, 1957.

Storey, L. R. O., An investigation of whistling atmospherics, *Phil. Trans. Roy. Soc. Londo 246,* 113–141, 1953.

Störmer, C., *Sur les trajectoires des corpuscul électrises dans l'espace sous l'action du magn tisme terrestre avec application aux aurores b réales,* Archives des sciences physiques et na urelles, Bureau des archives, Genève, 140 p 1907.

Vestine, E. H., I. Lange, L. Laporte, and W. Scott, *The Geomagnetic Field, Its Descripti and Analysis,* Carnegie Institution of Washin ton Publ. 580, Washington, D. C., 1947.

Vestine, E. H., and W. L. Sibley, Lines of for of the geomagnetic field in space, *Planetary a Space Science* (in press).

(Manuscript received July 27, 1959.)

Air Motions and the Fading, Diversity, and Aspect Sensitivity of Meteoric Echoes[1]

L. A. Manning

Radio Propagation Laboratory
Stanford Electronics Laboratories
Stanford University, Stanford, California

Abstract—A theory is presented which relates those properties of meteoric echoes that depend on distortion of the trail by winds. It is shown that existing results on the delay in the start of echo fading, the delay in echo appearance with aspect, the spectral composition of the received signal, and the regularity of the fading pattern are quantitatively explicable. In addition, the theory predicts that the ensemble-average rate of echo fading should rise characteristically with time and should then drop precipitously at the end of the ensemble echo; moreover, it predicts that the correlation of fading patterns at two ground receivers should be a gaussian function of the product of receiver spacing and echo fading cycle-number. Experimental results are given which confirm these predictions and make possible the determination of the principal properties of the wind profile. It is concluded that at the times of observation the small-scale cutoff wavelength of the turbulence spectrum was about a kilometer, that lack of correlation of wind velocities existed in a vertical range of about a scale height, that the rms variable component of N-S wind velocity was about 50 m/s, and that the rms value of the relative maxima of the vertical gradient of a component of the wind velocity was about 100 m/s. These figures agree with Whipple's photographic studies of meteor trails.

Introduction—Although columns of meteoric ionization are very straight when created, they do not stay that way. Wind shears and turbulence quickly warp the trails into complex serpentine shapes, and their radio-reflection properties are radically altered thereby. The major effects that result from the distortion are the fading of the echoes, gradual loss of aspect sensitivity, and the production of irregular variations in scattered signal amplitude with small changes in receiver position. The nature of the signal-strength decay-function is also influenced by trail distortion.

In the present paper an attempt will be made to explain qualitatively a new theory of meteoric reflection from distorted trails [*Manning*, 1957]. In addition to uniting earlier published observations concerning fading and aspect sensitivity, the theory has led to the discovery of a number of new experimental facts concerning meteoric echoes. These new results will be presented in their relation to the theory. Because the ideas which are presented cover a rather wide field, it has not been possible to present the full mathematical development in this single paper. It will be shown in future papers that the numerical results obtained from a variety of independent experiments yield consistent results. Here, for the sake of exposition, we shall avoid analysis based on a general form of wind velocity versus height function; instead, we shall draw upon the properties of a sinusoidal wind shear. It must be emphasized, however, that the general analysis does not restrict us to a particular Fourier spectrum in the analysis of turbulent wavelength, and it yields significantly different numerical answers than will the simple formulas given here.

Previous experimental results—The fading of meteoric radio echoes of sufficient duration has been evident to all workers. *Manning and others* [1952] have shown that a fading meteoric signal results from the superposition of two or more discrete Doppler-shifted frequency

[1] The work described in this paper was jointly supported by the U. S. Army Signal Corps, the U. S. Air Force, and the U. S. Navy (Office of Naval Research).

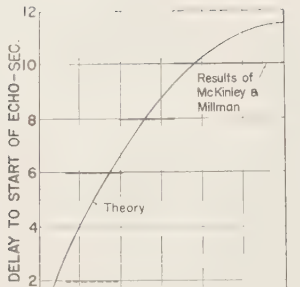

FIG. 1—The delay in the appearance of a radar echo from a visually observed column of meteoric ionization plotted versus the deviation of the reflection geometry from an initial specular condition [after *McKinley and Millman,* 1949].

components. *Greenhow* [1952a] has shown that when an ionization trail is formed in such a position as to present immediately a specular-reflection condition, the onset of fading is delayed an average of 0.4 sec after receipt of the echo. It is characteristic that early in the echo lifetime the fading is regular; deep regular minima are frequently seen that are similar to those of the function $|\sin t|$. Later in the echo lifetime a reduction in regularity is typical and Rayleigh fading is approached. Individual reflections, however, may be quite untypical. In the case of exceptionally long enduring echoes, lasting as much as a minute, the envelope of the usual rapid-fading pattern tends to fluctuate at a very slow rate. This long-period fading generally seems to get slower as time progresses; its origin has not previously been suggested.

In addition to those enduring echoes that are oriented with specular aspect and so produce echoes as soon as the trail is formed, many echoes are seen which do not appear at once. These so-called non-specular echoes appear up to about ten seconds after the trail is formed. *McKinley and Millman* [1949], in one of their remarkably useful papers, have presented data on the relation between the deviation of the radar line of sight from the specular-reflection condition and the delay between visual sighting and reception of the echo. In Figure 1 their results have been plotted as horizontal lines, indicating the observed variatio of delay that corresponds to a given deviatio of aspect. The curve fitted to the plot is derive from the general theory. The constants of th curve were obtained by applying the theory t other, quite independent, experimental result Notice that echoes may appear as much as 10 o 12 seconds after trail formation, if the aspe is unfavorable.

The air motions that cause the trail distor tions have been studied by both radar an photographic methods [*Manning and others* 1950, 1954; *Greenhow,* 1954]. The radar result have been based principally on Doppler-shifte echoes from short-duration, non-fading echoes Manning, Villard, and Peterson found that th major wind components were horizontal, wit an rms velocity of the order of 50 m/s; the vary from day to day. It was suggested that th winds were stratified in height. *Whipple* [1953 has photographed the contortions of long-en during meteor trails. He has presented record that show a minimum scale of about 3 km, a rms component of N-S velocity of about 5 m/s, and a lack of correlation between thes horizontal velocity components in a 5-km heigh change. The observed height profiles of th horizontal wind give the appearance of a randon function. From the photographs it is not possi ble to say whether turbulence exists with scale of less than about a kilometer. Thus, in th general theory, it is assumed that such short wavelength components in the Fourier spectrun of the wind profile may exist. However, it i found that to get experimental agreement, th amplitude of the small-scale components mus be greatly restricted.

Construction of a trail model—From th existing photographic and radar results, it ap pears reasonable to describe the verticle profil of a horizontal wind component in the iono sphere at a given time and place as a sampl of a gaussian noise function. The spectra curve of this function will be left completel arbitrary until restrictions based on experimen are discovered. That a component, say the N-S of the wind profile not be gaussian is hard t conceive. By 'gaussian' we merely mean tha magnitude of specific wind velocity taken fro a large number of uncorrelated measurement is distributed in gaussian form. Since man

tors presumably serve to influence the mag-ude of any single wind vector, we hardly ce assume otherwise. Note in particular that Kolmogoroff-Heisenberg spectrum of tur-lence is but a special case of the general ory, although it is not one that is consistent h the experimental results.

We have assumed a description of the verti-profile of the horizontal wind components. e shall next assume the vertical wind com-nents to be zero. As justification, we cite the lar and photographic studies that show that e bulk of the velocity components are hori-ntal. Perhaps the smaller-scale components e isotropic. If so, the conclusions of the study ll not be greatly altered. We shall assume that e profile does not change for the duration an echo. By comparing velocities and scales, e can show that this assumption is good for er a minute if the minimum scale is 1 km, d even longer for smaller scales. It is evi-ntly satisfactory for the scales we shall find, t in any case it is a convenience, not a ne-ssity.

Having made the above assumptions, we con-der what happens to an initially straight trail the wind. Because of the difference in direc-n and magnitude of the wind velocity with ight, the trail will assume a serpentine form. r the sake of argument, we shall leave the neral theory now and suppose that the trail formed in a vertical N-S plane and that echoes e observed by a radar which is also in that ane. For this geometry the E-W components trail drift do not affect the distance of the ail to the radar except to second order, so we ay neglect them. We are then concerned with geometry such as that in Figure 2. Parts of e trail are transported north or south in cordance with the wind profile; the sinusoidal rm is drawn purely for illustration. The ape of the trail reproduces that of the wind ofile in oblique coordinates, the axes being e trail axis as abscissa and the horizontal as dinate. As time advances, the scale of the dinate (trail distortion) increases, but the ape continues to be that of the wind profile. Except when considering aspect sensitivity, e may further simplify the model by removing e obliquity from the coordinate system in hich the trail distortion occurs. Suppose that

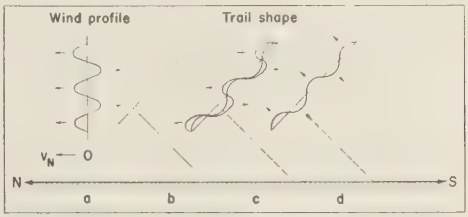

FIG. 2—(*a*) A sinusoidal wind profile, (*b*) the normal reflection geometry for a newly formed and undistorted trail, (*c*) the manner in which a horizontally stratified wind profile distorts a trail, (*d*) for small displacements the trail shape resembles that caused by motions normal to the trail.

we are concerned with the fading of echoes received at a radar so located that the wave path is normal to the trail at its center. Then we need to know only the displacement of the trail by the winds in the direction toward the radar; the fact that it is also transported a few hundred meters lengthwise along the trail is of only second-order importance, since such motion changes the length of the ray path but slightly. Hence, we shall generally assume that the wind distortion in the trail-radar plane is at right angles to the trail, in the direction to or from the radar (Fig. 2*d*). The magnitudes of the displacements are correspondingly reduced by the cosine of the zenith angle ζ of the meteor radiant. Precise justification of this simplification rests on comparison of the scale of the trail distortion, the wind velocity, and the echo duration.

Finally, we note that the model may be applied to oblique propagation with little change. If, for example, the meteor lies in a plane composed of perpendicular bisectors of the transmitter-receiver base line, the same components of velocity affect the phase path as if the transmitter and receiver were both at the path midpoint, although the phase-path variations are smaller.

The process of reflection for favorable aspect —Before a trail is distorted, the bulk of the received signal comes from the first Fresnel zone, which is centered at the perpendicular-reflection point. The length of the first zone depends on the radius of curvature of the trail (infinite) and that of the radiated wavefront (the radar range), and on the wavelength; it

is large, approximately a kilometer. The phase of the scattered signal differs by just 45° from the value it would have if it were all returned from the point on the trail nearest the radar. Thus reflection from the trail may be treated either as the sum of the contributions of the Fresnel zones, or else as a single contribution from the 'glint' at the specular-reflection point. The strength of the returned signal at a glint can be related simply to the curvatures; its phase can be related to its position. After the trail becomes warped, a first Fresnel zone may still be found wherever a glint or specular-reflection point exists. Provided that the size of the Fresnel zone does not approach too closely to the wavelength, it is still feasible to speak of reflection as coming from the specular point. This limit on the use of the glint idea is not violated for scales that are considerably smaller than those deduced from experiment. Thus we shall look upon the trail as a collection of glints of various intensities. Each of these glints is located at a specular-reflection point, and each returns a signal that is dependent upon the trail curvature in relation to that of the wavefront.

A feel for the development of the echo from a distorted trail can be most easily developed by considering first the unrealistic special case of a sinusoidal wind shear. Thus suppose that the component of wind velocity that is normal to the trail in the trail-radar plane is $v = V \sin(2\pi x/\Lambda)$ where V is the maximum wind velocity, x is the length measured on the trail from an origin at the original perpendicular-reflection point, and Λ is the wavelength of the shear profile on the trail. Then the radial displacement of the trail is

$$y(x) = Vt \sin(2\pi x/\Lambda) \qquad (1)$$

A first Fresnel zone and glint will appear at those points on the trail where the trail is tangent to a spherical wavefront centered at the radar. Figure 3 shows the development of the trail and the formation of glints. Notice that as the displacement of the trail becomes greater, new glints arise at points increasingly distant from the original specular-reflection point a. When a part of the trail, as at b, is first turned far enough to become parallel to the wavefront, a single new glint is produced. These new glints

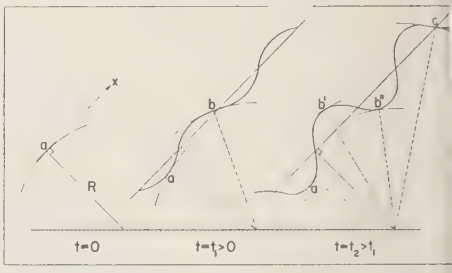

FIG. 3—The way in which additional reflectio points appear on a trail as distortion progresse

arise near the points where the wind gradien is maximum. As the trail continues to war the normal reflection geometry no longer hol at point b, but the required degree of trail r tation is found at two nearby points, b' and b The separation of these split glints usuall stays fairly small in comparison with the wav length. As time continues to advance, the exis ing glints, such as a, b', b'', shift their positio somewhat along the trail coordinate x, and ne glints c, d, etc., appear; at first they are singl but they quickly split into pairs c' and c'', and d''. The total length of trail over whi glints can be found increases, glint by glint, u til finally the whole trail is involved.

Mathematically, the condition for the pr duction of a glint is that the tangent of t angle of turning of the trail, $dy(x)/dx$, mu be equal to the tangent of the angle of deviati of the wavefront x/R, where R is the radius the wavefront. For the example of equation (1 a glint will occur if $x/R = (2\pi Vt/\Lambda)$ c $(2\pi x/\Lambda)$, which we may rewrite as

$$(x\Lambda)/(2\pi RVt) = \cos(2\pi x/\Lambda) \qquad (2)$$

If the two sides of equation (2) are plott versus x with t as parameter, the positions the glints are made evident as intersections the two curves. Figure 4a shows such a pl Directly below, in Figure 4b, are plotted t positions of the intersections, or glints, vers time. Note the way in which new glints pop as time advances and then split into two co ponents.

In general, a similar type of plot may used to study the formation of glints. If t velocity profile is $v(x)$, the displacement prof $y(x)$ equals x/R, so $x/(Rt)$ equals $v'(x)$. Figu

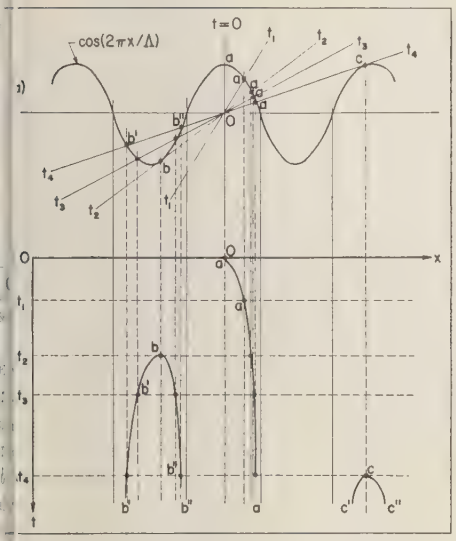

IG. 4—Determination of the locations of the ecting glints on a progressively distorted sinu- dal trail.

shows a more general plot of this sort, in ch the velocity-gradient function $v(x)$ is sumed to resemble band-limited gaussian se, or a typical trail distortion. It will be n that old glints can resolve and disappear much the same way that new glints form. instance, glints a and b are independent at e t_1. But branch b'' coalesces with a and ishes, while branch b' survives to join d'' r. From the point of view of continuity, we y distinguish three families of glints—the , and f groups. They are characterized by g isolated by the zeroes of the gradient ction $v'(x)$. In one sense there are but these e split groups. From another viewpoint, vever, each of the glint pairs a, b, d, and ust be considered in order to estimate the aber of glints, even though the glints are permanent. Note also that, in general, new ts are not necessarily produced at increasing ances from the original specular point. For ance, f is produced after c but is nearer the in.

lthough plots such as Figure 5 demonstrate type of behavior a distorted trail can pro- e, the lack of specific knowledge of the dient function makes exact prediction of echo properities in particular cases impossible. The general theory therefore treats the statistical properties of meteor echoes taken in quantity. By so doing, it is possible to consider that each trail is distorted by a wind profile that is a random sample from an ensemble of profiles which have the properties of gaussian noise and an arbitrary spectrum function. For each trail of the sample there will be a particular and undetermined distribution of glints along its length, developing in general as a function of time. To the receiver, each trail appears as a collection of reradiation points of varying strengths, capable of producing a signal with certain characteristics. The properties of the average signal, however, depend upon the properties of an ensemble-average trail, whose distribution of glints is the average of all the particular distributions of individual trails. For a sufficiently large ensemble, we may approximate the ensemble-average distribution of glints by a continuous distribution. We can say that, on the average, there is a certain probability of finding a glint within a certain length of trail versus time and position. The general theory shows that this probability distribution of en-

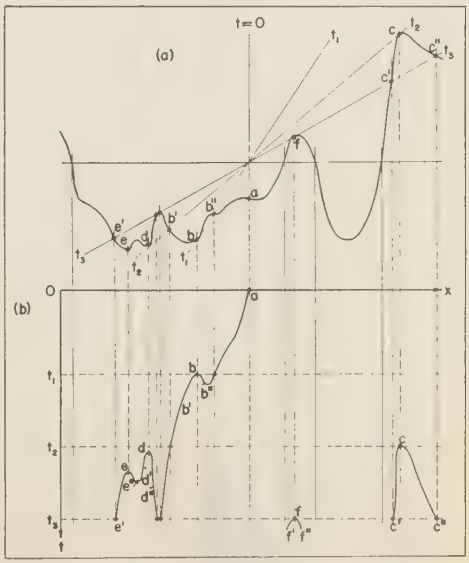

FIG. 5—Location of the position of the glints as a function of time for a trail distorted by an arbitrary wind profile.

ergy-scattering elements, or the 'trail aperture,' as it may be called, is a gaussian function of trail length centered about the initial perpendicular-reflection point. The probability of finding energy scattered far from the initial specular point is reduced in accordance with this gaussian error function, but the width of the distribution in the direction of the trail length increases linearly with time until it is limited by the trail length.

The spectrum of the wind profile does not enter the above argument, provided only that the smallest scale capable of turning the trail is large compared with the wavelength and the trail diameter. Examination of the implications, should that not be true, leads to unacceptable predictions with respect to the experimental results.

The production of fading and the fading rate —An echo fades because the received signal spectrum consists of two or more Doppler-shifted frequency components. If there is but one specular-reflection point on the trail, as prior to time t_1 (Fig. 5), the echo will not fade; however, the received echo does have a Doppler frequency shift, the 'body Doppler,' which is determined by the velocity of the trail at glint *a*. When a second glint is formed, a second received-echo component appears, with a different Doppler shift determined by the generally different trail velocity at the new glint *b*. The initial fading frequency is then determined by the difference in trail velocity at the two glints. As has been shown by *Greenhow* [1952a], fading does not start, on the average, until 0.4 sec after the production of an ionized trail. Hence, on the average, 0.4 sec is needed to produce the second glint. In the general theory, the mean delay is computed from the statistical properties of a general wind profile. To illustrate the rough order of magnitudes involved, we will consider again the unrealistic sinusoidal profile. Referring to Figure 4, note that had the phase of the sinusoid been random, the mean distance of the second glint *b* from the perpendicular-reflection point 0 would have been $3\Lambda/4$. Quite approximately, the value of cos $(2\pi x/\Lambda)$ at *b* is 1. Thus from (2) we have

$$(3\Lambda^2/4)/(2\pi R\, V t) \cong 1 \qquad (3)$$

and if we insert $R = 150$ km, $V = 30$ m/s, and $t = 0.4$, we find $\Lambda = 2.9$ km. Or for $V = 50$ m/s, $\Lambda = 3.8$ km. The scales are in the range known to exist from photographs of enduring meteor trains. The general analysis must be used for comparison of results, however, since the actual mean delay depends upon both the distribution in amplitude of the relative maxima of gradient and upon the associated scales. That is, the delay depends on the Fourier spectrum of the wind profile. If we use the sinusoidal model, a rough limit may be placed on the maximum velocity of smaller-scale Fourier components, since they cannot have more velocity in relation to their wavelength than is permitted by (3) without producing fading within 0.4 sec. Thus it would appear that the spectral velocities must die down as $V \propto 1/\Lambda$ in the small-scale region. Actually, consideration of the simultaneous turning effect of larger-scale components strengthens this result somewhat. A Kolmogoroff-Heisenberg spectrum is ruled out, however.

Once the second glint is formed, the echo starts to fade, and since at first only two components exist the fading tends to be deep and regular. As additional glints appear, the number of spectral components rises, and the fading eventually becomes Rayleigh. Because of the limited range of drift velocity of points on the trail, the received spectrum is band-limited, and the fading exhibits a quasi-period which is characteristic of the bandwidth of the spectrum. It is a property of a gaussian noise function such as the assumed wind profile, that the gradient of the function is not correlated with the function itself. Thus the location of glints depends on the wind gradient, but the values of wind at the glints are random samples with a gaussian distribution of magnitudes, provided only that the glints are not so close together that the auto-correlation of the profile produces dependence. When an echo first starts to fade, then, the mean fading frequency should depend on the expected difference in velocity from two samples from a gaussian distribution; this difference is 1.128 times the standard deviation of the sample, or the rms deviation of the wind component from the mean value. When a third glint is produced, the expected fading frequency will depend on the expected range in velocity of three samples from a gaussian distribution

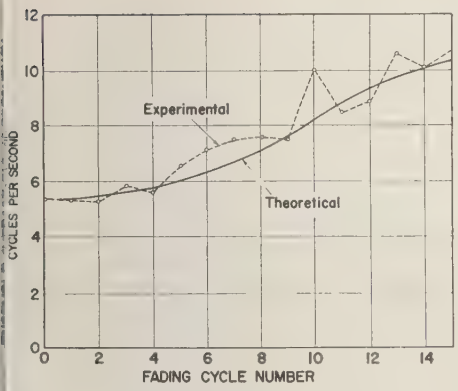

Fig. 6—Comparison of theoretical and experimental measures of ensemble-average fading frequency versus fading cycle-number, scaled from the start of the echoes.

is range is 1.693 standard deviations. As new nts are added, we should thus expect a adual increase in fading rate with time, until e length of the trail prohibits further lengthing of the effective aperture. Figure 6 shows analysis of fading frequency variation versus ne measured in fading cycle-number, which s carried out to test the hypothesis. Fading cle-number is used rather than time as abssa, since it normalizes changes in the rate of nt formation that are caused by geometrical ctors. The data were obtained over an oblique th using radiation from a 61-Mc/s television ation 1000 km to the east of Stanford Unirsity. (The author is indebted to V. R. hleman and O. G. Villard, Jr. for the experintal records.) The smooth curve is fitted to e data using the general theory and the above nsiderations relating fading speed to the mber of glints. The only constant that reires adjustment is the scale factor in time. s value depends on the rate at which glints e added. Upon close inspection, however, it ll be seen that the increase in expected velocspread in sampling a gaussian distribution pends not on the actual number of glints, t on the number of independent glints. Thus, two glints exist quite close together, because the auto-correlation of the wind profile the locities at the two glints will not be very ferent. By fitting the theoretical curve to the served fading-rate increase of Figure 6, the number of independent glints versus fading cycle-number is determined. From other experiments, such as the diversity measurements to be described, the total number of glints and their spacing can be found. Comparison of the results yields the height differential in the atmosphere within which the wind profile becomes uncorrelated. The value obtained from Figure 6 is 6.4 km, or very nearly the atmospheric scale height.

If the fading frequency truly does rise with time because of the creation of new glints over more and more of the trail, the fading frequency should drop when the echo duration is approached. The intensity of ionization along the length of the trail dies out towards both ends. Hence the duration of echoes from elements near the ends is not as great as that near the maximum of ionization. Near the end of the echo duration, glints formed near the end of a trail will cease to shine first. The effective length of the trail and the number of glints will rapidly drop to zero; according to the argument of the preceding paragraph, the fading frequency near the end of the echo should also drop to zero. Figure 7 shows a test of this prediction. The echoes that were scaled were selected so that the portions used were within four cycles of the start of the echo; therefore a fair length of trail would be covered with glints before decay. Special care was also used to estimate the location of the final fading cycle by extrapolating the generally linear decay of

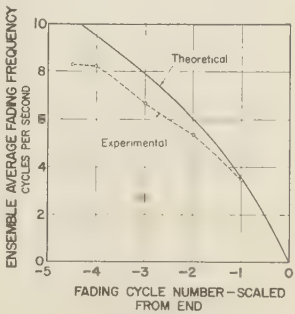

Fig. 7—Comparison of theoretical and experimental measures of ensemble-average fading frequency, scaled from the end of the echoes. The theoretical curve is high for early cycle numbers because of neglect of the effects of aperture formation.

echo amplitude to zero. It will be seen that a rapid, and indeed precipitous, drop in fading frequency occurs. The rate of drop corresponds closely to the predicted decrease in trail length based on the measurements of *Manning and others* [1953] and on the theory of *Eshleman* [1957].

Considering again a sinusoidal wind profile, recall that each new glint separates into two components immediately after formation (Fig. 4). The components of a split glint are separated by a distance along the trail that is generally small compared with the wavelength of the profile. As a result, rather small velocity differences exist between the motions of the halves of the glint, and a low-frequency beat is set up. The signal that is scattered from a split glint may therefore be treated as if it were a slowly fading signal from a single source. As time advances, the spacing of the halves of a split glint increases and, because of the drop in the autocorrelation function of the velocity profile with spacing, the rate of fading will go up. However, calculation shows that the fading from this cause is of the order of 30 times slower than the ordinary rapid fading. Since the echo from a long-duration echo will include returns from many split glints, each fading at a very slow but increasing rate, we may predict that the rapid fading will be modulated by a slowly fading envelope. This mechanism is suggested as the cause of the slow fade first described by *Greenhow* [1950]. The numerical values are of the right magnitude.

The diversity effect—In discussing the average properties of meteoric echoes, we pointed out that it is convenient to think of an ensemble-average distribution of glints along the length of trail. The effective reradiating aperture of the ensemble-average trail is gaussian for a wind profile that has a gaussian amplitude distribution, and the width of the aperture increases linearly with time until limited by trail length. At a single observing site a fading signal is received with a quasi-periodic fading frequency fixed by the range in velocity of glints within the scattering aperture of the trail. If a second receiver is located a few wavelengths from the first, a similar fading signal will be observed. However, because of the width of the trail aperture, the path lengths to the glints within the aperture are different for t two receivers. There should therefore be lo of correlation in the phase relation between t fading patterns in the two receivers. The grou spacing that is required to reduce the correl tion by a specified amount is a measure of t trail aperture.

To investigate this diversity effect in r flection, the correlation between fading patter for two spaced receivers was measured using 61-Mc/s television transmitter located 1000 k east of Stanford University. Receiver separ tions of 152.4, 228, and 304.8 meters were us across the path, and 304.8 meters along t path. In measuring the correlation betwe fading patterns, time was scaled in fading cyc number, starting with a value extrapolated the beginning of the echo. Cycle-number w used instead of time to normalize geometric factors that affect the growth of the apertu and the fading frequency in the same way. T cross-correlation was then scaled, cycle by cyc by taking a numbered cycle from one reco and comparing it with the amplitude variati in the record from the other receiver duri the same interval. The theoretical cross-correl tion function that results from a linear expanding aperture depends on the produ of fading cycle-number and receiver-spacin Hence scaled correlations corresponding to equ cycle-number times spacing products were a eraged over the ensemble, which was made of hundreds of meteors. The resultant plot shown in Figure 8. The smooth curve that fitted to the data is a gausian function, a

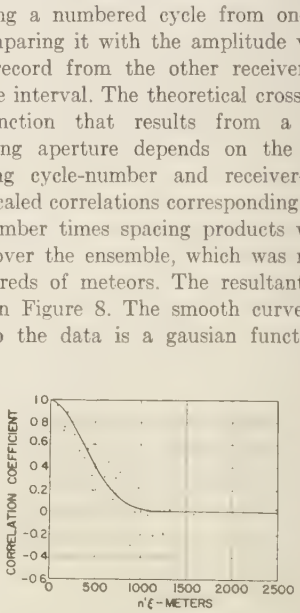

FIG. 8—Experimental determination of the e semble-average correlation coefficient between fa ing waveforms in two separated receivers vers the product of separation and fading cycle-nu ber. The solid curve is the gaussian correlati function best fitting the data. Each plotted poi represents an ensemble average.

s in agreement with the calculated gaussian rture distribution. That is, since the auto-relation function of the angular spectrum of radiation from an aperture equals the rier spectrum of the aperture distribution, gaussian aperture produces a gaussian ular auto-correlation function. The cross-relation of ground-fading patterns averaged r the ensemble gives a measure of the angu- auto-correlation; therefore it is also gaus- n. It may be noted that the points in Figure ith the largest deviations from the gaussian ve deserve relatively little weight, since they respond to smaller samples.

The standard deviation of the correlation ction depends on the rate of aperture growth, ich is in turn dependent on the ratio of mean ocity gradient to mean velocity. Since the an velocity is known from the mean fading quency, the rms value of the relative maxima wind gradient can be found from the diver- measurements. From the data of Figure 8, N-S component of this mean maximum dient was found to be very nearly 100 /s)/km, whereas the rms N-S velocity was y nearly 50 m/s. The ratio of velocity to dient gives some information on the nature the turbulent spectrum. For instance, for unrealistic assumption of a single spectral nponent, the velocity is $v = v_0 \sin (2\pi x/\Lambda)$ l the gradient is $v' = (2\pi/\Lambda)\, v_0 \cos (2\pi x/\Lambda)$. e ratio of mean velocity to mean gradient is $v') = \Lambda/2\pi$, leading to a value of Λ of out 3 km. If the general theory is applied, a stant is determined which gives a measure the short-wavelength 'bandwidth' of the ctrum. The small-scale cutoff for most as- ned spectral functions occurs at about 1 or 2 . A dropoff as slow as that of the Kolmogor- -Heisenberg spectrum is inconsistent with the erimental results.

Although the ensemble-average cross-correla- n function of Figure 8 is gaussian, the cor- ation observed in individual echoes is often illatory, although erratic. Such behavior can understood, since a trail with but two glints uld produce a sinusoidal correlation (the erferometer pattern).

Following the presentation of these results *Manning* [1957], *Landmark* [1958] con- cted a similar study, and he also found a gaussian correlation function. He observed as well, however, changes in the standard deviation of the correlation function with season. These results indicate the importance of making series of fading analyses as a way of studying the origins of the wind shears.

FIG. 9—The geometry of trail distortion in oblique coordinates.

Aspect sensitivity—In the analysis of fading and diversity effects it was convenient to neglect the component of trail drift in the direction along the trail axis. This longtitudinal component of drift cannot be neglected, however, in seeking to explain the aspect-sensitivity results in terms of horizontal wind shears. Refer to Figure 2 and consider the extreme case of a trail viewed end on. Notice that in (*d*), where the displacements are normal to the initial trail axis, it is never possible to achieve a perpendicular from the radar to the trail. In (*c*), however, where the displacements are at an angle to the trail axis, a perpendicular can be obtained from the radar within a finite period of time.

A rough explanation of the aspect effect can be given if one assumes sinusoidal trail distortion, although, as always, the general theory is needed for numerical study. Suppose, then, that the wind creates a trail that is distorted (Fig. 9). The trail displacement is y, the trail-length coordinate is x, and $y' = dy/dx$ is the wind gradient along the trail; y' will be less than the vertical gradient unless the trail axis is normal to the wind direction. If $m = dz/dx$ is the slope of the wavefront with respect to the rectangular trail coordinates x and z, the condition for production of an echo is $m = y' \sin \alpha/(y' \cos \alpha + 1)$ where α is the angle between the trail axis and the wind planes. The solution for the necessary wind gradient to produce reflection is $y' = m/(\sin \alpha - m \cos \alpha)$. The value of α that leads to the production of an echo with the smallest necessary gradient is tan $\alpha = -1/m$. For this α, the value of the mini-

mum y' is $y'_{\min} = m/\sqrt{1+m^2}$. If we call $\Delta\alpha$ the angle by which α differs from arctan $(-1/m)$, $y' = [m/(1+m^2)^{1/2}]/\cos\Delta\alpha$. Finally if θ is the angle by which the ray from the radar fails to meet the initial trail axis in a right angle, $\tan\theta = m$, and

$$y' = \frac{\sin\theta}{\cos\Delta\alpha} \tag{4}$$

Note that $\Delta\alpha$ is now the angle between the meteor-radar line and the direction of the wind component in the trail-radar plane.

Since the trail gradient $y' = v't$, where t is the trail age and v' is the gradient of the wind profile in the trail direction, we may find the delay to the start of the echo versus the orientation of the trail by using

$$t = \frac{1}{v'}\frac{\sin\theta}{\cos\Delta\alpha} \tag{5}$$

Using as orders of magnitude $v'_{\max} = 100$ m/s, as found from the diversity or delay-to-start of fading experiments, and assuming that $\cos\Delta\alpha$ for the glint on the trail created by the most favorably directed shear component is near 1.0, say 0.9, we find that

$$t = 11.1\sin\theta\sec \tag{6}$$

The experimental results of McKinley and Millman (Fig. 1, the horizontal lines) will be seen to be basically similar to the sinusoidal function of (6). The maximum delay of 11.1 sec predicted from the approximate analysis above is of the right magnitude. More exact statistical analysis yields the smooth curve shown in the figure, rather than the sine function of (6).

Conclusions—If it is assumed that the winds flowing at meteoric heights are horizontally stratified and that randomly selected velocity components from the velocity profile are distributed in gaussian form, it is possible to explain in detail the fading, diversity, and aspect-sensitive characteristics of meteoric echoes. In the present first paper, the mathematical development has been described only in qualitative terms or has been given only for restrictive special cases. From the general theory, however, it has been possible to find specific values for a number of the parameters of the wind profile. The Fourier spectrum of the wind profile must generally fall off in amplitu when the scale of irregularities is less than or 2 km. The rms N-S component of wi velocity was found to be about 50 m/s, a the rms N-S maximum wind gradient w found to be 100 m/s. A change in altitude about 6.4 km (a scale height) was found to required to eliminate correlation between t velocity of wind components in different ho zontal strata. The experimental results are excellent agreement with those obtained photographing enduring meteor trains in N Mexico. With those results, the theory c rectly predicts the delay in the start of fadi and the slow fade noted by Greenhow at Jodr Bank and the aspect sensitivity of detecti found by McKinley and Millman at Ottaw it also explains the detailed variation in fadi speed during the echo lifetime and the divers effect or angular-spectrum observation made Stanford and presented here.

A consequence of the experimental results, interpreted by the theory, is that the observ motions cannot be part of a Kolmogoroff sp trum; any turbulence generated by the served motions must be of quite low veloci

References

Eshleman, V. R., The theoretical length dist bution of ionized meteor trails, *J. Atmosphe and Terrest. Phys., 10,* 57–72, 1957.

Greenhow, J. S., The fluctuation and fading radio echoes from meteor trails, *Phil. Mag.,* 862–693, 1950.

Greenhow, J. S., Characteristics of radio ech from meteor trails: III The behaviour of electron trails after formation, *Proc. Phys. S London, B, 65,* 169–181, 1952a.

Greenhow, J. S., A radio echo method for the vestigation of atmospheric winds at altitudes 80 to 100 km, *Atmospheric and Terrest. Ph 2,* 282–291, 1952b.

Greenhow, J. S., Systematic wind measureme at altitudes of 80–100 km using radio echoes fr meteor trails, *Phil. Mag., 45,* 471–490, 1954.

Landmark, B., The fading of long duration met bursts in forward scatter propagation, *J. Atm pheric and Terrest. Phys., 12,* 341–342, 1958.

Manning, L. A., The fading of meteoric ra echoes, Talk presented at the 12th General sembly of URSI, Boulder, Colo., Aug. 195

Manning, L. A., A. M. Peterson, and O. Villard, Jr., Ionospheric wind analysis by me oric echo techniques, *J. Geophys. Research,* 47–62, 1954.

Manning, L. A., O. G. Villard, Jr., and A.

TERSON, Meteoric echo study of upper atsphere winds, *Proc. IRE, 38,* 877–883, 1950.
NING, L. A., O. G. VILLARD, JR., AND A. M. TERSON, Double-Doppler study of meteoric oes, *J. Geophys. Research, 57,* 387–403, 1952.
NING, L. A., O. G. VILLARD, JR., AND A. M. TERSON, The length of ionized meteor trails, *ns. Am. Geophys. Union, 34,* 16–21, 1953.
McKINLEY, D. W. R., AND P. M. MILLMAN, A phenomenological theory of radar echoes from meteor trails, *Proc. IRE, 37,* 364–375, 1949.
WHIPPLE, F. L., Winds in the upper atmosphere by meteor train photography, *J. Meteorol., 10,* 390–392, 1953.

(Manuscript received April 13, 1959.)

A Comparison of the Cosmic-Ray Intensity at High Altitudes with the Nucleonic Component at Ground Elevation*

J. E. HENKEL,† J. A. LOCKWOOD, AND J. H. TRAINOR

Department of Physics
University of New Hampshire, Durham, New Hampshire

Abstract—A series of balloon-borne soundings in the atmosphere with single Geiger tubes has been made during the period January to September 1958. The counting rate determined at the Pfotzer maximum is compared with that recorded by the nucleonic detector at Mt. Washington (1909 m; $\lambda = 55°$N). Large changes in the counting rate of each detector were observed, and the ratio of these changes is ~2-1. Several large deviations from this normal ratio were also observed; they occur for flights on which the shape of the intensity-altitude curve near the Pfotzer maximum is quite different from the normal. The changes are explained either in terms of depressions of the low-energy portion of the cosmic-ray spectrum following marked decreases in the nucleonic component or by the presence of excess low-energy radiation. An anomalous increase of ~100 per cent observed at high altitudes during one flight is attributed to high-energy X-radiation. It is found that the hemispherical average unidirectional intensity above the atmosphere derived from the counting rate at the Pfotzer maximum has decreased ~200 per cent from 1954 to 1958 at $\lambda = 53°$N, and this change is compared with results at other latitudes.

INTRODUCTION

is well established that the major portion he intensity-time variations of the cosmic ation is produced by a solar-controlled ulating mechanism. The magnitude of these ations is inversely related to the energy of cosmic-ray particles. Therefore, it is adageous to measure the low-energy part of primary cosmic-ray beam as well as the s that can be measured with nucleonic ctors and shielded ionization chambers. To e these measurements, high-altitude soundare necessary because the atmosphere abs the low-energy cosmic radiation. *Fonger* 3] has calculated the effective primary tra for neutron detectors and shielded ionon chambers located at geomagnetic latitude 48° and at altitudes corresponding to pres s of 680 and 1031 g cm^{-2}, respectively, asing the primary energy spectrum given by *lon et al.* [1952]. Fonger's calculations show that the effective primary proton spectrum for a neutron detector increases as a power series with decreasing proton energy down to about 2 bev. This is in contrast to the shape of the effective spectrum for a shielded ionization chamber which has a broad maximum about 10 to 20 bev. From these curves it is seen that the neutron detector has a greater response to the lower-energy part of the primary radiation. W. R. Webber (private communication, April, 1959) has recomputed the yield functions and effective primary spectra for nucleonic and meson detectors. He finds that the effective spectrum for meson detectors at sea level is unchanged but that the spectrum for a nucleonic detector exhibits a broad maximum at a rigidity of about 5 bev/c. For the results discussed here, Fonger's calculations are sufficient.

The cutoff imposed by atmospheric absorption for a neutron detector is about 1 to 2 bev. To measure the changes in the primary radiation of energies less than ~2 bev, a detector, such as a single Geiger tube, an unshielded ionization chamber, or Geiger tube telescope, must be used at high altitudes. The counting rate of such a detector is then from primary particles with energies above the cutoff imposed by the earth's magnetic field and second-

Supported by the Geophysics Research Dirate of the Air Force Cambridge Research ter, Air Research and Development Comd.

† Now at Yale University, New Haven, Conicut.

ary low-energy ionizing particles produced in the atmosphere by the primary radiation.

This study was undertaken to compare the intensity changes measured at the top of the atmosphere with those recorded deep in the atmosphere by a nucleonic detector. The difference between the intensity changes recorded by the neutron detector and the single Geiger tube at the top of the atmosphere is due to the changes in the low-energy radiation present, which does not reach the detector at ground elevation.

Experimental Procedure

It was desired to obtain a large set of measurements over a period of many months for the variation of the total cosmic-ray flux at the top of the atmosphere. Reliability, simplicity, and economy were required. Consequently, the conventional meteorological radiosonde system was used, modified only slightly to include the cosmic-ray detector.

Single 1B85 Victoreen Geiger counters were used as detectors. In order to compare flights, each tube was carefully calibrated with a Cs^{137} source, mounted in a cave of lead bricks with a vertical exit slit about 1 mm wide. With this apparatus, the effective length and the voltage plateau were determined for each tube. For all the tubes used the effective length was the same to within the resolution of the calibrating device (± 1 mm), and the plateaus were at least 120 volts long, centered at 900 volts, the operating voltage on all flights. Two Victoreen 1B85 tubes with good characteristics were chosen as standards and utilized as calibration checks throughout the experiment.

A circuit similar to that used by *Pomerantz* [1951] was designed. The circuit has a scale of 1, with a voltage pulse height discriminator. The modification of the radiosonde system was straightforward, the output of the Geiger counter circuit being capacitively coupled to the grid of the radiosonde transmitter tube. The radiosonde signals were picked up on the ground by a conventional radiosonde receiver, amplified, scaled, and finally recorded by a Brush paper-tape oscillograph. All counting rate and pressure data were taken from these tapes. Additional radiosonde equipment recorded the pressure contacts, temperature, and the counting rate as a frequency. Accurate tracking da were recorded for all flights, and it was deter ined that all balloon flights terminated geomagnetic latitude 53° ± 30′N, geomagne longitude 355° ±30′E.

Styrofoam boxes were used for thermal sulation, and in addition the entire equipme was enclosed in thin plastic. The balloons, ty ML-518, were launched from the facilities of t Test Engineering Section, Geophysics Resear Directorate, Air Force Cambridge Resear Center, Bedford, Massachusetts. Preliminary each flight, the baroswitch was calibrated in t laboratory to ±1 mm Hg. Out of the total twenty-one flights, only four were unsuccessf

Results

The results are summarized in Tables 1 a 2 and in Figures 1, 2, 3, 4, and 5. Figure 3 is summary plot containing data on solar flar geomagnetic storms, solar radio-frequency em sions, and the occurrence of auroras. Figure shows an anomalous increase occurring duri one flight; it is discussed in the next sectio The errors given in all figures and tables a the statistical errors plus any known expe mental errors. In Tables 1 and 2, N_0 refers the raw counting rate at the Pfotzer maximu and N_t is the counting rate N_0 corrected for t loss of counts due to the dead times of the 1B tube and the one-shot multivibrator (~1 mi sec), following the method suggested by *Ko* [1955]. N_c gives the normalized counting ra determined from the expression

$$N_c = KN_t \qquad (1$$

where K is the normalizing factor.

Hemispherical average unidirectional inte sity—Meredith et al. [1955] have discussed t relation between the observed counting ra N, of a Geiger counter and the hemispheri average unidirectional intensity, $\bar{J}$, given the expression

$$N = \epsilon G \bar{J} \qquad (2$$

where ϵ is the efficiency of the counter and G the geometry factor, related to the solid an subtended by the counter for a unidirectio beam. If $\bar{J}$ is independent of direction over t hemisphere, the geometry factor $G_{isotropic}$

TABLE 1—*Summary of the single geiger tube flights*

N_0 = raw counting rate at the Pfotzer maximum; $N_t = N_0$ corrected for loss of counts due to tube and quit dead times; MW_2 and MW_{12} refer to the average of the hourly counting rates for the neutron monitor at Mt. Washington for 2 hours and 12 hours respectively, centered about the time at which N_0 was recorded.

Flight No.	Date	Time of Pfotzer maximum, UT ± 0.04 hr	N_0, sec^{-1}	N_t, sec^{-1}	MW_2, scale of 64 ±0.2%	MW_{12}, scale of 64 ±0.1%
3	1/6/58	1942	23.9	24.6 ± 0.2	1943	1943
4	2/12	2022	23.4	24.0 ± 0.2	1818	1842
5	3/3	2101	26.9	27.7 ± 0.8	1962	1942
6	3/18	1932	25.2	26.0 ± 0.3	1965	1945
7	4/9	2011	25.3	26.1 ± 0.2	1947	1965
8	4/21	2107	23.8	24.5 ± 0.2	1969	1979
9	4/29	1546	23.7	24.4 ± 0.2	1954	1975
0	5/9	1934	23.6	24.3 ± 0.2	1942	1947
3	7/7	1830	23.8	24.5 ± 0.3	1944	1973
4	7/28	1920	24.5	25.2 ± 0.5	1948	1956
5	8/4	1830	26.1	26.9 ± 0.2	2026	2023
6	8/7	1850	25.0	25.7 ± 0.2	2055	2054
7	8/12	1825	26.6	27.4 ± 0.2	2077	2072
8	8/13	1836	27.3	28.2 ± 0.2	2115	2126
9	8/14	1830	26.2	27.0 ± 0.2	2084	2075
0	8/15	1830	26.9	27.7 ± 0.2	2082	2089
1	9/11	1836	25.4	26.1 ± 0.2	2014	1980
Mean			25.2	25.9 ± 0.3	1991	1993

TABLE 2—*Summary of the results of the single Geiger tube flights*

K is the calibration factor; $N_c = KN_t$; and $\bar{J}$ refers to the hemispherical average unidirectional intensity.

Flight No.	N_t, sec^{-1}	K	N_c, sec^{-1}	$\bar{J}$, cm^{-2} sec^{-1} $ster^{-1}$	
				At Pfotzer maximum	Extrapolated to above atmosphere
3	24.6 ± 0.2	0.973 ± 0.005	23.9 ± 0.3	0.338 ± 0.005	0.270 ± 0.004
4	24.0 ± 0.2	0.943 ± 0.005	22.6 ± 0.3	0.320 ± 0.005	0.256 ± 0.004
5	27.7 ± 0.8	0.982 ± 0.005	27.2 ± 0.9	0.385 ± 0.013	0.308 ± 0.011
6	26.0 ± 0.3	0.982 ± 0.005	25.5 ± 0.4	0.361 ± 0.006	0.289 ± 0.005
7	26.1 ± 0.2	1.000 ± 0.005	26.1 ± 0.3	0.369 ± 0.005	0.295 ± 0.004
8	24.5 ± 0.2	1.000 ± 0.005	24.5 ± 0.3	0.346 ± 0.005	0.277 ± 0.004
9	24.4 ± 0.2	1.000 ± 0.005	24.4 ± 0.3	0.345 ± 0.005	0.276 ± 0.004
0	24.3 ± 0.2	1.000 ± 0.005	24.3 ± 0.3	0.344 ± 0.005	0.275 ± 0.004
3	24.5 ± 0.3	0.990 ± 0.005	24.2 ± 0.4	0.342 ± 0.006	0.274 ± 0.005
4	25.2 ± 0.5	1.010 ± 0.005	25.4 ± 0.7	0.359 ± 0.010	0.287 ± 0.008
5	26.9 ± 0.2	1.020 ± 0.005	27.4 ± 0.4	0.388 ± 0.006	0.310 ± 0.005
6	25.7 ± 0.2	0.985 ± 0.005	25.3 ± 0.3	0.358 ± 0.005	0.286 ± 0.004
7	27.4 ± 0.2	1.042 ± 0.005	28.6 ± 0.4	0.404 ± 0.006	0.323 ± 0.005
8	28.2 ± 0.2	1.055 ± 0.005	29.8 ± 0.4	0.421 ± 0.006	0.337 ± 0.005
9	27.0 ± 0.2	1.071 ± 0.005	28.9 ± 0.4	0.409 ± 0.006	0.327 ± 0.005
20	27.7 ± 0.2	1.020 ± 0.005	28.2 ± 0.4	0.400 ± 0.006	0.320 ± 0.005
21	26.1 ± 0.2	1.046 ± 0.005	27.3 ± 0.4	0.386 ± 0.006	0.309 ± 0.005
Mean			26.1 ± 0.4	0.369 ± 0.006	0.295 ± 0.005

FIG. 1—The corrected counting rate of the Victoreen 1B85 Geiger counter at the Pfotzer maximum for the seventeen flights as compared with the nucleonic intensity at Mt. Washington for the 2-hr intervals centered at the time of the balloon observation.

given by the formula

$$G_{iso} = [\pi^2 aL/2][1 + (a/2L)] \qquad (3)$$

where a is the tube diameter and L is the tube length. G_{iso} can then be calculated, since a and L are known, and therefore $\bar{J}$ can be determined.

If it is assumed that the radiation is isotropic at the Pfotzer maximum, then G_{iso} is 70.7 ± 0.14 cm² steradian for these flights, where the parameters have the values

$$a = 1.91 \pm 0.02 \text{ cm}$$

$$L = 6.7 \pm 0.12 \text{ cm}$$

$$\epsilon = 1$$

By means of equation 2, the $\bar{J}$ at the Pfotzer maximum was determined for each flight.

In order to find the intensity above the atmosphere, the intensity-altitude curve must be extrapolated. A reasonable extrapolation can be obtained with the data given by *Van Allen* [1952] for the intensity in 1937 as a function of altitude at 51°N and 60°N geomagnetic latitudes. The ratios from these curves of intensity at the plateau to the intensity at the Pfotzer maximum are 1.29 at 51°N and 1.13 at 60°N. The interpolated ratio at 53°N is 1.25, and, thus, multiplying $\bar{J}$ at the Pfotzer maximum by 1/1.25 will give the hemispherical average unidirectional intensity above the atmosphere. The average value of this quantity for seventeen flights is 0.295 cm^{-2} sec^{-1} ster^{-1}. It should be noted that the errors assigned to the hemispherical average unidirectional intensities do not include an error due to a possible anisotropic distribution of

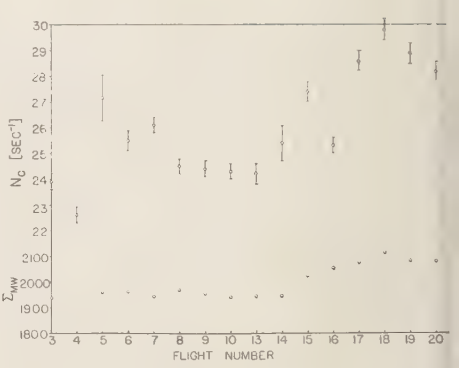

FIG. 2—The corrected counting rate at th Pfotzer maximum and the nucleonic intensity fo the corresponding 2-hr intervals in chronologica order.

radiation at the Pfotzer maximum. Further, i is assumed that the same ratio between th cosmic radiation intensity above the atmosphe and that at the Pfotzer maximum holds fo 1958 as for 1937. These points will be discusse in more detail in the next section.

DISCUSSION OF RESULTS

A. Latitude effect—Before making a detaile comparison of the high-altitude data with th surface neutron data, a possible geomagneti effect must be discussed. For this comparison the two measurements should be taken at th same time and at the same geomagnetic latitud and longitude. If the measurements are mad at different times or different magnetic lati tudes, corrections are necessary for possibl time variations or latitude effects, respectively Here the Geiger tube and neutron data wer compared at the same time.

However, the geomagnetic latitudes of th two measurements differed by about 2°, and therefore, an intensity difference arising from latitude effect could be present. This effec would be rather pronounced if the latitud curve in 1958 were the same as that obtaine by *Meredith et al.* [1955] in 1952 with Geige tubes flown in rockets at high altitudes. Th rate of change of intensity with latitude fo this curve is greatest in the region 53° to 55°N the latitudes of the balloon soundings and th neutron monitor, respectively. The 'knee' of thi

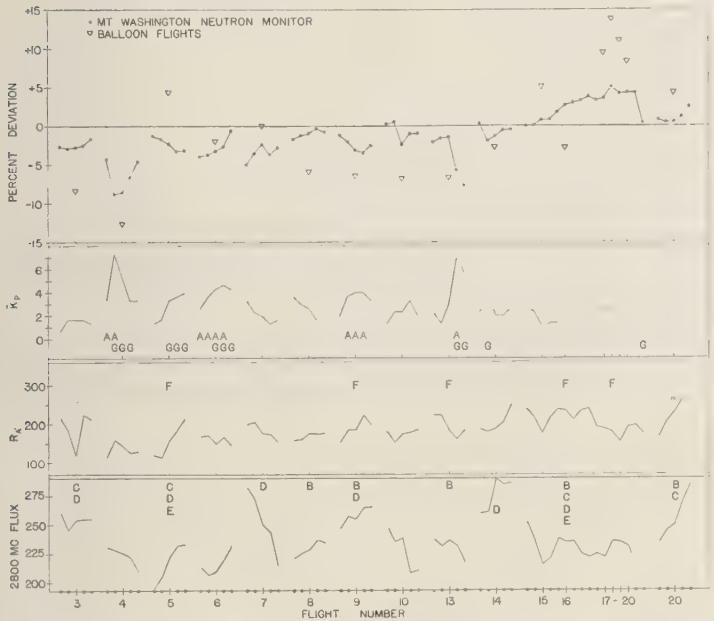

FIG. 3—The corrected counting rates at the Pfotzer maximum and the daily averages of the nucleonic intensity are given as a percentage deviation from their mean values. Also plotted are $\bar{K}_p$, the daily average geomagnetic activity index; R_A', the American relative sunspot numbers; and the daily average of the 2800-Mc solar flux. Capital letters refer to the following phenomena: *A*, aurora of strong intensity; *G*, principal geomagnetic storms; *F*, flares of magnitude >2 or large numbers of flares in the previous 30 hours; *B*, *C*, *D*, and *E*, strong outbursts of solar radio noise at 2800, 200, 67, and 470 Mc, respectively, near the time of the observation at the Pfotzer maximum.

urve, north of which there is no intensity hange with latitude, is at about 60°N.

In order to estimate the latitude curve for 958, a set of latitude curves for the nucleonic omponent prevailing at different times was tudied. *Meyer and Simpson* [1955, 1957] have ompared the latitude effect for the nucleonic omponent as measured in 1948, 1951, and 956. The essential feature of the data obtained y Meyer is the shift of the knee southward n periods of high solar activity and the shift orthward in periods of low solar activity. In 948, the last previous year of high solar activity, the knee of the latitude curve for the ucleonic component was at approximately 0°N. In 1956, it was at about 52°N, a atitude for which the magnetic cutoff (~1.3 ev) is greater than the atmospheric cutoff at he altitudes maintained in these flights (~300 g cm^{-2}). It can be inferred from the above tudy that in 1958, a period of higher solar activity than 1948 or 1956, the knee of the latitude curve is south of the location of the surface nucleonic detector and the high-altitude Geiger tube flights. Therefore, it is assumed that no correction for a latitude effect is necessary for these data. Measurements of the latitude curve of the nucleonic component in 1958 by Meyer and Simpson (private communication) tentatively place the knee south of $\lambda = 52°$N.

B. Unidirectional intensity—Gangnes et al. [1949] maintain that the isotropic intensity approximation is not valid in the lower atmosphere, and thus G_{iso} cannot be used. Hence, *Meredith et al.* [1955] have calculated $\bar{J}$ for the regions above the atmosphere where $\bar{J}$ is essentially independent of direction. For our experiment, the isotropic assumption in the transition region of the upper atmosphere must be justified. *Swann* [1939] and *Winckler and Stroud* [1949] have measured the direction dis-

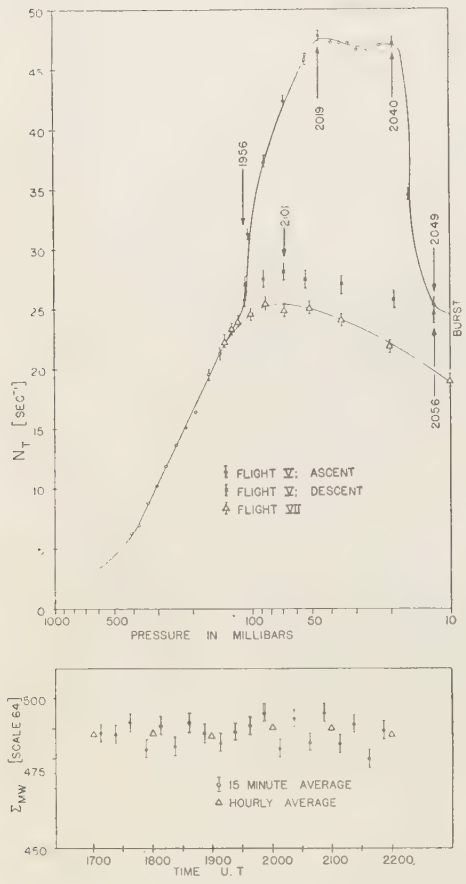

FIG. 4—The anomalous increase which occurred during flight 5 is shown, including ascent and descent with some significant times given in UT. Flight 7 is shown at the higher altitudes for comparison. Also given in the lower box are the Mt. Washington neutron monitor counting rates for 15-min and hourly intervals.

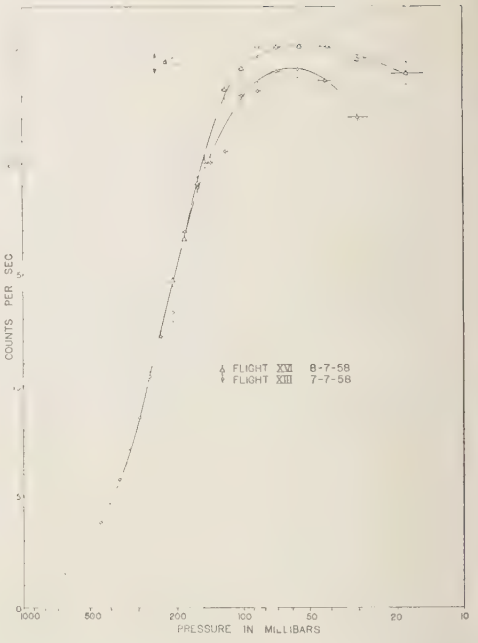

FIG. 5—The intensity-altitude curves are shown for the cases of a 'peaked' shape and a 'broad and flattened' shape.

tribution of the cosmic-ray intensity at high altitudes and find that at the Pfotzer maximum (~87 mb) the distribution is approximately isotropic. Below the Pfotzer maximum, the isotropy is not maintained, but, since in our experiment the counting rate is taken at the Pfotzer maximum, we shall assume that the distribution is isotropic.

The average value of $\bar{J}$ for the seventeen flights is 0.295 ± 0.005 cm^{-2} sec^{-1} ster^{-1}, with a range from 0.256 to 0.337. Comparison of this value with that obtained by *Meredith et al.* [1955] in 1954 above the atmosphere and north of the knee in the latitude curve shows that the intensity has decreased by ~200 per cent. This is considerably smaller than the 400 per cent change measured by *Neher* [1958] at $\lambda = 89.5°$N, with ion chambers flown to high altitudes comparable to the flights reported here. In 1954 Neher's data [1956] indicated that primary particles with energies down to 0.15 bev were present. Later results [*Neher*, 1957] in 1956 showed that this low-energy component was absent. Since the geomagnetic cutoff at $\lambda = 53°$, where our flights were conducted, is ~1 bev/c, based upon conventional geomagnetic theory, we would expect a smaller change in $\bar{J}$ between 1956 and 1958. Our results and those of Neher would also be different since they were not conducted at exactly the same time in the solar cycle of activity. It is interesting to note that *Lockwood* [1958], *Fenton et al.* [1958], and *Simpson* [1958] report that during the period 1954 to 1958 the intensity of the nucleonic com-

ponent measured deep in the atmosphere dropped about 20 per cent. Comparing the magnitudes of these changes, we can see the strong energy dependence of the long-term variation in the cosmic radiation. From these results the approximate energy dependence for the fractional change in intensity is given by $1/E^k$, where E is the energy in bev of the primary radiation and $k \simeq 2$. It should be noted that the exponent k is very sensitive to the mean energy of the effective primary spectra for the different detectors.

C. Anomalous increase—An anomalous increase in counting rate occurring during the flight on March 3 is shown in Figure 4. As this flight was approaching the 104-mb level, at 1956 UT, the counting rate rose abruptly, reaching a maximum at 2019 UT. At this time the counting rate was ~100 per cent higher than on previous flights. The duration of the maximum was approximately 21 minutes, during which the instrument rose from 45 mb to 19 mb. The shape of the curve at the maximum was quite flattened, even though the instrument continued rising. The counting rate then subsided rapidly to a more typical rate from 19 mb to 10 mb, where the balloon burst. On the descent, the Pfotzer maximum occurred at about the 65-mb level. This maximum was broad and flattened with a counting rate about 4 per cent higher than would be expected from the results of the complete series. The 15-minute average counting rates (corrected for barometric pressure) recorded by the Mt. Washington neutron monitor during this flight are also plotted on Figure 4. There is no significant increase in the nucleonic intensity.

To determine whether this increase was due to solar production of cosmic rays, solar-flare data were scanned for flares occurring before or at the time of the increase. Large flares occurred on March 1 at 0911 UT and on March 3, the day of the flight, at 1015 UT. Three subflares were reported by the U. S. Naval Research Laboratories, occurring at 1905, 1923, and 1942 UT on March 3. If a solar gas cloud was produced by the flare on March 1, a cloud transit time from sun to earth of ~60 hours is required, which seems long compared with the usual transit time of 20 to 30 hours. The short time interval between the flare at 1015 and the recorded increase suggests the arrival of solar-produced particles in advance of the main gas cloud, which arrived later on March 5 to produce the magnetic disturbances observed at several stations on that day. The flare occurring at ~1015 was accompanied by short-wave radio fadeouts of 3+ importance, which persisted until 1145 UT. The sudden commencement of a moderately severe geomagnetic storm was also noted by many stations at 0930 on March 3, the period of storminess continuing until March 8.

Unfortunately all solar radio-frequency emission data are not available at the times of these large flares, but the available data were checked for outbursts prior to the cosmic-ray increase, and are shown in Table 3. All four of these outbursts are large, especially the burst occurring at 167 Mc, which lasted throughout the period when the cosmic-ray increase was observed.

Several authors have reported the occurrence of such anomalous increases at high altitudes. *Meredith et al.* [1955] observed high-altitude bursts in Geiger counters, which they associated with 10 to 40-kev X-rays from electrons of auroral origin. *Pomerantz* [1956] reported occurrences of increased cosmic radiation, detected with a quadruple coincidence counter telescope. He correlated these events with solar radio noise, and found that some large solar flares gave no effect whereas other small flares produced a cosmic-ray increase, even though the measurement was made outside the impact zone. *Winckler and Anderson* [1957] found

TABLE 3—*Solar radio-frequency emission data, March 3, 1958*

Frequency and station	Start UT	Duration, min	Time of maximum	Maximum flux density, 10^{-22} m^{-2} $(c/s)^{-1}$
167 Mc; Boulder	1700	455	1803.3	1100
200 Mc; Cornell	1754	1		110
200 Mc; Cornell	1803.5	0.5		204
470 Mc; Boulder	1943.6	0.1		260

that very large increases in counting rate occurred during two balloon flights using Victoreen 1B85 Geiger tubes in triple coincidence. One of the increases was first observed at 8.7 g cm^{-2} and the other at 21 g cm^{-2}. *Winckler and Peterson* [1957] later reported sudden bursts associated with visible auroras and probably due to X-rays in the energy range of 50 to 70 kev.

Recent balloon flights at atmospheric depths of ~10 g cm^{-2} have disclosed two different types of increases. First, on August 29, 1957, *Anderson* [1957, 1958a] measured a large increase in cosmic radiation, occurring in conjunction with the sudden commencement of a geomagnetic storm. The increased radiation was probably X-radiation, its energy being approximately 100 kev. An event of a second type on August 22, 1958, detected by *Anderson* [1958b] and *Winckler et al.* [1959], was an increase due to the arrival at the earth of protons with energies of ~170 Mev, associated with a great solar radio noise storm. It should be noted that this event was preceded by a moderate geomagnetic storm approximately 13 hours earlier, which lasted for a considerable time. A similar event was observed by *Freier et al.* [1959] on March 26, 1958, where an increase of low-rigidity protons followed a three plus flare and associated solar radio noise storm.

We attribute the anomalous increase on March 3, 1958, to high-energy X-radiation, since it was observed deep in the atmosphere. For protons to be detected at ~108 mb, their energy at the top of the atmosphere must be ~450 Mev. As *Winckler et al.* [1959] found that the energy spectrum of the protons associated with the event on August 22, 1958, was very steep in the energy range 100 to 400 Mev, it does not appear that such a large increase at this depth could be produced by protons. The X-radiation observed could be due to the local acceleration of electrons, associated with large disturbances of the geomagnetic field.

D. Comparison of intensity changes with solar phenomena—It can be seen from Figure 1 that large changes in counting rate were recorded by both types of detectors. In this plot the amplitude of the changes in counting rate at the Pfotzer maximum is about twice that in the nucleonic component. It is evident that large deviations occur from this 'normal' ratio of ~2.0. Such deviations are probably due to changes in the lower-energy primary radiation to which the nucleonic detector does not respond.

Those flights shown in Figure 1 which are not within two standard deviations of the normal ratio are numbers 3, 5, 8, 9, 10, 13, and 16. Flight 5 has already been discussed; flight 16 is of especial interest and will be discussed later.

For the remaining five flights, it is seen from Figure 3 that there was considerable solar and geophysical activity at the times of the flights. Strong solar radio-frequency emissions were reported during four of these five flights; extended flare activity prior to the observation in two; and a geomagnetic storm was in progress for one observation. Flight 3 was made on January 6, 1958, during a period when the nucleonic component was slowly and erratically recovering from the large Forbush decrease which reached a minimum on December 22, 1957. At the time of flight 8 (April 21) the nucleonic intensity was slowly recovering from a large Forbush decrease several days earlier, but there was some indication of a change in the recovery rate on April 21. There were marked decreases in the nucleonic intensity amounting to about 3 per cent at the times of flights 9 (April 29) and 10 (May 10). On July 7 (flight 13) a large Forbush-type event occurred. Presumably the change in the low-energy primary radiation was much greater for these events than for the mean of the flights.

At the time of flight 16, August 7, the nucleonic intensity was increasing rapidly after a large Forbush decrease in mid-July, and the counting rate at the Pfotzer maximum is about 10 per cent less than we should expect. However, flight 14 on July 28, and flight 15 on August 4, had indicated that the primary spectrum had returned to normal after the decrease. This would indicate possibly that only the low-energy primary spectrum ($E < 2$ bev) was depressed at that time, and indeed, we find that there was a great deal of solar and geophysical activity before and at the time of the observation. However, the broad and flattened shape of the intensity-altitude curve above the Pfotzer maximum as shown in Figure 5 indi-

tes that, in addition, there was present low-
ıergy radiation (possibly protons with $E \lesssim$
50 Mev) in excess of that expected from a
ɔrmal spectrum.

Considerable flare activity was reported on
ugust 6 and 7; in particular, a large flare of
agnitude 3–2+ occurred about 3.5 hours be-
re the observation, and this was followed in
ıe afternoon by strong outbursts of solar r-f
nission at 167, 200, 470, and 2800 Mc. It is
ıite possible, therefore, that this excess lower-
ıergy radiation was solar-produced in conjunc-
on with the observed activity.

E. Comments on the shape of the intensity-titude curves—In analyzing the data from
ıe seventeen successful flights, it was noticed
ıat the shapes of the intensity-altitude curves
ere similar for ten flights, with the Pfotzer
aximum occurring at 70 to 65 mb pressure.
our of the other seven curves were character-
ed by a much more peaked shape at the
fotzer maximum, and the maximum was at
gher pressures (deeper in the atmosphere).
he three remaining curves showed a broad
nd flattened shape, with the maximum at lower
ressures, similar to the curves determined at
itudes farther north by *Winckler and Ander-
n* [1957]. An example of each of these ex-
eme cases is given in Figure 5. Table 4 sum-
arizes the characteristics of the intensity-
titude curves for all the flights.

The errors shown in Figure 5 are the statisti-
l errors in the counting rates and an estimated
aximum error of ±3 mb in the pressure. The
ue error for pressures less than 150 mb is
obably smaller than ± 3 mb, because each
ressure element was checked to ± 1 mm Hg
ith a manometer in the laboratory, and the

TABLE 4—*Intensity-altitude curve shapes*

Flight no.	Shape of curve	Pfotzer maximum pressure, ±5 mb
5	Flat	65
6	Flat	60
16	Flat	55
3	Peaked	85
8	Peaked	75
9	Peaked	80
13	Peaked	65
All others	Normal	65–70

temperatures in the gondola did not drop below 8°C at any time during the actual flights. It appears from Figure 5 and similar plots of the other flights in these extreme groups that the curves differ considerably in shape at higher altitudes and in the location of the Pfotzer maximum, as well as in the flatness of the maximum itself.

A possible change in the production of secondary particles above the 100-mb level due to changes in air density or the pressure-altitude relationship was investigated. It was found [*Cole et al.*, 1958] that the standard deviation of air density over North America at this latitude varies from 3 to 1.0 g m^{-3} between 70,000 ft and 100,000 ft, respectively, in January, and decreases to the values of 2 to 0.5 g m^{-3}, respectively, in July. The corresponding standard deviations in pressure are 2 to 0.7 mb in January, and 0.8 to 0.3 mb in July. Deviations larger than these would have appeared on the pressure-altitude plots obtained from regular radiosonde flights on most of the days of our cosmic-ray flights. Such small changes in air density do not appear to account for the observed changes in the shapes of the intensity-altitude curves above the Pfotzer maximum. For example, it can be seen from Figure 5 that this change is ~8 per cent between 65 and 30 mb for flights 13 and 16.

Temperature-altitude data were available from the same radiosonde flights, and, although the air temperature varied ±5°C from a mean temperature distribution for the flights, there was no correlation between shape of the counting rate vs. altitude curves and temperature variations.

Interpretation of these changes in shape of the Pfotzer maximum must, therefore, be based upon changes in solar and related geophysical conditions. The results of this analysis are shown in Table 5. Several points are immediately obvious:

1. Of the seven flights which we denoted as having a flattened or a peaked Pfotzer maximum, six fall more than 2 standard deviations away from the line of best fit on Figure 1.

2. Very little solar activity was observed on the days when the peaked curves were determined, and all four of these flights gave counting rates at the Pfotzer maximum which were

TABLE 5—*Summary of flight characteristics and associated solar and geophysical activity*

Curve shape	Flattened	Normal	Peaked
Number of flights	3	10	4
Location with respect to mean ratio (Fig. 1)	#5 and #16 off; #6 on	All on except #10	All below
Flares of magnitude 2 in previous 36 hr	#5, mag. 3 at ~1015 UT, on 3/3 #16, mag. 3 at 1500 UT, on 8/7	None	#13, 2+ flare about 1 hr before observatio
Geomagnetic storm within 12 hr before flight	#5, moderately severe sudden commencement storm began 3/3 at ~0930 UT and ended 3/8 at ~1500 #6, moderate storm of sudden commencement began on 3/18 at ~0200 UT and ended on 3/21 at ~2400	#4, storm ended ~5.5 hr before flight	None
$K_p \geq 5$	#5 and #6 at the time of the flight	#4 on day of flight (see above)	None
Remarks	Large solar r-f burst on several frequencies #6, ionospheric disturbance, G-S-SWF, at the time of the observation; 1+ flare 1905–1948 UT.	Several smaller solar r-f bursts occurred during flights (see Fig. 3)	

much lower than would be expected. As was noted in section D, the nucleonic component at Mt. Washington was considerably depressed at the times of these flights. It seems reasonable, then, that for these four events the change in the low-energy primary radiation was much greater than that in the radiation with $E \lesssim 1$ bev.

3. There was very little solar activity on the days when normal intensity-altitude curves were obtained; and, with the exception of flight 4, the nucleonic component showed only small variations for a few days before and after the flight.

4. Solar activity was high on the days of the three flattened curves. The presence of excess low-energy radiation in the case of flight 5 has already been discussed in section C, and that of flight 16 in section D. While flight 6 was in the altitude region of the Pfotzer maximum, a geomagnetic storm was in progress and an ionospheric disturbance was noted in conjunction with a 1+ flare. A flare of magnitude 3 also preceded the observation, and several large solar radio-frequency emissions were recorde just before and at the time of the observatio These three flights then indicate the arrival c presence of low-energy particles at the eart probably associated with the passage of a sola gas cloud, and, although the data from flight (Fig. 4) indicates that the time of the observa tion must be propitious in order to observe th major effects of this radiation, low-energy part cles are still present long after the burst ha ceased.

Conclusions— In the period January to Sep tember 1958, the ratio of the changes in coun ing rate measured by a Geiger tube at th Pfotzer maximum to those measured by th nucleonic detector at Mt. Washington is ap proximately 2.0. Several large deviations fro this normal ratio have been observed and in terpreted as follows.

Four flights have lower counting rates at th Pfotzer maximum than would be expected, an it is also found that the intensity-altitude curv are more peaked for these flights than for th others. All four of these flights occurred du

g, or just after marked decreases in the nu-
onic intensity. It is concluded that the low-
ergy portion of the spectrum is more highly
pressed during these events than for the
nger-term changes.

One flight revealed an increase of ~100 per
nt in counting rate at the Pfotzer maximum,
hich appears to be due to the presence of
-radiation with energies $E \leq 0.5$ Mev.

Two other cases of enhanced radiation above
e Pfotzer maximum were observed, as inter-
eted from the broad and flattened shape of
e intensity-altitude curves at low pressures.
hese flights were made at times when several
ents were in progress or had occurred which
e associated with the production of cosmic
ys or their arrival at the earth. These events
clude large solar flares, the associated solar
dio-frequency emission and ionospheric dis-
rbances, and geomagnetic storms.

The mean value of the hemispherical average
nidirectional intensity above the atmosphere
as derived from the corrected counting rates
the Pfotzer maximum. This value was com-
ared with that obtained in 1954 by *Meredith et al.* [1955]. It was found that the intensity
ad decreased by ~200 per cent from 1954 to
958.

Acknowledgments—We should like to thank
gt. Shipley and the men in the Test Engineering
ection, Geophysics Research Directorate, Air
orce Cambridge Research Center, for their valu-
ble assistance and advice in making the balloon
ights. We are indebted to the High Altitude
bservatory and the National Bureau of Stand-
rds for the Preliminary Report of Solar Activity
nd the monthly Solar-Geophysical Data. The
ssistance of Mr. Thomas Eichelberger in the con-
ruction of the instruments is also appreciated.

References

NDERSON, K. A., Occurrence of soft radiation during the magnetic storm of 29 August 1957, *J. Geophys. Research, 62,* 641–644, 1957.

NDERSON, K. A., Soft radiation events at high altitude during the magnetic storm of August 29–30, 1957, *Phys. Rev., 111,* 1397-1405, 1958a.

NDERSON, K. A., Ionizing radiation associated with solar radio noise storm, *Phys. Rev. Letters, 1,* 335–337, 1958b.

OLE, A. E., E. M. Darling, Jr., W. S. Ripley, and S. B. Solot, Atmospheric pressure and atmospheric density, Chapters 3 and 4, *Handbook of Geophysics for Air Force Designers,* Air Force Cambridge Research Center, Bedford, Mass., 1958.

Fenton, A. G., K. B. Fenton, and D. C. Rose, The variation of sea level cosmic ray intensity between 1954 and 1957, *Can. J. Phys., 36,* 824–839, 1958.

Fonger, W. H., Cosmic radiation intensity-time variations and their origin, II, Energy dependence of 27-day variations, *Phys. Rev., 91,* 351–361, 1953.

Freier, P. S., E. P. Ney, and J. R. Winckler, Balloon observation of solar cosmic rays on March 26, 1958, *J. Geophys. Research, 64,* 685–688, 1959.

Gangnes, A. V., J. F. Jenkins, Jr., and J. A. Van Allen, The cosmic-ray intensity above the atmosphere, *Phys. Rev., 75,* 57–69, 1949.

Kaplon, M. F., B. Peters, H. C. Reynolds, and D. M. Ritson, The energy spectrum of primary cosmic radiation, *Phys. Rev., 85,* 295–309, 1952.

Korff, S. A., *Electron and Nuclear Counters,* D. Van Nostrand Co., New York, pp. 256–258, 1955.

Lockwood, J. A., Variations in the cosmic-ray intensity, *Phys. Rev., 112,* 1750–1758, 1958.

Meredith, L. H., J. A. Van Allen, and M. B. Gottlieb, Cosmic-ray intensity above the atmosphere at high altitudes, *Phys. Rev., 99,* 198–209, 1955.

Meyer, P., and J. A. Simpson, Changes in the low-energy particle cutoff and primary spectrum of cosmic radiation, *Phys. Rev., 99,* 1517–1523, 1955.

Meyer, P., and J. A. Simpson, Changes in the low-energy particle cutoff and primary spectrum of cosmic rays, *Phys. Rev., 106,* 568–571, 1957.

Neher, H. V., Low-energy primary cosmic-ray particles in 1954, *Phys. Rev., 103,* 228–236, 1956.

Neher, H. V., Cosmic rays near the north geomagnetic pole in the summers of 1955 and 1956, *Phys. Rev., 107,* 588–592, 1957.

Neher, H. V., Cosmic-ray changes from 1954 to 1957, *Phys. Rev., 109,* 608, 1958.

Pomerantz, M. A., Cosmic-ray radiosonde and telemetering system, *Electronics, 24,* 88-92, April 1951.

Pomerantz, M. A., Cosmic-ray observations at very high altitudes during periods of intense solar activity, *Phys. Rev., 102,* 870–878, 1956.

Simpson, J. A., Cosmic ray program: First twelve months, *Bull. Intern. Geophys. Year, 15,* 11, 1958.

Swann, W. F. G., Showers produced by penetrating rays and allied phenomena, *Revs. Modern Phys., 11,* 242–254, 1939.

Van Allen, J. A., The nature and intensity of the cosmic radiation, chapter XIV, pp. 239–266, *Physics and Medicine of the Upper Atmosphere* (edited by C. S. White and O. O. Benson, Jr.), University of New Mexico Press, Albuquerque, 1952.

Winckler, J. R., and K. A. Anderson, High-

altitude cosmic-ray effect from 51° to 65°N geomagnetic latitude, *Phys. Rev., 108,* 148–154, 1957.

Winckler, J. R., and L. Peterson, Large auroral effect on cosmic-ray detectors observed at 8 g/cm² atmospheric depth, *Phys. Rev., 108,* 903–904, 1957.

Winckler, J. R., L. E. Petersen, R. Hoffman, R. Arnoldy, and K. A. Anderson, Observations of low-energy solar cosmic rays from the flare of August 22, 1958, Part II, *Bull. Phys. Soc. 4,* 238, 1959.

Winckler, J. R., and W. G. Stroud, A preliminary directional study of cosmic rays at high altitude, II, Experimental results and interpretation, *Phys. Rev., 76,* 1012–1019, 1949.

(Manuscript received July 2, 1959.)

Applications of the Molecular Refractivity in Radio Meteorology

B. R. BEAN AND R. M. GALLET

National Bureau of Standards
Boulder, Colorado

Abstract—Consideration of the molecular refractivity has led to a value of the radio refractive index referred to zero altitude or sea level that effectively removes the systematic altitude dependence of air density. The advantages of this new parameter are illustrated by two applications. The first application, the preparation of climatic charts of the radio refractive index, illustrates that this new parameter brings climatic differences into sharp relief. The second application deals with the vertical variation of air mass properties across a classic warm front and clearly delineates air mass differences, thus indicating the utility of this new parameter for synoptic studies.

The purpose of this paper is to present a method of minimizing the altitude dependence of the radio refractive index in order to emphasize climatic and synoptic differences in air masses. This method arises from consideration of the molecular refractivity of air and leads to a reduced value of the refractive index analogous to potential temperature as used in standard meteorological analysis. Although the concept of a potential refractive index was introduced some years ago by *Lukes* [1944] and *Katz* [1951], their development rests on use of the potential temperature in place of temperature in the equation for the refractive index; whereas the present method rests essentially on the average exponential decrease of the refractive index with height observed in practice. The present method has the added advantage of allowing the recovery of the refractive index at points above sea level from a knowledge of the height of the point alone without further knowledge of the potential temperature.

The molecular refractivity, R, is a constant, characteristic of each dielectric and is used in many branches of physics. By definition, R is given by

$$R = \frac{(\epsilon - 1)}{(\epsilon + 2)} \frac{M}{\rho} \tag{1}$$

where ϵ is the dielectric constant, relative to its value in free space, M the molar weight, and ρ the density. The molecular refractivity was derived from the Clausius-Mossotti equation [*Lorentz,* 1909, p. 145; *Frohlich,* 1949, p. 169]; when applied to gases it is known as the Lorenz-Lorentz formula [*Sommerfeld,* 1954, p. 93]. For a mixture the molecular refractivities are additive, the resultant being determined as the weighted average of the value for each constituent; the weights being proportional to the concentrations.

One may write

$$\frac{\epsilon - 1}{\epsilon + 2} = \frac{n^2 - 1}{n^2 + 2} \tag{2}$$

where n is the refractive index. For atmospheric gases n is very near unity and R may be expressed to a high degree of accuracy by

$$R = \left(\frac{2}{3} M\right) \frac{n - 1}{\rho}. \tag{3}$$

Although the quantity $(n - 1)$ is needed for some radio meteorological investigations, it is usually the variations of $(n - 1)$ from the local average that are ascribed to causing the variation of radio field strengths from their average level. By noting that $(n - 1)/\rho$ is a constant for dry, non-polar, atmospheric gases and inserting an average decay of ρ with altitude into (3), the large systematic variation of $(n - 1)$ due to systematic variation of density with altitude will be suppressed and the smaller but physically

more significant local departures of $(n - 1)$ will be emphasized.

The *average* variation of density with altitude in the atmosphere may be expressed in the first approximation as

$$\rho = \rho_0 \exp \{-z/H\} \tag{4}$$

where z is the altitude, ρ_0 the average sea level density of moist air and H the average scale height between zero and z. By analogy, suggested by (3), it is useful to introduce the concept of an *effective scale height*, H^*, for the average variation of refractive index in the atmosphere. Many studies have shown that the average refractive index variation with height is quite well represented, to a first approximation, by a formula similar to (4) [*Gerson*, 1948; *Bean*, 1953; *Misme*, 1958]. It is possible to calculate a theoretical value of this effective scale height using a distribution of water vapor. This is, however, quite a complex procedure. Furthermore, the value obtained depends upon the model of the water vapor distribution, and no definite conclusion can be justified considering the extreme variation of water vapor concentration with season, geographic location, and height above the earth's surface. A convenient and simple alternative is to adopt a value for H^* from the average $(n - 1)$ variation with height in the free atmosphere. Several such values of H^* were determined by reference to the NACA standard atmosphere [*Smithsonian Meteorological Tables*, 1951] and recent climatological studies of atmospheric refractive index structure [*Bean and Thayer*, 1959]. It is seen in Table 1 that H^* varies from 6.56 to 7.63 km in the NACA standard atmosphere, depending on the value of the relative humidity assumed. The value of $H^* = 7.01$ km for 80 per cent relative humidity is in close agreement with $H^* = 6.95$ km obtained from climatological studies of $(n - 1)$ variations over the first kilometer above the earth's surface from nearly 2 million radiosonde observations from many diverse climates.

TABLE 1—*Determination of the effective scale height*, H*, *for the radio refractive index*

Source	Humidity, per cent	H^*, km	Reference
NACA STANDARD ATMOSPHERE	100	6.56	[*Smith. Met. Tab.*]
	80	7.01	[*Smith. Met. Tab.*]
	60	7.63	[*Smith. Met. Tab.*]
Climatological data	As observed	6.95	[*Bean and Thayer*, 1959]
Adopted for this study		7.0	

In the light of this agreement the value of $H^* = 7.0$ km was arbitrarily adopted for use in the present studies. Note that this value is smaller than the usual scale height near sea level of 8.0 km for the density distribution of the air. Although the value H^* is quite arbitrary, it is evident from Table 1 that H^* should lie between 6.5 and 7.5 km. Further, as we shall see in subsequent applications, the advantage of adopting the molecular refractivity is relatively insensitive to the choice of H^*.

Using (4), the molecular refractivity for the atmosphere is approximated by

$$R \simeq \left(\frac{2}{3} M\right) \frac{n - 1}{\rho_0} \exp \{z/H^*\} \tag{5}$$

which characterizes immediately the departures of atmospheric moisture and temperature effects from the average, independent of the altitude of the point under consideration. Note that the molecular refractivity is now approximately expressed in terms of the local value of $(n - 1)$ and the altitude, all other factors being assumed constant. In order to emphasize this last consideration the notation

$$N \equiv (n - 1)\ 10^6 \tag{6}$$

will be adopted. Disregarding constant factors, (5) now becomes

$$N_0 = N \exp \{z/H^*\}, \tag{7}$$

the zero subscript drawing attention to the fact that $(n - 1)$ has been referenced to zero altitude, or sea-level. Since $R \propto N_0$, the remainder of this paper will be in terms of N_0.

As an illustration of the use of the concept of the molecular refractivity, consider the comparison of the refractive index at the earth's surface across the United States where the range

FIG. 1—Contours of average value of N_s for 0200 local time during the month of August.

of nonmountain relief is from 0 meters to 1600 meters (Denver) with many flat plateau regions over 3000 meters above mean sea level. The value of the refractive index may be determined from [*Smith and Weintraub*, 1953]

$$N \equiv (n - 1)\ 10^6 = \frac{77.6}{T}\left(P + \frac{4810 e_s RH}{T}\right) \qquad (8)$$

where P is the station pressure (mb), RH is the relative humidity expressed as a per cent of the saturation vapor pressure (e_s) for the temperature T (°K). The notation N_s is used to indicate the value of $(n - 1)\ 10^6$ obtained from the pressure, temperature, and humidity of the standard surface weather observation. Figure 1 presents a typical variation of N_s across the United States for the particular case of eight-year average values during the month of August at 0200 local time. The circles indicate the location of the 62 weather stations whose data were used. One notes that the coastal areas display high values of N_s, whereas inland areas have lower values. There are low values of N_s corresponding to the Appalachian and Adirondack Mountains, and a gradual decrease with increasing elevation of the great plains, until the lowest values are observed in the Rocky Mountain region and the high plateau area of Nevada. A corresponding gradient is observed from the West Coast eastwards. Cross-hatching indicates areas where the terrain changes so rapidly that it was felt the data were inadequate to obtain realistic contours of N_s. Note the great similarity between the contours of N_s on Figure 1 and the elevation of ground above sea level, Figure 2. The strong elevation dependence of N_s is due to the dominating effect of the changes of density with altitude. In fact, the information gained immediately from Figure 1 is essentially the general relief of the continent.

Consider, on the other hand, the rather open contours of

$$N_0 = N_s \exp\{z/7.0\} \qquad (9)$$

given on Figure 3. The removal of the station altitude dependence has produced a much simpler map with a considerably smaller range of variations. As a practical consequence the contours of N_0 may be obtained much more easily and more accurately than the more complicated contours of N_s. Further, N_s may be easily estimated from the smooth and slowly varying contours of N_0 and a knowledge of the station elevation. In fact, numerous tests using readings by several people have shown that N_s may be estimated four to five times more accurately from N_0 contours than from N_s contours for locations not used in the derivation of the contours [*Bean and Horn*, 1959].

Returning to the question of the appropriate

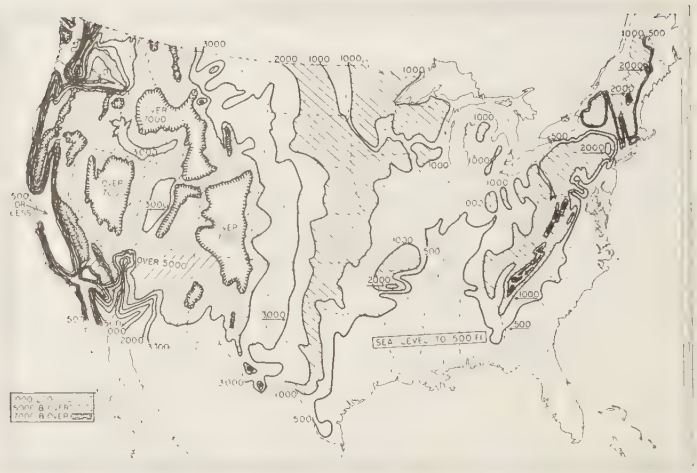

FIG. 2—Elevation of ground above sea level.

value of H^*; the adoption of any value of H^* between 6.5 and 7.5 km would have reduced the range of N_0 values on Figure 3 by no more than 2 N units. Since this reduction in range is more than an order of magnitude less than the original reduction accomplished by the use of N_0, it appears that the basic advantage of the method has been realized.

A map of N_0, such as that of Figure 3, which represents a large continental area, may easily be compared and merged with maps for ocean areas. This would be more difficult with N_s, since, for example, the strong gradient over California mainly represents the rapid altitude variations of the Sierra Nevada Mountains. It has also been demonstrated that N_0 is a better indicator of tropospheric storms and air masses than N_s when considered on a synoptic or 'daily weather map' basis [*Bean and Riggs*, 1959].

Also, (7) aids in comparing air properties as

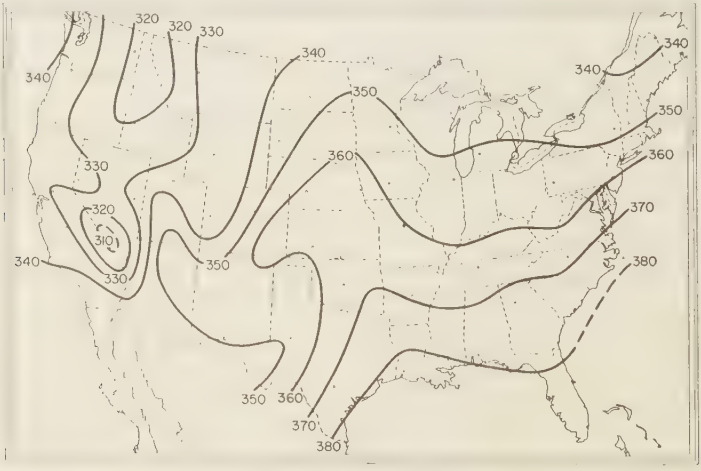

FIG. 3 Contours of average value of $N_1 = N_s \exp(z/7.0)$ for 0200 local time during the month of August.

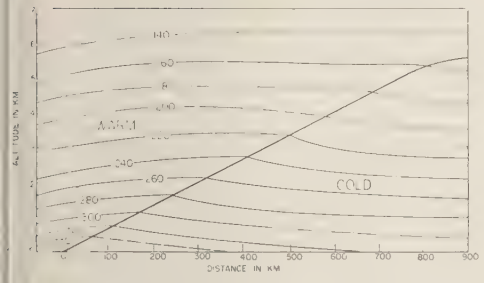

FIG. 4—Contours of $N = (n - 1)\ 10^6$ through a classic example of a warm front.

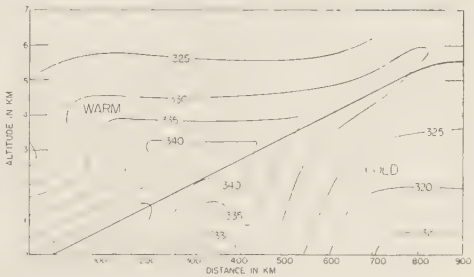

FIG. 5—Contours of N_0 for the same data as Fig. 4.

a function of altitude at the same position. The variations of N_0 will represents the local departures between this quantity and the value in a standard atmosphere and will show the perturbations in the structure of the atmosphere produced by fronts, air masses, etc. The variation of $(n - 1)\ 10^6$ as a function of height is shown by Figure 4 for the space cross-section through a classical warm front [*Byers*, 1944], and is characterized by a marked laminar structure with very little effect of the warm front in evidence. This marked height dependence disappears and the properties of the air masses appear when the same data are presented in terms of N_0, as in Figure 5. Note how much more clearly one can see the flow of warm moist air over the frontal interface and the region of maximum precipitation at about 400 km in advance of the front. It is interesting to note that this application of N_0 is opposite in objective to the first application. Namely, here we are interested in emphasizing air mass differences, whereas the climatic charts are desired to display a minimum of altitude-dependent air mass differences with fewer contours and with reduction of contouring and interpolation errors. Although any value of H^* between 6.5 and 7.5 km will remove the gross altitude dependence of the refractive index, the choice of value of H^* within this range could depend on the application. The synoptic application would be best served by a scale height near 8.0 km, whereas the objectives of the climatic chart usage would best be met by a scale height near 6.5 km. This seeming paradox is easily understood in terms of the physical interpretation of the various scale heights. For example, $H^* = 8.0$ km is typical of a perfectly dry atmosphere and its use results in emphasis of humidity differences between air masses, whereas $H^* = 6.5$ km corresponds to a saturated atmosphere and minimizes moisture differences. Thus it would appear that eventually one might use a value of H^* as indicated by the application at hand. As a practical matter, however, $H^* = 7.0$ km appears to reach a desirable compromise between the objectives of the two preceding examples.

The two illustrations above indicate the simplification introduced into climatological and synoptic studies of the radio refractive index of the atmosphere by the adoption of the concept of the molecular refractivity. In addition, it appears from research in progress that this concept will also be of use in the theory of scattering of radio waves by atmospheric turbulence.

The authors are grateful to the referees for bringing to their attention the earlier work by Lukes which was unknown to them at the time of the writing.

REFERENCES

BEAN, B. R., The geographical and height distribution of the gradient of refractive index, *Proc. I.R.E., 41*, 549–550, 1953.

BEAN, B. R., AND J. D. HORN, The radio refractive index climate near the ground, *J. Research Nat. Bur. Standards, Sec. D: Radio Propagation, 63D*, 1959, in press.

BEAN, B. R., AND L. P. RIGGS, On the synoptic variation of the radio refractive index, *J. Research Nat. Bur. Standards, Sec. D: Radio Propagation, 63D*, 91–98, 1959.

BEAN, B. R., AND G. D. THAYER, On models of the atmospheric radio refractive index, *Proc. I.R.E., 47*, 740–755, 1959.

BYERS, H. R., *General Meterology*, Chapt. 14,

McGraw-Hill Book Co., Inc., New York, 1944.

Frohlich, H., *The Theory of Dielectrics,* Oxford University Press, Oxford, 1949.

Gerson, N. C., Variations in the index of refraction of the atmosphere, *Geofis. pura e appl., 13,* 88–101, 1948.

Katz, I., Gradient of refractive modulus in homogeneous air, potential modulus, pp. 198–199 in *Propagation of Short Radio Waves* (by D. E. Kerr), McGraw-Hill Book Company, Inc., New York, 1951.

Lorentz, H. A., *Theory of Electrons,* Dover Publications, Inc., New York (reprint of 1909 edition).

Lukes, G. D., Radio meteorological forecasting by means of the thermodynamics of the modified refractive index, *Third Conference on Propagation,* November 16–19, 1944, Washington, D. C., Committee on Propagation, NDRC, pp. 107–113, 1944.

Misme, P., Essai de radio climatologie d'altitude dans le nord de la France, *Annals des Telecommunications, 13,* 303–310, 1958.

Smith, E. K., Jr., and S. Weintraub, The constants in the equation for atmospheric refractive index at radio frequencies, *Proc. I.R.E., 41,* 1035–1037, 1953.

Smithsonian Meteorological Tables, Smithsonian Institution, Washington, D. C., 1951.

Sommerfeld, A., *Lectures on Theoretical Physics: Vol. 4, Optics,* Academic Press, New York, 1954.

(Manuscript received June 8, 1959;
revised August 3, 1959.)

Atmospheric Radioactivity Levels at Yokosuka, Japan, 1954-1958

Luther B. Lockhart, Jr.

U. S. Naval Research Laboratory
Washington, D. C.

Abstract—For the past ten years the U. S. Naval Research Laboratory has had under way a program relating to the radioactivity of the atmosphere. This has involved the study of both natural and man-made radioactive materials in the air and their distribution, transport, and removal from the atmosphere. This report summarizes measurements made on the concentrations of some natural radioactive materials and of gross fission products in the air at ground level at Yokosuka, Japan, during the period 1954–1958.

These data support the conclusions that the concentrations of both natural radioactive products and fission products in the air at ground level vary widely from time to time, that the change in the concentration of the natural radioactivity is related in a general way to the phenomena that control precipitation, and that the trend of the fission-product concentration has been upward during the past few years as a result of increasing nuclear testing.

Introduction—Following the CASTLE series of nuclear tests held by the United States at the Pacific Proving Grounds in early 1954 and the resulting unfortunate incident involving Japanese fishermen on the *Fukuryu Maru,* the Japanese press for some time tended to credit the United States Government with most increases in radioactivity in the area around Japan. Partly as a consequence of this unfavorable publicity, the network of stations operated by the U. S. Naval Research Laboratory for the purpose of measuring the radioactivity of the air was expanded to include a station at Yokosuka, Japan.

Sufficient data is now at hand from atmospheric radioactivity monitor equipment operated for NRL by personnel of the Fleet Weather Facility at Yokosuka to make worth while a complete report of the radioactivity of the air at this site and to correlate the changes in the fission-product levels in the air with nuclear tests of the United States and the U.S.S.R.

Experimental procedure—The concentration of radon, thoron, and fission products in the air was obtained from the changes in the rate of decay over a 16-hour period of radioactive particulate matter collected on efficient filters as described in detail elsewhere. [*Lockhart and others,* 1958; *Blifford and others,* 1956]. During the 24-hour sampling period, 900 to 1300 cubic meters of air passed through the filter. Corrections were made for air-flow rate, geometry and energy dependence of the counter, and filter efficiency.

Filters were changed daily at 1600 local time. The reported radon concentrations are therefore representative of the radon levels in the midafternoon, the time of their usual minimum value. Temperature inversions cause entrapment of radon near the surface with resulting high concentrations at ground level during the early morning hours, whereas increased air turbulence and greater mixing during the late afternoons result in low concentrations at that time. The thoron and fission-product levels are generally representative of the average concentrations during the 24-hour collection period. Because the calculation of the thoron concentration depended on the rate of decay of the combined thoron–fission-product mixture on the filter, no determination of thoron was made in those collections having fission-product counts in excess of 1000 measured counts per minute. This eliminated those collections which contained sufficient short-lived fission products to give false indications of high thoron content.

Results—In Table 1, 2, and 3 are recorded the monthly averages of the fission products, thoron, and radon in the ground-level air at Yokosuka. A summary of this data for the years 1955–1958 together with pertinent rain data is given in Table 4.

TABLE 1—*Monthly average fission-product concentration in the air at Yokosuka, Japan*

Month	Radioactivity in $\mu\mu c/m^3$ of air				
	1954	1955	1956	1957	1958
January	...	0.17	0.56	0.71	0.79
February	...	0.14	0.36	0.30	0.43
March	...	0.27	2.9	0.45	4.0
April	...	1.49	1.13	1.36	3.0
May	...	0.45	0.58	1.46	1.83
June	...	0.50	0.56	0.46	1.17
July	0.20*	0.10	0.29	0.41	6.9
August	0.13	0.11	0.63	0.32	1.06
September	2.9	0.06	4.3	0.84	0.59†
October	1.7	0.05	1.38	0.98	10.3‡
November	3.0	0.21	0.46	0.37	3.6
December	0.39	0.64	0.42	0.25	2.0

* Collections started July 21, 1954.
† No data September 17–24, 27–30, 1958.
‡ No data October 1–14, 1958.

TABLE 2—*Monthly average thoron concentration in the air at Yokosuka, Japan*

Month	Radioactivity in $\mu\mu c/m^3$ of air				
	1954	1955	1956	1957	1958
January	...	0.55	0.43	0.77	0.51
February	...	0.51	0.48	0.52	0.40
March	...	0.48	0.43	0.56	0.52†
April	...	0.52	0.43	0.56	0.57‖
May	...	0.41	0.35	0.33	0.54
June	...	0.46	0.46	0.40	0.52
July	0.29*	0.36	0.46	0.30	0.51¶
August	0.50	0.41	0.65	0.29	0.56
September	0.26	0.53	0.54	0.46	0.37‡
October	0.53	0.36	0.52	0.55	0.42§
November	0.60	0.56	0.59	0.51	0.54
December	0.40	0.55	0.62	0.36	0.32

* Collections started July 21, 1954.
† Based on measurements during 17 days of month.
‡ Based on measurements during 18 days of month.
§ Based on measurements during 8 days of month.
‖ Based on measurements during 14 days of month.
¶ Based on measurements during 19 days of month.

TABLE 3—*Monthly average radon concentration in the air at Yokosuka, Japan*

Month	Radioactivity in $\mu\mu c/m^3$ of air				
	1954	1955	1956	1957	1958
January	...	89	77	90	47
February	...	76	77	74	50
March	...	81	60	81	44
April	...	54	54	51	43
May	...	43	45	48	29
June	...	48	60	50	31
July	17*	20	40	38	38
August	38	24	58	20	31
September	28	52	44	45	26†
October	61	54	85	51	45‡
November	74	60	120	56	66
December	81	70	131	49	63

* Collections started July 21, 1954.
† Based on measurements during 18 days of month.
‡ Based on measurements during 13 days of month.

TABLE 4—*Yearly averages of radioactivity and rain data from Yokosuka, 1955–1958*

Item	Year			
	1955	1956	1957	1958
Radon, $\mu\mu c/m^3$	56	71	54	43
Thoron, $\mu\mu c/m^3$	0.48	0.50	0.47	0.48
Gross fission products, $\mu\mu c/m^3$	0.35	1.13	0.66	2.96
Rainfall, inches	66.55	...	76.33	64.77
Days with rain	148	...	185	184
Percentage of fission products*	0.63	1.58	1.22	6.9

* Relative to radon in the air.
Note: 1 $\mu\mu c/m^3$ = 2.22 dis/min per m^3.

The average monthly gross fission-product concentrations in the air at Yokosuka and the highest daily average recorded during the month are shown in Figure 1. An attempt is made to assign the source of the recorded activity by indicating the periods when nuclear testing took place in the Northern Hemisphere. Previous work has shown that there is no discernable

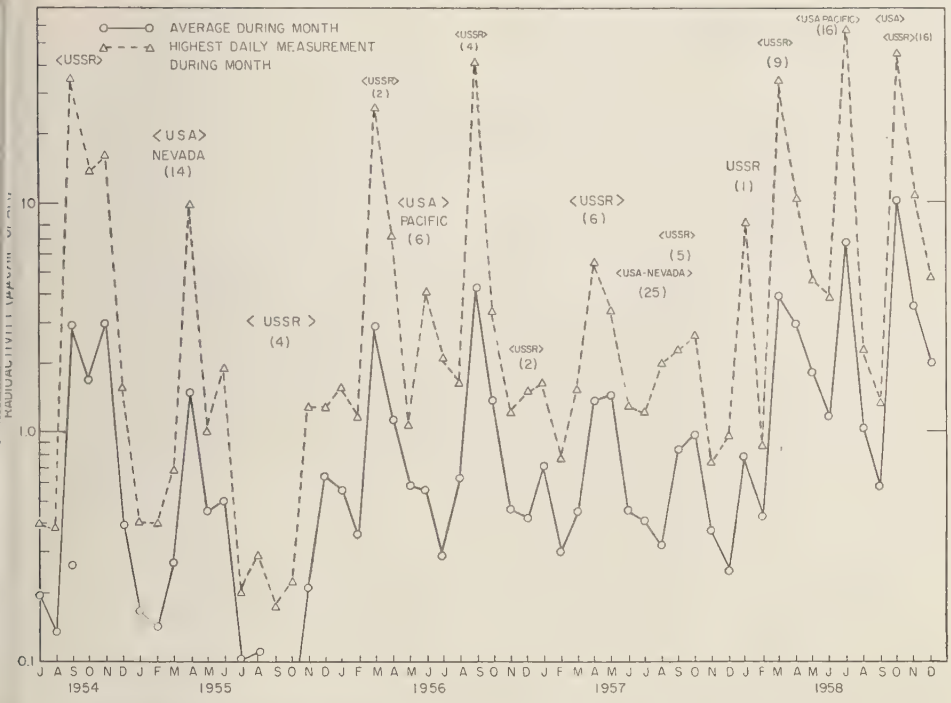

FIG. 1—Gross fission-product radioactivity in the air at Yokosuka, Japan, 1954–1958. Figures in parentheses refer to the number of nuclear tests in each series.

correlation between activity levels in the Northern Hemisphere and the nuclear tests conducted by the United Kingdom.

The results indicate rather clearly that most of the periods of peak activity are closely associated with nuclear tests in the Soviet Union. Higher activity from such tests is to be expected because of the closeness of Japan to the Soviet test sites and the generally prevailing winds that pass from west to east during much of the year. Further, the jet stream has a general west-to-east path. Debris which comes from the tests in the U.S.S.R. is thus generally fresher than that from the United States test sites and, for a given number of fissions, would contribute higher activity. There are cases, however, where substantial amounts of radioactive matter have been carried from the Eniwetok area to Japan. One such case occurred in July 1958; another evidently occurred in the spring of 1954 prior to the establishment of any routine air-monitoring stations in Japan. Because of the long path from Nevada to Japan and the small fission yield of weapons tested there, there has been only one occasion when a definite response to nuclear detonations in the continental United States has been recorded in Japan. This was during the TEAPOT series held at the Nevada Test Site from February to May, 1955, at a time when the general background of activity in the air was rather low. An even larger test program (PLUMBBOB, May to October, 1957) went undetected in Japan, possibly because of the high residual activity from an earlier test series of the U.S.S.R. but also because it coincided with the rainy season in Japan, with the resulting rapid wash-out of this activity from the air.

That the residual fission-product activity in the air has increased during the period of these measurements is apparent from the fact that no low monthly averages have been recorded since the end of 1955.

Included in Table 4 is a comparison of the

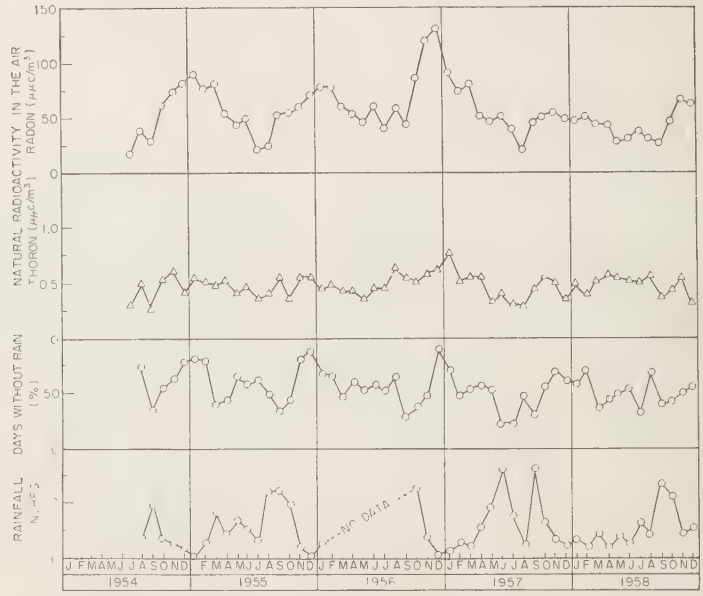

Fig. 2—Natural radioactivity in the air at Yokosuka, Japan, 1954–1958.

fission-product concentration in the air with that of the naturally occurring radon, as determined from measurement of its decay products. The radon level is variable, as can be seen from these averages and from Figure 2, where a plot of the monthly average radon concentrations is presented. Over the past four years the fission products averaged about 2.3 per cent of the radon activity, though during 1958 this percentage rose to 6.9. To get the relative contribution of fission products to the external dosage of γ-radiation which is received from all airborne radioactive matter, it is necessary to correct both for the number and the energy of γ-rays emitted by the short-lived radioactive descendents of radon and by the fission products. This has not been done. In any case, the relative dosage will be less by a factor of 2 or more than the activity ratio indicated above. Both the natural and the fission-product activity recorded in the Washington, D. C., area are generally considerably higher than at Yokosuka [*Lockhart and others*, 1958].

An attempt has been made to correlate the radioactivity data obtained at Yokosuka with the data reported in several Japanese publica tions. Data obtained by the operational net work of air monitor stations in Japan [*Centra Meteorol. Obs.*, 1955–1956] were not directl comparable with our data. There was no Japan ese station located at Yokosuka, and ther were differences in sampling times; further it is felt that relatively large errors were inher ent in the measurements made at these station because of the small volume of air sampled Better correlations were obtained with severa of the more comprehensive measurements re ported by *Tajima and Dôke* [1956] and b *Yano and Naruse* [1956].

Tajima and Dôke reported the gross fission product activity of the air at Tokyo to hav been 3 to 6 $\times$ 10^{-15} curies per liter (3 to 6 μ c/m^3) on April 12, 1955, with the activity re maining high during the period from Apr 12 to 15. Our comparable measurements a Yokosuka (about 20 miles southeast of Tokyo showed a maximum of 9.8 $\mu\mu$ c/m^3 for th collection ending at 1630 on April 11, 195 with high values during the period from Apr 11 to 14. These results are in reasonable agree ment when we consider the distance betwee

llection sites and the different procedures ployed.

Yano and Naruse reported high values of tificial radioactivity in atmospheric dust at kyo during the period from November 4 to 1954, with a maximum on November 5 and definite minimum on November 20—a rainy y. Our equipment at Yokosuka indicated a aximum of 10.6 $\mu\mu$ c/m^3 for the 24-hour llection ending at 1630 on November 5, with gh values during the period from November to 11. A minimum reading was likewise ob-ined on November 20 during a rainy period.

It has long been known that rain is the prime echanism by which the atmosphere is cleansed particulate matter. In fact, as long ago as 948 rain scavenging of fission products from ie atmosphere was under investigation at RL. Some information on the removal pro-ss and the lifetime of natural radioactivity in ne air was reported by *Blifford and others* 1952]. As a consequence of this interest, the don levels in the air at Yokosuka have been xamined for a possible correlation with rain ata. In Figure 2 are presented curves showing ne monthly average radon (RaB) and thoron ThB) concentrations, the rainfall in inches, nd the percentage of days without rain. Both f the natural radioactive products show sea-onal changes which are inversely related to eriods of rainfall and to the quantity of rain. The correlation is only a general one, however, nd it indicates that other meteorological param-ters are influencing both of these measure-nents. This was also evident from inspection f the daily radon levels as reported by *Lock-art and others* [1958].

The great variations in the radon level dur-ng the period of these measurements means hat measurements must be continued over a number of years before a satisfactory mean of natural radioactivity can be established for Yokosuka, or perhaps any other area. Natural radioactivity levels evidently require a statistical study, as do most other meteorological parameters.

Conclusions — Several conclusions are evident from the data presented: There are wide day-to-day variations in the level of both fission products and natural radioactive isotopes in the air at Yokosuka; the natural radioactivity of the air shows a general inverse relationship to the precipitation; the radioactivity of the air due to the fission-product concentration is negligible when compared with the total activity (this is even more evident when the total activity of its decay products are added to that of the radon); and finally, the average fission product concentration in the air has changed markedly during the past four years as the result of the increased incidence of nuclear testing.

References

Blifford, I. H., Jr., H. Friedman, L. B. Lockhart, Jr., and R. A. Baus, Geographical and time distribution of radioactivity in the air, *J. Atmospheric and Terrest. Phys., 9,* 1–17, 1956.

Blifford, I. H., Jr., L. B. Lockhart, Jr., and H. B. Rosenstock, On the natural radioactivity in the air, *J. Geophys. Research, 57,* 499–509, 1952.

Central Meteorological Observatory, Tokyo, *Bull. Atmospheric Radioactivity* (1955–1956, issued quarterly).

Lockhart, L. B., Jr., R. A. Baus, R. L. Patterson, Jr., and I. H. Blifford, Jr., Some measurements of the radioactivity of the air during 1957, *U. S. Naval Research Lab. Rept. 5208,* October 1958.

Tajima, Eizo and Tadayoshi Dôke, The airborne radioactivity, *Research in the Effects and Influences of the Nuclear Bomb Test Explosions,* Japan. Soc. Promotion Sci., Ueno, Tokyo, 1956.

Yano, Naoshi, and Hiroshi Naruse, Artificial radioactive dust—referring radioactive contamination in November 1954, *Research in the Effects and Influences of the Nuclear Bomb Test Explosions,* Japan. Soc. Promotion Sci., Ueno, Tokyo, 1956.

(Manuscript received June 1, 1959.)

Coastal and Inland Weather Contrasts in the Canadian Arctic[1]

C. I. JACKSON[2]

Department of Geography
McGill University, Montreal, Quebec

Abstract—A record of surface weather was maintained at the Canadian IGY base at Lake Hazen, Ellesmere Island, from August 1957 to August 1958. This is the first such record from the interior of any of the Canadian Arctic Islands and shows great differences from the permanent stations on the coasts. Winter temperatures were very much colder, and winds were very light, even during severe gales elsewhere. It is suggested that a continuing record from this or a similar location would be of great value, particularly if upper air soundings were also made.

The establishment of five permanent Canadian–United States weather stations in the Queen Elizabeth Islands of the Canadian Arctic has been of great value for high-latitude synoptic analysis. The stations are also providing continuous surface data and, finally, have been used as bases for general scientific studies in their vicinities.

None of the stations, however, were sited away from tidewater, and the surface records are essentially those of arctic maritime stations. On Ellesmere Island, for example, Eureka is located on an arm of Eureka Sound, 8 feet above sea-level on the west coast. Alert, on the north coast, is about a mile inland and 218 feet above sea level. All the earlier expeditions which made major contributions to the scientific discovery of the island—the British Admiralty Expedition of 1875–1876 under Nares [*Great Britain, Parliamentary Papers,* 1877], the American First Polar Year Expedition 1881–1883 led by *Greely* [1888], and Sverdrup's Second *Fram* Expedition 1898–1902 [*Mohn* 1907–1919]—were based at different points on the coast, and references to the weather experienced inland are generally few. The record of surface weather maintained at the Canadian IGY Expedition Base Camp at Lake Hazen from August 20, 1957, to August 10, 1958, is the first record from an inland station on any of the Canadian Arctic Islands for so long a period.

The Lake Hazen station was approximately 100 miles southwest of Alert and 220 miles northeast of Eureka, at 81°49′N, 71°18′W, and 528 feet above sea level. The lake itself, which is about 45 miles long, 7½ miles wide, and very deep, lies in a trough trending approximately northeast-southwest. On the northwest side of the lake, rising behind the Base Camp, is the Garfield Range, with peaks at about 3300 feet; on the southeast side is the much lower Greely-Hazen plateau. This is ice-free, whereas behind the Garfield Range lies a considerable icefield. Navigable tidewater extends to about 20 miles from the lake at the head of Chandler Fiord, but the station is far enough from the open sea to have a distinctly 'inland' climate.

Three-hourly observations were maintained throughout the period according to the practices of the Canadian Meteorological Service, and a microfilm copy of the records is deposited at its head office in Toronto. An extensive discussion of the records is being prepared by the author.

Of the various climatic parameters measured or observed at Lake Hazen undoubtedly the most significant were temperature and wind. It is these which provide the greatest contrasts with Alert and Eureka on the coasts and which, separately and in combination, are of most significance for human habitation in the Lake Hazen area.

The first few years of records from the Joint

[1] Sponsored by the Defence Research Board of Canada and based on a paper presented to a joint meeting of the Union and the American Meteorological Society, Washington, D. C., May 4–7 1959.

[2] Present address: 172, Forest Lane, Harrogate, Yorkshire, England.

TABLE 1—*Frequencies of temperatures below various limits*

Alert and Lake Hazen: August 21, 1957, to August 10, 1958; Eureka: September 1, 1957, to August 10 1958.

Limits	Lake Hazen		Eureka		Alert	
	Days in limits	In and below limits	Days in limits	In and below limits	Days in limits	In and below limits
Below freezing	294	...	289	...	320	...
0 to −20°F	38	225	33	204	62	206
−20 to −40	66	187	88	171	115	144
−40 to −50	48	121	57	83	28	29
−50 to −60	63	73	24	26	1	1
Below −60	10	10	2	2	0	0

Weather Stations have indicated that the cold pole of North America is in the vicinity of Ellesmere Island and not in the Barren Grounds of the continental mainland. Table 1 shows that very cold temperatures during the long winter are even more common inland than the coastal stations would suggest. The temperature reached −50°F on only 1 day at Alert during the winter of 1957–1958, but on 73 days at Lake Hazen, whereas temperatures of −40°F or below were recorded at the inland station on exactly one-third of the days in the year. The period of observations included the month of January 1958, which was remarkable for the high temperatures in the Canadian Arctic [*Thomas and Titus* 1958]. Freezing rain and above-freezing temperatures were recorded at Alert, and there can be no doubt that the number of days with very low temperatures would be considerably greater in a more normal winter. As the summers are generally cool (the maximum temperature at Lake Hazen in 1958 was only 59.2; in 1957, as recorded by an advance party, it was 62), the mean annual temperature in 1957–1958 of about −6°F makes it one of the coldest ice-free areas on earth.

To some extent these low temperatures are a result of the location of the inland station. Situated close to the foot of a mountain range, with an icefield behind, Lake Hazen is at the bottom of a gigantic frost hollow. But more important than the nearness of the mountains is the lack of moderate or strong winds which normally do much to 'roll up' an inversion by mechanical turbulence. The record of wind at Lake Hazen shows a remarkable number of calms and light winds, and presents even more of a contras with the coasts than the temperature record The lack of wind, it must be stressed, was no due to the poor exposure of the anemometer The presence of the mountains in the quadran between west and north might lead one t expect underrepresentation from that direction but otherwise the winds have a practically un interrupted flow along or across the lake. Ye 58 per cent of the more than 2800 three-hourl observations recorded either calms or winds o 1 mph. The months of November and Decem ber 1957 and February and March 1958 had a average of 66 per cent of calms, and wind above 20 mph were recorded only in Augus 1957 and January and July 1958. Winds of 2 mph or more occurred at 243 synoptic observa tions during the same period at Eureka and o 309 occasions at Alert, representing 11 per cen of all observations. The total number of oc casions at Lake Hazen was only 29, and 17 o these were in late August 1957. On several oc casions winds of 70 mph or more were recorde at Alert and Eureka, whereas Lake Hazer between them, recorded little or no air move ment. Even during the exceptional gale o January 1958, seventy-five years to the da after Greely's similar experience at Fort Conge practically calm conditions were recorded a Lake Hazen for 24 hours after the wind at Ale reached a steady speed of 40 mph and not unt it had risen to 90 mph on the coast did th wind reach 10 to 15 mph at Lake Hazen.

The reasons for this great contrast remai essentially unknown. It was at first believe that the strong winds on the coast, particularl

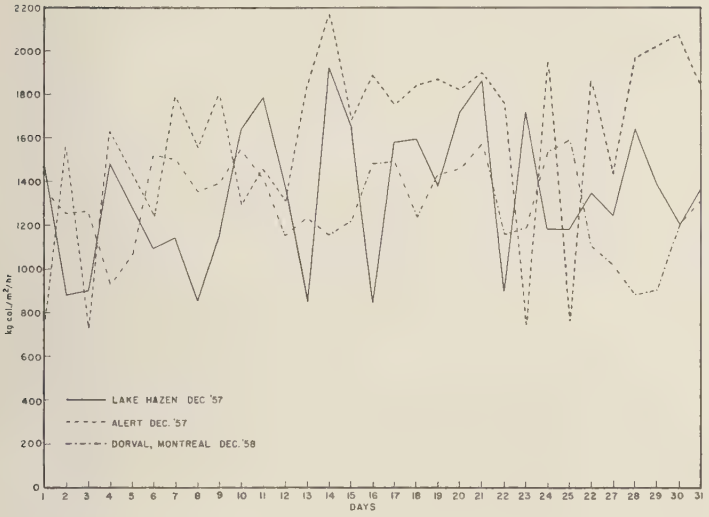

FIG. 1—Comparative values of windchill.

; Alert, might be local features peculiar to the ea of the weather stations. An examination of noptic maps, however, has shown that on ost occasions the high winds were associated ith strong pressure gradients and it is the ake Hazen station that is anomalous. *Wilson nd Markham* [1957] have in fact shown that ie ratio of surface to gradient wind at Alert relatively low. As the Lake Hazen station had either pilot balloon nor rawinsonde equipment ie height to which these calm conditions con- nue above the station is not known, but it is gnificant that snow lay apparently undis- rbed on the slopes of "Mount McGill," behind ie station, until it was blown off during the anuary gale. Therefore, fairly calm conditions ust be normal up to at least 3000 feet above ea level (about 900 mb).

The combination of these two elements, tem- erature and wind, is important from the uman aspect. There can be no doubt that, espite the very much colder temperatures, ving conditions are very much more pleasant t the inland site than on the exposed and indswept coast near Alert. Figure 1 shows indchill values for December 1957 at Alert nd Lake Hazen and, for comparison, for De- ember 1958 at Montreal Airport. The monthly ean temperatures were, respectively, −32°F, −48°F, and +11°F. The values shown in the figure are the highest windchills at any of the 8 observations made each day. It is apparent that the very much lower temperatures at Lake Hazen are balanced by the lack of wind; the great fluctuations in the curve for that station represent the difference between days of absolute calm and those with light winds. The usual values throughout the winter were between 1200 and 1400 units, relatively low values.

Although living conditions at a small station are hence usually favorable, the same conditions of low temperatures and light winds present a handicap to a larger installation, especially one involving frequent aircraft movements, because of the liability to ice fog. *Appleman* [1953] investigated the conditions under which such fogs develop; Figure 2 summarizes his findings. It will be seen that at a station such as Lake Hazen, where very low temperatures are a practically constant feature during the winter, the presence of hydrocarbon nuclei from heating units or aircraft engines would cause condensation and persistent ice fogs. These would be made worse by the lack of sufficient wind to disperse them. The only aircraft to visit Lake Hazen during the winter of 1957–1958, a C-130A Hercules of the U. S. Air Force, caused an ice

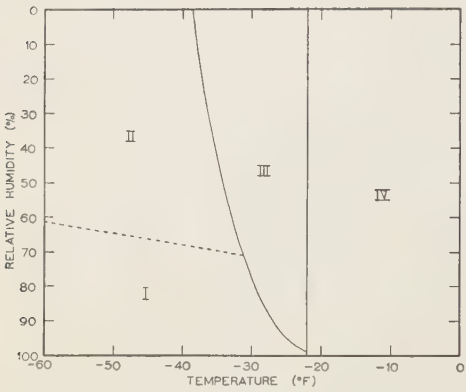

FIG. 2—Conditions necessary for the formation of ice fog (after Appleman).

I. Region of persistent ice fogs; atmosphere supersaturated with respect to ice.

II. Region of nonpersistent ice fogs; atmosphere subsaturated with respect to ice.

III. Region of no ice fog; combustion causes drying of atmosphere.

IV. Region of no ice fog; combustion causes drying of atmosphere; droplets will not freeze.

fog to develop on takeoff which did not clear for more than 4 hours.

Precipitation amounts at the three stations during the period are summarized in Table 2. Alert clearly had a much greater snowfall, and in particular a much greater rainfall, than either Eureka or Lake Hazen. The differences between Eureka and Lake Hazen are not so great as at first appears. Most of the excess snowfall at Eureka occurred in 1 month, September 1957, and on 1 day, September 2, the amount was one-quarter of the total throughout the 11 months and 10 days considered.

In Table 2 the measurable precipitation is slightly less than 1 inch at Lake Hazen, whereas the total fall was probably about 1.5 inches. The difference is contained in the 'traces' of precipitation, 187 in all, which did not reach a measurable amount (greater than 0.005 inch water equivalent). These traces are to a large extent due to the Canadian practice of taking measurements every 6 hours, and it seems desirable that this interval should be considerably longer in the Arctic, as clearly a significant proportion of the total fall goes unrecorded.

During the summers of 1957 and 1958, a glacial-meteorological station was maintained on the Gilman Glacier, about 20 miles north of the Base Camp and 3400 feet above sea level. *Sagar* [1959] has drawn attention to the contrast between the two stations in the matter of summer precipitation. Totals between May 5 and August 10, 1958, were 1.42 inches on the glacier and 0.17 inch by the lake, of which snow accounted for 1.11 inches and 0.10 inch (water equivalents) respectively. A study of synoptic conditions in the periods when the major falls took place showed that the precipitation was of essentially orographic origin. Occasional fronts were present, approaching Ellesmere Island either from the west or the south, but they would have had little effect had it not been for the presence of the mountains. The other lowland stations, Alert and Eureka, show few similarities to the Gilman Glacier, and the high rainfall at Alert is a product of the low cloud and fog which are frequent along the north coast in summer.

A study of the months of December 1957 and January 1958 revealed several features of interest concerning the relation of events in the lower troposphere to surface weather in midwinter. In particular, it showed that the mos

TABLE 2—*Precipitation during 1957–1958*

Station	Total, in.	Total days trace or more	Total days more than trace	(4) as percentage of (3)	Total rain, in.	(6) as percentage of (2)
(1)	(2)	(3)	(4)	(5)	(6)	(7)
Lake Hazen	0.98	134	39	29.1	0.07	7.1
Eureka	2.07	169	49	29.0	0.10	4.8
Alert	4.52	171	95	55.6	0.84	18.6

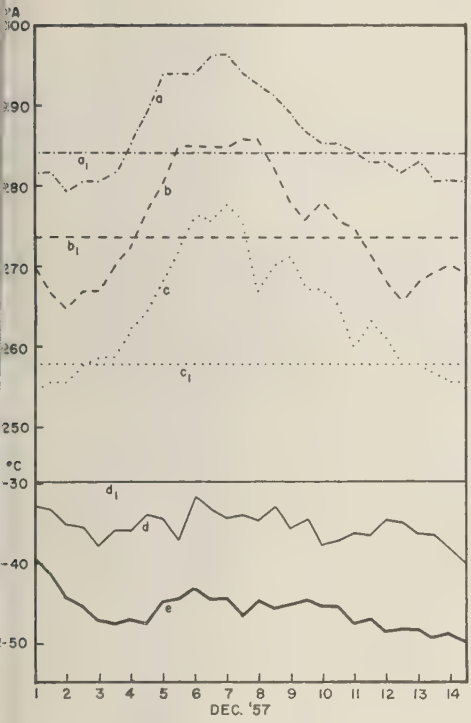

FIG. 3—Tropospheric warming in early December 1957. *a, b,* and *c* are twice-daily values of potential temperature over Alert at 500, 700, and 850 mb, respectively; *d* is the actual surface temperature; a_1–d_1 are mean December values, 1950–1953, for the various levels; *e* is the actual surface temperature at Lake Hazen.

important requirements for a rise in temperature at the surface are light surface winds or the presence of a cloud cover. A surface wind will cause mixing of the cold air near the ground with the warmer air aloft, and a cloud cover, or falling snow, will raise the surface temperature by long-wave radiation. By contrast, a warm lower troposphere by itself has little effect. Figure 3 shows conditions at Alert and Lake Hazen during the first half of December 1957. The free air over Alert was considerably warmer than is usual in December [*Canada, Department of Transport,* 1955]. The cause of the warmth, however, was subsidence in a polar anticyclone, and, lacking either surface winds or clouds, surface temperatures at both Alert and Lake Hazen were unaffected.

Another result of this synoptic study was to show that a considerable proportion of the midwinter snowfall of northern Ellesmere Island appears to be derived from the area of the Norwegian Sea, the moist air reaching Alert and Lake Hazen by way of north Greenland. At this period it is the nearest source of extensive open water and appears to have a significant effect on winter weather, although in summer disturbances from Baffin Bay or the Pacific-Alaskan region are much more important.

Conclusion—This summary of the results of a year's record from Lake Hazen has shown that contrasts between the coast and interior of Ellesmere Island are greater than might have been expected. The combination of low temperatures and light winds, particularly in winter, has considerable importance for human occupation. It is apparent that a continued record, including some form of upper-wind measurements, would be of considerable value.

REFERENCES

APPLEMAN, H., The cause and forecasting of ice fogs, *Bull. Am. Meteorol. Soc., 34,* 397–400, 1953.

CANADA, DEPARTMENT OF TRANSPORT, METEOROLOGICAL DIVISION, *Climatological Summary, Alert, N. W. T, Canada, June 1950–December 1953,* Toronto, 71 pp., 1955.

GREAT BRITAIN, PARLIAMENTARY PAPERS, *Journals and Proceedings of the Arctic Expedition 1875–76 under the Command of Capt. Sir George S. Nares,* LVI, 1877.

GREELY, ADOLPHUS WASHINGTON, *Report on the Proceedings of the U. S. Expedition to Lady Franklin Bay, Grinnell Land,* Govt. Printing Office, Washington, D. C., 2 vols., 1888.

MOHN, H., Meteorology, 389 pp., in *Norske Videnskaps-akad. Oslo,* 'Report of the Second Norwegian Arctic Expedition in the *Fram* 1898–1902', Vol. I, Kristiania, 1907–1919.

SAGAR, R. B., *Glacial-Meteorological Studies in North Ellesmere Island, 1958,* M.Sc. thesis, McGill University, Montreal, 181 pp., 1959.

THOMAS, MORLEY K., AND T. L. TITUS, Abnormally mild temperatures in the Canadian Arctic during January 1958, *Monthly Weather Rev., 86,* 19–22, 1958.

WILSON, H. P., AND W. E. MARKHAN, *A Study of Arctic Surface Winds,* CIR–2923, TEC–251, Canada, Dept. of Transport, Meteorological Branch, 1957.

(Manuscript received July 13, 1959.)

Underground Nuclear Detonations[1]

G. W. JOHNSON, G. H. HIGGINS, AND C. E. VIOLET

Lawrence Radiation Laboratory, University of California
Livermore, California

Abstract—Since 1952 eight nuclear explosions have been fired underground at the Atomic Energy Commission's Nevada Test Site. The explosions varied in energy release from 55 tons to 19,000 tons of TNT equivalent. Depths of burial varied from shallow, to produce cratering, to deep, where no visible effects appeared on the surface. The major experimental data from these explosions, as well as the phenomenology of the deeper shots, are summarized here.

INTRODUCTION

In 1955, during the nuclear weapons test series in Nevada, it became increasingly clear to the Lawrence Radiation Laboratory that concern over fallout would impose serious limitations on future weapons tests. Therefore, based on a suggestion of *Griggs and Teller* [1956], consideration was given to the possibility of underground testing at such depths that there would be no escape of radioactivity to the atmosphere. Further detailed consideration led to the design of an experiment, code-named Rainier, to test the feasibility of containment of the radioactive debris from a nuclear explosion. This experiment, conducted on September 19, 1957, was completely successful and all objectives of the experiment were achieved. The results of this 1.7-kiloton detonation have been previously reported in considerable detail [*Johnson and others,* 1958; *Johnson and Violet,* 1958; *Diment and others,* 1959]. Continued study has led to a fairly complete understanding of the physical and chemical processes associated with underground nuclear explosions. Subsequent to the Rainier detonation, five additional nuclear devices were fired underground at the Nevada Test Site during October 1958 in connection with weapons development programs. The preliminary results of these later explosions have been published [*Johnson and Violet,* 1958].

In this paper all major results presently available from these shots, as well as from three earlier cratering shots, are summarized, and the phenomenology of these events is discussed.

EXPERIMENTAL CONDITIONS

All the explosions, except the earlier cratering shots, took place in a thick formation of bedded tuffs. The three exceptions, which were detonated in a lightly cemented alluvium, will not be described in detail but are included for completeness. The coordinates and time of detonation for each explosion are listed in Table 1.

The geological structure in which the deep shots took place is characterized by 250 ft of welded tuff under which is 1700 ft of bedded tuffs and a thick bed of dolomite [*Diment and others,* 1958a]. The locations of the several shot points are illustrated in Figure 1. A stratigraphic feature of some importance in interpretation is the loosely consolidated zone in Tos_7, the limits of which are indicated by dashed lines in Figure 1. Rainier, Evans, Tamalpais, and Neptune were detonated in this lithologic unit about 100 ft below this lower limit. Blanca and Logan were donated in Tos_8 about 600 ft below this limit.

Physical and chemical properties of the medium, averaged in the vicinity of the Logan, Blanca, and Rainier detonation points, based on U. S. Geological Survey data, are listed in Tables 2 through 7.

GENERAL RESULTS

The gross results of the explosions will be described in terms of the visible behavior in the vicinity of the shot point, the escape of radioactivity, the air blast, and the ground

[1] This work was performed under auspices of the U. S. Atomic Energy Commission.

TABLE 1—*List of events, dates, times and locations of explosions*

Event	Date	Time (UT)	N Latitude ° ′ ″	W Longitude ° ′ ″	Elevation (ft)
Jangle-S	19 Nov. 51	1659:59.72	37 07 54	116 02 19	4214
Jangle-U	29 Nov. 51	1959:59.72	37 10 11	116 02 33	4298
Teapot-Ess	23 Mar. 55	2030:00.01	37 10 06	116 02 38	4226
Neptune	14 Oct. 58	1800:00.15	37 11 37.88	116 11 58.88	6716
Blanca	30 Oct. 58	1500:00.15	37 11 09.36	116 12 07.28	6138
Logan	16 Oct. 58	0600:00.140	37 11 03.03	116 12 04.04	6141
Rainier	19 Sept. 57	1659:59.454	37 11 44.800	116 12 11.35	6615
Tamalpais	8 Oct. 58	2200:00.131	37 11 43.10	116 12 01.64	6616
Evans	29 Oct. 58	0000:00.15	37 11 41.46	116 12 17.03	6620

shock. The explosions are listed in order of increasing scaled depth in Table 8. The scaled depth is defined as $D/W^{1/3}$, where D is the actual depth in feet and W is the energy release in kilotons (kt) of TNT equivalent. The depth D in the table is the distance to the nearest point on the surface. The column in the table entitled 'Measured radioactivity deposited on surface' represents the percentages of the total radioactivity which appeared on the surface, neglecting possible enrichment of particular isotopes.

One kiloton of TNT equivalent is defined as the prompt release of 10^{12} calories of energy (4.2×10^{19} ergs). This energy is determined by multiplying the number of fissions, as measured radiochemically, by the prompt energy release (179 Mev or 2.86×10^{4} ergs per fission). Prompt energy is the sum of the kinetic energy of the fission fragments, and the prompt neutron and prompt gamma-ray energies. The delayed release of energy due to radioactivity decay amounts to another 22 Mev per fission. About 15 Mev of this energy appears eventually as heat, of which about 7 Mev is released in the first 20 min.

Escape of radioactivity—In discussing the effectiveness of containment of radioactivity it is necessary to examine not only the escape through the surrounding formation but also the success of the stemming in the tunnels. For Rainier (1.7 kt) and Logan (5.0 kt) there was

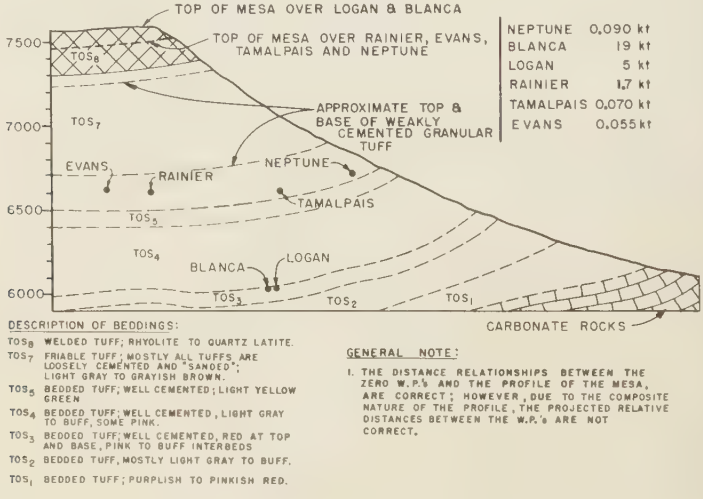

FIG. 1—Profile of mesa showing zero sites.

TABLE 2—*Average values of density, porosity and water content.*

Item	Logan*§	Blanca†§	Rainier‡§
ry bulk ensity m/cm³) atural state ılk density m/cm³) rain density m/cm³) orosity er cent) ater content veight r cent)	1.8±0.3 2.1±0.2 2.6±0.1 30.6±7.4 14.5±3.5	1.6±0.2 1.9±0.2 2.4±0.1 33.2±6.0 17.5±3.5	1.7±0.2 2.0±0.2 2.3±0.2 24.4±7.0 15.3±3.5

**Diment and others* [1958b].
†Unpublished USGS report.
‡*Diment and others* [1959].
§Errors are standard deviations.

TABLE 3—*Average chemical composition*

Constituent	Percentage by weight for air-dry samples	
	Logan*	Rainier†
SiO_2	71.5	66.9
Al_2O_3	13.0	12.3
CaO	0.7	2.3
Fe_2O_3	1.8	2.2
MgO	0.4	1.0
Na_2O	1.3	1.3
K_2O	6.6	2.2
H_2O	4.5	10.6
Balance	0.2	1.2

**Diment and others* [1958b].
†*Diment and others* [1959].

o detectable escape of radioactivity to the tmosphere or into the tunnels. For Blanca 19 kt) a chimney developed to the surface nd broke out 15 sec after the detonation. The loud rose about 1000 ft and deposited radio- ctivity on the ground. On integration of the adioactivity in the surveyed area it was found nat 0.3 to 0.5 per cent of the gross radioactivity ad escaped and had been deposited locally. olatile isotopes were enriched several-fold in ne vented radioactivity.

The tunnels collapsed at radii of 200 ft (Rai-

TABLE 4—*Mineral composition*

Mineral	Percentage by volume	
	Logan and Blanca*	Rainier†
Phenocrysts	19.4	17.4
Quartz	6.9	2.6
Alkali feldspar	5.6	6.1
Plagioclase	6.0	6.8
Biotite	0.5	1.3
Pyroxene and amphibole	...	0.2
Magnetite	0.4	0.4
Xenoliths	1.6	6.7
Shards and lapilli matrix	70.7	68.4
Heulandite	not differentiated	23
Montmorillomite	not differentiated	12
β-Cristobalite	not differentiated	11
Amorphous material	not differentiated	22
Vesicles	8.3	7.5

*Unpublished USGS report.
†*Diment and others* [1959].

TABLE 5—*Thermal properties*

A. Specific heat* for Rainier tuff (cal/gram/°C)†

Water content (grams H_2O/ grams dry sample)	Temperature °C				
	25	100	200	400	600
0	0.18	0.21	0.24	0.27	0.30
.15	0.28	0.31	...	...	...
.20	0.31	0.33	...	...	...
.30	0.34	0.36	...	...	...

B. Thermal conductivity (cal/cm²/sec/°C/cm)‡

	Rainier	Logan
Dry	0.0011	0.0014
Wet	0.0016	0.0020

C. Melting Range: 850 to 1500°C
D. Estimated enthalpy to molten state (≈1500°C): 700 cal/gm
Estimated enthalpy to vapor state (≈3000°C): 3000 cal/gm

*Calculated from chemical analysis. Does not include heat of vaporization of water.
†*Warner and Violet* [1959].
‡*Diment and others* [1958a].

TABLE 6—*Average values of strength and elastic properties*

A. Static tensile properties of Rainier tuff*

Air-dry tensile strength (psi)	165
Air-dry Young's modulus (psi)	0.46×10^6
Air-dry Poisson's ratio	0.12
Calculated rigidity modulus (psi)	0.22×10^6

B. Static compressive properties of Rainier tuff*

	Air dry	Natural state	Natural state under hydrostatic pressure 1000 psi
Compressive strength (psi)	4700	1200	5100
Young's modulus (psi)	1.1×10^6	0.18×10^6	0.37×10^6
Poisson's ratio	0.11		
Calculated rigidity modulus (psi)	0.50×10^6		

C. Dynamic properties of Rainier tuff†

f_L	f_T	b	v_L	v_T	$E \times 10^6$	$G \times 10^6$	σ
5900	4000	0.1	7940	5380	1.07	0.49	0.09

f is resonant frequency (cps)
L and T are longitudinal and torsional modes, respectively
b is specific damping capacity determined from width of resonance amplitude curve
v is calculated acoustic velocity (ft/sec)
E is calculated Young's modulus (psi)
G is calculated rigidity modulus (psi)
σ is calculated Poisson's ratio

D. Bulk modulus of Rainier tuff (psi)‡

	Unjacketed	Jacketed
Water-saturated sample	5.7×10^6	0.54×10^6
Average oven-dry sample	4.8×10^6	0.41×10^6

**Diment and others* (1959)
†*Diment and others* (1958a)
‡*Warner and Violet* (1959)

nier), 820 ft (Logan), and 850 ft (Blanca) from their respective centers of detonation. There was no detectable leak of radioactivity into the tunnels from any of these explosions. On digging back into the sites it was found that radioactivity had been projected down the tunnels 600 ft for Blanca and 190 ft for Logan.

From this experience it has been demonstrated that the radioactivity released by nuclear explosions can be successfully contained underground. It may be seen from Table 8 that the escape of radioactivity is small at a scaled depth of 300 $W^{1/3}$, and at a scaled depth of 500 $W^{1/3}$ it was not detectable.

Neptune, Teapot-Ess, Jangle-U, and Jangle-S all produced craters and released radioactivity to the atmosphere. In all these cases almost all of the radioactivity that escaped returned t earth within a few miles. For Neptune only per cent of the radioactivity escaped and wa deposited near the crater, although the volatil isotopes and those isotopes with gaseous pre cursors were enriched several-fold, as noted fo Blanca.

Local effects—The ground motion from Ra nier was barely felt at 2.5 miles and that fro Blanca at 16 miles. There was no structur damage to tunnels or to facilities at or beyon 2500 ft from Blanca. These facilities include a major electronic recording station and a ver tilation blower system for the tunnel. These ob servations give a rough indication of damag radii.

The airblast effects for all shots at scale

TABLE 7—*Miscellaneous properties of Rainier tuff*

A. Porosity at elevated pressures, (average of 2 samples of 28 per cent porosity).*

Pressure (psi)	0	1000	2000	3000	4000
Reduction in porosity (per cent)	0	6	8	10	12

B. Permeability to air (millidarcies)* to brine (millidarcies)

	Average†	Range‡	Average	Range
Rainier	6.0	0.95–41	1.4	0.084–27
Logan	0.81	0.14–2.4	0.036	0.00076–0.24

C. Seismic velocity, vertical distribution over Rainier.§

Interval depth below surface (ft)	Interval velocity (ft/sec)	Distance above Rainier shot room (ft)‖
230 to 270	7,150	665 to 625
270 to 310	13,700	625 to 585
310 to 395	6,650	585 to 500
395 to 525	7,070	500 to 370
525 to 675	7,180	370 to 220
675 to 775	5,850	220 to 120

**Warner and Violet* [1959].
†Averages are computed assuming log-normal distribution.
‡Ranges are the total ranges of values observed.
§*Swift and Sachs* [1959].
‖Shot room at 895 ft depth

TABLE 8—*Major features of underground nuclear explosions*

Event	Yield W (kt)	Medium	Depth D (ft)	Scaled depth ($D/W^{1/3}$)	Measured radioactivity deposited on surface (per cent)	Crater volume (yd^3)	Crater volume/kt (yd^3/kt)
Jangle-S	1.2±0.1	Alluvium	−3.5*	−3.3*	>65	1,650	1,400
Jangle-U	1.2±0.1	Alluvium	17	16	>80	37,000	31,000
Teapot-Ess	1.2±0.1	Alluvium	67	63	90	96,000	80,000
Neptune	0.090±.020	Bedded tuff	99	220	1–2	33,000	370,000†
Blanca	19.0±1.5	Bedded tuff	835	310	<0.5	0	0
Logan	$5.0^{+0.2}_{-0.4}$	Bedded tuff	830	485	0	0	0
Rainier	1.7±0.1	Bedded tuff	790	670	0	0	0
Tamalpais	0.072±.010	Bedded tuff	330	780	0‡	0	0
Evans	0.055±.030	Bedded tuff	840	2200	0§	0	0

*3.5 feet *above* surface.
†This explosion took place in bedded tuff under a sloping surface 1:3, hence the crater is probably larger than would be expected on a level surface.
‡No breakthrough to surface but radioactive gases in large quantities leaked into the tunnel.
§No breakthrough to surface but stemming failed, releasing gross fission activity into the tunnel.

depths of 200 $W^{1/3}$ or greater were negligible. These explosions were not audible at a distance of 2.5 miles, although some individuals reported hearing a dull boom from Rainier. While the explosions were not heard by ear, signals were detected by microbarographs in several locations, (Jack W. Reed, Sandia Corp., private communication).

The details of fracturing and bedding-plane shifts were mapped and have been described elsewhere [*Diment and others*, 1959; R. M. Foose and R. B. Hoy, Stanford Research Insti-

tute, private communication]. For Blanca a major section of the top of the mesa shifted down the slope and formed a scarp about 70 ft high.

Earth motion—Acceleration and displacement measurements for Rainier by the Stanford Research Institute [*Swift and Sachs,* 1959], Edgerton, Germeshausen and Grier, Inc. [1958]; and Sandia Corporation [*Perret,* 1958] indicated that a large earth cap beginning approximately 180 ft below the mesa surface separated from the mesa over the charge and subsequently fell back into place. The only significant vertical displacement occurred at or near surface zero and reached a maximum of 1 ft. The peak acceleration at surface zero was 6 g at 186 msec after zero time.

For Blanca [*Swift and others,* 1959; *Morris and Schneiderhan,* 1959; *Perret,* to be published], the accelerations measured on the mesa surface show vertical maxima that are consistently larger than the horizontal. The mesa surface directly above the Blanca detonation point was displaced vertically approximately 30 inches in about 400 msec.

Seismic signals from the Rainier event were detected at various stations in the continental United States and at distances up to 1000 miles [*Diment and others,* 1959; *Carder and others,* 1958]. Seismic signals were also detected (though barely resolved) at College Station in Fairbanks, Alaska, at a distance of 2200 miles.

Seismic effects [*Carder and others,* 1959, *Romney,* 1959] resulting from Blanca, Logan, Tamalpais, and events of Hardtack Phase-II underground explosions were measured by strong-motion and teleseismic seismographs out to distances of nearly 100 miles. In addition, many temporary seismographs were operated by a number of organizations to distances of nearly 2400 miles, and records from all over the world were available from regular seismograph stations.

Preliminary results indicate that the seismic effects were consistent with empirical formulas developed from Rainier data, except that attenuation of surface waves beyond 200 km may have been higher than the formula for that distance would indicate. Results obtained from the smaller shots require considerably more thought before appraisal. Preliminary seismic data on Logan, for example, indicate that the fraction of energy in the seismic waves is about twice as large as expected from the Rainier formulas.

Detailed Local Results

Of the underground explosions, the first one, Rainier, has been studied in the most detail and

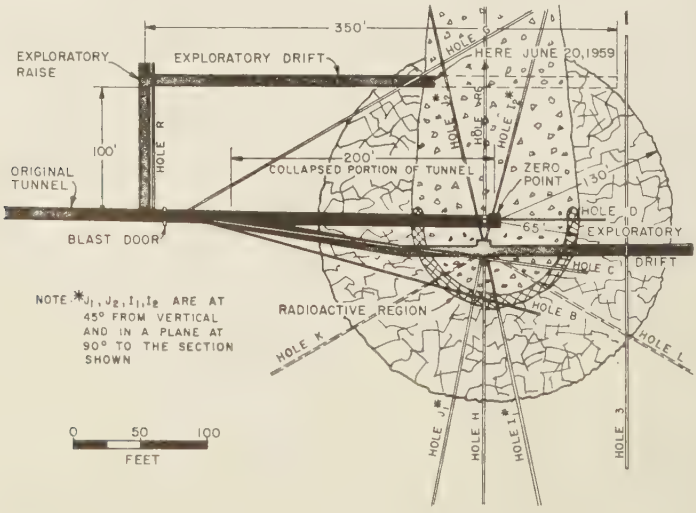

Fig. 2—Drifts and drill holes for post-shot studies of Rainier.

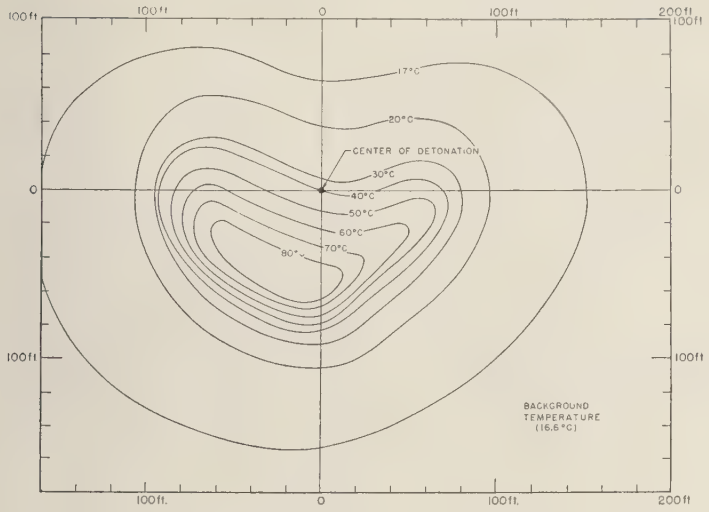

FIG. 3—Temperature distribution of Rainier, five months after detonation.

provides most of the data from which a model has been developed. Radioactivity and temperature distributions were determined by drilling and logging a series of holes through the active region. Cores were also recovered and analyses were made of their chemical, radiochemical, and physical properties. Similar work, although not in so much detail, has been accomplished for the other explosions. In addition to drilling, two drifts have been driven through the Rainier shot zone. One drift passed about 25 ft below and one about 100 ft above the center of detonation. The layout of drill holes and drifts is shown in Figure 2. Explorations by means of drill holes permitted the determination of the properties of the medium surrounding the center of the explosion.

Temperature distribution—The temperature distribution [*Goodale and others,* 1958; *Olsen and others,* 1959] for Rainier, measured five months after detonation, is shown in Figure 3.

The energy-content within the various isothermal contours calculated with a mean specific heat of 0.3 cal/gm/°C is listed in Table 9.

The maximum temperature measured within the 80°C contour was 94°C, which is the boiling point of water at the altitude of the explosion.

The temperature distributions for the other explosions have not yet been determined as completely as for Rainier, but at least one hole has been logged for each. The general features of the distributions, such as the geometry and the maximum temperatures observed, were similar to those of Rainier. For Logan and Blanca the minor asymmetry in the temperatures and radiation distributions indicates that there was movement of some of the gases along fissures and in the direction of the tunnels at early times.

For comparative purposes the approximate

TABLE 9—*Thermal energy distribution (Rainier)*

Isotherm (°C)	Average radius (ft)	Accumulated total energy within isotherm* (gram-calories)	Accumulated total energy within isotherm* (percentage of total prompt release)
20	100	10^{12}	60
40	80	7×10^{11}	40
60	55	3×10^{11}	17
80	30	6×10^{10}	3

*The temperature distribution was assumed to be axially symmetric.

TABLE 10—*Approximate average radii (ft) of various isotherms*

Isotherm (°C)	Blanca	Logan	Rainier	Tamalpais
20	240*	190*	100	...
40	120	100	80	...
60	...	80	55	...
80	...	70	30	...
R_T(ft)†	210	140	96	50
$\frac{R_T}{W^{\frac{1}{3}}}$ (ft/kt$^{\frac{1}{3}}$)	79	82	81	121‡

*The background temperatures for Blanca and Logan were 20°C and 18°C, respectively.

†R_T is the radius at which temperature first rises sharply.

‡Fired in a large room.

radii at which various temperatures were observed are listed in Table 10.

From these data R_T can be scaled according to the expression $R_T = 81\ W^{1/3}$.

The center of the Rainier temperature distribution appears to be displaced laterally about 20 ft. It is possible that the early gas venting took place in such a direction as to account for this effect. A large open vertical fault was found 50 ft from that side of the point of detonation, but whether venting actually occurred into this region is not known.

Distribution of radioactivity—The general distribution of radioactivity was determined by logging drill holes through the active region and by surveying the areas of fallout for those explosions that released activity to the atmosphere. The gross distribution [*Olsen and others,* 1959] as measured by thick-walled ion chambers for Rainier is shown in Figure 4. It is noted that the activity is concentrated in a bowl-like shell several feet thick. This same general distribution was noted for the other explosions. The mean radii of the radioactive zones are listed in Table 11 [*Olsen and others,* 1959]. A scaling law, $R = 50\ W^{1/3}$ ft, is derived from the scaled radii of the radioactive shells produced by the three large explosions.

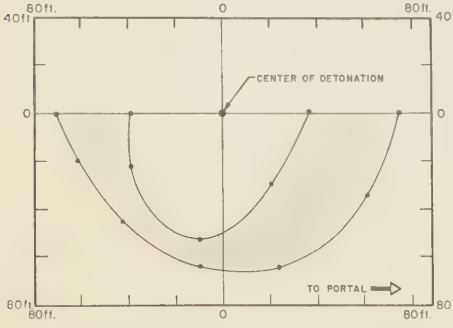

FIG. 4—Distribution of radioactivity, Rainier event.

It was determined that the bulk of the radioactivity was concentrated in glass that was formed by the explosion. From the radiochemical analysis of this material it was concluded that 500 ± 150 tons of rock were melted per kiloton of released energy. The glass contained between 60 and 85 per cent of the gross fission products. However, those materials with gaseous precursors were depleted in the glass by as much as a factor of 100 from the nonvolatile species. These volatile isotopes were correspondingly enriched outside the radioactive shells.

Since the fission products are composed of many elements, their volatilities range from very large (krypton, xenon) to very small (zirconium, cerium). The relative abundance of gaseous and refractory species changes as radioactive decay-processes proceed after the detonation.

Table 12 is a list of the parent-daughter relationships leading to some of the isotopes which were later determined radiochemically.

The effect of the gaseous ancestors in leading to the depletion of certain nuclides from the glass and their enrichment in the vented material is demonstrated in Table 13. These data are the summarized radiochemical results from all the explosions in tuff.

It should be noted that since Sr^{89} and Sr^{90} are

TABLE 11—*Radii of radioactive shells*

Event	Radius (ft)	Scaled radius (ft/kt$^{\frac{1}{3}}$)
Neptune	21	47*
Blanca	130	48
Logan	85	50
Rainier	62	52
Tamalpais	30	73†

*Cratering shot.

†Fired in a large room.

TABLE 12—*Decay chains leading to isotopes which have been measured in debris from underground explosions*

Mass	Element, half life, and measured isotope (underlined)				
85	As —0.43 sec→	Se —40 sec→	Br —30 min→	Kr	
89	Kr —3.2 min→	Rb —1.5 min→	Sr		
90	Kr —33 sec→	Rb —2.7 min→	Sr		
91	Kr —9.8 sec→	Rb —2 min→	Sr —9.7 hour→	Y	
95	Rb —sh*→	Sr —sh*→	Y —10 min→	Zr	
99	Zr —30 sec→	Nb —2.5 min→	Mo		
137	I —22 sec→	Xe —3.8 min→	Cs		
140	Xe —16 sec→	Cs —66 sec→	Ba		
141	Xe —1.7 sec→	Cs —sh*→	Ba —18 min→	La —3.7 hr→	Ce
144	Cs —sh*→	Ba —sh*→	La —sh*→	Ce	

*sh—short (compared with a few seconds).

strongly repleted in the glass debris, the gases must have escaped from the glass in times comparable to the half-lives of their krypton ancestors (3.2 min and 33 sec). At the temperatures in the cavity, around 1000 or 1500°C, several other fission products are volatile and also appear to be depleted from the glass and enriched in the vented materials. Arsenic, cesium, and uranium appear to behave in this way.

Phenomenology

The following discussion largely pertains to Rainier, since most of the measurements have been completed at that site. The nature of the radioactivity and the temperature distributions (Tables 10 and 11) and the marked increase in water permeability of the rock at the radii of the radioactive shells (Table 11) led to the conclusion that the explosions produced cavities of radius $R = 50\ W^{1/3}$ ft, which stood for a short time, and then collapsed.

In the case of Rainier, the state of the cavity at this time and its collapse has been described by *Kennedy and Higgins* [1958]. When first formed, the cavity was lined with about 4 inches of melted rock and filled with steam at a pressure of 40 atmospheres, which is approximately the lithostatic pressure. The cavity stood long enough, 30 sec to 2 min, for much of the fluid rock to flow down the sides and to drip from the roof. At this time the cavity began to collapse and to cool rapidly due to expansion of the steam. The sudden cooling quenched some of the droplets of rock in free fall, as well as some of the 'icicles' as they hung suspended from the cavity roof. The cavity was filled with broken rock from the collapse, and the caving progressed vertically to a distance of 386 ft above the point of detonation.

TABLE 13—*Summary of radiochemical data from several underground explosions*

Isotopes*	Percentage of total in fused material	Degree of enrichment in rubble chimney	Degree of enrichment in vented material‡
Kr^{85}	<1	~0	all in gas
Sr^{89}, As	3 to 10	>2	~10
Sr^{90}, Cs^{137} Y^{91}, Ba^{140}	20 to 40	>2	~5
Ce^{141}, Cs	30 to 60	>2	>2
U, Mo^{99}	50 to 100	<2	<2
Pu, A.E.† Pa, Hf Ta, Ce^{144}, Nd^{147}	~100	1.0	1.0

*Examples which have been measured.
†A.E. represents actinide earth.
‡Observed from Neptune and Blanca.

Inspection of the interior of the collapsed zone revealed the distribution in size of the blocks that were formed. The blocks in the lower drift varied from a few inches in diameter just inside the radioactive zone, to several feet in diameter near the center. The regions between the blocks were filled with pulverized material which had resolidified by the time re-entry was accomplished one year after the explosion. (Recementing is not surprising for material with high clay content.)

The drift, 100 ft above the zero point, first broke into a block-caved region 75 ft from the vertical line passing through the center of detonation. At this point the blocks were a few inches to a few feet in diameter, with open fractures, and then they graduated down to a fine powder at a distance of 65 ft. At a distance of 40 ft a large cavity was encountered. In summary, the collapse of the initial cavity produced a broken permeable zone that appeared to be cylindrical, with a radius of 65 to 75 ft for the first 100 ft of height, and with a total height of about 386 ft. The radius of the collapsed zone above 100 ft has not yet been measured.

Soon after detonation the high-temperature rocks rapidly cooled to the boiling point of water (94°C, at this altitude—6600 ft), because of the water content of the tuff and the large permeable zone which resulted from the collapse of the cavity. The diffusion of heat then took place at a lower rate, leading to the observed distribution measured five months after detonation (Fig. 3).

The Rainier device was detonated in a room 6 × 6 × 7 ft, which contained about 1 ton of material. The initial temperature and pressure in the room can be calculated as follows.

Energy density:

$$E = E_p + E_r + 3/2\, n\, kt + \frac{4\sigma T^4}{c}$$

where

E_p = energy density in the particles
E_r = energy density in radiation
n = $A_0\rho/M$ = number of particles per cm^3
k = 1.37×10^{-16} erg/°K (Boltzmann's constant)
T = temperature °K
σ = 5.74×10^{-5} erg/cm^2/°K^4 (Stefan-Boltzmann constant)
c = 3×10^{10} cm/sec (velocity of light)
A_0 = 6.04×10^{23} (Avogadro's number)
M = molecular weight
ρ = density in gm/cm^3

This can be put in the form

$$E = 3/2\, \frac{A_0\rho}{M}\, kT + \frac{4\sigma T^4}{c}$$

$$= 1.25 \times 10^8\, \frac{\rho}{M}\, T + 7.65 \times 10^{-15}\, T^4 \text{ erg/cm}^3$$

The pressure equals two-thirds particle energy-density plus one-third radiation energy-density, thus

$$P = 0.83 \times 10^8\, \frac{\rho}{M}\, T + 2.55 \times 10^{-15}\, T^4 \text{ dynes/cm}^2$$

The prompt energy release of the Rainier explosion was 7.2×10^{19} ergs. Since the mass of material in the room was about 10^6 gm and the volume was 7×10^6 cm^3, the mean density was 0.14 gm/cm^3. At extremely high temperatures essentially all electrons are stripped from nuclei, and, since the atomic weight is approximately twice the atomic number, the effective molecular weight is given by

$$M_{eff} \cong \frac{\Sigma N_i \times 2Z_i}{\Sigma N_i(Z_i + 1)} \approx 2$$

where N_i is the number of atoms of atomic number Z_i and the summation is taken over all nuclides in the zero room. From these expressions it follows that the temperature a few microseconds after detonation was about 1,000,000°K and the pressure 7,000,000 bars (atmospheres). The radiation pressure at this temperature is 2500 bars.

The calculation of the behavior of the medium from this point onward was carried out by *Nuckolls* [1959], who extended the earlier calculations of G. T. Pelsor (private communication). Nuckolls' treatment involved the development of a code for a computer calculation of the behavior of the medium from a few microseconds to about 100 milliseconds. This time was sufficiently long to permit calculation of all the dynamic behavior of the system. Only the general results of this calculation will be given here.

It was assumed that tuff has negligible large-scale tensile strength and behaves as a linear elastic solid as long as the tension does not exceed the stress due to overburden pressure. The elastic constants used in the calculations were the measured values for bulk modulus, shear modulus, and sound speed. After the tension in the spherical shell exceeds the lithostatic stress the components of the stress tensor are set equal to a pressure (shear modulus equal to zero) which is related to the volume by a bulk-modulus type equation of state.

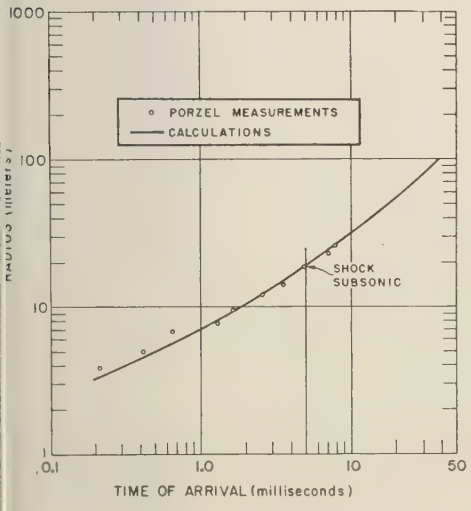

FIG. 5—Shock-time arrival, Rainier event.

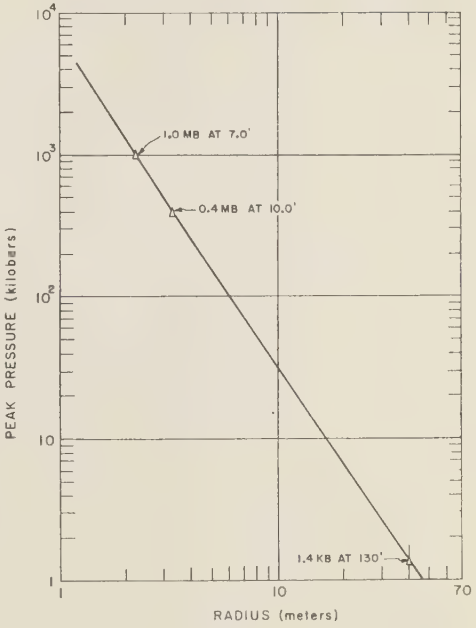

FIG. 6—Peak shock pressure, Rainier event.

From the calculations, the time of arrival of the shock wave was determined. This information together with the measured results of F. B. Porzel [*Cohn and others*, to be published] are shown in Figure 5. In Figure 6 the peak shock pressure as a function of radius is given. It decreases as $r^{-2.35}$ out to about 10 meters. The tuff was vaporized to a radius of 2.3 meters in 0.2 msec (peak pressure 1.0 megabar) and melted by shock wave to 3.3 meters (0.4 mb). Enough energy was deposited by the shock in the first 4.6 meters to melt all the tuff within this radius (660 tons). Radiochemical analysis on Rainier gave about 800 tons. The total amount that melted is the sum of the shock-induced melting (660 tons calculated) and the melting induced by the energy of fission-product decay and should be about 1.2 times larger than the shock-induced melting alone. The factor 1.2 is the result of the ratio of the percentage of

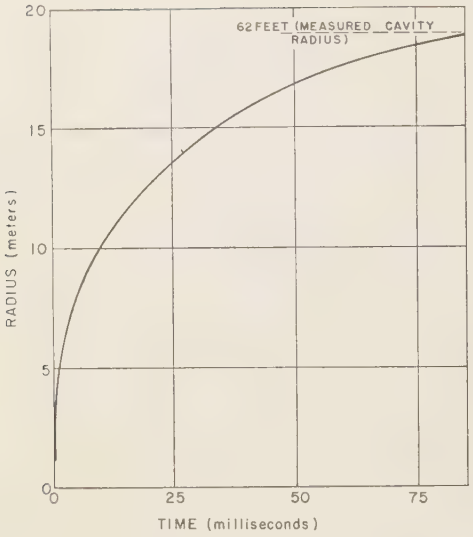

FIG. 7—Rate of growth of Rainier cavity.

prompt energy in gas + liquid + fission-product divided by the prompt energy in gas + liquid.

The shock wave progressed outward and crushed the medium to a radius of 130 ft where the pressure was 1.4 kilobars, or twice the static compressive strength. The elastic radius was calculated to be 285 ft horizontally and 305 ft vertically.

It was deduced that a spherical cavity was formed which expanded outward as the shock wave advanced. The melted tuff formed the inner surface of this cavity. The calculated rate of growth of the cavity is given in Figure 7. It is noted that it reached its maximum radius of 62 ft in about 80 msec. The radius that was determined experimentally is in agreement with this value.

TABLE 14—*Rainier energy distribution*

State	Radii (ft)	Percentage of prompt energy
Gas	0 to 62	8.2
Liquid	62 to 62¼	19.1
Crushed	62¼ to 130	47.0
Fractured	130 to 280	21.2
Elastic	280	4.5

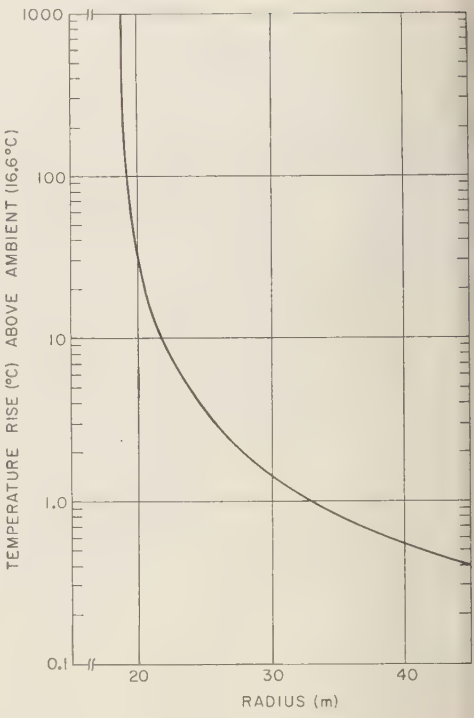

FIG. 8—Initial Rainier temperature distribution.

Nuckolls also calculated the energy and temperature distribution at 90 msec after detonation. At this time, less than 0.5 per cent of the energy was kinetic energy and therefore the system was essentially static (Table 14).

The calculated temperature distribution after the cavity had ceased to grow, but before it collapsed, is shown in Figure 8.

From the known melting properties of tuff, it was concluded [*Nuckolls*, 1959] that the melted material at this time must have been at a temperature of 1200 to 1500°C. To heat 800 tons of tuff (15 per cent water) to this temperature range would require about 5.7×10^{11} cal. This is 32 per cent of the total energy release (prompt plus fission-product heat) of the Rainier explosion (1.8×10^{12} cal). Nuckolls' calculation gives 27 per cent of the prompt release (1.70×10^{12} cal). Since the energy of fission-product decay should contribute between 3 and 4 per cent additional to the prompt melting energy, the numbers are consistent.

By assuming that all the water from the molten and vaporized rock remains in the cavity as steam and that the temperature is about the same as that of molten rock (1500°C), the pressure due to steam in the cavity can be calculated to be 40 bars, which can be compared with the lithostatic pressure of 50 to 55 bars. An experimental confirmation [*Kennedy and Higgins,* 1958] of this estimate was made by heating some of the glass which had condensed in free fall in a vacuum furnace to drive out the gas. From the measured quantity of trapped gas it was found that the pressure in the contained bubbles was 40 bars, which agrees with the calculated value.

Summary

1. The radioactivity of nuclear explosions in the kiloton range in tuff can be essentially contained underground at depths of $D = 400\ W^{1/3}$ ft or greater.

2. The initial cavity formed by the explosion has a radius of $R = 50\ W^{1/3}$ ft.

3. Initially melted rock, which is converted to glass on cooling, amounts to 500 ± 150 tons per kiloton of released energy.

4. The collapse of the cavity produces a zone of about 70,000 yds^3/kt (120,000 tons/kt) of broken permeable material.

5. The major portion (65 to 80 per cent) of the gross fission-product activity is in dilute (one part per 10,000,000) solution in glass. The remainder (20 to 35 per cent) is distributed throughout the collapsed zone of the chimney and is deposited on the surface of the broken material.

6. About 30 per cent of the total energy released by the explosion is initially deposited in steam and hot rock at a temperature in excess of 1200°C. This temperature rapidly degrades to the boiling point of water. One year after the Rainier explosion this energy resided within a volume whose radius was less than 80 ft.

References

Carder, D. S., and W. K. Cloud, Surface motion from large underground explosions, *J. Geophys. Research, 64,* 1471–1487, 1959.

Carder, D. S., W. K. Cloud, L. M. Murphy, and J. H. Hershberger, Surface motions from an underground explosion, *WT-1530,* 1958.

Carder, D. S., W. K. Cloud, T. H. Pearce, and L. M. Murphy, Surface motions from a series of underground nuclear tests, *ITR-1705,* 1959.

Cohn, S., A. Hoehn, R. G. Dickens, F. B. Porzel, T. Shiffman, S. Hoenig, N. Wilde, and C. Greenberg, Close-in time-of-arrival measurements for yield of UG shots, *WT 1495* to be published.

Diment, W. H., R. E. Wilcox, G. V. Keller, E. Dobrovolny, F. C. Kracek, J. C. Roller, L. C. Peselnick, E. C. Robertson, A. H. Lachenbruch, and C. M. Bunker, Properties of Oak Springs formation in Area 12 at the Nevada Test Site, *U. S. Geol. Survey, Trace Elements Rept. 672,* 1958a.

Diment, W. H., V. R. Wilmarth, F. N. Houser, F. A. McKeown, E. H. Hinrichs, T. Botinelly, R. E. Wilcox, A. Clebsch, Jr., I. J. Winograd, C. C. Hawley, and G. E. Manger, *U. S. Geol. Survey, Trace Elements Rept. 728,* 1958b.

Diment, W. H., V. R. Wilmarth, R. E. Wilcox, A. Clebsch, Jr., G. E. Manger, C. C. Hawley, G. V. Keller, E. C. Robertson, L. C. Peselnick, C. M. Bunker, D. L. Healey, M. F. Kane, E. F. Roth, S. W. Stewart, J. C. Roller, W. H. Jackson, H. W. Oliver, P. E. Byerly, and D. R. Mabey, Geologic effects of the Rainier underground nuclear explosion, U. S. Geol. Survey, *Trace Elements Rept. 355,* 1959.

Edgerton, Germeshausen & Grier, Inc., staff of, Photographic analysis of earth motion, shot Rainier, *WT 1532,* 1958.

Goodale, T. C., B. Ragent, A. H. Samuel, A. L. Anderson, D. E. Nielsen, and J. L. Olsen, Temperatures from underground detonation, shot Rainier, *WT-1527,* 1958.

Griggs, D., and E. Teller, Deep underground test shots, *Lawrence Radiation Lab., Univ. Calif., UCRL-4659,* 1956.

Johnson, G. W., G. T. Pelsor, R. G. Preston, and C. E. Violet, The underground nuclear detonation of Sept. 19, 1957, Rainier, *Lawrence Radiation Lab., Univ. Calif., UCRL-5124,* 1958.

Johnson, G. W., and C. E. Violet, Phenomenology of contained nuclear explosions. *UCRL-5124, Rev. I.* (Available from the Office of Tech. Services, Dept. Commerce, Washington 25, D. C.), 1958.

Kennedy, G. C., and G. H. Higgins, Temperatures and pressures associated with the cavity produced by the Rainier event, *UCRL-5281* (Available from the Office of Tech. Services, Dept. Commerce, Washington 25, D. C.), 1958.

Morris, R. H. and R. D. Schneiderhan, Earth motion studies, *ITR-1706,* 1959.

Nuckolls, J., Computer calculation of Rainier. Paper presented at Plowshare Symposium, San Francisco, California, May 13, 14 and 15, 1959 (to be published).

Olsen, J. L., W. P. Bennet, and D. E. Nielsen,

Paper presented at Plowshare Symposium, San Francisco, California, May 13, 14 and 15, 1959 (to be published).

Perret, W. R., Subsurface motion from a confined underground detonation—Part I, Sandia Corp., *ITR-1529,* 1958.

Romney, Carl, Amplitudes of seismic body waves from underground nuclear explosions, *J. Geophys. Research, 64,* 1489–1498, 1959.

Swift, L. M., and D. C. Sachs, Surface motion from an underground detonation, *WT-1528,* 1959.

Swift, L. M., D. C. Sachs, and W. M. Wells, Earth motion measurements, Part I. Seismic studies and cavity studies, *ITR-1702,* 1959.

Warner, S. E., and C. E. Violet, Properties of the environment of underground nuclear detonations at the Nevada Test Site, *UCRL-5542* (Available from the Office of Tech. Services, Dept. Commerce, Washington 25, D. C.), 1959.

Note: *ITR* and *WR* reports are available from the Office of Technical Services, Department of Commerce, Washington 25, D. C.

(Manuscript received July 13, 1959.)

Surface Motion from Large Underground Explosions

D. S. CARDER AND W. K. CLOUD

U. S. Coast and Geodetic Survey, Washington, D. C. and San Francisco, Calif.

Abstract—Seismic effects of several underground nuclear explosions were measured in terms of ground surface motion by suitable seismographs from 1200 ft to nearly 10 miles from the source and with teleseismic instruments at great distances. Prior to the Rainier explosion (a 1.7-kt nuclear shot detonated 900 ft underground) empirical formulas were developed which predicted ground effects from the Rainier shot and several of the larger HARDTACK II shots with fair accuracy but with certain limitations. The limitations were (1) that at distances greater than a few thousand feet, observed displacements were somewhat larger than the formula predicted, necessitating revision of the formula; (2) that frequencies of ground waves did not exceed 20 cps; and (3) that the source conditions and material were in fair duplication. Ground amplitudes on deep alluvium were, as expected, more than twice the amplitudes at nearly the same distance on rock. Velocity response spectrums of one of the shots have been made and reproduced. The magnitude of the Rainier shot was about 4.0, based on the assumption that the source was contained in a volume of rock comparable to that of an earthquake having the same magnitude. Local travel-time data indicate that the subbasement rock associated with a speed of about 6.2 km/sec is about 3600 ft beneath the shot points area.

Introduction—The U. S. Coast and Geodetic Survey, because of its long experience in measuring strong ground motion during earthquakes was given the assignment of measuring surface effects from a number of large explosions including the underground nuclear explosions of the PLUMBBOB and HARDTACK II series and certain other tests using high explosives. In this article some of the results which are of interest to the scientific public will be given and discussed.

The instruments used were the standard strong-motion seismographs which have been used for years by the Survey for measuring strong earthquake motion [*Cloud and Carder, 1956*]. They are direct-recording seismographs consisting of simply constructed compound pendulums damped by permanent magnets, together with timing clocks and 12-inch photographic tape cameras. Direct recording is accomplished by a foscused light beam reflected to the photographic tape from mirrors attached to the pendulums near the axes of oscillation. These instruments are capable of recording ground motion in the acceleration range from 0.001 g or less to 3.0 g, and transitory ground displacements of 6 inches or less. For this purpose, two sets of seisometers are required, one set having pendulum periods substantially less than the periods of expected ground motion and the other with periods substantially greater than the ground periods. Each set measures ground motion in the vertical and two horizontal directions. To accomplish this purpose, the periods of the accelerometer (short-period) pendulums ranged from 0.03 to 0.15 sec, depending on the distances from shot zero, and the displacement meter (long-period) pendulums were from 2 to 3 sec with magnifications from 0.5 to nearly 6. Nine stations were operated at distances of 930 feet to 3.2 miles from ground zero, or from 1240 feet to 3.2 miles slant distances from shot zero, and 2 stations 8 to 9 miles from shot zero, one during HARDTACK II on granite and the other during PLUMBBOB and HARDTACK II on deep alluvium in Yucca Flat. The station layout during the Rainier shot together with the underlying rock is indicated on the map in Figure 1.

Predictions of expected ground effects—During the preparation of instrumentation for the Rainier shot an estimate of expected ground accelerations and amplitudes was considered invaluable to insure that the records would be fully contained on the tapes yet large enough to be measurable. For this, advantage was taken of two sources of information.

1. On February 21, 1957 a 10-ton high-ex-

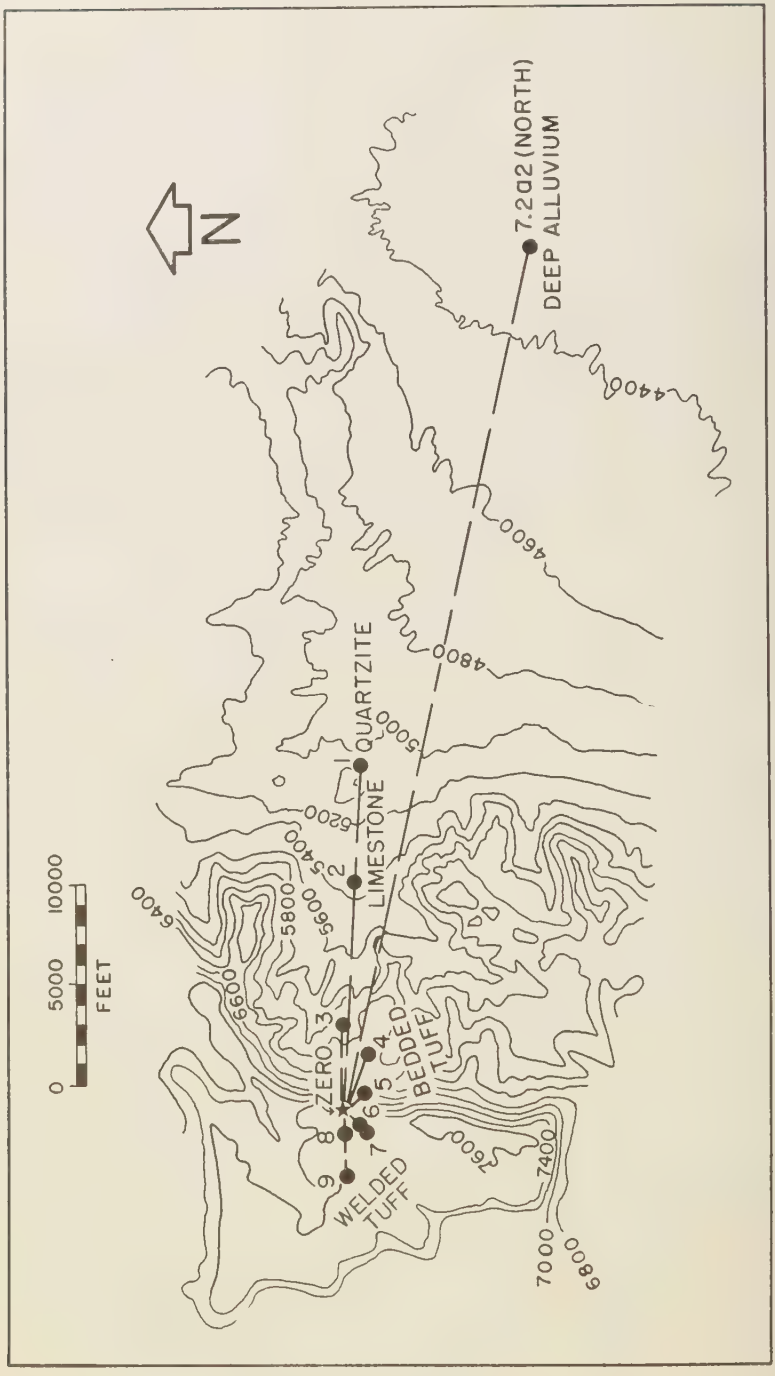

FIG. 1—Location of strong-motion seismograph stations, Rainier shot.

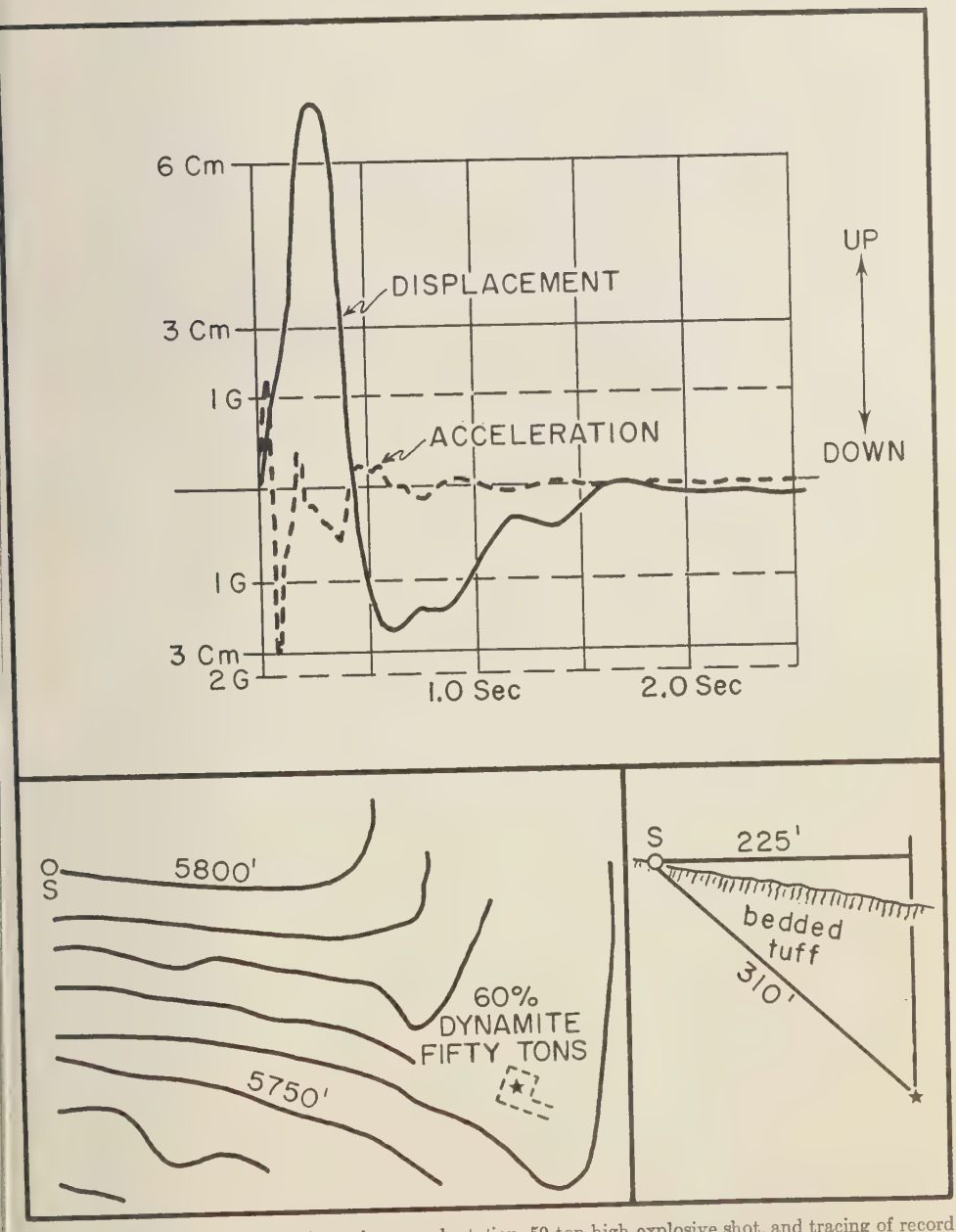

FIG. 2.—Location of strong-motion seismograph station, 50-ton high-explosive shot, and tracing of record.

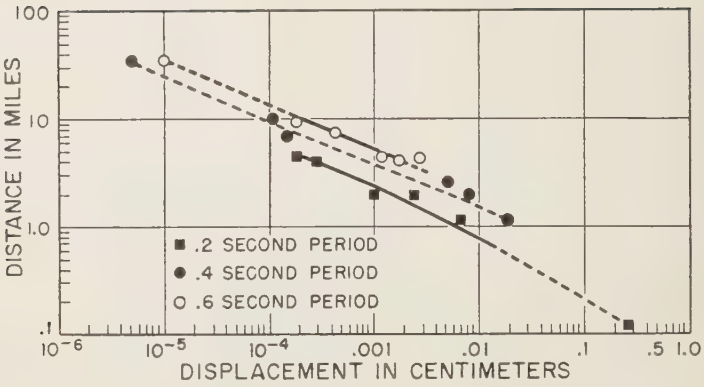

FIG. 3—Attenuation of displacement with distance

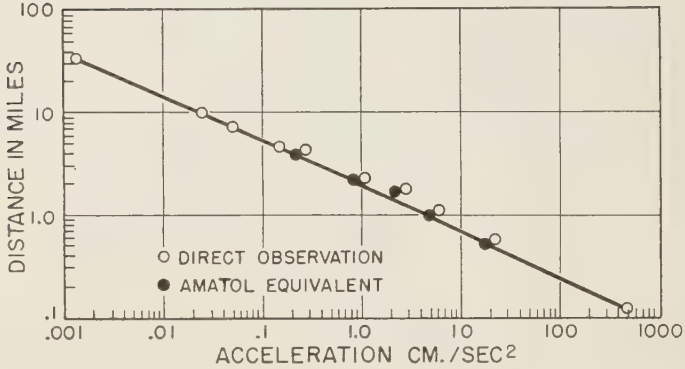

FIG. 4—Attenuation of acceleration with distance

FIGS. 3, 4—Ground effects data from 250,000 lb. surface explosions on U. S. Navy Proving Grounds, Arco, Idaho, 1945–46.

plosive shot was fired by the Geological Survey in the tuff near the Rainier site and on April 5, 1957 a 50-ton shot was fired in nearly the same location. Both of these shots were recorded at the Boulder City and Eureka, Nevada, Coast and Geodetic Survey teleseismic stations, and the latter was recorded by a strong-motion seismograph on the surface, 310 feet from the explosives charge. Figure 2 shows the station layout and the resulting record. The Eureka and Boulder City data indicated that ground amplitudes varied about as the ¾ power of the charge. This is in partial agreement with unpublished data collected by one of the authors (Carder) from a large number of explosions from which resulting ground amplitudes were observed to vary as the ½ to the 1.0 power of the explosives charge.

2. In 1945 and 1946, seismic measurements of ground effects from controlled explosions of ammunition dumps on the U. S. Navy Proving Grounds near Arco, Idaho, were made by the Coast and Geodetic Survey [*Carder*, 1948]. Since the reference article is out of print, two significant illustrations are reproduced here as Figures 3 and 4. From these illustrations it appears that acceleration varies inversely as the 2.2 power of the distance, but if data from 0.1 to 2.0 miles are used, variation as the inverse 2.0 power gives a good fit. If the wave periods

a the displacement data are ignored, displacements varying inversely as the 2.0 power also ive a good fit to the data.

Using the information just cited and putting W as he equivalent weight of the explosive in ons, D as the distance in feet, a as the acceleration in units of gravity, and A as the zero-to-eak ground displacement in centimeters, we ave

$$a_2/a_1 = A_2/A_1 = (W_2/W_1)^{0.75}(D_1/D_2)^2$$

nd more specifically by substituting information gained from Figure 2, we have

$$a = 1.85(W/50)^{0.75}(310/D)^2 g$$

nd

$$A = 7.15(W/50)^{0.75}(310/D)^2 \text{ cm}$$

r more simply

$$a = 0.95(W^{0.75}/D^2) \times 10^4 \text{ g} \qquad (1)$$

nd

$$A = 3.6(W^{0.75}/D^2) \times 10^4 \text{ cm} \qquad (2)$$

Acceleration data are for seismic waves having periods of 0.05 sec or greater, and displacement data are for periods of 0.5 sec or greater. Formulas (1) and (2) were used as guides n adjusting seismometer constants. However, haracteristics of the instruments in some cases revented fitting the constants to optimum alues set by the formulas.

It is of interest to compare formulas (1) and 2) with the data in Figures 3 and 4. The Arco xplosions were the equivalents of 125 tons of NT detonated on the ground surface of a baalt plain. The overburden was no more than .0 ft. Putting 125 as W in (1) and (2) we ave for $D = 5480$ ft., $a = 0.012$ g or 12 m/sec^2 and $A = 0.046$ cm. The ratio to observed values is about 2:1.

Test results, strong-motion data from the Rainier shot—Legible seismograms of Rainier vere obtained from ten Coast and Geodetic Survey strong-motion seismographs. Partial racings are shown in Figures 5 and 6. The ccelerometers measured accelerations only for round periods substantially larger than instrumental periods. Some of the highest accelerations were associated with sharp, high-frequency impulses. In evaluating these, ground period as well as trace amplitude was considered. Lower-frequency waves were measured directly from trace amplitudes and are considered reliable within 10 or 15 per cent. Periods for ground displacement in all cases were considerably less than instrumental periods; therefore, trace amplitude is proportional to displacement. Displacement results are considered reliable within 10 or 15 per cent, except for several cases where the zero positions of instrument booms were permanently shifted by high accelerations.

Acceleration data are summarized in Table 1 and displacement data in Table 2. Remarks in the summaries such as 'sharp spike' or 'poor record' indicate components for which estimated reliability might be less than 85 to 90 per cent.

As maximum acceleration attenuated to 0.13 g at 4390 ft, the radius within which damage might have occurred appears limited to about 1 mile. Very few of the observers stationed 2½ miles from the shot reported having felt any ground motion.

From an engineering standpoint, maximum acceleration alone is not a reliable criterion of structural damage. Relative maximum-velocity response of single-degree-of-freedom oscillators to an acceleration function offers a better approach [*Hudson*, 1956]. Utilizing the electric analog-type response spectrum analyzer system at the California Institute of Technology Earthquake Research Laboratory, several Rainier strong-motion records were subjected to such an analysis. The results are shown in Figure 7. For comparison, the velocity spectrum from an accelogram that was recorded about 7 miles from the epicenter of the San Francisco earthquake of March 22, 1957 (magnitude 5.3) is shown in Figure 8. Points on the curves give a relative measure of maximum kinetic energy that would have been attained during the time of ground motion by simple structures of various periods and damping. To illustrate, a structure with 0.5-sec period and 10 per cent critical damping at Rainier Station 09 (distance 3329 ft) would have experienced roughly $(0.6/0.3)^2$ or 4 times the kinetic energy of the same structure had it been located at Golden Gate Park during the earthquake of March 22, 1957. The same structure located at Taft during

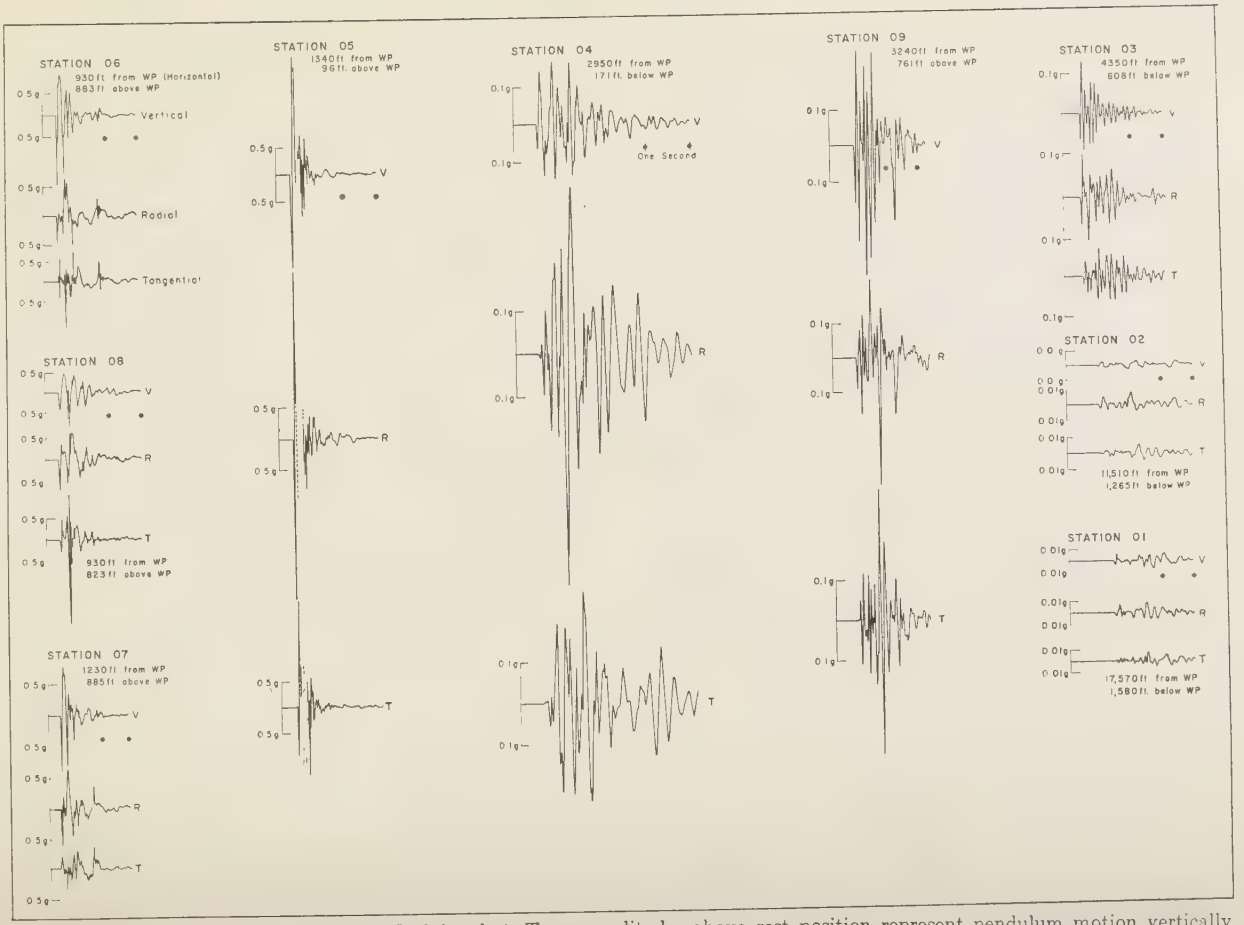

FIG. 5—Tracings of acceleration records, Rainier shot. Trace amplitudes above rest position represent pendulum motion vertically upward, radially away from zero, and tangentially to the left when facing zero.

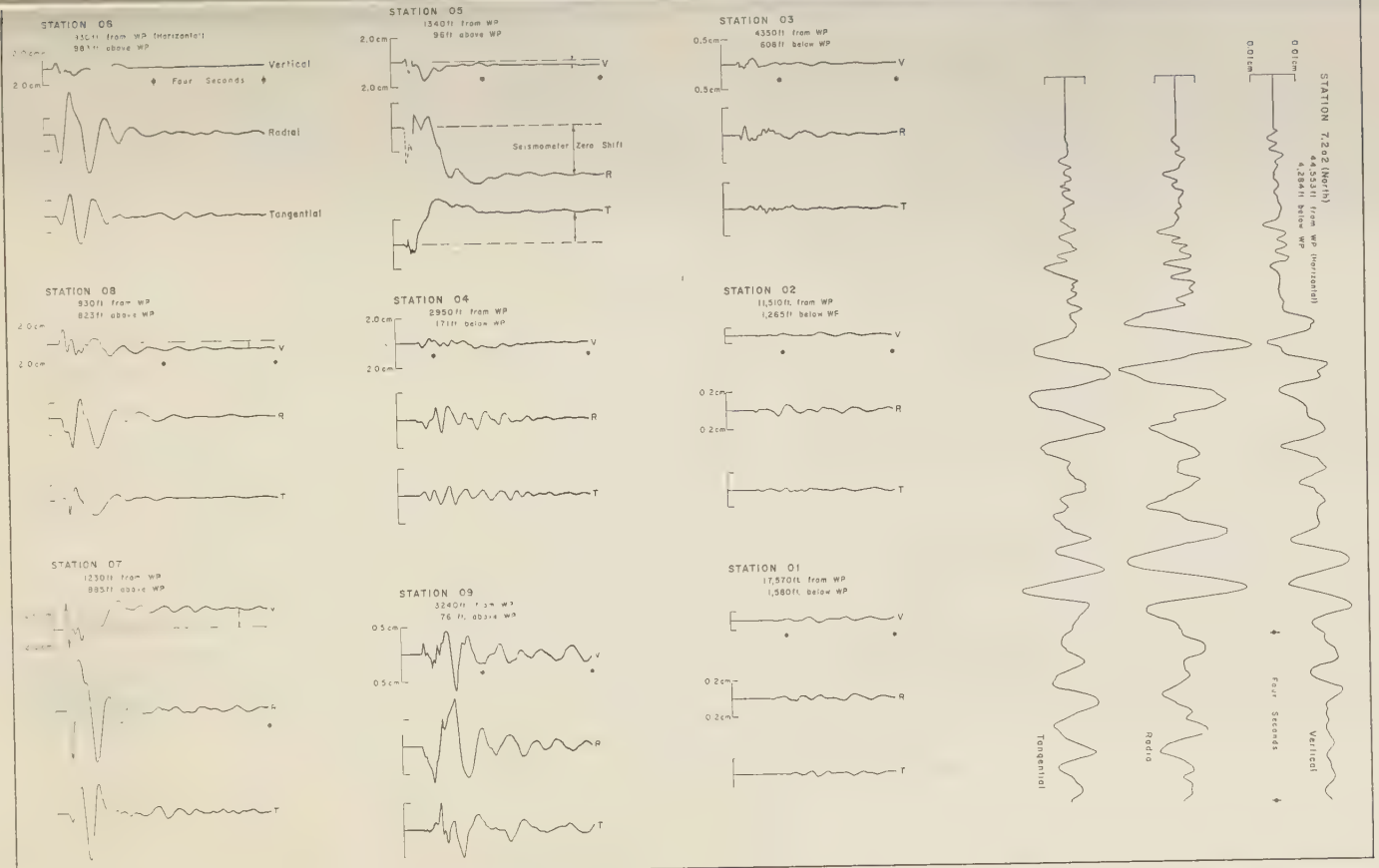

FIG. 6—Tracings of displacement records, Rainier shot. Trace amplitudes above rest position represent pendulum motion vertically downward, radially away from zero, and tangentially to the right when facing zero.

TABLE 1—*First-motion and maximum-acceleration data, Rainer shot*

Station No., distance, and foundation	Component	Period, sec	Acceleration, g	Time after first arrival, sec	First motion	Remarks
6003.01	Z	0.1	0.004	0	Up	
17569 ft (horiz.)		0.2	0.008	1.0		
17640 ft (slant)	R	0.1	0.004	0	Away	
Quartzite		0.2	0.009	1.04		
Cross-over	T	0.1	0.003	0	Right	
station with		0.1	0.007	1.03		
Geological						
Survey						
6003.02	Z	0.1	0.002	0	Up	
11508 ft		0.5	0.005	1.21		
11580	R	0.2	0.003	0	Away	
Dolomite		0.3	0.008	1.03		
	T	0.2	0.001	0	Left	
		0.3	0.005	1.25		
6003.03	Z	0.1	0.07	0	Up	
4348 ft		0.1	0.13			
4390 ft	R	0.1	0.06	0	Away	
Bedded tuff		0.2	0.10	0.17		
	T	0.09	0.016	0	Left	
		.15	0.07	.48		
6003.04	Z	0.2	0.07	0	Up	
2948 ft		0.25	0.19	0.8		
2950 ft	R	0.08	0.01	0	Away	
Bedded tuff		0.2	0.54	0.8		
	T		0.002	0	Right	
		0.3	0.27	0.9		
6003.05	Z	0.03	0.94	0	Up	
1338 ft		0.07	2.2	0.1		May be 1.4 g on one spike
1340 ft	R	0.1	2.6	0	Away	May be as high as 3 g
Bedded tuff	T		0.03	0	Right	
Tunnel station		0.01-	1.3	0.3		One spike may be 2.0 g or
Cross-over with		0.1				higher, Traces on this record
Sandia Corp.						were seriously overlapped.
6003.06	Z	0.1	1.6	0	Up	Cross-over station
932 ft	R	0.06	0.5	0	Away	with Stanford
1280 ft		0.05	0.65	0.3		Research Corp.
Welded tuff	T	0.02	0.14	0	Right	
on mesa		0.02	2.6	1		Sharp spike
6003.07	Z	0.1	0.91	0	Up	Cross-over station
1230 ft	R	0.1	0.59	0	Away	with Stanford
1516 ft		0.3	0.62	0.62		Research Corp.
Welded tuff	T	0.1	0.19	0	Right	Record from this
on mesa		0.07	0.41	0.2		station very similar
						to station 06 record.
6003.08	Z	0.2	0.42	0	Up	
932 ft		0.02-.06	0.90	0.25		
1242 ft	R	0.1	0.69	0	Away	
Welded tuff	T	0.25	0.4	0	Left	
on mesa		0.03	2.0	0.25		
6003.09	Z	0.1	0.16	0	Up	
3240 ft		0.1	0.36	0.4		
3329 ft	R	0.1	0.09	0	Away	
Welded tuff		0.1	0.34	0.7		
on mesa	T		0.11	0	Right	
		0.2	0.34			

TABLE 2—*Maximum-displacement data, Rainier shot*

Station No., distance, and foundation	Component	Maximum Displacement		Remarks
		Period, sec	Amplitude, cm	
6003.01	Z	0.7	0.045	
17569 ft (horiz.)				
17640 ft (slant)	R	0.7	0.030	
Quartzite	T	0.5	0.040	
6003.02	Z	1.0	0.043	
11508 ft				
11580	R	0.8	0.061	
Dolomite	T	0.4	0.022	
6003.03	Z	0.7	0.14	
4348 ft				
4390 ft	R	0.3	0.15	
Bedded tuff			0.06	
6003.04	Z	0.4	0.34	
2948 ft				
2950 ft	R	0.3	0.84	
Bedded tuff	T	0.4	0.60	
6003.05	Z		1.28	Poor record
1338 ft				
1340 ft	R		3.73	Poor record
Bedded tuff	T		3.16	Poor record
6003.06	Z		0.90	Poor record
932 ft				
1280 ft	R	1.3	5.40	
Welded tuff	T	.9	3.64	
6003.07	Z	1.0	3.01	Poor record
1230 ft				
1516 ft	R	1.1	3.46	
Welded tuff	T	.9	3.10	
6003.08	Z	.3	1.41	Poor record
932 ft				
1242 ft	R	1.2	3.90	
Welded tuff	T	1.9	1.96	
6003.09	Z	.7	0.70	
3240 ft				
3329 ft	R	1.5	0.85	
Welded tuff	T	.9	0.52	
7.2a2 (North)	Z	1.2	0.014	
44,553 (horiz.)	R	1.3	0.037	
Deep alluvium	T	1.3	0.025	

the Kern County, California, earthquake of July 21, 1952 [*Hudson*, 1956] would have experienced 2 to 3 times the Rainier kinetic energy. The damage at Taft was considered to be moderate [*Murphy and Cloud*, 1954]. The comparison is for one direction of horizontal motion.

In Tables 3 and 4, maximum acceleration and displacement recorded by 10 on-site strong-motion seismographs and by 7 off-site Wood-Anderson seismographs are compared with empirical formulas (1) and (2). The same data are illustrated in Figures 9, 10, 11, and 12.

Predictions within the ratio limits established by Rainier data were made for two unrelated underground explosions, as indicated in Tables

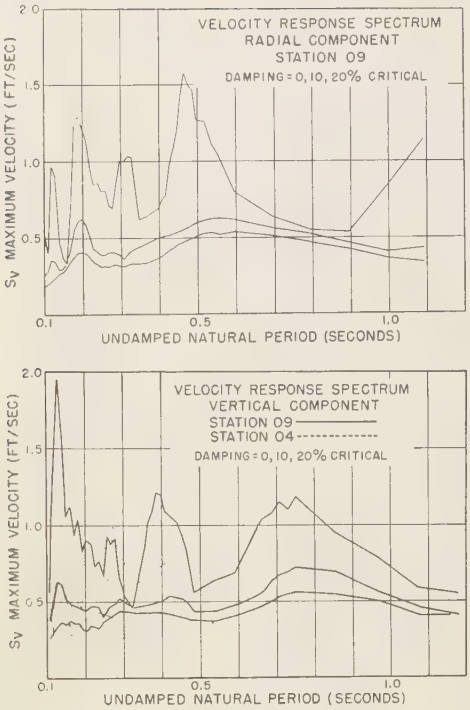

FIG. 7—Relative maximum velocity response spectrums, Rainier shot, of single degree of freedom oscillators to acceleration recorded at two Coast and Geodetic Survey stations in the directions indicated.

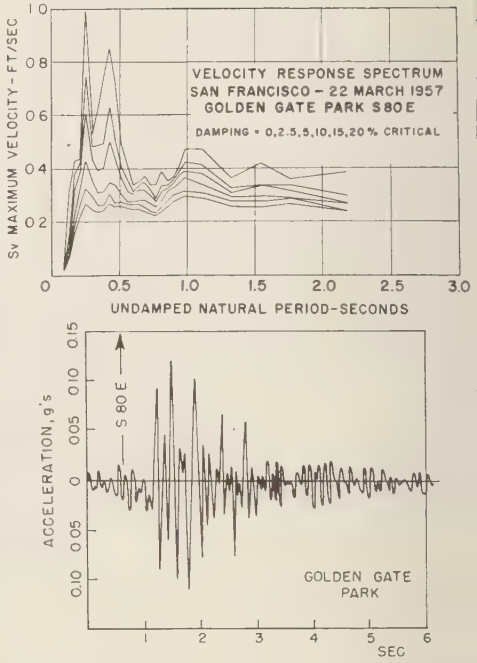

FIG. 8—Relative maximum velocity response spectrum of single degree of freedom oscillators to acceleration shown below.

5 and 6. At South Holston, it is believed that a large part of the energy was confined to a dolomite layer at the surface; this would account for the linear attenuation with distance.

Energy relationship, general—An earthquake or an explosion on or within the earth generates elastic waves that pass through the rock according to certain laws. These waves contain a certain amount of energy which can be measured in part as they pass a seismograph station located either on or within the earth. If the energy contained in the wave as it passes a seismograph station is known, the energy that enters the ground in the form of seismic waves at the source may be estimated if the wave paths and absorption and boundary losses enroute are known. Therein lies the uncertainty in estimating seismic energy at the source, and this uncertainty constitutes a part of our problem.

The energy contained in an elastic wave passing a point in a medium is represented by the well-known formula

$$E_s = 2\pi^2 \rho \Sigma v A_h^2/T$$

where E_s is the energy passing through a unit section, ρ is the density of the rock, v is the speed of the wave, A_h is its amplitude, and T is its period. The summation is over all the waves contained in a pulse. If the recording station is on the surface, as it usually is, the emergent wave usually has twice the amplitude of a wave confined underground. The energy formula measured from a pulse on the seismogram thus becomes

$$E_s = \frac{\pi^2}{2} \rho v \Sigma A^2/T \qquad (3)$$

if all waves are measured.

If we assume that seismic energy leaves the

TABLE 3—*Comparison of recorded and predicted maximum single component accelerations*

Station	Distance to source, ft	Distance to source, km	Maximum acceleration (gravity) recorded Z	R	T	Predicted	Ratio of recorded to predicted
01	17,640		0.008	0.009	0.007	0.008	1.1
02	11,580		0.005	0.008	0.005	0.019	0.42
03	4,390		0.13	0.10	0.07	0.130	1.0
04	2,950		0.19	0.54	0.27	0.288	1.8
05	1,340		2.2	2.6	1.3	1.39	1.8
06	1,280		1.6	0.65	2.6	1.53	1.7
07	1,516		0.91	0.62	0.41	1.9	0.83
08	1,242		0.90	0.69	2.0	1.62	1.2
09	3,329		0.36	0.34	0.34	.226	1.6
7.2a2 N*	44,553	13.6	0.00039	0.00088	0.00060	0.0013	0.68
Tinemaha*		180.7	East-West		0.000016	0.0000071	2.2
Hoover Dam*		185.4	East-West		0.0000046	0.0000068	0.34
Pasadena*		382.2	East-West		0.00000031	0.0000016	0.19
Mount Hamilton*		482.8	?		0.0000014	0.0000010	1.4
Palo Alto*		530.4	North-South		0.00000042	0.00000083	0.50
Berkeley*		540.5	East-West		0.00000020	0.00000080	0.25
San Francisco*		556.5	East-West		0.00000026	0.00000075	0.35

*Acceleration was computed from displacement by simple harmonic motion formula $a = 4\pi^2 A / T_c^2$.

TABLE 4—*Comparison of recorded and predicted maximum single component transient displacements*

Station	Distance to source, ft	Distance to source, km	Maximum displacement (cm) recorded *Z*	*R*	*T*	Predicted	Ratio of recorded to predicted
01	17,640		0.045	0.030	0.040	0.031	1.45
02	11,580		0.043	0.061	0.022	0.072	0.85
03	4,390		0.14	0.15		0.50	0.30
04	2,950		0.34	0.84	0.60	1.11	0.76
05	1,340		1.28	3.73	3.16	5.39	0.69
06	1,280		0.90	5.40	3.64	5.90	0.91
07	1,516		3.01	3.46	3.10	4.21	0.82
08	1,242		1.41	3.90	1.96	6.72	0.57
09	3,329		0.70	0.85	0.52	0.87	0.98
7.2a2 (North)	44,553	13.6	0.014	0.037	0.025	0.0049	7.6
Tinemaha		180.7	East-West		0.00025	0.000028	8.9
Hoover Dam		185.4	East-West		0.00011	0.000026	2.17
Pasadena		382.2	East-West		0.0000094	0.0000061	1.54
Mount Hamilton		482.8	?		0.000034	0.0000038	8.9
Palo Alto		530.4	North-South		0.000015	0.0000032	4.7
Berkeley		540.5	East-West		0.0000059	0.0000031	1.9
San Francisco		556.5	East-West		0.0000094	0.0000029	3.2

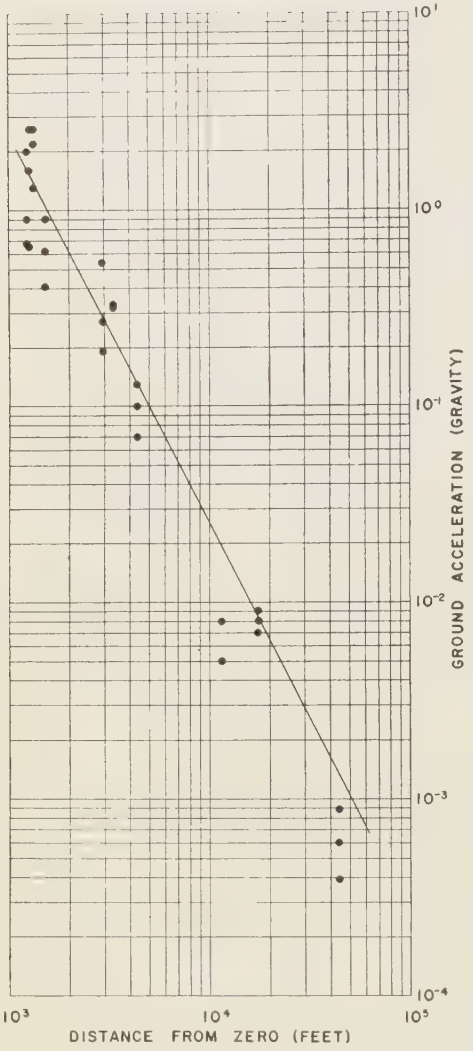

FIG. 9—Predicted and recorded accelerations, Coast and Geodetic Survey strong-motion stations, Rainier shot.

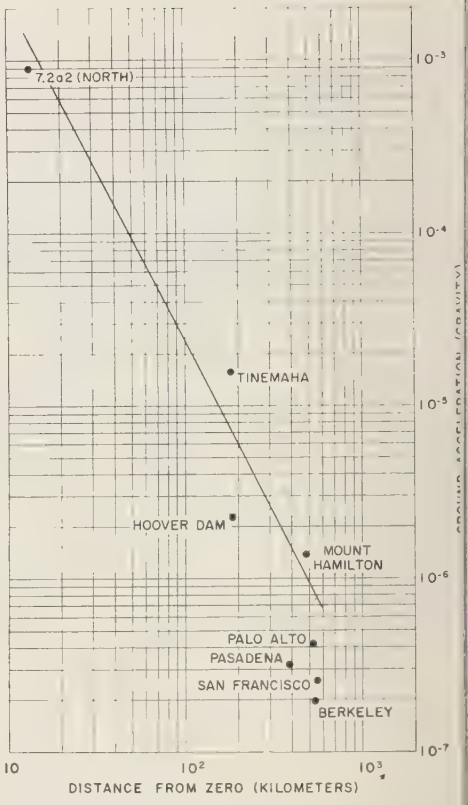

FIG. 10—Predicted and recorded accelerations, tele seismic station, Rainier shot.

source unimpeded the total seismic energy at any distance is determined from the area of the wave front multiplied by the ratio of the loss enroute. This may be represented by

$$E = E_s Q S\, e^{k_1 R}$$

where S is the area of the wave front; R is the distance, station to source; k_1 is an absorptio factor; and Q is a factor for loss by refractio or ratio of energy in the wave front as it leave the source to that which reaches as far as th station (horizontal homogeneity is assumed an absorption is neglected). All units are cgs, ex cept that R, when convenient, is in kilometer

If hemispherical wave fronts are assumed, $S = 2\pi R^2$. If measured energy is assumed to be con tained in body waves trapped in a surface laye of thickness h, $S = 2Rh$.

In empirical formulas, an exponential base 1 is more convenient to use. Therefore, if $k = 0.434k_1$,

$$E = 2\pi E_s Q R^2 \times 10^{kR} \qquad (4$$

if a hemispherical wave front is assumed; ar

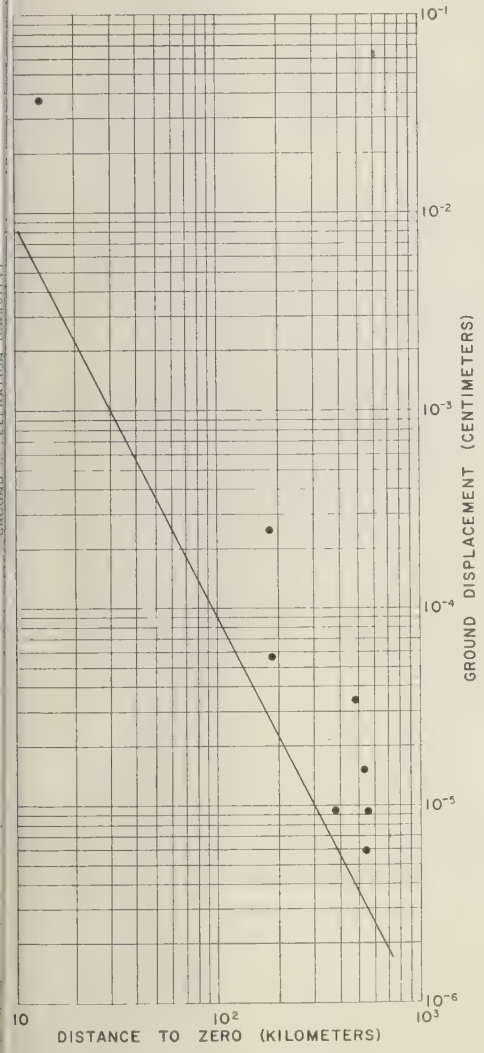

FIG. 11—Predicted and recorded displacements, strong-motion stations, Rainier shot.

$$E = 2\pi EQRh \times 10^{kR} \qquad (4b)$$

if a cylindrical wave front is assumed.

These energy formulas were utilized by the senior author (Carder) in an atempt to evaluate seismic energies at the source of earlier nuclear explosions detonated on the Nevada and Pacific-islands proving grounds. An absorption factor k was obtained from measurements of

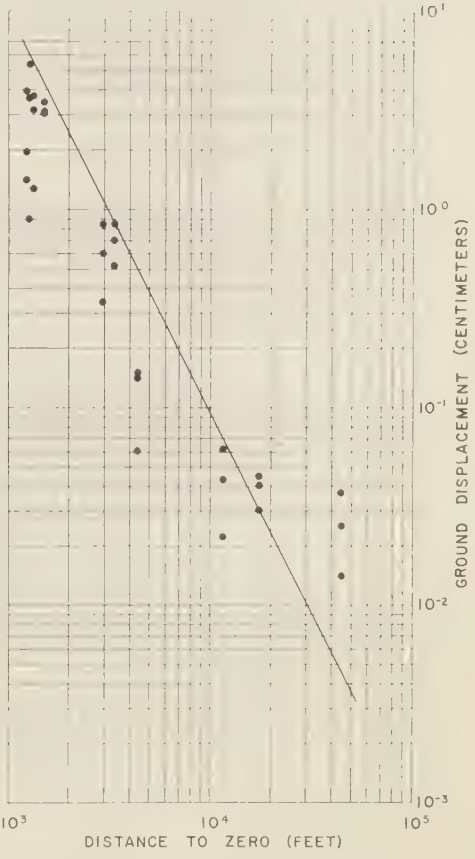

FIG. 12—Predicted and recorded displacements, teleseismic stations, Rainier shot.

S wavetrains (believed confined to the surface layers) resulting from the Trinity explosion of July 1945. This explosion was recorded by a number of Benioff seismographs at distances ranging from 437 to 1050 km. Their magnifications were estimated from a direct comparison with Wood-Anderson responses and trace amplitudes from the Bikini Baker explosion. The waves under study were assumed to be confined to surface layers. Using the relationship

$$k = \frac{\log (R_1 t_1 A_1^2 T_2^2 / R_2 t_2 A_2^2 T_1^2)}{R_2 - R_1}$$

with Trinity data, k was found to be about 0.0043 per km. Later a k of 0.005 per km seemed to give the better fit to most of the

TABLE 5—*South Holston Dam, Tennessee, explosion of February 5, 1949*

Distance, ft	Maximum displacement		Formula prediction, cm	Ratio of recorded to predicted
	Period, sec	Amplitude, cm		
8,000	0.33	0.068	0.128	0.53
11,500	0.33	0.046	0.062	0.74
38,500†	0.30†	0.018†	0.0033†	5.5

1,362,985 lb of high explosives were employed.
*Leet [1951].
†From an internal Coast and Geodetic Survey report by D. S. Carder.

Nevada data and will be used in this discussion.

Derivation of empirical amplitude relationships—Energy equations will be now applied to the Rainier problem. At distances of 180 km or greater, maximum amplitudes are in S or surface wavetrains of about 20-sec duration, and the period of the individual wave is about 1 sec. Further, the energy in the S surface group is considered only a part of the total. Consider it a third of the total, and if waves of only one component are measured, resultant energy is considered a ninth of the total. Represent this factor by $1/r$ (energy as measured from the seismogram near the source represents the total, if all components are measured). Within 1500 ft of the source most of the seismic energy is confined to a pulse of 2-sec duration and the component having the maximum amplitude contains from 0.4 to 0.5 of the total. We shall assume that $k = 0.005$ per km, that spherical wave fronts exist out to 150 km, that cylindrical fronts propagate beyond 150 km, and that the wave periods are 1 sec. We shall use as a base a ground amplitude of 1.9×10^{-4} cm at a distance of 180 km, and refer to data from this base with zero supscripts. This is an approximate square-root average between the amplitudes for Rainier from the Tinemaha and Hoover Dam records. From (3) and assuming the period $t = t_0$ and $v = v_0$ and equal layer thicknesses, we have

$$\frac{E_s}{rt} \propto A^2 = \frac{r_0 t_0}{rt} A_0^2 \frac{R_0}{R} 10^{k(R_0 - R)}$$

or

$$A^2 = \frac{k^2}{rtR} 10^{-kR} \qquad (5$$

where t and t_0 are durations of the pulse. Using $A^\circ = 1.9 \times 10^{-4}$ cm at 180 km and $k = 0.00$ per km, then $K = 0.1$, nearly. For R less tha 150 km, with the above data,

$$A^2 = \frac{N^2}{rtR^2} 10^{-kR} \qquad (6$$

where $N = 1$, nearly, and R is in kilometers.

In Figure 13, r and t are neglected in th dashed branch of the curve and the solid curv is a plot of equations (5) and (6), using $r_0 t_0 =$ 180 at 180 km and $rt = 6$ at 1 km, with th gradation of rt prorated between 1 km and 18 km. This solid curve from 3 to 150 km is con structed on the formula $(0.32/R) \times 10^{-0.00}$ which includes the gradations in rt.

The dotted line is the inverse-square relation ship modified from formula (2) by changin the coefficient 0.9 which would result from form ula (2), to 0.7.

The small circles are the amplitude maxim measured from strong-motion and teleseismi

TABLE 6—*Corona Quarry, California, explosion of February 18, 1959**

Distance	Maximum Acceleration		Ratio of recorded to predicted
	Recorded, g	Predicted, g	
1,200†	0.23	0.87	0.26
1,700‡	0.31	0.43	0.72

1,347,000 lb of high explosives were employed.
*Data recorded by the U. S. Coast and Geodetic Survey.
†On floor slab of heavy mill building.
‡On natural ground.

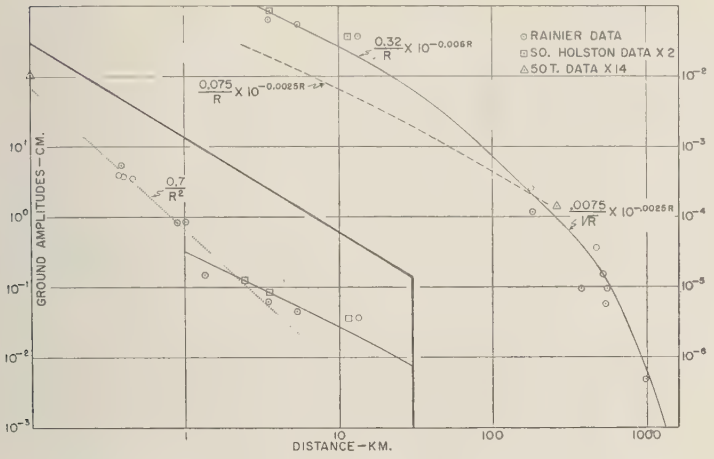

FIG. 13—Revised displacement attenuation formulas, Rainier shot. For use in extrapolation, values from curves should be multiplied by $(W(\text{tons})/1700)^{0.75}$.

data. The small squares are South Holston data multiplied by 2. The triangles are the measured or calculated displacement data from the 50-ton shot multiplied by 14.

Discussion of ground amplitude data, Rainier explosion—The fit of field data from 1 km and beyond to the solid curve in Figure 13 is certainly not perfect, but it is believed to be as satisfactory a fit as could be obtained from any other curve. One deviation is by a factor of 4; all others are well within a factor of 3. Without doubt slightly higher values for k would give more satisfactory results, and, certainly, body waves near the source would be expected to have a different absorption factor than S surface waves at some distance. Further refinements may result as more data are collected.

The Rainier data indicate a high absorption factor in the rock of the mesa from distances of about 1200 feet out to about 1.25 miles. From Figure 13, suppose $A = 7$ cm at 0.3 km and $A = 0.1$ cm at 3 km. If we assume transmission of energy outward in the form of spherical waves and no change in periods, we have from the energy equations,

$$k = \frac{\log\left(A_1^2 R_1^2 r_1 t_1 / A_2^2 R_2^2 r_2 t_2\right)}{R_2 - R_1}$$

$$= 0.40 \text{ per km.} \qquad (7)$$

The empirical formula (2), however, fits the close-in data—out to several kilometers—fairly well, although (7) will be used in later energy calculations.

Special mention of displacement data at Station 7.2a2N, distance 13.6 km, is in order. Here the amplitude is greater than the best empirical predictions by a factor of 2 and the duration of the wavetrain is probably 20 sec or more. This station is on deep alluvium. The results indicated here are therefore to be expected. This relationship was verified in later experiments, when it was observed that data from a station on rock at nearly the same distance fitted the empirical formula with fair accuracy and that the 7.2a2N data were again 2 to 3 times too high.

Discussion of acceleration attenuation—The empirical relationship in formula (1) fits nearby and teleseismic data fairly well. No attempt, therefore, will be made to refine it by using formulas based on energy absorption and distribution. However, a better fit to the data would result if the exponent of D were 2.2, as was observed from Figure 4.

Seismic energy at the source—Seismic energy is defined as the energy that leaves the source in the form of elastic waves in the rock. We shall assume for the Rainier explosion a spher-

ical wave front leaving the source in all directions and with uniform energy dissipation. We shall use a rock density of 2.0, a P-wave speed of 3.0 km/sec for tuff and 4.8 km/sec for limestone or quartzite, and a value for surface or near-surface amplitudes twice that of the confined amplitudes. We shall assume an absorption constant of 0.4 per km from 0 to 2 km and 0.005 per km beyond 2 km. Actually it is probably higher than this within the first thousand feet and somewhat lower near 2 km, but, until later refinements are made, this assumption seems to serve adequately for empirical purposes. We have then values for $\rho v_P^2/2$ of 30 $\times$ 10^5 for tuff and 48 $\times$ 10^5 for limestone and quartzite. No eneregy scatter other than absorption will be assumed. Pertinent data from close-in stations and the calculated logarithm of the seismic energy at the source, using formulas (3) and (4a), are listed in Table 7.

TABLE 7—*Seismic energy calculations from displacement data*

Station	R, km	$\Sigma A/T$	$E_s \times 10$, max.	10^{kR}	Log E
6003.01	5.38	0.033	1.60	10.3	18.48
.02	3.53	0.036	1.73	10.1	18.13
.03	1.34	0.30	9.00	3.44	17.54
.04	0.90	3.5	105	2.29	18.09
.05	0.41	40	1200	1.46	18.26
.06	0.39	52*	1560	1.43	18.33
.07	0.46	50*	1500	1.53	18.48
.08	0.38	34*	1020	1.42	18.12
.09	1.015	4.4	132	2.55	18.34

*Scaled in detail from records.

At present *Gutenberg and Richter* [1956] suggest the following formula relating the magnitude of M of earthquakes to energy

$$\log E = 9.4 + 2.14M - 0.054M^2$$

The median value of the exponentials in Table 7 is about 18.2. The Rainier shot is therefore equivalent to an earthquake of magnitude of 4.6 to 4.7. Earthquakes of lesser magnitudes are felt at distances somewhat greater than 2.5 miles. However, direct comparison with earthquakes is not entirely valid, since the energy calculations were based on high absorption near the source. In the calculations, high absorption, by assumption, ceases about 2 km from the source. The wave at this distance contains about 10 per cent of the estimated source energy. If the wave front at this distance is to be used for comparison purposes with earthquake magnitudes, log E is reduced by about 1.0, leaving 17.2 for the average exponential value. This corresponds to an earthquake of magnitude near 4.0. It is perhaps a more realistic figure, since the volume of ground involved at 2 km is probably comparable to the volume of ground involved at the focus of an earthquake.

Travel-time data.—The station distribution during the HARDTACK II series was much the same as for the Rainier shot (Fig. 1) with several stations on the mesa in which the underground explosions were fired and others on limestone and quartzite at lower elevations toward the east. During this series, greater precautions were taken to obtain reliable travel times. Travel times to the stations on tuff indicate average speeds of 2.8 to 3.5 km/sec, with a mean of 3.0 km/sec which fits most of these data. Speeds associated with stations on limestone and quartzite are 4.8 km/sec. The intercept at the time axis is about 0.03 sec. Beyond 10 km, more or less, to about 133 km, first arrivals are associated with a speed of 6.25 km/sec; the intercept time is 0.3 sec, and it follows that the depth under the shot points to the bottom of the 4.8 km/sec layer is about 1.1 km or about 3600 ft.

Discussion—Local ground effects from the Rainier and the larger HARDTACK II underground nuclear explosions have been predicted with fair accuracy with empirical formulas (1) and (2) which were derived from earlier work. The frequency ranges used to derive the formulas were from 1 to 20 cps for acceleration and from 0.5 to 2 cps for transitory ground displacement. The explosives were fully contained in moist volcanic tuff and the distance range was outside the zone of fracture, or greater than $80W^{1/3}$ ft, where W is the TNT equivalent in tons. For distances greater than 1 or 2 miles and less than 100 miles, formula (2) no longer fits observed data, and a substitute formula based on seismic wave propagation and absorption was derived:

$$A\ (\text{cm}) = \frac{8}{d} W^{0.75} \times 10^{-4-0.01d} \qquad (2a)$$

where d is in miles. From 100 to 600 miles, the ormula

$$A\ (\text{cm}) = \frac{2}{\sqrt{d}} W^{0.75} \times 10^{-5-0.004d} \qquad (2b)$$

eems to be the most applicable to 1- to 2-sec urface waves. Stations on deep alluvium would e expected to have two to three times the com- uted amplitudes, and poorly contained shots ould be expected to yield less ground effects. f the shot point is in crystalline or layered ock, the formulas would probably be changed n value or form because of the higher-frequency aves which might result or because of possible hanneling effects in a layer. It is believed that eismic energies assigned to large explosions are ot directly comparable with energies of earth- uakes because of the point source of explosions nd the large volume source of earthquakes. Comparable results may be obtained by using ormula (2a) rather than (2) and projecting it o zero distance. The calculated magnitude of he Rainier shot would then be about 4.0. Re- ulting ground effects at a distance were com- arable to those of an earthquake of that mag- itude.

One should be cautioned against the use of ormulas (1) and (2) or any other formula ased on an exponent of W of 0.75 or greater to igh yields, because eventually the predicted round accelerations and energy content will ecome unreasonably large.

Acknowledgments—The authors express appre- iation to the Atomic Energy Commission for ermission to republish a considerable portion of n earlier report [*Carder and others,* 1958] includ- ng eleven of thirteen illustrations.

Acknowledgments are due others of the staff of the Coast and Geodetic Survey for the collection and assembling of field data. Special mention is due E. B. Roberts, Chief, Division of Geophysics; to John Hershberger, L. M. Murphy, and F. H. Werner; and to T. H. Pearce and others of the Seismological Field Survey.

The authors are indebted to the following persons outside the Coast and Geodetic Survey who have contributed to the success of the projects covered in this article: R. G. Preston, Don Schueler, and Stanley E. Warner, University of California, Lawrence Radiation Laboratory; Frank Press, D. E. Hudson, and G. W. Housner, California Institute of Technology; and Perry Byerly, University of California.

This article was written by Federal Government authors as a part of their official duties. It is not copyrighted and is as much in the public domain as though published directly by the Government.

References

Carder, D. S., Seismic investigations of large explosions, *J. Coast and Geodetic Survey I,* 71–73, 1948.

Carder, D. S., W. K. Cloud, L. M. Murphy, and John Hershberger, Surface motions from an underground explosion, Operation PLUMBBOB Albuquerque Operations Office, *Atomic Energy Commission Report WT-1530,* November, 1958.

Cloud, W. K., and D. S. Carder, The strong-motion program of the Coast and Geodetic Survey, *Proc. World Conf. on Earthquake Engineering,* pp. 2–1 to 2–10, 1956.

Gutenberg, B., and C. F. Richter, Earthquake magnitude, intensity, energy, and acceleration, *Bull. Seis. Soc. Am., 46,* 105–145, 1956.

Hudson, D. E., Response spectrum techniques in engineering seismology, *Proc. World Conf. on Earthquake Engineering,* pp. 4–1 to 4–12, 1956.

Leet, L. D., Blasting vibration effects, *Explosives Engr.,* March-April, 1951.

Murphy, L. M., and W. K. Cloud, United States earthquakes 1952, *U. S. Coast and Geodetic Survey Serial No. 773,* 1954.

(Manuscript received July 20, 1959.)

Amplitudes of Seismic Body Waves from Underground Nuclear Explosions

CARL ROMNEY

Air Force Technical Applications Center, Headquarters, U. S. Air Force, Washington, D. C.

Abstract—Seismic waves from underground nuclear explosions in Nevada were observed at a number of temporary stations along a line extending eastward to Maine. A study of the seismograms from these stations and from a large number of permanent stations has shown that the amplitude of Pn varies inversely as the cube of the distance between 200 and 1100 km. Pn then disappears and a late-arriving higher velocity wave appears with relatively large amplitude. This later P wave has a slight amplitude maximum at about 2000 km, after which it decreases irregularly with distance.

Between 200 and 2000 km the amplitude of S (or Lg) varies inversely as the cube of the distance. The vertical, radial, and transverse components are of approximately equal size, and are about three times the amplitude of Pn between 200 and 1000 km.

At distances of 100 km or more the amplitudes of the body waves are proportional to the first power of the explosive yield. The explosions produced seismic waves equivalent in size to those from natural earthquakes of magnitude: $M = 3.65 + \log Y$, where Y is the energy of the explosion expressed in kilotons of TNT equivalent.

Introduction—Amplitudes of seismic body aves from earthquakes have been used as a ool for exploring the earth's interior at least nce the time of the Wiechert school of seis- ologists, about 1910. In principle, the relative nplitudes at all points on the earth's surface re predictable if the velocity structure and osorption within the earth are known [*Guten- erg*, 1944]. Amplitude measurements may thus e used to provide independent tests of con- usions on earth structure based on inferences om travel-time or other measurements.

Perhaps the earliest important application f amplitude information was in corroborating ie existence and probable fluid composition of ie core of the earth. For this purpose, it was iown that the amplitudes of longitudinal waves ecrease greatly beyond an epicentral angle of out 100°, at which distance the core inter- ipts transmission, and that shear waves are ot transmitted with observable amplitudes irough the core. Somewhat later, *Gutenberg* 1926] observed that longitudinal wave ampli- ides decrease with distance to about 15°, here the amplitudes suddenly increase; beyond out 20° the amplitudes decrease again. As is ell known from ray theory, a shadow zone will result if the velocity changes with depth in such a way that $dv/dr > v/r$, where v is the velocity at distance r from the center of the earth. The existence of such a low-amplitude zone between 5° and 15° was thus an essential part of Gutenberg's argument that a low-velocity region exists at a depth of about 80 km. Subsequent studies by *Richter* [1935], *Gutenberg and Richter* [1935, 1942, 1956], *Gutenberg* [1948], and *De Bremaecker* [1955] have tended to confirm the general conclusion stated above on the variation of P-wave amplitude with distance.

The remarkable nature of the amplitude studies just mentioned, and the conclusions drawn from them, becomes apparent when one considers the problems which beset seismologists working with earthquake sources. Since the seismologist has no control over the location of his energy source, he must accept amplitude measurements at distances where the seismographic stations happen to be. If he tries to supplement his data by using additional earthquakes, he is face to face with the problems of deciding how these earthquakes differ in energy or depth and how to allow for such differences. Moreover, it is known that earthquakes radiate

different amounts of energy in different directions; it is not certain that the exact radiation pattern at the source is known for any earthquake. A large proportion of the stations are equipped with instruments which differ from the instruments in the neighboring stations, with the result that the seismologist may be forced to view different portions of the spectrum of seismic motion at each of the various stations. To aggravate the problem, few of the seismographs are accurately calibrated. In spite of these difficulties, amplitude studies have produced information of great value to seismologists and others who seek to understand the nature of the earth.

Seismological studies of large explosions can overcome many of the problems mentioned, since the station (and sometimes the source) locations may be chosen, the energy and depth of the source are known, etc. The remaining problems, particularly the interpretation of the seismic data in terms of earth structure, are still formidable—see *Byerly's* [1956] review of general results from explosion seismology, for example. The intent of this report is to make available the results of an extensive program of measuring seismic-wave amplitudes from large explosions; it is hoped that this work will assist others in the more difficult problems of interpretation, which are not treated here.

The explosions—Seismic waves from six deep underground nuclear explosions in Nevada have been recorded sufficiently well at distances of 100 km or more to be of use in this study. Five of these explosions occurred during Octob 1958, as part of Operation HARDTACK; th sixth was an explosion named Rainier, fired as part of Operation PLUMBBOB during Sep tember 1957. The explosions were all fired in thick section of bedded tuff. Other informatio of interest to seismologists is contained in Tab 1. The 'depth' column gives the approxima distance to the nearest surface and is not nece sarily the vertical depth.

Sources of data—Seismograms from mo than 40 stations were studied at the time of th Rainier explosion. These were obtained fro university stations, stations of the U. S. Coa and Geodetic Survey, and stations of the D minion Observatory of Canada. Many of the 40 stations did not detect seismic waves fro Rainier. Some of the results of this study we reported by *Bailey and Romney* [1958]. Excep for the Wood-Anderson seismograms from se eral stations of the University of California an the California Institute of Technology, most the recordings were not suitable for amplitud studies.

When the Atomic Energy Commission an nounced that additional underground explosion would be conducted as a part of Operatio HARDTACK, the U. S. Air Force undertook program for the measurement of seismic wav from these shots. With the assistance of a co tractor (The Geotechnical Corporation), th Air Force was able to install 18 tempora seismographic stations. These stations were di posed at distances extending from 60 km fro

TABLE 1—*Characteristics of explosions**

Name	Date	Time Time GCT	North latitude	West longitude	Depth	Approx. yield kt
Tamalpais	8 Oct 58	22:00:00.1	37°11′43″	116°12′01″	330′	0.072
Evans	29 Oct 58	00:00:00.1	37°11′42″	116°12′17″	840′	0.055
Neptune	14 Oct 58	18:00:00 ± 1	37°11′38″	116°11′59″	99′	0.090
Rainier	19 Sep 57	16:59:59.4	37°11′45″	116°12′11″	790′	1.7
Logan	16 Oct 58	06:00:00.1	37°11′03″	116°12′04″	835′	5.0
Blanca	30 Oct 58	15:00:00.1	37°11′09″	116°12′07″	840′	19.0

* Sources of information:
Atomic Energy Commission [1959].
Johnson and Violet [1958].
Johnson, G. W., Summary of Experience Gained in Underground Nuclear Explosions, unpublished repo to the Second Plowshare Symposium, San Francisco, California, May 13, 1958.
Seismological Notes [1959].

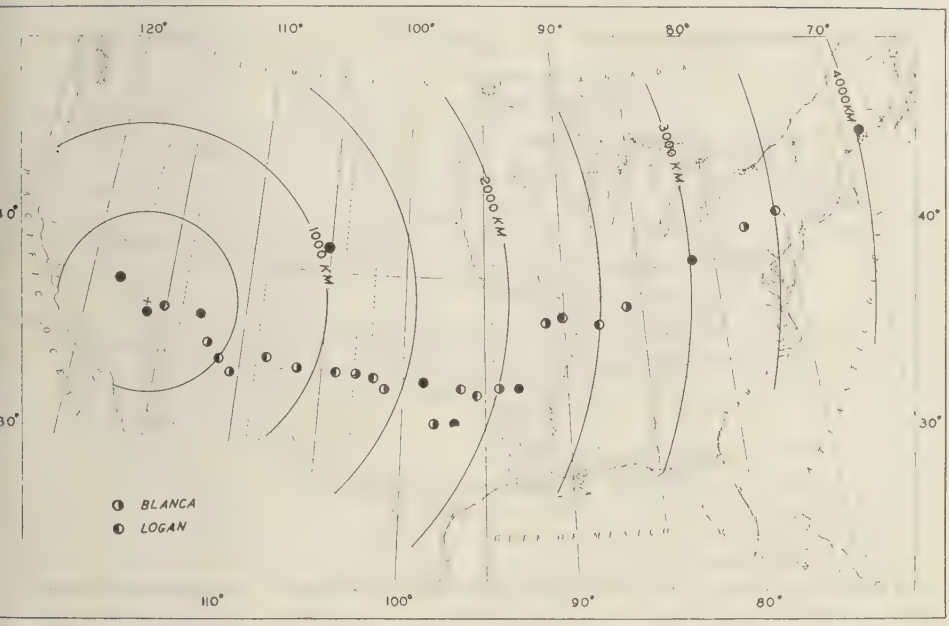

FIG. 1—Position of temporary stations during Operation HARDTACK, October 1958. Half-circles show the location of the mobile stations during the two principal explosions (as indicated in the figure); solid circles show the positions of stations which did not move. The cross indicates the position of the explosions.

the shot points to a distance of slightly more than 4000 km. Many of the stations were equipped with vehicles making it possible to move them to various locations as required. The stations were situated generally along a line extending eastward from the Nevada Proving Ground to Arkansas and thence northeastward to Maine (Fig. 1) with slight irregularities in the arrangement of stations to take advantage of the Geotechnical Corporation's offices near Dallas, Texas, and Laramie, Wyoming. Each operating site and alternate sites had been pre-selected by a team of geologists and geophysicists who located suitable outcrops of hard rock remote from obvious sources of man-made noise. It was planned that eight temporary stations would remain at fixed locations to provide control data on all shots, and it was hoped that the remaining ten mobile stations could be moved between shots in order to increase the amount of recorded data. These mobile teams were in fact able to move between shots Logan and Blanca. In all, recordings were made by the Air Force and the Geotechnical Corporation teams at 29 different distances from the shot point. Successful recordings were thus made at intervals of approximately 100 km out to 2300 km, and at intervals of about 250 km thereafter to a distance of 4000 km.

The temporary stations were all equipped with Benioff short-period vertical seismographs and most of them were additionally equipped with two horizontal components which were oriented along and transverse to the path from the shot point to the station. Each station was provided with a good timing device and means for recording time signals from WWV on a continuous basis. Each seismograph was calibrated under operating conditions by means of a Geotechnical Corporation ball-lift calibrator, which also gives the polarity of each instrument. In addition, special efforts were made to check both the calibration and the polarity by independent methods at one time or another during the course of the observations. Constants of the seismometers were $t_0 = 1.0$, $h_0 \simeq 0.7$

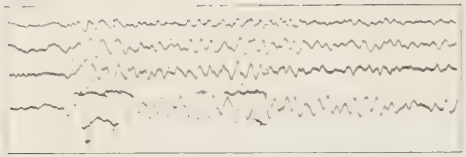

FIG. 2—P waves recorded at 1610 km. Top trace: recording of Logan on single vertical seismograph. Second trace: recording of Logan on array of four verticals. Third trace: recording of Blanca on single vertical seismograph. Bottom trace: recording of Blanca on array of four verticals. Compressional motion is upward; time marks at 10-sec intervals. Note the similarity of waveforms from both shots. Note also the emergence of smaller waves as a precursor to P as the signal-to-noise ratio increases from top to bottom.

(damping ratio of about 15:1); constants of the galvanometers were $t_g = 0.2$, $h_g \simeq 1.0$. The galvanometer and seismometer were loosely coupled in operation. It is believed that in most cases the magnifications of the instruments were known to within 5 to 10 per cent.

The results to be reported here depend to a large extent on the measurements from these temporary stations, supplemented, where possible, by data from many stations operated by universities, particularly those stations of the University of California and the California Institute of Technology, and stations of the U. S. Coast and Geodetic Survey. Seismograms for the largest explosions were available from more than 90 stations.

Amplitude-yield relationship for P waves—Each of the HARDTACK underground explosions produced almost identical waveforms at a given station (Fig. 2). It was therefore possible to measure the amplitude recorded from each shot at several identifiable points within the wavetrain. The separate measurements were then divided by the corresponding amplitudes recorded from the Logan shot, so that all results are normalized to Logan amplitude. For example, at the stations operated by the Air Force, the average ratio of the Blanca amplitudes to the Logan amplitudes was 2.36. At 12 stations of the California Institute of Technology and the University of California, the average amplitude ratio was 2.22. The results from these two sets of observations are thus in good agreement. Only Blanca, Logan, and Rainier produced measurable P waves at

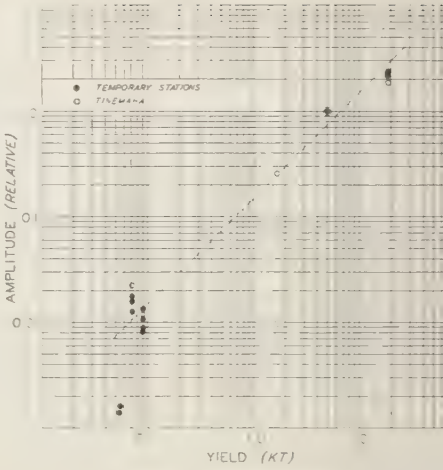

FIG. 3—Amplitude of underground explosions a function of yield. All measurements are re tive to Logan (5 kt) amplitudes. Solid circles Blanca (19 kt) are averages of university a temporary stations; solid circles for other sh are for individual station measurements.

distances beyond about 300 km. Amplitu ratios on the smaller shots are thus somewh less well determined. The results of these o servations are shown in Figure 3. It may seen that the points describe an approxima first-power relationship between amplitude a yield. A theoretical discussion of the reasons this relationship will shortly be published *Latter, Martinelli, and Teller* [1959]. It is o vious that the first-power scaling law cannot used to predict the amplitudes of very lar explosions, since the energy computed to be the seismic waves would ultimately exceed t total energy of the explosion. For reasons whi are not understood, the amplitudes from Eva were less than one-tenth of those from Tam pais, although the two shots released appro mately the same amount of energy (55 and tons, respectively). This phenomenon has be termed "The Evans Mystery."

For a comparison, the amplitudes record on the Wood-Anderson torsion seismograph Tinemaha are plotted on the same graph. The measurements are of the maximum amplitud in the shear waves rather than in the P-wa group. It may be seen that the Tinemaha shea wave amplitudes have about the same depen

TABLE 2—*Amplitude of P waves versus distance*

Logan		Blanca	
Distance km	Amplitude[a] mμ	Distance km	Amplitude[a] mμ
96.2	1,860 (P̄)	203.5	3,330
	14,500 (Pn?)	300.6	1,160
203.5	1,500	395.1	400
300.6	528	599.7	148
498.9	107	908.9	7.7
714.5	41	1036.0	5.2
1036.0	3.1	1215.1	49
1111.5	...[b]	1398.3	67
1313.1	17.4	1610.1	16
1610.1	5.1	1707.0	37
1803.7	6.3	1842.0	60
1902.1	13.9	2011.2	14
2111.3	11.4	2111.3	34
2305.0	64	2208.8	53
2506.0	19.5	2665.3	60
3017.4	<10[c]	3017.4	32
3502.0	<10[c]	3308.9	<10[c]
3717.5	~21[d]	3717.5	~44[d]
4020.6	17.2	4020.6	30.5

[a] P-wave amplitudes measured as half the maximum peak-to-trough displacement in the first few cycles of motion.

[b] Beginning P waves lost in noise from passing train.

[c] Signal not detected; noise estimated at 5 to 10 millimicrons.

[d] Estimated from College records.

nce on yield as the amplitudes of P waves.

Amplitude-distance relationship for P waves—The maximum vertical amplitudes in the first three cycles of the P waves are given in Table 2. These measurements, obtained from the temporary stations discussed previously, were computed by dividing the recorded amplitude by the seismograph magnification (for displacements) for sine waves of 1.0-sec period. Since all the recorded P waves had dominant periods of 1 second, or slightly less, the resulting amplitude may be considered to be roughly the peak earth displacement in the first part of the P waves. However, in the 0.5- to 1.0-sec period range, the response of the Benioff seismograph is more nearly proportional to earth particle velocity than to displacement, so that the amplitudes in Table 2 are more correctly considered to be equal to ground displacement divided by period. This quantity, A/T, is convenient for use in computing magnitudes, as discussed in a later section, and is more directly related to energy than is the displacement. For convenience, and since it is not a true velocity measure, A/T will simply be called 'amplitude' in the remainder of this report.

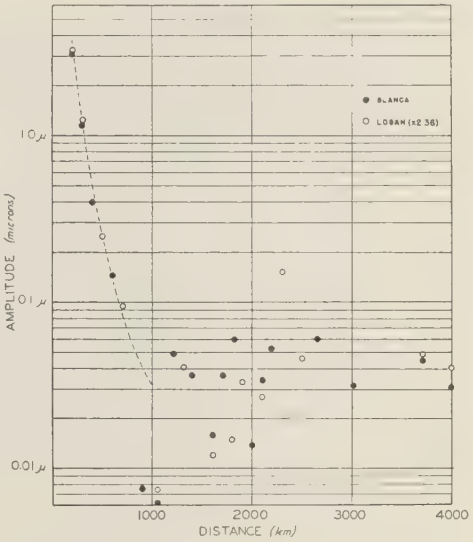

FIG. 4—Amplitude of P waves from a 19-kt underground explosion as a function of distance. The dashed curve is drawn proportional to the inverse cube of the distance.

The amplitudes from Table 2 are shown as a function of distance in Figure 4. The data indicated by the solid circles are from Blanca (19 kt). Logan data, indicated by open circles, were used to help define this curve by multiplying each observed Logan amplitude by 2.36, which was the average amplitude ratio of Blanca to Logan observed at fixed stations. Curves for other yields may be constructed by using the first-power scaling law (amplitude-yield relationship) mentioned in the preceding section. For example, the amplitude-distance curve from a 1 kt explosion in the same medium is estimated to be given by the amplitudes of Figure 4 divided by 19.

At distances between about 200 km and 1000 km the amplitudes of Pn are found to be inversely proportional to the cube of the distance, confirming measurements made from earthquakes and previously reported in the literature

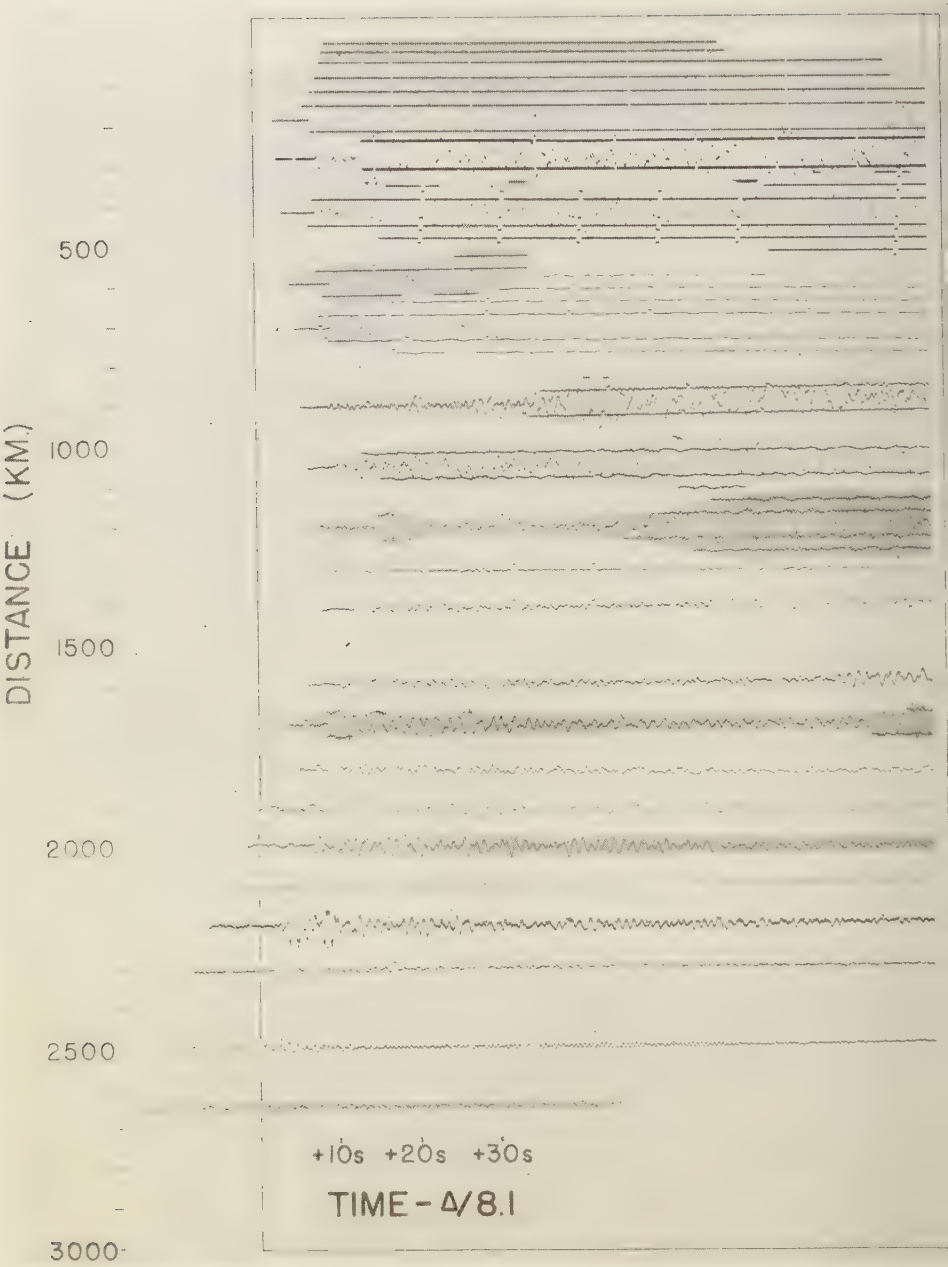

Fig. 5—Vertical-component seismograms from Logan and Blanca. Time marks are at 10-sec interval except the 0-sec mark is omitted each minute. Compressional motion is upward. Note the break in the travel-time curve and the late arrivals commencing at about 1200 km. Note $\bar{P}$ (6 km/sec) near the right-hand margin on the 1700-km record and on records of closer stations at successively earlier times.

of seismology [*Gutenberg and Richter*, 1956].

Beyond about 1000 km, Pn apparently decreased to such small amplitudes that it became undetectable at most stations. However, other strong P waves were detected several seconds after the expected time of Pn. Generally, these late waves had longer periods than Pn, and the travel times indicated a higher apparent surface velocity. The abrupt change in the amplitude-distance relationship, the longer periods, the higher speeds, and a break in the travel-time curve all indicate the arrival of a new wave. Similar observations were first noted by Gutenberg and discussed extensively by him in a paper on structure of the earth's mantle [*Gutenberg*, 1954].

Beyond 2000 km the amplitudes fall off about as expected from earthquake studies, except that there is a low-amplitude region at 3300 and 3500 km. Logan was not detected at 3500 km and Blanca was not detected at 3300 km. In each case, measurements of microseismic noise showed that the P-wave amplitudes must be less than 10 millimicrons.

Figure 5 shows a selection of the vertical-component seismograms obtained at distances from 200 through 2650 km; the figure includes recordings of both Logan and Blanca. The seismograms are arranged in order of distance and aligned in time so that the arrivals should all lie along a straight line parallel to the distance axis if the speed of the P waves is 8.1 km/sec. The time marks on the seismograms are at 10-sec intervals except that one mark is omitted each minute; upward motion on the seismograms is compressional motion of the earth. The preceding remarks concerning the late arrivals and higher apparent surface velocities of the waves beyond 1000 km may be confirmed by inspection of Figure 5.

The seismograms shown in Figure 5 also illustrate the problem of determining the direction of first motion. In principle, the first motion from a blast should always be compressional. It may be seen that the first motion is recorded as compressional at some stations and rarefactional at others. There seems to be no systematic dependence upon the distance, with the obvious exception that the first wave is strong and compressional at small distances (less than about 700 km). At distances greater than 1100 km and less than 2650 km, it is not known with certainty whether the first motion was observed at any station on either Logan or Blanca. At some stations, (for example, the station at 2300 km) there is apparently clear, rarefactional first motion in spite of a signal-to-noise ratio of at least ten. The problem of identifying the direction of first motion may perhaps be better understood by a study of Figure 2, which shows the emergence of new and smaller waves ahead of the main P pulse as the signal-to-noise ratio is improved. It is clear from this illustration that the direction which will be read and reported can be expected to be a function of the signal-to-noise ratio. It is also clear that there must be a very large signal-to-noise ratio indeed if first motions at this distance (about 1600 km) are to be considered meaningful. This particular distance, of course, is particularly troublesome from this standpoint, since the first waves in the Pn shadow zone may well be diffracted and hence unusually weak. Direct measurements were made of first motion at distances less than 1000 km. Here, there is no reason to expect diffracted arrivals, and the waveforms are relatively simple. It was found that first motion decreases with distance relatively faster than the total P-wave motion decreases. At 200 km, first motion was about one-third of the total amplitude, whereas at 1000 km first motion decreased to less than one-fifth of the total motion.

Shear waves—Short period (1- to 1.5-sec period) shear (or Lg) waves, arriving at a speed of about 3.5 km/sec, were observed to a distance of about 2000 km. These waves have not been analyzed in detail at the present time. As a general observation, however, it can be stated that the radial- and transverse-horizontal components of motion are approximately equal in amplitude, and that these, in turn, are approximately equal in size to the vertical component of motion. Amplitudes are shown in Figure 6. Logan amplitudes were normalized to Blanca with a normalizing factor of 2.25, which was the average amplitude ratio observed at fixed stations. Note that the shear waves have about three times the vertical amplitude of the Pn waves. At some distances there is the appearance of several discreet arrivals which might help to confirm the conclusion that these waves are high-mode surface waves propagated

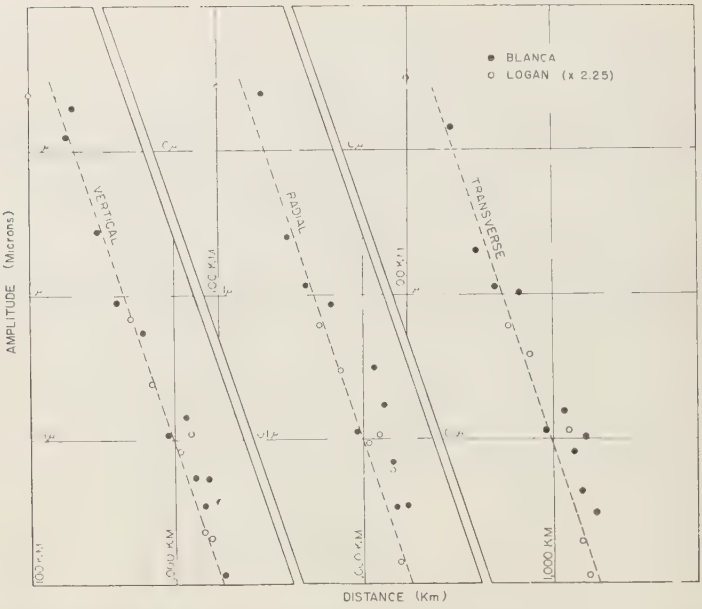

FIG. 6—Amplitudes of 3.5-km/sec shear waves from a 19-kt underground explosion. Curves are drawn proportional to the inverse cube of the distance.

in accordance with a method suggested by *Oliver and Ewing* [1957]. The fact that these amplitudes vary as the inverse cube of the distance may not be consistent with the interpretation that these are high-mode surface waves, however.

Surface waves—Rayleigh waves were detected by long-period seismographs at Berkeley, California; Laramie, Wyoming; Fort Sill, Oklahoma; and Palisades, New York. In addition, there are clear indications of Love waves at Berkeley and Palisades; and at Resolute Bay the surface wavetrain consists predominately of Love waves of 10- to 15-sec period. These latter waves were completely unexpected from blasts, and their presence on the seismogram is believed to be due to mode conversion near the source, by processes which are not understood at the present time. The amplitudes of surface waves were not measured.

Magnitudes—Three variations of the magnitude scale are in use today [*Gutenberg*, 1956]. These scales are designed to give concordant results at about magnitude six, but may disagree slightly at other magnitudes. One scale which is of interest in the present problem makes use of measurements of maximum amplitude recorded on standard Wood-Anderson torsion seismographs from sources at small distances. The other scale of interest makes use of the amplitude of longitudinal waves measured on calibrated vertical seismographs at greater distances.

Magnitudes were first determined for all shots recorded by Wood-Anderson torsion seismographs according to the method given by *Richter* [1935]. It should be emphasized here that these magnitudes merely serve for comparison of the size of the seismic waves from blasts with those from earthquakes; it is not believed that the energies released can be compared by this means. The complete results are shown in Table 3.

The magnitude of Blanca, determined from the torsion seismographs, was found to be 4.8 ± 0.4* based on measurements from ten stations. The magnitude of Logan was found to be 4.4 ± 0.4* based on measurements from the same ten stations. Only seven stations with torsion seismographs recorded measurable ampli-

TABLE 3—*Magnitudes from torsion seismographs based on shear-wave amplitudes*

Station	Distance km	Magnitude				
		Blanca	Logan	Rainier	Tamalpais	Neptune
Tinemaha	180.7	5.1	4.8	4.2	3.1	2.9
Woody	289.1	4.2	3.9			
Riverside	370.8	4.7	4.4			
Pasadena	382.2	4.8	4.4	4.0		
Mt. Hamilton	482.8	5.4	5.0	4.7		
Barrett	502.8	3.9	3.7			
Palo Alto	530.4	5.2	4.8	4.4		
Berkeley	540.5	4.9	4.5	4.1		
San Fran.	556.6	4.9	4.5	4.2		
Mineral	583.0	4.8	4.4	4.3		

Note: Blank spaces in the table mean signals were not detected or were not measurable for other reasons.

tudes for Rainier; these gave a magnitude of $4\frac{1}{4} \pm 0.2$*. The magnitudes for the smaller shots were observable at only one station, and reliance should not be placed on these single estimates. It is important to note that if the Rainier magnitude is computed by differences from Logan and Blanca, it is found to be about 4.05, rather than $4\frac{1}{4}$. It thus appears that the magnitude was originally overestimated because the amplitudes at three stations were not included in the calculation; a revised magnitude of 4.0 or 4.1 is now preferred for Rainier.

Magnitudes were next computed for Blanca and Logan from eight and six stations, respectively, at greater distances (Table 4). In the computation the procedures and the table given by *Gutenberg* [1956] were used. The results are: for Blanca $M = 4.8 \pm 0.4$*; and for Logan $M = 4.4 \pm 0.5$*. Thus, magnitudes estimated by the two methods are in agreement. According to Gutenberg, such agreement is not expected—at least not from earthquakes. His studies show that estimates of earthquake magnitudes by the two procedures will disagree by nearly one magnitude unit, since the two scales have diverged by that amount at magnitude 4.5. This discrepancy may not be significant, however, because of the uncertainty of the relationship between the two magnitude scales.

TABLE 4—*Magnitudes from Benioff seismographs based on P-wave amplitudes*

Distance km	Magnitude	
	Blanca	Logan
1706.9	4.5	...
1803.7	...	3.8
1842.0	4.7	...
1902.1	...	4.1
2011.2	4.1	...
2111.3	4.5	4.0
2208.8	4.7	...
2305.0	...	4.9
2506.0	...	4.5
2665.3	5.1	...
3017.4	5.0	...
4020.6	5.1	4.9

Since it appears that the measurements given in Table 3 and Table 4 are a homogeneous set, all measurements were combined to give

$$\text{Blanca Magnitude} = 4.8 \pm 0.1$$

$$\text{Logan Magnitude} = 4.4 \pm 0.1$$

where the precision index is the standard deviation of the mean.

The magnitudes of smaller shots may be computed from their amplitudes, the established magnitude of Logan, and the relation,

$$M_1 - M_s = \log \left(\frac{A}{T}\right)_1 - \log \left(\frac{A}{T}\right)_s$$

where the subscripts refer to Logan and the shot in question. The origin of this expression may be seen from the definition of magnitude in the next section. Results are

$$\text{Rainier Magnitude} = 4.1$$

$$\text{Neptune Magnitude} = 2.4$$

$$\text{Tamalpais Magnitude} = 2.6$$

Magnitude-yield relationship—A magnitude-yield relationship can be derived from the data so far presented. The basic definition of magnitude is

$$M = \log \left(\frac{A}{T}\right)_d - \log \left(\frac{B}{T}\right)_d \qquad (1)$$

where $(A/T)_d$ is the 'amplitude' at distance d and $(B/T)_d$ is the 'amplitude' of a zero magnitude shock at the same distance. The observed relationship (Fig. 3) between amplitude and

* Standard deviation of a single observation.

yield (Y) is given by

$$\left(\frac{A}{T}\right)_d = K_d Y \qquad (2)$$

where K_d is the amplitude observed at a distance d from an explosion of 1 kiloton yield. From (1) and (2), it may be seen that

$$M = C + \log Y \qquad (3)$$

where C is a constant which can be evaluated if the magnitude is known for a given yield. Estimates for C can be made, based on the known yields and magnitudes. Values of C are found to be: for Blanca 3.5; for Logan 3.7; for Rainier 3.9; for Neptune 3.4; and for Tamalpais 3.7. Equation (3) is thus found to be

$$M = 3.65 + \log Y \qquad (4)$$

where Y is the yield in kilotons. Shot Evans was not used in the determination. This relationship may not apply for shots in other localities or in other media within the Nevada Test Site.

Acknowledgments— It is a pleasure to acknowledge the difficult but excellent work of all members of the field teams who obtained the basic information used here. Joe Whalen and Wayne Helterbran of the Geotechnical Corporation deserve special thanks, as do Lt. Col. Benjamin Grote and Major John Bush of the U. S. Air Force. I also wish to extend my appreciation to Leonard Murphy of the U. S. Coast and Geodetic Survey for collecting and making available the records from many stations, and to the operators of those stations for supplying the records. Finally, many of my colleagues deserve credit for assisting in the reduction and interpretation of the data.

References

Atomic Energy Commission, *Atomic Energy Commission Release on HARDTACK Bomb Tests,* No. B-39, March 10, 1959.

Bailey, L. F., and C. F. Romney, Seismic waves from the Nevada underground explosion of September 19, 1957, *Bull. Geol. Soc. Am., 69,* 1672, 1958.

Byerly, P., Subcontinental structure in the light of seismological evidence, *Advances in Geophys., 3,* 1956.

De Bremaecker, J. Cl., Use of amplitudes, Part I: Pn from 3° to 23°, *Bull. Seis. Soc. Am., 45,* 219–244, 1955.

Gutenberg, B., Untersuchungen zur Frage bis zu welcher Tiefe die Erde kristallin ist, *Z. Geophys., 2,* 24–29, 1926.

Gutenberg, B., Energy ratio of reflected and refracted seismic waves, *Bull. Seis. Soc. Am., 34,* 85–102, 1944.

Gutenberg, B., On the layer of relatively low wave velocity at a depth of about 80 kilometers, *Bull. Seis. Soc. Am. 38,* 121–148, 1948.

Gutenberg, B., Low-velocity layers in the earth's mantle, *Bull. Geol. Soc. Am., 65,* 337–348, 1954.

Gutenberg, B., Magnitude and energy of earthquakes, *Ann. geofis., Rome, 9,* 1–15, 1956.

Gutenberg, B., and C. F. Richter, On seismic waves (second paper), *Gerlands Beitr. Geophys., 45,* 280–360, 1935.

Gutenberg, B., and C. F. Richter, Earthquake magnitude, intensity, energy, and acceleration, *Bull. Seis. Soc. Am. 32,* 163–191, 1942.

Gutenberg, B., and C. F. Richter, Earthquake magnitude, intensity, energy, and acceleration (second paper), *Bull. Seis. Soc. Am., 46,* 105–145, 1956.

Johnson, G. W., and C. E. Violet, *Phenomenology of Contained Nuclear Explosions,* UCRL-5124 Rev. I, University of California, Lawrence Radiation Laboratory, Livermore, 27 pp., 1958.

Latter, A. L., E. A. Martinelli, and E. Teller, A seismic scaling law for underground explosions, *Physics of Fluids,* 1959 (in press).

Oliver, J., and M. Ewing, Higher modes of continental Rayleigh waves, *Bull. Seis. Soc. Am., 47,* 187–204, 1957.

Richter, C. F., An instrumental earthquake magnitude scale, *Bull. Seis. Soc. Am., 25,* 1–32, 1935.

Seismological Notes, *Bull. Seis. Soc. Am., 49,* 205, 1959.

(Manuscript received July 10, 1959)

Note on the Tectonics of Kern County, California, as Evidenced by the 1952 Earthquakes[1]

A. E. SCHEIDEGGER[2]

California Institute of Technology
Pasadena, California

Abstract—A statistical analysis has been made of the mechanisms of the aftershocks of the Kern County, California, earthquake of July 21, 1952. A method the writer developed earlier shows the direction of tectonic motion to be at N 32° W, approximately normal to the strike of the White Wolf fault. This is in agreement with Gutenberg's fault-plane solution for the main Kern County earthquake which yielded an overthrust in a northwesterly direction. It therefore appears that the Kern County earthquake and its aftershocks were caused by the same tectonic effects.

It stands to reason that the recent tectonics f an area is somehow connected with the arthquakes that occur in that area. In par- cular, one would suspect that the fault-plane olutions of the earthquakes would have a irect correlation with recent tectonic displace- ents. However, if one plots the available fault- lane solutions in an area, one does not, in eneral, obtain a consistent picture: the fault- ig indicated by the earthquakes appears to ccur in a more or less random fashion with o obvious connection with the tectonic pic- ure.

In this connection, the writer has shown *Scheidegger,* 1958a] that a correlation with ie tectonics does, in fact, exist, if the fault- lane solutions are treated statistically. The ethod is based upon the assumption that the ull axes of the fault-plane solutions (being the ntersection between the fault plane and the lane that is normal to the displacement vector) re, on the average, orthogonal to the mean di- ection of tectonic motion of the area. Thus, if a eries of fault-plane solutions of earthquakes is vailable in an area, it is possible to determine ie direction of tectonic motion of that area. his method was applied to the Northwest Pa- fic Ocean [*Scheidegger,* 1958b]. In that case, however, the number of fault-plane solutions of earthquakes was not large enough to actually substantiate the method in the light of known tectonics. In order to attain the latter aim, a large number of fault-plane solutions in a very small area must be available. Such a possibility existed in central and western Asia [*Scheidegger,* 1959], where many fault-plane solutions of small 'local' seismic shocks are readily accessible in the literature. The statistical analysis of these fault-plane solutions has completely justified the method by demonstrating that the seismically postulated tectonic motions are in full agreement with the recent tectonic displacements as determined from geological field observation.

Central Asia was chosen as a test area for the writer's statistical method because of the many fault-plane solutions which were available. There is another instance where a similar number of fault-plane solutions per unit of area is available: the aftershocks of the Kern County earthquake which occurred in California in 1952. However, the nature of the Kern County data is quite different from that of the central Asian earthquakes.

In central Asia, small 'local' earthquakes occur almost every day. If a group of portable instruments is in operation for a few months in this area, enough data for the analysis of several hundred earthquakes can be collected. As stated, the situation in Kern County is quite different. Here, a large earthquake occurred on

[1] Contribution No. 928 from the Division of eological Sciences, California Institute of Tech- ology, Pasadena, California.

[2] On leave of absence from Imperial Oil Lim- ed, Calgary, Canada.

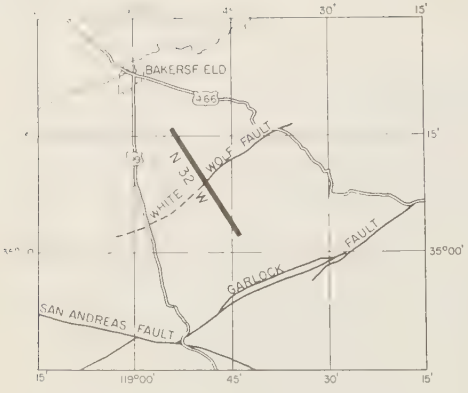

FIG. 1—Tectonic motion as determined from the aftershocks of the Kern County earthquake of 1952, in relation to the known tectonics of the area.

July 21, 1952, with many aftershocks following in its wake. Only the regular station-network could be used for collecting data, since the operation could not be planned in advance as had been done in central Asia. The regular net work is very dense, but not quite dense enoug for actual fault-plane solutions to be obtaine

The Kern County data have been analyze by *Båth and Richter* [1958]. These autho determined the position of the nodal lines o the surface of the earth and made an estimat as to whether there are one or two nodal line If there are two nodal lines, it must be assume that one represents the strike of the fault plan and the other the strike of the plane normal t the motion, so that the null axis points verti cally downward. If there is only one nodal lin it represents the null axis itself. Needless to say this interpretation is somewhat crude; on really would like to know the dip and strik of both the fault and the auxiliary plane. How ever, one still has reason to believe that th above interpretation should lead to a genera picture of the tectonics of the area if the sta tistical analysis is performed with the null axe as indicated above.

Because of the simple nature of the nul

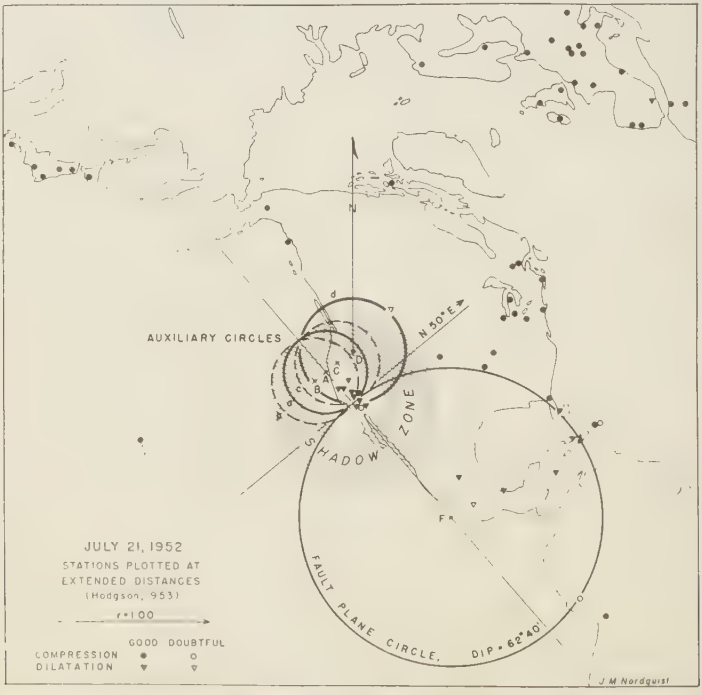

FIG. 2 Gutenberg's fault-plane solution of the main Kern County shock of 1952 [from Gutenber 1955].

es (vertical or horizontal), the statistical alysis (which ordinarily is a rather compli- ted procedure, best executed on an electronic mputer) becomes very simple indeed. The ane normal to the direction of tectonic mo- on must be vertical (so as to contain all the ll axes corresponding to the bi-nodal solu- ons), and its strike must be equal to the erage strike of the uni-nodal solutions.

Båth and Richter [1958] list 57 fault-plane lutions of aftershocks. Of these, 13 are uni- odal and the average strike of their nodes is 58°E. Hence, the direction of tectonic motion which is normal to the former direction) turns ut to be N 32°W. Naturally, the seismic ethod can give no indication as to the sense the motion along this direction. The relation- ip of the motion direction with the tectonics Kern County is shown in Figure 1.

At first glance, it might appear to be some- hat odd that the direction of tectonic motion, s calculated from the aftershocks, is almost ormal to the White Wolf fault—an indication at the latter is a normal fault or an over- rust. Perhaps one would rather expect a trike-slip motion. However, it should be noted at the direction thus calculated from the ftershocks is well-nigh identical to that ob- ained by *Gutenberg* [1955] by performing a ault-plane solution on the main shock. Guten- erg's fault-plane solution of the main Kern ounty earthquake is reproduced in Figure 2. ne sees from this figure that the main shock orresponds to an overthrust in a northwesterly irection. The auxiliary circle (representing he plane that is normal to the tectonic motion) s somewhat ambiguous (represented by the possibilities *a*—*d* in Fig. 2); one possibility is a pure overthrust with no lateral component (circle *a* in Fig. 2). The resulting direction of the thrust is then N 40°W, which is 8° west of what has been calculated from the aftershocks. In view of the various uncertainties in the interpretation, this discrepancy is very minor indeed.

It therefore appears that the Kern County earthquake and its aftershocks were caused by the same areal tectonic effects.

In conclusion, the writer wishes to acknowledge that it was the kind invitation of R. P. Sharp, Chairman of the Division of Geological Sciences, and F. Press, Director of the Seismological Laboratory, to spend a period as a visitor at the California Institute of Technology, which enabled him to complete the present study. Discussions of the subject matter with C. F. Richter have been of invaluable help.

References

Båth, M. and C. F. Richter, Mechanisms of the aftershocks of the Kern County, California earthquake of 1952, *Bull. Seis. Soc. Am., 48,* 133–146, 1958.

Gutenberg, B., The first motion in longitudinal and transverse waves of the main shock and the direction of slip, *Calif. Dept. Nat. Resources, Div. Mines, Bull., 171,* 165–170, 1955.

Scheidegger, A. E., Tectonophysical significance of fault plane solutions of earthquakes, *Geofis. pura e Appl., 39,* 19–25, 1958a.

Scheidegger, A. E., Seismological evidence for the tectonics of the Northwest Pacific Ocean, *Bull. Seis. Soc. Am., 48,* 369–375, 1958b.

Scheidegger, A. E., Seismic evidence for the tectonics of Central and Western Asia, *Bull. Seis. Soc. Am.,* 1959 (in press).

(Manuscript received April 22, 1959.)

Earthquake Waves Reflected at the Inside of the Core Boundary*

B. GUTENBERG

Seismological Laboratory
California Institute of Technology
Pasadena, California

Abstract—Travel times of waves generated by an earthquake at a depth of 600 km and reflected from the inside of the core boundary as well as the epicentral distances of the caustics of PKKP, SKKP, and PKKS agree within the limits of error with those calculated on the basis of velocity-depth curves. This applies also to the travel times of SKKS and SKKKS for which poor agreement was reported before the inner core was established. The periods of all waves traveling through the outer core seem to be shortened. In the outer core the attenuation is possibly smaller than in the mantle.

Symbols and materials used—For brevity in he following discussion, waves which have raveled through the outer core, but not through he inner core, are indicated by one prime, hose which have entered the inner core, by wo primes. Thus, for example, P′ ≡ PKP, P″ ≡ PKIKP, SKKP″ ≡ SKIKKIKP. Symbols with a subscript 1 (for example, P_1') refer o the earlier of two branches connecting at a ocal point, those with a subscript 2 to the later. An asterisk indicates an epicentral distance over 80° (for example, SKKS*).

Unless it is stated otherwise, all data refer o the earthquake of 1957, April 16, 4:04:04, vith an adopted epicenter at 4.5°S, 107.5°E, ocal depth 600 km. The elements of this shock nave been redetermined. Considering the expected systematic errors involved in the calculation (for example, in the assumed travel imes or resulting from the assumption that the nternal structure of the earth is spherical), he coordinates of the adopted epicenter are probably correct within a few tenths of a legree, the origin time within 2 or 3 seconds, nd the focal depth within about 20 km. Records of this shock from 55 stations at listances from 119° to 178° have been used previously by Gutenberg [1958a, p. 244]. Additional records have been made available upon equest by the following stations (epicentral listance in degrees in parentheses): Brisbane (48.9), Matsushiro (49.9), Jerusalem (77.4), Kiruna (93.0), Uppsala (93.8), Honolulu (95.7), Skalstugan (96.3), College (100.3), Sitka (108.1), Alberni (117.3), Victoria (118.5), Banff (121.3), Saskatoon (124.8). The author is very grateful for the speedy response from all stations.

Theoretical travel times of waves originating at the earth's surface have been calculated on the basis of the tables of *Jeffreys and Bullen* [1940] for waves through the mantle. For those through the core the same procedure has been followed as described by *Gutenberg* [1958a, p. 241]. This is based on the travel times of *Gutenberg* [1958b, Table 4] for the portion of the waves through the core and on the travel times of *Jeffreys and Bullen* [1940] for PcP, ScS, and ScP for zero focal depth. Corrections for the focal depth of 600 km have been taken either from tables of *Jeffreys and Bullen* [1940] or from tables of *Gutenberg and Richter* [1936]. The resulting differences between the two procedures are small and within the limits of errors. Corrections for the effect of the focal depth on distances of the focal points have been taken from tables of *Gutenberg and Richter* [1936]. Errors in the assumption of corresponding portions of PcP, ScS, and PcS on the one hand and of the portions of the paths inside the core on the other rarely affect the resulting travel-time curves by more than 2 seconds; moreover, they may shift the calculated distance of focal points by

* Contribution No. 933, Division of Geological Sciences, California Institute of Technology.

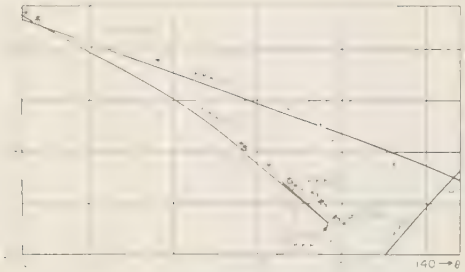

FIG. 1—Travel times t of the PKKP group for epicentral distances Θ in degrees, observed for earthquake 1957, April 16, at 4:04:04, focal depth $h = 600$ km, and calculated curves for $h = 600$ km. Symbols as in Fig. 3.

about one degree and even more under unfavorable circumstances; for example, for repeated reflections. The calculated travel-time curve then either extends beyond the actual curve in the preceding direction or ends at a shorter distance with a focal point practically on the actual curve.

The PKKP group—Travel times and amplitudes of PKKP′ and PKKP″ have been studied previously by the author [*Gutenberg,* 1951, pp. 381, 383; *Gutenberg,* 1958a, p. 246]. Most of the travel times of PKKP′ observed for the shock 600 km deep are within a few seconds of the calculated values (Fig. 1). There are a few observations which closely fit the travel times calculated for PKKP″, but this phase is never conspicuous. Some of the PKKP′ phases, however, are very clear (Fig. 2). According to *Jeffreys and Bullen* [1940, p. 42] the focus of

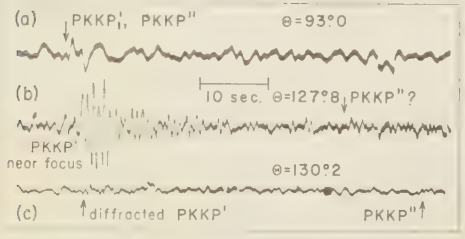

FIG. 2—Portions of records of shock 1957, April 16, 4:04:04, focal depth 600 km, showing waves of the PKKP group. (a) Grenet vertical, Kiruna, 93.0°; (b) and (c) short-period Benioff verticals; (b) Woody, 127.8°; (c) Barrett, 130.2°, about 2½° beyond focus of PKKP′.

PKKP′ for shocks at zero focal depth should be at 234° (126°), whereas the new calculations give about 127°. The decrease in distance connected with a focal depth of 600 km is about 2°, so that theoretically the caustic of PKKP′ should be expected at 232° to 231°; that is, near 128° to 129°. Actually, no PKKP′ waves have been observed beyond 130.2° (Fig. 2c), although there are records available for 130.7°, 132.2°, 133.9°, 134.2°, 134.7°, etc.

The ratio of the amplitude a to the period T of PKKP′ has been compared with the corresponding ratios for PP and for P″. Unfortunately, the travel-time curve of PP crosses that for pP″ near 130° and follows it at greater distances. Consequently, amplitudes of PP cannot be found with confidence for distances exceeding about 128½°. For distances less than 128°, the ratio a/T for PKKP′ to that for P″ was found to increase on seismograms for the short-period vertical instruments from about 0.1 to 0.2 at distance between 121° and 127° to 0.4 at 127.5° and 0.5 at 127.8° (Fig. 2b) and then to drop to less than 0.1 beyond 128° (Fig. 2c). Similarly, the ratio of a/T for PKKP′ to that for PP was 1 or more at distances less than 128° but only about 0.5 between 128° and 128½°. Thus the focal point of PKKP′ in the shock 600 km deep has been at about 127¾°, and diffracted PKKP waves have been observed for about 2½° beyond. Thus, the travel-time curve for PKKP, calculated on the recent assumptions of the velocities of longitudinal waves in the core, agrees with the observations well within the limits of error.

PKKKP should have a caustic at distances near 315° (45°) with travel times near 36 minutes in shallow shocks (near 35 minutes in shocks 600 km deep), with both branches extending towards the epicenter. Apparently it has not been observed; in the present research no records obtained at such short distances have been used.

SKKS and SKKKS—Gutenberg and Richter [1939, p. 126] found noticeable differences between the observed and calculated travel times of SKKS and SKKKS; however, their travel times were calculated prior to the discovery of the inner core. A comparison of observed and calculated travel times of these phases was made by *Nelson* [1954], who found that the

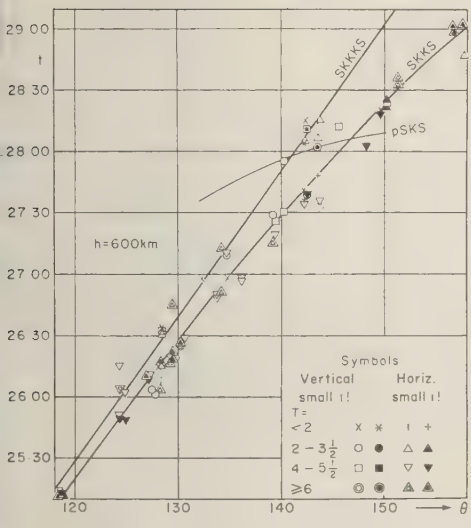

FIG. 3—Travel times t of SKKS and SKKKS, details as in Fig. 1.

residuals for SKKS and SKKKS never exceeded 7 seconds, relative to the improved travel-time curves. Figure 3 shows a portion of the recently calculated travel times of the two phases for shocks at a focal depth of 600 km and the times observed on seismograms of the shock of April 16, 1957. The agreement is good. On seismograms recorded near a distance of 180°, where both phases should have a focal point, SKKS, SKKS*, SKKKS, and SKKKS* are clearly recorded with relatively large amplitudes. At distances beyond 180° there are some observations near the calculated curves for SKKS'* and SKKKS'*, and also a few near the calculated curve for SKKS''*, but in several instances these observed waves may belong to different phases with travel-time curves crossing that of the phase under consideration. SKKKS''* should start near a distance of 60° with a travel time of about 43½ min for $h = 600$ km, and its travel-time curve should continue across the epicenter where its travel time is about 45 minutes.

It is surprising how relatively large the amplitudes of SKKS and SKKKS are (compare Fig. 4 with Figs. 2 and 6). *Nelson* [1954, p. 46] found that in shallow shocks the observed amplitudes of the vertical component of SKKS'

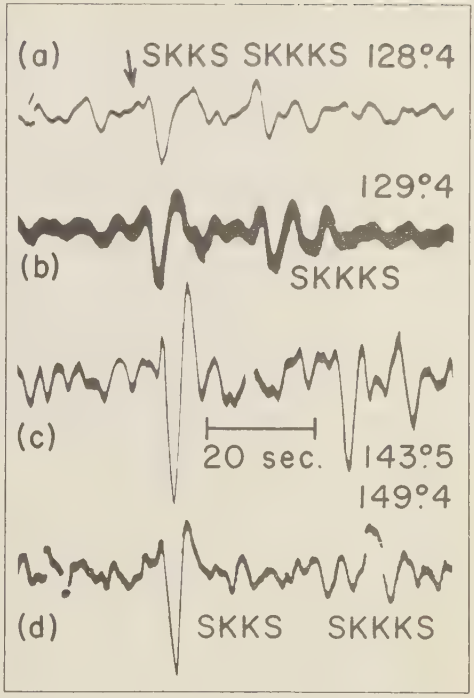

FIG. 4—Portions of records as in Fig. 2, showing SKKS and SKKKS. (a) long-period Benioff NS, Pasadena, 128.4°; (b) McComb-Romberg EW, Salt Lake City, 129.4°; (c) and (d) Wilson-Lamison NS; (c) Fayetteville, 143.5°; (d) Columbia, 149.6°.

at distances between 90° and 135° are between 1½ and 3 times the calculated amplitudes. The amplitudes of the horizontal components are close to the calculated values near 95° and between 140° and 150°, but are otherwise too small up to 170° and only about one third of the calculated amplitudes near 120° and 170°. *Nelson* [1954, p. 48] found an appreciable effect of prevailing directions of faulting for different locations of the sources. The remaining discrepancies at least partly may be the result of errors in the quantities assumed for the calculation of the observed amplitudes as well as for those found theoretically. Major errors in theoretical calculations may result from the fact that the periods T of SKKS and SKKKS are between 1 and more than 10 seconds, so that the corresponding lengths of the

waves which arrive at the surface of the earth are between a few and more than 30 km. The longer wavelengths are of the order of the thickness of the earth's crust. Consequently, the angle of incidence i_0 at the surface to be used for calculations, especially for the ratio of the ground displacement to the incident amplitude, may vary considerably as a function of T. Moreover, the ratio of the observed horizontal component H to that of the vertical component Z depends considerably on the angle of incidence i_0; in a homogeneous material this ratio may vary from about 5 for an angle i_0 near 10° (short waves) to 2½ for an angle of 17°, which has to be assumed for relatively long waves as a first approximation. There are other sources of error in the theoretical calculations.

The fact that SKKS is rather large as compared with PKKP depends partly on the percentage of energy reflected at the core boundary (KK). For PKKP, the ratio of the amplitude of the reflected K wave to that of the incident K wave should rarely if ever be greater than 0.1 [*Gutenberg*, 1951, p. 387]. On the other hand, in SKKS (and similarly in SKKKS) this ratio is 0.8 or more, if the angle of incidence i inside the core boundary is between about 35° (critical angle for P waves refracted into the mantle) and about 70° [*Dana*, 1944, p. 194]; these conditions are fulfilled for SKKS at epicentral distances up to about 180° and for SKKKS up to about 250° (all observed SKKKS waves and SKKKS* have distances between about 180° and 110°). Theoretically the factor F for the decrease in amplitudes at all refractions and reflections at the core boundary is less than about 0.08 for practically all PKKP waves, near 0.5 for SKKS and near 0.4 for SKKKS as well as for SKKKS* at distances over 100°, but much smaller for SKKS*.

The relatively large amplitudes of SKKS and SKKKS indicate that the attenuation in the outer core is relatively small. Unfortunately, the travel-time curve for SKKKS* intersects so many travel-time curves of other phases that it is difficult to decide how much these phases contribute to the observed amplitudes atttributed to SKKKS*. On the other hand, the ratio of the amplitudes of SKKKS to those of SKKS or of SKS varies too much for a reliable calculation to be made of the absorption coefficient in the outer core. However, most calculated values for the absorption coefficient in the outer core for the shock of April 16, 1957, indicate that its value is smaller than in the mantle. If the absorption coefficients were equal in the mantle and outer core, SKKKS* should be about 0.5 of SKKS at 150°, if both have the same periods.

PKKS, SKKP and related phases—Travel times of waves belonging to this group have been calculated, but little research has been done to find the relationship of the observed to the calculated times. "There is a long train of these waves with an indefinite beginning, so that the readings scatter very much when plotted, and do not serve to define a travel time curve" [*Gutenberg and Richter*, 1934, p. 118]. Figure 5, which shows a portion of the travel-time curves of this group but does not contain waves of the type pPKKS, etc., explains the long duration and the complicated appearance of this group (Fig. 6). Moreover, these waves have the same small ratio of the reflected to the incident amplitudes at the core boundary (KK) as PKKP, and the amplitude loss factor F for refractions and reflections at the core boundary is even slightly smaller than that for PKKP.

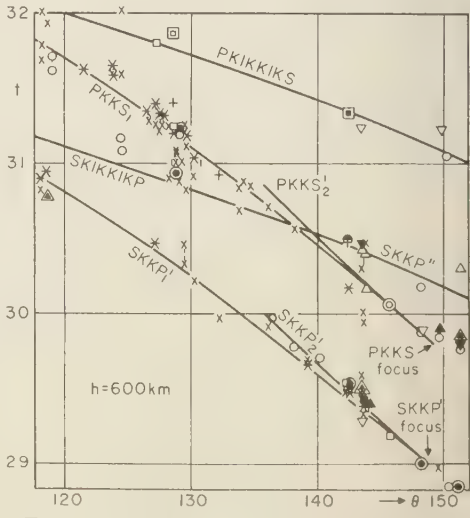

FIG. 5—Travel times t of SKKP-PKKS group, details as in Fig. 1.

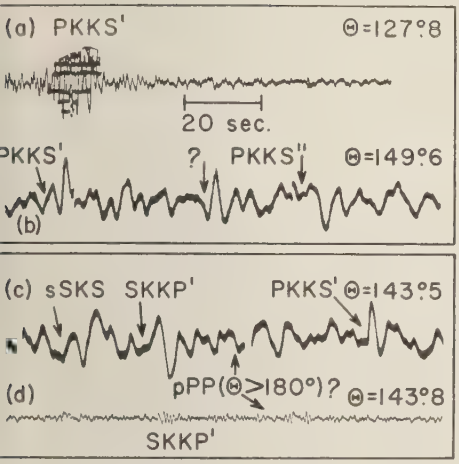

FIG. 6—Portions of records as in Fig. 2, showing waves in PKKS-SKKP group. (a) and (d) short-period Benioff vertical; (b) and (c) Wilson-Lamion NS; (a) Woody, 127.8°; (b) Columbia, 149.6°; (c) Fayetteville, 143.5°; (d) Dallas, 143.8°.

A number of travel-time curves of other waves (for example, sPS, SPP, PS, PSKS, SP, SKSP) intersect those of the group, but the relatively small periods of the waves under consideration and the fact that the travel times of the other waves increase with increasing distance, thus contrasting with those of the waves considered here, aids a definite identification of the waves in most instances. For most of the phases of the SKKP-PKKS group there are enough definite observations (Fig. 5) to establish that the observed and the calculated travel times agree within the limits of error and that the same is true for the distances of the focal points. Again, there are no observed waves along the trend of the curves at distances over about 2° beyond the calculated focal points; that is, there is no indication of appreciable diffraction.

The fact that PKKS is frequently clear not only on the horizontal but also on the vertical components, in spite of the relatively steep arrival of the waves at the earth's surface, is explained by the theoretical ratio of the vertical ground motion to the amplitudes of the incident SV waves. This increases rather rapidly with increasing angle of incidence of SV and reaches about 0.7 for SV waves which have an angle of incidence at the surface of slightly less than 20° [*Gutenberg,* 1944, p. 99].

SKKKP and PKKKS theoretically have a focal point at a distance of about 290° (70°) with a travel time of 38¼ min for shocks originating at the surface. The factor F for the amplitude reduction at the refractions and reflections at the core boundary should be noticeably smaller than 0.01, so that it is unlikely that these phases are observed.

The wave periods—PKKP "has a short period" [*Gutenberg and Richter,* 1934, p. 116]. "In PKKP, waves with periods of three seconds or more are extremely rare on all records" [*Gutenberg,* 1951, p. 380]. Usually, PKKP waves are immediately identified on records of short-period instruments on the basis of their short periods (Fig. 2); PKKP′ is rarely found on records of long-period instruments. No definite reason for the short periods of PKKP′ nor of those of P′P′ has been given thus far. On the records of the shock of April 16, 1957, periods of all well-recorded waves which had been reflected at the inside of the core boundary have been measured. In some instances, periods of waves from other phases, superposed on the waves under consideration, may have been measured, so that the 'observed' periods are rather too large than too small.

It was found that for statistical purposes the periods observed in PKKP′ and PKKP″ may be combined, though those of PKKP″ are on the average slightly longer than those of PKKP′. Similarly, it was found that, within the limits of error, periods of PKKS′, PKKS″, SKKP′, and SKKP″ may be combined, and also those of SKKS with those of SKKKS and SKKKS*. The respective period frequencies are given in the first three columns of Table 1, followed by those found for PP. The following columns are based on results of previous research. Where data from shocks at various focal depths are combined ("all" in Table 1), most refer to shallow shocks, and the number of data from deeper shocks decreases with focal depth [see, for example, *Gutenberg,* 1958c, Table 3, p. 277]. Usually, in deep shocks the periods are slightly smaller than the corresponding periods in shallow shocks.

Gutenberg [1958c, p. 275] has concluded that "the smallest periods observed regularly

TABLE 1—*Frequencies (in per cent) of periods T in seconds observed in records of various phases, h = depth of focus in km, n = number of observations*

Phase	PKKP	SKKP PKKS	SKKS SKKKS	PP	PKKP	PKKP	P'P'	P' P''	SKP PKS	P	S	P	S
h	600	600 (1957, April 16)	600	600	<70	all	all	all	all	all	all	>300	>300
T													
≤1	70	41	3	15	43	47	27	42	17	22	0	35	3
1.1–3	24	39	23	49	56	52	66	51	51	24	1	31	5
3.1–6	6	13	56	31	1	1	7	7	28	26	20	27	53
6.1–10	0	7	15	3	0	0	0	1	3	23	44	7	32
>10	0	0	3	2	0	0	0	0	1	5	35	0	8
n	33	101	117	61	96	109	154	183	90	368	410	45	38

in S waves at distances between 20° and 100° are about 4 seconds, while periods in P waves of 1 to 3 seconds are frequently reported for all these distances." Table 1 shows that the shortest periods are observed in longitudinal phases which have traveled through the core (PKKP and P'P'); slightly greater periods are found in those waves which have traversed the mantle once as longitudinal and once as transverse waves (SKP, PKS, PKKS, SKKP). SKKS and SKKKS have still longer periods, but, in contrast with S, frequently show periods of between 1 and 3 seconds.

It is difficult to explain these results. It is possible but not likely that greater attenuation of long waves than of short waves in the core is the main cause; it rather seems that a relative increase in the number and amplitudes of waves having shorter periods plays the main role (compare SKKS with S.) The fact that there seems to be little difference between the waves which have traveled through portions of the inner core and those which have not entered the transition zone between the outer and the inner core, puts the source of the short waves in the outer core or in the core boundary. In the records of the shock 600 km deep that is under special investigation, about 24 per cent of SKKS, but 39 per cent of SKKKS waves which have passed a portion of the outer core three times, had periods of 1 to 3 seconds; if the corresponding waves beyond 180° are included, the corresponding figures are 22 and 39 per cent respectively. However, the number of observations (*n* in Table 1) is too small to prove that the shortening of the periods of SKKS and SKKKS occurs in the outer core, although the figures in Table 1 strongly support this conclusion; neither the SKKS nor the SKKKS waves involved have entered the inner core.

REFERENCES

DANA, S. W., The partition of energy among seismic waves reflected and refracted at the earth's core, *Bull. Seis. Soc. Am., 34,* 189–197, 1944.

GUTENBERG, B. Energy ratio of reflected and refracted seismic waves, *Bull. Seis. Soc. Am., 34,* 85–102, 1944.

GUTENBERG, B., PKKP, P'P', and the earth's core, *Trans. Am. Geophys. Union, 32,* 373–390, 1951.

GUTENBERG, B., Caustics produced by waves through the earth's core, *Geophys, J., 1,* 238–248, 1958a.

GUTENBERG, B., Wave velocities in the earth's core, *Bull. Seis. Soc. Am., 48,* 301–314, 1958b.

GUTENBERG, B., Attenuation of seismic waves in the earth's mantle, *Bull. Seis. Soc. Am., 48,* 269–282, 1958c.

GUTENBERG, B., AND C. F. RICHTER, On seismic waves (First paper), *Gerlands Beitr. Geophys., 43,* 56–133, 1934.

GUTENBERG, B., AND C. F. RICHTER, Materials for the study of deep-focus earthquakes, *Bull. Seis. Soc. Am., 26,* 341–390, 1936.

GUTENBERG, B., AND C. F. RICHTER, On seismic waves (Fourth paper), *Gerlands Beitr. Geophys., 54,* 94–136, 1939.

JEFFREYS, H., AND K. E. BULLEN, *Seismological Tables,* British Assoc. Advance. Sci., 48 pp., 1940.

NELSON, R. L., A study of the seismic waves SKS and SKKS, *Bull. Seis. Soc. Am., 44,* 39–55, 1954.

(Manuscript received June 13, 1959.)

Evaluation of the Ground-Water Contamination Hazard from Underground Nuclear Explosions[1]

GARY H. HIGGINS

Lawrence Radiation Laboratory, University of California
Livermore, California

Abstract—Radioactivities in ground water collected at Nevada Test Site since the underground nuclear explosions in Operations Plumbbob and Hardtack Phase II have not been significantly above background, due to the formation of silica glass by the explosion, and the ion-exchange properties of fission products in normal earth minerals and water. The glass formed by the high shock pressures releases less than 10 per cent of its radioactivity when leached with water, and the rock minerals crushed by the explosive-forces adsorb several tens of milliequivalents of fission products per 100 g. The distribution coefficients for adsorption range from 50 to 500,000, depending on the particular fission product and mineral. A theory pertaining to the flow of activity in an ion-exchange medium is developed, and equations for application of laboratory data to field experiments are included. Some of the available distribution coefficients are tabulated from the literature on waste disposal. It is concluded from existing information that hazards arising from underground explosions in other media will not give rise to serious contamination problems. Until more experience is gained, measurements of aquifer properties should be made prior to planned explosions to determine that safe conditions exist in each particular case.

INTRODUCTION

Several underground explosions at the Nevada Test Site during Operations Plumbbob and Hardtack Phase II occurred in a volcanic tuff. Subsequent to the detonations water has been sampled from drill holes transecting the explosion sites, and from tunnels which have been dug into the crushed and collapsed zones close to the explosion sites. The radioactivity in this water has ranged from 1 to 10 μ-μc per ml. This range of radioactivity is about that expected as background in southern Nevada and is below the maximum allowable for human consumption.

This low radioactivity in the ground water is understandable from consideration of the effects of the explosions on the medium, of the ion-exchange behavior of minerals, and of the nature of underground water flow. The details of these three areas of considerations are discussed separately.

[1] This work was performed under the auspices of the U. S. Atomic Energy Commission.

THE NUCLEAR EXPLOSION AND ITS EFFECT ON THE IMMEDIATE SURROUNDINGS

If nuclear explosions are triggered underground, they produce local effects that are thought to be relatively independent of the rock type and geological formations present. In most, if not all, of the envisioned applications of nuclear explosives, the explosion will occur at depths that will be sufficiently large to contain more than 99 per cent of the radioactive debris in the formations immediately adjacent to the explosion. At the same time these formations will necessarily be subjected to the heats and pressures developed during the explosion.

When a nuclear explosive is fired in a small chamber surrounded by a dense material, such as rock or soil, the walls are subjected to shock pressures in the order of several million atmospheres and are heated to several thousand degrees C. This high pressure and temperature serves to melt and vaporize the first few feet of material outward from the explosion chamber, and the bulk of the radioactive debris is contained in this fused material [*Johnson and*

Violet, 1958]. Beyond the melted region, the shock pressure continues to do considerable damage to the surrounding formations as it passes through them, and its intensity falls off rapidly since work is done on the medium until the pressure reaches a value equal to the crushing strength of the rock. Thus one would expect the fused material containing the bulk of the radioactive debris to be surrounded by a zone of finely pulverized, unclassified, highly compressed material.

The extent of these several regions depends on the rock type and amount of explosive. In tuff in which the Nevada experiments in Operations Plumbbob and Hardtack Phase II were conducted, the radius of the fused region amounted to about 15 $W^{1/3}$ ft and the radius of the highly compressed pulverized region extended to about 100–150 $W^{1/3}$ ft, where W is the amount of nuclear explosive in kiloton equivalents. The difference between tuff and other rocks or aggregate materials should not account for very large differences from these radii since the radii are related to the cube root of the energy or pressure, and changes of a factor of 8 in the mechanical properties of rock should account for changes of a factor of 2 in the boundary radii at which various effects are noted.

Another noticeable effect produced by the underground explosion is the formation of a cavity. The momentum imparted by the high shock pressures and the gases left at the center of the explosion chamber at high temperatures and pressures combine to form the cavity, and the gaseous fission products, such as krypton and xenon, are trapped in this cavity. If the cavity collapses, these radioactive gases escape. Fortunately, the fission products that are permanent gases, such as Kr^{85}, are not biologically dangerous because they are rapidly diluted if the gases reach the atmosphere and are biologically inert. Some of the gases present during times shorter than a few minutes, however, decay into isotopes, which are of concern in their effect on the biosphere. Most important among these are the 33-sec Kr^{90}, which ultimately decays to Sr^{90}; and 3.8-min Xe^{137}, which decays to Cs^{137}.

In cases in which the collapse of the cavity does not reach the ground surface, the Sr^{90} and Cs^{137} would be adsorbed by fragment surfaces throughout the collapsed permeable region but contained from escape to the atmosphere. The degree to which the gaseous products would be contained in the fused material would depend primarily on the length of time the cavity stood before collapse. Analysis of debris from the Rainier explosion fired during Operation Plumbbob indicates that a large percentage of the Sr^{90} and Cs^{137} was contained in the glass. Glass debris from larger explosions that occurred in the same material as Rainier seems to contain less Sr and Cs, indicating earlier collapse.

In case of vented underground nuclear explosions the gaseous activities would escape and decay and should rapidly adhere to the surfaces of the relatively large dust particles that will be formed when the gases break through the ground surface. These large particles should fall out relatively close to the site of the detonation because the dust cloud should be relatively cool compared with the cloud produced by a nuclear explosion that occurs in air above ground, and therefore should not rise to an appreciable altitude, and because they are probably ten times larger (1000 times heavier) than ordinary fission product debris from air or near-surface bursts [*Lapple,* 1958]. Activity that is deposited on the ground surface does not reach the ground water supply in any reasonable length of time. *Russell and others* [1955] state that 'the very small amount of leaching observed in soil is indicative that the movement of fallout in subsoil drainage water is likely to be a very minor source of hazards, at any rate in soils of high base-exchange capacity.'

The production of fused material is important in reducing the potential contamination of ground water, since even at early times 65 to 80 per cent of the fission products are not gaseous.

If the medium in which the explosion occurs contains appreciable alumina and silica, and does not contain excessive sodium or potassium, a glass results from the melting, and these glasses have been shown in several experiments to be extremely impervious to leaching. *Amphlett and Warren* [1956] found that sands that had adsorbed activity by ion-exchange processes and were then sintered at 1000°C for 8 hr retained 99.87 per cent of all fission products as well as Sr^{90} and Cs^{137} even after being equilibrated with

times their volume of water for 4 months. vas also evident from their experiments that rate of extraction of additional activity was pping from the initial rate of 0.1 per cent week to well below 0.003 per cent per week 4 months so that something like 99.5 per cent all the activity contained in the glass would be available to ground water in the next centuries. The data of *Bond and Clark* 958] confirm that these data apply in gen- l to the fused materials produced by an un- ground nuclear explosion in Oak Springs tuff. f the explosion took place in a limestone me- m, the fused material might not be so in- ctable to leaching since fused calcium and gnesium oxides tend to react with water and nporarily release the trapped radioactivities. The effects of the explosion may be summar- d by saying that the explosion itself serves to event the contamination of ground water in o ways. This occurs first because the bulk the activity is bonded in an insoluble, un- chable glass produced from many materials; d second because a zone of finely divided un- ssified material is produced, which should act an effective aquiclude (impermeable barrier water flow) [*Tolman*, 1937] between possible ound-water flow and the activity. The effects this crushed region on water flow are dis- ssed below.

Flow of Radioactive Ions in the Earth's Crust

In every case minerals and soils that have been idied adsorb and exchange a significant number free ions. This effect was noted and has been der more or less constant study since 1850, en the first studies on soil ion exchange were orted by H. S. Thompson and by J. T. Way in e Journal of the Royal Agricultural Society. e remarkable thing about this is that at that ne the science of chemistry was not well organ- d, so that even such now obvious things as e existence of acid hydrogen ions were not spected. In spite of this, more than half of e work performed in the first 10 years of vestigation has withstood later scrutiny and accepted today [*Kelley*, 1948].

At the present time it is sufficient to say that act relationships between minerals and ions water can be stated, and that if the general nature of the minerals and flow of water is determined experimentally, the transport of fission products or induced activities can be calculated with sufficient accuracy and dependability to guarantee radiological safety.

The rules that govern transport of ions in soils and minerals may be divided into three general subcategories. These apply to the capacity of the minerals for ion exchange, the distribution of various ionic species between the aqueous and solid phases, and the kinetics of ion transport in an ion-exchange medium. These rules apply both to radioactive species and inert ions and form the basis for understanding low-temperature mineralization.

The capacity of minerals for ion exchange—Soils and mineral particles or fragments acquire their ion-exchange capacity from two distinctly different sources. The first is the ability of impervious crystalline assemblages of atoms to hold charged ions by electrostatic attraction. In this way the outer negative oxygen atoms of finely divided pure quartz produced by grinding large crystals hold ions on the surfaces [*Evans*, 1956].

The second source of ion-exchange capability comes from actual stoichiometric chemical reaction. In this way montmorillonite clays exchange a part of their inter-crystalline Na^+, K^+, Ca^{++}, or Mg^{++} with ions in solution. This kind of ion exchange is more nearly a volume phenomenon in that there are exchangeable ions throughout the crystal volume. If the particle sizes are large, however, the rates of exchange with interior ions are very slow so that not all are available to water flowing at an appreciable rate. A certain amount of ion migration goes on within the crystal, though, so that different ions are in the outer available sites at various times.

It is evident that any sample of naturally occurring material will exchange ions by both mechanisms, since in general many different minerals and particle sizes will be present. The range of experimentally determined capacities for naturally occurring and artificial minerals of clay-particle-size range varies from about 1 to 150 milliequivalents per 100 g. The portion of this capacity due entirely to surface electrostatic effects can be determined from the data of *Evans* [1956] and is about 0.5 meq per square meter of surface on quartz. In the particle size

TABLE 1—*Capacities and distribution coefficients for several radioactive ions on several kinds of soils and minerals in water*

Material*	Capacity, meq/100 g	K_d-Distribution Coefficients						References
		Cs	Sr	Y	Pu	Ce	Ru	
1.	—	>90	>90	>90				*Tesdahl and others* [1952]
2.	18.3	100,000	576	8,270		50,000	505	*Nishita and others* [1954]
3.	8.2	4,490	416	2,890		12,500	97	*Nishita and others* [1954]; *McHenry* [1954, 1955]; *Rhodes and others* [1957]
4.	14.6	4,490	645	4,950		5,510	112	*Nishita and others* [1954]
5.	17.4	3,530	221	16,600		12,500	166	"
6.	6.0	4,490	35	408		545	92	"
7.	15.1	4,110	505	12,500		12,500	120	"
8.	14.3	100,000	666	7,100		50,000	273	"
9.	68.2	16,600	259	5,510		12,500	172	"
10.	—	7,590	2470	33,200	50,000	49,900	1560	*Evans* [1956]; *Nishita and others* [1954]
11.	—	1,290	233	49,900	550	200,000	1560	*Rhodes* [1952]
12.	2				150			*Evans* [1956]
13.					171			"
14.	1				82			*Evans* [1956]
15.					4,900			*Rhodes* [1952]
16.	Average K_d for mixed 1-yr-old fission products: 370.							*Stettes and Straub* [1958]

*Description of the soils and minerals listed by number:

1. Mixed surface organic and inorganic "red" soils from Savannah River.
2. Aiken clay loam (kaolinite), *p*H 5.7, 4 per cent organic, exchangeable ions Ca and Mg.
3. Hanford composite soil (primary illitic), *p*H 6.6, 1.45 per cent organic, exchangeable ion Ca.
4. Nevada sandy loam, *p*H 8.6, 0.52 per cent organic, exchangeable ions Ca and Na.
5. Panoche clay loam (<21μ particles), *p*H 7.7, 0.47 per cent organic, principal exchangeable ion Na and Ca.
6. Sassafras sandy loam (kaolinite), *p*H 4.6, 1.58 per cent organic, principal exchangeable ions, N and Ca.
7. Sorrento fine (kaolinite with montmorillonite), *p*H 8.0, 1.52 per cent organic, principal exchangeab ion is Ca.
8. Vina fine (montmorillonite with kaolinite), *p*H 6.5, 0.18 per cent organic, principal exchangeab ions are K and Ca.
9. Egbert muck, *p*H 3.9, 32 to 35 per cent organic, principal exchangeable ion is Ca.
10. Pure Colorado bentonite (montmorillonite), *p*H 8.2, <21μ size, principal exchangeable ions a Na and Ca.
11. Kaolinite, <21μ, *p*H 4.3; principal exchangeable ions are Na, Ca, and Mg.
12. Chalk River 'soil,' 80 per cent sand of quartz, feldspar, and hornblende; 2 per cent clay of illite type
13. Separated feldspar 2 to 0.2μ size.
14. Separated quartz 2 to 0.2μ size.
15. Separated glauconite (illitic mineral) 2 to 0.2μ size.
16. Meteoric dust and rhyolite roofing granules. Not separated for particle size but all less than 1 mm

range for which the capacities are stated above, surface effects account entirely for the values from 1 to 2 meq/100 g of sample quoted as the lower limit of capacity.

Since 1 megaton of fission produces about 1×10^6 meq of fission products which would be distributed in at least 5×10^{21} g of material, only 2×10^{-4} of the capacity would be used for complete adsorption even if the minimum capacity (1 meq/100 g) is assumed. Under these conditions the chemical effect of the fissio products on the soil and ground-water chemistr is seen to be negligible and in fact 'trace conditions are reached.

Table 1 contains a list of several experimentall determined ion-exchange capacities. These a

licative of the usual variation, and much re extensive information is available in several ndard references on either ground water or y mineralogy [*Grim*, 1953; *Tolman*, 1937].

The distribution of various ions between solutions d earth minerals—In any chemical reaction, ch as the adsorption and desorption of an ion to a solid, an equation can be written to present the process. The usual equilibrium uations must apply and a reaction constant can derived.

Thus, if M^{+m} and A^{+n} represents ions of fission oduct activities and naturally occurring exangeable minerals carrying charges $+m$ and n, and X is assumed to be a reactive chemical dical in the earth mineral, the equation for change is

$$M^{+m} + m(AX_n) \rightleftarrows n(MX_m) + mA^{+n} \quad (1)$$

nd

$$K = \frac{[MX_m]^n[A^{+n}]^m}{[M^{+m}]^n[AX_n]^m} \quad (2)$$

Ordinarily it is difficult to apply this equation mineralogical processes because the effective tivities of ions in solids are difficult to deterine. Since only 2×10^{-4} of the active sites e occupied by fission products, $[A^{+n}]$ and $[X_n]$ may be assumed constant. The distribuon coefficient K_d can therefore be written as

$$K_d = \frac{MX_m}{M^{+m}} \frac{V}{W} \quad (3)$$

here V is the volume of solution and W is the eight of minerals. The ratio of MX_m/M^{+m} is ie fraction of radioactive ions in the mineral ase divided by the fraction of radioactive ions the water.

The value of K_d is easily determined in the boratory by equilibrating a sample of mineral ixed with water with a small amount of tracer tivity of the desired ion. These measurements ave been made on many ions with many difrent kinds of soil and minerals and a few are mmarized in Table 1.

The implication of equation 3 is that in any ineral-water system, such as an aquifer, there a fixed ratio between the radioactivities in ie liquid and solid phases. The values of K_d Table 1 fall generally in the order of 100 to veral thousand so that at least 100 times as much of the radioactivity is adsorbed as is in solution. Since only the solutions are moving in the earth, only a small portion of the ions adsorbed are transferred with the water.

Two generalizations about the values of K_d can be made from the data presented in Table 1. First, the value of K_d for the same isotope in different minerals correlates generally with the capacity of the mineral. This is easily understood since the K_d is expressed as a ratio per gram of mineral while the chemical equation requires that the concentration of active sites in the mineral be used. The ion-exchange capacity is in reality an expression of the concentration of active sites. Since the exchangeable ion may be Ca^{+2}, Mg^{+2}, K^{+1}, or Na^{+1} in varying amounts, the correlation cannot be exact and it is not practical to try and define K_d in terms of the more proper variables. In general, K_d quartz < kaolin < illite < montmorillonite, although this relationship does not hold for all ions.

Second, the relative values of K_d for different ions in the same mineral or soil are such that Ru < Sr < Cs < Y < Pu ≈ Ce, so that as the radioactive ions of these elements elute through soils or minerals, they will appear in this order at any point along their path, and the first element to appear would be Ru.

It is implicit in the foregiong statements that the minerals that weather to the clay minerals discussed (i.e., illite, kaolinite, and montmorillonite) will be as effective or perhaps more effective as ion exchangers than their clay daughters, providing sufficient surfaces are available for exchange. At least in the region in near proximity to the explosion site, the high shock pressures are sure to produce sufficient surfaces by crushing.

While the K_d's listed in Table 1 apply in relatively pure water (~0.001 M impurities) several investigators have studied the effects of varying salt and pH [*Evans* 1956; *McHenry*, 1954, 1955; *Nishita and others* 1954; *Rhodes*, 1952; *Rhodes and Nelson*, 1957]. The effect of added salt in the water is not the same for each ionic species, but in general K_d decreases logarithmically with increasing salt concentration. Thus, while K_d for the tracer Cs is about 5000 in relatively pure water on Hanford soil, it decreases to about 15 in saturated sodium chloride

solution [*Rhodes and Nelson*, 1957]. This effect is not so pronounced with Pu and Ce. Varying *p*H has very small effect between *p*H 2 and about 9, and causes a decrease in K_d as it varies beyond these limits. Most ground water would fall within this *p*H range.

This discussion has been confined to the adsorption of cationic species (base exchange) even though minerals also display some anionic exchange properties. Fortunately, the only fission product whose half life is longer than 1 yr and which displays anionic properties is Ru, and it has been adequately studied [*Nishita and others*, 1954] to demonstrate that it behaves primarily as a cation in soils although its adsorption is not entirely reversible.

There are a few radioactive species that are inert as regards their behavior in soil minerals. Tritium and the noble gases Kr and Xe would not be affected by ion-exchange processes, so that tritium should be the best ground-water tracer available.

The kinetics of ion transport in an ion-exchange medium—The potential hazard arising from ground-water contimination is reduced by ion-exchange processes in two ways. First, the flow of a particular ion is markedly inhibited so that instead of moving with the ground water, cationic radioactivities move at most only about 1 per cent as fast as the ground water. Second, the concentration of the radioactivity is reduced as it finds its way through the aquifer materials because the movement of any particular ion from the soil into the water is a statistical matter and a group of ions that start out together will move further and further apart after they exchange on and off the soil several times. These two effects are considered in detail below.

If the distribution coefficient K_d and flow rates of water F_w are known in a particular aquifer, it is a simple process to calculate the flow rates of any ionic species, F_a, from the expression

$$F_a = \frac{F_w}{1 + K_d\rho} \qquad (4)$$

where ρ is the ratio of the weight of mineral to volume of water per unit volume of aquifer material. Since ρ is not known exactly, it is convenient and very conservative to use a value of unity in calculation since the usual value is 5 to 10.

Using values from Table 1 and assuming a water flow of 10 ft per day in Hanford composit soil, the flow rate of Cs^{137} is 0.027 in. per day whereas the flow of Pu^{239} on pure crushed quart would be as large as about 1.5 inches per day.

Even this small retardation noted on quart is sufficient to delay the appearance of plutoniu at a well 1 mile from the source of contaminatio for 120 years. Cs^{137} would not be easily detectabl 1 mile from the source of contamination in soil similar to the Hanford material since i would take 6600 years to get there and by tha time it would have undergone radioactive deca by a factor of about 10^{-90}.

The flow calculated from equation (4) i the *average* rate of transfer of ions. There wi be some ions that flow slightly faster on th average, and some slightly slower. The effect c this random statistical motion is one of reducin the concentration at any point in the aquife after some flow has occurred. It is possible t calculate the distribution of activity as a functio of distance and time. If it is assumed that a the radioactivity is in a plane zone of arbitrar thickness oriented at right angles to the dire tion of flow, and that if it were possible to sto all time-dependent processes, the radioactivit in the water, A_w, would be

$$A_w = \frac{A_s}{\rho K_d} \qquad (5$$

where A_s is the activity in soil or mineral. A_s very nearly the total activity when K_d is larg and the fraction of radioactivity in the wate may be represented by

$$\overline{A_w} = \frac{1}{\rho K_d} \qquad (6$$

Now if the zone is restricted so that it cor tains a unit mass of mineral, and a time cycl (c) is defined so that a unit volume of wate just flows through the unit zone, ρ become 1 and

$$A_w = \frac{1}{K_d} \qquad (7$$

will be transferred to the next zone along th path of flow. The process is repeated in the secon time cycle so that the fraction of activity i the third zone is $1/K_d$ times that in the secon which is $1/K_d$ times that in the first or $(1/K_d)$

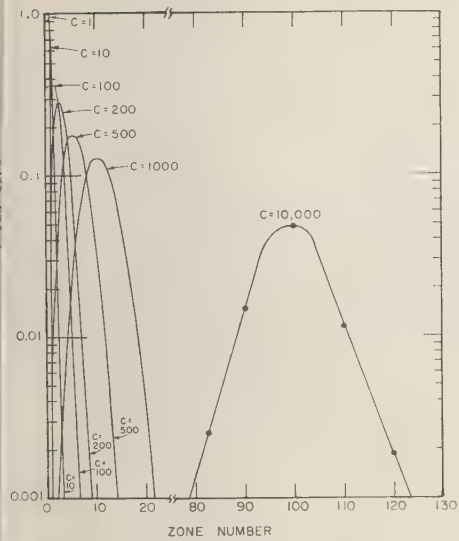

IG. 1—Distribution of exchangeable ions after arying numbers of exchange contact cycles (c).

nd the activity in the second zone is

$$A_2^2 = \frac{1}{K_d} + \left(1 - \frac{1}{K_d}\right)\frac{1}{K_d} - \left(\frac{1}{K_d}\right)^2$$

nd that in the first zone is

$$A_1^2 = 1 - \frac{1}{K_d} - \left(1 - \frac{1}{K_d}\right)\frac{1}{K_d}$$

nd likewise in the third time cycle.

By repetition of this process the distribution f activity up to 1000 time cycles has been alculated, and the result is shown in Figure 1 or $c = 1$, 10, 100, 500, and 1000. These curves ave been calculated so that they may be applied o a real case by letting one time cycle equal he time to flow one unit distance, and the length f zone be equal to $100/K_d$ units distance. Thus or an aquifer flowing at 10 ft per day one time ycle would be 1/10 of one day. The length of one for Sr^{90} in montmorillonite would be $100/2470 = 0.0405$ ft, using the value of K_d rom Table 1. In this example after 100 days the distribution will be given by the curve for $= 1000$ (10 cycles per day $\times$ 100 days) and the distance covered by the average or peak of the distribution will be 10 zones of 10 times 0.0405 ft = 0.405 ft, but 10 per cent of the activity will have travelled 18 or 19 zones or 0.73 ft. The concentration in the peak zone, however, is only 12 per cent as large as it was before the flow began to spread the activity and after many thousands of cycles the radioactivity will be dispersed so that its concentration at any point is a few orders of magnitude lower than when it started. This calculation does not take into account the lateral diffusion of the ions that would further disperse the radioactivity, and assumes completely laminar flow. It is also assumed that the range of particles present is large enough so that not all the ion-exchange sites are at equilibrium with the solution ions.

The result of a calculation using equation 4 may be checked against the results using Figure 1. Using the same example of Sr^{90},

$$F_a = \frac{10}{1 + 2470} = 4.05 \times 10^{-3} \text{ ft per day}$$

and after 100 days the average distance travelled is 0.405 ft, which was also calculated from the curve in Figure 1.

The fraction of the initial radioactivity in any zone (n) after any number of time cycles (c) may be calculated from the expression

$$A_n^c = \left(1 - \frac{1}{K_d}\right)^{c-n} \times \left(\frac{1}{K_d}\right)^{n-1}$$

$$\times \binom{c-1}{n-1} \left[\begin{array}{l}\text{Private communication,}\\ \text{J. L. Brady, Lawrence}\\ \text{Radiation Laboratory}\end{array}\right] \qquad (8)$$

where $\binom{c-1}{n-1}$ is the binomial coefficient of $c - 1$ and $n - 1$ and is equal to

$$\frac{(c-1)!}{[(c-n-2)!(n-1)!]}$$

However, this expression is cumbersome to calculate for large values of c and n. The curve for $c = 10{,}000$ in Figure 1 was calculated from this equation.

It should be noted that the studies done at Hanford [*McHenry*, 1954, 1955; *Rhodes*, 1952; *Rhodes and Nelson*, 1957] with flowing columns should not be expected to fit these calculations because the Hanford studies were performed in such a way that additional activity was introduced into the soil continuously until the

soil was saturated, whereas the calculation here assumes that after flow starts no activity is introduced.

In summary it may be said that the ion-exchange behavior of the major fission product radioactivity is well understood, and that their behavior serves to essentially eliminate the potential hazard from ground-water contamination with debris produced by an underground nuclear explosion. This results from the restriction of movement of cationic fission products to generally less than 1 per cent of the water flow and from their gradual dispersion over large areas so that future withdrawals from the contaminated aquifer region could never contact more than a very small portion of the total activity.

The Occurrence and Flow of Underground Water

This section contains a brief description of the nature of aquifers and has been largely summarized from *Tolman* [1937] and *Meinzer* [1942].

Occurrence and nature of aquifers—Ground water occurs in three different types of aquifers. These are water table aquifers, confined water aquifers (artesian or pressure systems), and solution channel or fissure aquifers. The first two are by far the most important water sources for commercial and domestic use since they are easiest to encounter in drilling, but there are areas where the only ground water which exists occurs in fissure and solution channels of the third type.

Water table aquifers consist of porous pervious materials generally of the alluvial type where some classification of particle size has occurred. A water table aquifer is characterized by being in more or less direct pressure contact with the soil surfaces so that the level of water is fixed by the quantity of water and available void space. Void spaces in this kind of aquifer cannot exceed about 40 per cent of the total volume and are generally about 20 per cent or less. The profile of the water table is in general a subdued replica of the surface profile. That is, the distance from the ground surface to the water table does not change as much as would be expected from surface feature variations assuming a flat water table. The depth to th water table on the top of a hill might be onl slightly more than the depth in an adjacer valley.

Confined aquifers are like water table aquife in that they consist of the same kinds of ma terials, but differ in the fact that their uppe surfaces are bounded by impermeable beds (fo instance fine clay) so that their physical limi are not determined by the available volume water but by the available space. Since th permeable water-containing strata are generall not level, pressure gradients are developed fro point to point by gravity, and a spatial repr sentation of the pressure in a confined aquif is called a pressure surface. When the pressu surface is higher than the ground surface, art sian flow occurs when the aquifer is penetrate

Perched water tables are like confined wat systems except that the impermeable beds pr vent the water from freely flowing at the bo tom and sides instead of the top. In this wa an ancient stream bed of permeable grav surrounded by impermeable silt might produce perched water table separated by many fe from the general water table in the same are All of the available connected pores will b filled with water below the water table eve though not all strata can be considered aquifer The aquifer must also be permeable.

Solution channel and fissure water syste develop in rocks along fissures and beddin planes. Most of the water which is encountere in lava and in carbonate rocks exists in th kind of aquifer. The primary difference be tween fissure water and water table or co fined aquifer water is that the local direction flow is determined primarily by the structure the fissure, and there may be little or even n exchange between relatively close lying fissure Fissure aquifers in general are not necessaril filled with porous conglomerate so that ion ex change takes place on exposed surfaces rathe than throughout the aquifer volume. Flow rat in the channels may be very much larger tha through alluvial or conglomerate materials.

Source and quantity of ground water—Groun water derives from two primarily differen sources. The most important source is from rai fall. The path from surface runoff to a particula aquifer may involve transfer through a strea

d, but lakes and streams ultimately derive their water from rainfall also. The other urce of water is from mineral decomposition. ater is an essential part of the structure of ost earth minerals, and heating or compressing em causes physical and chemical changes hich may involve the release or uptake of ater. It is probable that all the water presently the earth's surface originally came from this urce during the formation of the earth. It is probable that much water is presently leaving entering the total free water inventory from ck decomposition.

Water does not exchange between the earth d atmosphere or ocean rapidly. It is estiated that at any one time about 0.1 per cent all free non-saline water is atmospheric; 1.5 er cent is on the surface in lakes, streams, land seas, etc.; about 45 per cent is in the ound within 2500 ft of the surface; and the mainder is between 2500 and 12,500 ft below ie surface. (Water below 12,500 ft it not included in the estimate as 'free' water and may ly exist in rock solutions.) It is also estiated that about 1 per cent of the total free ater 'exchanges' per year. That is, 1 per cent the total 'free' water is transferred from ceans into the ground water supply, and about per cent leaves fresh water storage and reirns to the oceans [*Nace*, 1959].

The flow of ground water—Only a part of ie water contained in aquifers is free to flow. art is held by the surfaces of the mineral parcles. In fine clay that contains as much as 30 er cent water, none may be removed by centrifuging at 1000 g. Coarse gravel, on the other and, will release nearly all the water it conains. The quantity of water a given volume f a particular aquifer material will release is ermed its 'specific yield,' and the quantity it etains, its 'specific retention.'

In general the flow of water in an aquifer is etermined by Darcy's law, which may be stated s

$$v = P\frac{h}{l} \qquad (9)$$

here v is velocity, h is the hydrostatic head, is the distance of flow, and P is the constant f permeability. This constant is related to the pecific retention noted above. The usual units of h and l are feet and miles, whereas v is expressed in feet per day.

The constant of permeability determines the flow of water and is primarily a product of two factors. The first factor that affects the permeability is particle size. The finer the particles of an aquifer material, the slower the flow of water under a given hydraulic gradient. *Tolman* [1937; pp. 219, 220, and 387] indicates that under a 1 per cent hydraulic gradient ($h/l = 0.01$ in equation 9) water will flow 0.001 ft per day in clay whose average particle size is a few microns, and 110 ft per day in coarse gravel whose average particle size is several mm.

The second factor that affects the permeability constant is the particle classification or porosity. If an aquifer consists of spherical particles of equal sizes, the porosity has been shown to be equal to between 0.26 and about 0.48 depending on the symmetry of packing [see discussion on p. 103 ff, *Tolman*, 1937]. The permeability of such a material is ideal and quite high. If, however, smaller or irregularly shaped particles are also present, they may move into the openings between the major matrix particles and markedly reduce the permeability and porosity. In nature there is always some variation in particle size, but the variation is small in good aquifers.

Of course some aquifers existing in solution channels and fissures are restricted only by their "orifice" dimensions, and the flow-determining size may exist only in a few places over the length of the aquifers.

In nature the largest underground flow rate yet observed is 212 ft per day, and the slowest is below 1 ft per yr. 'In recognized water-bearing formations from which wells obtain their water supplies, the natural rate of movement of ground water is generally not greater than 5 feet per day nor less than 5 feet a year' [*Meinzer*, 1942]. An average flow rate would be about 50 ft per yr.

Relationship between the occurrence and flow of ground water and hazards from radioactive contamination.—As water moves in an aquifer, only that fraction which is determined from the specific yield measurement is in motion, while the remainder is loosely bound to the solid particles. From time to time the water on the surfaces, or the bound water, freely exchanges with

the free or mobile water. The effect of this exchange is to cause dissolved radioactivities to become more and more disperse as transfer continues. In fact the same equations of distribution and flow, which were stated in the previous section of this paper, apply to this dispersion. The value of K_d in this case is the ratio of specific retention to specific yield and can vary all the way from zero to infinity. Values of 1 or 2 would not be unusual in aquifers from which water is obtained and the flow of completely neutral chemical species (such as tritiated water for example) would be one-half or one-third as large as the flow of water. Although this concept is difficult to accept on face value, it is easier to understand if the water is thought of as if it consisted of discrete particles. It may be imagined that a restriction is placed on the particles such that at any one time only a given fraction of them are allowed to move and all the rest must stand still. Then, if a small volume of aquifer material is represented by a box containing these discrete particles and the flow is represented by addition and subtraction of particles, it is not hard to imagine a specific particle being introduced into the box and staying there for some time while new particles are placed into and then withdrawn from the box.

Since ground water generally moves a few hundred feet per year or less, hazards from short-lived fission products are practically nonexistent. Radioactivities that decay with half-lives shorter than 1 yr would generally not leave an explosion control area even if they were not adsorbed by the minerals of the aquifer, so that studies of adsorption may well be restricted to the longer-lived fission products.

Production of shattered, irregular shaped, finely divided debris, such as that described in the first section, will produce a condition in which permeability is very low by aquifer standards since all these factors act to reduce the permeability constant in equation 9. This will be especially true if most of the water transfer is in fissures or solution channels that may be easily clogged with debris or closed by the pressure produced by nuclear explosions. In this way the radioactive debris should be left in a ground water 'island' even when the explosion site is in an active aquifer.

It may be concluded, then, that under most conditions the nature of ground-water flow wil aid in containing and diluting radioactivity pro duced by underground nuclear explosions.

Conclusion

There are three major conclusions that ca be drawn from the foregoing discussion. Th first is that the absence of water contaminatio from the underground explosions in Nevad should have been expected because of the for mation of insoluble glasses, the ion-exchang property of the tuff and the nature of wate flow in finely divided materials. Expressed i percentages, the insolubility accounts for re moving about 90 per cent from availability, io exchange removes more than 99 per cent o the remaining 10 per cent or 9.9 per cent fo every zone of thickness traversed away fron the contaminated area, and the water distribu tion probably removes 60 per cent of the re maining 0.1 per cent for each zone traversed In short, within a few feet *all* the radioactivity is adsorbed in the mineral.

Second, the principles discussed in connectio with the restriction of flow of radioactivity apply to all earth minerals. Certainly man minerals when fused will not form such insol uble glasses as the high-silica, low-sodium-con taining tuff, but the restrictions due to ion ex change and water division apply to all mineral investigated so far. This implies also that studie of ion-exchange distribution constants should b extended to as many soils and minerals as pos sible. Data are especially sparse for high-carbon ate minerals such as marble, dolomite, calcite and magnesite. It is safe to say that sufficien data exist so that no hazard would be expecte in water of average composition flowing in an mineral.

The third conclusion is that studies of th ground-water situation should be made as par of every pre-explosion investigation. These stud ies should include measurements of the loca flow rate, direction, and ion-exchange distribu tion coefficients in the aquifer materials an local ground water. These distribution coeffi cients should be measured with all the long-live fission products, especially strontium and ru thenium. From these measurements it shoul be possible to reliably predict the behavior o

ll important radioactivities before contamination is released underground.

Acknowledgments—The author wishes to acknowledge the help and valuable criticism of Ir. D. E. Rawson, and many helpful discussions ith Drs. R. E. Batzel and R. H. Goeckermann f the Lawrence Radiation Laboratory.

References

MPHLETT, C. B., AND D. T. WARREN, Fixation of activity in solid form by adsorption on soils. Part I. Firing and leaching tests, Harwell, *AERE C/R-1686,* 1956.

OND, W. D. AND W. E. CLARK, Results of leaching experiments on debris from the Rainier Event, Oak Ridge, *ORNL-58-7-101,* 1958.

VANS, E. J., Plutonium retention in Chalk River soil, Chalk River Project, Canada, *CRHP-660,* 1956.

RIM, R. E., *Clay Minerology,* McGraw-Hill, New York, 1953.

OHNSON, G. W. AND C. E VIOLET, Phenomenology of contained nuclear explosions, *Lawrence Radiation Lab., Univ. Calif., UCRL-5124, Rev. 1,* 1958.

ELLEY, W. P., Cation exchange in soils, *Am. Chem. Soc. Monograph 109,* Reinhold Pub. Corp., New York, 1948.

APPLE, C. E., Fallout control, final report, Stanford Research Institute for U. S. AEC, done under project agreement No. 5 of contract *AT(04-3)-115,* 1958.

McHENRY, J. R., Adsorption and retention of cesium by soils of the Hanford Project, *Hanford Atomic Products Operations, HW-31011,* 1954.

McHENRY, J. R., Adsorption and retention of strontium by soils of the Hanford Project, *Hanford Atomic Products Operations, HW-34499,* 1955.

MEINZER, O. E., *Hydrology,* McGraw-Hill, New York, 1942.

NACE, R. L., Water management, agriculture and ground water supplies, *U. S. Geological Survey,* 1959.

NISHITA, H., B. W. KOWALEWSKY, AND K. H. LARSON, Fixation and extractability of fission products contaminating various soils and clays. I. Sr^{89}, Sr^{90}, Y^{91}, Ru^{106}, Cs^{137}, and Ce^{144}, *Univ. Calif., Los Angeles, UCLA-282,* 1954.

RHODES, D. W., Preliminary studies of plutonium adsorption in Hanford soil, *Hanford Works, HW-24548,* 1952.

RHODES, D. W. AND J. L. NELSON, Disposal of radioactive wastes from the uranium recovery plant, *Hanford Atomic Products Operation, HW-54721,* 1957.

RUSSELL, R. S., H. M. SQUIRE, AND R. P. MARTIN, The effects of operation Hurricane on plants and soil, Harwell, *AERE/SPAR/3,* 1955.

STETTES, L. R. AND C. P. STRAUB, The distribution of radioactivity from rain, *Trans. Am. Geophys. Union,* v. *39,* 451, 1958.

TESDAHL, T. C., C. S. LOWE, F. C. MEAD, AND E. L. MURPHY, Fixation of mixed fission product activity by soils of the Savannah River Project, Mound Laboratory, *AECD-3629(MLM-665),* 1952.

TOLMAN, C. F., *Ground Water,* McGraw-Hill, New York, 1937.

(Manuscript received August 6, 1959.)

Crustal Structure from Gravity and Seismic Measurements

G. P. WOOLLARD

Department of Geology, University of Wisconsin
Madison, Wisconsin

Abstract—Gravity data indicate that there is a regular relationship between crustal structure, crustal density (composition), and surface elevation. Earthquake and surface seismic refraction and reflection evidence as to the composition and structure of the earth's crust have not yielded a simple, unambiguous relationship to the surface elevation. The velocity dispersion of earthquake surface waves, on the other hand, indicates variations in the thickness and composition of the crust that are in general accord with the variations in surface elevation and the Bouguer gravity anomalies. Why seismic refraction measurements have not agreed everywhere with gravity and surface wave indications of crustal structure appears to be a result of masking of crustal layering. On the basis of the slope of the curve that describes the relationship between the seismic depth to the Mohorovicic discontinuity and Bouguer gravity anomalies, the density difference between the crust and the mantle appears to decrease as the thickness of the crust increases. On the assumption that the mantle has a constant mean density of 3.32 gm/cc, the mean crustal density would appear to increase from a minimum value of 2.86 gm/cc in the oceans to about 3.08 gm/cc beneath the high plateaus and mountains. If the mean crustal density is essentially constant, the effective density of the mantle must decrease by a comparable amount. The existence of a low-density zone in the upper part of the mantle, as suggested by the velocity dispersion of very long period Rayleigh waves, would explain the relationships observed. Isostatic relationships suggest that the mean density of the continental crust is essentially constant (2.85 gm/cc to 2.88 gm/cc). These values imply that a basaltic layer is present everywhere. That there is possibly an increase in mean crustal density as the crust thickens is suggested by U.S.S.R. seismic studies in Central Asia. These show that the intermediate (basaltic) layer is usually thicker beneath areas of uplift. Although the origin of the basaltic layer can only be surmised, its general inhomogeneity, as indicated by variations of seismic velocity from 6.4 to 7.3 km/sec, and its varying thickness suggest that it may be a zone of phase transformation within the underlying mantle rock. Despite the lack of homogeneity in the crust, it appears possible that empirical relationships may be used to predict approximate crustal thickness from the regional Bouguer gravity anomalies or from surface elevations with a reliability approaching that for seismic measurements.

INTRODUCTION

Seismology is the discipline that has revealed he most information about the internal structure and composition of the crust. Although, n general, the various seismic methods of study refraction and reflection measurements and elocity dispersion of surface waves) give simiar pictures of crustal structure, in certain areas, iotably the plateaus, the results are at varance. To resolve these uncertainties, other neasurements intimately related to crustal conlitions at depth must be utilized. The most iseful of these auxiliary studies is gravity. Taken alone, gravity data offer no unambiguous olutions, but they can be used to support or lisprove a given crustal model suggested by eismic data. As crustal structure is intimately related to surface elevation through the phenomenon of isostasy, and as surface elevation is also related to geologic factors, any crustal model derived must be geologically reasonable. Although there are other observable physical phenomena that might be related to crustal composition and structure—heat flow, for example—knowledge concerning these fields and their variations is still too limited to permit any general applications. The present discussion is restricted to relations observed in the fields of gravity, seismology, and geology as they pertain to the earth's crust.

ISOSTASY, GRAVITY ANOMALIES, AND THE CRUST

From seismic evidence we know that the earth consists of essentially uniform, concentric

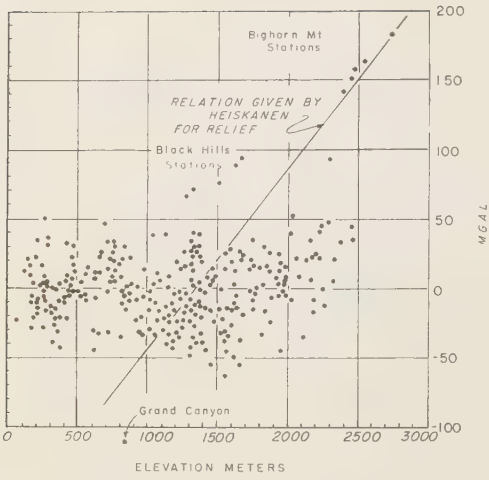

FIG. 1—Relation of free-air anomalies to elevation.

layers, increasing in density with depth. The crust is the outermost layer, and it has the greatest variations in homogeneity of all the earth's layers. Despite the marked variations in surface elevation, mineralogic composition, and thickness of the crust, gravity and seismic data indicate that hydrodynamic equilibrium is approximated and that the crust appears to float on the denser mantle rocks. As a consequence, equal pressure (isostasy) is approximated everywhere at some depth beneath the crust.

As free-air, Bouguer, and various isostatic anomalies have all been used in the study of crustal structure, a few remarks concerning these anomalies appear to be justified. In areas of low relief, such as plains and plateaus, free-air anomalies are a direct measure of the degree of isostatic equilibrium. In mountain areas the free-air anomaly values show a dependence on relief that is related to the regional compensation for the average elevation of the area rather than to the elevation of the observation site. Figure 1 shows that despite a ±50-mgal scatter in values, caused mostly by variations in surface and near-surface geology, the mean anomaly value approaches zero. The effect of relief (mountain and deep-valley observations) is also shown for data in the Black Hills, the Bighorn Mountains, and the Grand Canyon. Bouguer anomalies, in contrast with free-air anomalies, show an inverse dependence upon regional elevation everywhere (Fig. 2). Since the effects of surface masses have been allowed for down to sea level, the Bouguer anomalies are principally related to deep compensating masses which are associated with changes in crustal structure and composition. Isostatic anomalies represent the departures of the actual compensating mass distribution from that assumed in the calculations. That concepts which vary as widely in physical assumptions as those of Airy and Pratt should yield isostatic anomalies close to zero, as do the free-air anomalies in areas of low relief, is merely proof that isostasy is a real phenomenon and, as long as the depth of isostatic equilibrium chosen is deep enough, the crustal model used in deriving the isostatic correction is not important.

In order to study crustal structure from gravity anomalies it is necessary to start with the Bouguer anomalies or their equivalent derived from free-air anomalies incorporating suitable corrections for known surface and near-surface mass distributions. As the crust is not homogeneous in composition and as there is no fixed relationship between crustal thickness and the anomaly values, one cannot hope to derive an exact determination of changes in crustal structure from the variations in the regional gravity anomaly values alone. Fortunately, the composition of the crust appears, on the whole, to vary with thickness in a systematic manner. By using supplementary seismic data it is possible to derive a first approximation of crustal structure from gravity data. For example, on the basis of earthquake seismology and the results of a transcontinental gravity traverse across the United States [*Woollard,* 1943], the writer computed as early as 1942 the probable variations in crustal thickness across North America. The reality of these (unpublished) results has been borne out subsequently by both surface refraction studies of crustal structure and studies of the velocity dispersion of earthquake surface waves. As will be shown, the use of more recent seismological data permits a more comprehensive and significant analysis of the gravity data to be made than was formerly possible.

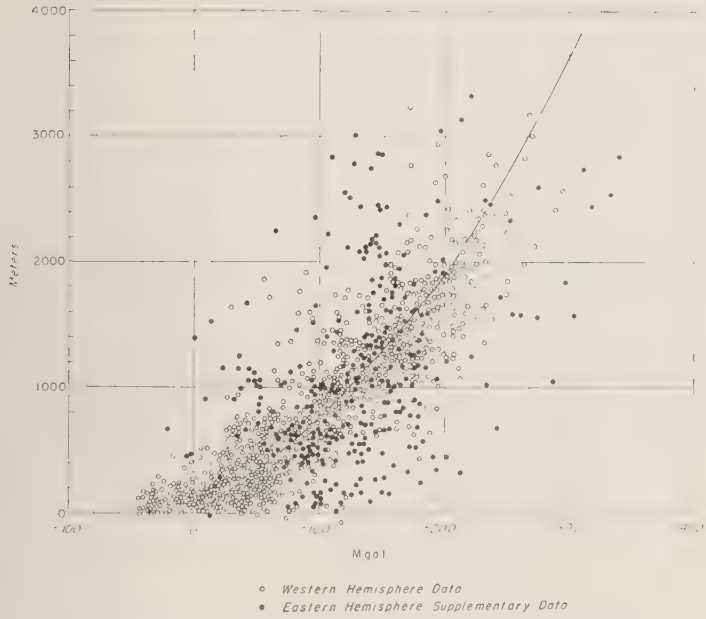

FIG. 2—Relation of Bouguer gravity anomaly to surface elevation.

SEISMIC STUDIES OF THE CRUST

Earthquake seismology—Seismic studies of ıstal structure and composition can be sub-ıided into observatory studies of earth-ake waves and field measurements based explosive blasts and rock bursts. It was rough the analysis of earthquake waves re-rded at short distances from earthquake epi-nters that the first clue regarding crustal ucture was obtained. The discovery by Mo-rovicic of the 8-km/sec seismic velocity dis-ntinuity, which has been found to be of iversal extent, gave an easily recognized uctural marker because of its characteristic locity (appreciably greater than the 5.5 to 5-km/sec values for the near-surface crustal aterial). This discontinuity, now identified by e discoverer's name and commonly referred as the 'Moho,' occurs at a depth of about 35 n beneath the continents. It has come to be entified with the base of the crust. Laboratory udies of the velocities associated with different ck types suggest that the underlying mantle aterial is ultrabasic in composition. *Conrad* 925] identified a second velocity discontinuity, having a value of 6.3 km/sec, which defines an intermediate crustal layer beneath the continents. This seismic horizon, which bears Conrad's name, has come to be identified as the 'basaltic layer' of the crust; and the overlying material, having a velocity of 5.5 to 6.2 km/sec, is known as the 'granitic layer.' The depth and velocity of the Conrad discontinuity are not as consistent as those of the Mohorovicic discontinuity, and in some areas the Conrad layer appears to be missing. In oceanic areas, the granitic layer is totally missing. As these seismic horizons can only be identified through refracted wave arrivals observed over a sufficient distance to verify the velocity of propagation, their recognition from earthquake wave arrivals is dependent upon both the distribution of the observatory sites and their distances from the points of origin. Because the experiment is not a controlled one in terms of location, depth of origin, or time of impulse, the data obtained from earthquake body waves have not been as complete as one might wish. It is not surprising, therefore, that the results of recent experiments with explosion seismology

TABLE 1—*Summary of results of surface seismic measurements in North America*

Area	Velocity km/sec				Depth to Mohorovicic discontinuity km			Surface elev. m.	Observer
	P_0	P_1	P_*	P_n	Vel. const.	Incr. vel.	Refl. depth		
Atlantic Seaboard									
(Md.—Va.)	5.5	6.1		8.1	26–29	30–33	30–35	30	Carnegie Inst
Appalachian Highland									
New York		6.2		7.8		38		25	Slichter
New England		6.2		7.8	25			15	Slichter
New England		6.1	6.8	8.4		36		50	Leet
Pennsylvania		6.0		8.2		33		230	Katz
Appalachian Mts.									
(Tenn.)		6.0		8.1	39	42	45–50	820	Carnegie Inst
Mid Continent Shield									
Ontario		6.2	7.0	8.2	36			330	Hodgson
Adirondacks, N.Y.		6.4		8.2		35		360	Katz
Adirondacks, N.Y.		6.0		8.1		36		350	Katz
No. Michigan	4.2	6.2		8.2	36	41		190	Slichter
No. Michigan	4.7	6.3		7.9	36			360	U. of Wis.
No. Wisconsin	4.6	6.2		8.2	36	37		320	Slichter
No. Wisconsin	5.2		6.5	8.2	38			330	U. of Wis.
Minnesota		6.1		8.1	37		40	430	Carnegie Inst
Iowa	4.5	6.2		8.2	37	44		170	Slichter
Arkansas	5.2		6.9	8.2	43			100	U. of Wis.
Alberta	3.6	6.2	7.2	8.2	43			1000	Richards and Walker
Plateau Area									
Utah	5.5			8.0	28			2000	U. of Utah
Utah	5.5			8.0	29			2000	Carnegie Inst
Arizona-N. Mex.		5.8		8.1	34			2100	Carnegie Inst
Arizona-N. Mex.		5.8		8.1	29			1400	Carnegie Inst
Mexico	5.1	6.1		8.2	39			2100	U. of Wis.
Pacific Coast									
(California)		5.9	6.6	8.2	35		25–30	450	Gutenberg
Pacific Coast									
(California)		6.0		8.0	23–32			450	Carnegie Inst
Washington		6.0		8.0	30			360	Carnegie Inst
Puget Sound		6.0		8.0	19			25	Carnegie Inst
British Columbia		6.4		8.2	33			5	Milne

have not agreed in detail with the earlier conclusions of *Jeffreys* [1926] and *Gutenberg and Richter* [1945].

Surface refraction and reflection measurements—Several groups of investigators have carried out surface seismic measurements of crustal structure by explosion techniques, and the advantages of controlled, repeatable experiments have been realized. About twenty sets of such measurements have now been made in the United States, and the results are summarized in Table 1. *Byerly* [1956] has given an excellent review of foreign measurements. The reliabilit of these measurements depends upon mar basic assumptions, such as homogeneous crust layers and increasing velocity with depth, bu in general the depths so obtained seem to b accurate to about ±10 per cent. An exceptio are the plateaus, where depths are general too shallow to conform either to the gravit data or to values determined from analysis earthquake surface waves.

A series of similar measurements, with ap propriate changes in technique, has been mad

TABLE 2—*Typical seismic results in marine areas*

Area	Velocity			Depth to Moho km	Depth of water km	Observer
	P_0	P_1	P_n			
W. Atlantic		6.4	8.0	12.0	5.2	Lamont Geol. Obs.
res Basin	4.5	6.5	8.5	11.1	5.3	Lamont Geol. Obs.
rth Atlantic		7.2	8.3	9.5	4.8	Lamont Geol. Obs.
lf Mexico	3.2	6.2	8.3	17.5	3.7	Lamont Geol. Obs.
ribbean		5.9	7.8	13.5	4.0	Lamont Geol. Obs.
onson Deep	4.3	6.6	7.9	10.4	5.3	Lamont Geol. Obs.
ntinental Slope	4.9	6.8	8.5	15.9	2.8	Lamont Geol. Obs.
lf Maine	5.3	6.2	7.5	16.5	0.02	Lamont Geol. Obs.
Pacific		6.8	8.1	12.0	5.5	Scripps Inst.
kini flank	5.1	6.5	8.2	13.0	4.6	Scripps Inst.
ntral Pacific		6.8	8.1	10.8	5.5	Scripps Inst.
ariannas		6.0	8.0	9.4	4.9	Gaskell and Swallow

the oceans. Although the upper mantle locity is the same as that obtained for the ntinents, the velocity of the overlying crust the oceans averages about 0.3 km/sec higher. ese results are summarized in Table 2. A ther complete tabulation of crustal thickness r the Atlantic Ocean and the Mediterranean a is given by *Ewing and Ewing* [1959].

Relations of seismic depths to Bouguer anomies—The relations of the seismic depths to the gional Bouguer gravity values in the same eas are shown in Figure 3. The general corlation between the depth of the Mohorovicic scontinuity and the Bouguer gravity anomies strongly suggests that the gravity values e controlled primarily by the mass variations sociated with changes in crustal thickness. hat the relationship is not perfect everywhere indicated by the data for the plateau areas, hich appear to have a crust somewhat thinner an would be anticipated from the gravity alues and elevation. *Tatel and Tuve* [1955] ggested that this anomalous relationship in e plateaus may be due to changes in mean nsity of the crust or of the underlying mantle ck in these areas; but, as will be shown ter, it is more likely that crustal layering in ese areas was not detected in the refraction ismic measurements.

The pressures and temperatures 6 km beath the oceans must be different from those 5 km beneath the continents. But since the ismic velocities are the same (a little over 8 km/sec), the Mohorovicic discontinuity must be a change in mineralogic composition rather than a change in physical state. That this discontinuity does not represent a boundary for plastic flow is suggested by both gravitational and seismic studies of oceanic islands [*Woollard*, 1954]. In all cases studied to date (Oahu, Bermuda, Kwajalein) the island mass appears to be carried as if on an elastic crustal plate, flexed downward over an area 300 to 500 km in diameter. As the average island platform is no more than 100 km in diameter at its base, this regional distribution of the compensation signifies a crustal sheet having a thickness considerably greater than the 5 to 6 km defined by the Mohorovicic discontinuity.

Surface-wave studies—Press and Ewing [1955] have shown that the earthquake surface waves with periods of 8 to 140 sec have a velocity dispersion pattern that coincides with that theoretically to be expected where crustal structure is known from surface refraction measurements. Departures from this pattern can therefore be interpreted in terms of crustal abnormality. It is also found that the very long period shear waves, identified as Lg waves, are restricted in occurrence to the continents. These waves appear to be propagated in a wave guide in the upper part of the crust. *Birch* [1958], on the basis of laboratory studies of rocks under high pressure, suggested that the Lg waves may be trapped within the upper 10 km of the crust because of strong upward refraction which is

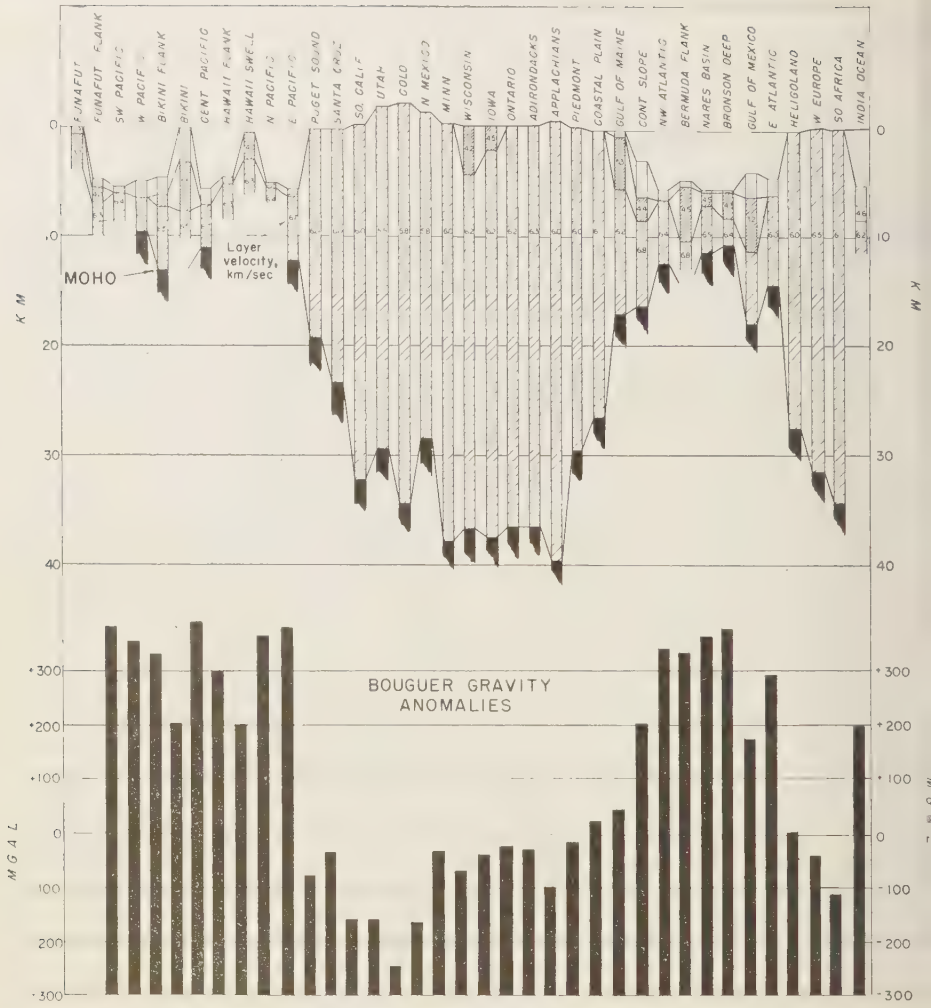

FIG. 3—Relation of crustal thickness obtained from seismic measurements to Bouguer gravi anomalies.

due to a marked change in compressibility with pressure. Propagation would be by a combination of upward refraction and surface reflection. Their absence in the oceans would be explained by the pressure effect of the water column and sediments which would raise the velocity values of crystalline rock nearly to the terminal velocity so that the remnant upward refraction would not be sufficient to give a similar confinement of energy. Since the velocity dispersion for these earthquake surface waves gives t general crustal conditions over long paths, the measurements furnish a technique for studyi over-all crustal structure in inaccessible regio

Press [1956] has used the phase veloci dispersion for Rayleigh waves of 10- to 30-s periods in conjunction with the results for su face refraction measurements in South Afri to establish a standard set of relationshi between phase velocity, period, and crus

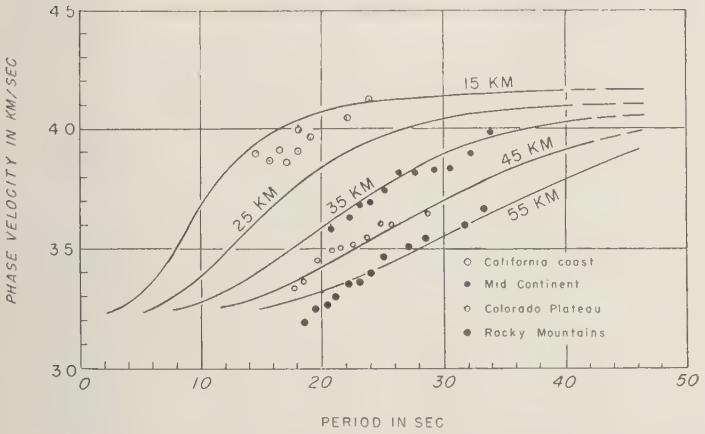

FIG. 4—Phase-velocity dispersion of Rayleigh waves and variations in crustal thickness in different physiographic areas.

hickness. These have been extended mathematically to determine the relationships for different values of crustal thickness, and *Ewing nd Press* [1959] have determined variations f crustal thickness in various parts of the Inited States. Figure 4 shows the consistency f these data for different physiographic provnces and the results are given in Table 3.

It will be noted that, whereas the values of rustal thickness obtained by refraction measrements in the plateau areas average close to 5 km, the surface-wave measurements average bout 48 km. The latter figure is in substantial greement with the results deduced from ouguer gravity anomalies, as will be shown ter.

ABLE 3—*Crustal thickness derived from phase elocity dispersion of Rayleigh waves in the United tates (after Ewing and Press, 1959, and Press, 1957)*

Area	Kilometers
acific Coast–Southern California	20
ransverse Ranges	38
oastal Range	45
an Joaquin Valley	43
outhern Sierra Nevada	40–49
asin and Range and Plateau areas	42–53
ocky Mountains	38–43
igh Plains	34–39
nterior Low Plains	35
anadian Shield	37–41
ppalachian Mountains	

It should also be noted in connection with surface-wave studies that, since the parameters involved include density as well as the elastic properties of the crust and mantle, the thickness determination is influenced by the assumed mean density for the standard column and by assumptions made regarding crustal structure and density variations with thickness.

Analysis of Data

Density-velocity equivalents—As mentioned earlier, in order to interpret realistically the gravity anomalies in terms of crustal structure, it is necessary to have a starting point where the crustal thickness and the difference in density between the crust and mantle rocks are known. It is from seismic measurements that both quantities are obtained. The seismic velocities, though not attributable to unique rock associations, can be used with a certain degree of confidence to deduce the probable density values. The relation between density and seismic velocity for compressional waves is given by $V_p^2 = (K + 4/3G)/d$, where V_p is the compressional velocity; K is the bulk modulus, the reciprocal of the compressibility; G is the modulus of rigidity; and d is the density of the material. If the elastic quantities K and G remained constant, then any increase in the density would result in a decrease in velocity. Actually, the elastic properties for all crystalline silicate rocks change with density in such

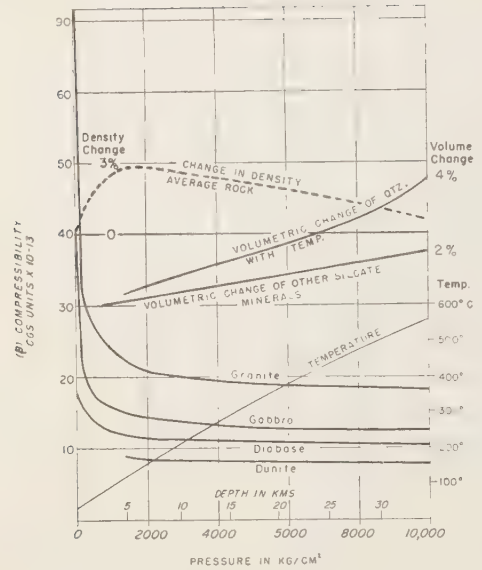

FIG. 5—Effect of pressure and temperature on density of rocks.

a way that velocity and density vary directly and approximately in the ratio of 3 km/sec to 1 gm/cc. For unconsolidated materials the velocity is governed not only by the mineral constituents present but also by the porosity of the aggregate and the nature of the material occupying the voids. A dry sand may have a velocity of only 0.6 km/sec; the same sand, water saturated, will have a velocity of 1.7 km/sec. If the sand becomes poorly cemented with calcium carbonate, it may have a velocity of 3.2 km/sec; if cemented with silica, it may be indistinguishable in velocity from a granite. Porosity, which is directly related to the compressibility and the bulk modulus, is therefore a major determinant of velocity. For the crystalline rocks with porosity values of usually less than 3 per cent the elimination of the voids by pressure leads to large changes in the elastic constants K and G. Although this effect is offset somewhat by thermal expansion, since temperature also increases with depth, the temperature effect is small compared with that for pressure. The effect of these same factors on density, on the other hand, is negligible (Fig. 5). The elimination of an initial porosity of 3 per cent or less by pressure is almost exactly offset by thermal expansion at depth. That the velocity is greatly affected is shown in Figure 6, which represents the results of experimental laboratory studies by *Birch* [1958]. From Figures 5 and 6 it is clear that granite at a depth of 10 km will have a velocity approaching that of gabbro at the surface, but the density will still be close to the value of 2.65 gm/cc at atmospheric pressure. These observations explain why the average velocity of crystalline rocks at the surface is about 5.4 km/sec and the crustal values at depths greater than 5 km appear to be 6.4 km/sec or somewhat greater. The observed change in velocity is related to the elimination of porosity rather than to a change in crustal composition. If the velocity at depth, however, is of the order of 6.4 km/sec, as observed in Wisconsin, or 6.9 km/sec, as observed in Arkansas [*Steinhart and others* 1958], these velocities are too large to be attributed to the elimination of porosity and are indicative of a change in mineral composition. As the observed velocity for the oceanic crust is about 6.52 km/sec, this value can also be examined as to its mineralogic significance in terms of the confining pressure at the base of the oceanic sediments. As shown in Figure 6, the velocity value for the oceanic crust falls about halfway between the curves for granite and gabbro. This suggests that material of intermediate composition forms the oceanic crust.

When all the experimental results on density-velocity relationships are assembled and plotted as a graph it is found that there is a considerable amount of scatter in values and that there is no simple over-all relationship. With unconsolidated saturated sediments, both velocity and density increase with depth of burial. With consolidated sediments the increase in both parameters can be correlated with geologic age. With whole crystalline rocks there is an apparent linear relationship between density and velocity but the slope of the curve for surface pressures differs from that for depths greater than 8 km. For mineral assemblages rich in spinels, in particular those with high accessory iron, a third set of relations is applicable because of the resultant high density. The uncertainty as to the prevalence of this group of rocks at depth poses a major problem in interpreting seismic velocities in terms of density. It is thus obvious

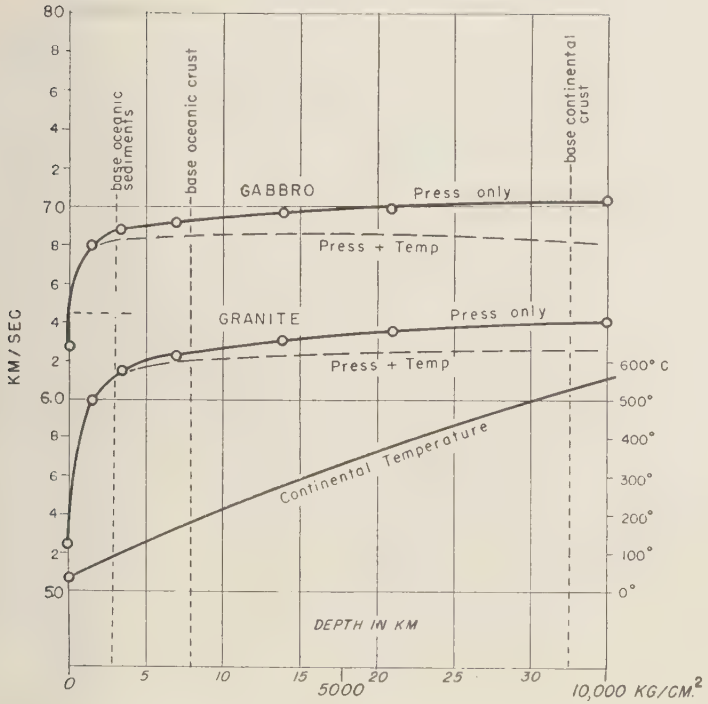

FIG. 6—Effects of pressure and temperature on compressional wave velocity in rocks.

hat it will never be possible to assign a unique ock type to any velocity value, and the only st of the reality of any density interpreta- on of seismic velocities is to make trial com- utations to see how well the implied mass stribution agrees with the gravity data. Fig- re 7, which shows the relationship between ismic velocity and density, is based on all vailable data for normal rock types. The source aterial is principally *Birch and others* [1942] us field and laboratory measurements con- ucted by the University of Wisconsin. Although nly a small percentage of the actual points are own, enough are indicated to show the prob- ble uncertainty. The value for oceanic sedi- ents is an approximation based on core values r fine-to-coarse clastics kept in open packing y the dilatent pressure of the overlying water olumn and by a minor clay fraction that has a gh density because of the collapse of its aled cell structure.

Mean crustal density—From Figure 7 and the seismic data for an average oceanic crustal section the following densities are obtained: bottom sediments, 2.0 gm/cc; crustal material, 2.86 gm/cc; and mantle material, 3.32 gm/cc. These are minimum density values—any accessory magnetite would raise the values.

Using the same approach on the continents leads to rather confusing results, as the crust has a layered structure and is composed of materials having various velocities. An indirect approach on the assumption of isostasy, however, can be made by using the observed crustal thickness values and the density data derived for the oceanic section. A crustal thickness of 34 km was used for the continents. It is the average thickness determined from refraction and reflection measurements for those parts of the continent which are below 400 meters in altitude, excluding areas, such as are found in Arkansas, which show evidence of abnormality. When the weight of this column is equated to the weight of the average oceanic column with

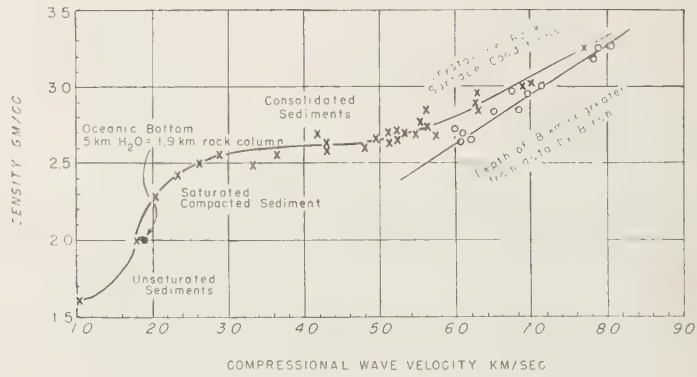

FIG. 7—Relation of density to compressional wave velocity in rocks.

densities as shown in Table 5, the derived density of the continental crust is 2.87 gm/cc and the mantle-crust density differential is 0.45 gm/cc. In a similar manner but using slightly different thickness and density values, *Worzel and Shurbet* [1955] found the density differential to be 0.43 gm/cc. With this value, and on the assumption of a homogeneous crust, it is possible to evaluate changes in crustal thickness on the basis of the change in Bouguer gravity anomaly values. The average anomaly for the seismic sites used in determining the continental crustal column was −34 mgal. On the basis of the gravity effect of a horizontal slab and a density differential of 0.45 gm/cc, the decrease in crustal thickness is 1.8 km at the coast where

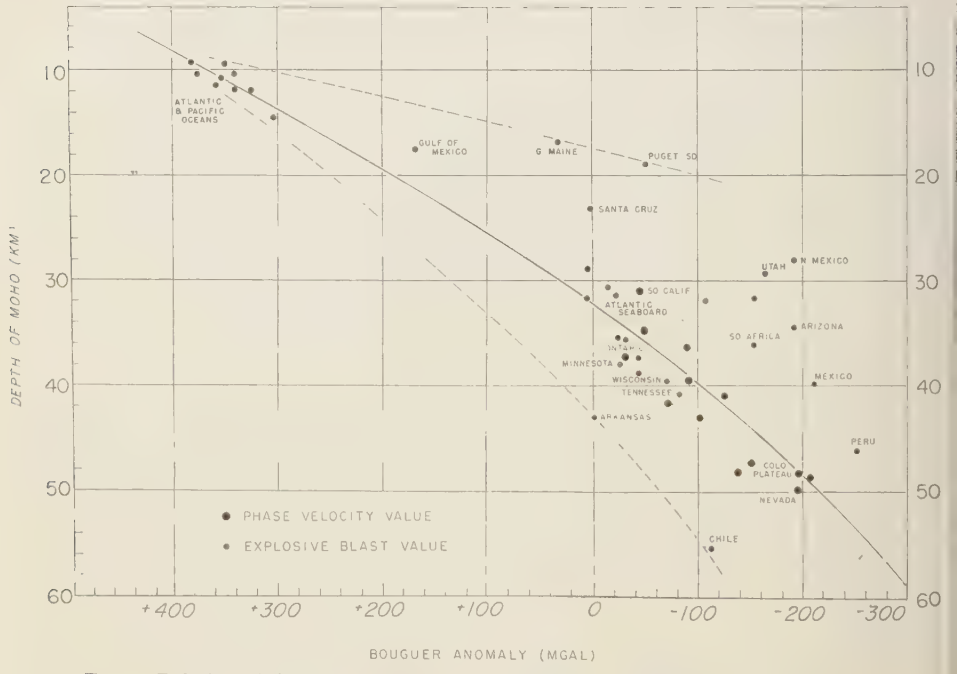

FIG. 8—Relation of depth of Mohorovicic discontinuity to Bouguer gravity anomaly.

ne mean anomaly is zero (Fig. 2). This would ndicate a continental sea-level crustal column f approximately 32 km. This value falls near ne midpoint of the observed depths of 30 to 3 km calculated from refracted arrivals with n assumed velocity increase with depth. This lso is in the middle of the 30- to 35-km depths omputed from reflected arrivals. In the Rocky Mountains, with a regional anomaly of −260 ngal, the increase in thickness of the crust be- ow sea level is 14.5 km. This gives a crustal hickness of approximately 46 km, which is in eneral agreement with the 45- to 53-km depths etermined by *Ewing and Press* [1959] from he velocity dispersion of Rayleigh waves.

A plot of the relationship between the depth f the Mohorovicic discontinuity, as determined rom surface refraction measurements, and the Bouguer anomalies (Fig. 8) shows that the situ- tion is not so simple, however. This plot indi- ates a nonlinear relationship and also a wide catter in the data for the continental area. 'art of this scatter is related to the fact that efraction measurements in the plateau regions ive abnormally shallow depths in comparison ith those derived from surface waves. If these iscrepancies are discounted for the moment as eing related to masking of an intermediate ve- ocity layer within the crust and only measure- nents obtained from the velocity dispersion of urface waves are used for these areas, it is seen hat a curve of exponential type can be used o describe the general relationship.*

From the slope of the curve it appears that as the crust becomes thicker its mean density increases, if it is assumed that the underlying mantle rock is characterized by a constant density, as is indicated by its uniform velocity. This suggestion of an increase in mean crustal density with thickness is also indicated by other data. A plot of the depth of the Mohorovicic discontinuity as a function of elevation (Fig. 9) also shows an exponential relationship between crustal thickness and elevation. If the mantle has a fixed density, this is evidence of increasing crustal density with elevation and crustal thickness. A similar plot of Bouguer anomalies as a function of elevation (Fig. 2) likewise suggests that there is an increase in mean crustal density beneath the areas of highest elevation. This last, however, can also be related to the regionality of the gravity compensating effect of the mass distribution associated with the configuration of the base of the crust. This effect, however, is less than that shown in Figure 2. Therefore, on the basis of these independent relationships, it appears that the hypothesis of a decreasing contrast in density between the crust and the mantle with increasing elevation and crustal thickness is well supported.

In order to describe the magnitude of the postulated change in density contrast between the crust and the mantle with crustal thickness, two approaches can be used. The first is based upon the density equivalents for the seismic velocities (Fig. 7). The second is based upon the density contrast derived from the slope of the empirically determined curve (Fig. 8). A log-log plot of this curve shows that an exponential relation holds for the continental observations. But if the oceanic values are to fit exponentially with the continental data, it is necessary to use a density of 2.48 gm/cc rather than 2.67 gm/cc in calculating the density deficiency of the water column relative to that of rock. Such a low density for the enclosing rock does not appear to be geologically probable. Slope values were therefore determined graphically rather than by analytical computation, and the density contrast which was derived on the basis of the gravitational attraction of a slab was compared with that based on the equivalent velocity values shown in Figure 7. For the oceanic

*It might also be thought that three distinct near relationships could be described: one for he oceans, one for the stable continental areas, nd one for the plateaus. This, however, would ead to unlikely conclusions. For example, from he slope of any curve which relates the change n regional gravity to the change in crustal thick- ess, the density contrast between the crust and nantle rock can be determined. In the oceans, or the linear alignment suggested between Santa Cruz and the deep ocean values, the slope would e about 30 mgal/km, from which it is found hat the density contrast between the crust and he mantle would be 0.72 gm/cc. In the con- inental plateau areas the suggested alignment as a slope of less than 4.0 mgal/km, from which t is found that the density contrast between the rust and the mantle would be less than 0.096 m/cc. Both values are geologically improbable. These apparent alignments are therefore thought o be more fortuitous than real.

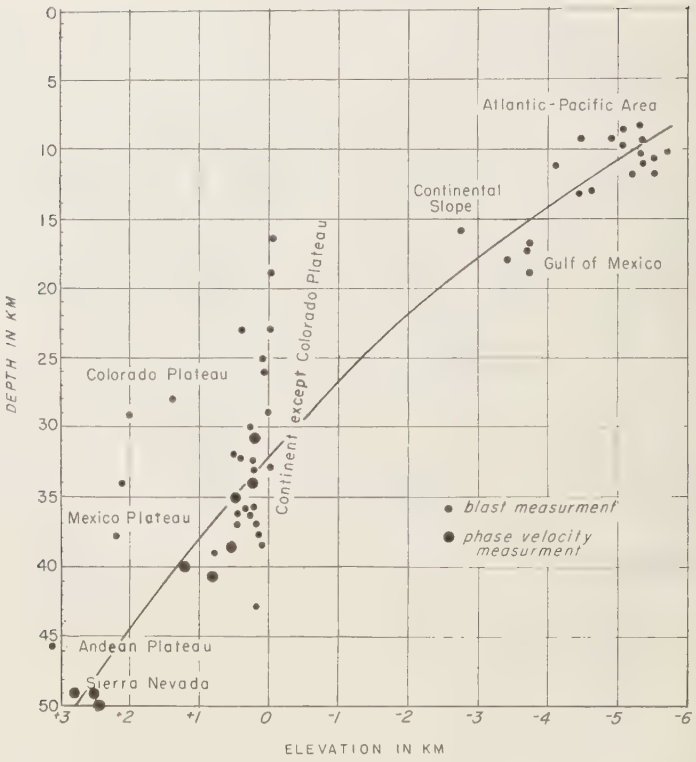

FIG. 9—Relation of depth of Mohorovicic discontinuity to surface elevation.

part of the curve, with anomalies close to +350 mgal, the slope is 19 mgal/km, which corresponds to a density differential of 0.455 gm/cc between the crust and the mantle. If the mantle rock is taken to have a density of 3.32 gm/cc, the density of the oceanic crust would be 2.86 gm/cc. This is the same value that was deduced earlier from Figure 7 for the oceanic crustal velocity of 6.52 km/sec.

However, when the slope of the curve is used to determine continental crustal density it is found that at sea level the continental crust has a density of 2.98 gm/cc; beneath the Colorado plateaus, where the average anomaly is −200 mgal, the crustal density is 3.07 gm/cc; and beneath the Rocky Mountains, with an anomaly of −260 mgal, the density is 3.09 gm/cc. These values all appear to be geologically unlikely and all are greater than those which would be derived from the seismic values of crustal thickness and the velocity-density equivalents given by the high-pressure curve of Figure 7.

To test the validity of the density contrast these density values were used with the characteristic regional Bouguer gravity anomalies for the different physiographic provinces to compute the depth to the base of the crust, and these depths were then compared with the seismic ones (Table 4). Depths were also computed for the same areas on the basis of Archimedes' principle for a floating crust in hydrostatic equilibrium; the same density values and the values of crustal thickness derived from the gravity anomalies (Table 5) were used. As shown in Table 4, the gravity depths agree to within 1 km with those determined seismically except in the Rocky Mountains where the velocity dispersion of earthquake surface waves indicated no significant increase in crustal thickness. This is regarded as unlikely in view of the

TABLE 4—*Crustal parameters derived from gravity data.*

Area	Bouguer anomaly mgal	Slope of curve Fig. 11 mgl/km	Density contrast, crust & mantle gm/cc	Crustal density Mantle = 3.32 gm/cc	Average density contrast gm/cc	Δh* km	Elevation of Moho km	
							Gravity data	Seismic data
Ocean	+350	19	.455	2.86			−11.5 (base)	−11.5
					.40	20.9		
Seacoast	0	14.5	.345	2.98			−32.4	−32.0
					.297	15.8		
Colorado Plateau	−200	10.5	.250	3.07			−48.2	−48.0
					.238	6.0		
Rocky Mts.	−260	9.5	.225	3.09			−54.2	−49.0

* $\Delta h = \dfrac{\text{Bouguer anomaly}}{2\pi G \times \text{density contrast}}$; i.e., $\dfrac{+350 \text{ mgal}}{41.85 \times .40 \text{ gm cm}^{-3}} = 20.9$ km.

tation array that was used in making this determination and the results of seismic refraction measurements in other mountain areas. The results shown in Table 5 for a floating crust in equilibrium indicate that the mean crustal density values used are too high. In order to obtain equilibrium for the values of crustal thickness shown, and with the mantle having a density of 3.32 gm/cc, the sea-level column would have to be 2.85 gm/cc and that for the plateaus and Rocky Mountains about 2.88 gm/cc.

If these density values are used with the Bouguer anomalies to compute crustal thickness it is found that in order to obtain agreement with the seismic value for the change in crustal thickness between the continents and ocean basins it is necessary to use the mean crustal density of 2.85 gm/cc rather than 2.67 gm/cc in correcting for the mass deficiency of the oceanic water column. It is also found that the increase in crustal thickness beneath the plateaus and mountains is significantly less than that indicated by the seismic data. Therefore, although the concept of increasing density with

TABLE 5—*Elevation of Mohorovicic discontinuity on basis of isostasy and Archimedes' principle.*

Area	Crustal elevation km	Elevation of Moho km (Gravity)	Column density gm/cc	Displacement of mantle column km	Δh* km	Elevation of Moho km (Arch. Prin.)
Ocean Floor	−5 (−3.2 rock equivalent)	−11.5	Mantle 3.32 5 km Water 1.03 1 km Seds. 2.00 5.5 km Crust 2.86	6.9		−11.5 (base)
					21.8	
Seacoast	0	−32	2.98	28.7		−33.3
					17.3	
Colorado Plateau	+2.0	−48	3.07	46.0		−50.6
					6.8	
Rocky Mts.	+3.2	−54	3.09	52.8		−57.4

* $\sum \rho h = \bar{\rho} h$; i.e., $h = \dfrac{\bar{\rho} h \text{ (crust)}}{\bar{\rho} \text{ (mantle)}}$; for seacoast, $\dfrac{2.98 \times 32}{3.32} = 28.7$ km.

increasing thickness of crust appears to be verified, there is considerable uncertainty regarding the density values to be assigned to the continental crust.

Andreev [1958], in a recent paper on this same subject, relates variations in crustal thickness on the continents to the Bouguer gravity anomaly as a linear function, $H = 0.1\Delta g + 30$, where H is the crustal thickness in kilometers and Δg is the Bouguer anomaly. The slope of this relation (10 mgal/km) suggests a mean density contrast of 0.24 gm/cc between the crust and the mantle. This implies a mean density for the continental crust of 3.08 gm/cc, if the mantle density is 3.32 gm/cc. In a more recent paper *Andreev* [1959] calls attention to the fact that with a layered crust the use of mean density values in computing crustal thickness from Bouguer anomalies leads to incorrect results where anomaly structures of limited width are involved.

Although this is generally known, Andreev is the first to publish specific examples related to crustal structure and to present an equation dealing with a compound layered structure. The general relation developed by Andreev is $\Delta g = 2\pi GS(H)$ where $S = \sum_{k=1}^{n} \Delta d \exp(-2\pi Z_k/L)$. In the latter expression, Δd = density contrasts between layers, k = layer designation, Z = depth of layer interface, and L = 'wavelength' of anomaly. For the case of mountain areas with anomaly structures ranging in wavelength from 200 to 400 km and with a crustal section composed of 15 km of rock of density 2.7 gm/cc and 30 km of rock of density 2.9 gm/cc overlying mantle material of 3.3 gm/cc, the following are found: when $L = 200$ km, $S = 0.12 + 0.16 = 0.26$; when $L = 400$ km, $S = 0.16 + 0.25 = 0.41$. For both conditions, the contribution from the upper interface approximates that from the lower one, although Z_1 and Δd_1 are each only one-half of Z_2 and Δd_2. If these values of S are substituted in the general equation for a conformable displacement of 10 km, Δg for $L = 200$ km is 105 mgal, and Δg for $L = 400$ km is 176 mgal. If a single layer with the mean density for the above crustal section (2.83 gm/cc) is used ($\Delta d = 0.47$ gm/cc), the computed value of Δg for $H = 10$ km is 197 mgal. It would not be until $L = 500$ km that the compound layer solution would yield the same value as that for a single layer of the mean density. This example therefore illustrates that it is necessary to use regional gravity anomaly values over an area about 400 km in width in relating changes in gravity to crustal thickness where crustal structure is not known. As the area gravity coverage adjacent to each of the seismic measurements used in constructing Figure 8 averaged about 200 km × 350 km, the nonlinearity of the plot is not believed to be related to this representation-factor.

In Figure 2, which relates Bouguer anomalies to elevation, the nonlinear relationship likewise might be thought to be related to a similar cause because at high elevations the associated crustal root is restricted in width and has a smaller gravitational effect than a similar increase in crustal thickness of greater width would have beneath an area of lower elevation. However, the curvature of this plot at low elevations is greater than that at high elevations. This is in the zone where the thickness of the crust is relatively uniform and all transitions in thickness are of a regional nature. The changes in slope indicated in Figure 2 for the section below an elevation of 1000 meters are from 14.2 mgal/km at sea level to 11.0 mgal/km at 1000 meters. These are the same values that are indicated for these physiographic provinces by the relation between the Bouguer anomalies and the seismic values of crustal thickness plotted in Figure 8. Both sets of relationships therefore indicate that the density contrast between the crust and the mantle decreases as the thickness of the crust increases and as elevation increases. As there is no independent evidence of a significant increase in the mean density of the crust with increasing thickness, it appears that there must be an anomalous negative mass within the upper part of the mantle whose proximity where the crust is thickest is sufficient to lower the apparent mean density contrast between the crust and the mantle. A similar concept was proposed by *Daly* [1940] as a means of explaining isostasy. He assumed differences in the concentration of radioactive heat that would lead to the formation of anti-roots of vitreous, low-density material beneath the areas of greatest crustal thickness. More convincing are the results of isostatic studies conducted by *Bowie* [1917], who found

at the most probable depth of isostatic com-
nsation beneath the Rocky Mountains was
2 km, in contrast with a depth of 57 km be-
ath the continental lowlands. More recently
ismic evidence has also shown that there may
a low-density layer within the upper part of
e mantle. This is suggested by the velocity
spersion of very long period Rayleigh waves
om earthquakes. *Dorman, Oliver, and Ewing*
959] (unpublished) have postulated that these
aves are propagated in a wave guide formed
a reversal in seismic velocities in the upper
art of the mantle. If this is true, it would
expected that this zone should also be one
lower than normal density. Because of the
crease in thermal conductivity with increasing
mperature above 600°C (at about 25 km, as
ostulated by *Lubimova* [1958]) it would be
pected that where the crust is thickest the
otherms would be distorted in the underlying
antle so as to cause a thickening of the low-
elocity layer in the mantle. The thickening
fect would be roughly proportional to the
ickness of the overlying crust. Therefore, in-
ead of attributing the observed density change
an increase in mean crustal density as the
ickness of the crust increases, it appears that
should be attributed to a decrease in mean
antle density as the crust thickens. This ex-
lanation not only resolves the discrepancy
rought out by Tables 4 and 5 but also explains
hy analytical studies based upon the density
quivalents of seismic velocities did not appear
be applicable in explaining the gravity anom-
lies.

As determined earlier, there is probably some
inor increase in mean crustal density (2.85
o 2.88 gm/cc) as the thickness of the crust on
he continents increases, but in gross form it
ppears that the crust is characterized by a
early constant mean density.

Determination of crustal thickness—Despite
he complexity of relations brought out above,
t is possible to make an empirical approxima-
ion of crustal structure from the relationships
f the gravity anomaly values and surface
levation to crustal thickness. In Figure 10
wo curves are shown which give the observed
elationship between the elevation of the Mo-
orovicic discontinuity and the Bouguer anom-
ly and the elevation of the rock surface (sea

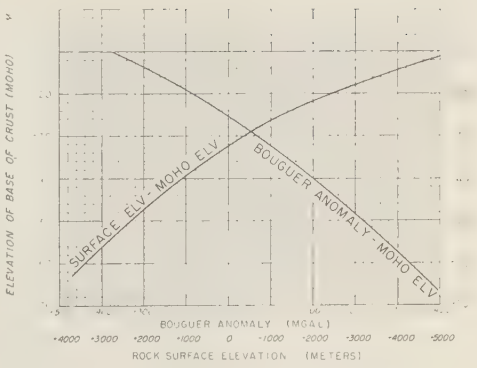

FIG. 10—Plot of depth of Mohorovicic discontinuity as a function of Bouguer gravity anomaly and surface elevation.

floor in the ocean). To determine crustal thickness with either parameter it is necessary to add the surface elevation to the values indicated for the elevation of the Mohorovicic discontinuity.

Where there are marked local departures in either the Bouguer anomalies or elevation from the regional values, a certain amount of discrimination must be exercised in using the relations shown in this figure. As shown in Figure 11 for the Bighorn Mountains region, many rather large topographic features are not compensated by a local thickening of the crust to form roots. A general rule is that if the width of the feature does not exceed three times the regional crustal thickness defined by Figure 10 it is probably compensated on a regional basis over a wide area rather than locally. The width of the Bighorn Mountains is about 85 km, the average regional elevation is 1800 meters, and the indicated crustal thickness (Fig. 10) for this elevation is 47 km. A local crustal root for these mountains therefore would not be expected. That there is regional compensation through crustal flexure in a manner analogous to that observed when one steps on a thin sheet of pond ice is indicated by the profile of the Bouguer gravity anomaly (Fig. 11). For the case of marked local changes in anomaly values, the Rocky Mountains in Colorado can be used. Here the regional Bouguer anomaly value is about −260 mgal and the indicated elevation of the base of the crust (Fig. 10) is −53 km. Beneath the continental divide the anomaly is

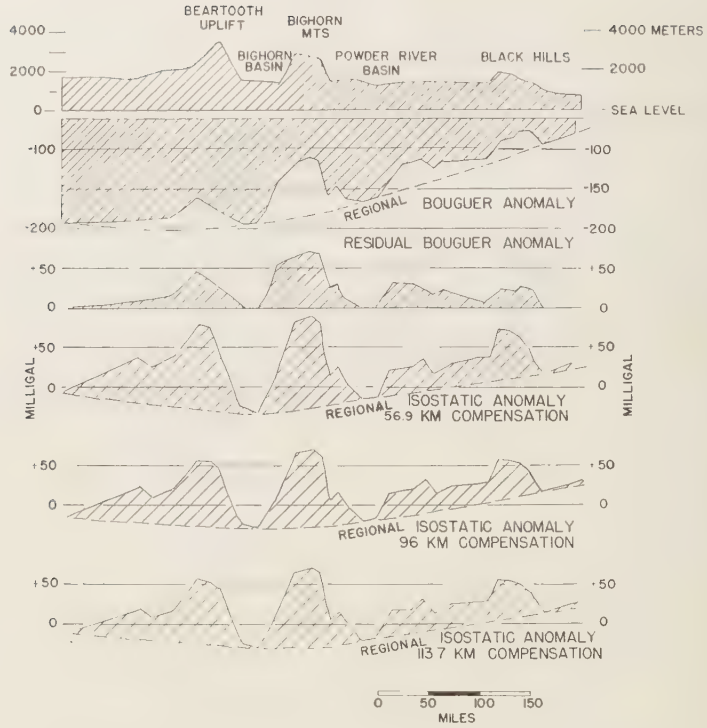

FIG. 11—Relation of gravity anomalies in Bighorn Mountains.

about −300 mgal. This local anomaly increment of −40 mgal could be caused by the surficial geology, intrusive granite, or a local thickening of the crust. Examination of the geological data suggests that either intrusive granite or local crustal thickening is the cause of the gravity effect. The problem of which of the two possibilities pertains can be resolved on the basis of the gravity effect of a simple geometric form such as a sphere or a horizontal cylinder. From the width of the 40-mgal anomaly increment at half amplitude the depth to the center of the anomalous mass is found to be about 45 km. As this lies above the regional depth to the Mohorovicic discontinuity, at about −53 km, the cause of the anomaly is probably an intracrustal granitic intrusive. If the depth had fallen below −53 km, the cause of the local increase in anomaly could definitely be attributed to crustal thickening, and its dimensions could be computed.

Because of nonsystematic variations in crustal composition (layering), a more sophisticate analysis of gravity anomalies in terms of crus tal thickness than that outlined above an incorporated in Figure 10 does not appear t be justified at this time. Figure 12 shows tha results comparable to those derived from ana lytical procedures can be obtained. The ob served Bouguer anomalies in each case wer corrected for abnormal masses which were in dicated by appreciable isostatic anomalies On the assumption of a homogeneous crust an a density differential of 0.40 gm/cc, and wit the Gulf of Mexico seismic section as a startin

* In the Gulf of Mexico the seismic studies *Ewing* and others [1955] show that the isostat anomaly of +80 mgal cannot be attributed t the section of sedimentary rock, but an abnorm crust of high density is indicated by a seism velocity of 7.07 km/sec near the site of the gra ity observation. In the Balsas Basin on the we side of the Plateau of Mexico the local isostat anomaly of approximately −25 mgal is believe to be related to the surficial geology of the are

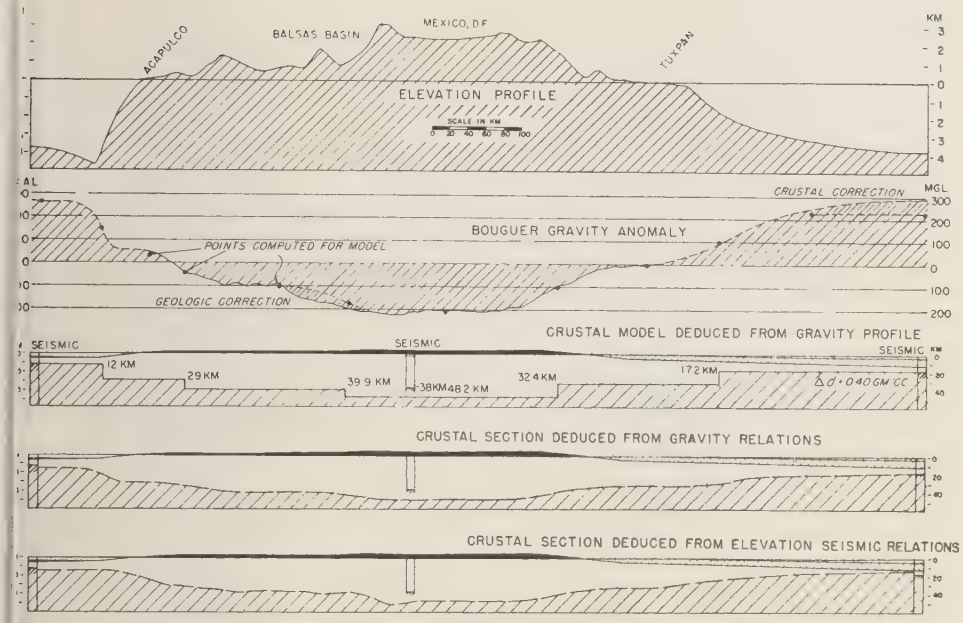

COMPARATIVE CRUSTAL SECTIONS, MEXICO

FIG. 12—Comparative crustal cross section of Mexico based on gravity and elevation data.

point, a crustal section was derived (Crustal model deduced from gravity profile, Fig. 12) which extends across Mexico into the Pacific Ocean. In the high plateau there is a lack of agreement with the seismic refraction measurement made by the University of Wisconsin. The elevation for the base of the crust from the refraction measurement is −38 km rather than −48 km. However, in the Pacific area the agreement with the seismic value of −12 km is excellent. The comparative section (Crustal section deduced from gravity relations, Fig. 12), based on the relation of the Bouguer anomaly to crustal thickness from Figure 10, agrees in over-all depths to within 2 km with those described above, and it is only in the transition from one level to another that a difference in structure is indicated. If abrupt changes in the level of the M discontinuity with near vertical boundaries exist at depth as implied under the assumption of local isostatic equilibrium, cognizance should be taken of the gravity effect produced by such boundaries. Except for this boundary effect and situations involving possible sharp local protuberances of the crust into the mantle (which would have a regional low-amplitude gravity effect at the surface), the relationship of gravity to crustal thickness given in Figure 10 appears to yield a realistic first approximation to crustal structure. That the relationship of surface elevation to crustal thickness is not quite the same as that based on the gravity anomalies is indicated in the last section of Figure 12. This section was derived from the relationship of elevation to crustal thickness shown in Figure 10.

If isostatic equilibrium kept pace with erosion and if the crust were homogeneous, variations in regional elevation would be a sensitive indicator of variations in crustal thickness. Despite these limitations, it appears that elevation can be used as a rough gauge of crustal thickness where other data are missing. A rule of thumb based on Figure 10 is that a change of 1 km in surface elevation is equal to a change of 6.8 km in crustal thickness. Applying this

change to a base value of 32 km at sea level gives the depth to the base of the crust. In the Rocky Mountains, with a mean elevation of about 10,500 ft (3.2 km), for example, the indicated increase in thickness is 22.7 km, which places the Mohorovicic discontinuity at about −55 km. In the oceans the same procedure can be used if the layer of water is converted to an equivalent rock layer and a synthetic elevation is obtained. For example, under oceanic conditions, 5 km of water equals in mass approximately 1.9 km of rock of density 2.67 gm/cc. The synthetic elevation would therefore be −3.1 km. The crustal thinning indicated is 21 km, and the elevation for the base of the crust is thus −11 km. These values check very well with those derived from gravity and seismic measurements and are further proof that isostasy is more than just a theory and that the crust everywhere appears to be floating on the mantle.

Remarks on Results of Analysis

Seismic refraction measurements reported by *Veytsman and others* [1957] suggest that there is also probably a limited increase in mean crustal density with increasing thickness of crust. In the northern Tien Shan Mountains, the southern Tien Shan Mountains, and in western Turkemenia of central Asia, it was found that, although the crust thickens beneath the mountains with a downward displacement of the Mohorovicic discontinuity, the overlying Conrad basaltic layer thickens disproportionately and bulges upward beneath the mountains. In western Turkemenia, beneath the Bolshoi Balkan Ridge, both the Conrad and Mohorovicic discontinuities are displaced downward beneath the mountains. *Balavadze and Tvaltvadze* [1957], discussing seismic refraction studies in the Georgia-Caucasus region of southern Europe, noted that the basaltic layer, with a velocity of 6.7 km/sec, varies between 24 to 35 km in thickness in this region and that the over-all thickness of crust varies from a maximum of 50 to 67 km beneath the Caucasus Mountains to a minimum of 40 to 45 km beneath the Dzirnula crystalline massif. Both groups of authors stressed the fact that the gravity anomalies are strongly influenced by the variable thickness of the basaltic layer.

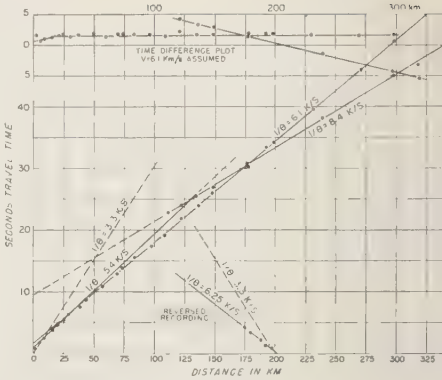

Fig. 13—Travel-time plot for Durango, Mexi seismic refraction study.

Refraction measurements made by the U versity of Wisconsin also indicated that basaltic layer is thickest where the crust thickest [*Steinhart and others*, 1958].

On the basis of a mean crustal density 2.85 to 2.88 gm/cc derived earlier, it appe that a basal crustal layer of 'basaltic' mate is present everywhere. However, published sults of refraction studies in North Amer have not, for the most part, reported such layer. The most likely explanation is that layer is present but is masked.

A re-study of the seismic data for some ar has shown that an intermediate layer could defined, but its inclusion has not always remov the discrepancy between the gravity and surf wave results. For example, the anomalous sult from the refraction studies in the plate region of Mexico, as compared with that rived from gravity (Fig. 12), has been stud by *Meyer and others* [1958]. The travel-ti plot of the field data obtained in this measu ment by the University of Wisconsin (Fig. 1 shows that if layering is present it is effectiv masked. On the assumption that such an int mediate layer exists, calculations were ma which show that a 14-km layer of material w a velocity of 7 km/sec could be present witho showing as a first arrival. Its effect would be deepen the crustal column by 4 km, wh would still leave a discrepancy of nearly 6 relative to the depth derived from the grav data. This suggests that the layer is actua

much thicker than 14 km, and failure to detect its presence either as a first or second arrival implies that its onset is not marked by a well-defined acoustic boundary such as is associated with the Mohorovicic discontinuity, which shows up as a second arrival 65 km prior to the cross-over range at 175 km.

In a recent re-study of crustal measurements in the plateau region of South Africa, *Hales arnd Sacks* [1959] found that an intermediate layer with a velocity of 6.7 to 7.2 km/sec might be defined. However, the increase in crustal thickness by the inclusion of this layer would be only 4 km over that originally reported. The revised elevation of −36.6 km for the base of the crust would still be about 3 km less than that suggested by the mean Bouguer anomaly value of −120 mgal.

That masked layering where the acoustic boundary is sharp can be readily detected through both reflected and refracted late arrivals is shown by the results reported by *Richards and Walker* [1959] for crustal structure in Alberta, Canada. Structure here was determined entirely on second and third arrivals for defining the Conrad and Mohorovicic discontinuities.

In addition to the masking of second arrivals by first arrival motion, masking may also be caused by variations of horizontal velocity, particularly in fan-recording. Such a situation is apparent in the results for the Patuxent, Maryland, crustal study reported by *Tatel and others* [1953]. In the published results a single-layer crust of 6.2 km/sec overlying mantle rock of 8.1 km/sec is reported. However, as shown in Figure 14, these data could also be interpreted as indicating a surface layer of 1.8 to 2.7 km/sec (sediments), a basement rock layer of 6.2 km/sec, an intermediate layer of 7.1 km/sec, and then the M discontinuity with a velocity of 8.1 km/sec. In a preliminary interpretation of this material, these investigators identified layers having velocity values of 6.1, 6.7, and 7.05 km/sec above the M discontinuity. They also pointed out that the reflection depths obtained indicate a crustal thickness about 4 km greater than that based on the refraction interpretation for a single-layer crust.

The nature of the 'basaltic' layer and why it thickens with crustal thickness can only be surmised at this time. In view of the geologic evidence of a 'pulsating' crust, it would appear that whatever mechanism controls regional uplift and subsidence also controls changes in crustal structure and density. If the intermediate basaltic layer is not an inherited feature from magmatic differentiation on a primeval

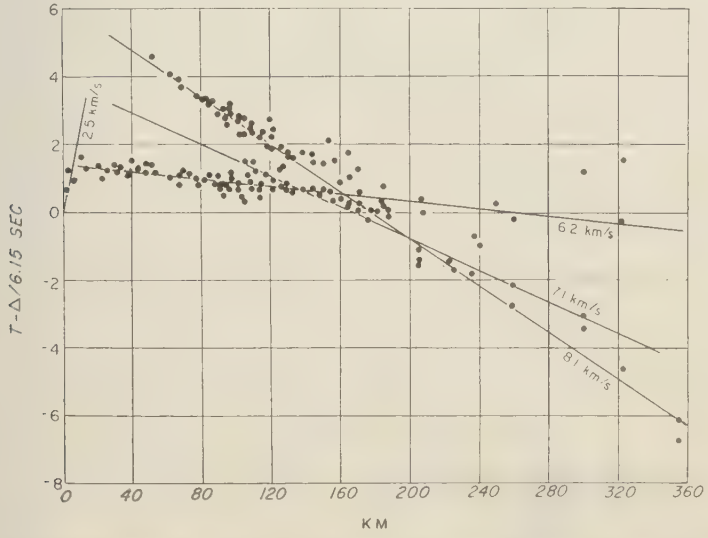

Fig. 14—Reduced travel-time plot for Patuxent, Maryland, seismic refraction study.

earth but is rather a phase transformation of the mantle, its apparent variations in thickness with over-all thickness of the crust can be readily explained by the concept developed by G. Kennedy (unpublished Sigma Xi lecture). Under this concept, which involves the phase transformation of eclogite to basalt at the Mohorovicic discontinuity, base leveling of any mountain by erosion would reduce the pressure at the base of the crust and lead to a crustal thickening, eustatic uplift, and bowing upward of the granite-basalt interface. An alternate transformation is that of dunite to serpentine, as suggested by *Hess* [1955]. This depends upon water vapor being available and the temperature being below 500°C. Serpentinization of the mantle rock would result in a volumetric increase of 25 per cent in the affected zone. Density would likewise decrease by 25 per cent, as would the seismic velocity. Even partial serpentinization of a limited zone of mantle material would cause a sufficiently large change in velocity for the material to lose its identity as mantle material. The resulting increase in thickness of the crust would result in eustatic uplift and also in a bowing upward of the granite-basalt interface.

As the intermediate (basaltic) layer varies in velocity from about 6.4 to 7.3 km/sec, it does not appear to represent any one kind of material. Also, it does not appear to be as marked an acoustic boundary as the Mohorovicic discontinuity, and it cannot always be found even though gravity data suggest its existence. Both facts indicate that it may represent a transitional zone with a well-defined lower boundary but a gradual transition upward. Although the writer is in no position to argue for either the Hess or the Kennedy concept, it seems likely that a phase transformation is involved. It also seems that the degree of development, both in terms of thickness and change in mineralogy, is a function of time as well as of the prevailing temperature and pressure conditions and the amount of free water vapor available. The longer a transformation has been operating in a given direction, the more complete the transformation will be. This is certainly suggested by the seismic velocity values observed over the Wisconsin Arch and the Adirondack Dome, the two areas of long-term structural uplift which have been studied to date. Both in the Wisconsin area and in the Adirondacks, the near-surface crustal velocities of 6.4 and 6.5 km/sec, respectively, are anomalous and well above those normally associated with the continental crust, which is 6.0 to 6.2 km/sec. The values are also at the low end of the spectrum reported for the basaltic layer, which ranges from about 6.4 to 7.3 km/sec. Although it can be argued that the situation in the Adirondacks is a special one because of basic rocks in the area, this cannot be claimed for Wisconsin where the crust is abnormally thick (38 to 40 km) for the elevation and the gravity anomalies substantiate this value. Unfortunately there are not yet enough seismic data to establish any reliable relationships such as the one suggested above, but at least the relation is one to be looked for.

Whether the process of serpentinization can operate at the temperature conditions found at depths of 45 to 50 km beneath the plateaus cannot be demonstrated. In the mountain regions of geosynclinal origin the problem is not so controversial, since the geologic evidence indicates that at one time in the orogenic cycle invasion of mafic material took place. Further, the occurrence of belts of serpentine bodies in mountain regions is a characteristic feature [*Hess*, 1955]. Both transformation theories are supported by the U.S.S.R. seismic studies in mountains, as well as by the gravity data, and the greatest development of the intermediate layer appears to be beneath the areas of highest elevation. This suggests that elevation may have resulted, in part at least, from growth of this layer and its possible upward migration because of gravitational instability. On the basis of the subnormal crustal velocities of 5.5 to 5.8 km/sec reported in the Colorado Plateau (*Tatel and Tuve* [1955]; and *Berg*, unpublished), it might appear also that the plateaus are characterized by crustal material of lower than normal density. However, the seismic measurements in the plateau areas of Mexico and South Africa do not support this relationship as being general. A normal crustal velocity of 6.1 km/sec is observed in both areas. If there is any general mass abnormality associated with the plateaus, it must lie within the basaltic layer or in the underlying mantle rock.

Summary

(1) Isostasy, on the basis of both isostatic nd free-air anomalies, is a real phenomenon n a regional basis.

(2) The inverse relationship of Bouguer ravity anomalies to elevation on the basis of eismic data is attributable principally to thickning of the crustal layer with increasing ele- ation.

(3) The densities of crustal materials can be leduced from seismic velocities with sufficient ccuracy to permit their use in most analytical tudies of gravity data.

(4) The interrelationships between Bouguer gravity anomalies and the thickness of the rust suggest either that the mean density of he upper part of the mantle decreases or that f the crust increases with increasing thickness f the crust.

(5) If it is assumed that the mantle rock is homogeneous and has a constant density of 3.32 gm/cc, as suggested by its characteristic velocity of about 8.1 km/sec, the mean density of the crust would appear to increase from a value of 2.86 gm/cc beneath the oceans to approximately 3.1 gm/cc beneath the high mountains. If it is assumed that the mean density of the crust remains essentially constant (2.85 to 2.88 gm/cc), then the mean density of the mantle decreases by equivalent amounts in the same areas. This latter situation appears to be the more probable because of seismic indications of a velocity reversal in the upper part of the mantle.

(6) On the basis of Archimedes' principle for a floating crust, values of crustal thickness can be obtained which are in agreement with seismic measurements. The average ratio of freeboard to submerged root for the crust is approximately 1:6.8. This strongly implies that the mean density of the crust is essentially constant.

(7) Isostasy appears to be best explained by (a) a floating crust of constant mean density whose dimensions are defined by the configuration of the Mohorovicic discontinuity and (b) a systematic decrease in the mean density of mantle material with increasing crustal thickness.

(8) On the basis of either regional Bouguer gravity anomalies or regional values of surface elevation, it is possible to derive empirically a first-order approximation of crustal thickness. If corrections are applied for surface geologic effects and cognizance is taken of general gravity anomaly relations to be expected for a few geometric mass distributions at depth, a more exact picture of crustal structure can be derived. In general, analytical methods are not justified in the light of present knowledge because of nonsystematic variations in crustal homogeneity.

(9) There appears to be a slight increase in mean crustal density with increasing thickness of the crust because of a thickening of a basal layer whose velocity averages about 6.7 km/sec but reaches values as high as or higher than 7.3 km/sec.

(10) Crustal structure deduced from Bouguer gravity anomalies agrees closely with that deduced from the velocity dispersion of surface earthquake waves. The agreement with refraction measurements is good everywhere except in the plateau areas.

(11) The present ambiguity between seismic refraction measurements and other methods of crustal measurement (surface-wave, velocity-dispersion, and gravity) in the plateaus appears to be related to the masking of layering within the crust. Failure to recognize this layering through second arrivals (although those from the Mohorovicic discontinuity are prominent) suggests that the upper surface of the postulated layer is not always well defined acoustically and may be transitional in nature.

(12) Surface refraction measurements indicate that in some areas, such as Arkansas, the crust is thick and is composed, for the major part, of high-density material. This results in positive gravity anomaly values which normally would be interpreted as evidence of a thinner than normal crust. Similar relationships have been detected from refraction measurements in northern Wisconsin and Michigan, Alaska, Washington, and in the Adirondack region of New York.

(13) Whereas the apparent systematic relationship between the thickness of the basal layer of the crust and the over-all thickness of the crust appears to be real, the cause of the development of this layer can only be surmised.

A phase transformation, such as serpentinization of mantle material, as suggested by *Hess* [1955], or an eclogite-basalt transformation, as suggested by G. Kennedy (unpublished Sigma Xi lecture), would create such a layer, and the accompanying volumetric expansion and possible upward migration of material would explain many of the relations observed in plateaus. Situations such as in Arkansas, however, where there is a thick crust of high-density material, would call for a special set of conditions—possibly crustal foundering following crystallization because of gravitational instability, as suggested by *Van Bemmelen* [1957].

(14) The problem of crustal structure is far from resolved. Only through a continued program of analytical studies of surface waves, careful seismic refraction and reflection measurements (with improved recording techniques in 'type' areas chosen because of the known geologic structural setting) and regional gravity anomaly measurements will a better understanding of the crust become possible.

Final Note—Since completing this paper, the writer's attention has been called to a report by *Wilson* [1959] covering his recent visit to Russian and Chinese scientific establishments. From this report it appears that Russian scientists have come to some of the same general conclusions reached by the writer regarding the relation of the Bouguer gravity anomalies and elevation to crustal thickness.

Wilson cites two equations in use in Russia for determining the approximate crustal thickness (H) from the elevation (Δh) and the Bouguer gravity anomaly (Δg). They are based on empirical relations, as has been done in this paper. From elevation data, $H = 33 \tanh (0.38\Delta h - 0.18) + 38$. From gravity data, $H = 35(1 + \tanh 0.0037\Delta g)$. At sea level, if the gravity anomaly is zero the crustal thickness is 35 km, in contrast to our value of 32 km, but this discrepancy is small compared with that found when data for the high plateaus are considered. For example, assume an average plateau of 2-km elevation with an average Bouguer anomaly approaching −200 mgal. Substitution in the elevation equation yields a crustal thickness of 55.2 km versus 49.5 km, as derived from the elevation curve of Figure 10 of the present paper. Substitution in the gravity equation yields a crustal thickness of 57 km versus 50 km, as derived from the gravity curve of Figure 10. If the gravity relation to crustal thickness derived by *Andreev* [1958] is used ($H = 0.1\Delta g + 30$), $H = 50$ km, which agrees with the value derived by the writer. If the elevation relation to crustal thickness derived by *Heiskanen and Vening Meinesz* [1958] is used ($H = H_0 + 4.45\ \Delta h + \Delta h$), $H = 41$ km, which falls considerably below all the above values. If their alternate density contrast of 0.6 gm/cc is used, giving the equation $H = H_0 + 8.9h + h$, $H = 60$, which value is about as much too large as the former was low. To test the degree of agreement of the Russian equations cited by Wilson, the writer prepared Table 6 which covers the full range of anomaly and elevation conditions.

These comparisons show that the over-all agreement is better than that indicated by the test situation used for the plateaus, although for all continental situations the Russian values tend to run higher.

However, the relationship established by *Andreev* [1958] between the Bouguer anomalies and crustal thickness on the continents does agree everywhere with those of the writer to within about 1 km.

Another point brought out by Wilson's report is the complexity of layering found within the crust and in the upper part of the mantle by Russian investigators. This is well illustrated by the section for the Russian platform cited, which is reproduced below.

Crustal Section Russian Platform Area

0–5 km Sedimentary rocks 4.5 km/sec (average)
5–10 km 1st Granitic layer 6.0 km/sec
10–19 km 2nd Granitic layer 6.75 km/sec
19–28 km 1st Basaltic layer 7.2 km/sec
28–40 km 2nd Basaltic layer 7.75 km/sec
40–50 km 1st Mantle layer 8.15 km/sec
50–90 km 2nd Mantle layer 9.2 km/sec
90 + km 3rd Mantle layer 9.6 km/sec

As Wilson cites first-arrival distances for all the above layers, and as the average thickness of each layer above the Mohorovicic discontinuity is less than 10 km, one wonders about the reality of the structure depicted. The pat-

TABLE 6—*Comparisons of crustal thickness.*

A. Based on Bouguer gravity anomalies

Anomaly	Crustal thickness $H = 35\,(1 + \tanh 0.0037\Delta g)$	Crustal thickness Gravity curve (Moho elev.) Fig. 10			
		Moho elev.	− surface elev.	=	thickness
mgal	km	km	km		km
+300	7	−13	−4	=	9
+200	13	−19	−2.5	=	16.5
+100	22	−25	−1	=	24
0	35	−32	0	=	32
−100	47	−40	+1	=	41
−200	57	−48	+2	=	50
−300	63	−57	+4	=	61

B. Based on elevation

Elevation	Crustal thickness $H = 33 \tanh (0.38\Delta h - 0.18) + 38$	Crustal thickness Elevation curve (Moho elev.) Fig. 10			
		Moho elev.	− surface elev.	=	thickness
km	km	km	km		km
−5	6	−11	−5	=	6
−3	9.5	−18	−3	=	15
−1	21	−26	−1	=	25
0	32	−32	0	=	32
+1	44.5	−39.5	+1	=	40.5
+2	55	−47.5	+2	=	49.5
+3	59	−56.5	+3	=	59.5

tern is very suggestive of an exponential increase in velocity with depth, and resolution of the layers would depend upon extensive correlations of second, third, and fourth arrivals. To the writer's knowledge, no similar structure has been reported elsewhere. In view of the great detail shown, one wonders why the compressional effect noted in the upper part of the crust by the University of Wisconsin measurements and called for by the laboratory studies of Birch is not noted. It would appear that lack of detail in the shot-point area has caused this effect to be averaged in with the velocities for sedimentary rock, and a hybrid value of 4.5 km/sec was obtained. If the indicated layering is real, the geologic explanation for its existence poses a much greater problem than that for a two-layer crust. Further, in the writer's opinion, it must be a situation that is not of general occurrence, since it is hard to see how it could be missed. The only measurement the writer knows of that even suggests a similar complex-layered structure in North America is that reported by *Richards and Walker* [1959] for Alberta. These authors, however, made no attempt to establish more than two layers for the crust, although evidence of three layers appears to be present.

REFERENCES

ANDREEV, B. A., Gravity anomalies and crustal thickness of continental regions, *Doklady Akad. Nauk SSSR, 119,* 255–256, 1958.

ANDREEV, B. A., Relation between structural relief and gravity anomalies for the case of some density layer boundaries, *Doklady Akad. Nauk SSSR, 124,* 311–313, 1959.

BALAVADZE, B. K., AND G. K. TVALTBADZE, Structure of the earth's crust in Georgia from geophysical evidence, *Abstr. of Repts., XI Gen. Assembly, IUGG, Toronto,* 16–18, 1957.

BIRCH, F., Interpretation of the seismic structure of the crust in the light of experimental studies of wave velocities in rocks, *Contributions in*

Geophysics, 1, Pergamon Press, New York, 158–170, 1958.

Birch, F., J. F. Schairer, and H. C. Spicer, Handbook of physical constants, *Geol. Soc. Am. Spec. Pap. 36,* 325, 1942.

Bowie, W., Investigations of gravity and isostasy, *U. S. Coast and Geodetic Survey, Spec. Publ. 40,* 196 pp., 1917.

Byerly, P., Subcontinental structure in the light of seismological evidence, *Recent Advances in Geophys., 3,* Academic Press, 106–148, 1956.

Conrad, V., Laufzeitkurvën des tauernbebens vom 20 November 1923, *Mitt. Erdb. Komm., Wein Akad. Wiss., (N.F.),* no. 59, 1-23, 1925.

Daly, R. A., *Strength and structure of the earth,* Prentice Hall, New York, 434 pp., 1940.

Ewing, John, and W. M. Ewing, Seismic refraction measurements in the Atlantic Ocean basins, in the Mediterranean Sea, on the Mid-Atlantic ridge and in the Norwegian Sea, *Bull. Geol. Soc. Am., 70,* 291–318, 1959.

Ewing, M., and F. Press, Determination of crustal structure from phase velocity of Rayleigh waves, Pt. III, The United States, *Bull. Geol. Soc. Am., 70,* 229–244, 1959.

Ewing, M., J. L. Worzel, D. B. Ericson, and B. C. Heezen, Geophysical and geological investigations in the Gulf of Mexico, I, *Geophysics, 20,* 1–18, 1955.

Gutenberg, B., and C. F. Richter, Seismicity of the earth, II, *Geol. Soc. Am. Spec. Pap. 34, Suppl., Bull. Geol. Soc. Am., 56,* 603–668, 1945.

Hales, A. L., and I. S. Sacks, Evidence for an intermediate layer from crustal studies in the eastern Transvaal, *Geophys. J., 2,* 15–33, 1959.

Heiskanen, W. A., and P. A. Vening Meinesz, *The earth and its gravity field,* McGraw-Hill, New York, 467 pp., 1958.

Hess, H. H., Serpentiners, orogeny and epeirogeny, *Geol. Soc. Am. Spec. Pap. 62,* 391–408, 1955.

Hodgson, J. H., A seismic survey in the Canadian shield I: refraction studies based on rockbursts at Kirkland Lake, Ontario, *Publs. Dominion Observatory Ottawa, 16,* 111–163, 1953.

Jeffreys, H., On near earthquakes, *Monthly Notices Roy. Astron. Soc. Geophys., Suppl., 1,* 385–402, 1926.

Katz, S., Seismic study of crustal structure in Pennsylvania and New York, *Bull. Seis. Soc. Am., 45,* 303-326, 1955.

Leet, L. D., Seismological data on surface layers in New England, *Bull. Seis. Soc. Am., 26,* 129–145, 1936.

Lubimova, H. A., Thermal history of the earth, *Geophys. J., 1,* 115–134, 1958.

Meyer, R. P., J. S. Steinhart and G. P. Woollard, Seismic determination of crustal structure in the central Plateau of Mexico (Abstr.), *Trans. Am. Geophys. Union, 39,* 525, 1958.

Press, F., Determination of crustal structure from phase velocity of Rayleigh waves, Pt. 1—Southern California, *Bull. Geol. Soc. Am., 67,* 1647–1658, 1956.

Richards, T. C., and D. J. Walker, Measurements of the thickness of the earth's crust in the Albertan plains of western Canada, *Geophys., 24,* 262–284, 1959.

Shor, G. J., Jr., Deep reflections from Southern California blasts, *Trans. Am. Geophys. Union, 36,* 133–138, 1958.

Skeels, D. C., Gravity in sedimentary basins, *Trans. Am. Geophys. Union,* 182–201, 1940.

Steinhart, J. S., R. P. Meyer, and G. P. Woollard, Crustal studies and associated gravity anomalies in selected areas (Abstr.), *Geophysics, 23,* 1063, 1958.

Tatel, H. E., L. H. Adams, and M. A. Tuve, Studies of the earth's crust using waves from explosions, *Proc. Am. Phil. Soc., 97,* 658–669, 1953.

Tatel, H. E., and M. A. Tuve, Seismic exploration of a continental crust, *Geol. Soc. Am. Spec. Pap. 62,* 35-50, 1955.

Van Bemmelen, R. W., Magmatic diapirism and tectonic deformation, *Madjalah Ilmu Alam Untuk Indones., 113,* 1–5, 1957.

Veytsman, P. S., I. P. Kosminska, and Y. W Riznichenko, New evidence for the structure of the earth's crust and mountain roots in central Asia from data in seismic deep sounding, *Abstr. of Repts., XI Gen. Assembly, IUGG., Toronto,* 34–36, 1957.

Wilmore, P. L., A. L. Hales, and P. G. Gane, A seismic investigation of structure in the Western Transvaal, *Bull. Seis. Soc. Am., 42,* 53–80, 1952.

Wilson, J. T., Geophysical institutes of the U.S.S.R., *Trans. Am. Geophys. Union, 40,* 3–24, 1959.

Woollard, G. P., Transcontinental gravitational and magnetic profile of North America and the relation to geologic structure, *Bull. Geol. Soc. Am., 54,* 746–790, 1943.

Woollard, G. P., Crustal structure beneath oceanic islands, *Proc. Roy. Soc. London A, 222,* 361–387, 1954.

Worzel, J. L., and G. L. Shurbet, Gravity interpretations from standard oceanic and continental crustal sections, *Geol. Soc. Am. Spec. Pap. 62,* 87–100, 1955.

(Manuscript received May 6, 1959.)

A Crustal Section across the Puerto Rico Trench[1]

MANIK TALWANI, GEORGE H. SUTTON, AND J. LAMAR WORZEL

Lamont Geological Observatory
(Columbia University)
Palisades, New York

Abstract—A crustal section across the Puerto Rico Trench, from 450 km north to 250 km south of San Juan, was deduced from seismic refraction and gravity data. The result, a refinement of previous work, was made possible through more complete seismic refraction coverage and a program for high-speed electronic computation of two-dimensional gravity problems. On the basis of refraction data, the crust was divided into five layers having compressional wave velocities of 1.54, 2.1, 3.8, 5.6, and 7.0 km/sec. Densities taken from a density-velocity curve compiled by Nafe and Drake are 1.03, 2.0, 2.4, 2.7, and 3.0 gm/cc, respectively. Depths to the Mohorovicic discontinuity were computed from the gravity data using sub-crustal density of 3.4 gm/cc, which corresponds to 8.2 km/sec on the density-velocity curve. (A similar calculation was made using a sub-crustal density of 3.3 gm/cc). Depth to M under the trench is about 20 km decreasing sharply on both sides. Northwards, it reaches a minimum of about 10 km under the Outer Ridge and then deepens gradually to about 13 km beneath the southern margin of the Nares Basin. South of the trench M rises under the Puerto Rico Shelf to about 17 km and then deepens sharply to about 30 km beneath Puerto Rico. South of Puerto Rico the depth decreases again to about 14 km under the Venezuelan Basin.

Depths to M were also obtained by using Airy isostatic anomalies and assuming constant crustal density of 2.67 gm/cc over a mantle of density 3.27 gm/cc. The crustal section thus deduced differs significantly from that obtained when the density structure within the crust was considered.

Introduction—A crustal section across the Puerto Rico Trench from the Nares Basin, 450 km north of San Juan, to the Venezuelan Basin, 250 km south of San Juan, was deduced from seismic refraction and gravity data. The resultant section, a refinement of previous work [*Ewing and Worzel,* 1954; *Worzel and Ewing,* 1954; and *Shurbet and Ewing,* 1956], was made possible through more complete seismic refraction coverage [*Officer and others,* 1957; *Officer and others,* in press; *Sutton and others,* in preparation] and a program for high-speed electronic computation of two-dimensional gravity problems [*Talwani and others,* 1959].

Locations of the seismic refraction stations and gravity stations in the vicinity of the section are shown in Figure 1. Interface depths from the refraction stations along the section, shown as points in the upper part of Figure 3, furnish the control for the deduced structure down to the top of the high-velocity basement layer (7.0 km/sec, 3.0 gm/cc.) Compressional wave velocities and layer identifications are listed in Table 1. Densities were determined from an empirical density versus seismic-velocity curve (Fig. 2) compiled from various sources by J. E. Nafe and C. L. Drake (unpublished). The position of the top of the mantle, the Mohorovicic discontinuity[2], was obtained from the gravity data with the crustal layering taken into account. Depths to M, determined seismically, serve as a check on the method.

Airy isostatic anomalies based on the assumption of a two-dimensional structure were computed, and they agree well with the three-dimensional Airy isostatic anomalies, computed by Heiskanen (Table 2).

Seismic and gravity data—The seismic stations used for determining the crustal layering of the section and as a check on the gravity determination of depth to M are numbered on Figure 1. Station *H* is from *Hersey and others*

[1] Lamont Geological Observatory Contribution No. 374.

[2] Hereafter, for brevity, the Mohorovicic discontinuity is referred to as M.

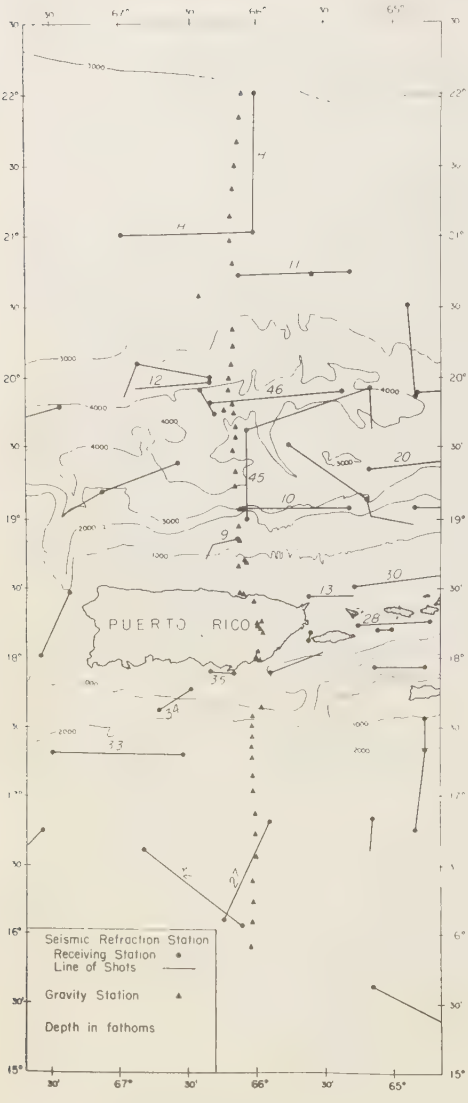

FIG. 1—Location of seismic refraction and gravity stations.

[1952]; stations 11, 12, 45, 10, 9, and 13 are from *Sutton and others* (in preparation); stations 46, 35, 34, 33, and 32 are from *Officer and others* [1957]; and stations 27, 20, 30, and 28 are from *Officer and others* (in press). Stations 20, 30, and 28, which are some distance from the section line, are shown on Figures 1 and 3, since the seismic interface shown for them (Fig 3) was not observed at stations closer to th profile. The densities used in the gravity calcu lations and the representative velocities for th layers are given in Figure 3. A density of 1.0 gm/cc was used for the water layer. The veloci ties used were based both on the seismic observa tions discussed here (Table 1) and those at othe nearby stations. A velocity of 2.1 km/sec wa used in determining the density of the uncon solidated sediment layer (2.1 km/sec, 2.0 gm/cc rather than the 1.8 km/sec usually used fo the calculation of seismic layer thickness wher the velocity was not directly observed. The for mer value is believed to be a better averag [*Nafe and Drake*, 1957] density because of th effect of increasing velocity with depth. This dif ference would not appreciably affect the calcu lations of thickness.

There is little seismic control on the low velocity basement layer (5.5 km/sec, 2.7 gm/cc under the Outer Ridge. It was not directly ob served on either stations *H* or 11. Station 1 showed a poorly determined 4.1-km/sec laye under the unconsolidated sediments. Thi velocity is closer to that which is representativ of the consolidated sediments(volcanics?) (3. km/sec, 2.4 gm/cc) than to the low-velocit basement. The adopted interpretation is base on information on sub-bottom reflections nea station *H* [*Hersey and Ewing*, 1949] and in formation from stations east of the section lin [*Officer and others*, in press]. Essentially, it rep resents the greatest thickness of material abov the high-velocity basement (7.0 km/sec, 3. gm/cc) that is consistent with the seismic ar rivals. Other possible interpretations would ten to reduce the depth to M determined both fro the seismic and the gravity observations. Th seismic control on the interface between the low and high-velocity basement under Puerto Ric is limited to stations quite distant from th section line. They show rather steep east-wes plunges of this interface. The interface betwee the low- and high-velocity basements is appar ently missing at station 32, although it is pres ent at the adjacent station 27. Since an inter mediate velocity is observed for the single laye the effect on the gravitational attraction woul be small.

The gravity data used in this paper are liste

TABLE 1—*Compressional wave velocities (km/sec)*

Refraction station	Unconsolidated sediments	Consolidated sediments (volcanics?)	Low-velocity basement	High-velocity basement	Mantle
H	1.7*		4.3*	6.6	7.9
11	1.8*		5.4*	7.2	8.3
12	1.8*		4.1	7.0	8.7
46		3.4		6.3	7.9
45	1.8*	4.1	5.2	6.7	
10		3.8*	5.3	7.3	
9	1.8*	3.8*	5.3	7.3*	
13		3.8	5.6	6.5*	
35	2.0		5.2		
34	1.9*	3.8	4.8		
33		3.2	5.1	6.9	7.8
27	1.8*	3.3	6.5	7.1	7.9
32	1.9*	3.8	← 6.7 →		8.0
20				6.8*	8.4
30			5.8	7.0	
28			5.7	6.6	

*Velocity not measured; assumed for thickness calculations.

n Table 2. The data at sea were obtained on U.S.S. *S-21* by Vening Meinesz [*Heiskanen, .939*] and on the U.S.S. *Diablo* [*Shurbet and Worzel,* 1956]. Isostatic reductions for the *Diablo* stations were made by Heiskanen at the Isostatic Institute, Helsinki. Simple Bouguer anomalies on Puerto Rico were obtained for selected stations of *Shurbet and Ewing* [1956] along the profile line. In order to reduce the terrain effect of the Puerto Rico topography to a negligible amount, only stations in areas of low relief were used. Simple Bouguer anomalies for these land stations are comparable to free-air anomalies at sea in the sense that both of these anomalies can be attributed to anomalous masses below sea level. Hereafter, in this paper, the term free-air anomalies will tacitly include simple Bouguer anomalies on Puerto Rico. This is to avoid confusion with Bouguer anomalies at sea in which sea water is replaced by crustal rocks and to which we shall refer later on.

Computational procedure—Computations of the vertical component of gravitational attraction and the location of M were made following the method described by *Talwani and others* [1959]. The computations assume two-dimensionality; that is, there are no variations of structure transverse to the section. Because of this assumed symmetry, the volume integral for the gravitational attraction of a body of uniform density can be reduced to a line integral. A program has been written for the IBM 650, which, given the densities of two-dimensional layers and the coordinates of polygons of arbitrary complexity representing the boundaries of these layers, computes the appropriate line integrals and sums them for each point of observation. M is determined by adjustment to fit the residual anomalies obtained by subtracting the effects of the 'known' crustal layers from the observed free-air anomalies.

In the present problem the four top layers (water, unconsolidated sediment, consolidated sediment, and low-velocity basement) are the 'known' layers. It is also necessary to compute the attraction of the high-velocity basement, assuming that its base lies at an arbitrary but constant depth. The combined gravitational attraction of all these layers was obtained at close intervals along the length of the section and subtracted from the free-air anomalies to obtain residual anomalies. These are shown in Figure 4 (the zero of the milligal scale is arbitrary). The residual anomalies can be thought of as two-dimensional Bouguer anomalies which in addition to variations of water depth also include density variations within the crust as deduced from seismic information. Under the as-

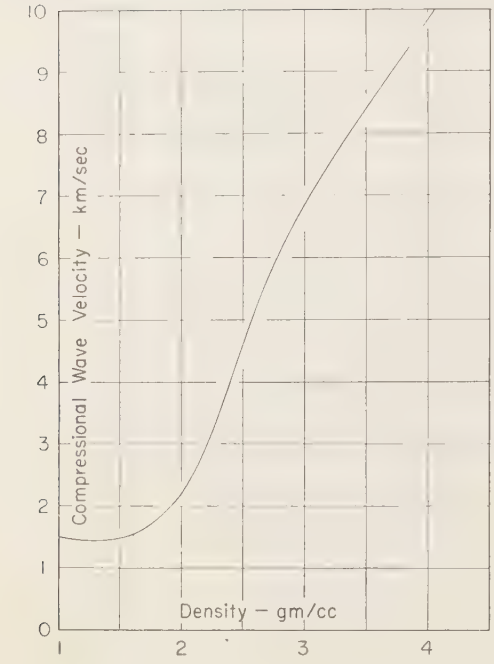

FIG. 2—Experimental relationship between compressional wave velocity and density (*Nafe* and *Drake*, unpublished) which was used for gravity calculations.

sumption that the layers are homogeneous with no lateral variations of density and that there are no undetected interfaces within the crust, the residual anomalies represent directly the relative elevations of M at the base of the crust, since the effect of all the known layers has been removed. With the $(\sin x)/x$ method [*Tomoda and Aki*, 1955; *Tsuboi*, 1956] which was also programed on the IBM. 650 by *Talwani and others* [1959], an approximate solution for the location of M was obtained. For this computation it is necessary to fix the depth to the mantle at one point. A depth of 11 km was chosen between seismic stations *H* and 11 under the Outer Ridge. The location of M as determined by the $(\sin x)/x$ method was used as a first approximation and then adjusted by trial and error until its computed gravitational effect fitted the residual anomalies as well as desired. This procedure was followed using both 3.4 gm/cc, predicted by the velocity-density relationship, and the more commonly used 3.3 gm/cc as densities for the upper mantle material. The computed mantle surfaces and the residual anomalies are compared in Figure 4.

The fit of the gravitational effect of M to the residual anomalies is, of course, exactly equivalent to the fit of the total gravitational attraction of the entire section, from sea level to a fixed depth, to the free-air anomalies after subtracting a constant. This constant is proportional to the average density to the fixed depth in an area where the free-air anomaly is zero. Our choice of 11 km as the depth to M between seismic stations *H* and 11 fixes the value of this constant for our problem. The constant obtained indicates an average density of 2.87 gm/cc for a crust 32 km thick. It follows then, that if we subtract 2.87 gm/cc from the densities of all the layers in the section to a fixed depth of 32 km and compute the attractions of these layers using these reduced densities, the sum of their attractions will give the free-air anomalies. This is shown in Figure 3. The solid line represents the sum of the attractions of the different layers and fits the observed free-air anomalies well.

In order to compare the procedure discussed above with conclusions based upon isostatic anomalies and to check the validity of the two-dimensional analysis the following computations were made, using densities of 1.03, 2.67, and 3.27 gm/cc for water, crustal rock, and mantle material, respectively. (The results are summarized in Figure 5.)

1. Assuming a two-dimensional configuration the position of the theoretical Airy isostatic M (dashed line, Figure 5) is computed on the principle of constant total mass using a depth of compensation $T = 32$ km (the thickness of a sea-level crustal section). This thickness is used rather than 30 km, which is often used for isostatic calculations, in order to keep the theoretical interface below the ocean bottom in the Puerto Rico Trench. Using a T of 20 km, also commonly used in isostatic computations, would require the theoretical M to be above the ocean bottom at normal ocean depths when in isostatic balance.

2. The isostatic anomalies are then computed two-dimensionally by adding to the free-air anomalies the computed effect of the attraction of the water layer (using a differential density of $2.67 - 1.03 = 1.64$ gm/cc) and subtracting the effect of the attraction of the compensation

TABLE 2—*Summary of gravity data*

Station	Latitude deg	Latitude min	Longitude deg	Longitude min	Depth meters	Anomalies mgal: Free-air†	Anomalies mgal: Isostatic‡ 3-dim. (T = 30)	Anomalies mgal: Isostatic 2-dim. (T = 32)	Distance N of 18°N km	Source
Diablo 3	22	01.0	66	07.0	5641	−24	−16	−22	447	Shurbet & Worzel 1956
Diablo 4	21	51.0	66	08.0	5650	−18	−9	−16	428	" "
Diablo 5	21	41.0	66	09.0	5498	−13	−8	−11	410	" "
Diablo 6	21	30.0	66	10.0	5640*	3	10	4	389	" "
Diablo 7	21	20.0	66	11.0	5549	0	7	1	371	" "
Diablo 8	21	09.0	66	12.0	5466*	5	11	6	350	" "
Diablo 9	20	59.0	66	12.0	5461	13	21	13	332	" "
Diablo 10	20	49.0	66	11.0	5379*	28	30	28	313	" "
S-21 35 (Vening Meinesz)	20	35.0	66	25.5	5340	21		25	287	Heiskanen 1939
Diablo 11	20	21.0	66	11.0	5766*	8	11	13	261	Shurbet & Worzel 1956
Diablo 12	20	14.0	66	11.0	6081*	−31	−25	−24	248	" "
Diablo 13	20	06.0	66	12.0	6278*	−83	−81	−75	234	" "
Diablo 14	20	00.0	66	13.0	7260*	−144	−138	−127	222	" "
Diablo 15	19	55.0	66	13.0	8367*	−201	−166	−166	213	" "
Diablo 16	19	49.0	66	11.0	8061*	−252	−220	−221	202	" "
S-21 36 (Vening Meinesz)	19	46.5	66	14.0	7699	−264		−236	197	Heiskanen 1939
Diablo 17	19	45.0	66	11.0	7659*	−283	−257	−255	195	Shurbet & Worzel 1956
Diablo 18	19	39.0	66	10.0	7659*	−306	−278	−278	184	" "
Diablo 19	19	35.0	66	10.0	7460*	−323	−297	−293	176	" "
Diablo 20	19	29.0	66	11.0	7600	−333	−303	−296	165	" "
Diablo 21	19	20.0	66	10.0	7860*	−346	−307	−291	148	" "
Diablo 22	19	14.0	66	10.0	7343	−320	−278	−258	137	" "
Diablo 23	19	04.0	66	08.0	6003	−213	−177	−163	119	" "
Diablo 24	18	57.0	66	08.0	3302	−84	−105	−95	106	" "
Diablo 25	18	51.0	66	08.0	2629	−36	−71	−51	95	" "
Diablo 26	18	42.0	66	06.0	1735	31	−16	4	78	" "
Diablo 52	18	41.4	66	05.3	1343	42	−22	15	77	" "
Diablo 27	18	40.0	66	08.0	1548	37	−10	3	70	" "
S-21 37 (Vening Meinesz)	18	27.8	66	06.8	9	129		42	52	Heiskanen 1939
Diablo 51	18	27.7	66	05.5	10	119	32	31	51	Shurbet & Worzel 1956
Puerto Rico 29	18	23.95	66	01.51	−35.2	142		58	47	Shurbet & Ewing 1956
Puerto Rico 53	18	15.18	65	58.83	−63.8	153		84	29	" "
Puerto Rico 54	18	14.59	66	00.58	−56.5	143		75	28	" "
Puerto Rico 136	18	13.29	66	00.67	−61.1	137		69	26	" "
Puerto Rico 137	18	12.33	65	59.40	−72.6	144		77	24	" "
Puerto Rico 139	18	10.39	65	58.64	−94.8	134		67	20	" "
Puerto Rico 145	18	02.21	66	00.48	−99.6	141		68	4	" "
Puerto Rico 81	18	00.24	66	01.45	−18.0	138		61	0	" "
Puerto Rico 146	17	58.88	65	59.92	−8.9	134		55	−2	" "
Diablo 50	17	38.8	65	57.3	1931	−12	−44	−30	−39	Shurbet & Worzel 1956
Diablo 49	17	34.8	66	01.6	2503	−41	−51	−43	−47	" "
Diablo 48	17	30.3	66	01.7	3314	−67	−54	−48	−55	" "
Diablo 47	17	26.0	66	01.7	4073	−82	−50	−48	−63	" "
Diablo 46	17	21.1	66	01.9	4778	−91	−47	−41	−72	" "
Diablo 45	17	16.6	66	01.8	4900	−85	−42	−34	−80	" "
Diablo 44	17	09.0	66	01.8	4764	−66	−34	−30	−95	" "
Diablo 43	17	02.2	66	01.7	4595	−47	−27	−25	−107	" "
Diablo 42	16	52.2	66	00.3	4473	−29	−17	−15	−126	" "
Diablo 41	16	43.7	66	00.6	4368	−20	−10	−12	−141	" "
Diablo 40	16	33.6	65	59.9	4221	−7	0	−1	−160	" "
Diablo 39	16	23.1	66	01.9	4418	−4	6	1	−180	" "
Diablo 38	16	13.9	66	01.7	4437	−7	1	−1	−197	" "
Diablo 37	16	05.0	66	01.8	4384	−13	−10		−213	" "
Diablo 36	15	54.2	66	02.6	4535	−17	−7		−233	" "

*Depths corrected after original publication.
†Simple Bouguer anomalies for Puerto Rico stations.
‡Reduced by Heiskanen.

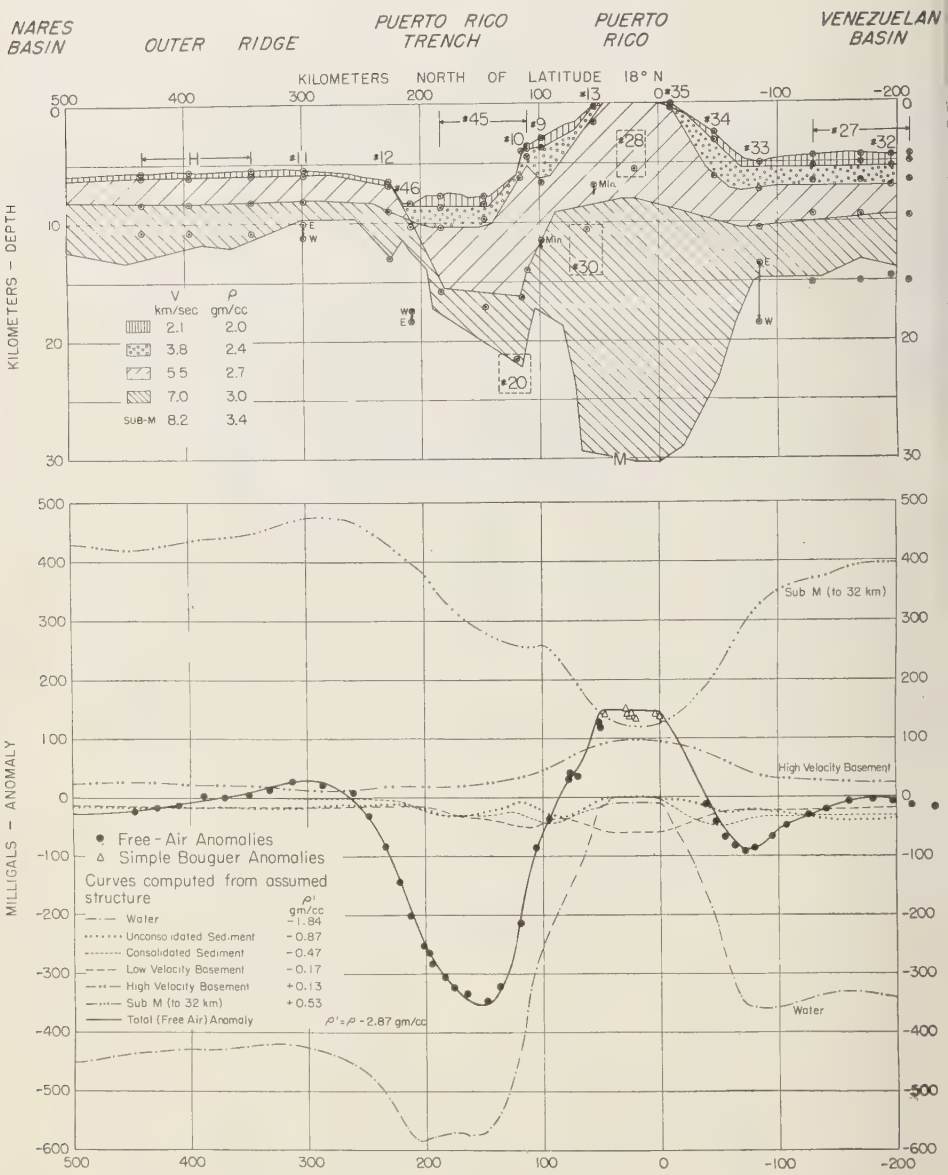

FIG. 3—*Upper*—Computed crustal section. Crustal layering is from seismic data; M is from gravity data; points are seismic interfaces. *Lower*—Computed attraction of layers to 32-km depth using reduced densities ρ'. Solid curve is total attraction (computed free-air anomaly) which is compared with observed anomalies.

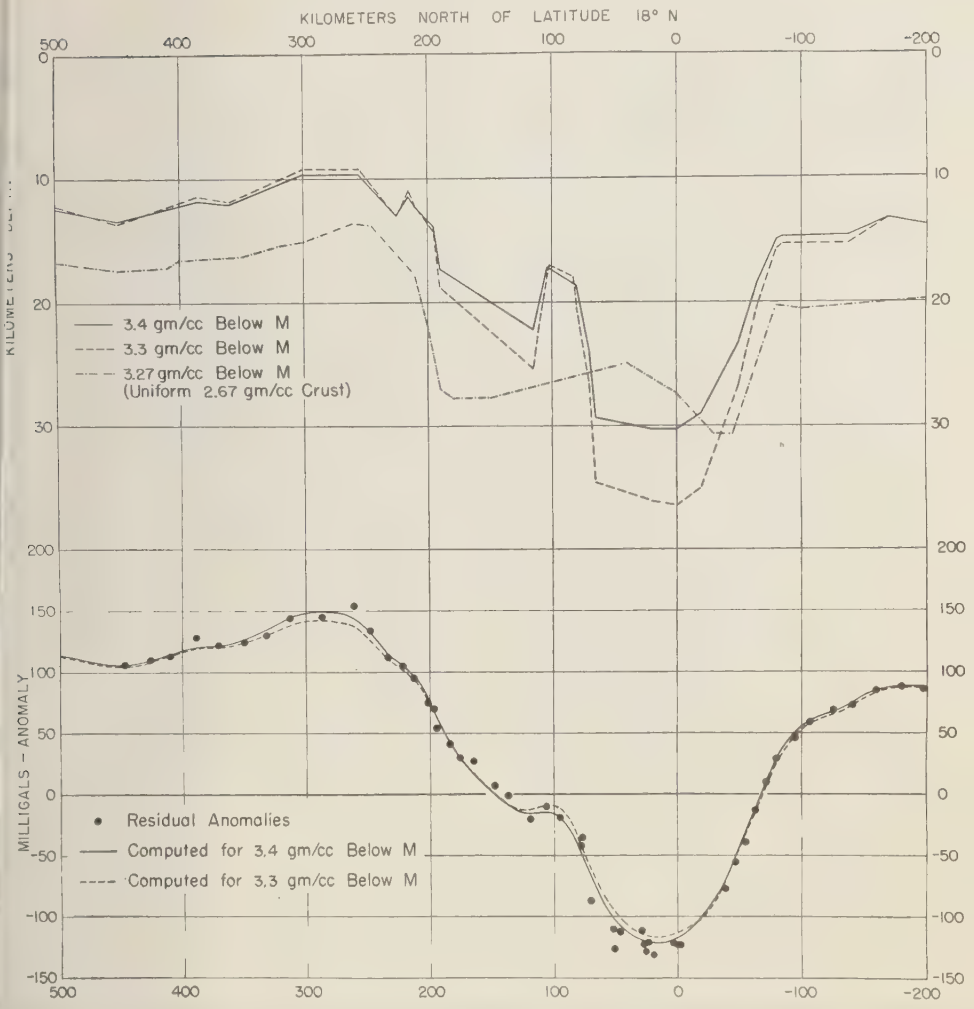

FIG. 4—*Upper*—Depths to M for three cases computed. *Lower*—Fit between attraction and residual anomalies for two cases involving layered crust.

of the water layer, that is, of the material between the theoretical isostatic M and a constant depth of 32 km (using a differential density of $3.27 - 2.67 = 0.6$ gm/cc). The values obtained are listed in Table 2 and shown in Figure 5. Three-dimensional Airy isostatic anomalies, computed by Heiskanen for $T = 30$ km and also shown in the figure, agree well with the results of the two-dimensional analysis.

3. The computed M from the isostatic anomalies is obtained by trial and error in such a way that the gravitational attraction of the material between the theoretical isostatic M and the computed M fits the isostatic anomalies. This fit is not very good in the immediate vicinity of Puerto Rico. A better fit would have necessitated a large up-and-down fluctuation in the depth of the computed M.

The depths to M computed under different assumptions are compared in Figure 4. It can be seen that the depths obtained from the assumption of a uniform crust of density 2.67 gm/cc

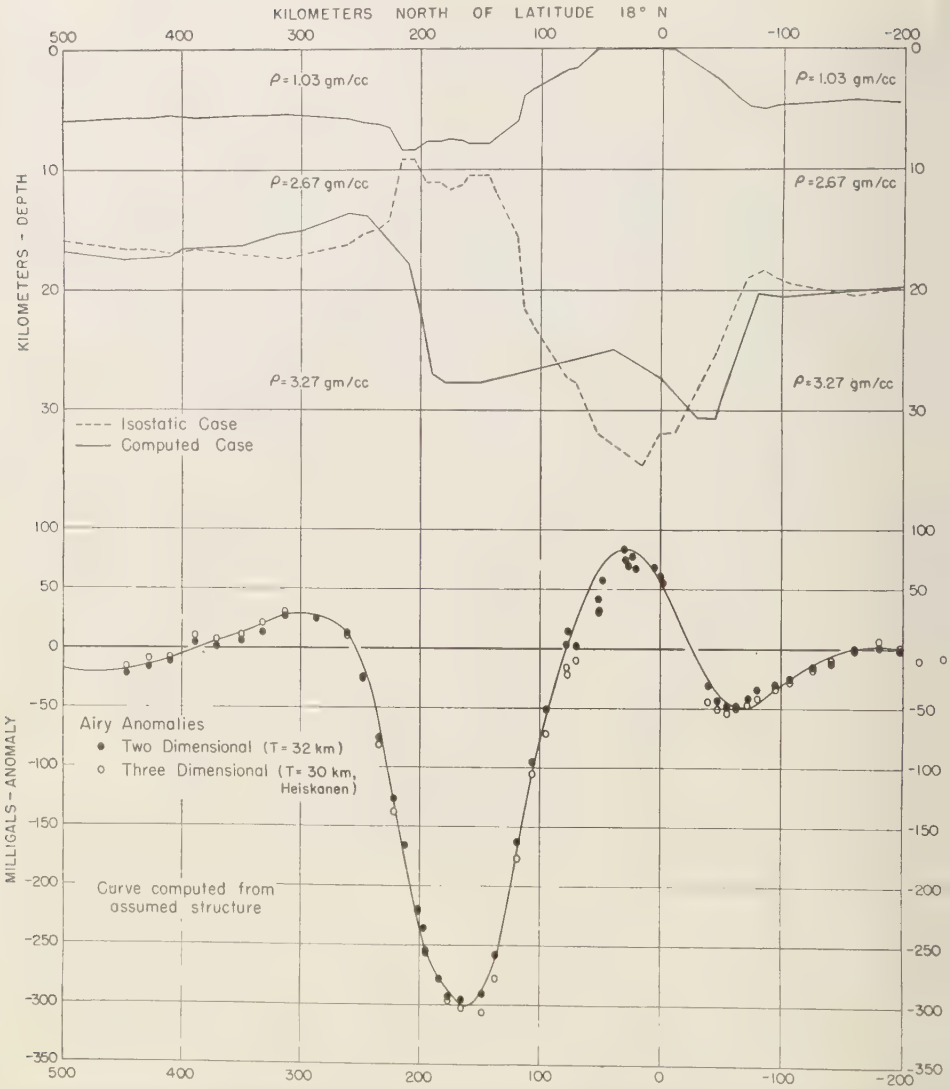

FIG. 5—Summary of results assuming uniform crustal density 2.67 gm/cc and mantle density 3.27 gm/cc.

over a mantle of density 3.27 gm/cc diverge considerably from those obtained with the assumption of a density structure within the crust which is correlated with seismic observations.

Results—In contrast with free-air anomalies, which show sharp minima under the trenches north and south of Puerto Rico with a large positive over Puerto Rico, the residual anomalies vary more or less smoothly between high values in the open ocean north and south of Puerto Rico and a low value under the island, with no large deviation in the trench areas. This implies that the large free-air minimum over the Puerto Rico Trench and the smaller minimum over the trench south of Puerto Rico are caused mainly by the thick, partially compensated water and

sedimentary column. However, when examined in detail the residual anomaly curve has some irregularities, notably in the region between 220 and 70 km north of 18°N. The deviation from a smooth curve can be viewed as either a minimum between 220 and 100 km or a maximum between 130 and 70 km of approximately 50 mgal amplitude. Before interpreting this deviation as being entirely caused by variations in M elevation we must consider the possibility that it arises from poor choices of thicknesses and densities of the upper crustal layers. We can discount erors in gravity observations because many observations from different cruises have shown that 50 mgal is much larger than the probable errors of gravity measurements at sea. To have the deviation caused by errors in elevation of the 2.4 to 2.7 gm/cc interface would require increasing its depth under the Puerto Rico Trench, or decreasing its depth just south of the trench by about 5 km, or some combination of the two. This appears unlikely since the seismic control is fairly reliable for this interface. Approximately the same variations would be needed on the 2.7 to 3.0 gm/cc interface and of course both interfaces could be in error. Some reasonable modifications in the upper crustal layers could be made without violating the seismic data. However, it is extremely unlikely that the general configuration of M deduced from the residual anomalies would be changed significantly.

At the bottom of Figure 3, the relative attractions are given for the individual layers which are shown in the section at the top. It is obvious from these curves that the major contributions to the free-air anomaly come from the water layer and the variations in the depth to M. The details of the crustal structure modify the anomaly curve to a smaller extent. For example, the effect of replacing all the consolidated sediments by low-velocity basement material near 100 km north of 18°N, where the sediment has a maximum in thickness, would reduce the residual anomaly by about 27 mgal. This would lower M by about 3 km.

Provided that the seismic control for the upper layers is adequate and the depth to M at one point and the densities used are reliable, the section shown in Figure 3 represents a unique solution for the crustal thickness. As mentioned earlier the absolute depth to M, which is not uniquely determined from gravity, is fixed at one point on the basis of seismic evidence. The depth to M has been observed at several different locations along the section, and comparison between the depths obtained by seismic and gravity measurements provides a check on the reliability of the depth determinations.

Starting at the north, the depth of M is about 12.5 km under the southern portion of the Nares Basin. This is about 3 km deeper than that obtained from seismic observations by *Ewing and others* [1954] farther north in the basin. The difference could be partially caused by the low-velocity basement layer which was not observed by them. The depth to M under the northern portion of the Outer Ridge is greater than Hersey's value. The depth decreases southward to a minimum of about 9.7 km at the southern edge of the Outer Ridge. The depth found seismically at station 11 in this area varies between 10 and 11 km (from east to west). The decrease in depth southward across the Outer Ridge, indicated by the gravity calculations, may be partially explained by lateral variations in density within the layers. Density variations are indicated by the variations of seismic velocities and have not been considered. The observed seismic velocities in the high-velocity basement and upper mantle increase southward in this area (Table 1). An equivalent change in the density of these layers would make the computed depth to M somewhat less than the actual value. Also, as noted previously, the seismic evidence for the low-velocity basement layer under the Outer Ridge is not very definite [*Sutton and others*, in preparation]. Even if we allow for these possible variations, the depth to M under the southern margin of the Outer Ridge is among the smallest ever observed.

M drops sharply under the north wall of the Puerto Rico Trench. The correlation between the depths obtained by seismic and gravity methods is surprisingly good for such a complicated area. The depth from seismic measurement at station 12 agrees exactly with the depth obtained gravimetrically; that of station 46 is considerably deeper, but the difference could be caused by structural variations transverse to the section. M reaches a maximum depth of 22.2

km under the south wall of the trench. There is no seismic value for the depth at this location. However, the mantle depth from profile 20, which is an equivalent location about 100 km to the east, is 21.5 km and is in agreement with the depth from gravity. Between the trench and Puerto Rico there is a rise in M to about 17 km. M then drops sharply to about 29.5 km near the north shore of Puerto Rico. A maximum depth of 30.3 km is reached near the south shore of the island. South of Puerto Rico M rises to about 15 km. The negative anomaly associated with the trench south of Puerto Rico is not directly reflected in the M topography. This is in agreement with the M depth from station 33. Farther south, under the Venezuelan Basin, M rises to about 14 km, in agreement with the seismic results from stations 27 and 32, although station 32 shows only one layer beneath the consolidated sediment (volcanics?) layer. As mentioned previously, the velocity found at station 32—6.7 km/sec—is approximately the mean of the velocities observed in the two layers and would have a similar gravitational effect. These sharp variations in crustal structure in the Venezuelan Basin appear to be real; however, the effect on the depth of M should be minor.

There is no seismic check on the depth of the mantle under Puerto Rico. Also the rises in M near the north and south sides of the Puerto Rico Trench have no seismic confirmation. The existence of the northern feature, about 210 km north of 18°N, is subject to some doubt. The residual anomaly curve shows that the irregularity to be fitted is quite small. However, as discussed above, it is probable that the prominent rise south of the trench exists.

If a mantle density of 3.3 gm/cc is assumed, the depths to M have the same general configuration but greater relief than those obtained using 3.4 gm/cc (Fig. 4), as would be expected, and reach a maximum depth of about 37 km under Puerto Rico. Except for station 20, the stations are located so that seismic checks on the depth to M do not indicate which choice of density is preferable. Station 20, which is some distance from the section line, agrees better with the 3.4 gm/cc results. The principal reason for preferring the 3.4 gm/cc solution is that this density is predicted by experimental velocity-density data.

The good agreement between two-dimensional and three-dimensional Airy isostatic anomalies is a check on the assumption of two-dimensional structure. The slightly different choices of T do not appreciably affect this comparison.

As mentioned earlier, there is considerable difference between the position of M as located from a consideration of density structure derived from seismic results and as located on the assumption of a homogeneous crust of density 2.67 gm/cc overlying a mantle of density 3.27 gm/cc. This difference can be thought of as arising partly from the different choices of density contrast between crust and mantle and partly from the density variations within the crust. A choice of 2.87 gm/cc for the average crust overlying a mantle of 3.40 gm/cc would improve the agreement considerably, and, in fact, in the absence of seismic information this choice of densities would give a good first approximation to the actual structure. It should be noted that in the homogeneous case as well as in the more complicated case the shallowest depth to M is under the southern portion of the Outer Ridge.

For a feature like the Puerto Rico Trench, which is out of isostatic balance, the derivation of isostatic anomalies does not particularly help in determining the depth to M. The straightforward use of Bouguer anomalies is preferable.

The crustal section in Figure 3 differs in detail from those given by *Shurbet and Ewing* [1956] and in the earlier papers by Ewing and Worzel because of the additional seismic control and closer fit between computed and observed anomalies. In general the results they presented are substantiated by this work. Among the principal differences from the previous results are the steep slopes found for the interfaces near the margins of the trench. Their values range between approximately 10° and 30°. In many cases, these slopes could be increased considerably without violating the seismic or gravity data, and the resemblance to a down-faulted structure would be more striking.

Acknowledgments—The advice and encouragement of M. Ewing, Director of Lamont Geological Observatory, during the course of this research is gratefully acknowledged. Many discussions with our co-workers at Lamont, expecially B. C. Heezen and J. Ewing, were profitable. E. S. Skinner and G. E. Quest assisted with the computations and drafting. The computing facilities of the

'atson Scientific Computing Laboratory and evis Cyclotron Laboratory, both of Columbia niversity, were used in this work. W. Heiskanen ade isostatic reductions for the *Diablo* stations the Isostatic Institute, Helsinki. This research as carried out under contracts from the Office Naval Research and the Bureau of Ships of the .. S. Navy.

References

WING, M., G. H. SUTTON, AND C. B. OFFICER, JR., Seismic refraction measurements in the Atlantic Ocean, Part VI: Typical deep stations, North American Basin, *Bull. Seis. Soc. Am. 44,* 21–38, 1954.

WING, M., AND J. L. WORZEL, Gravity anomalies and structure of the West Indies, Part I, *Bull. Geol. Soc. Am., 65,* 165–174, 1954.

EISKANEN, W., Catalogue of the isostatically reduced gravity stations, *Isos. Inst. Inter. Assoc. Geod. Pub.,* no. 5, p. 139, 1939.

ERSEY, J. B., AND M. EWING, Seismic reflections from beneath the ocean floor, *Trans. Am. Geophys. Union, 30,* 5–14, 1949.

ERSEY, J. B., B. C. OFFICER, JR., H. R. JOHNSON, AND S. BERGSTROM, Seismic refraction observations north of the Brownson Deep, *Bull. Seis. Soc. Am., 42,* 291–306, 1952.

AFE, J. E., AND C. L. DRAKE, Variation with depth in shallow and deep water marine sediments of porosity, density and the velocities of compressional and shear waves, *Geophysics, 22,* 523–552, 1957.

AFE, J. E., AND C. L. DRAKE, Physical properties of crustal materials as related to compressional wave velocities; paper presented at Annual Meeting of *Soc. Expl. Geophys.,* 1957, Dallas, Texas (unpublished).

OFFICER, C. B., JR., J. I. EWING, R. S. EDWARDS, AND H. R. JOHNSON, Geophysical investigations in the eastern Caribbean: Venezuelan Basin, Antilles Island Arc, and Puerto Rico Trench, *Bull. Geol. Soc. Am., 68,* 359–378, 1957.

OFFICER, C. B., JR., J. I. EWING, J. F. HENNION, D. G. HARKRIDER, AND D. E. MILLER, Geophysical investigations in the eastern Caribbean: Summary of 1955 and 1956 cruises, *Physics and Chemistry of the Earth, 3,* Pergamon Press, London (in press).

SHURBET, G. L., AND M. EWING, Gravity reconnaissance survey of Puerto Rico, *Bull. Geol. Soc. Am., 67,* 511–534, 1956.

SHURBET, G. L., AND J. L. WORZEL, Gravity observations at sea in U.S.S. *Diablo, Bull. Geodesique, 42,* 51–60, 1956.

SUTTON, G. H., M. EWING, AND W. J. LUDWIG, Seismic refraction measurements in the Puerto Rico Trench area (in preparation).

TALWANI, M., J. L. WORZEL, AND M. LANDISMAN, Rapid gravity computations for two-dimensional bodies with application to the Mendocino submarine fracture zone, *J. Geophys. Research, 64,* 49–59, 1959.

TOMODA, YOSHIBUMI, AND KEIITI AKI, Use of the function sin x/x in gravity problems, *Proc. Japan Acad., 31,* 443–448, 1955.

TSUBOI, CHUJI, Crustal structure in Northern and Middle California from gravity-pendulum data, *Bull. Geol. Soc. Am., 67,* 1641–1646, 1956.

WORZEL, J. L., AND M. EWING, Gravity anomalies and structure of the West Indies, Part II, *Bull. Geol. Soc. Am., 65,* 195–200, 1954.

(Manuscript received June 30, 1959; presented at the Fortieth Annual Meeting, Washington, D. C., May 4, 1959.)

The Measurement of Thermal Conductivity of Deep-Sea Sediments by a Needle-Probe Method[1]

R. VON HERZEN

Scripps Institution of Oceanography
La Jolla, California

AND

A. E. MAXWELL

Office of Naval Research
Washington, D. C.

Abstract—The transient heating of a needle probe is used to measure the thermal conductivity of deep-sea sediments in 10 minutes or less. An accuracy of 3 to 4 per cent compares favorably with steady-state methods, and measurements by both methods on the same sediments show good agreement. Thermal diffusivity of deep-sea sediments is shown to be proportional to thermal conductivity, in agreement with theoretical expectations.

INTRODUCTION

Until recently, apparatus for the measurement of thermal conductivity of solid materials of lower conductivity than metals, such as soils and clays, has generally been of one type; namely, the steady-state hot-plate method. This consists of a small cylindrical prism of the sample, the ends of which are bound by metal slabs of higher conductivity. Heat is supplied at a known rate to one of the slabs and taken away at the other, so that the specimen is a part of the path of uniform flow of heat. Under these conditions, the temperature difference on both sides of the specimen is measured, and the conductivity can readily be calculated. Several hours may be required for the determination of the conductivity of a specimen with this method because of the long time necessary for the attainment of equilibrium and the need for several samples to be measured. Recent improvements [*Beck*, 1957] have reduced this time somewhat.

Measurements of heat flow through the floor of the ocean require an accurate determination of the thermal conductivity of the sediment where the thermal-gradient measurement is made. The sediment is brought to the ocean surface in a coring tube, where there is a need for rapid determination of the conductivity at many points without serious disturbance of the core sample. These requirements have led to the development of a transient technique for measuring thermal conductivity.

DESCRIPTION AND THEORY

Thermal conductivity—Basically, the transient technique closely approximates an infinitely long, continuous line source of heat in an infinite medium, the temperature near the line source being measured as a function of time. The method was first used to measure the thermal conductivity of liquids [*Van der Held and others*, 1953], although convection posed difficulties not encountered with soil and deep-sea-sediment measurements. Similar techniques have been developed for measuring the thermal conductivity of insulating materials by *D'Eustachio and Schreiner* [1952], who used thermocouples as temperature-sensing elements. Likewise, equipment for this measurement has been successfully applied to the determination of thermal conductivity of soils [for example, *Mason and Kurtz*, 1952; *Beuttner*, 1955; *Lachenbruch*, 1957].

The measurement of thermal conductivity of a deep-sea sediment contained in a tube 2 inches in diameter requires similar, but some-

[1] Contribution from Scripps Institution of Oceanography, New Series.

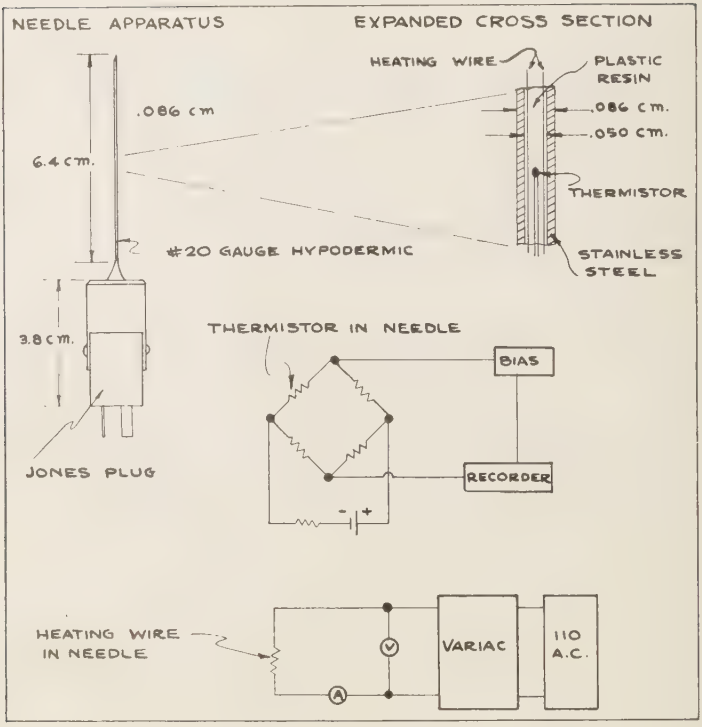

FIG. 1—Needle-probe apparatus for measuring conductivity.

what smaller apparatus than is used for soils. Figure 1 shows the first instrument developed for this use by *Maxwell* [1958] and described by *Bullard and others* [1956]. Briefly, the probe of Figure 1 is a hypodermic needle enclosing a single loop of heating wire and a temperature sensing thermistor placed at the middle of the needle.

The theory for the apparatus has been worked out in considerable detail by *Jaeger* [1956, 1958], among others. Their analyses have shown that the rise of temperature of the probe is given to a good approximation by

$$T = \frac{q}{4K\pi} (\ln 4\alpha t/Ba^2$$

where

t = time
q = heat input per unit length per unit time
K = thermal conductivity of sediment sample
α = thermal diffusivity of sediment sample
a = probe radius
B = constant = 1.7811

This relationship is valid when t is large com pared with a^2/α. A plot of T versus ln t w then give a straight line, the slope of whic determines K, for known values of q. Dependin on the sediment, a^2/α for this needle prob ranges between ½ and 1 second. It is experi mentally observed that the linear asympto on a plot of T versus ln t is closely approache after 10 seconds. This is consistent with the th oretical analysis [*Jaeger*, 1958] in which, for cylinder with the dimensions of the probe use an approach is given to this asymptote with 3½ per cent at 10 seconds, and within 1½ p cent at 20 seconds. The linearity is valid up about 10 minutes; for longer times the samp boundaries and finite length of the needle prob begin to affect seriously the approximation

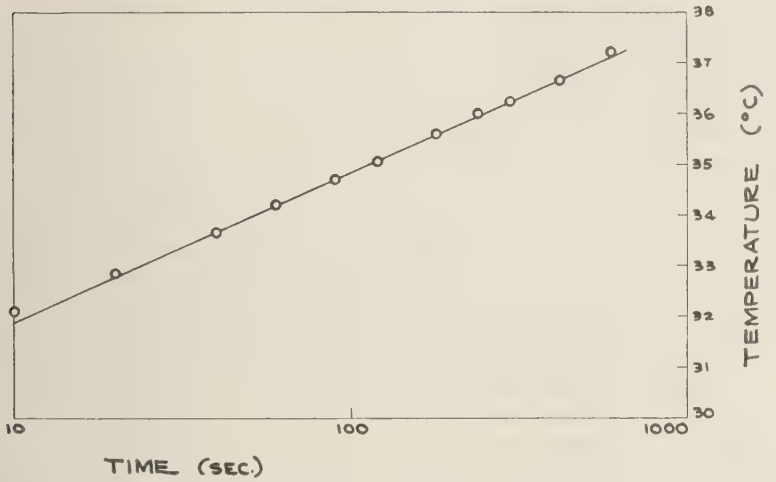

FIG. 2—Temperature versus time for a needle-probe measurement of *DWBG* 137.

a infinitely extended line source in an infinite edium.

. A typical record for one of the needle-probe easurements is shown in Figure 2, where, with . 2-watt power input, the 10-minute time inter- al is found to be adequate for a determination f K. During this time, K is integrated over sediment sample of approximately 2-cm ra- ius, which approaches the radius of the core mple. Concurrently, there is a temperature ncrease at the needle probe of 5 to 7°C. As K as a small temperature coefficient—approxi- ately that of water as determined by D. W. utler (private communication) and verified by ne authors—this temperature change would ncrease K by 1 to 2 per cent at the needle, and y lesser amounts at greater distances from the eedle. No systematic increase of K with time as been noted during the measurements, and o corrections have been made for this effect. n the other hand, to correct the measurements f K to the near-freezing ambient temperature f the ocean bottom requires a reduction of 5 o 10 per cent of the measured value.

Thermal diffusivity—A knowledge of the ermal diffusivity, $\alpha = K/\rho C$, is required for ne extrapolation of the records of temperature radient obtained in oceanic heat-flow measure- ents. This has been determined for five samples f sediment material by independently measuring he conductivity K, the density ρ, and the water fraction by weight w. As the thermal capacity C depends largely upon the water content, and very little on the mineralogical composition of the solid fraction, C has been obtained from w in the manner described by *Bullard* [1954].

A plot of experimentally determined values

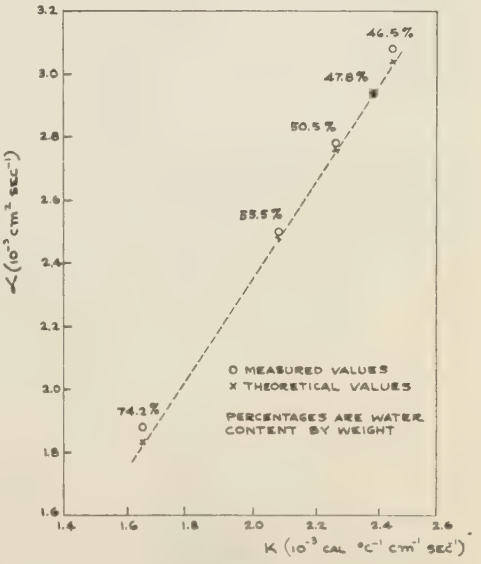

FIG. 3—Thermal diffusivity α versus thermal conductivity K of deep-sea sediments from the southeastern Pacific Ocean.

of α against K (Fig. 3) shows the relationship to be nearly linear for the range of measured values, suggesting that α might be determined simply from a knowledge of K.

If it is assumed that the sediments can be represented as solids in a fluid medium, it is then possible to determine a theoretical relationship between α and K. For example, the density may be written as

$$\frac{1}{\rho} = \left(\frac{1}{\rho_w} - \frac{1}{\rho_s}\right)w + \frac{1}{\rho_s}$$

$$= \frac{w}{\rho_w}\left[1 + \frac{1 - w}{w}\left(\frac{\rho_w}{\rho_s}\right)\right] \qquad (2)$$

Where ρ_w is the density of water fraction and ρ_s is the density of the solid fraction. Similarly, the heat capacity is given by

$$C = C_w w + (1 - w)C_s$$

$$= wC_w\left[1 + \frac{1 - w}{w}\left(\frac{C_s}{C_w}\right)\right] \qquad (3)$$

where C_w is the heat capacity of the water fraction and C_s the heat capacity of the solid fraction. From equations (2) and (3) the relation between α and K is given by

$$\frac{\alpha}{K} = \frac{1}{\rho_w C_w}\left[\frac{1 + \frac{1 - w}{w}\left(\frac{\rho_w}{\rho_s}\right)}{1 + \frac{1 - w}{w}\left(\frac{C_s}{C_w}\right)}\right] \qquad (4)$$

The following values have been used for the densities and specific heats:

ρ_w = 1.03 gm/cm³ (density of sea water)
ρ_s = 2.50 gm/cm³ (determined by plotting $1/\rho$ versus w for a series of deep-sea sediments from the Pacific and using the $1/\rho$ intercept as given in equation (2))
C_w = 0.94 cal/gm°C [*Sverdrup and others*, 1942, p. 61]
C_s = 0.18 cal/gm°C [*Bullard*, 1954]

With these values, equation (4) has been used to compute the theoretical values of α in Figure 3 from the corresponding measured values of K and w. The best-fitting least-squares linear relationship, which allows for interpolations of sufficient accuracy, is given by

$$\alpha = 1.53\ K - 0.70 \times 10^{-3} \qquad (5$$

and shown as the dashed line. The agreemen between the theoretical and experimental value is reassuring and lends strength to the suggestio that α can be predicted with sufficient accurac from a knowledge of K.

Another method of determining α directly b the needle method is described by *Jaeger* [1958 Use is made of the theoretical intercept on th ln t axis of the asymptote of T versus ln t, whic is given by $Ba^2/4\alpha$. However, several objection arise in applying this method to the needl probe. Errors of conductivity, or slope of th line, of 2 per cent will produce errors in th intercept, and hence in α, of 10 per cent. Th method of making successive graphical approx mations to the true value of K suggested b *Jaeger* [1958] is not particularly applicabl because the transient approach to a linea asympotote is not well determined for small This is because t is not measured accuratel while T is changing rapidly. Another difficult lies in the radius of the small probe (abou 0.043 cm) which is known only with an accurac of about 3 per cent. Finally, correction mus be made for the finite conductivity of the prob by substracting a constant temperature fro the experimental plot of T versus ln t. Th correction has the effect of reducing the temper ture at the sensing thermistor to that of th boundary of the cylindrical probe, thereb allowing a fit to the theory of the perfectly co ducting cylinder. To determine this constan temperature correction, it is necessary to measu several specimens of known K and α. Because these difficulties and limitations we have co cluded that it is simpler to utilize the form method of determining α. For our purpose the accuracy of α obtained in this manner adequate.

Experimental Results and Comparisons

In connection with an ocean floor heat-flo program carried out on several cruises of th research vessels of the Scripps Institution Oceanography in the past few years, the autho used the needle-probe method for determinin the thermal conductivity of many sedime cores from the Pacific Ocean floor. To establis the validity of the results, it was thought prude to establish the accuracy of the technique. Goo

TABLE 1—*Description of sediment sample*

Core number	Position Latitude	Longitude	Ocean depth, m	Date taken	Description of core
WBG 84	42°44′S	96°06′W	4700	1957 Dec. 15	Uniform dark brown zeolitic clay
WBG 130	14°44′S	112°06′W	3120	1958 Feb. 11	Light brown clayey calcareous ooze, mottled
WBG 135	11°42′S	109°43′W	3230	Feb. 14	Buff calcareous ooze
WBG 137	09°53′S	110°41′W	2770	Feb. 15	Dark brown clayey calcareous ooze, color banding
WBG 147-B	1°27′N	116°13′W	4000	Feb. 20	Mottled buff calcareous-siliceous ooze

DWBG refers to cruise, ship, and type of core taken: *DW*, DOWNWIND Expedition; *B*, S. F. BAIRD; gravity core.

reement has been obtained on some samples easured by both the needle-probe and the ady-state methods. For example, bentonite y had a K of $(1.83 \pm .02) \times 10^{-3}$ cal/cm°C by the steady-state method, and $(1.82 \pm .03) \times 10^{-3}$ by the needle probe. An additional eck was made by molding a cylinder of solid phthalene, similar in shape and size to a sedi- ent core sample, around the needle probe. his gave a K of $(.805 \pm .008) \times 10^{-3}$cal/cm°C which compares favorably with the value $.804 \times 10^{-3}$ listed in the *International Criti- l Tables* [1929].

A more extensive check was made by select- five sediment samples obtained during the Y DOWNWIND cruise to the southeastern Pacific Ocean for comparison of the needle-probe steady-state methods. Table 1 gives a brief description of the sediment cores from which the samples were selected. Conductivities were first determined by the needle-probe method in the laboratory in the same way as was done aboard ship. These various samples were then sent to three separate laboratories for independent steady-state measurements of thermal conductivity. When the core samples were returned they were again measured by the transient-state method. The results are summarized in Table 2. The first column gives the shipboard determination made by the needle-probe technique immediately after the cores were brought aboard. Shipboard measurements were made

TABLE 2—*Thermal conductivities*

Core number	K, 10^{-3} cal/°C cm sec					
	Shipboard	Lab *A* (before)	Lab *B*-1	Lab *B*-2	Lab *B*-3	Lab *A* (after)
WBG 84	1.63	1.65	1.66	1.65	1.70	...
WBG 130	2.33	2.38	2.53	2.6	2.28	2.33
WBG 135	2.35	2.26	2.53	2.5	...	2.29
WBG 137	2.14	2.08	2.13	1.95	1.98	2.07
WBG 147-B	2.07	2.44	2.44	...	...	2.44
stimated accuracy, %	∓3–4	∓3–4	∓4–5	∓4–5	∓3	∓3–4

three to five months prior to the laboratory determinations. Lab-*A* measurements are the needle-probe values obtained by the authors. The 'before' and 'after' values were made in an attempt to determine the effects of shipment and aging during steady-state measurements. Labs *B*-1, *B*-2, and *B*-3 refer respectively to the steady-state measurements on the same sediment samples by A. Beck, (University of Western Ontario, London, Canada), E. Robertson, (Geophysics Lab., USGS, Silver Spring, Maryland), and E. Ratcliffe, (National Physical Lab., Teddington, England). The need for measuring the conductivity as soon as possible after a core is retrieved is emphasized by these results. Changes in conductivity up to 20 per cent are possible in relatively short times because of evaporation and gravity settling in the core samples. Estimates of the accuracy of the needle-probe determinations were derived from the largest variations found on individual samples, and estimates of the accuracy of the steady-state measurements were provided by the respective investigators.

The water content and specific gravities were determined along with the thermal conductivities of the five samples. These values are given in Tables 3 and 4. Lab *B*-1 did not measure the water content of the samples, and water had to be added to *DWBG* 135 because of accidental dehydration during shipment. This may account for some of the discrepancy of the needle-probe measurements for this sample. Lab *B*-2 measured the densities and water contents before and after measurements of thermal conductivity were made. Although the water contents and densities were determined in slightly different ways by each laboratory, Tables 3 and 4 show that these parameters were sufficiently constant for comparisons of thermal conductivity to be made.

Comparative results for the transient and steady-state techniques show good agreement, except perhaps for *DWBG* 130 and 135. Independent steady-state measurements by Lab *B*-1 and Lab *B*-2 for *DWBG* 130 and 135 were consistent with each other but were about 10 to 12 per cent higher than the needle measurements. This suggests a possible systematic error between the two types of measurements. On the other hand, the Lab *B*-3 determination is

TABLE 3—*Water-content determinations*

Core number	Water content, percentage of wet weight			
	Lab *A*	Lab *B*-2 Initial	Lab *B*-2 Final	Lab *B*
DWBG				
84	74.3	78	76	71
130	47.8	48	46	43
135	50.5	51	50	...
137	55.5	56	53	56
147-B	46.5	...	...	...

TABLE 4—*Density determinations*

Core number	Specific gravity				
	Lab *A*	Lab *B*-1	Lab *B*-2 Initial	Lab *B*-2 Final	Lab *B*-3
DWBG					
84	1.19	1.19	1.14	1.17	1.17
130	1.50	1.50	1.51	1.60	1.56
135	1.45	1.42	1.48	1.58	...
137	1.39	1.41	1.37	1.43	1.36
147-B	1.50	1.51	...	...	...

consistent with the needle measurement f
DWBG 130. One explanation of the discrepanc
is strongly suggested by the fact that durin
shipment these two specimens showed a lar
water separation from the solid fraction of sed
ment material. This was probably due to an u
stable water saturation and high permeabilit
the water separation occurring with the distur
ance and time involved during the shipment.

Successive determinations of needle condu
tivity at the same place on *DWBG* 135, ma
after the steady-state measurements, gave i
creasingly higher results. The magnitude
these approached the steady-state values. Th
is probably due to a migration of water by gra
ity, or perhaps more likely because of migrati
in the vapor phase away from the warm need
toward the cooler parts of the core; eith
would tend to increase the measured therm
conductivity. Significant errors of this effect f
a single needle measurement have not be
noted. This effect may be larger for a stead
state measurement, since a longer time is i

ved during the measurement. Lab *B*-2 ac-lly noticed an increase in conductivity with ie during some of the measurements. The ect could also be due to heat losses from the paratus, which would be expected to be ger for the steady-state apparatus than for needle probe. However, this effect was not iced for all samples, and it is more likely roperty of a particular type of sediment.

Conclusions

The comparative results between the needle d steady-state determinations are nearly all hin the errors estimated for the respective asurements. The error of 3 to 4 per cent for needle measurements has been estimated m the combination of possible errors in cali-ation and random errors on repeated measure-nts. Random errors are probably only 1 or 2 r cent on repeated measurements, and care-calibration can probably reduce the sys-natic errors to even lower values. Care must taken on repeated measurements that the liment material in the immediate vicinity of e needle probe does not dehydrate and thereby crease the apparent conductivity. It is ncluded that the needle method of determin-g thermal conductivity of deep-sea sediments as accurate as steady-state methods, and it s the advantages of being much more quickly ade and more conveniently used on board ship. The method also lends itself to the measure-ent of thermal conductivity *in situ* on the ean floor at the same time that a temperature adient measurement is made; this would rgely eliminate the difficulties and uncertain-es involved in raising a sediment sample to the rface.

Acknowledgments—This investigation has been ade possible with equipment and sediment cores llected by many persons at the Scripps Institu-n of Oceanography, University of California. ntracts with the Office of Naval Research and e Bureau of Ships have helped to support many ases of the project, and a grant from the Insti-te of Geophysics, University of California, has materially aided the laboratory work. Russell W. Raitt and Robert Arthur have provided many helpful comments and discussion on the manuscript.

The authors are especially indebted to A. Beck, E. Robertson, and E. Ratcliffe for many measurements of thermal conductivity by the steady-state method.

References

Beck, A., A steady-state method for the rapid measurement of the thermal conductivity of rocks, *J. Sci. Instr., 34,* 186–189, 1957.

Beuttner, K., A small portable meter for soil heat conductivity and its use in the O'Neill test, *Trans. Am. Geophys. Union, 36,* 827–830, 1955.

Bullard, E. C., The flow of heat through the floor of the Atlantic Ocean, *Proc. Royal Soc. London A, 222,* 408–429, 1954.

Bullard, E. C., A. E. Maxwell, and R. R. Revelle, Heat flow through the deep sea floor, *Advances in Geophys., 3,* 1956.

D'Eustachio, D., and R. E. Schreiner, A study of a transient heat method for measuring thermal conductivity, *Trans. Am. Soc. Heat. and Vent. Engr., 58,* 331–342, 1952.

International Critical Tables, vol. 5, McGraw-Hill Book Co., New York, 1929.

Jaeger, J. C., Conduction of heat in an infinite region bounded internally by a circular cylinder of a perfect conductor, *Australian J. Phys., 9,* 167–179, 1956.

Jaeger, J. C., The measurement of thermal conductivity and diffusivity with cylindrical probes, *Trans. Am. Geophys. Union, 39,* 708–710, 1958.

Lachenbruch, A. H., A probe for measurement of thermal conductivity of frozen soils in place, *Trans. Am. Geophys. Union, 38,* 691–697, 1957.

Mason, V. V., and M. Kurtz, Rapid measurement of the thermal resistivity of soil, *Elec. Eng., 71,* 985–992, 1952.

Maxwell, A. E., *The outflow of heat under the Pacific Ocean,* Ph.D. dissertation, Scripps Inst. Oceanog., 1958.

Sverdrup, H. U., M. W. Johnson, and R. H. Fleming, *The Oceans,* Prentice-Hall, Inc., 1087 pp., 1942.

Van der Held, E. F. M., J. Hardebol, and J. Kalshoven, On the measurement of the thermal conductivity of liquids by a non-stationary method, *Physica, 19,* 208–216, 1953.

(Manuscript received May 16, 1959.)

Magnetic Anisotropy and Remanent Magnetism in Hemo-Ilmenite from Ore Deposits at Allard Lake, Quebec

ROBERT B. HARGRAVES[1]

Princeton University, Princeton, New Jersey

Abstract—The anisotropism of magnetic susceptibility of nearly pure hemo-ilmenite ore from deposits in the Allard Lake area consists of a distinct plane of maximum susceptibility (defined by maximum and intermediate axes along which the susceptibility is of similar magnitude) with a minmum susceptbility axis at right angles. This plane coincides with a preferred crystallographic grain-orientation indicated by the parallelism of titanhematite lamellae which have exsolved on the basal plane of the ferrianilmenite host grains. Measurement of the remanent magnetism (RM) shows a striking tendency for the RM vectors to lie in or near this preferred plane. On the assumption that hematite (if not ilmenite as well) is potentially ferromagnetic in the basal plane only (paramagnetic parallel to the *c*-axis), it was inferred that the RM vectors could represent the resolved component of the magnetizing field which tended to lie in the plane of maximum susceptibility. Under this hypothesis, it is possible to resolve the broad spread shown by the RM vectors of samples from one deposit in terms of a single magnetizing field direction. The variation of the intensity of RM of otherwise similar samples can also be explained on this basis.

With one exception, the RM of 47 measured samples of hemo-ilmenite ore was reversely polarized (N-seeking pole up). Additional 'natural history' evidence bearing on the problem of self-reversal of thermo-remanent magnetism (TRM) is provided by this study.

Introduction—An aeromagnetic survey of the Allard Lake area in 1947 [*Bourret*, 1949] disclosed strong negative anomalies over all the massive hemo-ilmenite deposits. Association of negative anomalies with rocks containing members of the hematite-ilmenite series as the exclusive or predominant oxide mineral has, since that time, become more widely recognized [*Balsley and Buddington*, 1958]. It is now acknowledged that reverse polarization may result from self-reversal of the natural remanent magnetism of the hematite-ilmenite mineral. Nagata, Uyeda, and others have effectively demonstrated this property in natural and artificial hematite-ilmenite solid solutions [*Uyeda*, 1958] of a certain limited range in composition, and they attribute the self-reversal to a magnetic interaction between two phases so intimately mixed that the Weiss-Heisenberg exchange interaction could take effect [*Uyeda*, 1958, p. 56]. The Allard Lake hemo-ilmenites are not now of a composition equivalent to the solid-solution range for which self-reversal has been demonstrated (for example, in Haruna dacite), but Uyeda (p. 119) has evidence suggesting that the cause of the Allard Lake self-reversal lies in the 'tendency for reverse TRM' of the titanhematite phase. Additional 'natural history' evidence bearing on the problem of self-reversal is provided by this investigation.

General geology—The specimens utilized in the magnetic work were collected during the course of a detailed study of the geology of the Allard Lake ilmenite deposits and associated rocks. Retty's reconnaissance survey in 1941 [*Retty*, 1944] first drew attention to the existence of massive ilmenite deposits in the area, and intensive ground and airborne exploration programs were undertaken in 1946 and 1947, respectively. *Bourret* [1949] published an account of the aeromagnetic survey, and *Hammond* [1952], upon the completion of the surface exploration, gave a generalized account of the regional geology with a more detailed account of the Lac Tio ore deposit. Lac Tio is the largest ilmenite deposit in the Allard Lake area, and is at present being worked by the Quebec Iron and Titanium Corporation. The following is a brief description of the rocks in

[1] Present address: Department of Geology, University of Witwatersrand, Johannesburg, Transvaal, South Africa.

the area and their mutual relations as understood at present.

The anorthosite suite consists essentially of two distinct members:

(1) Predominantly massive, grey to pinkish-grey, coarse-grained, almost pure anorthosite (An 40 to 60 per cent), with occasional hypersthene-rich phases.

(2) Coarsely foliated, blackish-grey, medium-grained, oxide-rich norite, containing substantial magnetite and hemo-ilmenite in about equal proportions.

The oxide-rich norite, considerably less abundant than the pure anorthosite, occurs as a series of thick sheets which appear to transgress primary foliation in the anorthosite. It is thought to represent a somewhat younger, though consanguineous, intrusion into the anorthosite.

The massive hemo-ilmenite deposits occur usually as irregular sheets or discontinuous lenses within (1) the foliated oxide-rich norite or (2) the barren anorthosite 'below' the foliated norite. These ore concentrations seem to be genetically related to the oxide-rich norite.

To the east and southeast of the Allard Lake area, the anorthosite suite is in contact with pyroxene syenite gneiss.

Although fault planes are rarely exposed, the surface geology and the conspicuous lineaments evident on aerial photographs suggest that the area has been broken by block faulting. The magnitude and hade of the displacement between adjacent block is, however, indeterminable.

The structural attitude most common in the area, as evident from foliation in the anorthosite suite and in the syenite gneiss, is one of steep to gentle easterly dip.

General magnetic results—The natural remanent magnetism and, where possible, the susceptibility anisotropy of two or more cores from 121 specimens has been measured. This total includes 56 specimens, of which 28 consist essentially of massive hemo-ilmenite, from the Lac Tio deposit. The remaining specimens, collected throughout the area, are massive ilmenite, anorthosite, oxide-rich norite, and pyroxene syenite gneiss.

Preliminary analysis of the RM of all specimens showed a considerable spread of orientation (Fig. 1), with both normal and reverse polarization. It was evident, however, that with one exception cores from all 47 specimens of massive hemo-ilmenite were reversely polarized. Anticipating the possibility of deviations caused by contrasting mineralogy and differential tilting of separate structural blocks, an analysis was initially made of samples of single mineralogy (massive hemo-ilmenite) from a single locality (Lac Tio, 28 specimens) in an endeavor to elucidate their magnetic properties.

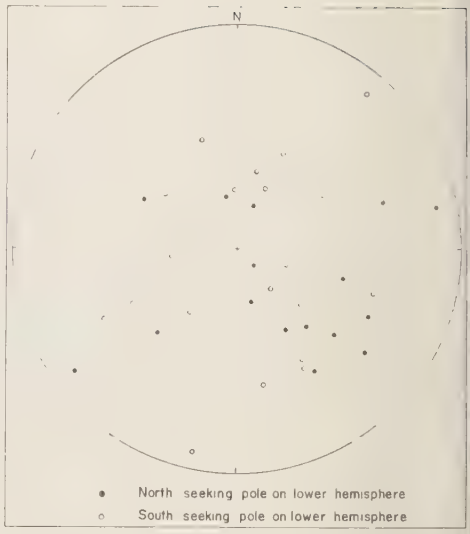

FIG. 1—Equal-area plot of a selection of RM vectors from all rock types throughout the area, deliberately chosen to illustrate the broad spread.

Geology of Lac Tio hemo-ilmenite deposit—The deposit may generally be described as a somewhat irregular, sheet-like body of essentially massive hemo-ilmenite, 3600 ft by 3400 ft in surface area and up to 300 ft thick, which dips gently to the east. The ore occurs in pure anorthosite with local hypersthene-rich zones. Particularly towards the hanging wall, coarsely banded hemo-ilmenite and anorthosite overlie massive ore. Drill-holes through pure anorthosite east of the exposed ore zone encountered first, banded ore, followed by massive ore. This confirmed the extension of the deposit down dip to the east (Fig. 2).

More detail as to the geology and structure

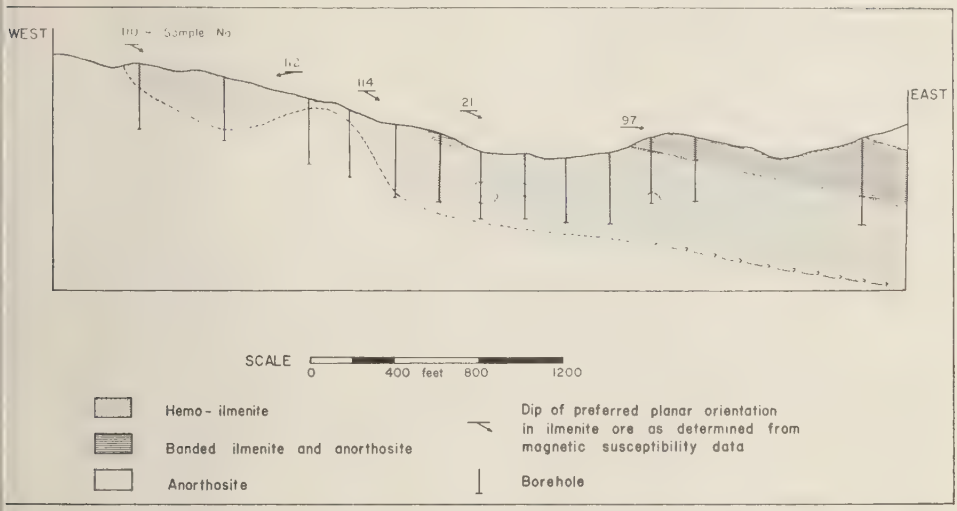

FIG. 2—Geological cross section through Lac Tio ilmenite deposit. Note general parallelism between preferred planar orientation in hemo-ilmenite ore (as determined from magnetic susceptibility data) and foot wall of ore body.

of the deposit is given by *Hammond* [1952, pp. 639–644].

Mineralogy of the hemo-ilmenite in Lac Tio ore—Analyses of two pure hemo-ilmenite samples (concentrated with Clerici solution S. G. 3.10; Analyst: F. Ridgley, Supervisor, Analytical Research, Quebec Iron and Titanium Corp.) are given in Table 1.

TABLE 1—*Analyses of two pure hemo-ilmenite samples*

Oxide	Sample 23	Sample 33
TiO_2	38.2	38.10
FeO	28.05	29.20
Fe_2O_3	31.00	28.70
MgO	2.55	2.80
MnO	1.03	1.02

If one assumes MgO and MnO to substitute for FeO in ilmenite, the proportion of ilmenite to hematite in the samples may be computed and the result expressed as a value of (x) in the solid-solution formula

$$(x)\ FeTiO_3 \cdot (1 - x)\ Fe_2O_3$$

For sample 23 $(x) = 0.70$, and for 33 $(x) = 0.72$.

Uyeda [1958, p. 114] gives the results of a partial analysis of a sample of Allard Lake ore (MgO and MnO were not reported) for which $(x) = 0.71$, in excellent agreement with the results above.

Ilmenite and hematite form a completely isomorphous series at elevated temperatures, unmixing into two phases when cooled slowly to lower temperatures. The subordinate component in the original solid solution is invariably reported to exsolve parallel to the basal plane of the host crystal [*Ramdohr*, 1955, p. 747; *Nicholls*, 1955, p. 137].

In polished section, the hemo-ilmenite grains show thin to broad (depending on orientation) parallel exsolution lamellae of titanhematite enclosed in a ferrian-ilmenite host. Measurement of the lamellae in sections cut perpendicular to their plane, gave widths varying up to 0.03 mm. In polished sections of single grains, cut as nearly parallel to the plane of the lamellae as was possible, the lamellae are irregular in outline but appear effectively equidimensional in this plane. This form may be seen in several grains illustrated in Figure 4 (section 4). Thus, the lamellae are judged to have the general shape of thin, circular disks. It should be noted that unless the section is cut precisely parallel

TABLE 2—*X-ray determination of unit cell dimensions*

Source of sample	Parameter	Ilmenite	Hematite
Lac Tio	a_{rh} (*A*)	5.528	5.439
	α_{rh}	54°45′	55°17′
	V_{rh} (A^3)	104.80	101.31
	(*x*)*	0.89†	0.19‡
Allard Lake	a_{rh} (*A*)	5.521	5.438
	α_{rh}	54°48′	55°14′
	V_{rh} (A^3)	104.59	101.11
	(*x*)*	0.87†	0.14‡

* Ilmenite fraction in each phase.
† Ferrian-ilmenite.
‡ Titanhematite.

to their plane, the lamellae will inevitably appear to be elongated and to have the form of thin, elliptical disks, as was suggested by *Carmichael* [1959]. This appearance is also demonstrated by certain grains in Figure 4 (section 3).

At least two distinct generations of hematite exsolution may be observed, with thin hematite lamellae present in the ferrian-ilmenite host between coarser segregation. In turn, fine lamellae of ilmenite may be present in the coarser hematite lamellae [*Hammond,* 1952].

X-ray determination of the unit-cell dimensions of these two components in one specimen (H33) and estimation of the composition of the two phases from Nagata's graph [*Nagata and Akimoto,* 1956] are given in Table 2 together with a determination for a sample of Allard Lake ore [*Uyeda,* 1958, p. 117]. There is reasonable agreement between the two determinations.

All research work performed during development of the Lac Tio property indicated that the bulk Fe and Ti ratio of the ore was essentially constant throughout [*Hammond,* 1952]. Therefore, as magnetite is extremely rare in the deposit, the bulk hematite-ilmenite ratio is also constant. The two independent X-ray determinations suggest that the degree of exsolution of the two components is the same throughout, which is to be expected on the basis of equilibrium considerations. No distinct variation in the proportion of coarse-to-fine hematite lamellae was discerned when different polished sections of the ore were studied.

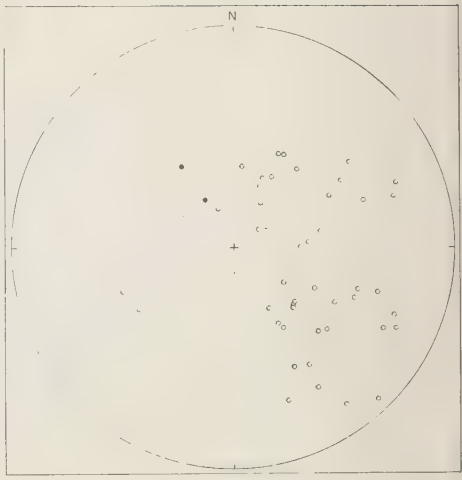

FIG. 3—Equal-area plot of RM vectors from 26 Lac Tio hemo-ilmenite samples (51 cores). Legend as in Fig. 1.

All the above evidence points to a uniform mineralogy of the hemo-ilmenite, which varies only in bulk grain size.

Remanent magnetism of Lac Tio ilmenite ore—The RM of 51 cores of more than 90 per cent pure hemo-ilmenite from 26 separate specimens was measured (Table 3) using a spinner magnetometer.[2] The broad scatter of the RM orientations is illustrated in Figure 3. However, with the exception of cores from one sample (No. 35), which was collected within 9 inches of a post-ore pegmatite dike, all the cores are reversely polarized (that is, North-seeking pole up).

Susceptibility anisotropy of Lac Tio ilmenite ore—The susceptibility anisotropy of the cores described above was measured (Table 3) using an ac bridge method. In almost all cases maximum and intermediate axes along which the susceptibility was of equal or of very similar magnitude were recorded, with a minimum susceptibility axis of significantly smaller magnitude. This relationship suggested that some

[2] The equipment which was used for this study is in the Geophysical Laboratory, U. S. Geological Survey, Washington, D. C. It will be described in a forthcoming publication by J. R. Balsley and A. F. Buddington.

TABLE 3—*Magnetic data obtained for all Lac Tio massive ilmenite samples*

Sample no.	Remanent magnetism* Azim.	Inclin.	Moment emu 10^{-3} per cc	Direction of min. suscept.† Azim.	Inclin.	Susceptibility per core, emu 10^{-3} Min.	Max.	Int.	Volume susc.‡ emu 10^{-4}/cc	Suscept. anisotropy factor
20c	339	75	4.28	151	25	.440	.610	.580	4.16	1.40
d	300	68	4.90	160	15	.280	.480	.460	3.10	1.70
21c	68	22	4.04	256	70	.220	.540	.390	2.78	2.49
d	72	25	4.66	264	65	.140	.330	.300	1.84	2.43
23a	26	51	5.99	240	60	.060	.089	.084	.596	1.48
c	148	54	6.45	302	26	.036	.060	.060	.396	1.68
26b	125	67	7.07	300	00	.046	.084	.084	.535	1.83
33a	39	52	4.43	201	38	.102	.196	.196	1.23	1.92
b	79	57	3.66	345	70	.100	.153	.153	1.03	1.53
35a	327	54	5.45	156	69	.025	.043	.043	.278	1.69
b	330	70	6.53	150	55	.024	.040	.037	.253	1.68
36a	237	47	1.79	Vertical		.023	.035	.030	.236	1.56
b	248	45	2.10	00	70	.030	.037	.035	–.262	1.22
46a	86	62	2.18	214	54	.360	.450	.390	3.10	1.25
b	90	65	2.80	275	36	.400	.540	.480	3.66	1.35
85a	135	58	4.12	00	30	.110	.350	.340	1.82	3.11
b	149	57	4.90	357	24	.170	.440	.430	2.48	2.56
86a	23	65	6.07	222	32	.069	.145	.143	.837	2.10
b	31	71	6.46	239	27	.039	.100	.098	.565	2.56
90a	53	35	3.89	265	70	.760	1.360	1.200	8.33	1.79
95c	147	37	3.89	22	48	.340	.690	.640	4.12	2.03
d	153	39	4.35	20	43	.210	.500	.470	2.86	2.42
96a	118	24	4.28	346	39	.260	.560	.540	3.34	2.15
b	134	45	5.14	329	41	.230	.550	.520	3.14	2.38
97a	112	22	3.81	Vertical		.580	1.240	1.240	7.50	2.13
b	116	19	3.73	Vertical		.680	1.500	1.390	8.73	2.21
98a	131	43	3.50	307	59	.175	.330	.320	2.06	1.89
b	118	47	3.96	304	65	.187	.348	.340	2.19	1.87
105a	160	27	2.96	07	68	.205	.560	.560	3.11	2.73
b	149	27	2.80	11	62	.190	.460	.450	2.65	2.43
110a	66	49	4.66	217	55	.187	.536	.508	2.89	2.87
b	61	49	4.66	219	57	.170	.484	.460	2.61	2.85
112a	144	13	1.35	75	70	.198	.710	.680	3.56	3.60
b	136	06	1.40	Vertical		.208	.740	.680	3.66	3.55
114a	58	42	3.11	215	55	.120	.300	.260	1.64	2.50
b	70	37	3.50	201	58	.091	.260	.250	1.41	2.85
206a	05	60	3.42	230	27	.086	.248	.244	1.35	2.89
b	22	62	3.50	242	30	.063	.205	.199	1.06	3.26
207a	107	32	1.71	228	42	.244	.580	.570	3.37	2.38
b	108	40	2.14	228	42	.234	.560	.540	3.22	2.39
210a	28	51	3.58	264	38	.193	.372	.302	2.16	1.93
b	28	60	4.28	303	17	.100	.368	.308	1.74	3.68
212a	131	59	3.03	01	55	.120	.230	.190	1.35	1.91
b	131	59	2.49	327	54	.150	.310	.260	1.79	2.06
213a	116	56	2.12	00	65	.207	.380	.350	2.35	1.83
b	112	40	1.57	00	70	.198	.375	.370	2.34	1.89
214a	55	79	6.85	270	10	.210	.560	.540	3.10	2.66
b	57	76	6.37	270	00	.175	.360	.340	2.16	2.05
216a	149	64	3.43	38	56	.065	.098	.094	.660	1.51
b	100	69	3.73	348	29	.078	.097	.094	.695	1.25
c	172	80	3.51	03	33	.083	.118	.115	.810	1.40

* All cores are reversely polarized (south-seeking pole down) except for cores from sample 35. The azimuth and inclination refer in each case to the lower hemisphere intersection of the RM vector; that is, with the exception of sample 35, the azimuths are those of the south-seeking poles.

† On a projection, the direction of the axis of minimum susceptibility is also the pole of the 'plane of maximum susceptibility.'

‡ Values in excess of 4.0×10^{-4} emu/cc indicates the presence of magnetite.

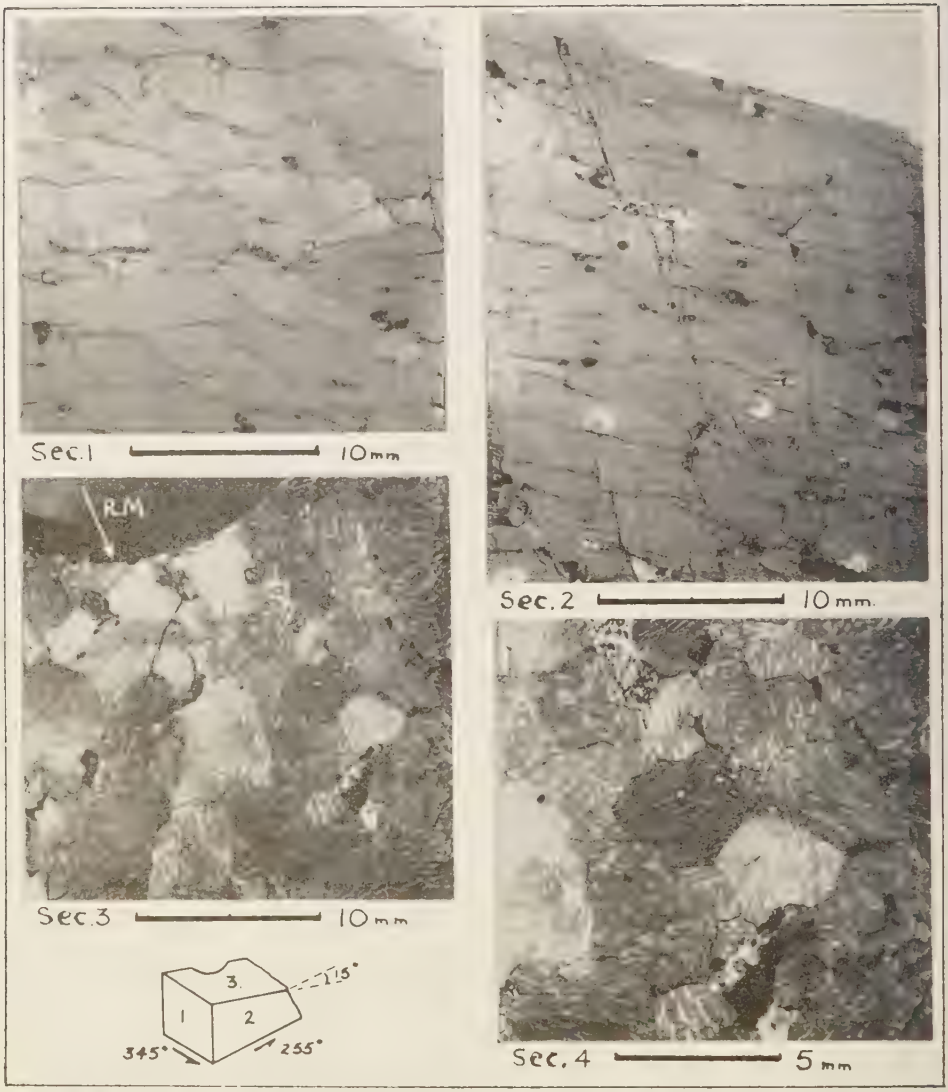

FIG. 4—Polished sections of hemo-ilmenite sample 112, oriented as in sketch, illustrating marked preferred planar orientation of titanhematite lamellae. Susceptibility anisotropy factor 3.6. Sections cut according to susceptibility data: average strike of plane of maximum susceptibility 345°; average dip of plane of maximum susceptibility 10°; azimuth 255°. Note horizontal parallelism of hematite lamellae in section 1 (vertical), cut parallel to strike, and slightly inclined parallelism in section 2 (vertical), cut parallel to dip direction. Section 3 (cut 15° from horizontal) is nearly parallel to the plane of maximum susceptibility and to the plane of the lamellae, as indicated by their relatively greater width and irregular orientation. The RM vector of the sample also lies nearly in the plane of section 3, and its orientation is indicated. Section 4 is an enlargement of part of section 3, in which several grains, cut almost parallel to their basal plane, show lamellae which are irregular to roughly equidimensional in outline.

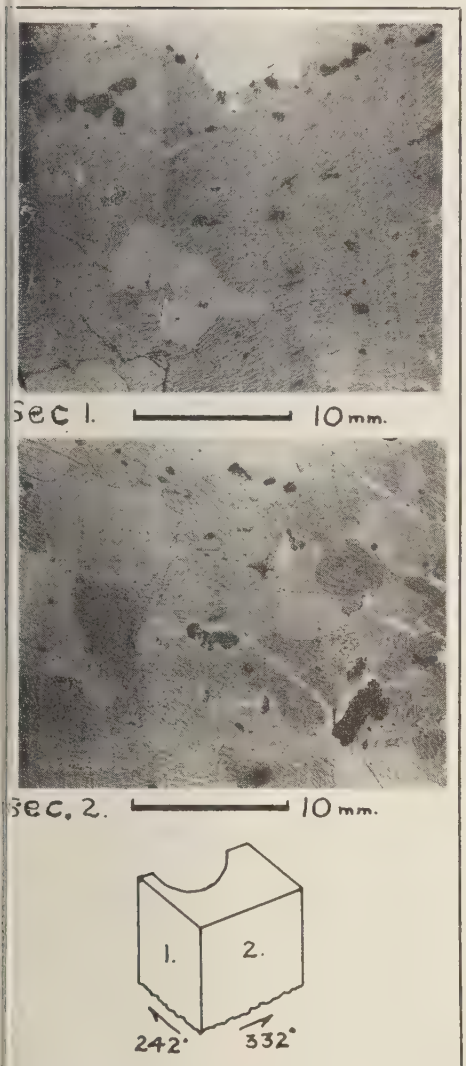

Fig. 5—Vertical polished sections of hemo-ilmenite sample 36, oriented as in sketch, illustrating preferred planar orientation of titanhematite lamellae. Susceptibility factor 1.4. Susceptibility data from two cores are inconsistent (see Table 3) but suggest plane of maximum susceptibility within 20° of horizontal. Vertical sections cut according to RM data: azimuth 242°; inclination 3°. Preferred orientation of lamellae is much less perfect than in sample 112 (Fig. 4), consistent with low susceptibility anisotropy factor of sample 36. However, the rough parallelism in both sections indicates planar structure, and its relatively low inclination is in general agreement with that suggested by the susceptibility data.

form of preferred planar orientation existed in the apparently massive ore.

Preferred crystallographic orientation in Lac Tio ilmenite ore—Hematite lamellae exsolve parallel to the basal plane of the ilmenite host [*Ramdohr*, 1955], and a megascopic check on the possible existence of a preferred orientation can be made by polishing a sample on two surfaces at right angles to each other. *Tuttle* [1943] used this technique to demonstrate a preferred orientation in the St. Urbain ilmenites. This test, applied to several samples, confirmed a preferred orientation of the hematite lamellae, and hence a preferred crystallographic orientation (Figs. 4 and 5). Furthermore, this preferred planar orientation was found to coincide in attitude with that indicated by the susceptibility data.

In some samples a dimensional orientation of somewhat platy grains, parallel to the preferred orientation of hematite lamellae, is evident; however, this dimensional orientation is not always apparent. In the St. Urbain ilmenite deposit, *Tuttle* [1943] found a preferred hematite lamellae orientation which was oblique to the platy-grain orientation.

The magnitude of the difference between maximum-intermediate and minimum susceptibility varied among the samples, and a 'susceptibility anisotropy factor' was arbitrarily obtained by dividing the maximum susceptibility by the minimum. This susceptibility anisotropy factor varied from 1.2 to 3.8. The interpretation of this factor as reflecting a variation in the degree of preferred orientation was also confirmed in the polished sections, as may be seen by comparing the samples illustrated in Figures 4 and 5. Cores from these two samples had factors of susceptibility anisotropy averaging 3.6 and 1.4, respectively.

In general, the attitude of the planes of maximum susceptibility of the samples, plotted on a geological plan, are roughly parallel to the structural contours of the foot wall of the ore body, as indicated by borehole data (Fig. 2). There is no geological evidence of post-ore metamorphism, and therefore this relationship implies that the preferred crystallographic orientation is due to some feature associated with the original emplacement and consolidation of the ore. Departures from this tendency can

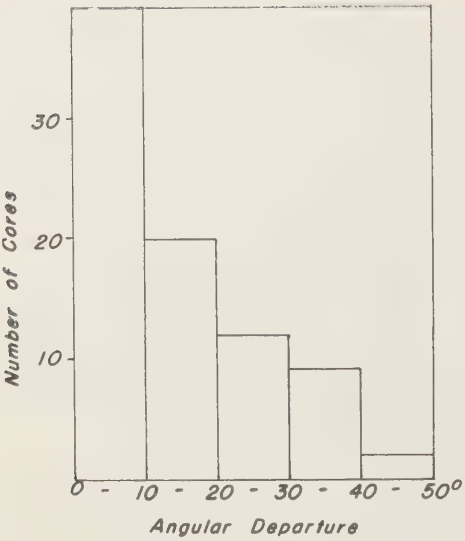

FIG. 6—Histogram of angular departure of RM vectors from plane of maximum susceptibility for all massive hemo-ilmenite samples.

reasonably be ascribed to local irregularities and contortions in the ore zone.

Relation between remanent magnetism and susceptibility anisotropy in Lac Tio ilmenite ore—Comparison of the RM of the samples with their susceptibility anisotropy showed that, within the limits of experimental error, the RM vector tended to lie in, or slightly below, the plane of maximum susceptibilty (Fig. 6). As the susceptibility is related to the preferred basal plane orientation of grains in the ore, as indicated by the parallelism of hematite lamellae, the correlation between RM and the plane of maximum susceptibility suggests that the orientation of RM is also controlled by this basal plane. Evidence in support of this interpretation is provided by current concepts of the relation between magnetic properties of hematite and ilmenite and their crystal structure.

Magnetic properties of hematite and ilmenite—*Shull* and others [1951] have shown, by means of neutron diffraction, that between the Curie point of 950°K and a transition ('Morin') point of 250°K, magnetic moments of the Fe^{3+} ions of α hematite are oriented anti-ferromagnetically parallel to the basal plane of a hexagonal unit cell. In this temperature range α hematite has an anisotropic ferromagnetism which is held very strongly in the basal plane [Neel, in *Williams and others*, 1958]. In taking photomicrographs of the magnetic domains in α hematite, *Williams and others* [1958] used thin platy specimens, the plane of which corresponded to the basal hexagonal plane. These authors reported (p. 1773): "Since the magnetization vectors lie in the plane of a specimen it was necessary to incline the specimen at an angle of 45° to the light beam in order to observe the domains."

The above evidence would lead one to expect, therefore, that any remanent magnetism a natural hematite crystal may possess may well be oriented parallel to its basal plane. This possibility was anticipated by *Howell and others* [1958].

Although the anti-ferromagnetic arrangement of the cations is somewhat different in ilmenite [*Bozorth and others*, 1957], with Fe^{3+} ions coupled anti-ferromagnetically within each cation layer instead of in alternate layers as in hematite, it again seems likely that any RM which a natural ilmenite crystal may possess may likewise be oriented parallel to the basal (hexagonal) plane.

Furthermore, as it has been proposed that the α Fe_2O_3 structure is paramount in solid solutions of hematite and ilmenite [*Bozorth and others*, 1957] up to the limit of 15 molecular per cent Fe_2O_3, it is considered most likely that natural crystals of hematite-ilmenite solid solutions would manifest this strong magnetic anisotropism and would tend to have the RM vectors restricted to the basal plane.

Interpretation of magnetic data—The crystal structure evidence cited above permits the following interpretation of the observed magnetic data to be made. The susceptibility anisotropism of the ore samples is due to preferred basal plane orientation of composite hemo-ilmenite grains which individually are ferromagnetic parallel to their basal plane (plane of maximum susceptibility) and paramagnetic parallel to their *c*-axis (axis of minimum susceptibility). It has been demonstrated that the variation in the susceptibility anisotropy factor is due to variation in the degree of preferred orientation of the gneiss. Similarly, because of this mag-

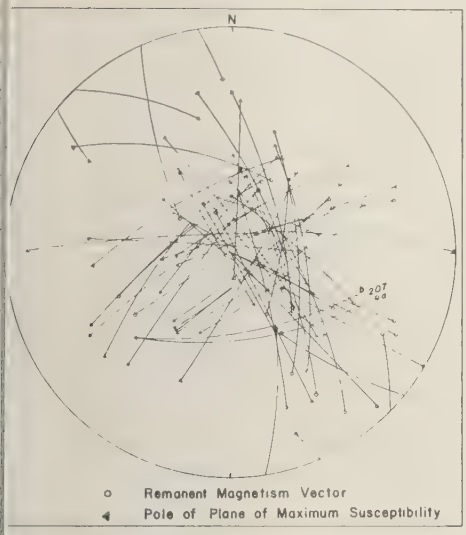

FIG. 7—Equal-area plot of segments of great circles, less than 90°, drawn perpendicular to planes of maximum susceptibility (i.e. from their poles to the remanent vector) for all Lac Tio massive hemo-ilmenite samples. The distinctly anomalous positions of the segments for sample 207 suggest an error in field-orientation.

FIG. 8—Equal-area density diagram obtained by plotting, counting, and contouring all intersections in Fig. 7. Maximum point concentration of 18 per cent.

netic anisotropy, the grains can only retain a permanent magnetization which is oriented parallel to their basal plane.

Regardless of the precise cause of the preferred crystallographic orientation in the ore, the exsolution into two phases indicates that the ore was originally deposited as a homogeneous solid solution of hematite in ilmenite; that is, at a temperature at least in excess of 600°C (see hematite-ilmenite solvus curves by *Nicholls* [1955]; *Uyeda* [1958]). In the absence of any geological evidence of post-ore metamorphism, it is probable that the preferred crystallographic orientation existed in the one-phase mineral grains prior to magnetization. In fact, magnetization of the titanhematite lamellae may have occurred as they were being exsolved. Therefore, in view of the near coincidence between the RM vector and the maximum susceptibility plane, it may be postulated that the RM vector represents the resolved component of the magnetizing field which lay in the plane of maximum susceptibility.

Testing of the hypothesis—Because of the variation in the degree of preferred orientation of the grains in different ore samples, the coincidence between the RM vector and the plane of maximum susceptibility is not, nor can it be expected to be, perfect (Fig. 7). For practical purposes, however, the RM vector may be considered as having 'migrated' from the magnetizing field direction toward the plane of maximum susceptibility, the path of migration lying in a plane perpendicular to the plane of maximum susceptibility.

Graphical application of this hypothesis to a particular sample may be described as follows. In a stereographic or equal-area projection, a great circle perpendicular to the plane of maximum susceptibility which passes through the RM vector should include the magnetizing field direction. In detail, the great circle should be a segment only, 90° or less, drawn from the pole of the plane of maximum susceptibility to the RM vector. The great-circle segments obtained from all the samples should intersect at a point which would represent the direction of the magnetizing field. The results of this treatment, as applied to the Lac Tio ilmenite samples are shown in Figure 7. Every intersection in this figure represents a valid solution for two cores.

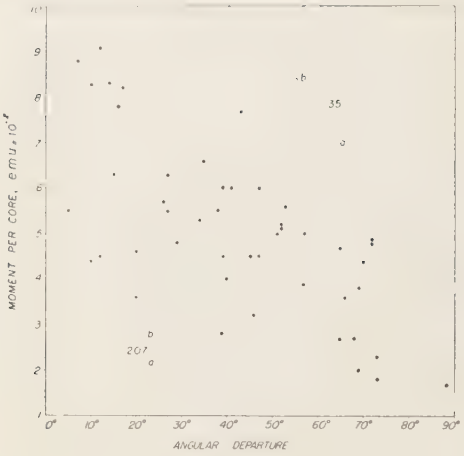

FIG. 9—Curve showing variation of RM moment (core diameter 1 in., length 1 in.) with angular departure of plane of maximum susceptibility from inferred magnetizing field direction. Sample 35 (cores a and b) was collected within 9 in. of a pegmatite dike and was the only normally polarized hemo-ilmenite ore sample recorded. Sample 207 (cores a and b), from its position in Fig. 7, is suspected of having been grossly misoriented in the field.

The intersections on an equal-area projection were traced as individual points and counted (a 1 per cent circle was used according to standard statistical procedure [*Fairbairn*, 1949, p. 285]. The resulting density diagram, contoured as illustrated in Figure 8, shows a maximum point concentration of 18 per cent. On this interpretation, the magnetizing field had an azimuth of 73° with an inclination of 72°. The position of the present earth's field is shown for comparison in Figure 8.

Examination of the RM results reveals a significant variation in the moment or intensity of magnetization. Under the above hypothesis, a sample with a maximum susceptibility plane which included the direction of the magnetizing field should have a maximum intensity of RM, and one with a plane perpendicular to the magnetizing field should have minimum intensity. Figure 9 is a plot of the intensity of RM of the samples against the angular departure of their plane of maximum susceptibility from the estimated magnetizing field direction. A tendency toward the expected relationship is evident. Anomalous departures from the general rule could be due to error in field orientation (for example, see position of great-circle segments for cores from sample 207, Fig. 8), experimental measurement, or natural causes. It is estimated that at best an accuracy of 5° can be claimed for original orientation and RM determination, and 10° for the directional susceptibility. Some of the samples are somewhat weathered, and sample 35, the only massive ore sample to give a normally polarized RM, was collected within 9 inches of a pegmatite dike. The points representing two cores from this sample are also conspicuously above the curve in Figure 9.

Application of this approach to the relatively few massive ilmenite samples available from all other individual deposits, or groups of deposits which could reasonably be presumed to belong to the same structural block, gave results in fair agreement as individual groups. However, the apparent mean of the intersections in some of the groups appears to show a small but significant departure from the result obtained for the Lac Tio deposit. This departure could be interpreted in terms of differential structural tilting of separate blocks within which the deposits lie.

Significance of shape effect—Carmichael's work [1959], whereby he measured the RM of thin plates of the Allard Lake ore before and after dissolving out the hematite lamellae, has shown that at least the greater part of the RM in the ore is due to the titanhematite. His work also confirms the fact that the RM vector lies in the plane of the lamellae.

However, Carmichael also states that "the lamellae have the general shape of thin elliptical discs with one long, one intermediate and one short axis" and "there is a high correlation between the direction of the remanent magnetization of a specimen of the ore and the average direction of the long axis of the hematite lamellae in the crystals which make up the specimen. . . . Because of the shape effect, the lamellae should retain only the component of their magnetization parallel to the long axis of each lamellae regardless of the direction of the magnetizing field."

It is this author's conclusion that the hematite lamellae in Allard Lake hemo-ilmenite ore samples are effectively equidimensional in the basal plane. (See description given above; see

lso Fig. 4.) The lamellae are considered to have he general shape of thin, circular platelets. lthough it may be argued that the restriction f the RM vector to the plane of the lamellae s a consequence of shape effect, there is no onspicuous shape element within this plane hich could control the orientation of the RM ector. Thus the graphical technique for de-ermining the magnetizing field direction and he principle on which the technique is based re still valid.

From Figure 9 it is concluded that the in-ensity of RM of a hemo-ilmenite sample is rimarily a function of the attitude of its plane f maximum susceptibility with respect to the agnetizing field direction. This is contrary to he conclusion of Carmichael, who attributes he variation in intensity to a variation in the egree of preferred orientation of grains in the ample. An objection to this conclusion is articularly illustrated by the results obtained or sample 112 (Fig. 4) which shows an ex-eptionally high degree of preferred orientation susceptibility anisotrophy factor for two cores verages 3.57) and yet has about the lowest in-ensity of RM recorded in Lac Tio ilmenite amples (average 1.37 $\times$ 10^{-3} emu/cc). This esult is in complete agreement with the fact hat the plane of maximum susceptibility of ample 112 is oriented very nearly perpen-icular to the inferred magnetizing field direc-ion (Fig. 9).

With regard to the restriction of RM to the asal plane, however, it is the basal crystallo-raphic plane of the original one-phase hemo-lmenite grain which determines the platy shape nd crystallographic orientation of the exsolved ematite lamellae. This is also the plane to hich the remanent magnetic vectors are the-retically restricted on the hypothesis of crys-al-structure control of magnetic properties.

From the data presented in this study it is ot easy to decide which of the two possibili-ies—grain shape or crystal-structure control f orientation of RM—is correct. At least as egards reversed RM the exsolution itself is a anifestation of an ionic ordering to which *yeda* [1958] attributes the mechanism of elf-reversal. Ionic ordering is controlled by rystal structure, which therefore seems likely o control the orientation of reversed RM. The discrete hematite lamellae are only an end product of this ordering process. Thus, to the author it seems probable that RM may at least start to reverse, and its orientation be fixed, even before hematite appears as a discrete phase.

TABLE 4—*Comparison of samples*

Sample	Susceptibility anisotropy factor	Intensity of rm emu $\times$ 10^{-3}/cc	Volume susceptibility emu $\times$ 10^{-4}/cc
86a	2.10	6.07	.857
b	2.56	6.46	.565
207a	2.38	1.71	3.37
b	2.39	2.14	3.22

Because ilmenite, relative to hematite, tends to have higher susceptibility and lower intensity of RM [*Balsley and Buddington*, 1958] it has been suggested that whereas the intensity and orientation of RM are due to the hematite phase, the intensity and anisotropy of susceptibility are due largely to the ilmenite phase and its shape in the preferredly oriented grains.

However, the hematite-ilmenite ratio in the ore appears to be constant (see above). Thus, it is not possible to interpret the variation in volume susceptibility (cube root of maximum $\times$ intermediate $\times$ minimum susceptibility) as being due to a variation in the relative proportion of ilmenite. Despite the constant mineralogy, comparison of some samples suggests that there might be a general inverse relation between intensity of RM and volume susceptibility (Table 4).

These results may be interpreted as reflecting a subtle and indeterminable variation, unrelated to the intensity of RM in the number of minute single-domain-sized exsolution lamellae in the samples. On the other hand, if there is any significance in the inverse relationship, it would appear to be consistent with a fundamental crystal-structure control common to both hematite and ilmenite.

Effect of magnetic anisotropy of hematite-ilmenite on paleomagnetic orientations—Because of the unusual magnetic properties of hematite-ilmenite minerals, justifiable doubt has been

cast on the validity of paleomagnetic interpretations based on results obtained from any rock containing minerals of this series [Nagata and others, in *Uyeda*, 1958, p. 87]. The hypothesis presented in this paper is that the susceptibility and RM in these minerals is controlled by their inherent magnetic anisotropism. If this hypothesis is correct a graphical technique is available whereby it is possible to correct for any deviation from the true direction of magnetization which might result from the unusual properties of the mineral series.

In summary, the precise RM vector orientation of any hematite or ilmenite grain is determined by the attitude of its basal plane to the magnetizing field direction [*Howell and others*, 1958]. If the crystallographic orientation and direction of magnetization of several crystals of diverse attitude are known, the true direction of the magnetizing field can be obtained by the graphical method outlined previously.

In the hemo-ilmenite samples used in this study, the existence of a preferred crystallographic orientation coincident with the measured plane of maximum susceptibility was demonstrated. The measured RM of any sample, therefore, could be regarded as a resultant vector of the magnetizing field which tended to move directly *away* from the direction of minimum susceptibility of the samples until the two were perpendicular.

If this is the general case, in any rock containing hematite-ilmenite as the only ferromagnetic constituent and in which a susceptibility anisotropy can be detected, deviation of the RM vector from the magnetizing field direction can be expected to occur in a direction away from the direction of minimum susceptibility. With a sufficiently varied scatter of directions of minimum susceptibility, which existed before magnetization occurred, the true field direction may be solved graphically.

Whereas susceptibility anisotropism may be expected in a hematite-ilmenite assemblage, the susceptibility of magnetite is, for practical purposes, isotropic. Any susceptibility anisotropism which may be detected in a magnetite assemblage can therefore reflect only gross fabric distribution such as grain shape, foliation, lineation. This should cause negligible deviation of the RM vector from the external field direction. In any rock containing both minerals the very much larger susceptibility of magnetite may well obscure any anisotropy due to hematite-ilmenite; but if susceptibility anisotropy is recorded, one of three conditions may obtain:

(1) The rock has a gross fabric distribution of magnetite in no way related to any preferred orientation of hematite-ilmenite grains.

(2) The rock has a gross fabric distribution of magnetite with which a preferred basal-plane orientation of hematite-ilmenite grains coincides.

(3) In the event of an isotropic distribution of magnetite, the anisotropy reflects a preferred crystallographic orientation of hematite-ilmenite grains.

If paleomagnetic results from appropriate rocks show erratic deviations, the anisotropy of hematite-ilmenite may be responsible. The correction test, based on the susceptibility anisotropy of the bulk samples, may be tried in the hope that conditions (2) or (3) above do actually obtain.

This test was applied to all remaining Allard Lake samples for which susceptibility data were available. Many of the samples (for example, the oxide-rich norite) are known to contain up to 15 per cent magnetite in addition to a similar amount of hemo-ilmenite. The position of the resulting intersections suggested a magnetizing field of steep inclination, similar to that determined from the massive ilmenite samples; but the paucity of samples from individual structural blocks precluded a satisfactory statistical estimate of azimuth.

The susceptibility of hematite and ilmenite at room temperature is so low that when these minerals are present as minor accessories only, any susceptibility anisotropy which may exist is likely to be beyond the resolving power of most susceptibility-measuring apparatus. This situation holds for all the pure anorthosites sampled in this study (characterized by minute accessory grains of ilmeno-hematite) and the spread of the remanent vectors cannot be resolved in the manner outlined for the massive hemo-ilmenite. The same obstacle will frustrate the application of this principle to most hematite-ilmenite bearing rocks sampled for general

TABLE 5—*Oxide mineralogy and remanent magnetism in different oxide-rich norite samples*

Sample	Percentage by Weight		Ratio magnetite/ ilmenite	Polarization of RM
	Magnetite	Ilmenite		
211	6.5	47.6	0.14	Reversed
143	3.4	16.5	0.2	Reversed
160	7.0	24.4	0.3	Reversed
159	10.8	34.9	0.3	Reversed
120	14.0	22.0	0.7	Reversed
164	11.6	16.8	0.7	Normal
165	16.4	18.8	0.9	Normal
187	11.3	6.0	1.8	Normal
179	10.6	5.5	1.9	Normal

paleomagnetic determinations. To overcome this problem more sensitive measuring instruments are needed.

Remanent magnetism of oxide-rich norite—Samples of oxide-rich norite, known to contain both magnetite and hemo-ilmenite, have both normally and reversely polarized RM. Modal analyses of thin sections cut from some of these samples provide quantitative mineralogical data from which the ratio of magnetite to ilmenite can be determined. Although these ratios are not necessarily precisely the same as those in the cores cut from the same samples, they are assumed to be roughly comparable.

In Table 5 the relative proportions of magnetite and ilmenite in nine samples of oxide-rich norite are listed and the normal or reverse polarization of the RM of cores cut from the same samples is indicated. The samples are listed in increasing order of the ratio of magnetite to ilmenite.

In general, the azimuth and inclination of RM in these samples is highly erratic, even in different cores cut from the same sample. The magnetite and hemo-ilmenite are both primary minerals and are present as separate grains. There is no geological reason to doubt that these samples were not magnetized contemporaneously. In consequence the results in Table 5 strongly suggest an interaction between two oppositely magnetized mineral constituents: normally polarized magnetite and reversely polarized ilmenite. The data suggest further that the intensity of magnetization of the hemo-ilmenite is roughly 0.7 times that of the magnetite. Similar relations were found by *Balsley and Buddington* [1958] in Adirondack rocks with both magnetite and members of the titanhematite-ilmenite system.

Qualitative degaussing experiments were performed on some oxide-rich norite samples by William Huff of the U.S.G.S. Geophysical Laboratory. The samples were reversely polarized to start with, but progressive degaussing at higher field strengths resulted in increasing intensity of RM. The azimuth and inclination of RM of the samples also changed, but insufficient work was done to reach any conclusion on this aspect. However, the increase in intensity of reverse RM as the strength of the degaussing field was increased (maximum 200 gauss) is judged to indicate progressive preferential demagnetization of the minor, normally polarized, magnetite component.

Bearing of results upon cause of reverse remanent magnetism in the hematite-ilmenite mineral series—It appears from the literature that there is still some difference of opinion as to the precise nature of the magnetic properties of hematite and ilmenite at room temperature. This makes understanding of the mechanism of self-reversal of TRM even more hypothetical. In general, however, the reversed RM is thought to be the result of a negative exchange interaction with an initially acquired, normally directed 'parasitic ferromagnetism' [*Uyeda*, 1958].

It is clear that experimental work on appropriate materials is necessary to confirm, or deny, the hypothesis of crystal-structure control of magnetic properties of hematite and ilmenite (in preference to shape control) employed in this study. Nevertheless, two empirical relationships are suggested which, if correct, must be borne in mind in any hypothesis explaining TRM.

(1) The reversed TRM vector lies in the basal plane of each hemo-ilmenite grain.

(2) The intensity of reversed TRM is directly related to the attitude of the basal plane of the grain with respect to the magnetizing field direction.

Acknowledgments—Research has been made possible through the generosity of the Kennecott Copper Corporation, who, in addition to financing

both field and laboratory work, made arrangements for the author to work on the property of the Quebec Iron and Titanium Corporation.

The enthusiastic advice and stimulation of A. F. Buddington, who suggested and supervised the study, is gratefully acknowledged.

All magnetic measurements were made at the Geophysical Laboratory of the U. S. Geological Survey through the courtesy of James R. Balsley. Instruction by William Huff in the use of the instruments is much appreciated.

The author wishes to thank James R. Balsley, C. M. Carmichael, S. Uyeda, and F. B. Van Houten, who collectively reviewed and edited the manuscript.

References

Balsley, J. R., and A. F. Buddington, Iron-titanium oxide minerals, rocks and aeromagnetic anomalies of the Adirondack area, New York, *Econ. Geol., 53,* 777–805, 1958.

Bourret, W., Aeromagnetic survey of the Allard Lake district, Quebec, *Econ. Geol., 44,* 732–740, 1949.

Bozorth, R. M., Dorothy E. Walsh, and A. J. Williams, Magnetization of ilmenite-hematite system at low temperatures, *Phys. Rev., 108,* 157–158, 1957.

Carmichael, C. M., Remanent magnetism of the Allard Lake ilmenites, *Nature, 183,* 1239–1241, 1959.

Fairbairn, H. W., *Structural petrology of deformed rocks,* Addison Wesley Publishing Company, 344 pp., 1949.

Hammond, P., Allard Lake ilmenite deposits, *Econ. Geol., 47,* 634–649, 1952.

Howell, L. G., J. O. Martinez, and E. H. Statham, Some observations on rock magnetism, *Geophysics, 23,* 285–298, 1958.

Nagata, T., and S. Akimoto, Magnetic properties of ferromagnetic ilmenites, *Geofisica pura e appl.,* 34, 36–50, 1956.

Nicholls, G. D., The mineralogy of rock magnetism, *Phil. Mag. Suppl., 4,* 113–190, 1955.

Ramdohr, P., *Die erzmineralien und ihre verwachsungen,* Akadamie-Verlag-Berlin, 875 pp., 1955.

Retty, J. A., Lower Romaine River area, *Quebec Bur. Mines Geol. Rept., 19,* 3–29, 1944.

Shull, C. G., W. A. Strausser, and E. O. Wollan, Neutron diffraction by paramagnetic and ferromagnetic substances, *Phys. Rev., 83,* 333, 1951.

Tuttle, O. F., Orientation of ilmenite and andesine from the St. Urbain, Quebec titaniferous iron-ore deposit, *Trans. Am. Geophys. Union, 24,* 280, 1943.

Uyeda, S., Thermo-remanent magnetism as a medium of paleomagnetism with special reference to reverse thermo-remanent magnetism, *Japan J. Geophys., 2,* 1–123, 1958.

Williams, H. J., R. C. Sherwood, and J. P. Remeika, Magnetic domains in αFe_2O_3, *J. Appl. Phys., 29,* 1772–1773, 1958.

(Manuscript received March 23, 1959; revised June 26, 1959.)

An Investigation of Shear Strength of the Clay-Water System by Radio-Frequency Spectroscopy

A. G. Pickett and M. M. Lemcoe

Southwest Research Institute
San Antonio, Texas

Abstract—This paper summarizes a soil mechanics study of the clay-water system made with steady-state nuclear magnetic resonance as the analytical tool. Although the study was limited to measurements of the contribution of water-lattice strength to the shear strength of clay soils, the results demonstrate the utility of the techniques of radio-frequency spectroscopy in such investigations. The authors conclude that water-lattice strength is of negligible significance in determining the shear strength of wet clay soils.

Introduction—The study of the strain response of materials to applied stress is a science of fundamental importance to disciplines ranging from animal husbandry to zeppelin design. Historically, that study began as mathematical exercises known as the classical theories of elasticity and hydrodynamics. Today, these theories are recognized as the limiting cases of rheology (the science of flow) wherein investigators attempt to develop stress-strain equations from knowledge of the constitution of real materials instead of by abstract mathematical analysis alone [*Freudenthal,* 1950]. This realistic approach is required in such fields as glaciology, plastics engineering, and soils engineering—fields in which the inelastic behavior of solid materials is of far greater significance than is the elastic behavior.

In order to use a realistic approach, one must begin with relationships obtained from laboratory studies of the material and a concept (or model) of the material which will predict (or explain) the behavior of the material when the empirical relationships are fitted to the concept. This places a heavy burden upon the investigator because he is required not only to choose an accurate model of the material but also to devise and interpret laboratory experiments which will measure the physical constants needed to transform this model into usable mathematical equations. Laboratory measurements are limited by the tools which are used for empirical evaluation of these physical constants, especially when the measurement involves identification of mechanism as well as functional relationship between stress, strain, and time.

An excellent example of the difficulties which may be encountered is provided by the studies of the creep of ice which were made with the ordinary tools of materials laboratories (tools which were evolved for metals testing) [*Dorsey,* 1940]. Here, James Clerk Maxwell's theory of viscosity (a liquid is considered to be an elastic solid with a high rate of stress relaxation) seems to furnish an adequate model for the material, and one needs but to measure a single material property—the relaxation time—that is a function of temperature, pressure, structure, purity, and stress orientation. The product of relaxation time and the modulus of rigidity is called viscosity. Attempts to measure either viscosity or relaxation time by traditional methods proved unsuccessful because of the inability of the investigator to isolate and identify the various mechanisms which contribute to the results of stress or strain relaxation experiments on ice. If Maxwell's concept of flow as being stress relaxation in an elastic body is restated so that we consider the body to be a liquid with hindered internal motion (the same mathematical model is used for both concepts), the problem of evaluating the macroscopic property of viscosity seems to be reduced to that of measuring molecular mobility. Statistical mechanics provides a mathematical basis for the correlation between viscosity and hinderances of internal motions if the duration of molecular orientation is measured [*Bloembergen and others,* 1948].

One method of measuring this time is steady-state nuclear magnetic resonance (NMR).

The publications listed in the bibliography present both mathematical models and the quantum-mechanics theory of NMR [*Andrew,* 1955; *Bloembergen and others,* 1948; *Pake,* 1950].The following descriptive model, developed by analogy, has been found helpful as an introduction to the techniques and is presented for that purpose.

Imagine the hydrogen nucleus to be a bar magnet spinning about its longitudinal axis. Because of thermal movements, the hydrogen nuclei in water will have completely random distribution of axis directions. If the water is immersed in a constant magnetic field, a force will be exerted on each nuclear magnet which will cause the nucleus to precess around the field direction at an angular velocity (frequency) which is proportional to the strength of the field (the frequency is independent of the angle between the magnetic field and the nuclear magnet axis but is dependent on the strength of the constant magnetic field). Now on this system superimpose an oscillatory magnetic field of the same frequency as the precessional angular velocity of the nuclei and perpendicular to the constant magnetic field. This added force will cause an increase in the angle of precession, and, since this increase will require energy, energy will be absorbed from the oscillatory magnetic field. Measurement of the energy so absorbed will give a measure of the number of nuclei per unit volume which are absorbing energy.

The precessing nuclei come into equilibrium with the neighboring nuclei and the surrounding lattice shortly after being placed in the fixed magnetic field. When the oscillating magnetic field is added, this equilibrium is disturbed, and a finite time is required for the energy absorbed by the nucleus to be dissipated to the lattice. This time is called the thermal relaxation time T_1. If energy is fed into the precessing nuclei at a rate faster than they can dissipate it, saturation will result and no energy will be absorbed. Therefore, by drawing saturation curves, T_1 can be measured, and the coupling between the atom, which contains the absorbing nuclei, and the lattice can be determined.

Precessing nuclei which are close together will influence each other. The magnetic field of one nucleus will cause an additional field at the other nucleus which can either add to or subtract from the fixed and externally applied magnetic field. Therefore there will be a slight shift in the precession frequency of neighboring nuclei. Over the whole sample, the summation of all these shifts will cause the resulting absorption curve for the whole sample to have a finite width. The width will be a measure of the proximity of the nuclei, and therefore a measure of the tightness of their bonding. There is a time constant associated with this internuclear coupling, known as the spin-spin relaxation time T_2, which is related to the line width in that the line width is equal to a constant times the reciprocal of T_2.

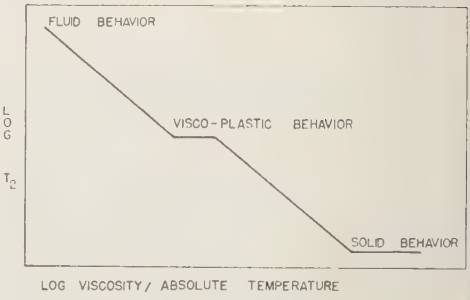

FIG. 1—The relationship between T_2 and viscosity for H_2O.

It is therefore possible, using the NMR technique, to measure the energy absorbed by the nuclei, and therefore the number of nuclei. It is also possible to measure T_1 and T_2 to determine their chemical and physical environment or the bond strength of the atoms that contain the nuclei. Figure 1 shows the type of relationship which exists between T_2 and viscosity for water and ice (T_1 is also a measure of viscosity and can be used for correlation in the solid-behavior region when T_2 becomes constant).

Study of the condition of water in clay—The usefulness of this technique for measuring the mobility of molecules, and their consequent participation in resisting shear forces, is not restricted to studies of pure hydrogen-bearing compounds. This parameter can also be measured in solutions, mixtures, gels, and other complexes that contain such compounds. And,

f course, since the parameter which is really eing measured is bond strength, the informa- on gained from NMR studies of physically nd chemically bound hydrogen-bearing com- ounds can be used for the analysis of addi- .onal material properties.

The clay-water system is considerably more omplicated than ice. It is fairly easy to list he forces which bond the discrete clay parti- les to each other (electrostatic, London–Van er Waals, ionic, and polar) but it is very ifficult to isolate and measure them. The rystal structure of clay [*Grim*, 1953] indicates hat two specific kinds of bonds are of funda- nental importance:

(1) Those bonds which result from crystal mperfections.

(a) Broken edge. A perfect clay crystal vould be electrically neutral. If such a crystal s broken into pieces, there will be unsatisfied onds at the broken edges where atoms are eparated from their partners. Although this s not the usual mechanism which creates these onds, the result is the same.

(b) Isomorphic substitution. A metallic ion n the lattice of the perfect clay crystal is re- placed with an ion of similar properities but of lower valence.

The real (and imperfect) clay crystal there- fore behaves as a large, insoluble, weakly charged ion whose surface has a negative charge. This negative charge may be satisfied by a screen of cations in the soil solution or by posi- tive broken-edge charges of other clay crystals [*Schofield and Samson*, 1954], and the charge sites are excellent potential bonding sites for naturally occurring chemical compounds as well as for soil modifiers.

(2) Those bonds which result from the crys- tal surface.

(a) Hydroxyl (OH) groups in clay-crystal surfaces provide a bonding site by replacement of the hydrogen ion.

(b) The forces which act on surface ions are not as balanced as those which act on interior ions (analogous to the cause of surface tension at a water-air interface). This causes a distor- tion of the spatial distribution of electrons at the surface of solids. Even in perfect and

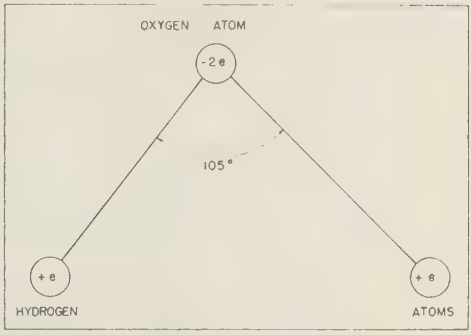

FIG. 2—Water molecule.

electrically neutral crystals, such distortion causes these surfaces to behave as if they were electrostatically charged.

The valence bond that is attainable by re- placement of the hydrogen ion can result only from a chemical reaction and is probably the strongest bond in which a clay crystal can participate. The electrostatic bond to the crys- tal surface that is attainable because of electron distribution is probably the weakest bond in which the clay crystal can participate, but, because of the enormous surface area of clays (a typical estimate is 8×10^6 cm²/gm [*Hend- ricks and others*, 1940]), the sum of these bonds can be a large force.

The water molecule is asymmetric (Fig. 2) and, consequently, polar. That is, the spatial distribution of electrons is distorted so that the molecule behaves as a body with oppositely charged ends. The polar nature of the water molecule, which causes many of the anomalies of the physical behavior of water, [*Dorsey*, 1940], is an orienting influence which opposes the tendency of the Brownian movement to create random molecular orientation. The polar nature of the water molecule also causes it to be attracted to and oriented by the clay-crystal surface which, in addition to exerting a force on the water molecule because of electron dis- tribution, has an almost perfect atom spacing for the creation of an ice lattice [*Forslind*, 1952].

The strikingly similar mechanical behavior of ice and clay has been remarked by many in- vestigators, and the bonding together of clay

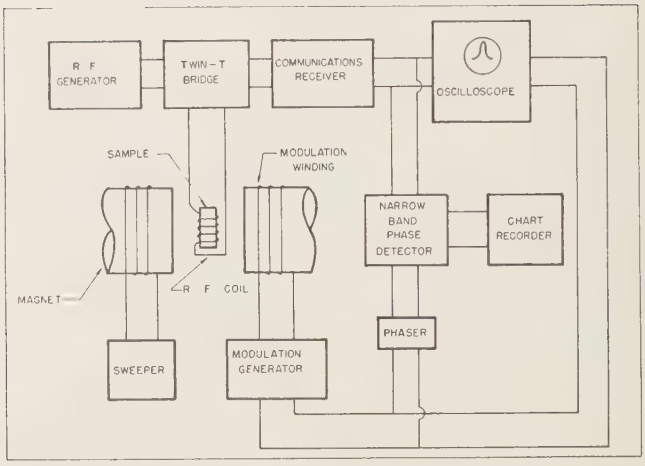

FIG. 3—Block diagram of NMR equipment.

particles by a lattice of water molecules has for many years been suggested as a significant source of the shear strength of clays [*Terzaghi,* 1931; *Winterkorn,* 1943; *Grim and Cuthbert,* 1945; *Haefeli,* 1953]. The orienting and immobilizing force exerted by clay-crystal surfaces on water has been the subject of considerable debate; in particular, the amount of this force, the manner and rate of decay of this force in successive water layers away from the clay-crystal surface, and the role of the cations in disrupting or tightening the water lattice have been discussed. To the authors' knowledge the magnitude of water-lattice forces in wet clays had never before been directly measured, because of the inherent difficulties in isolating it from other forces. NMR provided a suitable tool for measuring this parameter and was used for this purpose.

Figure 3 depicts the equipment used in this experiment. This equipment, designed and built at Southwest Research Institute after *Bloembergen and others* [1948] for developmental studies of the measurement of the water content of solids (such as for continuous sampling of grain during processing), was easily modified during the course of the experiment to fit the idiosyncrasies of the clay-water system as they were encountered.

In this equipment, a twin-T bridge fed from a crystal-controlled oscillator measures the Q of the radio-frequency (rf) coil. Q is the ratio of the energy stored in the electromagnetic field of the coil to the energy lost from the electromagnetic field (which is a measure of the energy absorbed by the hydrogen nuclei). The increase in the bridge output voltage is directly proportional to the decrease in Q. Since the frequency of the rf energy is fixed (because a crystal-controlled oscillator is used), the magnetic field must be varied to traverse through a resonance curve of finite width. The steady magnetic field is supplied by a 1180-gauss permanent magnet. Coils are wound around the pole pieces to which a sinusoidally varying current (modulation) is applied. Another set of coils is fed from a very slowly, but linearly varying current (sweep). As a result, the magnetic field is slowly swept through the resonance condition and is sinusoidally modulated at the same time. The amplitude of the sinusoidal output of the bridge is directly proportional to the slopes of the absorption curve, and its phase is such that it is in phase with the modulation for the positive slope and 180 degrees out of phase for the negative slope. The sinusoidally varying output of the bridge is amplified by an rf amplifier, and the sinusoidal variation is stripped off by a detector. This sinusoidal variation is, in turn, detected by a phase-sensitive detector. The output, plotted as a function of the sweep current, is the derivative curve (Fig. 4).

The line width, a function of T_2, is measured

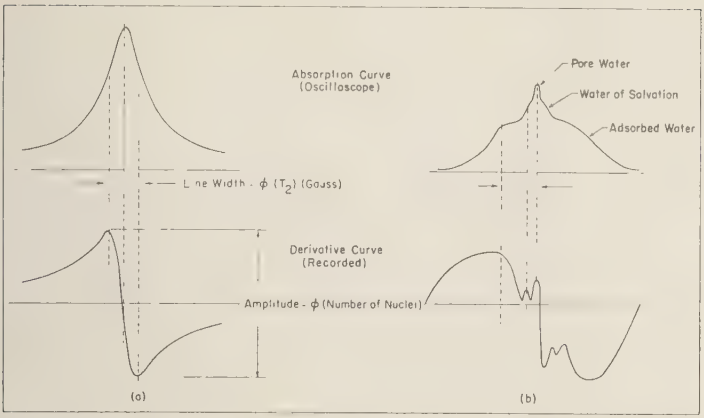

FIG. 4—Typical NMR signals; frequency constant, field strength varied. (a) NMR signals for hydrogen nuclei in single bound state. (b) NMR signals for hydrogen nuclei in two bound states.

is the width of the absorption curve at half amplitude, which is also the inflection point at which maximum slope is reached and the line width is measured as shown in Figure 4. The modulation frequency was 100 cps. The frequency of the crystal oscillator was 4.97 Mc/s. The sweep rate was 260 milligauss per minute. The chart speed for the recorder on which the derivative curve was drawn was 0.5 inches per minute; thus one inch on the chart is equal to 520 milligauss. Distances on the chart between the two peaks of the derivative curve can therefore be converted to milligauss, from milligauss to cycles, and from cycles to T_2 in seconds, according to the relation (if the absorption curve is considered to be Lorentzian in shape) that the line width in cycles per second equals $1/\sqrt{3\pi T_2}$.

The line width was also influenced by the inhomogeneity of the magnetic field, which also causes a spread in the precession frequencies for the nuclei over the sample volume. The inhomogeneity in the magnet was approximately 50 milligauss, and a correction was made for this. The amount of water on the clay was determined by the ordinary soils-laboratory technique (oven drying and weighing) instead of from the NMR curves.

In order to limit the variables, clays of well-known properties were prepared and tested. These clays were (1) a Georgia kaolin, (2) homionic Wyoming bentonites, and (3) treated homionic montmorillonites. These clays were prepared at various moisture contents, and the line width of the derivative signal (equal to $1/\sqrt{3\pi T_2}$) was measured and plotted as a function of moisture content. Stored at constant moisture content (in sealed bottles) the samples exhibited no change in line width despite noticeable changes in strength properties (caused by thixotropic behavior and remolding) which resulted from quiescent aging for periods of as long as six months and from agitation. Figures 5, 6, and 7 show the experimental curves of line width versus moisture content which summarize the results of this experiment.

The magnitude of the bonding force, expressed here as line width, is low in wet clay and, in fact, surprisingly low in dry clay. For example, ice at −2°C [*Bloembergen and others*, 1948] has a line width of 4000 milligauss, whereas sodium montmorillonite has line widths of 1600 milligauss at 0.48 per cent moisture content (based on oven-dry weight of the sample) and 950 milligauss at 3.46 per cent. A comparison between the line widths and shear strengths of ice and the clays that were studied indicated that the water film on clay crystals contributed little to the shear strength of wet clays (Fig. 1).

The modified clays were prepared for the purpose of investigating the differences in the condition of water on the different surfaces of montomorillonite crystal stacks. When the water is driven from between the layers of lithium montmorillonite, the lithium ions prevent the

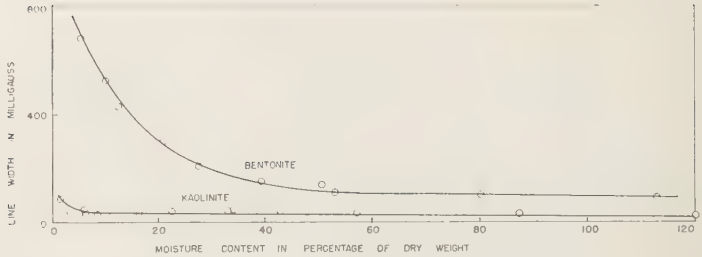

FIG. 5—Natural bentonite and natural kaolinite.

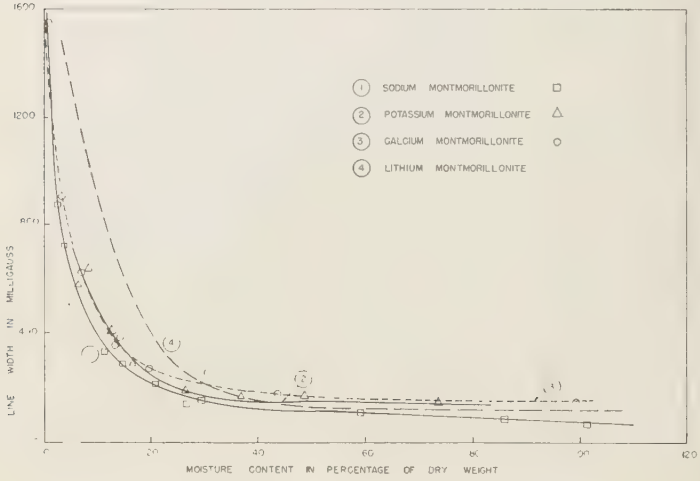

FIG. 6—Homionic clays.

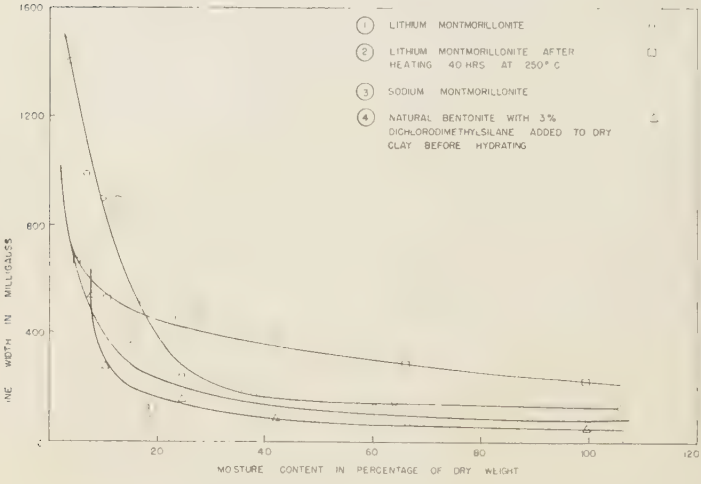

FIG. 7—Modified clays.

ystal sheets from separating enough to per- rehydration; this clay has an exterior water ilm but no intralayer water [*Greene-Kelly,* 52, 1953]. The silane reacts with clay sur- ces and forms a water-repellent coating, but t cannot enter between the crystal sheets; ds clay has intralayer water but no exterior ater film [*Rochow,* 1946]. No difference was served in mode or energy of bonding between e two systems (the cause of the broad line dth of the heated lithium montmorillonite is t understood but it does not indicate differ- ces in these parameters).

Conclusions—The experiment described in s paper was a feasibility study limited to an vestigation of the utility of radio-frequency ectroscopy as an analytical tool in soils udies. Complete quantitative data essential to e proper evaluation of such parameters as nd type and bond energy were not obtained. he measurement of the viscosity of the liquid ase in various clays (at moisture contents om the oven-dry state to saturation), the ferences which may be drawn from the shape the NMR derivative curve, and the plots line width versus moisture content are ought to be worth-while contributions to the derstanding of clay-water systems. These ta provide an opportunity for the study of isting concepts of the clay-water system in e following respects.

(1) The bonding of water to clay. The evi- nce of the derivative curve (Fig. 4) is that e water exists in a single bound state. From evious work [*Dorsey,* 1940], it appears evi- nt that the molecular orientation induced by e polar nature of water results in the forma- on of an ice lattice in free water. The mecha- sm of clay-water bonding (if only the water volved in the interval between oven-dry and turated clays is considered) seems to be lim- ed to accentuation of this effect by polar rces, since these forces exist and only one pe of force is present. This type of curve is contrast with that which would be obtained for example, the clay formed a hydrate hich was enclosed in a double-layered 'hull', is the case with many true colloids.

(2) The viscosity of the liquid phase of the ay-water system. That the viscosity of the water at the clay surface is greater than that of free water and that it decreases uniformly with increasing distance from the clay surface is clearly shown by the plots of line width versus moisture content.

(3) The contribution of the viscosity of the liquid phase to the shear strength of wet clay soils. The small measured viscosity of ice compared with that of clays of low moisture content and the relative magnitudes of the viscosities of ice and the liquid phase evaluated by comparison of line widths indicate that the contribution of the viscosity of the liquid phase to the shear strength of wet clays is negligible.

(4) The influence of exchangeable cation on viscosity of the liquid phase. The viscosity of the liquid phase is altered by a cation exchange in the same sense as is the shear strength. The magnitude of this change in viscosity is far less than that of the change in shear strength, however, and is further evidence of the insignificant contribution of the viscosity of the liquid phase to the shear strength of wet clay soils.

Acknowledgments—The experiment reported here is a part of a fundamental research study into the physical properties of clay soils. The study was sponsored at Southwest Research Institute by the Geophysics Research Directorate of the Air Force Cambridge Research Center, Air Research and Development Command. Particular credit is due to William L. Rollwitz, William H. Storey, Jr., Ray Garren, and I. G. Peters, who contributed necessary technical assistance with respect to the NMR techniques and the preparation of samples.

References

Andrew, E. R., *Nuclear magnetic resonance,* Cambridge University Press, 265 pp., 1955.

Bloembergen, N., E. M. Purcell, and R. V. Pound, Relaxation effects in nuclear magnetic resonance absorption, *Phys. Rev., 73,* 679–712, 1948.

Dorsey, N. E., *Properties of ordinary water-substance,* Reinhold Publishing Corp., New York, 673 pp., 1940.

Forslind, E., Clay-water system. 1. Crystal structure and water adsorption of clay minerals, *Svenska Forskningsinst. Cement Betong vid Kgl. Tek. Högskol. Stockholm, Medd. 11,* 20 pp., 1948. II. Water adsorption and cation exchange in montmorillonite, *Acta Polytech., Chem. Met. Ser., 3,* 3–12, 1952.

Freudenthal, A. M., *The inelastic behavior of*

engineering materials and structures, John Wiley & Sons, New York, 587 pp., 1950.

Greene-Kelly, R., Irreversible dehydration in montmorillonite, *Clay Minerals Bull., 1,* 221–225, 1952; *2,* 52–56, 1953.

Grim, R. E., *Clay mineralogy,* McGraw-Hill Book Company, New York, 384 pp., 1953.

Grim, R. E., and F. L. Cuthbert, Bonding action of clays, I. Clays in green molding sands, *Illinois State Geol. Survey, Rept. Invest. 102,* 55 pp., 1945.

Haefeli, R., Creep problems in soils, snow, and ice, *Proc. Intern. Conf. Soil Mech. and Foundation Eng., 3rd Conf., Switzerland,* 238–251, 1953.

Hendricks, S. B., R. S. Nelson, and L. T. Alexander, Hydration mechanisms of the clay mineral montmorillonite saturated with various cations, *J. Am. Chem. Soc., 62,* 1457–64, 1940.

Pake, G. E., Fundamentals of nuclear magnet resonance absorption, I and II, *Am. Jour. Phy ics, 18,* 438–452, 473–486, 1950.

Rochow, E. R., *An introduction to the chemistr of the silicones,* John Wiley & Sons, New Yor 137 pp., 1946.

Schofield, R. K., and H. R. Samson, Flocculatio of kaolinite due to the attraction of opposite charged crystal faces, *Discussions Faraday So 18,* 135–145, 1954.

Terzaghi, Charles, The static rigidity of plast clays, *J. Rheol. 2,* 253–263, 1931.

Winterkorn, H. F., The condition of water porous systems, *Soil Sci., 56,* 109–115, 1943.

(Manuscript received February 14, 1959; r vised June 17, 1959.)

Effects of Microrelief on Distribution of Soil Moisture and Bulk Density

A. W. Krumbach, Jr.

Vicksburg Research Center[1]
Southern Forest Experiment Station
Forest Service, U. S. Department of Agriculture

Abstract—A plot of moderately dissected bottom-land soil in west-central Mississippi was divided into 120 sampling areas, on each of which soil moisture samples were taken from the 6- to 12-inch layer below the surface (at the point of sampling). Topography was mapped at contour intervals of 0.3 ft and soil moisture and bulk density were analyzed in relation to microelevation. The total difference of elevation on the plot was 1.8 ft. Two shallow drainages divided the plot.

Very small changes in elevation caused significant changes in moisture and bulk density for the 6- to 12-inch layer. The variation in moisture appeared to be greater when measurements were by volume than by weight.

Introduction—Most considerations of variation in soil moisture content and associated physical properties have been concerned with differences between soil types, physiographic areas, or climatic regions; and little attention has been paid to effects of microtopography on moisture variation. This study, a portion of a comprehensive investigation of soil strength, was limited to the 6- to 12-inch layer because the moisture content and resultant strength of that layer are assumed to govern the capacity of soils to support overland vehicle traffic [*Carlson and others,* 1956].

Description and methods—A 50 by 60 ft plot was located on Falaya silt in a forested area in Warren County, Mississippi. The site had never been cultivated. This bottom-land soil is deep and imperfectly drained. Sediments from loess are continually being added, and small rills or drainage channels are characteristic (Fig. 1).

Two small channels ran through the plot. Rill *A* was wide and filled with sediment. It normally would not be noted as a depression. Rill *B* had steeper slopes and was eroding sufficiently to be bare of vegetation. A topographic map was constructed with contour intervals of 0.3 ft, starting with the lowest point on the plot as zero (Fig. 2). The highest elevation was 1.8 ft. For convenient reference the plot was divided into six elevation zones (Fig. 3).

The plot was laid out in 5-ft squares to make 120 sampling areas. Each square was divided into four quadrants 2.5 ft square. Moisture content and physical properties were sampled in one randomly selected quadrant of each square.

Moisture was sampled on two occasions. The first sample was secured when the 6- to 12-inch

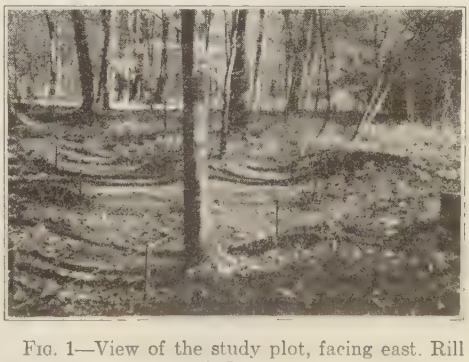

Fig. 1—View of the study plot, facing east. Rill *A* is to the right, rill *B* to the left. Rills have been cleared of litter. Rill *A* flattens until it becomes imperceptible to casual observation.

[1] Maintained at Vicksburg, Missisippi, in cooperation with the Engineers Waterways Experiment Station, Corps of Engineers, U. S. Army.

FIG. 2—Plot topography.

layer averaged 29.44 M_w[2], and the second when this layer was near field maximum, 36.08 M_w (Table 1).

The relative terms 'dry' and 'moist' will henceforth be used when discussing moisture contents of the first and second samples, although it is recognized that 29.44 M_w is by means low.

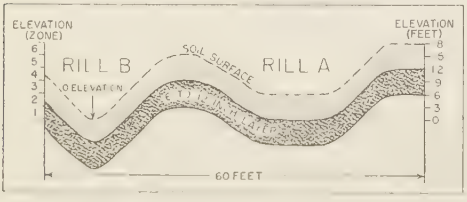

FIG. 3—Profile of plot showing elevation zones. Elevation is always specified in reference to the lowest point on the surface of the plot. Samples were obtained from the 6- to 12-inch layer.

The 120 observations of the dry conditio were taken in 1.5 hours; those of the moi condition were taken in 2.5 hours. Probab little moisture movement occurred during san pling.

Soil texture was uniform in the upper inches. Bulk density[3] increased slightly wi depth, whereas organic content, liquid limi plastic limit, and plasticity index decreas with depth (Table 2).

Differences in moisture and bulk density f the 6- to 12-inch layer were determined fro the following comparisons: (1) between elev tions within the same rill, (2) for the san elevation between rills, and (3) between t rill bottoms (which were not at the same el vation).

Results and discussion—Significant differenc (t test at 0.05 level) in M_w showed up on under the dry condition (Table 3). In rill

[2] The symbols M_w and M_v are used throughout this paper to indicate moisture content per unit weight and moisture content per unit volume, both expressed as percentages. This usage is consistent with the proposals in the report of the Joint ASAE-SSSA Soil Compaction Committee, 'Concepts, terms, definitions and methods of measurement for soil compaction,' *Agr. Eng., 39,* 173–176, 1958.

[3] For bulk density determinations, soil cores inches in diameter and 1⅝ inches long were take with the Vicksburg modification of the San Dim soil core sampler [*Andrews and Broadfoot,* 1958

BLE 1—*Moisture content (M_w) by layers, means of 120 observations*

yer, n.	Mean M_w	Standard deviation of individual observation	Standard deviation of the mean	Coefficient of variation
		Dry condition		
to 6	32.17	2.83	0.26	8.79
to 12	29.44	2.17	0.20	7.37
to 18	28.90	2.27	0.21	7.85
		Moist condition		
to 12	36.08	3.33	0.30	9.22

BLE 2—*Soil properties, means of 120 observations*

Property	Layer: 0 to 6 inches	6 to 12 inches	12 to 18 inches
	Percentage by weight		
nd, >0.05-mm dia.	5.14	5.03	4.90
t, 0.02- to 0.05-mm dia.	84.52	83.98	83.23
ay, <0.002-mm dia.	10.34	10.99	11.87
ganic matter	2.14	1.19	.94
quid limit, M_w	36.86	33.12	31.93
astic limit, M_w	30.32	27.41	26.42
asticity index, M_w	6.54	5.71	5.51
	Grams per cubic centimeter		
ılk density	1.28	1.32	1.33

e fifth elevation had significantly less moisre than the third, and in rill *B* the fourth evation had less moisture than the first or cond. Comparisons between rills showed the bottom and the third and fourth elevations of rill *A* to have significantly more moisture than rill *B*.

Explanation of these variations is not possible on an M_w basis because M_w, unlike M_v, does not measure the amount of water in a given unit of space within the soil mass. For that reason, the remainder of the soil-moisture computations were by volume.

The M_v values are the product of mean bulk density and mean M_w for each elevation. Individual products were not calculated and averaged because M_w was not derived from the same soil sample as was the bulk density, and because some M_w observations were at one microelevation whereas the accompanying bulk density sample fell in another (but still in the same sampling quadrant). Consequently, M_v means could not be analyzed statistically.

M_v distribution patterns between elevations in the same rill as well as for the same elevations between rills were similar to M_w *patterns*, but differences were generally greater. Moreover, in moist sampling, M_v differences were generally evident, whereas M_w differences were very small (Table 4).

Under both moisture conditions, the third elevation of rill *A* had more moisture than that of rill *B*, but the bulk densities were essentially the same (Table 5). The explanation may be in the fact that the third elevation generally lay in the bottom of rill *A* with its shallower gradient, but it lay along the sides of rill *B* with its steeper gradient and sides.

Perhaps for the same reason, the rill *A* bot-

TABLE 3—*Moisture content (M_w) of 6- to 12-in. layer in relation to microrelief*

Zone	Elevation, ft	Dry condition: Rill *A*		Rill *B*		Moist condition: Rill *A*		Rill *B*	
		N*	M_w	N	M_w	N	M_w	N	M_w
6	1.5–1.8	2	29.20	...	...	2	37.00	...	...
5	1.2–1.5	18	29.42	3	28.97	18	35.74	4	35.62
4	0.9–1.2	20	30.68	11	28.01	22	35.83	11	36.00
3	0.6–0.9	10	31.88	19	28.80	8	37.16	17	35.38
2	0.3–0.6	...	...	11	29.37	...	...	10	37.06
1	0.0–0.3	...	...	3	30.23	...	...	3	36.37
ill bottom		11	31.85	11	29.06	11	36.64	11	36.76

*N = number of observations.

TABLE 4—*Soil moisture (M_v) of 6- to 12-in. layer in relation to microrelief*

Elevation zone	Dry		Moist	
	Rill *A* M_v	Rill *B* M_v	Rill *A* M_v	Rill *B* M_v
6	36.79	...	46.62	...
5	39.01	36.79	47.39	45.37
4	40.92	36.07	47.79	46.36
3	41.67	37.49	48.57	46.06
2	...	40.17	...	50.69
1	...	42.01	...	50.55
Rill bottom	40.53	38.88	46.63	49.21

TABLE 5—*Bulk density in 6- to 12-in layer*

Elevation zone	Rill *A*		Rill *B*	
	No. of observations	Bulk density, gm/cm³	No. of observations	Bulk density gm/cm
6	2	1.26	...	...
5	21	1.33	3	1.27
4	20	1.33	11	1.29
3	10	1.31	19	1.30
2	...	...	7	1.37
1	...	...	4	1.39
Rill bottom	11	1.27	11	1.34

tom under the dry condition was wetter than the rill *B* bottom, even though its bulk density was lower.

Under the wet condition, the 6- to 12-inch layer below the bottom of rill *B* was 2.58 M_v higher than the same layer in rill *A*, probably because the water table was nearer the surface in portions of rill *B*.

As is common in soils of uniform texture, bulk densities increased with depth from 0 to 18 inches. However, two additional phenomena were observed. First, bulk density of the 6- to 12-inch layer of rill *B* decreased as the elevation of the layer increased. If the soil had once been of uniform level, the 6- to 12-inch layers now under lower elevations would be further from the original soil surface and would have higher bulk densities.

The second observation was that for the same elevation the bulk densities in rill *A* were higher than those of rill *B*. A possible explanation is that rill *A* soil was deposited more recently than rill *B* soil and has not been subjected as long to the action of flora and fauna.

These are merely conjectures, for bottom areas continually undergo alluvial and erosive action.

Conclusions—This study indicates that, in a soil of uniform texture and at a given time changes in microrelief may cause significant variations in the moisture content of the 6- to 12-inch layer. The variation appeared to be greater if measured by M_v than by M_w.

Although the variations are small in the absolute sense, it is possible that gross errors in estimation of water content or water yield for an area could develop from such small variations, and small changes in moisture content can be associated with appreciable changes in soil strength.

These findings probably explain some of the variation commonly ascribed to instrumental or experimental error. They suggest that microrelief must be taken into consideration when plans are made for moisture sampling, at least in the surface foot.

REFERENCES

ANDREWS, L. A., AND W. M. BROADFOOT, The Sandia Dimas soil core sampler, *Soil Sci., 85,* 297–301, 1958.

CARLSON, C. A., K. G. REINHART, AND J. S. HORTON, Predicting moisture in the surface foot of soil, *Soil Sci. Soc. Am. Proc., 20,* 412–415, 1956.

(Manuscript received April 2, 1959; revised June 30, 1959; presented at the Fortieth Annual Meeting, Washington, D. C., May 4, 1959.)

Precipitation and the Levels of Lakes Michigan and Huron

Ivan W. Brunk

U. S. Weather Bureau, Chicago, Illinois

Abstract—A number of correlations of precipitation and the levels of Lakes Michigan and Huron indicated a computable relationship and also an apparent lag between precipitation and its effect. When land-area precipitation only was considered, a correlation of lake level with four-year precipitation data gave a correlation coefficient of 0.69. A correlation of precipitation and the difference in annual mean levels indicated a correlation coefficient of 0.68.

In order to include the effect of additional variables, a correlation of water-year precipitation on a two-year basis and net basin supply was made. A correlation coefficient of 0.79 was obtained, and a lag between precipitation and its effect was again indicated. Monthly precipitation values were correlated with seasonal changes in level, and correlation coefficients of 0.85 and 0.81 were obtained with antecedent precipitation and the seasonal rise and antecedent precipitation and the seasonal fall in levels, respectively. Finally, it is pointed out that geological conditions in the Michigan-Huron basin provide a physical reason for the indicated lag between precipitation and its effect.

Introduction—In 1904 it was reported that a markably close relationship between precipitation and the levels of the Great Lakes from 83 to 1898 had been found [*U. S. Chief of ngineers*]. *Day* [1926] reached the following onclusion: 'The water levels seem to be closely lated to the quantity of precipitation, delays a year or more often appearing in the reponse of the levels, since the run-off is not mediate.'

However, *Pierce and Vogt* [1953] stated: ccording to the literature many unsuccessful tempts have been made to correlate rainfall ith lake levels' and 'no correlation between infall and lake levels can be found from avail-le data.' In *Senate Document No. 28,* [1957] was stated: 'The relationship between the ctors influencing the rise and fall of levels is complex that no satisfactory method has been roduced by the various studies of the subject hich will permit computations of future levels om measurements of causative factors.' Furermore, *Bingeman* [1953] quoted one authory as indicating that raw precipitation data annot be applied directly to the lake levels, nd *Freeman* [1926] said, '. . . the ratio of nnual rainfall by itself is found to be an unertain index to the run-off of any one of the reat Lakes in any particular year.'

The intuitive unreasonableness of precipitation having no detectable effect on lake levels prompted this study. It will be demonstrated that there is a computable effect of precipitation on mean annual lake levels, changes in mean annual levels, and seasonal changes in levels, insofar as Lakes Michigan and Huron are concerned. (Lakes Michigan and Huron are considered hydraulically as one lake because of the broad and deep connection through the Straits of Mackinac.)

Data used—The precipitation we are concerned with is of two types: (1) that which falls directly on the lake and thus has an immediate effect upon the level of the lake and (2) that which falls on the drainage basin, a portion of which sooner or later finds its way into the lake. The relative effect of these two depends on the ratio of drainage area to lake area, the proportion of drainage-area precipitation that finally reaches the lake, and any difference between amounts of precipitation on land and on lake.

The land area of the Michigan-Huron drainage basin is approximately twice the size of the lake area, but, since a considerable portion of the precipitation on land is evaporated, and since there probably is little difference between amounts of precipitation on land and on lake, at least in the annual means, the magnitude of the effect of precipitation on lake levels may well

be about the same for land and lake precipitation. However, since accurate data exist for the land-area precipitation but not for lake precipitation or for evaporation, these last two effects are not considered. One or more of the following assumptions will then apply to all the correlations given below: (1) the effect of precipitation on the lake is neglected; (2) the amount of precipitation on the land is representative of that on the lake and thus represents the average precipitation over the combined land and water area; or (3) the precipitation on the lake surface is of approximately the same order of magnitude as the evaporation from the lake surface, and these two items cancel each other. Assumption (2) appears to be the most valid, but (3) cannot be ruled out as a possibility. The effect of flow in rivers connecting the lakes is considered in one correlation.

The lake-level data, the precipitation averages, and net values for basin supply (defined later) used in this study were obtained from the U. S. Lake Survey, Corps of Engineers. Unless otherwise indicated, the records for 1903–1957 were used as dependent data and the records for 1883–1902 as independent data. The monthly and yearly precipitation values were based upon a varying number of stations —in 1957 approximately 300 stations were used. The average yearly precipitation over the Michigan and Huron basins was practically the same (about 31 inches), with an average yearly difference of a little over 2 inches. Since the ratio of the land areas of the drainage basins was essentially 1 (actually 0.92), and since differences in stream flow and movement of ground water are unknown, an unweighted average of the precipitation over the two basins was used.

Precipitation and annual lake levels—From a multiple linear correlation of mean annual Michigan-Huron level L, with calendar year precipitation, the following regression equation was obtained:

$$L = 0.51I + 564.01 \qquad (1)$$

where

$$I = .09A + .37B + .34C + .20D$$

and

A = current year's precipitation

B = precipitation one year ago

C = precipitation two years ago

D = precipitation three years ago

L is in feet when precipitation amounts are i inches. The effect of precipitation beyond thre years ago was not included because the correla tion with precipitation four years ago gave negative coefficient.

This equation indicates a computable rela tionship between precipitation and its effe upon lake levels. The multiple correlation co efficient was 0.69, which would normally ind cate that approximately half of the variatio in levels is explained by precipitation. How ever, this may be too high because of seri correlation of the yearly values of the leve (persistence).

A year-by-year computation of levels, usin equation (1), gave an average error of 0.66 for dependent data and 0.67 ft for independen data. However, when determined by comparin the difference between computed yearly valu with the actual change in level of succeedin years, the average yearly errors are only 0.36 and 0.37 ft, respectively. The average differenc between mean levels of succeeding years approximately ½ ft (absolute value).

The following is a comparison of the co relation coefficients of year-by-year lake lev and precipitation for the period 1903–195 with those obtained by *Day* [1926] for 187 1924:

Period	*Lake level and precipitation*			
	Current year	One year ago	Two years ago	Thre year ago
1903–1957	0.11	0.45	0.39	0.2
1875–1924 [*Day*]	−.28	.52	.36	.1

Except for the current year, there is goo agreement between the correlations for the tw periods. The fact that the precipitation valu used by Day were based upon relatively fe stations compared with the number used in th present study is probably not significant.

Precipitation and annual change in lake leve —In order to eliminate most of the effects serial correlation, a multiple linear correlatio

the yearly *change* in mean annual lake level (difference between mean annual levels of succeeding years, Y), with calendar year precipitation was made. The regression equation was

$$Y = 0.23I - 7.27 \qquad (2)$$

where Y = yearly difference in feet, and I = $.4A + .6B$, with A and B in inches. (Correlations were negative for precipitation two and three years ago). The multiple correlation coefficient of 0.68 here also apparently indicates that nearly one-half of the variance is explained by the precipitation. A year-by-year computation of yearly differences using equation (2) gave an average error of 0.39 ft with dependent data and 0.35 ft with independent data.

Obviously the change in the lake level (difference between annual mean levels) is a function of more than the effect of precipitation on the drainage basin. A more complete equation can be given as

$$\Delta L = I - O + R_1 + R_2 - E \qquad (3)$$

where ΔL is the change in level over the period of time considered; I is the inflow from Lake Superior only; O is the outflow, including diversion and domestic pumpage at Chicago; R_1 is inflow by streams and ground water from precipitation within the drainage basin; R_2 is the precipitation that falls directly on the lake surface; and E is the evaporation from the lake surface. This equation can be rearranged as $\Delta L + O - I = R_1 + R_2 - E$.

The terms on the left side now represent the water production of the basin. The quantity is usually defined as the net basin supply, or water yield. A correlation of R_1 with the net basin supply is more appropriate than correlation with ΔL, since the effect of more factors is included. Of course if $I - O \approx 0$ and $R_2 - E \approx 0$, the resulting relation would be essentially the same as equation (2). $R_2 - E$ is difficult to evaluate, but conceivably it could be near zero, as mentioned earlier. Values of $I - O$, however, are available, are not near zero, and are not insignificant compared with ΔL.

If variations in I and O occurred only through natural processes, there would probably be some effect of serial correlation introduced by the inclusion of these factors. However, while variations in O are essentially natural, those of I are definitely not, because of the regulation of flow from Lake Superior.

Precipitation and annual changes in net basin supply—In addition to including the effect of I, O, and the change in level, the next correlation eliminates the effect of one other factor, namely snow which accumulated in the late months of the calendar year melting in the following year. This was accomplished by using precipitation for 12-month periods beginning October 1 (water year). The correlation coefficient relating the current water-year precipitation and net basin supply for the 69-year period 1883–1952 was 0.73. Inclusion of the precipitation of the preceding year gave a coefficient of 0.79. The latter figure indicates that over 60 per cent of the variation in net basin supply is explained by the precipitation data used. The increase from 0.73 to 0.79 indicates a lag between precipitation and its effect, since the inclusion of the precipitation for two years explains an additional 9 per cent of the variance. The regression equation was

$$S = 0.17A_w + 0.06B_w - 4.44 \qquad (4)$$

where

S = net basin supply in feet

A_w = precipitation of current water-year in inches

B_w = precipitation of preceding water-year in inches

Computed values of the net basin supply from equation (4), when compared with actual values, indicated an average yearly error of only approximately 10 per cent of the average yearly net basin supply.

Monthly precipitation and seasonal changes in lake levels—While the relationship of precipitation and the lake levels, as discussed in the previous sections, may be of some interest, the seasonal changes and the association with precipitation may be of more practical importance. Therefore, correlations were next made with monthly precipitation and the seasonal changes. The changes were considered from the low in December, January, or February, to the high in June, July, or August and the inverse. Eighty-three per cent of the lows and 90 per cent of

the highs occurred in the respective months indicated during the period 1900–1957.

Using single months, the best correlations obtained were 0.40 with April precipitation and the seasonal rise, and −0.55 with September precipitation and the seasonal fall (positive values given to seasonal fall). Using various combinations of a number of factors and the seasonal rise, a number of regression equations were developed from multiple linear correlations. Of these, the following regression equation indicated the best relationship

$$R = 0.16X_1 + 0.21X_2 + 0.26X_3 + 0.17X_4 + 0.19X_5 + 0.19X_6 - 1.18 \quad (5)$$

where

R = rise, in feet, winter low to summer high

X_1 = January precipitation in inches

X_2 = February precipitation in inches

X_3 = March precipitation in inches

X_4 = April precipitation in inches

X_5 = May precipitation in inches

X_6 = yearly change of index I of equation (1)

The multiple correlation coefficient of 0.85 indicates that 72 per cent of the variation in the seasonal rise is explained by the precipitation. The average error of the computed yearly values from equation (5) for dependent data was 0.21 ft. For comparison, use of the average yearly rise of 1.1 ft instead of equation (5) would give an average error of 0.37 ft. A check of equation (5) with the independent data indicated an average yearly error of 0.23 ft.

Similarly, the best equation obtained for the seasonal fall was

$$F = 3.31 - 0.224X_1 - 0.194X_2 - 0.139X_3 - 0.217X_4 \quad (6)$$

where

F = fall, in feet, summer high to winter low

X_1 = August precipitation in inches

X_2 = September precipitation in inches

X_3 = October precipitation in inches

X_4 = November precipitation in inches

The multiple correlation coefficient was — 0.8 and the average yearly error, computed fro equation (6), was 0.20 ft. This can be cor pared with an average error of 0.37 ft, obtain if the average yearly fall of 1.1 ft was used i stead of equation (6). A check of this equati with the independent data gave an avera yearly error of 0.23 ft. The index I from equ tion (2) was used in equation (5) but not us in equation (6), as it did not improve the r sults. (The correlation of the index I and t seasonal rise is 0.47, whereas the correlati with the seasonal fall is only — 0.11.)

It should be noted that some of the variati from predicted values in most of the precedi equations could be caused by the varying *cha acter* of the precipitation. *Freeman* [192 stated that the run-off depends as much up the concentration of rainfall and upon the tim of year in which it falls as upon the total dept For example, a monthly total of five inches rainfall, concentrated mainly in one or tw storms, will produce a far greater and fast run-off than the same total precipitation that the sum of many smaller amounts. This w demonstrated in October 1954 when two u usually heavy rains resulted in large immedia run-off which caused the level of Michiga Huron to rise from September to October, spite of a fall from July to September.

Summary and conclusions—Precipitation da for the land area of the Michigan-Huron drai age basin was used to demonstrate a number relationships with lake levels. A correlatio when only the effect of precipitation was co sidered, indicated not only a relationship b also a lag. A correlation of precipitation and r basin supply included the effect of a number additional factors and further substantiated t evidence for the lag between precipitation a its effect. A lag is certainly reasonable, for the is general agreement [for example, *McDona* 1954, and *Hough*, 1958] that precipitation h a delayed and variable effect on lake levels b cause of variations in run-off.

It appears that geological conditions in t Michigan-Huron basin provide a physical re son for the lag between precipitation and effect. *Freeman* [1926] indicated that the la surface is largely a deposit of glacial sands a gravel, which, when not frozen, absorbs t

nfall with more than common facility and ds to conserve it while it is slowly percolating ard the main stream beds and into the lakes. considerable portion may therefore take eral years in underground transit and may ry a part of the rainfall of one year into the -off of a later year.

cknowledgment—The assistance of Lawrence Hughes, Research Forecaster, U. S. Weather reau, Chicago, Illinois, in the preparation of s manuscript, is gratefully acknowledged.

References

NGEMAN, M. E., Two studies concerning the evels of the Great Lakes, *Proc. Rochester Acad. ci., 10,* 120 pp., 1953.

Y, P. C., Precipitation in the drainage area of Great Lakes, 1875–1924, *Monthly Weather ev., 54,* 85–106, 1926.

EEMAN, J. R., *Regulation of elevation and discharge of the Great Lakes,* (A report to the Chicago Sanitary District), Chicago, Ill., 548 pp., 926.

Hough, J. L., *Geology of the Great Lakes,* Univ. of Illinois Press, Urbana, Ill. 313 pp., 1958.

McDonald, W. E., Variation in Great Lakes Levels in relation to engineering problems, *Proc. 4th Conf. on Coastal Engineering, Council on Wave Research,* Univ. Calif., Richmond, Calif., 1954.

Pierce, D. M., and J. E. Vogt, Method for predicting Michigan-Huron lake level fluctuations, *J. Am. Water Works Assoc., 45,* 502–520, 1953.

Senate Document No. 28 (85th Congress, 1st Session) *Effects of diverting an additional diversion of water from Lake Michigan at Chicago,* U. S. Govt. Printing Office, Washington, D. C. 74 pp., 1957.

U. S. Chief of Engineers, Annual Report, Appendix EEE, 4057–4132, 1904.

(Manuscript received October 2, 1958; revised May 11, 1959; an adaptation of a paper presented at the Second National Conference on Applied Meteorology: Engineering; sponsored by the American Meteorological Society and the American Society of Civil Engineers, Ann Arbor, Michigan, September 10, 1958.)

Water Deficits and Irrigation Requirements in the Southern United States[1]

C. H. M. van Bavel

Southwest Water Conservation Laboratory, Tempe, Arizona

Abstract—The frequency of exhaustion of available moisture supplies and the attendant water deficits have been determined for 9 southern states. The results are based upon estimated daily moisture balances computed for 25 years at 264 stations. Evapotranspiration was estimated with the Penman formula.

Results are given in terms of two parameters: storage capacity of the root zone and recurrence probability. Therefore, the values obtained have immediate practical value for a number of agrohydrological and agronomical applications. Among these are the estimation of irrigation requirements for river basins, farms, and individual fields, as well as estimation of drought hazard.

Generalized, the results indicate typical occurrence of severe drought throughout the South during the growing season. It appears that soil moisture storage capacity and recurrence frequency are more important than geographical location in determining water deficits.

Introduction—Even though it is generally recognized that in the eastern United States soil moisture reserves are often depleted during the growing season, until recently no quantitative descriptions of drought occurrence have been given. This report summarizes a series of studies made by the author, his associates, and others for the southern half of the humid section of the United States. Several developments have made quantitative information on drought occurrence an urgent need in agriculture.

First, increased efficiency of farm production has made supplemental irrigation more attractive, but for sound farm-management decisions, the need for irrigation should be accurately known.

Further, the associated requirements for irrigation water should be available for planning on-the-farm water supplies and in determining water needs in large areas. This is particularly true when public works that will make irrigation water available are being considered or designed.

Finally, studies of drought and water needs are a part of the evaluation of an important national resource, and they can contribute to better utilization of land, water, and capital.

The need for such research has been painfully demonstrated by large-scale crop failures and local water shortages for domestic and industrial purposes. Further, on the positive side, remarkable results have been obtained with crop irrigation in the 'humid' South.

Method—A realistic criterion for drought must be based upon soil moisture availability, and, therefore, it must consist of three elements: amount and distribution of rainfall, evapotranspiration, and the amount of water that the soil can store in a form that is available for plants. The last factor entails both the physical nature of the soil and the depth of root penetration.

Compared with rainfall, the evapotranspiration and storage factors are relatively unchanging, and certain simplifying assumptions can be made. However, rainfall is so erratic that its variation from day to day and from year to year cannot be neglected. This means that studies of drought and water needs cannot be based on anything but actual, daily records of precipitation, as contrasted with the use of average values for daily or monthly quantities.

Therefore, the author proposed earlier to estimate and study daily soil moisture balances [*Van Bavel*, 1953] in order to arrive at the prevalence of drought at a location. Others

[1] Contribution from the Soil and Water Conservation Research Division, Agricultural Research Service, United States Department of Agriculture.

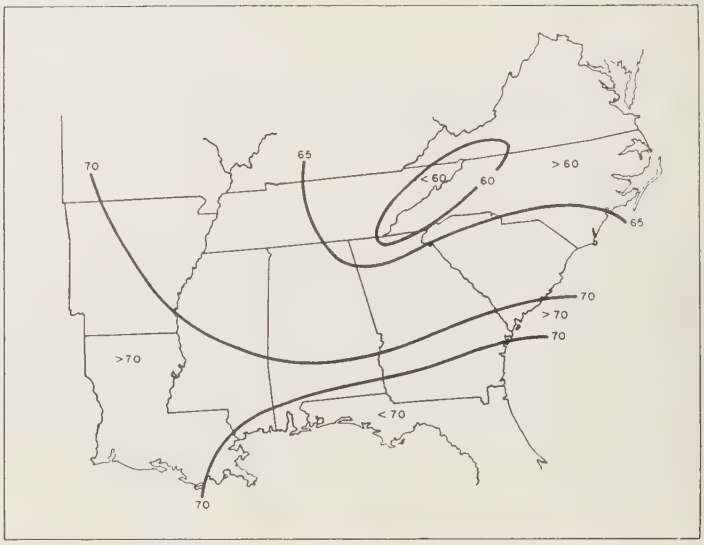

FIG. 1—Seasonal (April through September) values of evapotranspiration in centimeters as computed with the Penman formula.

have suggested essentially identical procedures [*Allred and Chen*, 1953; *Pengra*, 1958]. In all of these procedures, a daily balance is made by adding measured rainfall and subtracting estimated evapotranspiration, subject to the upper and lower limit of the soil moisture reservoir.

The number of times that the soil reservoir is reduced to its lower limit is indicative of the intensity of drought, which may be characterized by noting the number of 'drought-days' in a particular month or season.

The water requirement may be approximated by finding the amount of water that would have evaporated on the drought-days as estimated, had soil moisture been available for evaporation.

In the procedure followed by the author the evapotranspiration is estimated as the maximum or potential value found from the formula by *Penman* [1956]. Seasonal values thus found are shown in Figure 1. However, for calculations, average monthly values, based upon available data on sunshine duration, air temperature, humidity, and wind speed, were used. A typical set of values by months is shown for four stations in the area under study (Table 1).

TABLE 1—*Typical values of daily amount of evapotranspiration in centimeters by months for four locations as calculated with the Penman formula*

Month	Location			
	Shreveport, La.	Mobile, Ala.	Columbia, S. C.	Richmond Va.
Apr	0.32	0.33	0.33	0.27
May	.39	.39	.39	.34
Jun	.50	.44	.43	.40
Jul	.50	.41	.42	.39
Aug	.46	.37	.40	.33
Sep	.36	.33	.32	.27

The upper limit of the soil's storage capacity for water is realistically represented by the field capacity[2] of the root zone. It is more difficult to fix the lower limit. The wilting percentage is an obvious criterion but there are many indications that it is desirable to replenish soil moisture at a much earlier point in depletion

[2] Soil Science Society of America definition (1955): Amount of water remaining in a well drained soil when the velocity of downward flow into unsaturated soil has become small.

drought may then be said to occur before the ilting percentage has been reached.

A common practice, reflected in many Soil onservation Service Irrigation Guides, is to rigate when 50 per cent of the water held by le soil between its field capacity and its wilt- g percentage is depleted. The moisture ten- on that corresponds to the 50 per cent deple- on level varies with soil type but will likely between 0.5 and 1.5 bar.

Regardless of the choice of the lower limit storage capacity, the actual amount of stor- e will vary with different soils and crops. herefore, the drought studies reported here ve been carried out for a number of values the storage capacity varying from 2.5 to 7.5 n of water. Accordingly, drought incidence d water requirements can be ascertained only hen a dependable estimate of the soil's storage pacity is available.

A further question arises with respect to the lation between soil moisture content and apotranspiration. This point is still contro- ersial [*Veihmeyer and Hendrickson,* 1955]. udies with weighing lysimeters, which supply e most accurate information in this matter, nerally indicate that soil moisture tension ust be very high before any perceptible de- crease in transpiration under field conditions is noted. After this point is reached, transpiration decreases rapidly to a small and often negligible quantity at the wilting percentage. The supposition has been made [*Thornthwaite and others,* 1958] that evapotranspiration might be proportional to the fraction of available soil moisture remaining. This assumption is without experimental foundation and is contrary to such dependable measurements as are available. Admittedly, further precise measurements concerning this point are badly needed.

In view of the foregoing considerations the following procedure was adopted for computing daily moisture balances. A figure was assumed for the storage capacity of the soil; for example, 5 cm. Further, it was assumed that at the beginning of the growing season, such as April 1, the soil would be at its maximum moisture content, that is, at field capacity, and that, therefore, the amount of available water would be equal to the value of the storage capacity (field capacity minus wilting percentage). Then, on a daily basis, precipitation, as recorded, was added, and evapotranspiration, as estimated, was subtracted. If a zero value resulted, no further subtraction was carried out. No allowance was made for surface runoff, and no stor-

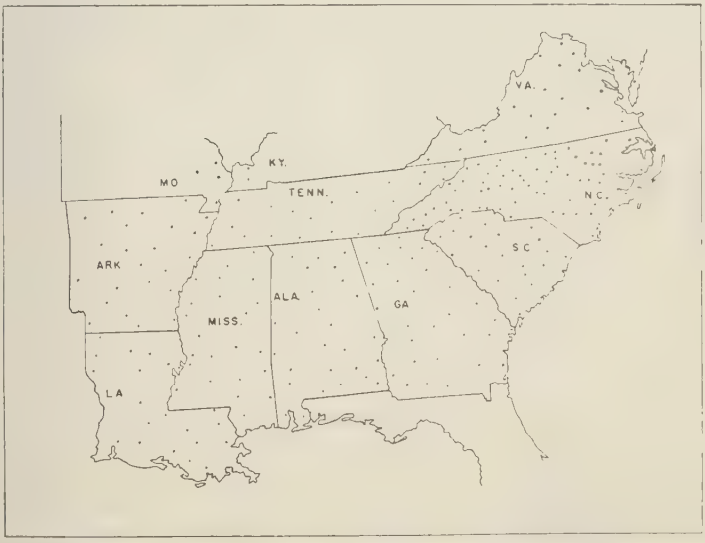

Fig. 2—Stations for which analysis of drought frequencies and water deficits were made.

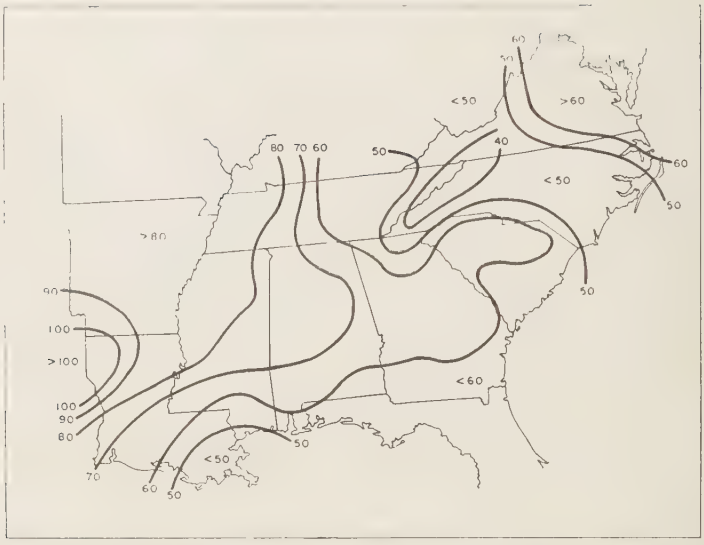

FIG. 3—The least number of drought-days at a probability of 0.1 for a soil moisture storag capacity of 7.5 cm.

age in excess of capacity (in this case 5 cm) was permitted.

This procedure was carried out for five values of storage capacity between 2.5 and 12.5 cm and for time periods varying from April through September in Virginia to the entire year in Louisiana, Arkansas, and Mississippi. The number of drought-days thus found was determined by months and by years for 256 stations (Fig. 2) and for 25 years of record. All computations of some 8 million daily water balances were made by machine methods.

Water deficits were obtained by accummulating the potential evapotranspiration amounts on the drought-days as recorded. Frequency distributions were prepared of drought-day occurrence and water deficits at each of the 256 stations under study. These, in turn, were generalized into maps and tables. For the purpose of the present report, a common time period of April through September was selected to show data for the entire region, but information for additional months is available for some of the individual states.

Results—The results presented are only a very condensed abstract of the total body of available information. Complete data have been published in a series of reports dealing wit individual states [*Van Bavel and others*, 195 1957a, 1957b, 1958; *Knetsch and Smallshau* 1958].

To convey a general impression, two map of drought-day occurrence are shown. Both o these are for a storage capacity of 7.5 cm. Thi is a rather high figure for typical soil condition in the Southeast and in the South. In man cases, the root zone of agricultural crops ca barely store 2.5 cm of available moisture, an 5.0 cm is a quite common value. The princip reason for the low storage capacity is the sha low depth of root penetration that is commonl observed on the prevalent Red-Yellow Podzol soils in the area. However, there are also exce tions to this general observation. In any pa ticular case the value of the soil's storag capacity may be taken into account by the us of detailed data as explained above.

Figure 3 shows the minimum number drought-days that occurs at a probability 0.1. That is, the figures displayed will be equale or exceeded in one out of ten years. In contra with the somewhat exceptional nature of th data of Figure 3, Figure 4 shows the sam situation at a probability of 0.5. As one migh

Fig. 4—The least number of drought-days at a probability of 0.5 for a soil moisture storage capacity of 7.5 cm.

pect, the drought hazard depends markedly probability, and the limited value of 'aver-e' figures is hereby well demonstrated.

The occurrence of drought-days as illustrated Figures 3 and 4 is a quantitative measure of drought as it affects crop production. The corresponding amounts of water needed to alleviate the water deficits are shown in Figures 5 and 6. Both figures apply, again, to a storage capacity of 7.5 cm; Figure 5 shows the minimum deficit for a probability of 0.1, whereas Figure 6 shows the deficit at a 0.5 probability.

Space does not permit a full portrayal of the results obtained. However, Table 2 demonstrates, in a typical case, the effect of both probability and storage capacity on the minimum number of drought-days. Water deficits show a similar variation.

TABLE 2—*Least number of drought-days during the period of April through September in central North Carolina*

Probability	Available moisture storage capacity of the soil, cm				
	2.5	5.0	7.5	10.0	12.5
0.1	85	65	45	40	35
0.2	75	55	40	35	25
0.3	65	50	35	25	20
0.5	55	45	25	15	5

Discussion—Even though only typical and generalized data can be presented here, it appears obvious that lack of soil moisture for plant growth is a characteristic feature of the growing seasons in the South. Even on the better soils this seems true, and on sandy and shallow soils drought often has disastrous proportions.

First of all, then, the present studies provide a means of classifying the various soil conditions with regard to drought hazard and their suitability for different uses. Second, a measure is provided of the extent to which drought may interfere with certain management aspects of crop production, such as fertilization or selection of crop variety. Third, a measure is given of the water requirements of agriculture if production at optimum levels is to be maintained through irrigation.

This last point has far-reaching consequences. Farmers must compete with other users for limited supplies of water, on the basis of anticipated needs. In arid regions, this may be done

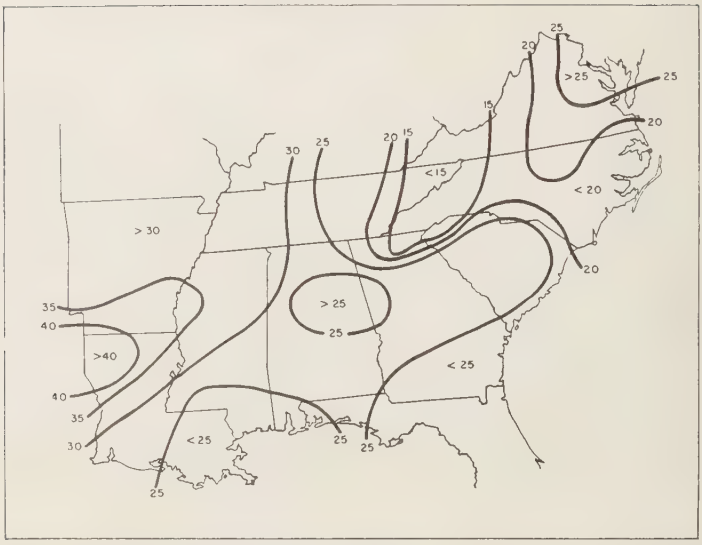

FIG. 5—The least seasonal water deficit at a probability of 0.1 for a soil moisture storage capacity of 7.5 cm.

by simply considering total consumption of water by crops. In humid areas the situation depends upon soil conditions as well, and, furthermore, in estimating water needs a sufficient margin must be allowed to provide for insurance against the consequences of a very unfavorable season.

It is believed that the present method supplies reliable data on the basic irrigation requirements of agriculture in the South. De-

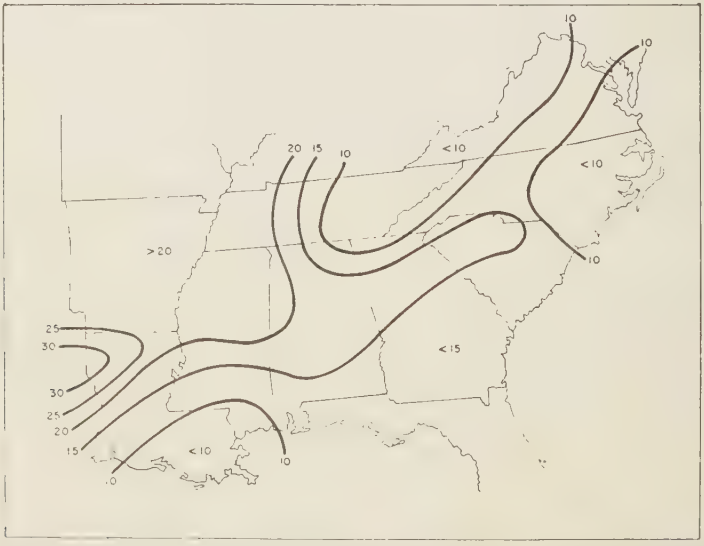

FIG. 6—The least seasonal water deficit at a probability of 0.5 for a soil moisture storage capacity of 7.5 cm.

ending upon the actual method of irrigation, ae requirements of farms may be higher than ae figures given here. This is considered an ngineering problem that is outside the scope f the present studies. Lysimetric studies of ae validity of Penman's formula [*Gilbert and an Bavel,* 1954; *Harris and Van Bavel,* 1959] or estimating evapotranspiration confirm its eliability, at least for agricultural crops. Studes of the water-storage properties of soils ndicate that in many southern states soils will all within the range considered here [*Carlson,* 955; *Doss and Broadfoot,* 1956; *Lund,* 1959].

A major criticism of the approach used here ould be that runoff is not accounted for, prinarily by default of a generally applicable unoff-rainfall relationship. Surface runoff often occurs in connection with storms that are in excess of storage capacity, but not always. Exploratory studies by the author have shown hat an error of from 5 to 10 per cent may be ncurred by neglecting surface runoff from ypical Piedmont soils. In some instances this error may be larger, and application of present data should be made with care.

Seasonal irrigation requirements in the South vary in the same way as the drought-days. Typical values range from 8 to 32 cm per season, depending upon soil and location. 'Safe' values are from 25 to 50 cm, corresponding to the greatest need in nine out of ten years.

This range of values corresponds well to actual amounts of water applied in various irrigation experiments [see, for example, *Tharp and Crickman,* 1955]. A recent study [*Thornthwaite and others,* 1958] indicates that the 'mean' annual deficit for the South varies from 0 to 10 cm. These figures are greatly at variance with our results, but the difference may be explained by the fact that Thornthwaite's work is based on average monthly water balances rather than on actual daily balances and also by the fact that 30 cm was used as the storage capacity of the soil. The 30 cm figure is not representative for agricultural soils in the South, as was pointed out before.

The generalized data which are supplied in this report are not suitable for many individual applications. Often, crops are in the field for a brief period only. Further, the soil's storage capacity must be considered in each case and it may need adjustment as a crop develops. Therefore, in the detailed reports on each of the southern states, drought-days and irrigation requirements are given for individual months, for limited geographical areas, for a range of moisture storage capacity of the soil, and for different probabilities.

In detailed form, therefore, the present studies make possible rather careful planning and engineering of land use, cropping systems, irrigation facilities, and water-supply sources. As such, the data are now being used by the Soil Conservation Service in planning farm irrigation systems. Furthermore, these data, used in conjunction with data from irrigation experiments, permit the forecasting of the chance of economic returns from irrigation. Various State and Federal planning agencies are using these data to project the benefits to agriculture of large reservoirs and to estimate agricultural needs for water in the future.

The present studies were intended as a survey of water deficits and needs, and it is recognized that refinements are possible and needed. Several of these are considered in an earlier report [*Van Bavel and Verlinden,* 1956]. In particular, the estimation of evapotranspiration from different crops at varying stages of development requires much more study. Also, a broader knowledge and appreciation of the water-storage capacity of different soils under varying management is a continuing need.

Nevertheless, the supposition that soil moisture conditions in the South are often a limiting factor in crop production appears to be well founded in quantitative fact, and an order of magnitude for the water needs for crop production has been established.

Acknowledgments—These studies were carried out by the Agricultural Research Service in cooperation with the Agricultural Experiment Stations of North Carolina, Virginia, South Carolina, Georgia, and Alabama, the Soil Conservation Service, and the Tennessee Valley Authority. The help of many persons in the cooperating agencies is gratefully recognized. Regional summarization of the data was carried out by F. D. Whisler, ARS, USDA.

References

Allred, E. R., and R. Chen, Evaluating irrigation needs in humid areas, *Agr. Eng., 34,* 611–615, 1953.

Carlson, C. A., and R. C. Pierce, The field maximum moisture content, *Soil Sci. Soc. Am. Proc., 19,* 81-83, 1955.

Doss, B. D., and W. M. Broadfoot, Properties of 91 southern soil series, Southern Forest Experiment Station, *Forest Serv.-U. S. Dept. Agr. Occasional Pap. 147,* 1956.

Gilbert, M. E., and C. H. M. van Bavel, A simple field installation for measuring maximum evapotranspiration, *Trans. Am. Geophys. Union, 35,* 937-942, 1954.

Harris, D. G., and C. H. M. van Bavel, Evapotranspiration of Bermuda grass and corn, *Soil Sci. Soc. Am. Proc.,* (in press) 1959.

Knetsch, J. L., and J. Smallshaw, The occurrence of drought in the Tennessee Valley, *Tenn. Valley Authority Rept. T 58-2AE,* 1958.

Lund, Z. F., Available water-holding capacity of alluvial soils in Louisiana, *Soil Sci. Am. Proc., 23,* 1-3, 1959.

Pengra, R. F., Agricultural drought in South Dakota, *S. Dakota Agr. Expt. Sta., Agr. Econ, Pamphlet 94,* 1958.

Penman, H. L., Estimating evaporation, *Trans. Am. Geophys. Union, 37,* 43-46, 1956.

Tharp, M. M., and C. W. Crickman, Supplemental irrigation in humid regions, *Yearbook Agr., U. S. Dept. Agr.,* 252-258, 1955.

Thornthwaite, C. W., J. R. Mather, and D. B. Carter, *Three water balance maps of eastern North America,* Resources for the Future, Inc., Washington, D. C., 1958.

Van Bavel, C. H. M., A drought criterion and its application in evaluating drought incidence and hazard, *Agron. J., 45,* 167-172, 1953.

Van Bavel, C. H. M., Agricultural drought and water surplus in the Lower Mississippi Valley, *U. S. Dept. Agr. Tech. Bull.,* (in press) 1959.

Van Bavel, C. H. M., and J. R. Carreker, Agricultural drought in Georgia, *Georgia Agr. Expt. Sta. Tech. Bull. New Ser. 15,* 1958.

Van Bavel, C. H. M., L. A. Forrest, and T. C. Peele, Agricultural drought in South Carolina, *S. Carolina Agr. Expt. Sta. Bull. 447,* 1957a.

Van Bavel, C. H. M., and J. Lillard, Agricultural drought in Virginia, *Virginia Agr. Expt. Sta. Tech. Bull. 128,* 1957b.

Van Bavel, C. H. M., and F. J. Verlinden, Agricultural drought in North Carolina, *N. Carolina State Coll., Agr. Expt. Sta. Tech. Bull. 122,* 1956.

Veihmeyer, F. J., and A. H. Hendrickson, Does transpiration decrease as the soil moisture decreases? *Trans. Am. Geophys. Union, 36,* 425-448, 1955.

(Manuscript received June 10, 1959; presented at the Fortieth Annual Meeting, Washington, D. C., May 4, 1959.)

Reducing Lake Evaporation in the Midwest

W. J. ROBERTS

State Water Survey Division
Urbana, Illinois

Abstract—During the summers of 1957 and 1958 studies were conducted on two lakes in central Illinois to determine a practical method of applying monomolecular layers and to learn the effectiveness of the layers in reducing evaporation. Results showed a saving of 43 per cent in 1957 and 22 per cent in 1958 of the water normally lost to evaporation. A method was developed for determining the strength of the monolayer by measuring the heat gradient near the water surface.

Introduction—Reducing evaporation from water surfaces has been studied extensively in the arid regions of Australia, Africa, and the United States, and interest in the subject is developing in humid regions as well. In the United States, for example, dry climatic conditions that are ordinarily associated with the Southwest have, during drought periods, extended into normally humid areas. Thus in Illinois where the rainfall is generally favorable, averaging from forty-seven inches in the south to thirty-two inches in the north, experiments in retarding evaporation were begun following the severe drought of 1951–1955.

Project area—In an earlier paper [*Roberts*, 1957] chemical studies and field research on this subject were reviewed, and a report was made on work done in 1956 by the Illinois State Water Survey with a fatty alcohol called hexadecanol. In the present paper a summary is given of results obtained during the summers of 1957 and 1958 when two adjacent lakes in central Illinois were made available for a study of ways of applying monolayers for suppressing evaporation from water surfaces. The lakes are located at the Department of Conservation fish hatchery near Mattoon in east central Illinois (Fig. 1). The north lake covers 2.8 acres and receives runoff from 2.4 acres of sodded grass. The south lake extends over 2.3 acres and has a watershed of 1.4 acres of relatively flat sod. The area which contributes runoff is west of the lakes, and the opposite shores of the lakes are bordered by levees. The lakes are adjacent to Paradise Lake, the municipal water source for Mattoon. Water from Paradise Lake can be pumped into either of the small lakes to compensate for water losses.

Each lake was equipped with an instrument pier on which automatic water-level recorders were installed. At various times, water-temperature and air-temperature recorders were located on the piers. A weighing-bucket rain gage was located to the west, near both lakes.

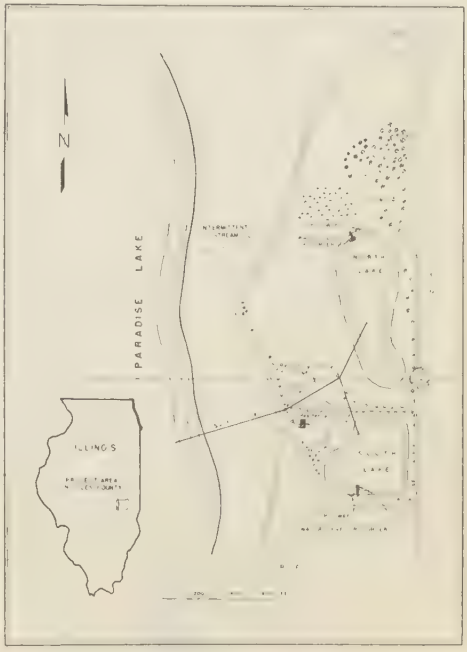

FIG. 1—Research area.

During the 1957 test, the south lake was used as a control, and all experiments with fatty alcohols were performed on the north lake. In 1958 this procedure was reversed; the south lake was used for testing and the north lake was a control.

Preliminary study—Six weeks of study preceded application of the first monolayers. The charts of lake level fluctuation showed nearly constant seepage from both lakes. This was determined by comparing the nighttime slope of the lake-level curves, when evaporation was negligible, with the daytime traces, which included evaporation. The same rate of evaporative loss from both lakes was assumed in order to study the seepage rate for different lake levels. Within measurable limits, no significant change in seepage rate could be detected. Water losses from both lakes were the same except after heavy rains, when the north lake, with its larger watershed, showed an apparent reduction in water-loss rate because additional runoff reached it. This effect seldom persisted for over 36 hours. During times when water was being added to one of the lakes, the water-level records were of little value for determining evaporative losses.

Application program—Beginning in late June 1957 various forms of hexadecanol and octadecanol were, in turn, spread on the lake. These included extrusions, flakes, beads, and powders. They were dispersed from mesh-float containers anchored in the lake, applied to the lake surface from a boat, or fed from slurry pots. Detection of film strength was made by tests already described [*Crow and Daniel,* 1957; *Bur. of Reclamation,* 1957].

Although normal dispersion tests work well under laboratory conditions, water surfaces can become coated with dust films which, by action of innumerable wicks of dust particles, increase evaporation rather than retard it. Under such conditions a temperature test, developed on this project, is a valuable tool. It has been demonstrated [*Roberts,* 1957] that a strong monolayer cover traps heat that is normally lost by evaporation. By measuring under shade and using a sensitive temperature probe in conjunction with a high-accuracy thermistor thermometer, it was possible to measure temperatures in the ¼ inch of water immediately below the monolayer surface which were 4° to 7°F warmer than in the control lake. Water temperature

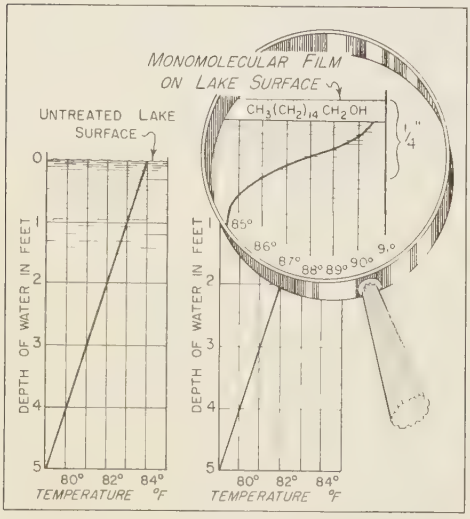

Fig. 2—Graphs of lake water temperatures with and without monomolecular film.

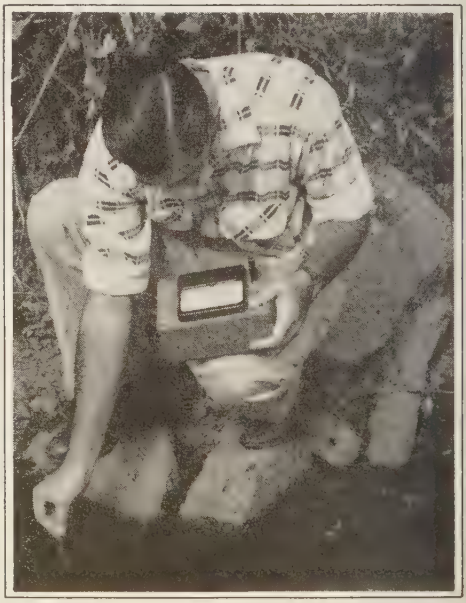

Fig. 3—Thermistor thermometer and temperature probe used to measure film temperature.

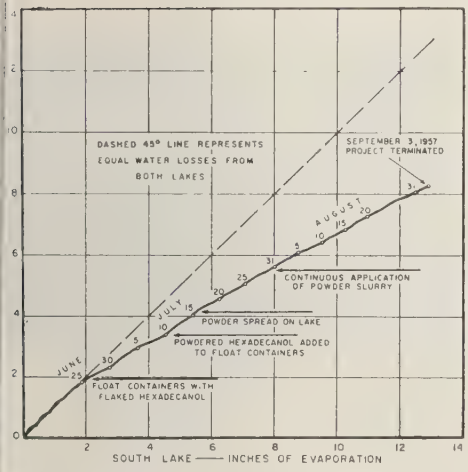

FIG. 4—Double-mass graph of 1957 experiments.

gradually decreased below that depth. This temperature difference could be detected whenever a strong film was present, and its absence indicated a weak or non-existent monolayer. The temperature curve is shown schematically in Figure 2. Apparatus for measuring temperature is shown in Figure 3.

The results of the 1957 tests are shown in Figure 4. This is a double-mass analysis [*Kohler*, 1949] in which the accumulated total of one series of observations is compared with the concurrent values of a second series. In the graph, daily amounts of evaporation from each of the lakes are plotted as rectangular coordinates, the north lake data being ordinates and the south lake data abscissas. Points falling on the 45° dashed line represent equal water losses. A section of the preliminary calibration period is included in the lower left of the double-mass plot to show that water losses from both lakes were practically equal before hexadecanol was used.

On June 26, 1957, two mesh-float containers, each holding 8 ounces of extruded hexadecanol, were placed in the north lake. In addition, one pound of hexadecanol in fine bead form was applied to the lake from a boat. The combination produced a strong monolayer as evidenced by tests on the following day. However, on the night of June 27 a storm deluged the area with 8 inches of rain. The chemical film was impaired, but it reformed during the following day.

FIG. 5—Hexadecanol cover in foreground produces calm water (compare with rippled surface).

On July 9 two new floats, each containing 10 ounces of powdered hexadecanol, were placed in the lake. Also, one pound of beaded hexadecanol was spread over the lake from a boat. This combination produced a strong monolayer which could be observed spreading against a 20-mile-per-hour wind (Figs. 5 and 6).

Although the powder in the floats spread when first put in the water, it tended to cake and remain in the floats. Also the floats accumulated growths which clogged the screens.

One week later tests indicated poor film coverage, so it was decided to omit the floats and spread the chemical manually from a boat rowed around the lake. This produced a good

FIG. 6—Same view as Fig. 5 taken fifteen minutes later. The monolayer had spread over all but a small central area of the lake.

monomolecular cover, but it was necessary to add the chemical daily in order to maintain measurable film strength.

Chemical life of film—A search of the literature showed that the dosage required for any water surface depends not only upon the quantity of the hexadecanol but also on the perimeters of the individual particles. The rate of spreading varies with the total length of the contact between the particles and the surface of the water. Therefore powdered hexadecanol was used to provide a very large perimeter for a given amount of material.

The rate at which a monomolecular layer of hexadecanol spreads [*Mansfield,* 1956] is 1.01 $\times$ 10^{14} molecules per centimeter per second, and the number of molecules required to form a complete monolayer of hexadecanol is 5.14 $\times$ 10^{14} molecules per square centimeter. Thus 5 cm of perimeter of solid should be sufficient to generate approximately 1 cm^2 of complete film per second.

Up to this point in our testing we had found that the physical form of hexadecanol had little effect on its active life. A study of the water-level recorders showed that there was appreciable reduction of evaporation from the treated lake for a maximum period of three days after each application of hexadecanol. After that time, biological attrition, together with physical factors such as wind and rain, removed the protective layer. It was apparent that before hexadecanol could retard evaporation efficiently it would be necessary to apply the chemical continuously.

Continuous film application—The month of August 1957 was spent in testing the effect of continuous application of powdered hexadecanol to the north pond. On July 30, 1957, a 20-gallon open-end tank (Fig. 7) was installed on the east shore of the north pond, and two similar tanks were installed on the west shore. These were filled with slurries of powdered hexadecanol which were permited to enter the lake through ¼-inch discharge pipes. Flow was controlled through valves so that approximately 100 drops of slurry per minute were permitted to enter the pond from each tank. Copper sulfate was added to each of the slurry pots to counteract biological attrition of the hexadecanol. The initial charge to each tank was 3 pounds of

FIG. 7—Hexadecanol slurry from tank generates monolayer as indicated by calm water. Fingers of monolayer from other tanks show at sides of pictures.

powdered hexadecanol mixed in a slurry with lake water. The tanks were inspected and serviced twice daily.

Theoretically, 0.02 lb of hexadecanol forms a compact monolayer film on an acre of water surface. In practice considerably more chemical is required. For instance, the three slurry pots discharged 6 pounds of powdered hexadecanol in 7 days, or enough chemical to cover nearly 100 acres of water at maximum efficiency.

In accounting for the wasted chemical, it is estimated that approximately one half collected along the leeward shores, where it was removed by birds and insects. Ducks taking off from the lake opened long gaps in the monolayer by removing the film on their feathers. Aquatic life nibbled at the surface frequently and biologic attrition of the layer was probably continuous. Thus only a small percentage of the original slurry was available to maintain the monolayer on the lake.

Cost of applying hexadecanol—The 25 pounds of hexadecanol which were used during the month of August 1957 cost sixty cents per pound or about fifteen dollars. As the north lake covered approximately three acres, 8 pounds per acre were required for the month. One third of a pound was left in each tank at the end of the testing period. Examination of the water-level records during August 1957 showed that the water which was saved was approximately 1/5 ft, or 43 per cent of the water which is

FIG. 8—Applying algaecide to south lake. Note heavy cover of aquatic growth.

normally lost to evaporation. The total saving amounted to 65,171 gallons per acre, or 7,600 gallons for each pound of hexadecanol used. Thus, the cost of saving 1000 gallons of water amounted to 8 cents, approximately $26 per acre-foot. This figure does not take into account the cost of the slurry tanks and fittings or the time necessary for servicing.

Research program for 1958—Aquatic vegetation was an objectionable factor during the 1958 study. Some algae growths developed on the periphery of both lakes during the 1957 experiments but these were controlled by application of copper sulfate. In September 1957 a heavy growth appeared on the south lake. This condition persisted throughout the winter, and in May 1958, 80 per cent of the lake was covered with aquatic growths. An algaecide was applied to the south lake on May 20 and one day later all aquatic growths submerged and were not in evidence throughout the summer of 1958 (Figs. 8 and 9).

FIG. 9—Same view as Fig. 8 taken one week later shows no evidence of algae growth.

During the summer of 1958 the experiments were repeated, with the north lake used as a control. Unfortunately, there were nearly 22 inches of well-distributed rainfall during the four months, May through August. In addition, temperatures were below normal. Consequently, natural evaporation was greatly reduced and there was little need for or effect from using monomolecular layers. However, the 1958 tests were valuable because they led indirectly to the finding of an effective means of removing algae growths from lake surfaces. They also provided additional evidence that the slurry method, as used in Texas [*Dressler and Johanson,* 1958; *Chem. Eng. News,* 1958], has advantages over other methods of generating monomolecular layers on small lakes in Illinois.

Figure 10 shows the results of the work in 1958. The water that was saved represents 22 per cent of that which was normally lost by evaporation.

Conclusion—Experience with the lakes at

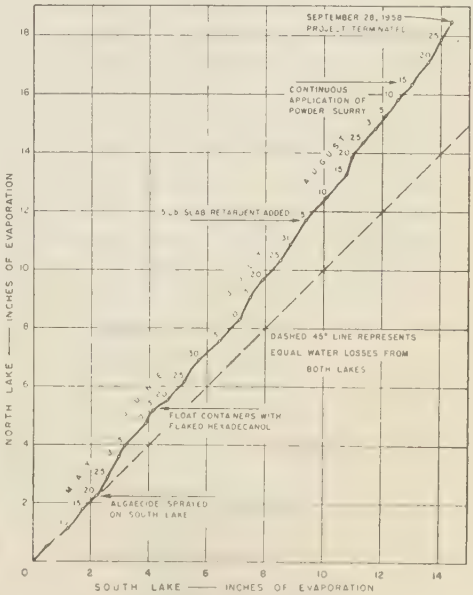

FIG. 10—Double-mass graph of 1958 experiments.

Mattoon indicates that the estimated cost is conservative. No attempt was made to limit the amount of hexadecanol used in order to arrive at a minimum cost. A stricter rationing of the chemical might have effected some saving of the monolayer which was washed up on the windward shore. Problems that ordinarily would not confront owners of small lakes occurred at these lakes because they were used constantly in the fish hatchery program. Thousands of fingerlings were added or removed from the lakes during the periods of testing. These plus other aquatic life, such as turtles, fed on the monolayer constantly. It seems reasonable that on an average small lake it would be possible to double the effect of the monolayer so that applying hexadecanol worth one cent at the present price would result in a saving of perhaps 250 gallons of water.

Acknowledgment—Arrangements for using the lakes were made through the cooperation of Sam A. Parr of the Illinois Department of Conservation. Richard Wiley, Fish Hatchery custodian, and his assistants cooperated constantly during the testing program. Their enthusiastic interest added greatly to the success of the project. This research was done under the general direction of William C. Ackermann and H. F. Smith.

References

Bureau of Reclamation, *Chem. Engineering Lab. Rept. SI-9,* January 1957.

Chemical and Engineering News, *Film Protects Climates' Prey,* 44–45, June 30, 1958.

Crow, F. R., and E. R. Daniel, Chemical means of controlling evaporation from open water surfaces, Paper presented at annual meeting of Amer. Soc. Agr. Engrs., East Lansing, Michigan, June 25, 1957.

Dressler, R. G., and A. G. Johanson, Water Reservoir evaporation control, *Chem. Eng. Progr., 54,* 66–69, 1958.

Kohler, M. A., Double-mass analysis for testing the consistency of records and for making required adjustments, *Bull. Am. Meteorol. Soc., 30,* 188–189, 1949.

Mansfield, W. W., The use of hexadecanol for reservoir evaporation control, *Proc., Intern. Conf. on Reservoir Control,* San Antonio, Texas, 1956.

Roberts, W. J., Evaporation suppression from water surfaces, *Trans. Am. Geophys. Union, 38,* 740–744, 1957.

(Manuscript received April 18, 1959; revised July 8, 1959; presented at the Fortieth Annual Meeting, Washington, D. C., May 4, 1959.)

A Note on the Field Use of a Theoretically Derived Infiltration Equation

K. K. WATSON

School of Civil Engineering, University of New South Wales
Sydney, Australia

Abstract—The use of equations of the diffusion type as a means of solving certain flow problems in porous media has recently led to a convenient analytical solution for the infiltration of water into an homogenous soil of uniform initial moisture content. From the general solution a simplified infiltration equation is obtainable. This simplified equation is tested against field infiltration curves in order to investigate its possible use for the expression of these field curves with a greater degree of accuracy that has hitherto been possible with the commonly known empirical equations, in particular the Horton equation.

Introduction—Many situations arise in field studies connected with applied hydrologic research and investigation in which it is most desirable to characterize the entry of water into the soil as infiltration by a small number of parameters. Generally these parameters are the coefficients of an algebraic equation, and they represent the variation of the cumulative infiltration or rate of infiltration with time. Until recently the available equations have been of an empirical nature; however, *Philip* [1957a] formulated from a fundamental theoretical approach an equation which expresses the relationship between the cumulative infiltration and the time from the start of infiltration. If certain terms in this equation are neglected, a simplified, manageable, and yet sufficiently accurate infiltration equation results. The application and possible use of this equation in expressing the results obtained in experiments with a sprinkling infiltrometer on a small rural catchment is considered in this paper.

The available infiltration equations—Brief mention must be made of the available infiltration equations and their limitations. Recently *Swartzendruber and Huberty* [1958] detailed some aspects of these equations; therefore the discussion here will be kept to a minimum.

Probably the infiltration equation which has found the widest usage in applied hydrologic studies is that which was first suggested in one form by *Gardner and Widtsoe* [1921] and was later, with some small modifications, well applied by *Horton* [1940].

$$f = f_c + (f_0 - f_c)e^{-\beta t} \tag{1}$$

where f is the infiltration rate at time t, f_0 and f_c are the initial and final values of the infiltration rate, and β is a constant.

In particular, the equation has been applied as a convenient and reasonably rapid method of expressing the results of experiments with a sprinkling infiltrometer. Because of this fact the data which have been chosen from the field experiments for the purpose of testing the theoretically derived equation have also been subjected to expression by equation (1).

This equation has the advantage that in the limit as t approaches infinity the infiltration rate does not approach zero. However it also has the two serious limitations that the representation is poor at small times (when there is a very rapid decrease of the infiltration rate from high values) and that three parameters are needed.

A simpler equation of the form

$$i = ct^{\alpha} \tag{2}$$

where i is the cumulative infiltration at time t and c and α are parameters, was first suggested by *Kostiakov* [1932]. The differential form of this equation yields the infiltration-rate equation

$$f = \alpha c t^{\alpha - 1} \tag{3}$$

The disadvantages of this equation lie in the fact that the parameters α and c vary according

to the range of t. It can be readily shown [*Philip*, 1957b] that for small times α has the value of $\frac{1}{2}$, whereas for large times α becomes unity and c assumes the value of the saturated hydraulic conductivity of the material.

Philip [1954] proposed a simplified physical model of infiltration in which he considered the application of Darcy's law to a system of vertical flow under gravity and under a constant capillary potential, which was considered to operate at the 'wet front.' By introducing approximations concerning the average moisture content down the profile and the status of the 'wet front,' he obtained an equation of the following form

$$t = Y\left[i - Z \log\left(1 + \frac{i}{Z}\right)\right] \qquad (4)$$

where Y and Z are constants.

The accuracy of the equation in any particular circumstance naturally depends on the validity of the simplifying assumptions for the physical conditions prevailing in that circumstance. Of importance in this regard is the degree of correspondence between the actual shape of the curve which represents the diffusivity function and the ideal shape assumed in the analysis. It may be noted that the use of t as the dependent variable results in the equation being awkward to handle.

The diffusion approach—Infiltration is one particular example of the general phenomenon of water movement in porous media, and accordingly in recent years the process has been studied utilizing the concept that soil-water movement may be satisfactorily expressed by equations of the diffusion type. In particular, we may state that there exists a general partial-differential equation of parabolic second order which describes liquid-phase water movement in a porous medium and which, for the case of vertical infiltration, may be expressed by equation (5) below. The total potential here comprises the gravitational and capillary pressures only and is a single valued function of the moisture content.

$$\frac{\partial \theta}{\partial t} = \frac{\partial}{\partial x}\left(D \frac{\partial \theta}{\partial x}\right) - \frac{\partial K}{\partial x} \qquad (5)$$

where

$D = K(\partial \Psi / \partial \theta)$ = diffusion coefficient

K = unsaturated hydraulic conductivity
θ = volumetric moisture content
x = vertical ordinate, positive downwards
Ψ = capillary potential

If the uniform initial moisture content is θ and there is free water available at the surface giving θ the value of θ_{sat} when $x = 0$, then the boundary conditions to the problem are

$$\theta = \theta_n, \qquad t = 0, \qquad x > 0$$

$$\theta = \theta_{sat}, \qquad x = 0, \qquad t \geq 0 \qquad (6$$

The most convenient and efficient solution o equation (5), subject to boundary conditions (6 is a numerical procedure developed by *Philip* [1957c]. As a first approximation to the solutio the transformation $\phi = xt^{-\frac{1}{2}}$ is employed i conjunction with equation (5), however neglect ing initially the gravitational term $\partial K/\partial x$. B iterative procedures the final solution of (5) i eventually obtained in the form

$$x = \phi t^{-1/2} + \chi t + \psi t^{3/2} + \cdots \qquad (7$$

where ϕ, χ, and ψ are functions of the moistur content θ.

The cumulative infiltration may then be ex pressed as

$$i = t^{1/2} \int_{\theta_n}^{\theta_{sat}} \phi \, d\theta + t\left(K_n + \int_{\theta_n}^{\theta_{sat}} \chi \, d\theta\right) + t^{3/2} \int_{\theta_n}^{\theta_{sat}} \psi \, d\theta + \cdots \qquad (8$$

where K_n = unsaturated hydraulic conductivity when $\theta = \theta_n$.

In general the expression for i may be safely limited to the first two terms in the series giving

$$i = t^{1/2} \int_{\theta_n}^{\theta_{sat}} \phi \, d\theta + t\left(K_n + \int_{\theta_n}^{\theta_{sat}} \chi \, d\theta\right) \qquad (9$$

Philip [1957b] proposes the term *Sorptivity* fo $\int_{\theta_n}^{\theta_{sat}} \phi \, d\theta$ and denotes it by S. It is a functio of θ_{sat} and θ_n and is a measure of the capillar uptake or removal of water. In this regard S i a property of the medium with some resemblanc to permeability, however its units are cm sec$^{-\frac{1}{2}}$. If $K_n + \int_{\theta_n}^{\theta_{sat}} \chi \, d\theta$ is denoted by A, then

$$i = St^{1/2} + At \qquad (10$$

id the infiltration rate is given by

$$f = \tfrac{1}{2}St^{-1/2} + A \qquad (11)$$

Equation (11) is a simple equation which is based on physical theory and is accurate for all but very large t, since as $t \to \infty$ equations (10) and (11) must fail.

The influence of field conditions—Two matters must be touched upon as a necessary preface to the consideration of the influence of field conditions. First, the analytical solution of the infiltration problem as summarized above has not gone uncompared with laboratory experiments. *Youngs* [1957], with careful instrumentation, carried out a series of infiltration experiments and compared the developed moisture profiles with those computed by the analytical solution. The agreement was found to be very good. The second matter concerns the testing of the available equations against the analytical solution. *Philip* [1957b], using the laboratory data of *Moore* [1939] on the moisture characteristic and the relationship between the moisture content and the unsaturated hydraulic conductivity, carried out such a test. Of import for this discussion is the comparison of the Horton equation and the simplified Philip equation with the full analytical solution. The latter may be summarized by saying that the simplified equation gave almost exact correspondence, whereas the Horton equation gave very considerable errors in the cumulative infiltration at times up to 10^6 seconds.

With this recent laboratory and analytical support for the simplified theoretical equation, one mechanism which was present in the laboratory experiments and is implicit in the mathematical approach must not be lost sight of. It concerns the removal of the air from the pore spaces during the downward movement of the wet front.' This air is free to escape from the media via the open end of the column; there is no counterpart to this in infiltration into field soils. This fact, together with the poor result obtained in attempting to fit the Horton equation to the analytically computed cumulative infiltration curve as mentioned above, must be considered, for, in defence of the Horton equation, many results have been presented in the last two decades in which the Horton equation has represented field infiltration curves quite reasonably. Does the mechanism of the air removal and the influence of field conditions, such as sub-surface cracking, root penetration, raindrop compaction, and like effects so modify the situation that the equation, which gave poor results from the analytical viewpoint, may be used with confidence with field curves? The other side of the argument is also of the utmost importance here, namely the adequacy of the analytically derived equation to express the field infiltration curves when factors other than those covered in the basic assumptions are operative. Naturally the degree to which the field soils simulate the analytical model, particularly as regards a constant moisture profile, will have a prominent bearing on the result.

Comparison of the curves—The method of approach in obtaining the required comparisons was to compute the various parameters of the equations in question so that the best fit would be obtained with the field infiltration curve. This curve was determined from an analysis of the plot rainfall and runoff curves, due allowance being made for the effects of depression storage and surface detention.

The method of least squares appeared to be the most satisfactory means of determining the parameters S and A in the Philip equation. However, this method of determination is time consuming by ordinary procedures, and, since the merit of an algebraic expression is greatly diminished unless it can be rapidly obtained, an alternative means of applying the method was sought. A suitable program was worked out for a DEUCE-type electronic computer in which the ordinates of the field curve were used, and the least-square analysis and the parameters were determined in a matter of minutes. The form of the Horton equation is such that greatly increased benefit would not have occurred by using the computer, and accordingly the necessary parameters in the equation were determined by the available published methods [*Horton*, 1940].

This short paper is intended to be only a note on this work; accordingly, a number of the available curves for different soil types and antecedent moisture conditions are not included but only one average case is considered. The three curves of interest for this one case are given in Figure 1.

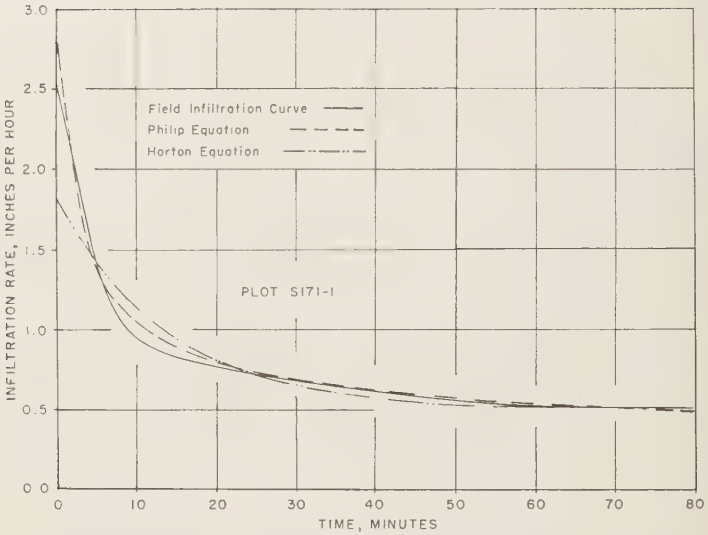

FIG. 1—The field infiltration curve compared with best-fit curves determined by the Horton equation and the simplified Philip equation.

Before commenting on these curves a brief note is necessary regarding the physical conditions on this plot at the time of the experiments with the sprinkling infiltrometer. The soil profile may be summarized as

0″–5″ Surface soil; brown silty clay loam
5″–6″ Transition horizon of red medium clay; barely evident
6″–16″ Sub-soil of red heavy clay
16″–72″ Deep sub-soil of grey heavy clay

Due to a prolonged dry period before the test the moisture profile was reasonably uniform to a depth of 18 inches. At this prevailing moisture content some cracking was evident in the clay but this was not excessive. The surface was well grassed.

From a study of the curves given in Figure 1 attention is initially focused on the early section of the infiltration curve where there is a rapid decrease of the infiltration rate with time. As the comments on the Horton equation earlier in this paper indicated, this equation is of such form that it does not represent this section of the curve with accuracy. In contrast to this, the degree of correspondence of the Philip equation at small times is very good.

It is common in most sprinkling-infiltrometer experiments that derived infiltration curves become sensibly parallel to the time axis at relatively small times, say of the order of 90 minutes. The form of the Horton equation is such that this value f_c can be fully characterized by the equation, and it yields an exact correspondence at the particular time t_c of constancy of the infiltration rate. The Philip equation however requires additional comments on this matter. The position is that in the majority of cases the least-square analysis results in the equation closely representing the field curve in the vicinity of the f_c value. However at times greater than t_c, particularly when t_c is small (such as 90 minutes), the computed curve will continue to slope towards the time axis and will result in an increasingly greater deviation from the sensibly constant f_c value. The solution to this aspect lies in specifying that the computed equation is only valid in the range of 0 to t_c. Such a 'limit of validity' for the computed equation would also naturally require the least-square analysis to be carried out only over this range.

In conclusion, therefore, it may be stated that the theoretically derived Philip equation represents the field infiltration curve particularly well at small times when the infiltration rate is changing rapidly with time. In addition, the

egree of representation is good over other sec-ons of the curve, although the stipulation must e made that it can only be applied up to time . For times greater than t_o the infiltration rate assumed to be the f_o value. The use of the ethod with other soil types and other ante-edent conditions has yielded similar results.

References

ARDNER, W., AND J. A. WIDTSOE, The movement of soil moisture, *Soil Sci., 11,* 215–232, 1921.

ORTON, R. E., Approach toward a physical interpretation of infiltration capacity, *Soil Sci. Soc. Am. Proc., 5,* 399–417, 1939.

OSTIAKOV, A. N., On the dynamics of the coefficient of water-percolation in soils and on the necessity for studying it from a dynamic point of view for purposes of amelioration, *Trans. Sixth Comm. Intern. Soc. Soil Sci., Russian pt. A,* 17–21, 1932.

MOORE, R. E., Water conduction from shallow water tables, *Hilgardia, 12,* 383–401, 1939.

PHILIP, J. R., An infiltration equation with physical significance, *Soil Sci., 77,* 153–157, 1954.

PHILIP, J. R., The theory of infiltration: 1, *Soil Sci., 83,* 345–357, 1957a.

PHILIP, J. R., The theory of infiltration: 4, *Soil Sci., 84,* 257–264, 1957b.

PHILIP, J. R., Numerical solution of equations of the diffiusion type with diffiusity concentration-dependent, *Australian J. Phys., 10,* 29–42, 1957c.

SWARTZENDRUBER, D., AND M. R. HUBERTY, Use of infiltration equation parameters to evaluate infiltration differences in the field, *Trans. Am. Geophys. Union, 39,* 84–93, 1958.

YOUNGS, E. G., Moisture profiles during vertical infiltration, *Soil Sci., 84,* 283–289, 1957.

(Manuscript received June 4, 1959.)

Variations in the Net Exchange of Radiation from Vegetation of Different Heights[1]

WAYNE L. DECKER

Department of Soils, University of Missouri
Columbia, Missouri

Abstract—The measurements of net radiation from one ventilated and two unventilated radiometers were compared, and instrumental corrections were made. Using these radiometers, net radiation was measured from a short grass turf, an alfalfa field, and a corn plot. The magnitude of the net radiation term from the three covers decreased with decreasing height of the vegetative cover. The possible effect which these radiation differences might have on evapotranspiration is discussed.

Introduction—Varying quantities of energy each the surface of the earth through radiative ransfer of heat. A portion of this energy is ceived as radiation of short wavelengths from ae sun and sky, and the remainder is the radia- on of energy in the long wavelengths from the tmosphere. The surface of the earth constantly ssipates the heat received through radiative rocesses. The earth reflects a portion of the nergy of short wavelengths it receives and diates energy of long wavelengths. The heat hich remains or is required by the surface of ie earth after all radiative exchange has oc- urred is called the net radiation.

The net radiation is thermal energy and may e mathematically defined as

$$H = I - rI - R_e \qquad (1)$$

here

I is the short-wave energy from the sun and sky

r is the albedo of the surface for short-wave radiation

R_e is the net longwave radiation

he term R_e is not the simple black-body radia- ion from the familiar relationship of the fourth ower of the absolute temperature. It is the et exchange of energy radiated in the long avelengths between the earth, the clouds, and he atmospheric gases. The net exchange of ng-wave energy is the black-body radiation corrected for moisture content of the atmosphere and cloud cover.

Net radiation is an important concept to geophysics because it represents the amount of energy available for thermal and biological processes. The direction and amount of the sensible heat transferred between the earth and the atmosphere is determined by the sign and magnitude of the net radiation term. In

FIG. 1—A ventilated net radiometer (Beckman & Whitley).

[1] Contribution from the Missouri Agricultural Experiment Station. Journal Series No. 2013.

addition, net radiation supplies the energy for the evaporation of water at the surface of the earth.

Measurement of net radiation—Radiometers for measuring all the components of equation (1) are not commercially available. Indeed, the components of this relationship are not important, and instruments are available for direct measurement of the net radiation. Such instruments have been described by *Gier and Dunkle* [1951], and by *Suomi and others* [1954]. These instruments are ventilated to maintain a constant air movement over the heat-exchange plate. In Figure 1, a commercial adaptation of a ventilated net radiometer is shown.

In order to overcome the expense of the ventilated radiometer and to make possible net radiation measurements without ventilation, *Suomi and Kuhn* [1958] designed an economical net radiometer. This instrument utilizes the temperature of two blackened plates of copper which have been thermally insulated from one another. One is exposed to the sky and the other is exposed to the earth's surface. The use of the economical radiometer must be limited to hours of daylight because the accumulation of dew on the instrument at night impairs its accuracy. An economial radiometer is pictured in Figure 2.

Instrumental corrections for economical radiometers—In order to compare the response of the economical radiometer with that of a ventilated radiometer, simultaneous measurements were taken over a short bluegrass turf. Two economical radiometers, which were designated *A* and *B*, were exposed near a single ventilated radiometer. Upon reviewing the series of observations, *Decker and Gerber* [1959] noted that consistent differences existed between the economical and ventilated radiometers over the entire range of values.

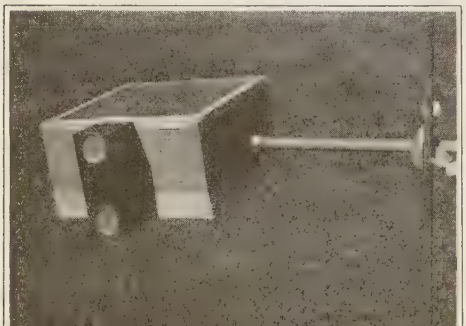

Fig. 2—An economical net radiometer (Ag-met).

Radiometer *A* averaged 3.1 langleys per hour and radiometer *B* averaged 1.5 langleys per hour below the net radiation indicated by the ventilated radiometer. When tested, the mean differences between the measurements from the economical and ventilated radiometers were significant at the 1 per cent level. The responses of the two economical radiometers also differed by a significant amount. These statistical tests indicated that the responses of the radiometers were not the same.

Net radiation from vegetative covers of different heights— Measurements of net radiation were taken from three types of cover, using the two economical radiometers and one ventilated radiometer. The ventilated radiometer was permanently installed above a bluegrass turf, which was cut to a height of 2 to 4 inches. The two economical radiometers were exposed periodically over either an alfalfa field or a corn field. The alfalfa ranged in height from 1 to 3 feet and the corn was about 10 feet high at the time the observations were made. All observations with the economical radiometers were made during the daylight hours.

The comparisons of the mean values obtained from each cover are shown in Table 1. It was necessary to include in these calculations the correction for instrumental differences.

During the daylight hours higher values of net radiation occurred with the taller types of vegetative cover. It is uncertain whether these results would be duplicated in other years and other locations. Since replicated observations were not made, statistical tests are not available for determining the significance of the mean difference between covers. When the economical and ventilated radiometers were exposed over the bluegrass cover the standard error of the mean differences was 0.5 langley per hour. If the standard error of the mean difference between radiometers is of the same order of magnitude when bluegrass is compared with the other covers, these results are significant.

Interpretation of results—The net radiation term is positive during the daylight hours; in

E 1—*Computation of the difference in the average net radiation received from over alfalfa and corn covers when compared with a short turf of bluegrass*

Item	Measurements from economical radiometers over *corn* and ventilated radiometer over grass		Measurements from economical radiometers over *alfalfa* and ventilated radiometer over grass	
	Economical *A* versus ventilated	Economical *B* versus ventilated	Economical *A* versus ventilated	Economical *B* versus ventilated
ber of observations	29	33	58	9
n economical diometer ly/hr	50.9	52.4	44.6	35.5
n ventilated diometer ly/hr	*45.4*	*49.1*	*44.7*	*31.0*
nomical minus ntilated ly/hr	5.5	3.3	−0.1	4.5
umental difference ly/hr	*+3.1*	*+1.5*	*+3.1*	*+1.5*
l net radiation fference ly/hr	8.6	4.8	3.0	6.0
ghted mean of difference in t radiation from selected ver and grass ly/hr	6.8		3.4	

r words, heat is being supplied to the vege- ve region of the soil and atmosphere. This e warms the soil and the atmosphere and porates moisture.

he results indicate that more heat is avail- in the case of corn and alfalfa covers than bluegrass. If the amount of heat supplied he soil and atmosphere were the same for three covers, the extra energy would be l in the evapotranspirational processes. As sult the taller covers would transpire more er than the shorter vegetation. This con- ion is contrary to the assumptions of the t-balance technique for estimating evapo- nspiration as described by *Penman* [1956]. t is interesting to contemplate how much er could be evaporated by the reported dif- nces in net radiation. Since 1500 langlies e required to evaporate an inch of water, the ess of net radiation for the corn and alfalfa ld evaporate an average of 0.0045 and 23 inch of water per hour more than the egrass cover. These averages seem small, but number of daylight hours during late sum- r ranges from 13 to 15 hours. These small erences may reflect evaporation differences 0.03 to 0.06 inch per day. These daily values of considerable size when compared with average evapotranspiration of 0.17 inch per y, which was measured from the corn and alfa covers.

The results are speculative and are presented primarily to stimulate thought and measurements by others. The excess of net net radiation for the taller plant covers may not have been used in the evaporative process. Further studies are planned which will include estimates of heat transfer by mechanisms other than evaporational processes. Also under consideration are measurements of net radiation from different types of covers during the hours of darkness.

Acknowledgment—Partial support for the research reported in this paper was obtained from the U. S. Weather Bureau through contract cwb-9296.

References

Decker, W. L., and J. F. Gerber, Field measurements of evapotranspiration as related to environmental factors, *Final Rept. U. S. Weather Bur. Contract cwb-9296*, University of Missouri, Columbia, Missouri, 1959.

Gier, T. T., and R. V. Dunkle, Total hemispherical radiometers, *Trans. Am. Inst. Elec. Engrs. 70*, 339–343, 1951.

Penman, H. L., Estimating evaporation, *Trans. Am. Geophys. Union, 37*, 43–50, 1956.

Suomi, V. E., M. Frassila, and N. F. Islitzer, An improved net-radiation instrument, *J. Meterol., 11*, 276–282, 1954.

Suomi, V. E., and P. M. Kuhn, An economical net radiometer, *Tellus, 10*, 160–163, 1958.

(Manuscript received June 15, 1959.)

Extension of a Definition of Constancy to Noncircular Normal Distributions

C. E. ABRAHAM AND W. H. BRADFORD

Sandia Corporation
Albuquerque, New Mexico

Abstract—British meteorologists have extensively used a measure of wind constancy based on the assumption of circular normal distribution of wind velocities. In the present paper the definition is extended to include the noncircular case and results are exhibited in the form of graphs and nomographs.

Introduction—Workers in fields involving vector statistics may encounter situations in which circularity commonly required of normal distributions of vectors is too restrictive. Meteorologists, in particular, may have occasion to analyze sets of winds which are more adequately described by the noncircular normal distribution than by the more specialized circular case. A series expansion for computing the distribution of wind speeds for noncircular normal distributions has been derived [*Davies*, 1958]. *Scott* [1956] has derived a formula for the probability that a vector of the distribution has its end point on a given contour of the distribution. *Van Becklin and Murray* [1956] have discussed applications of the noncircular normal distribution related to the bombing of offset circular targets; alternate methods are given by *Groves* and *Smith* [1957]. A measure of wind constancy based on the assumption of a circular normal distribution of wind velocities is defined and tabulated by *Brooks and Carruthers* [1953] on page 198.

The purpose of the present paper is to extend this definition to the noncircular case. Also, it is suggested that the constancy number associated with a noncircular normal distribution of vectors may be useful in certain Monte Carlo processes as a measure of the expected straightness of broken-line paths generated by choosing vectors of the distribution and laying them end to end.

The noncircular normal distribution—Figure 1 presents the essential idea of the distribution to be considered. A constant vector $\mathbf{V}_r$, called the vector mean, is chosen along the positive x-axis.

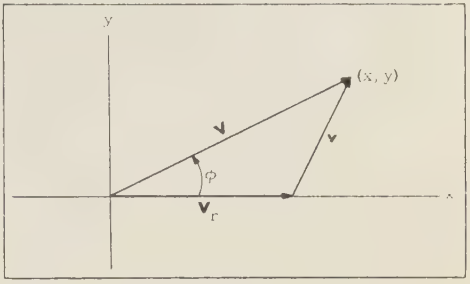

FIG. 1—Wind vector **V**.

The frequency distribution of end points of vectors is assumed to be given by the expression

$$\frac{1}{2\pi\sigma_x\sigma_y}\exp\left\{-\frac{1}{2}\left[\frac{(x-V_r)^2}{\sigma_x^2}+\frac{y^2}{\sigma_y^2}\right]\right\} \quad (1)$$

where V_r is the magnitude of $\mathbf{V}_r$ and where σ_x and σ_y denote standard deviations of velocity components along and perpendicular to $\mathbf{V}_r$. The vector deviation of a particular vector **V** from the vector mean $\mathbf{V}_r$ is represented by **v**. The angle ϕ is used later in the polar coordinate form of (1). The mean value V_s of the magnitudes of the vectors of the distribution is given by the integral

$$V_s = \frac{1}{2\pi\sigma_x\sigma_y}\int_{-\infty}^{\infty}\int_{-\infty}^{\infty}\sqrt{x^2+y^2}\cdot\exp\left\{-\frac{1}{2}\left[\frac{(x-V_r)^2}{\sigma_x^2}+\frac{y^2}{\sigma_y^2}\right]\right\}dx\,dy \quad (2)$$

The ratio $q = V_r/V_s$—As a measure of wind constancy, meteorologists use the ratio $q =$

V_r/V_s; that is, the magnitude of the mean vector of a set of vectors divided by the mean of their magnitudes. There is also a sense in which this ratio applied to a set of displacement vectors in a plane provides a measure of 'straightness' of the broken line formed by placing the vectors end to end. Consider, for example, the broken line of Figure 2. The value of the ratio

$$q = \frac{|\mathbf{V}_1 + \mathbf{V}_2 + \mathbf{V}_3|}{|\mathbf{V}_1| + |\mathbf{V}_2| + |\mathbf{V}_3|} \tag{3}$$

is a measure of the straightness of the broken line *ABCD*. This definition associates $q = 1$ with a set of displacement vectors all having the same sense and direction. The ratio q has been defined for theoretical distributions of vectors [*Brooks and others*, 1950] and is developed here for the noncircular normal distribution in a plane.

Although the principal interest in the above notion has been among British meteorologists, it may be useful in the following context. Suppose it is desired to simulate a large number of ground paths of floating particles carried by a wind whose direction and velocity features are described satisfactorily by a noncircular normal distribution. Paths having some natural degree of straightness are generated if each leg of each simulated path is obtained by adding some deviation vector $\mathbf{v}$, with components $\mathbf{v}_x$ and $\mathbf{v}_y$ chosen at random from normal distributions $(0, \sigma_x)$ and $(0, \sigma_y)$, respectively, to the constant mean vector $\mathbf{V}_r$. The straightness number of each path generated by the above process converges, in probability, to the ratio $q = V_r/V_s$, where V_s is given by (2), as the number of its legs increases.

A series expansion of V_s—The integral defining V_s for the noncircular normal case, (2), is written conveniently in polar form using V as the radius vector and ϕ as the polar angle of the transformation. With this transformation,

$$V_s = \frac{\exp\left\{\frac{-V_r^2}{2\sigma_x^2}\right\}}{2\pi\sigma_x\sigma_y} \int_0^{\infty}\int_0^{2\pi} V^2 \exp\left\{-\frac{V^2}{2\sigma_y^2}\right\} \cdot \exp\left\{\frac{V V_r \cos\phi}{\sigma_x^2} + \frac{V^2\cos^2\phi}{2}\left(\frac{1}{\sigma_y^2} - \frac{1}{\sigma_x^2}\right)\right\} dV\, d\phi \tag{4}$$

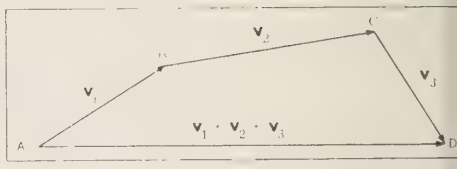

FIG. 2—Vector addition of $\mathbf{V}_1$, $\mathbf{V}_2$, and $\mathbf{V}_3$.

It can be shown by elementary theorems tha the above integral can be evaluated by expandin the integrand in series and integrating term wise. By this means the following series positive terms are obtained.

$$V_s = \frac{\sqrt{\pi}\,\sigma_y^2}{\sqrt{2}\,\sigma_x} \exp\left\{-\frac{V_r^2}{2\sigma_x^2}\right\} \cdot \sum_{i=0}^{\infty}\sum_{j=0}^{j=i} a_{ij}\left[1 - \left(\frac{\sigma_y}{\sigma_x}\right)^2\right]^{i-j}\left[\frac{\sigma_y V_r}{\sigma_x^2}\right]^j \tag{5}$$

where

$$i = 0, 1, 2, 3, \cdots,$$

$$j = 0, 2, 4, 6, \cdots,$$

and

$$a_{ij} = \frac{(2i - j + 1)!(2i - j)!}{2^{4i-5/2i}[(i - j/2)!]^3(i - j)!j!}$$

for $\sigma_y \leq \sigma_x$; and

$$V_s = \frac{\sqrt{\pi}\,\sigma_x^2}{\sqrt{2}\,\sigma_y} \exp\left\{-\frac{V_r^2}{2\sigma_x^2}\right\} \cdot \sum_{i=0}^{\infty}\sum_{j=0}^{j=i} b_{ij}\left[1 - \left(\frac{\sigma_x}{\sigma_y}\right)^2\right]^{i-j}\left[\frac{V_r}{\sigma_x}\right]^j \tag{6}$$

where

$$i = 0, 1, 2, 3, \cdots,$$

$$j = 0, 2, 4, 6, \cdots,$$

and

$$b_{ij} = \frac{(2i - j + 1)!(2i - 2j)!}{2^{4i-5/2i}[(i - j/2)!]^2[(i - j)!]^2(j/2)}$$

for $\sigma_x \leq \sigma_y$. (The computation program requir positive terms.)

When $\sigma_x = \sigma_y$, (5) and (6) reduce to

$$V_s = \frac{\sqrt{\pi}\,\sigma}{2} \exp\left\{-\frac{V_r^2}{\sigma^2}\right\} \sum_{n=0}^{\infty} \frac{(2n + 1)!V}{(2\sigma)^{2n}(n!)^3}$$

$$= \frac{\sqrt{\pi}\,\sigma}{2} \exp\left\{-\frac{V_r^2}{\sigma^2}\right\} {}_1F_1\left(\frac{3}{2}, 1; \frac{V_r^2}{\sigma^2}\right)$$

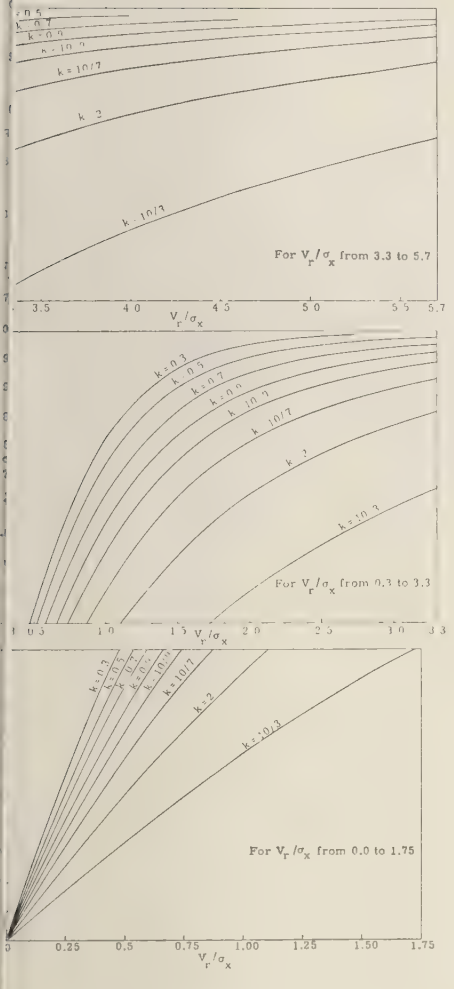

FIG. 3—The constancy ratio q for three ranges of V_r/σ_x.

ere ${}_1F_1(3/2, 1; V_r^2/\sigma^2)$ is the confluent hyper-ometric function, and $\sigma = \sqrt{2}\,\sigma_x = \sqrt{2}\,\sigma_y$.

Results—It is convenient to estimate q by t estimating its reciprocal. For this purpose and (6) are divided by V_r and the series nputed for various ratios of $k = \sigma_y/\sigma_x$. Figure hows q versus V_r/σ_x for the following values k: 3/10, 1/2, 7/10, 9/10, 10/9, 10/7, 2, and /3.

Summation of the series for values of k out-le the range 3/10 to 10/3 was not attempted, since it is thought that such values of k would not often be of interest and also because the summation was made somewhat prohibitive by a decreasing rate of convergence; for $k = 3/10$ it was necessary to sum 73,768 terms to find $q = 0.992$.

Nomograms for the above-mentioned values of k are given in Figures 4 and 5, which show the relation between q, V_s, V_r, and σ, where σ is defined by

$$\sigma_x^2 + \sigma_y^2 = \sigma^2$$

These nomograms show that if one of the four values of q, V_s, V_r, and σ is selected, a range of values exists for the other three, whereas if any two values are selected, the remaining two are uniquely determined. For example, in the noncircular normal distribution if $\sigma_y = 0.5\sigma_x$ (Fig. 4), $\sigma = 4$, and $V_r = 3$, $q = 0.697$ and $V_s = 4.3$. Also, values of V_r, V_s, and σ outside the range shown may be scaled so that the nomograms will apply. Thus, $V_r = 20$ and $\sigma = 30$ correspond to $V_r = 2$ and $\sigma = 3$ to yield $V_s = 31$ and $q = 0.643$.

For $\sigma_x = \sigma_y$ our results agree with those of *Brooks and others* [1950].

Details concerning computational techniques, IBM 704 EDPM program, accuracy criteria, convergence of the double series, additional nomograms, and numerical tables are found in another publication [*Abraham and Bradford*, 1959].

Acknowledgment—This work was performed at Sandia Corporation under AEC Contract AT-(29-1)-789.

References

Abraham, C. E., and W. H. Bradford, Extension of a definition of constancy to noncircular normal distributions, *Sandia Corporation Tech. Mem. SCTM 54–59(51)*, 57 pp., 1959.

Brooks, C. E. P., and N. Carruthers, *Handbook of Statistical Methods in Meteorology*, Her Majesty's Stationery Office, London, 412 pp., 1953.

Brooks, C. E. P., C. S. Durst, N. Carruthers, D. Dewar, and J. S. Sawyer, Upper winds over the world, *Geophys. Mem. 85*, His Majesty's Stationery Office, London, 150 pp., 1950.

Davies, M., Noncircular normal wind distributions, *Quart. J. Roy. Meteorol. Soc., 84*, 277–279, 1958.

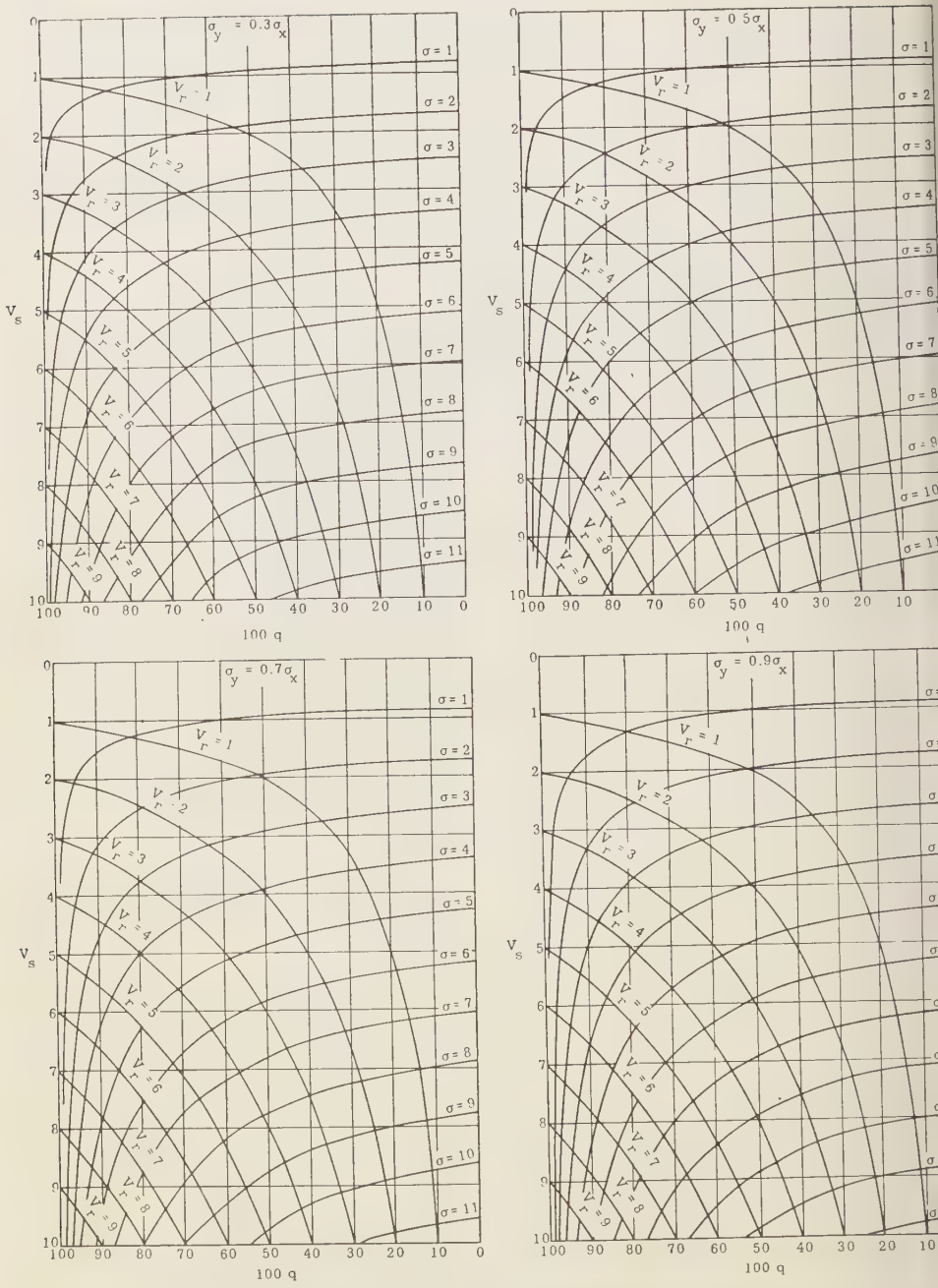

FIG. 4—Nomograms of $q = V_r/V_s$ for $\sigma_y = 0.3\sigma_x$, $0.5\sigma_x$, $0.7\sigma_x$, and $0.9\sigma_x$, where $\sigma = \sqrt{\sigma_x^2 + \sigma_y^2}$.

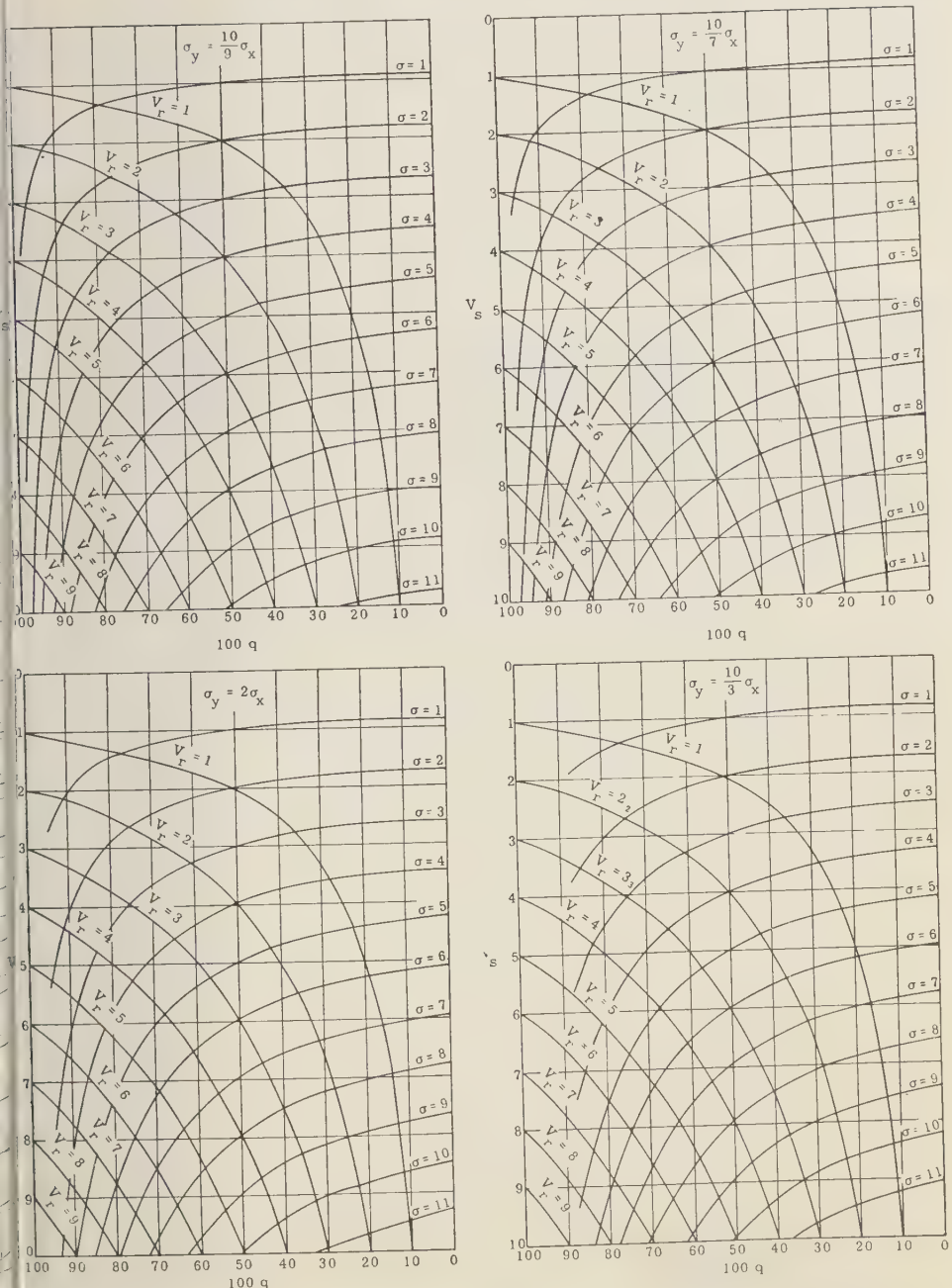

FIG. 5—Nomograms of $q = V_r/V_s$ for $\sigma_y = 10/9\sigma_x$, $10/7\sigma_x$, $2\sigma_x$, and $10/3\sigma_x$, where $\sigma = \sqrt{\sigma_x^2 + \sigma_y^2}$.

Groves, A. D., and E. D. S. Smith, Salvo hit probabilities for offset circular targets, *Operations Research, 5,* 222–228, 1957.

Scott, J. R., A note on the parametric representation of noncircular wind distributions, *Quart. J. Roy. Meteorol. Soc., 82,* 87–88, 1956.

Van Brocklin, G. R., and P. G. Murray, A polar planimeter method for determining the probability of hitting a target, *Operations Research 4,* 87–91, 1956.

(Manuscript received April 30, 1959.)

Letters to the Editor

LANGMUIR PROBE MEASUREMENTS IN THE IONOSPHERE[1]

R. L. Boggess, L. H. Brace, and N. W. Spencer

Department of Electrical Engineering
University of Michigan, Ann Arbor, Michigan

The electron temperature and positive-ion number density of the ionosphere E layer were measured above Fort Churchill, Manitoba, Canada, on November 30, 1958, through the use of a rocket-borne adaptation of a Langmuir probe. The design adopted was considered an exploratory experiment that would provide a basis for future ionospheric probes. Therefore establishing the reasonableness of the theoretical treatment [*Hok and others,* 1953],[2] developing an appropriate experimental technique, and determining ionospheric parameters were regarded as equally important.

Earlier attempts [*Hok and others,* 1951] to use a rocket-borne probe were hampered by design concessions made for other experiments on the same rocket and by aerodynamic considerations important during the early part of the flight. Such probes generally yielded ambiguous results; thus the present probe was ejected from the rocket both to avoid the need for such design compromises and to permit complete isolation in the ionosphere. Other objectives in the design were to provide a simple geometry for mathematical convenience, to prevent overlap of the sheaths and gas contamination of the environment, and to investigate the telemetry-antenna field disturbance of the plasma and possible photoelectric effect.

The bipolar arrangement that was chosen consisted of two 6-in. spheres separated by a 1-in. long, 2¼-in.-diameter cylinder (Fig. 1).

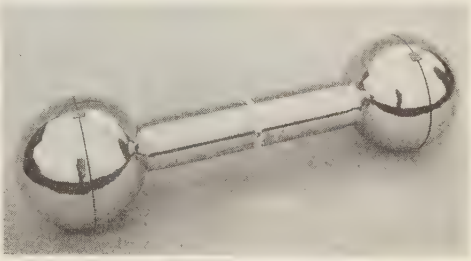

Fig. 1—Photograph of ionosphere Langmuir probe.

This configuration permitted fewer theoretical assumptions and minimized the practical problems encountered in the design of the probe circuits and the telemetry antenna. Each sphere was composed of two electrically insulated hemispheres; the outer hemispheres acted as information electrodes, and the inner 'funnels' (the inner hemisphere plus half the cylindrical section) acted as guard electrodes. A volt-ampere curve was obtained by varying the voltage between the information electrodes and between the guard electrodes while measuring only the current between the information electrodes. The resulting volt-ampere characteristic is a function of electron temperature, ion number density, electron number density, ion temperature, particle energy distribution, and probe geometry, as well as other, less significant factors.

In data reduction, the electron current to the electrode drawing a net positive-ion current from the ionosphere is measured by the difference between the extended ion-current saturated region and the volt-ampere characteristic. A typical experimental curve (AC) with the ion-saturated part (BC) extended is shown in Figure 2.

The electron temperature is determined, as in

[1] This work was made possible by the joint support of the Ballistic Research Laboratory of Aberdeen Proving Ground and the Geophysics Research Directorate of the Air Force Cambridge Research Center.

[2] A technical report on design and analysis is in preparation.

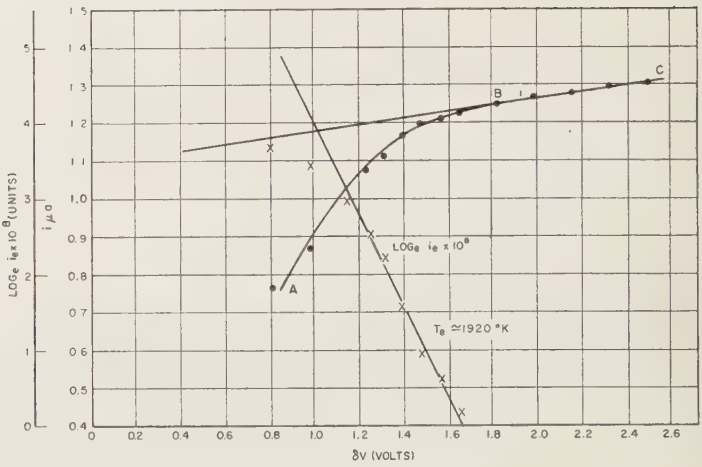

FIG. 2—Typical experimental volt-ampere characteristic and corresponding log I vs. E curve.

other Langmuir probe applications, from the slope of the log of the electron current, also shown in Figure 2. The log of the current was found to be a nearly straight line, thus indicating a Maxwellian energy distribution among the electrons measured.

The validity of the current magnitude measured could be verified periodically throughout the flight by substituting a known resistance 'for the ionosphere.' Calibration of the equipment in terms of electron temperature and density was not considered feasible, owing to the difficulties and uncertainties in simulating an ionospheric environment in the laboratory.

The electron temperatures shown in Figure 3 (each volt-ampere curve yields a temperature) are, in general, the average of three measurements taken during a small altitude interval. The spread indicated on each point represents an attempt to evaluate the standard deviation. Temperatures below 111 km were not obtained, owing to too low currents, indicating that the probe had not entered the E layer below this altitude (corroborated by simultaneously recorded ionograms). Temperatures above 177 km could not be determined on account of saturation of the current-measurement system.

Several interesting ionospheric features are suggested by these data: (*a*) the electron temperature is higher than the predicted kinetic gas temperature (1956 ARDC); (*b*) the temperature gradients are greater than tho normally expected; and (*c*) the apparent ter perature minimum at 175 km, previously su pected,[3] has not been seen in model atmosphere

High kinetic gas temperature and temper

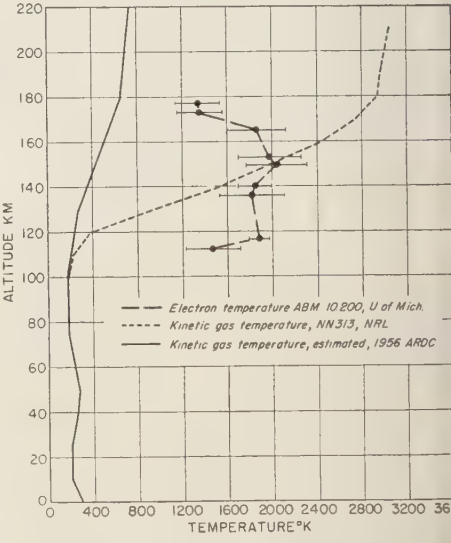

FIG. 3—Electron and neutral particle temper ture vs. altitude, November 30, 1958, Fort Churc ill, Canada.

[3] Informal, personal discussion with H. Kallma RAND Corporation, and H. E. Newell, NASA

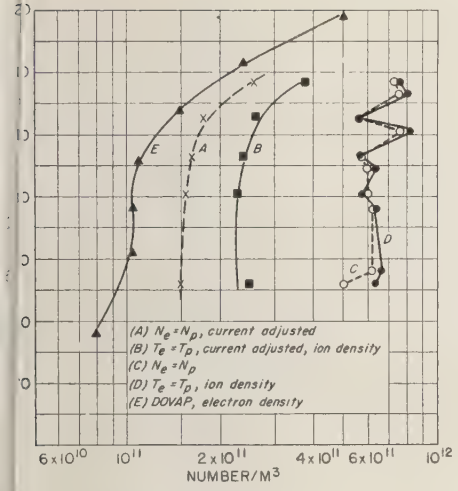

. 4—Electron and ion density vs. altitude, November 30, 1958, Fort Churchill, Canada.

e gradients over Fort Churchill have been orted by *Horowitz and LaGow* [1958]. How- r, close correlation between those data and probe data is not feasible since they were tained at different times. Also, the equiva- ce of electron and neutral-particle tempera- es in the ionosphere has not been firmly ablished.

The positive-ion number density shown in gure 4 was estimated from the volt-ampere aracteristic by two methods, both dependent the electron-temperature data. The first thod, which depends on the slope, the voltage, d the current at any single point in the ion- turation part of the curve, assumes that the n and electron temperatures are equal; the ond method [*Allen, Boyd, and Reynolds,* 57] assumes not only that the ion and elec- on number densities are equal but also that e current to the electrode is relatively inde- ndent of the ion temperature.

Curves *A* and *B* show the number density en the volt-ampere curves were corrected for apparently high current ascribed at present photoelectric emission. Curves *C* and *D* show e number density reduced by both the above ethods directly from the volt-ampere curves. olt-ampere characteristics calculated from rve *B* and the corresponding temperatures most closely approximate the experimental curves. The electron density, curve *E*, resulted from a preliminary study of DOVAP data taken on the same flight.[4] An electron density of 9×10^{10} el/m^3 at approximately 120 km was indicated by the ionograms.

The results obtained from the probe experiment described here seem to the authors to demonstrate the applicability of the Langmuir probe technique to the measurement of various properties of the ionosphere. That ionospheric parameters were measured is indicated by the facts that the currents increased with altitude and that all available experimental data (electron temperature, ion number density, electron number density from the probe, DOVAP, and ionograms) are consistent. The high electron temperatures are in reasonable agreement with higher gas temperatures discovered over Fort Churchill [*Horowitz and LaGow,* 1958; see also *Krassovsky,* 1959], which is located in the auroral zone. In this regard, it has been suggested by *Jastrow* [1959] that the temperature of the upper atmosphere in the auroral zone is controlled by the intensity of the particles in the outer Van Allen belt, and thus that the properties of the auroral-zone upper atmosphere differ entirely from those of the atmosphere at lower latitudes. Thus, correspondence between the temperature in the auroral zone and that at lower latitudes is not necessarily expected. It is clear, however, that more measurements are necessary before these conclusions can be firmly established.

Besides the flight reported, three other probes have been similarly flown in the ionosphere. One of them was spherical with protruding cylindrical electrodes which, because of a large ratio of electrode areas, permitted sampling of a greater percentage of the available electrons. The results of these experiments are being studied.

It is planned to fly several additional experiments with different geometries to higher altitudes.

References

Allen, J. E., R. L. F. Boyd, and P. Reynolds, The collection of positive ions by a probe im-

[4] Personal communication, W. W. Berning, Ballistics Research Laboratory.

mersed in a plasma, *Proc. Phys. Soc. London, B, 70,* 297, 1957.

Hok, G., and others, Dynamic probe measurements in the ionosphere, *Univ. Mich. Eng. Research Inst. Rept.,* Ann Arbor, August 1951. Reprinted as *Univ. Mich. Research Inst. Rept.* 2521-5-S, AFCRC TN-58-616.

Hok, G., N. W. Spencer, and W. G. Dow, Dynamic probe measurements in the ionosphere, *J. Geophys. Research, 58* (2), June 1953.

Horowitz, R., and H. LaGow, Auroral-zone a mosphere-structure measurements, *J. Geoph Research, 68,* 757, 1958.

Jastrow, R., Density and temperature of the upp atmosphere, *Astronautics, 4,* (7), 24, July 19

Krassovsky, V. L., Exploration of the upper a mosphere with the help of the third Sovi sputnik, *Proc. IRE, 47,* (2), 293, February 19

(Received July 21, 1959; revised July 29, 1959.)

NOTE ON QUIET-DAY VERTICAL CROSS SECTIONS OF THE IONOSPHERE ALONG 75°W GEOGRAPHIC MERIDIAN

J. W. WRIGHT

National Bureau of Standards
Boulder Laboratories
Boulder, Colorado

Programs are now under way at several institutions for the systematic reduction of ionospheric vertical soundings to electron density profiles, N (h) curves, thereby making available for the first time adequate numerical data on electron densities throughout the lower ionosphere at many dates, times, and places (see *Thomas* [1959] for a complete bibliography of work in this field). In undertaking a similar program, the National Bureau of Standards has had two immediate objectives: to develop efficient methods by which *hourly* ionospheric soundings may be systematically reduced to N(h) profiles from a number of sounding stations, making these data available regularly to research workers; and to carry out a study of ionospheric morphology along a chain of stations stretching nearly from pole to pole along the 75°W geographic meridian. It is planned to combine these objectives by concentrating a systematic hourly reduction program on the 75th meridian stations. Already, stations at Fort Monmouth, New Jersey; Grand Bahama Island; St. Johns, Newfoundland (U. S. Army Signal Corps); and Puerto Rico (NBS), are preparing hourly virtual height data in the form required for N (h) analysis.

The method of calculation, using an IBM 650 computer, is the familiar one due to *Budden* [1954]. Results of the true height calculation, giving the heights of reflection at 60 closely spaced frequencies between 1.8 and 17.6 Mc/s, are run through another calculation that provides the electron densities at each 10 km of height above 100 km. A parabola fitted to two of the true heights and the measured value of f_0F_2 is used to determine the height of the peak density (h_{max}) and any values of N (h) falling

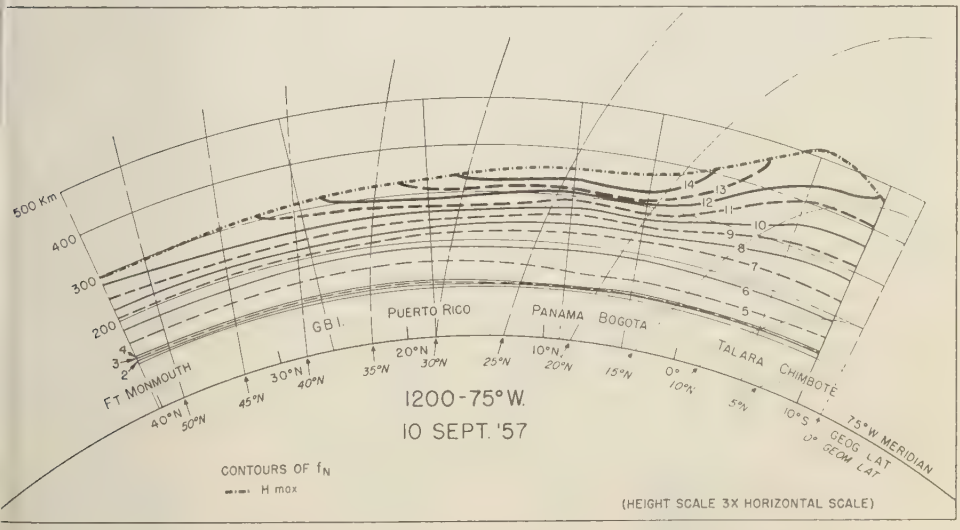

FIG. 1—Instantaneous ionospheric section along 75°W geographic meridian.

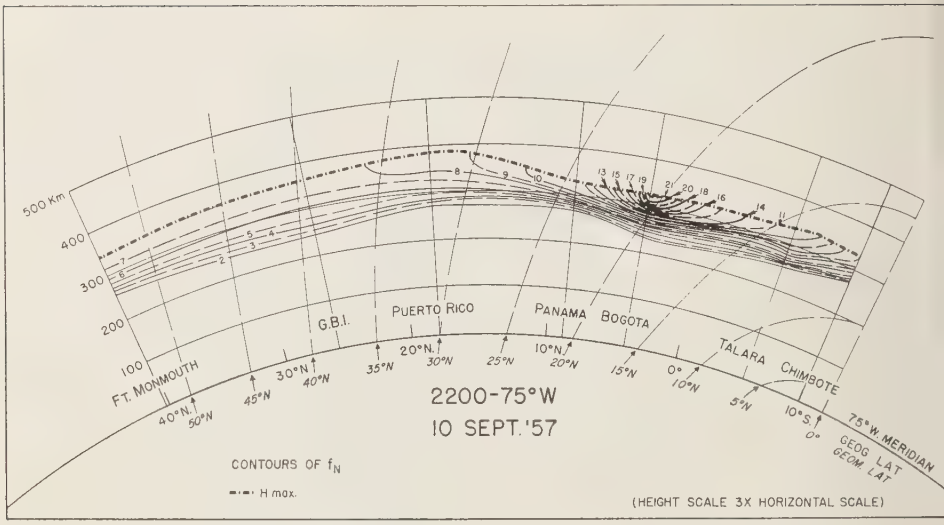

FIG. 2—Instantaneous ionospheric section along 75°W geographic meridian.

above the highest true height. In additional steps in the program, not further discussed here, the N (h) distribution is integrated in 10-km steps, to give the electron content up to each level. The integrated electron density up to $h_{max}F_2$ is called Sh_{max}.

Some results for one magnetically quiet day in September 1957 are shown in Figs. 1 and 2. Contours of plasma frequency f_N, related to electron density by N (electrons/cm^3) = $12{,}400f_N$ Mc/s, are shown in a vertical plane along the 75th meridan between geographic latitudes 10°S and 40°N. The dashed limiting curve represents h_{max}, the height of maximum electron density, above which no direct information can be obtained from conventional vertical soundings. The f_N contours intersecting h_{max} indicate the *penetration frequency*, f_0F_2, at that point; these contours form closed loops above h_{max} in an unknown way, although reasonable inferences can be drawn from the spacing of the contours below h_{max} and from recent satellite results which indicate that the integrated electron content above the maximum is roughly three times that below. Lines of force of the geomagnetic field are shown on the figure at each 5° of geomagnetic latitude. The present note is confined to a few qualitative remarks on these figures.

By graphically illustrating the presence of large horizontal ionization gradients, the contours account for a puzzling kind of ionogram frequently observed at low latitudes; a typical example (Panama, 2000 September 10, 1957) is shown in the upper part of Figure 3. No well-defined f_0F_2 can be observed here; the virtual height curve fades out to higher frequencies and heights. An explanation is obtained from the lower part of Fig. 3, which shows the ionospheric structure at the time the vertical sounding was obtained. It seems probable that, at frequencies above about 9 Mc, echoes observed at Panama are progressively more oblique as the probing frequency increases; that is, they come from the intense "cloud of ionization" over Bogotá. Of course, this casts doubt on the profile of ionization deduced from the Panama sounding, but it is believed that an approximately correct value of overhead maximum electron density is obtainable from the first multiple echo, and that a useful virtual height curve is observed at lower frequencies.

Two interesting features of the equatorial ionosphere also are immediately apparent from these illustrative cross sections:

The equatorial "bulge" or great thickness of the ionosphere over the geomagnetic equator (*Figure 1*). It has been shown by *McNish and*

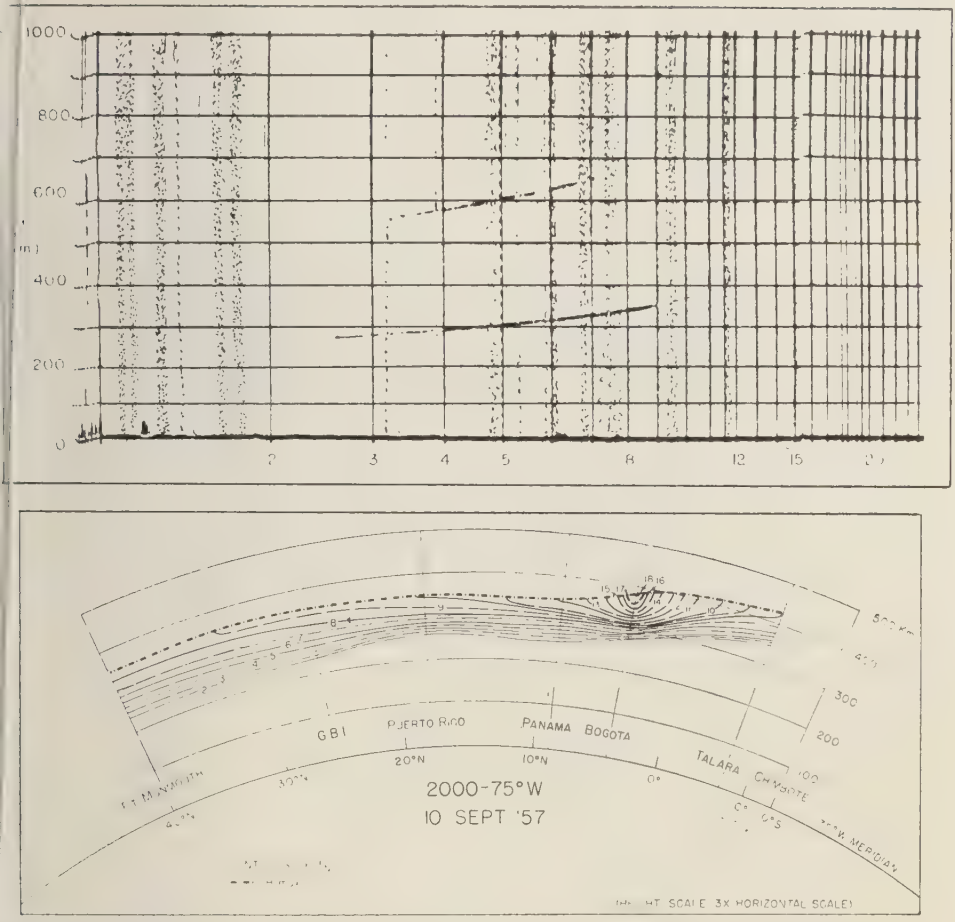

FIGURE 3—*Upper:* Ionospheric sounding obtained at Panama 2000 September 10, 1959. *Lower:* Ionospheric structure at the same time.

Gautier [1949] that vertical drift forces produced by the diurnal variation of the earth's magnetic field can account for the considerable distention of the daytime equatorial ionosphere. *Martyn* [1954], in discussing this process in greater detail, points out that the absence of vertical diffusion at the equator permits upward drift to take full effect. In the evening, the *F* region is left at a very great altitude, where it decays slowly until brought to lower altitudes by downward drift.

The region of intense ionization at about 17° from the geomagnetic equator. It is especially prominent over Bogotá at 2200, in Figure 2. The mechanism has been suggested by Mitra [1946] and discussed further by *McNish and Gautier* [1949] and by *Martyn* [1954]. It is supposed that the ionization diffuses *horizontally,* from the high, thick equatorial ionosphere, along the converging magnetic lines, to neighboring higher latitudes. The geomagnetic line passing through the 300-km over Bogotá reaches 800 km over the geomagnetic equator, not a great distance above the daytime peak of the equatorial *F* region.

A quantitative investigation of these two

features of the equatorial ionosphere is the subject of a current study at this laboratory.

Acknowledgment—The development of the NBS $N(h)$ facilities receives the valued assistance of G. H. Stonehocker, T. E. Van Zandt, and H. H. Howe. The work was supported largely by funds made available to NBS by the National Science Foundation.

References

Budden, K. G., A method for determining the variation of electron density with height ($N(z)$ curves) from curves of equivalent height against frequency (h', f curves), *Report of the Physical Society Conference on the Physics of the Ionosphere*, p. 320, The Physical Society, London September 1954.

Martyn, D. F., Theory of height and ionizatio changes at the maximum of a Chapman-lik region, taking account of ion production, de cay, diffusion, and tidal drift, *Report of th Physical Society Conference on the Physics o the Ionosphere*, p. 254, The Physical Society London, September 1954.

McNish, A. G., and T. N. Gautier, Theory o lunar effects and midday decrease in F_2 ion density at Huancayo, Peru, *J. Geophys. Re search, 54*, 181–185, 1949.

Mitra, S. N., Geomagnetic control of region F_2 o the ionosphere, *Nature, 158*, 668–669, 1946.

Thomas, J. O., The distribution of electrons i the ionosphere, *Proc. IRE, 47*, 162–175, 1959.

(Received June 27, 1959; revised July 24, 1959.

COSMIC RADIO NOISE ABSORPTION ON 25 MC/S AND *F* SCATTER

K. R. RAMANATHAN AND R. V. BHONSLE

Physical Research Laboratory, Ahmedabad, India

In a previous communication [*Bhonsle and Ramanathan,* 1958], the authors have reported on the measurements of cosmic radio noise on 25 Mc/s at Ahmedabad over a period of 1 year from March 1957 to February 1958 and have given estimates of the values of the attenuation of cosmic radio noise in the atmosphere. On the assumption that the attenuation occurs mainly in the *D* region and *F* regions of the ionosphere, it was shown that the total attenuation could be divided into two components, a *D*-region and an F_2-region component. On examination of the mean diurnal and seasonal variations, the curves of total attenuation (Fig. 1) showed the following features: (1) minimum attenuation occurs before sunrise; (2) a daytime maximum in the attenuation occurs near or shortly after noon; and (3) a second maximum in attenuation occurs after sunset and before midnight, usually between 20 and 22 hours local time, in the winter equinoctial and months.

Adopting a method previously used by *Mitra and Shain* [1953], *D*-region absorption and *F* attenuation were separately estimated. The *D*-region absorption was found to be directly dependent on solar zenith distance with maximum amplitude in summer and minimum in winter. The deviative *F*-region attenuation was not a simple function of the solar zenith distance; above a certain minimum value of the critical frequency f_0F_2, it increased rapidly with increase in f_0F_2. The F_2 attenuation in the first half of the night often exceeded its maximum daytime value by about 2 db. It was evident that the increase in the value of f_0F_2 in the early part of the night and its nearer approach to 25 Mc/s were inadequate to account for the premidnight peak in F_2 attenuation during winter and equinoctial months. There was some evidence to show that the premidnight peak was connected with *F* scatter. But the occurrence of a rather sharp rise in attenuation shortly after sunset and its reaching a maximum at 21 to 22 hours were puzzling features.

The view that the additional nighttime peak is due to *F* scatter is strongly supported by some new evidence brought out recently by *Bateman and others* [1959] from their observations of *F* scatter during IGY in the Philippines-Okinawa area. They observed anomalous enhancements, during the evening hours, of the signals transmitted at VHF between the Philippines and Okinawa. The enhancements were found to occur with greatest frequency in September and October. They usually lasted several hours, beginning at about 19 hours at the midpoint of the transmission path. The signal intensity usually increased rapidly, then leveled off, and finally dropped back below the normal scatter level around midnight. The first measurements of this anomaly were made over an experimental circuit operating at 36.4 Mc/s between Poro Point, Philippine Islands, and Sobe, Okinawa. A second circuit at 49.84 Mc/s over an almost identical path commenced operating in September 1957. During the year of operation at 36.4 Mc/s, the frequency of occurrence of evening enhancements reached a peak during each equinoctial period. During 1958–1959 at 49.84 Mc/s, however, only the peak in the autumn could be observed. At vernal equinox, there appeared, if anything, to be a minimum.

Bateman and his co-authors have examined the ionospheric data from Baguio, Philippine Islands, and Okinawa ionospheric stations during September 1957, a period of anomalous propagation. No association between the anomaly and *E*-region effects could be detected, but the periods of anomalous propagation did correspond to those of spread-*F* at Baguio and high F_2 critical frequencies at Okinawa. They suggested that the enhanced signal was propa-

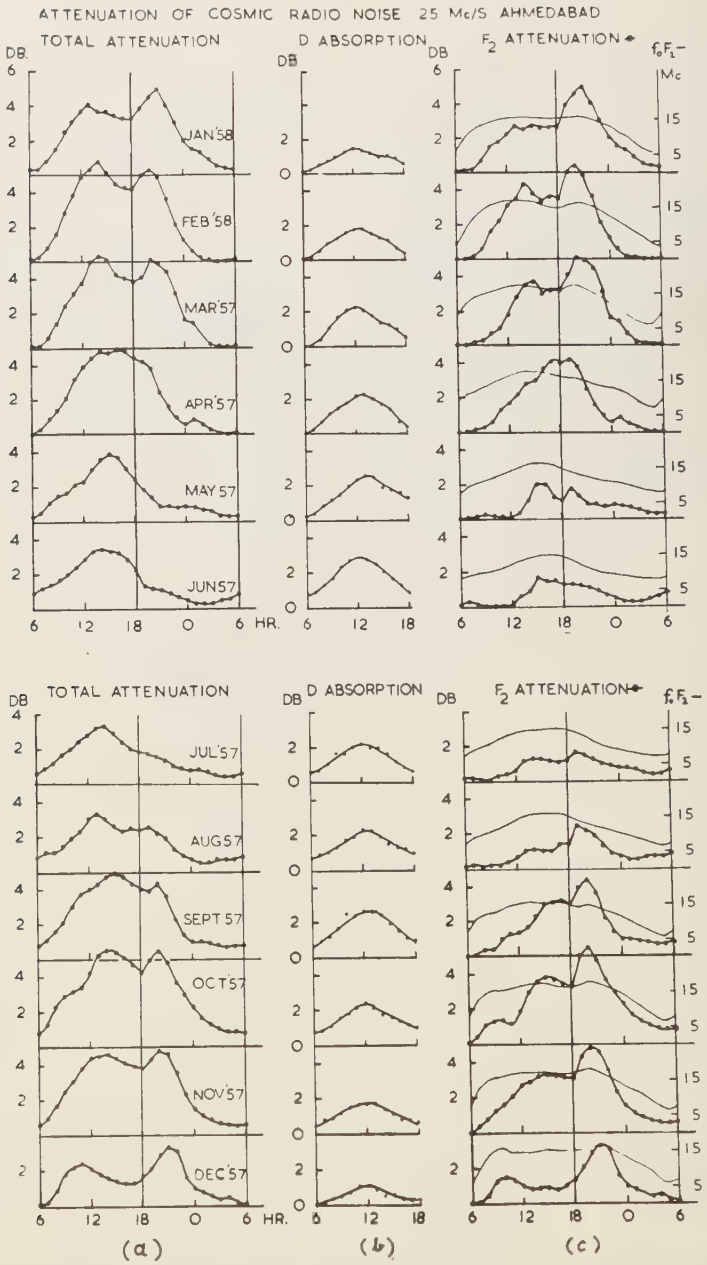

FIG. 1—Monthly mean hourly values of (*a*) total attenuation, (*b*) D absorption, and (*c*) F_2 attenuation (median values of f_0F_2 are also shown by thin lines). (From *J. Sci. Ind. Research, India 17A*, 1958.)

ated via the F region and was enhanced when here was low-latitude spread-F

We are of the view that the anomalous hancement of scattered VHF signals observed these authors and the sharp post-sunset crease in the attenuation of cosmic noise served at Ahmedabad are due to the same ysical cause. The agreement in the times of mmencement of these two independent effects, the time taken for reaching their maximum tensity, and in the time of their subsequent ecline is very striking. It is physically understandable that ion clouds of appropriate size in ae F region can increase the scattered VHF gnal strength from a ground transmitter and the same time attenuate the noise signals ceived from extraterrestrial noise sources. easonal variation of spread-F echoes at Ahedabad shows a maximum in equinoxes in igh-sunspot years and also shows a negative rrelation with magnetic activity [*Kotadia nd Ramanathan,* 1959]. It may be mentioned ere that the cosmic noise absorption on 25 Mc/s at Ahmedabad decreases markedly on days of magnetic storms, a fact that can be correlated with the known absence of F scatter on magnetically disturbed days in low latitudes.

One of the authors, R. V. Bhonsle, is the recipient of a Senior Research Fellowship from the Council of Scientific and Industrial Research, Government of India.

References

Bateman, R., and others, IGY observations of F-layer scatter in the Far East, *J. Geophys. Research, 64,* 403–405, 1959.

Bhonsle, R. V., and K. R. Ramanathan, Studies of cosmic radio noise on 25 Mc/s at Ahmedabad, *J. Sci. Ind. Research, India, 17A,* 40–45, 1958

Kotadia, K. M., and K. R. Ramanathan, Magnetic and ionospheric disturbances in low latitudes (in press).

Mitra, A. P., and C. A. Shain, The measurement of ionospheric absorption using observations of 18.3 Mc/s cosmic radio noise, *J. Atmospheric and Terrest. Phys., 4,* 204–218, 1953.

(Received June 27, 1959).

SOME EFFECTS OF PRESSURE ON THE THERMOLUMINESCENCE OF LIMESTONE

Ernest E. Angino

Department of Geology, University of Kansas
Lawrence, Kansas

In the course of studies on the effects of pressure on the thermoluminescence of limestones, certain phenomena have been observed that are relevant to work now being conducted at various institutions on the different aspects of thermoluminescence.

The first investigation of the effects of deformation on thermoluminescence was that of *Zeller and others* [1955]. Recent work by *Angino* [1959], *Handin and others* [1957], and *Debenedetti* [1958] has furnished further information on some of the processes at work in pressure-induced thermoluminescence.

In an effort to ascertain the nature of the effects of pressure *alone* on the thermoluminescence of limestones, a preliminary study was made on seven limestones of different geologic age (Table 1). The samples were preheated in a muffle furnace to 300°C for 18 hours. This treatment is considered sufficient to drain completely all of the thermoluminescence occurring naturally in the 0 to 400°C temperature range. These samples were then pressed at 7720 bars for increasing lengths of time (2, 5, 10, 15, 30 minutes), and a glow curve was plotted for each sample to determine the amount of thermoluminescence present after pressure. Pressure was applied vertically by a Rogers 50-ton Universal hydraulic press and was not truly hydrostatic. Three of the samples gave no indi cation of thermoluminescence after pressure but the remaining four exhibited considerabl thermoluminescence.

Pressure activates thermoluminescence i some limestones and not in others. The reaso for these differences in pressure activation i not presently known. Further work indicate that the length of time of pressure applicatio is a more critical factor than the actual pressur applied.

The thermoluminescence observed after hea and pressure treatment was of the high-tem perature type. The peaks in all cases wer above 300°C, actually 345°C in three instance and 320°C in the fourth. Pressure-induce thermoluminescence was not observed belo 200°C. Figure 1 shows a comparison of th glow curves of natural and pressed thermolumi nescence for the same sample and illustrate the different character of the two types o curves.

In all cases, when the thermoluminescenc (as measured by planimetry) was increase with increasing time of pressure application, i took place by an increase in light intensity an not by any broadening of the peak. This woul seem to indicate narrow trapping levels rathe than broad ones.

Table 1—*Ratios of pressed to natural thermoluminescence* Tl_p/Tl_u

Name	Age	Tl_p/Tl_u	Location
Kimmswick	Ordovician	0.15	Cedar Hill, Missouri
Sundance	Jurassic	0.00	Crow Heart, Wyoming
Nummulitic	M. Eocene	0.00	Ddjurdjura Mts., Algeria
Sierra Blanca	U. Eocene	0.00	San Rafael Mts., California
Eniwetok	Miocene	0.84	Eniwetok, Marshall Islands
Tavenier	Pleistocene	0.45	Tavenier Creek Bridge, Florida
Tufa	Recent	1.08	Yellowstone Park, Wyoming

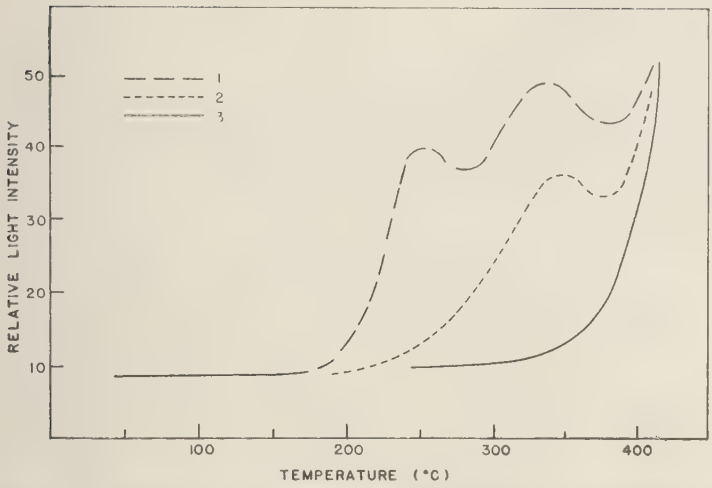

Fig. 1—Glow curves. (1) Natural curve of Eniwetok sample before heat and pressure treatment. (2) Curve of same sample after heat and pressure treatment. (3) Black body radiation curve.

The maximum pressure-induced thermoluminescence was obtained after 30 minutes of pressure application and ranged from 15 per cent of the natural thermoluminescence in the Ordovician sample to 108 per cent in the Recent sample. These observations imply that similar results could be expected if limestones were subjected to pressures smaller than 7720 bars for long periods of time. For example, if we assume an average density of 2.5 for sedimentary material, then at a depth of 10,000 feet (3050 m) a pressure of 745 bars would be developed. Such pressure over a long period of time may be sufficient to develop enough pressure-induced thermoluminescence to constitute a relatively large percentage of the observed natural thermoluminescence of the sample.

The reason for the by-passing of low-temperature trapping levels is unknown. Possibly the trapping mechanisms for high- and low-temperature peaks are different and independent of one another. *Debenedetti* [1958] has postulated that the high-temperature peaks are activated by less energetic agents (like deformational ones) than low-temperature peaks.

The general shape of the pressure-induced curve is similar to that of a crystallization-induced glow curve. It is now thought possible that some type of secondary reaction occurs in the pressed sample during pressure application, so that what we observe may actually be a crystallization effect induced by pressure.

It has been noted that the peak temperatures of the pressure-induced glow curves do not coincide with the peaks of the natural thermoluminescence of the sample. The pressure-induced peak is from 15 to 20°C higher. This can be interpreted as substantiating evidence that the same trapping mechanism is not at work in the two instances.

Certain of the phenomena observed cannot be fully explained by the gliding mechanisms of *Handin and others* [1957] or the electrostatic effects postulated by *Zeller and others* [1955]; consequently, more experimental data are being gathered in the hopes that an acceptable theory to explain these pressure effects can be formulated. Evidence is accumulating, however, to show that the effects of pressure are not as small as originally thought, and these effects will have to be taken into account or serious errors could be introduced into any age-determination method based on thermoluminescence.

The author expresses his thanks to E. J. Zeller and William C. Pearn for discussions on this subject. Financial assistance under Contract AT(11-1)83, Project 5, from the Atomic Energy Commission is gratefully acknowledged.

References

Angino, E. E., Pressure effects on thermoluminescence of limestone relative to geologic age, *J. Geophys. Research, 64,* 569–573, 1959.

Debenedetti, A., On mechanical activation of thermoluminescence in calcite, *Nuovo cimento, 7,* 251–254, 1958.

Handin, J., D. V. Higgs, D. R. Lewis, and P. K. Weyl, Effects of gamma radiation on the experimental deformation of calcite and certain rocks, *Bull. Geol. Soc. Am., 68,* 1203–1224, 1957.

Zeller, E. J., J. L. Wray, and F. Daniels, Thermoluminescence induced by pressure and crystallization, *J. Chem. Phys., 23,* 2187, 1955.

(Received June 26, 1959.)

CONTAMINATION OF THE INTENSITIES OF THE OXYGEN LINES BY THE NEIGHBORING OH EMISSION BANDS IN THE NIGHT AIRGLOW

M. W. CHIPLONKAR AND P. V. KULKARNI

Department of Physics
University of Poona, Poona 7, India

In the course of our investigations of the night airglow at Poona, we have come across certain results that point to the significance of the emission of the OH bands in the upper atmosphere.

At Poona a photoelectric photometer was used to scan the whole dome of the sky in an almucantar manner several times during a clear night. From these observations and by using the Van Rhijn formula the height of the λ5577 Å emission layer was estimated to be 220 km and 190 km during the clear seasons of 1956 and 1957–1958, respectively [*Kulkarni*, 1958]. Workers in the higher latitudes have obtained practically the same values (between 200 and 250 km) for the height of λ5577 Å layer [*Chamberlain and Meinel*, 1954]. From more recent observations much lower values (68 to 112 km) have also been deduced [*Roach*, 1955]. Similarly, for the λ6300 Å emission layer, heights ranging from 180 km to 270 km had been deduced earlier [*Chamberlain and Meinel*, 1954], and in later investigations they were found to lie between 116 and 143 km [*Roach*, 1955]. Using the rocket techniques these two layers were found to be at about 100 km and 162 km respectively. Apart from the actual heights of the layers it is significant to note the very large difference between the heights of these two emission layers, whether obtained by the Van Rhijn method, the triangulation method, or the rocket technique.

Further, using a fast spectrograph (glass, *f*/2,5) the spectrum of the night airglow was photographed at Poona on many clear moonless nights during the period December 1956 to April 1957 [*Chiplonkar*, 1957], and from the 21 pairs of the intensity measures for the two radiations λ5577 Å and λ6300 Å a high coefficient of correlation, 0.62, and a rather low value for their intensity ratio, 100 : 24, were obtained. On the other hand, Roach and coworkers have obtained a much smaller value for the correlation coefficient [*Roach*, 1955], namely 0.3, between the intensities of the two oxygen lines, and a relatively higher ratio (100 : 60) of their intensities [*Roach*, 1956].

If the stepwise process of emission for the atomic oxygen lines is accepted, it is difficult to understand why in the higher latitudes such *large differences* between the heights of the two emission layers and such *low* correlations between their intensities are observed.

These discrepancies between the observations in the tropics and the higher latitudes can be explained satisfactorily if we take into account the effect of contamination due to the OH emission bands in the upper atmosphere. According to *Meinel* [1950], apart from the very bright and numerous OH bands in the near and far infrared regions there are OH bands at λ5593 Å ($v' = 7, v'' = 1$) and at λ6257 Å ($v' = 9, v'' = 3$) that are sufficiently bright and nearly coincident with the two atomic oxygen emission lines. For instance, the intensity of the OH band at λ5593 Å has been estimated to be approximately 6 per cent of the average observed intensity of the oxygen green line λ5577 Å, and that of λ6257 Å to be 115 per cent of the red oxygen line λ6300 Å [*Roach*, 1956]. Naturally, the green-line intensity is much less affected than red-line intensity by the neighboring OH band.

We suggest that the OH emission is probably

much greater and more variable in the higher latitudes than in our latitudes. Such large contaminations by the OH bands, especially of the red oxygen line, will naturally give a low correlation and also a different (possibly lower decause the height of the OH emission has been estimated at 70 km [*Roach et al.*, 1950]) value for the height of the λ6300 Å emission layer.

In our present photometer we could not measure the intensities of the red line along with the green, and hence height for the λ6300 Å layer is not available for our station. Efforts are, therefore, being made in that direction for further confirmation of this hypothesis.

References

Chamberlain, J. W., and A. B. Meinel, *The Earth as a Planet* (ed., G. P. Kuiper), p. 561, table 1, University of Chicago Press, Chicago, 1954.

Chiplonkar, M. W., *J. Poona Univ.* (*Sci. & Tech.*), *12*, 123, 1957.

Kulkarni, P. V., Thesis submitted for Ph.D. degree, Poona University, 1958.

Meinel, A. B., *Astrophys. J.*, *111*, 555, 1950.

Roach, F. E., *Ann. géophys.*, *11* (2), 214–230, 1955.

Roach, F. E., *IGY Instruction Manual for the Night Airglow*, pp. 75–76, Pergamon Press, New York, 1956.

Roach, F. E., H. Pettit, and D. R. Williams, *J. Geophys. Research*, *55* (2), 183–190, 1950.

(Received May 8, 1959; revised June 27, 1959.)

HYDROMAGNETIC PROPAGATION OF SUDDEN COMMENCEMENTS OF MAGNETIC STORMS

W. E. FRANCIS, M. I. GREEN, AND A. J. DESSLER

Lockheed Aircraft Corporation, Missiles and Space Division
Palo Alto, California

The curve for the hydromagnetic wave velocity function of altitude, shown in Figure 1, was computed from preliminary ion density calculations of *F. S. Johnson* [1959] and the observations of *C. Y. Johnson and others* [1958]. This curve replaces the one previously reported [*Dessler*, 1958]. Table 1 gives the ion number density, the average ionic molecular weight, and the velocity of hydromagnetic waves as functions of altitude in the equatorial plane. It is likely that the ion density figures used in computing the hydromagnetic wave velocity above 2000 km will be modified (W. B. Hanson and F. S. Johnson, private communication). The expected changes are such as to reduce the calculated delay time from the 11 sec given here. The hydromagnetic wave velocity V in the equatorial plane was calculated from the relation

$$V = B/(\mu_0\rho)^{1/2}$$

$$= KR^{-3}(mn)^{-1/2} \quad \text{(MKS units)}$$

where B is the magnetic field strength (taken to have a value $B_0 = 0.315$ gauss at the earth's surface); μ_0, the permeability of a vacuum; ρ, the ionic mass density; R, the distance from the center of the earth; m, the ionic molecular weight; n, the ion number density; and $K = 1.789 \times 10^{32}$.

The ray paths, shown in Figure 2, and the transit times, given in Table 2, of hydromagnetic waves traveling in the equatorial plane between points several earth radii distant on the noon meridian to points immediately above the

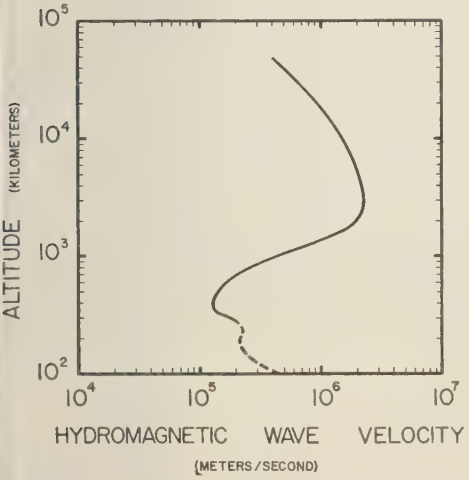

FIG. 1—Velocity of hydromagnetic waves in the equatorial plane vs. altitude. This curve applies for both longitudinal and transverse waves. The curve is dashed in the lower altitude region where dissipation becomes important and the wave propagation becomes complex.

TABLE 1—*Ion number density, average ionic molecular weight, and hydromagnetic wave velocity vs. altitude above earth's surface*

Altitude, km	Ion number density, ions/m³	Average ionic molecular weight	Velocity, m/sec
150	2.09×10^{11}	29.5	2.47×10^5
200	3.31×10^{11}	23.0	2.17×10^5
250	3.72×10^{11}	18.1	2.26×10^5
300	6.76×10^{11}	16.3	1.72×10^5
400	1.10×10^{12}	16.0	1.30×10^5
500	8.70×10^{11}	16.0	1.40×10^5
700	3.62×10^{11}	15.4	2.04×10^5
1,000	8.78×10^{10}	10.6	4.39×10^5
2,000	1.45×10^{10}	1.43	2.01×10^6
3,000	8.3×10^9	1.00	$2.27 \times 10^{6*}$
4,000	5.1×10^9	1.00	2.13×10^6
5,000	3.3×10^9	1.00	2.02×10^6
10,000	6.5×10^8	1.00	1.51×10^6
25,000	5.0×10^7	1.00	7.78×10^5

*Maximum.

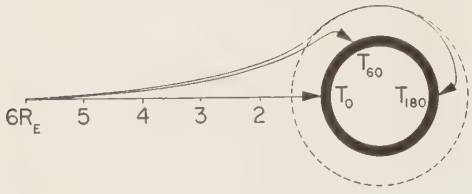

FIG. 2—Three paths in the equatorial plane of hydromagnetic waves generated at 6 earth radii. The dashed line indicates the altitude of maximum velocity (3×10^3km). Note that the ray paths traveling around the earth remain very near this altitude in accordance with Fermat's principle. For these ray paths, T_0 is 33.1 sec, T_{60} is 35. 4 sec, and T_{180} is 43.6 sec.

earth's surface were computed utilizing Fermat's principle. The transit time T for the above ray paths, between the points S_i and S_f expressed in polar coordinates (R, θ), is

$$T = \int_{S_i}^{S_f} \frac{dS}{V} = \int_{\theta_i}^{\theta_f} \frac{(R^2 + R'^2)^{1/2}\, d\theta}{KR^{-3}(mn)^{-1/2}}$$

$$= \int_{\theta_i}^{\theta_f} F(R, R')\, d\theta$$

where R is the distance from the center of the earth, θ is the polar angle, $R' = dR/d\theta$, and dS is the differential of arc. The application of Fermat's principle results in the Euler equation [*Courant and Hilbert*, pp. 183–187, 1953],

$$\frac{d}{d\theta}\left(\frac{\partial F}{\partial R'}\right) - \frac{\partial F}{\partial R} = 0$$

Since the function F does not contain the independent variable θ, it follows that

$$R'\left[\frac{d}{d\theta}\left(\frac{\partial F}{\partial R'}\right) - \frac{\partial F}{\partial R}\right]$$

$$= \frac{d}{d\theta}\left[R'\frac{\partial F}{\partial R'} - F\right] = 0$$

thus it is apparent that

$$R'\frac{\partial F}{\partial R'} - F = \text{constant} = C$$

from which R' and $d\theta$ may be obtained [*Courant and Hilbert*, pp. 206–207, 1953]. Substituting for F yields

$$R' = \pm R[mn(R^4/KC)^2 - 1]^{1/2}$$

and

$$d\theta = \pm [mn(R^4/KC)^2 - 1]^{-1/2}(dR/R)$$

The equation for the transit time then becomes

$$T = \left| \int_{R_i}^{R_f} \frac{1}{K}\left(\frac{1}{KC}\right) \frac{mnR^7\, dR}{[mn(R^4/KC)^2 - 1]^{1/2}} \right|$$

The constant $1/(KC)$ can be determined from the relation

$$1/KC = -(R^2 + R'^2)^{1/2}/[R^5(mn)^{1/2}]$$

The ray paths were chosen so that time differences could be obtained for the vertical arrival of a hydromagnetic wave on the noon meridian as compared with the later time of arrival on other meridians. Calculation of the transit time for the ray path of vertical descent offers no problem. The equation for the transit time in

TABLE 2—*Transit and delay times for waves traveling in the earth's equatorial plane*

T_θ represents the transit time for hydromagnetic waves generated at the noon meridian, and traveling in the equatorial plane, to reach the earth's surface at an angular distance of $\theta°$ from the noon meridian. The angular displacement is thus represented by a subscript; e.g., T_{60} represents the transit time to the meridian 60° from the noon meridian. ΔT_θ is the delay time or time difference between the arrival of a hydromagnetic wave on the noon meridian and its arrival at a meridian θ degrees away, $\Delta T_\theta = T_\theta - T_0$.

Distance of generation from earth's center, earth radii	Transit time, seconds				Delay time, seconds		
	T_0	T_{60}	T_{120}	T_{180}	ΔT_{60}	ΔT_{120}	ΔT_{180}
2	7.5	10.3	14.4	18.5	2.8	6.9	11.0
4	17.0	19.4	23.5	27.6	2.4	6.5	10.6
6	33.1	35.4	39.5	43.6	2.3	6.4	10.5
10	89.1	91.3	95.4	99.5	2.2	6.3	10.4

this case becomes

$$T = \int_{R_i}^{R_f} \frac{dR}{KR^{-3}(mn)^{-1/2}}$$

The calculation of transit times for other ray paths requires a proper choice for the constant $1/(KC)$. All rays traveling at the altitude of maximum velocity will be refracted away from this altitude except the path satisfying the condition $R' = 0$. Since here we are only interested in rays converging slowly toward the earth, it is necessary to choose a very small negative value of R' at the altitude of maximum velocity. The constant $1/(KC)$ is then fixed by this choice of R'. The numerical integration of the transit times for the above ray paths requires the use of a very small increment, ΔR, near the maximum velocity altitude. The computations were done on a Univac 1103AF digital computer.

The difference in transit times for waves generated at 6 earth radii to reach the earth's surface at the noon meridian and at the midnight meridian in the equatorial plane is found to be approximately 11 sec. It will be noticed in Table 2 that there is a difference in delay times of only a few tenths of a second for waves originating between 2 and 10 earth radii. This would seem to indicate that the delay times for the sudden commencements of weak and strong magnetic storms will not vary appreciably.

Gerard [1959] has compiled data on the arrival times of world-wide sudden commencements for three magnetic storms. On the basis of *Dessler's* [1958] original estimate of the delay time for sudden commencements (computed from ray paths which violated Fermat's principle), Gerard concluded that the hydromagnetic mechanism for the propagation of sudden commencements was not valid. Gerard's data, however, show an average delay time of about 11 sec between sudden commencements on the dark and sunlit hemispheres for the three storms. This delay time is in good agreement with our present results which were obtained in accordance with Fermat's principle.

The results presented here are to be regarded as an approximation, since: (1) the ray paths were confined to the equatorial plane, (2) the earth's magnetic field was approximated as a centered dipole, (3) diffractive and dispersive effects were not considered, (4) the impact of the solar wind on the geomagnetic field will produce an extended source whereas we considered only point sources, and (5) the hydromagnetic wave velocity above the 2000 km may be modified. Nevertheless we believe that the results of calculations taking the above effects into account will not differ significantly from the preliminary findings presented here.

Hydromagnetic ray tracing calculations for the full three-dimensional case are being carried out by W. Hess and collaborators at the Lawrence Radiation Laboratory, Berkeley, California.

References

Courant, R., and D. Hilbert, *Methods of Mathematical Physics*, vol. 1, Interscience Publishers, New York, 561 pp., 1953.

Dessler, A. J., The propagation velocity of world-wide sudden commencements of magnetic storms, *J. Geophys. Research, 63,* 405–408, 1958.

Gerard, V. B., The propagation of world-wide sudden commencements of magnetic storms, *J. Geophys. Research, 64,* 593–596, 1959.

Johnson, C. Y., E. B. Meadows, and J. C. Holmes, Ion composition of the arctic ionosphere, *J. Geophys. Research, 63,* 443–444, 1958.

Johnson, F. S., The structure of the outer atmosphere including the ion distribution above the *F*-2 maximum, *Tech. Rept. LMSD 49719,* Lockheed Missiles and Space Division, Sunnyvale, Calif., 29 pp., 1959.

(Manuscript received August 3, 1959.)

Information for Contributors
to the *Journal of Geophysical Research*

Manuscripts—Send manuscripts to J. A. Peoples, Jr., Department of Geology, University of Kansas, Lawrence, Kansas. Manuscripts, including proof copies of figures, should be submitted in triplicate to expedite review and publication. Manuscripts should be in English, typewritten on heavy paper on one side of page only, double spaced (including abstracts and references), with generous margins.

Ample space should be allowed for mathematical expressions, which should be typed or very plainly written by hand. Particular attention should be given to legibility of subscripts and superscripts and to differentiation between capital and lower case letters. Unusual symbols and cumbersome notations should be avoided. Fractional exponents should be used in preference to root signs, and the solidus (/) should be used for fractions wherever its use will save vertical space.

Authors are urged to have their papers critically reviewed by their associates for scientific validity, manner of presentation and use of English before submitting them for publication.

Abstracts—An abstract must accompany each manuscript. It should be a concise but comprehensive condensation of the essential parts of the paper, suitable for separate publication, and adequate for the preparation of general indexes to geophysical literature.

References and footnotes—References should be indicated in the text by the insertion in brackets of the author's name and the year of publication, thus: [*Trelease*, 1951]. If the author's name is part of the text, only the year is bracketed. If there are two or more references citing different papers published in the same year by the same author, distinguish them by the letters a, b, c after the year. At the end of the paper, list all references alphabetically by the authors' names. Include in each entry the following: name of senior author, followed by his initials; names of junior authors, each preceded by his initials; title of paper (or book); title of publication or journal; volume number; inclusive page numbers; year of publication. Abbreviations of journals follow the style used in *Chemical Abstracts*. If in doubt, give the full title of the publication or journal. When a book is cited, add the publisher's name, the city of publication, and the total number of pages. Reference to specific pages may be made in the text if appropriate. Acknowledge unpublished reports and private communications in the text, not as references. Avoid footnotes to the text; use parenthetic sentences instead of footnotes if possible.

Tables and figures—Material suitable to tabular form should be arranged as a table and may be typewritten on a separate page, Tables must be numbered according to their sequence in the text, and each table should have a title. Column headings should be short and self-explanatory; more complete explanation may be given in footnotes to the table. Authors should avoid repeating in the text material which is given in tables or figures.

Figures should be prepared with the column width of this Journal in mind (a scale of two to four times that of the published figure is usually adequate). Lettering and symbols should be large enough to stand reduction and remain legible. Captions should be typed on a separate page, not lettered in the figures. Necessary legends or lettering in the figures should be executed to meet competent drafting standards, not typewritten. If the author cannot arrange for suitable lettering, he may send the drawings with the lettering lightly penciled in or shown on a proof copy, and the lettering will be done at the editorial office.

Line drawings should be in India ink on white paper or tracing cloth. Coordinate paper should be avoided, but, if used, it must be blue-lined and the coordinate lines which are to show must be inked.

Photographs are acceptable only if they have good intensity and contrast. They should be unmounted, glossy prints.

Figures should be identified by numbering lightly in pencil, and 'top' of each figure should be indicated.

Acknowledgments—Acknowledgments should be made only for significant contributions by the author's professional associates. A brief closing statement will usually suffice.

References

American Chemical Society, *List of periodicals abstracted by Chemical Abstracts*, Chemical Abstracts Service, Ohio State Univ., Columbus, 314 pp., 1956.

American Institute of Physics, *Style Manual*, American Institute of Physics, New York, 28 pp., 1951.

American Mathematical Society, A manual for authors of mathematical papers, *Bull. Am. Math. Soc.*, 49, no. 3, pt. 2, 1–16, 1943.

Emberger, M. R., and M. R. Hall, *Scientific writing*, Harcourt, Brace and Co., New York, 469 pp., 1955.

Taft K. B., J. F. McDermott, and D. O. Jensen, *The technique of composition*, 3rd ed., Farrar and Rinehart, New York, 628 pp., 1941.

Trelease, S. F., *The Scientific paper —how to prepare it, how to write it*, Williams and Wilkins Co., Baltimore, 175 pp., 1951.

U. S. Geological Survey, *Suggestions to authors of the reports of the United States Geological Survey*, 5th ed., U. S. Govt. Printing Office, Washington, 255 pp., 1958.

William Byrd Press, *Mathematics in type*, Richmond, 58 pp., 1954.

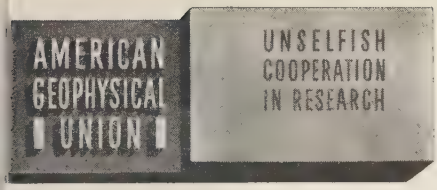

AMERICAN GEOPHYSICAL UNION

1515 Massachusetts Avenue, N.W., Washington 5, D. C.

Established by the National Research Council in 1919 for the development of the science of geophysics through scientific publication and the advancement of professional ideals.

APPLICATION FOR MEMBERSHIP

Please refer to qualifications on reverse side and designate below type of membership desired:

Member ($10) ☐ Associate ($10) ☐ Student ($3) ☐

Application forms for Corporation Membership are available upon request.

1. _____
Surname *First Name* *Middle Name*

2. _____
Preferred mailing address for publications

_____
Permanent address

3. _____ 4. _____
Place *Month* *Day* *Year of Birth* *Country of citizenship/naturalization*

5. _____
Nature of work and title and/or military rank; name and address of organization with which you are associated.

6. Check section or sections with which affiliation is desired.

☐ Geodesy
☐ Seismology
☐ Meteorology
☐ Geomagnetism and Aeronomy
☐ Oceanography
☐ Volcanology, Geochemistry, and Petrology
☐ Hydrology
☐ Tectonophysics

7. **EXPERIENCE (List below)**

Dates: From To Name and address of organization Title, duties, nature of work

8. **EDUCATION (List below)**

Dates: From To School Address Major Subject Degree, if any

*9. References: Please list below names and addresses of two or three references; include members of the AGU or others who know you well.

*10. Titles of technical contributions or publications, particularly those in the geophysical sciences, and where published.

*11. Brief statement of any special interests or qualifications in the geophysical sciences.

Date_____ _____
Written Signature

* Applicants for student membership may omit Questions 9, 10, and 11, but must fill in Question 12. Please return form with check or money order payable to American Geophysical Union, 1515 Massachusetts Ave., N.W., Washington 5, D. C

(over)

12. (STUDENT MEMBERS ONLY) The person whose signature appears on the reverse side is known to me and is a student majoring in _____ (subject) at _____ (Name of college or university) expected to graduate in _____ (year) with the degree of _____

☐ He is a full-time student, or ☐ a teaching or research assistant enrolled in more than half of a full-time academic program.

_____
(Signature of faculty sponsor)

☐ Check here if faculty sponsor is a member of AGU and willing to act as a regular sponsor for associate membership as well.

_____
(Typed or printed name of sponsor)

_____
(Title)

QUALIFICATIONS FOR MEMBERSHIP IN THE AMERICAN GEOPHYSICAL UNION

The membership of the AGU shall consist of Members, Associate Members, Student Members, and Corporation Members.

Those eligible as candidates for election to the grade of MEMBER shall be:

Member (a) Persons who have made an active contribution to geophysical research through observation, publication, teaching, or administration. Definite evidence should be presented to the Membership Committee. "Publication" may include books, articles, unpublished manuscripts, inventions, or development of geophysical instruments.

(b) Persons who have made active practical application of geophysical research. It should be shown that the nominee's work has not been purely routine, but that it has tended to create new knowledge of, or to broaden or strengthen the application of, geophysical research. In general, the minimum qualifications for membership will be not less than three years of professional experience in some phase of geophysics.

Those eligible as candidates for election to the grade of ASSOCIATE MEMBER shall be:

Associate Member Persons who have an active interest in physical processes of the Earth or technical assistance in the application of geophysics. In general, the minimum qualification for associate membership will be acceptable training or experience in some field of geophysics or allied science.

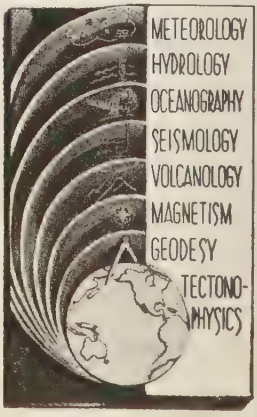

Corporation Member Corporations and other interested organizations shall be eligible as candidates for election to CORPORATION MEMBERSHIP. They shall have the privilege of designating a representative who has the rights and privileges of Members (use special form).

Student Member Those eligible as candidates for election to the grade of STUDENT MEMBER shall be persons who are graduate or undergraduate students in residence at least half-time and who are specializing in the geophysical sciences. Teaching or research assistants enrolled in more than half of a full-time academic program may also be eligible for Student Membership. Student Members shall have all the privileges of Members except that they shall not vote or hold office.

American Geophysical Union

PROPOSAL FOR CORPORATION MEMBERSHIP

To the Executive Committee, American Geophysical Union
1515 Massachusetts Ave., N.W., Washington 5, D. C.

Gentlemen:

As an indication of our interest in the aims and activities of the American Geophysical Union, and to assist in maintaining and extending its program of publication and other work in the development of the geophysical sciences, the undersigned applies for Corporation Membership in the AGU and, until further notice, agrees to pay annual dues, currently at the rate of $100 per unit of corporation membership, in accordance with the information set forth on the back of this sheet.

Company or Organization _____

By _____ Title _____
(Signature)

Address _____

City _____ State _____

General fields of activity _____

_____

_____

_____

The following person is designated as our representative in this membership _____
_____ Title _____

Number of units of membership desired (this will be taken as one unless otherwise indicated) _____

Place _____

Date _____

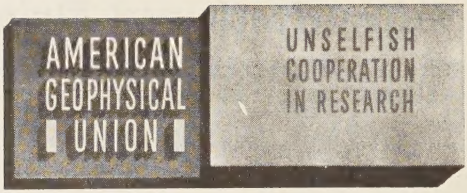

INFORMATION CONCERNING CORPORATION MEMBERSHIP

The American Geophysical Union is a non-profit scientific organization established by the National Research Council. It is the American National Committee of the International Union of Geodesy and Geophysics, and its Executive Committee is the Committee on Geophysics of the National Research Council.

Extracts from the Statutes:

Article 3. Membership—The membership of the American Geophysical Union shall be as follows:

(e) *Corporation Members*—Corporations and other organizations interested in geophysics elected by the Executive Committee of the Union. The designated representative of each such organization shall enjoy the privileges of a Member.

Extracts from the By-Laws:

(2) . . . Members of class (e) shall pay dues of not less than $100 for each calendar year; . . .

(21) One copy of each issue of (a) the *Transactions*, (b) *Journal of Geophysical Research*, (c) any published *List of Members and Officers*, and (d) any other publication which may be approved for *free distribution* to the membership by the Executive Committee of the Union, shall be sent to each . . . Corporation Member. . . . Each . . . organization in good standing may purchase any available publication of the Union at a discount from printed price list to non-members. The General Secretary is authorized to establish discounts for sales of publications.

Action of the Executive Committee, November 29, 1946:

(1) A list of corporation members shall be published on one or more pages immediately after the final page of text in each issue of the *Transactions*.

(2) A list of corporation members shall be included in the Membership Directory as a distinct unit.

AMERICAN GEOPHYSICAL UNION

1515 Massachusetts Ave., N.W.
Washington 5, D. C.

Contents

(*Continued from back cover*)

(Journal of Geophysical Research, Vol. 64, No. 10, October 1959)

Contents

(Continued inside back cover)